The Supramolecular Modification of *trans*-Resveratrol and Related Antioxidant Molecules

Lee Elizabeth Hunt

Thesis presented for the degree of

DOCTOR OF PHILOSOPHY

In the Department of Chemistry

University of Cape Town

March 2017

Supervisors:

Professor M.R. Caira

Professor S.A. Bourne

ACKNOWLEDGEMENTS

The author would like to thank:

- My supervisors, Professors M. R. Caira and S. A. Bourne, for their supervision, guidance and support throughout this project. Thank you for your patience and for having faith that I could cross this finishing line.

- Dr C. L. Oliver for the numerous conversations about the trials and tribulations of thesis writing and for advising me when challenges arose.

- Dr H. Su and Ms. D. L. Cruickshank for single crystal diffraction data-collection and processing.

- Dr. M. Bogdan and his group at the National Institute for Research and Development of Isotopic and Molecular Technologies, Cluj-Napoca, Romania for hosting me in September 2009 and for their invaluable assistance with the solution NMR studies performed in this project.

- The members of the Centre for Supramolecular Chemistry Research for their support, friendship and assistance. It has been a pleasure to work with you and be a part of a rather extended CSCR family.

- My parents for always being there for me, for being my pillars of strength, for their generous financial support of my tertiary education and constant, unconditional love. I could not have progressed this far without you.

- My husband, Julian, for his love and support, his encouragement and positivity.

- My sweet baby Rebecca who surprised us in the middle of trying to wrap up this project! Thank you for giving me a new perspective of life, love and what it means to be selfless. You are such a blessing.

- The National Research Foundation and the University of Cape Town for financial support.

Parts of this thesis have been published

- L. Trollope, D. L. Cruickshank, T. Noonan, S. A. Bourne, M. Sorrenti, L. Catenacci and M. R. Caira, Inclusion of *trans*-resveratrol in methylated cyclodextrins: synthesis and solid-state structures, *Beilstein J. Org. Chem*., 2014, **10**, 3136-3151.

Parts of this thesis have been presented at the following international conferences

- XXII Congress and General Assembly of the International Union of Crystallography (22–30 August 2011) – Oral presentation: “The Supramolecular Modification of Hydroxymethoxy Acetophenone Isomers by Cyclodextrin Inclusion” by Lee Trollope, Mino R. Caira, Susan A. Bourne.

- XXII Congress and General Assembly of the International Union of Crystallography (22–30 August 2011) – Poster: “Inclusion of a series of hydroxymethoxy acetophenone isomers in Cyclodextrins: a Solution NMR and X-ray study” by Lee Trollope, Mino R. Caira, Susan A. Bourne, Mircea Bogdan.

- Processes in Isotopes And Molecules Conference, Cluj-Napoca, Romania (24-26 September 2009) – Poster: "Inclusion of trans-Resveratrol in Cyclodextrins: a Solution NMR and X-Ray Study" by Lee Trollope, Sorin I. Farcas, Irina Kasco, Mino R. Caira, Susan A. Bourne, Mircea Bogdan.

- 2nd Romanian-South African Seminar, Sovata, Romania (18-23 September 2009) – Oral presentation: "Cyclodextrin Inclusion of antioxidants and related molecules" by Lee Trollope, Mino R. Caira, Susan Bourne.

- 12th International Seminar on Inclusion Compounds, Stellenbosch, South Africa (4-9 April 2009) – Poster: "The Solid State Chemistry of trans-Resveratrol" by Lee Trollope, Mino R. Caira, Susan A. Bourne. (Poster Prize awarded from the New Journal of Chemistry - http://www.njc.cnrs.fr/spip.php?article181).

Abstract

Lee Elizabeth Hunt **March 2017**

The Supramolecular Modification of *trans*-Resveratrol and Related Antioxidant Molecules

The naturally occurring phytoalexin *trans*-Resveratrol (RES) is known to be a powerful antioxidant and is used as a nutraceutical. It is considered to be one of the factors contributing to the beneficial effects of red wine. The phenolic hydroxycinnamic acids caffeic acid (CAF), ferulic acid (FA), *p*-coumaric acid (PCA) and sinapic acid (SA) are found in a wide variety of plants and also have antioxidant activity. The acetophenone derivatives paeonol (2H4M) and vanillin (4H3M) display antioxidant, anti-inflammatory and antihypertensive activity. The use of these compounds as food fortifiers and nutraceuticals is limited as they exhibit adverse physical properties such as low aqueous solubility and low bioavailability. These properties may be improved by inclusion complex formation with cyclodextrins (CDs) and by cocrystallisation with generally regarded as safe (GRAS) coformers. A study of the CD complexation of RES, CAF, FA, PCA, SA, 2H4M and 4H3M was carried out both in solution and in the solid state. The solubility enhancement of the nutraceuticals by CD inclusion and by cocrystallisation was evaluated. The compounds hydrocaffeic acid (HCA), hydroferulic acid (FA), 2-hydroxy-5-methoxy acetophenone (2H5M) and 2-hydroxy-6-methoxy acetophenone (2H6M) have little or no known bioactivity but were included in the study as structural analogues for comparative purposes.

Inclusion complexes were formed with the nutraceuticals and the native CDs (β- and γ-CD) by kneading and coprecipitation, as well as with methylated CDs by coprecipitation. The resulting inclusion complexes were characterised using powder X-ray diffraction (PXRD), ^{1}H nuclear magnetic resonance spectroscopy (^{1}H-NMR), thermogravimetric analysis (TGA), differential scanning calorimetry (DSC) and hot stage microscopy (HSM). Single crystal X-ray diffraction was used to elucidate inclusion complex structures. Three novel RES inclusion complexes were formed with methylated CDs having common modes of inclusion and hydrogen bonding motifs. Inclusion complex formation with the methylated CDs also produced six new hydroxycinnamic acid complexes and five new hydroxyacetophenone complexes. The results of phase solubility studies revealed that, in general, CD inclusion complex formation improves the aqueous solubility of RES [randomly methylated CD (RAMEB) effecting a maximum increase of 63 times that of free RES] and hydroxycinnamic acids.

The thermodynamic parameters and association constants for complexation between hydroxycinnamic acids and both β- and γ-CD were determined by isothermal titration calorimetry (ITC). For β-CD a 1:1 host-guest ratio was found with association constants in the range 246-774 M^{-1}. The interactions between the guests and β-CD were found to be enthalpy-driven, except for that of SA and β-CD which was entropy-driven. With γ-CD a 1:1 host to CAF ratio was found (K = 475 M^{-1}) while PCA, FA and SA interact with γ-CD in a 2:1 molar ratio. The association constants were in the range 228-543 M^{-2}. The formation of 2:1 complexes in solution was found to be enthalpy-driven while that of 1:1 complexes was entropy-driven.

^{1}H NMR spectroscopy was used to study the interaction of the acetophenone derivatives with β- and γ-CD in solution. Job plot analyses confirmed 1:1 host-guest complex ratios. The association constants spanned the range 145-336 M^{-1}. Similarly for γ-CD, complex stoichiometries were confirmed to be 1:1 with 2H6M and 4H3M with association constants 67 and 125 M^{-1}, respectively.

Eight cocrystals were prepared with hydroxycinnamic acids and the GRAS compounds nicotinamide (NIC) and isonicotinamide (ISO) by coprecipitation, and were fully characterised. Single crystal X-ray diffraction confirmed the formation of cocrystals rather than salts. Analysis using ^{1}H NMR spectroscopy for quantitation revealed that the aqueous solubilities of FA and PCA were enhanced approximately ten-fold when tested in the form of their cocrystals with the coformer NIC.

Table of Contents

Chapter 1: Introduction

Supramolecular Chemistry

Supramolecular chemistry focuses on the study of the phenomenon of interactions between molecules. In this branch of chemistry it is the non-covalent interactions that are of interest, not covalent bonds. The interactions taking place are well-defined, including van der Waals forces, hydrophobic forces, hydrogen bonding, electrostatic forces and π-π interactions. These interactions lead to the formation of molecular crystals where the regularity of these assemblies is defined by the principle of close packing.[1] The importance of these interactions is obvious as their effects can be seen everywhere over many centuries. Emil Fischer (1852-1919) discovered the so-called 'lock and key' mechanism to depict how enzymes react.[2] The identification of the base pairs or 'building blocks' of DNA (guanine and cytosine, adenine and thymine) and how they interact illustrates the specific molecular recognition that all biological entities depend on.[3] Molecular recognition, self-assembly and self-organisation by design are key principles in crystal engineering, such that the observation of a single molecule (the bottom-up approach) is just as important as the study of the entire complex (the top-down approach). While the field of supramolecular chemistry spans many research fields, this contribution will focus on the phenomena of cyclodextrin (CD) inclusion and cocrystallisation.

Cyclodextrin inclusion

Cyclodextrins (CDs) are macromolecules utilized by the pharmaceutical and food industries (as well as others) to alter the physical, chemical and biological activities of hydrophobic guest molecules by forming inclusion complexes, both in solution and in the solid state.[4] The formation of a CD inclusion complex occurs when a guest molecule interacts with a host molecule, which contains a cavity into which a complementary guest molecule may fit. The guest molecule is held in the cavity by intermolecular interactions through space. The process of inclusion can therefore be said to be dynamic and the resulting supramolecular structures are formed by both additive and cooperative interactions with their properties being dependent on the structural features of the host and guest molecules.

CDs are generally described as having the shape of a truncated cone and the parent (or 'native') CDS, namely α-CD, β-CD and γ-CD, are made up of six, seven and eight α-(1,4)-linked glucopyranose units respectively (Figure 1.1).[5] CDs have two distinct faces, the narrower side known as the primary hydroxyl face (containing the C6 hydroxyl group) and the wider side known as the secondary hydroxyl face (containing the C2 and C3 hydroxyl groups).[6,7] The CDs are stabilized by a series of intramolecular O-H···O hydrogen bonds between the secondary hydroxyl groups of contiguous glucopyranose units, making the CD highly rigid. The cavity is lined with hydrogen atoms making it hydrophobic while the outer edges are hydrophilic, due to the hydroxyl groups.[5] This characteristic of CDs makes them ideal for increasing the apparent solubility of water-insoluble molecules *via* their inclusion within the CD cavity.

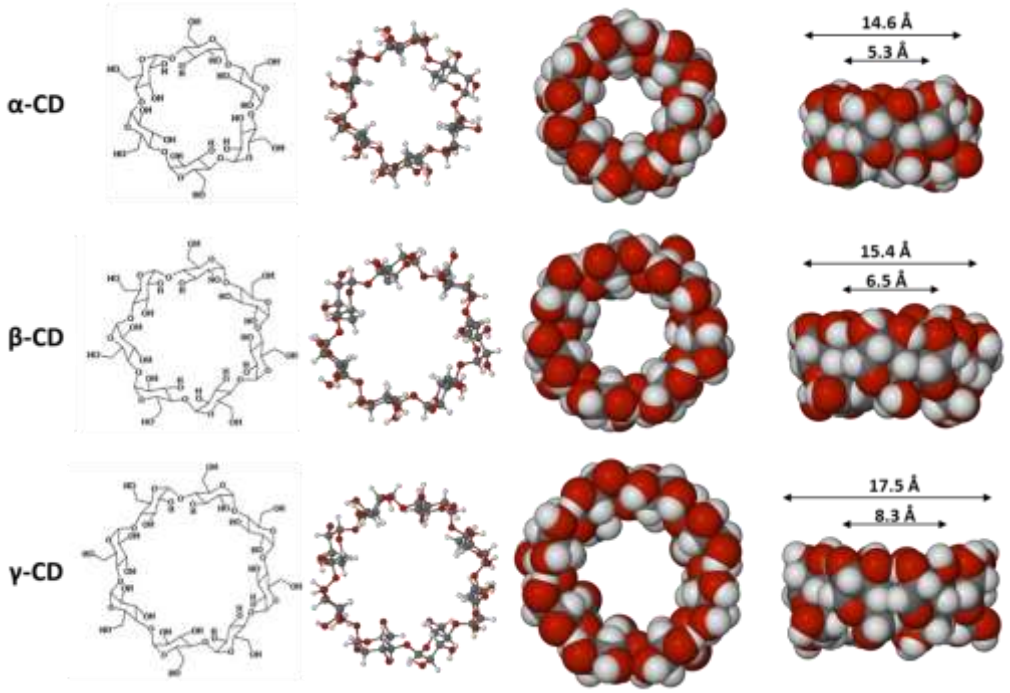

Figure 1.1: From left to right: The chemical structures of the host molecules α-, β- and γ-CD, the macrocyclic structures, CPK diagrams viewed onto the secondary rim and side-on CPK diagrams with inner and outer cavity width dimensions.

Derivatised CDs have also proven useful when attempting to modify the properties of hydrophobic molecules. By substituting the hydroxyl groups on the native CDs with methoxy groups one can effect significant changes to the host physical properties. One such change is that methylated CDs have a negative temperature coefficient, i.e. they crystallise from solution at high temperatures but remain in solution at lower temperatures.[8] This property lends these methylated CDs to overcoming the insolubility of hydrophobic molecules. Derivatised CDs used in this study include DIMEB [heptakis-(2,6-di-*O*-methyl)-β-CD], TRIMEB [heptakis-(2,3,6-tri-*O*-methyl)-β-CD], RAMEB (randomly methylated β-CD), HP-β-CD [(2-hydroxypropyl)-β-CD, with a degree of substitution of 4.6] and TRIMEA [heptakis-(2,3,6-tri-*O*-methyl)-α-CD].

Structural features

The conformation of the CD molecule is described by a number of structural parameters.[9,10] The deviations from idealized symmetry of the molecule may be assessed with relation to the glycosidic (O4) atoms of the polygon by measuring the parameters *r* (the 'radii' drawn from the O4 atoms to the polygon centroid), *D* (the glycosidic O4···O4' distance), *a* (the O4···O4'···O4''angle) and *d* (the O4···O4'···O4''···O4''' torsion angle) (Figure 1.2, in which β-CD is shown as representative). The planarity of the molecule is described by the deviation of the O4 atoms from the O4 least-squares plane (α). The respective orientation of each glucopyranose unit is measured by the tilt angles τ_1 or τ_2, where τ_1 is the angle between the mean plane through C1-C2-C3-C4-C5-O5 (see Figure 1.2 for atom labels) of the glucopyranose ring and the line orthogonal to the O4 mean plane, and τ_2 is the angle between the least-

squares O4 plane and the mean O4-C4-C1-O4' plane of the glucopyranose ring. These parameters may be compared with mean values shown in Table 1.1, in order to assess similarities or differences in these structural parameters in different inclusion complex structures.

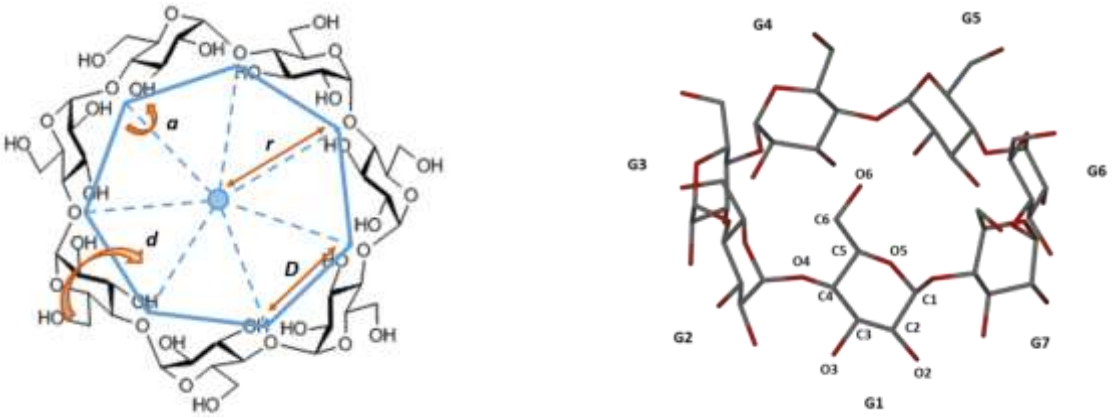

Figure 1.2: The geometric parameters of the O4-heptagon of β-CD used to describe the geometry of the macrocycle (left) and the glucopysranose unit and atom labels used (right).

Table 1.1: Literature values of average geometrical parameters describing the macrocyclic conformation of selected host molecules.

Parameters	β-CD[11]	TRIMEA[12]	TRIMEB[12,13]	DIMEB[14,15,16]
r (Å)	5.0	4.2	4.9	5.0
D (Å)	4.4	4.2	4.4	4.4
a (°)	128	118	126	128
d (°)	6	17	22	7
α (Å)	0.15	0.32	0.44	0.13
τ_1 (°)	12.6	17.4	27.7	13.3
τ_2 (°)	13.9	21.5	31.6	14.6

Crystal packing and isostructurality

In monomeric and dimeric structures with native CDs, the latter generally pack in one of two broad categories: cage type or channel type. Monomeric cage type structures include herringbone (HB), layer (LY), brickwork (BW) and zigzag (ZZ) packing motifs while the channel type structures form helical channel (HC) motifs. Dimeric channel type structures form channel (CH), intermediate (IM), screw channel (SC) and chessboard (CB) motifs. CD structures with similar packing arrangements will have similar powder X-ray diffraction (PXRD) patterns as a result of a phenomenon termed isostructurality.[17] Isostructural phases have very similar unit cell dimensions and internal molecular arrangements. This implies that such closely related structures have common CD host atoms with very similar three-dimensional coordinates. In the area of CD inclusion studies, this has a very useful application such that a new form of a CD-guest compound may be readily identified as an inclusion complex simply by comparing its PXRD pattern with those of known isostructural series until a match with a specific series is found. This will enable deduction of approximate unit cell dimensions, space group and details of host assembly from the single experimental PXRD pattern of the new complex.

Pharmaceutical co-crystals

Efforts to develop new crystalline forms of active pharmaceutical ingredients (APIs) and nutraceuticals have increased in the last decade, after it was discovered that the physicochemical properties of a drug may be modified by generating new solid forms of the drug. It is also useful to be able to fully characterise and control new solid forms. One significant approach is to generate cocrystals by crystal engineering, molecular assembly based on the use of supramolecular synthons.[19] Cocrystals are multi-component molecular crystals, in most cases formed from two solid components at room temperature.[18] Recently, the FDA defined pharmaceutical cocrystals as crystalline materials containing APIs and a physiologically acceptable coformer ("generally recognized as safe" or GRAS compound) within the same crystal, interacting through non-covalent, non-ionic bonds.[20] It was further proposed that, in physical terms, a cocrystal may be classed as a solvate in which the coformer is nonvolatile,[21] although this has not been the accepted norm in research and academia.

APIs and nutraceuticals contain functional groups through which molecular recognition events can occur between such molecules and biologically active sites. These same functional groups can therefore also undergo molecular recognition with other molecules to form supramolecular homosynthons (formed with identical functional groups) or heterosynthons (formed with different but complementary functional groups) via highly directional intermolecular hydrogen bonds (Figure 1.3).[22]

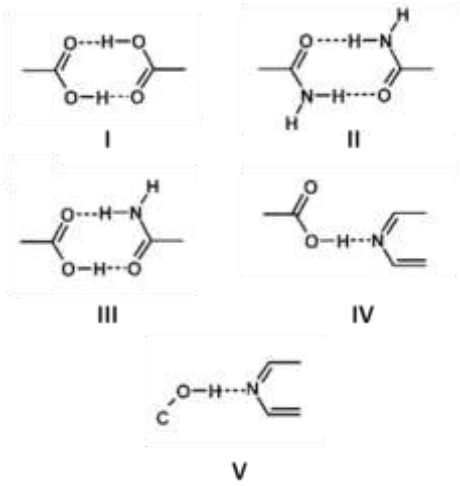

Figure 1.3: Some frequently occurring supramolecular synthons, where I and II are homosynthons and III-V are heterosynthons.

Cocrystal screening using various methods of preparation is most commonly used to produce new solid forms. This is often time-consuming and has a low hit rate, among other problems. By making use of the knowledge-base available it is possible to facilitate rational selection of potential coformers based on structural similarities with known cocrystal structures.[23] The results presented in Chapter 4 involve caffeic acid and its analogues which contain hydroxyl and carboxylic acid groups which interact most favourably with e.g. amides, pyridyls and diazines, the most stable resulting cocrystal structure being

that in which the best hydrogen-bond donor and the best hydrogen-bond acceptor interact preferentially.[24,25] Different solvent systems are also significant in generating new solid phases, even of known cocrystals. Thus far there is no method to identify the best solvent or solvent system for a given API and coformer, but it has been suggested that mixed solvent systems are more effective in generating a new solid form than single solvent systems.[26]

Cocrystal polymorphism may occur due to conformational flexibility of the components or structural changes in packing. Less frequently, polymorphism is effected by the formation of less favourable synthon interactions.[27] Cocrystal polymorphs have pharmaceutical interest due to their potential to enhance API dissolution rates, absorption and bioavailability in their metastable and even amorphous forms.[28,29]

trans-Resveratrol

trans-Resveratrol (_trans_-3,5,4'-trihydroxystilbene) is a naturally occurring phytoalexin (Figure 1.4), a product synthesized by various plant species in response to injury or fungal infection, exposure to ultraviolet light and ozone or to heavy metal ions.[30] It is found in grapes, peanuts and mulberries, and is considered to be one of the factors contributing to the beneficial effects of red wine.[31-32] It is used as a nutraceutical, a substance extracted from foods that is claimed to have a medicinal effect on human health.[33] It has been widely researched regarding its biological activity and was found to be a powerful antioxidant.[32,34] It has been found to have neuroprotective,[35] cardioprotective,[36] and anti-inflammatory,[37] as well as antioxidant[38] properties as a free radical scavenger.[39] _Trans_-Resveratrol also has the ability to inhibit platelet aggregation and lipid peroxidation.[30]

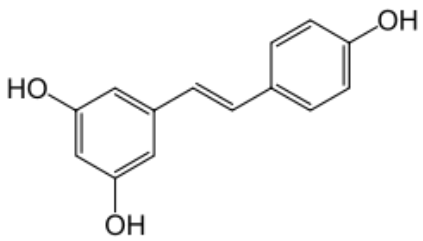

Figure 1.4: _trans_-Resveratrol

Phenolic compounds which have antioxidant activity function by two main mechanisms. The first is H-atom transfer, where the radical removes a hydrogen atom from the antioxidant molecule. The radical is neutralized and the antioxidant molecule becomes a radical. The second mechanism involves a one-electron transfer from the antioxidant to the free radical with the antioxidant becoming a radical cation. Using computational methods, Leopoldini _et al_. determined that _trans_-resveratrol acts via the former mechanism.[40] The reasons for this are that _trans_-resveratrol is a planar, highly conjugated molecule, stabilized by delocalization and hydrogen bond formation. The most likely site of radicalization is the hydroxyl 4'-OH at the _para_-position. This hydroxyl was found to generate the most stable radical because the hydroxyl hydrogen atom is the most acidic.[6,7] The _cis_-isomer is a much less effective antioxidant.[30]

However, while *trans*-resveratrol has high oral absorption, it is so rapidly metabolized systemically that it exhibits low bioavailability.[32] It is also poorly soluble (reported to be less than 0.05 mg/mL in water) which limits its use in pharmaceutical preparation processes as a food fortifier and nutraceutical.[4] These issues may be overcome by making use of supramolecular methods.

Other monophenolic compounds

Caffeic acid and its derivatives

Polyphenolic compounds such as *trans*-resveratrol have become known as powerful antioxidants contributing to their anti-carcinogenic and cardioprotective properties. Unfortunately, the compounds have low bioavailability making polyphenols less effective.[41] However, it has been noted that small monophenols also exhibit antioxidant, anticancer, antimutagenic and antimicrobial activities.[42] The phenolic acids caffeic acid (CAF), ferulic acid (FA), *p*-coumaric acid (PCA) and sinapic acid (SA) are found in a wide variety of fruits, vegetables and medicinal plants (Figure 1.5).[43] These compounds act very similarly to polyphenols as they have free radical scavenging activity, forming resonance-stabilized phenoxyl radicals.[44] The hydroxycinnamic acids are poorly soluble in water and may exhibit low oxidative stability.[45] These issues may be overcome by CD inclusion and cocrystallisation. Hydrocaffeic acid (HCA) and hydroferulic acid (HFA) were also studied for comparative purposes.

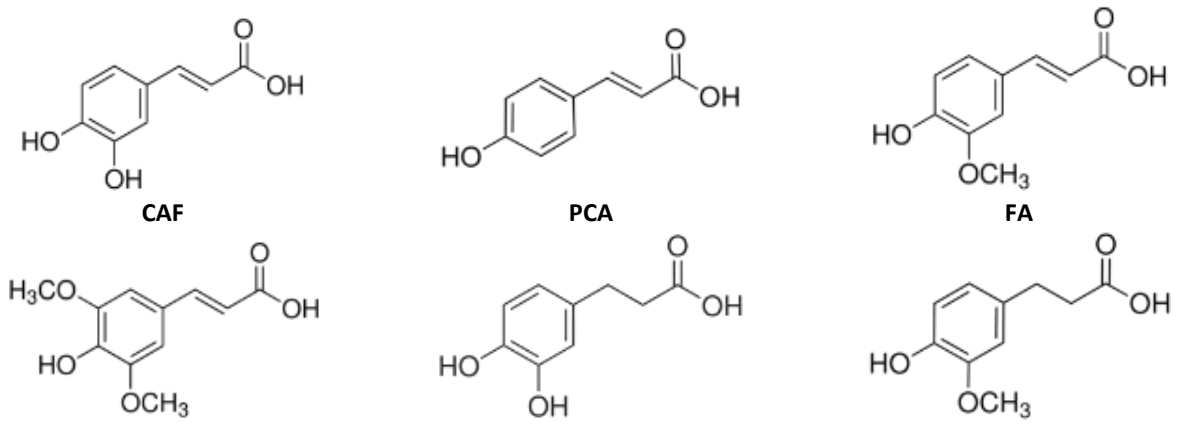

Figure 1.5: The chemical structures of the related antioxidant molecules.

Isomeric acetophenone derivatives

Chemical structures of relevant compounds in this category are shown in Figure 1.6. 2-hydroxy-4-methoxy acetophenone (common name: paeonol, here abbreviated to 2H4M) displays antioxidant, anti-inflammatory and antihypertensive activity.[46,47] 2H4M is lipophilic and has a low solubility in water, which may limit its application as a nutraceutical. 4-hydroxy-3-methoxy acetophenone (common name: vanillin, here abbreviated to 4H3M) displays antioxidant and antimicrobial properties and may be used as a food preservative.[48] There is evidence for anti-carcinogenic and antimutagenic effects of 4H3M; however, it

has a short shelf life due to its thermal instability and volatility, which limits its use in the nutraceutical industry.[49] These limitations may be reduced by the formation of CD inclusion complexes. Two derivatives, namely 2-hydroxy-5-methoxy acetophenone (2H5M) and 2-hydroxy-6-methoxy acetophenone (2H6M), have little or no bioactivity and are also subjects of the present study for comparative purposes.

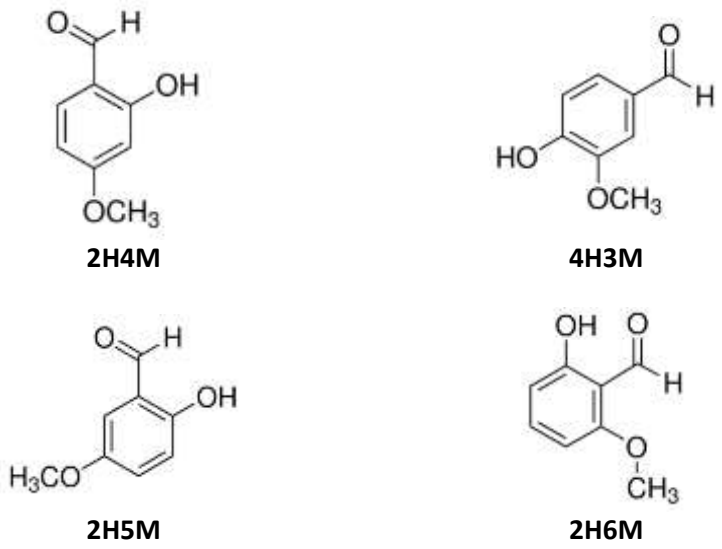

Figure 1.6: The chemical structures of the isomeric acetophenone derivatives.

Objectives

The aim of the project on which this thesis is based was to generate novel solid forms of the bioactive compounds *trans*-resveratrol, caffeic acid and its analogues, and a series of isomeric acetophenone derivatives using CDs and GRAS coformers, and to investigate possible changes to the physicochemical properties of the bioactive compounds effected by forming multi-component systems. Specific objectives were to:

- Prepare the desired multi-component systems by environmentally friendly methods
- Investigate the solid-state structures of such novel derived solid forms using single crystal X-ray diffraction.
- Characterise the novel solid forms by proton nuclear magnetic resonance (where appropriate), thermal analysis and powder X-ray diffraction.
- Investigate, where possible, the solubilizing effects of CD inclusion or cocrystallisation of the compounds studied
- Evaluate the thermodynamic parameters and association constants of selected CD complexes in solution.

In Chapter 2, the materials and experimental methods used in this study are summarised.

REFERENCES

1. A. I. Kitajgorodskij, *Acta Cryst*., 1965, **18**, 585-590.
2. E. Fischer*, Berichte der Deutschen chemischen Gesellschaft zu Berlin*, 1894, **27**, 2985-2993.
3. J. D. Watson and F. H. Crick, *Nature*, 1953, **171**, 737-738.
4. J. M. López-Nicolás, E. Núñez-Delicado, A. J. Pérez-López, A. C. Barrachina and P. Cuadra-Crespo, *J. Chromatogr. A*, 2006, **1135**, 158-165.
5. K. Uekama, *Adv. Drug Del. Rev.*, 1999, **36**, 1-2.
6. J. Szejtli, *Pure Appl. Chem*., 2004, **76**, 1825-1845.
7. J. Szejtli, *Chem. Rev*., 1998, **98**, 1743-1754.
8. A. Kusmin, R. E. Lechner, M. Kammel and W. Saenger, *J. Phys. Chem. B*, 2008, **112**, 12888-12898.
9. K. Harata, *Bull. Chem. Soc. Jpn.*, 1988, **61**, 1939-1944.
10. D. Mentzafos, I. M. Mavridis, G. Le Bas and G. Tsoucaris, *Acta Cryst*., 1991, **B47**, 746-757.
11. T. Steiner and G. Koellner, *J. Am. Chem. Soc.*, 1994, **116**, 5122-5128.
12. T. Steiner and W. Saenger, *Angew. Chem., Int. Ed.*, 1998, **37**, 3403-3407.
13. M. R. Caira, S. A. Bourne, W. T. Mhlongo and P. M. Dean, *Chem. Commun.*, 2004, 2216-2217.
14. J. J. Stezowski, W. Parker, S. Hilgenkamp, and M. Gdaniec, *J. Am. Chem. Soc.*, 2001, **123**, 3919-3926.
15. T. Aree, H. Hoier, B. Schulz, G. Reck and W. Saenger, *Angew. Chem., Int. Ed*., 2000, **39**, 897-899.
16. T. Aree, W. Saenger, P. Leibnitz and H. Hoier, *Carbohyd. Res*., 1999, **315**, 199-205.
17. M. R. Caira, *Rev. Roum. Chim.*, 2001, **46**, 371-386.
18. J. M. López-Nicolás and F. García-Carmona, *Food Chem*., 2008, **109**, 868-875.
19. a) E. J. Corey, *Pure Appl. Chem.,* 1967, **14**, 19-38. b) G. R. Desiraju, *Angew. Chem*., *Int. Ed. Engl.,* 1995, **34**, 2311-2327.
20. U.S. Food and Drug Administration, http://www.fda.gov/downloads/Drugs/.../Guidances/UCM281764.pdf (accessed April 2013)
21. U.S. Food and Drug Administration, http://www.fda.gov/ucm/groups/fdagov-public/@fdagov-drugs-gen/documents/document/ucm516813.pdf (accessed August 2016)
22. G. Springuel, B. Norberg, K. Robeyns, J. Wouters and T. Leyssens, *Cryst. Growth Des*., 2012, **12**, 475-484.
23. Cambridge Structural Database and Cambridge Structural Database System, Version 5.37, May 2016, Cambridge Crystallographic Data Centre, University Chemical Laboratory, 12 Union Road, Cambridge, England
24. H. D. Clarke, K. K. Arora, H. Bass, P. Kavuru, T. T. Ong, T. Pujari, L. Wojtas and M. J. Zaworotko, *Cryst. Growth Des.*, 2010, **10**, 2152-2167.
25. M. C. Etter, *Acc. Chem. Res.*, 1990, **23**, 120-126.
26. T. Rager and R. Hilfiker, *Cryst. Growth Des*., 2010, **10**, 3237-3241.

27. A. Mukherjee and G. R. Desiraju, *Chem. Commun*,. 2011, **47**, 4090-4092.
28. A. J. Aguiar, J. Krc Jr., A. W. Kinkel and J. C. Samyn, *J. Pharm. Sci.*, 1967, **56**, 847-853.
29. I. Kushida, M. Ichikawa and N. Asakawa, *J. Pharm. Sci.*, 2002, **91**, 258-266.
30. L. Fremont, *Life Sci.*, 2000, **66**, 663-473.
31. C. Lucas-Abellán, I. Fortea, J. M. López-Nicolás and E. Núñez-Delicado, *Food Chem.*, 2007, **104**, 39-44.
32. T. Walle, F. Hsieh, M. H. DeLegge, J. E. Oatis and U. K. Walle, *Drug Metab. Dispos.*, 2004, **32**, 1377-1387.
33. S. H. Zeisel, *Science*, 1999, **285**, 185-186.
34. S. Ślusarczyk, M. Hajnos, K. Skalicka-Woźniak, and A. Matkowski, *Food Chem.*, 2009, **113**, 134-138.
35. H. Li, Z. Yan, J. Zhu, J. Yang and J. He, *Neuropharm.*, 2011, **60**, 252-258.
36. M. Mokni, F. Limam, S. Elkahoui, M. Amri and E. Aouani, *Arch. Biochem. Biophys*., 2007, **457**, 1-6.
37. O. H. Kang, H. J. Jang, H. S. Chae, Y. C. Oh, J. G. Choi, Y. S. Lee, J. H. Kim, Y. C. Kim, D. H. Sohn, H. Park and D. Y. Kwon, *Pharmacol. Res*., 2009, **59**, 330-337.
38. J. Yao, J. Y. Wang, L. Liu, Y. X. Li, A. Y. Xun, W. S. Zeng, C. H. Jia, X. X. Wei, J. L. Feng, L. Zhao and L. S. Wang, *Arch. Med. Res.*, 2010, **41**, 288-294.
39. F. Caruso, J. Tanski, A. Villegas-Estrada and M. Rossi, *J. Agric. Food Chem*., 2004, **52**, 7279-7285.
40. M. Leopoldini, T. Marino, N. Russo and M. Toscano, *J. Phys. Chem.*, 2004, **108**, 4916-4922.
41. L. N. Bell, *Handbook of nutraceuticals and functional foods*, ed. R. E. C. Wildman, CRC Press, New York, 2001, 501-516.
42. a) J. Tabart, C. Kevers, D. Evers and J. Dommes, *J. Agri. Food Chem.*, 2011, **59**, 4763-4770. b) G. Xu, X. Ye, J. Chen, and D. Liu, *J. Agri. Food Chem*., 2007, **55**, 330-335.
43. a) S. A. Heleno, A. Martins, M. J. Queiroz, and I. C. Ferreira, *Food Chem*., 2015, **173**, 501-513. b) K. Sevgi, B. Tepe, and C. Sarikurkcu, *Food Chem. Toxicol*., 2015, **77**, 12-21.
44. A. S. Pannala, R. Razaq, B. Halliwell, S. Singh and C. A. Rice-Evans, *Free Radic. Biol. Med*., 1998, **24**, 594-606.
45. a) A. Crozier, I. B. Jaganath and M. N. Clifford, *Nat. Prod. Rep*., 2009, **26**, 1001-1043. b) A. Munin and F. Edwards-Lévy, *Pharmaceutics*, 2011, **3**, 793-829. c) J. Nichols and S. K. Katiyar, *Arch. Dermatol. Res*., 2010, **302**, 71-83. d) L. -J. Yang, S. -X. Ma, S. -Y. Zhou, W. Chen, M. -W. Yuan and Y. -Q. Yin, *Carbohydr. Polym*., 2013, **98**, 861-869.
46. Y. Dobashi, J. Kondou and Y. Ohkatsu, *Polym. Degrad. Stab.*, 2005, **89**, 140-144.
47. T. -C. Chou, *Br. J. Pharmacol.*, 2003, **139**, 1146-1152.
48. J. Burri, M. Graf, P. Lambelet and J. Löliger, *J. Sci. Food Agric*., 1989, **48**, 49-56.
49. F. Kayaci and T. Uyar, *J. Agric. Food Chem*., 2011, **59**, 11772-11778.

Chapter 2: Experimental

MATERIALS

Trans-Resveratrol, the hydroxyacetophenone isomers and the hydroxycinnamic acids were obtained from Sigma-Aldrich (Germany) and were used as received. The host compounds β-CD, γ-CD, DIMEB [heptakis-(2,6-di-*O*-methyl)-β-CD], TRIMEB [heptakis-(2,3,6-tri-*O*-methyl)-β-CD], TRIMEA [hexakis-(2,3,6-tri-*O*-methyl)-α-CD], HP-β-CD [(2-hydroxypropyl)-β-CD, D.S. 4.6] and RAMEB [randomly methylated β-CD] were obtained from Cyclolab (Hungary) and were also used as received. Deuterated dimethyl sulfoxide (DMSO-d_6) and deuterium oxide (D_2O) used in ^{1}H NMR spectroscopy studies were obtained from Sigma-Aldrich (USA) and used as received.

PREPARATION OF CYCLODEXTRIN INCLUSION COMPLEXES

Inclusion complexes were prepared using three methods, namely kneading, co-precipitation and slow cooling.

Kneading method

The respective guest compound and the CDs (γ- and β-CD, respectively) were ground together in a 1:1 molar ratio in a mortar for 15-20 minutes. Distilled water was added dropwise so as to maintain a paste-like consistency. The pastes were then analysed using powder X-ray diffraction (PXRD).

Co-precipitation method

A hot (≈50-60 ˚C) saturated solution of CD (γ- and β-CD, respectively) was made by dissolving the CD in distilled water at elevated temperature with stirring until the solution went clear. The respective guest compound was added to this solution in a 1:1 host:guest ratio. The suspension was heated slightly, with stirring, and the resulting clear hot solution was filtered into a clean vial and left to cool at room temperature. A variation on this method, namely slow cooling, was also used to prepare complexes. This method involved preparing the hot solution (as above) and leaving it to cool from 100°C to ambient temperature over two days in a Dewar flask.

The inclusion complexes with the derivatised CDs DIMEB, TRIMEB and TRIMEA required a different method of preparation as these compounds dissolve in water at low temperature and tend to crystallise at higher temperatures. The derivatised CDs were dissolved in distilled water (1-2 mL) at low temperatures (4-6 °C) with stirring. Once the solution cleared, the respective guest was added in a 1:1 host:guest molar ratio and stirred at low temperature. The resulting solution was then filtered into a clean vial and left to crystallize in an oven at 50-70 ˚C. In some cases crystals were obtained at room temperature.

PREPARATION OF COCRYSTALS

Co-grinding method

The hydroxycinnamic acid guest compounds were ground together in a 1:1 molar ratio with nicotinamide and isonicotinamide, respectively, for 15-20 minutes. The resultant product was analysed using PXRD.

Co-precipitation method

A solution of the cocrystal former (nicotinamide or isonicotinamide) was prepared using ethanol or an ethanol/water 50/50 v/v mixture. Once dissolved, the respective hydroxycinnamic acid component was added in a 1:1, 2:1 or 1:2 molar ratio. The solution was filtered into a new vial and allowed to evaporate at room temperature.

ANALYSIS AND CHARACTERISATION

THERMAL ANALYSIS

Three thermal analytical techniques were used, namely thermogravimetric analysis, differential scanning calorimetry and hot stage microscopy.

Thermogravimetric analysis (TGA) records the mass changes of a sample of material as a function of temperature. Mass loss occurring as a result of dehydration, solvent loss, loss of the guest or decomposition can be measured and is determined by a highly sensitive microbalance. From this loss it is possible to calculate the number of solvent or guest molecules per host molecule. The TGA measurements were performed using a TA Instruments TGA Q500 with dry N_2 purge gas flowing horizontally over the sample at a rate of 60 mL min^{-1}. Samples were surface dried on filter paper and placed on an open platinum pan. The samples were then heated in the furnace at a rate of 10 K min^{-1} from 30 to 350 ˚C.

Differential scanning calorimetry (DSC) experiments measure the amount of energy absorbed or released by a sample as it is heated or cooled as compared to a reference. The onset temperature, temperature range and the enthalpy change of a thermal event can be determined by taking the derivative of the endothermic and exothermic peaks. The heat of fusion of a sample and the enthalpy change for a phase transition can be determined by integrating the area under the curve. DSC experiments were carried out on a TA Instruments DSC Q200 with a dry N_2 purge gas flowing at a rate of 50 mL min^{-1}. The Q200 is also capable of performing modulated DSC (MDSC). This method enables separation of the reversible and the irreversible thermal events which may not be distinguishable from one another, e.g. a melt from a phase transition occurring at the same temperature. Samples were surface dried on filter paper and sealed in a

Tzero aluminium pan. The samples were then heated at a rate of 10 K min^{-1} from 30 to 350 ˚C, unless otherwise stated.

The TGA and DSC curves were analysed using the TA instruments software Universal Analysis 2000 for Windows.[1]

Hot stage microscopy (HSM) was used to observe the physical changes in a sample, which are often related to the thermal events measured by TGA and DSC. Physical changes mainly observed and recorded during performance of the studies reported in this thesis are bubbling due to organic solvent or water loss from crystals, and melting and colour changing due to degradation. Samples were immersed in silicone oil on a cover slip and viewed with a Nikon SMZ-10 stereoscopic microscope fitted with a Linkam THM hot stage and a Linkam TP92 temperature control unit. Images were captured with a real-time Sony Digital Hyper HAD colour video camera and viewed with the Soft Imaging System program, analySIS.[2]

POWDER X-RAY DIFFRACTION (PXRD)

PXRD patterns were recorded for the products obtained after attempting to form inclusion complexes and cocrystals. PXRD patterns of CD inclusion experiment products were compared with a set of reference patterns from a known series of isostructural inclusion complexes. Two crystalline phases are isostructural when they have identical or nearly identical crystal packing motifs, having similar unit cell dimensions and arrangements of molecules.[3] PXRD gives a two-dimensional representation (intensity as a function of the angle 2θ) of this information and therefore may be used to identify isostructurality. If a match between the experimental and reference patterns was obtained, complexation was confirmed. If the patterns did not match, the experimental pattern was examined to see whether it matched patterns of the native CDs or if superimposed peaks of the guest and the CD were visible. If the experimental PXRD of the product did not match either of those of the starting materials or a pattern from an isostructural series, it indicated that the product could be an inclusion complex requiring further investigation. The PXRD patterns of the cocrystal products were compared with those of the starting materials. If the experimental PXRD pattern did not match either of the PXRD patterns of the starting materials it was deduced that the product represented a new crystalline phase e.g. a cocrystal product or a polymorph of either of the starting materials.

Powder X-ray diffraction measurements were performed using a Bruker D8 Advance X-ray diffractometer equipped with a $CuK\alpha_1$ X-ray source and a LYNXEYE 1-D detector. A Göbel mirror was used to create parallel X-ray beams. Samples were sprinkled onto the 25 mm diameter high-index silicon surface of a zero background sample holder and mounted onto a rotating stage. The voltage was set to 30 kV and the

current to 40 mA. An air-scatter screen was introduced to reduce the amount of background noise. The 2θ range measured was 4° to 40° with a step size of 0.01°. The diffractometer was controlled by the DIFFRAC^{plus} suite which includes DAVINCI and EVA software for equipment operation and data analysis.

SINGLE CRYSTAL X-RAY DIFFRACTION

Data collection

Single crystals of adequate size, quality and optical uniformity were obtained for the inclusion complexes and cocrystals. These crystals were between 0.1 mm and 0.5 mm in all directions and the quality was determined under the polarising microscope. The crystals were covered in Paratone N oil to prevent loss of crystallinity due to dehydration and mounted on a cryoloop. The nylon loop was then mounted on a goniometer head and the data collected. Two single crystal X-ray diffractometers were used to perform full intensity data collections, namely a Bruker KAPPA APEX II DUO diffractometer and a Nonius Kappa CCD diffractometer, both using 1.2 kW graphite-monochromated MoKα-radiation (λ = 0.71073 Å). All collections were performed at low temperature by cooling the crystals using a constant stream of nitrogen vapour produced by a Cryostream cooler (Oxford Cryosystems, UK). Preliminary unit cell parameters and space group symmetry were determined for all crystals to ensure that inclusion complexes or cocrystals were formed as these parameters would be different from those of the starting materials. These data were checked at both ambient and low temperatures to ascertain whether any phase transitions occurred in this temperature range. The intensity data were scaled and multi-scan absorption corrections were applied using SADABS.[4] Space groups were determined by examining systematic absences and comparing them with those for known space groups.[5]

Structural solution and refinement

The data files for each structure were prepared using the program XPREP.[6] Simultaneously the space group was confirmed by inspecting systematically absent reflections as well as the value of $|E^2 - 1|$ in cases where it was necessary to distinguish centrosymmetric from non-centric space groups. The structures were solved either by isomorphous replacement or by direct methods using the program SHELXD.[7] The isomorphous replacement method makes use of the principle of isostructurality, whereby the co-ordinates of the CD host non-hydrogen atoms of an inclusion complex with similar unit cell dimensions and therefore similar atomic coordinates are employed in a trial model for initial refinement.[3] SHELXD was used for structure solution when either no isostructural complex existed or when the atomic coordinates of the isostructural complex did not match those of the unknown structure to sufficiently high accuracy. The algorithm employed is an *ab initio* method which uses the dual space strategy where the structure is solved by alternating the data between real and reciprocal spaces.

SHELXD makes use of the Patterson function, which provides better than random starting phases for the dual-space recycling (other methods assign entirely random phases). In reciprocal space the phases are refined using a tangent expansion, while selecting the largest *N* independent peaks in real-space.

The refinement of the structures was initially carried out using the program SHELXH-97[8] which was accessed using the X-SEED[9] interface. After the release of SHELX-2013[10] the structures were re-refined using SHELXL in order to generate the required CIF file format. Refinement involves minimising the function $\Sigma\ w\ (F_o^2 - F_c^2)^2$ using the full-matrix least-squares technique. The agreement between the observed (F_o) and calculated (F_c) structure factors is given by the residual index R_1, which is defined as $R_1 = [\Sigma\ ||F_o|-|F_c|| / \Sigma\ |F_o|]$. The agreement between intensities for the refinement against F^2 is given by the residual index wR_2, where $wR_2 = \{[\Sigma\ w\ (F_o^2 - F_c^2)^2] / [\Sigma\ w\ (F_o^2)^2]\}^{½}$. The default weighting scheme (w) and the parameters a and b were refined for each structure using $w = 1 / [\sigma^2 (F_o^2) + (aP)^2 + bP]$ and $P = [\max (0, F_o^2) + 2\ F_c^2] / 3$. The goodness-of-fit (S) is defined as $S = [\Sigma\ w\ (F_o^2 - F_c^2)^2) / (n - p)]^{½}$ where n is the number of reflections and p is the total number of refinement parameters.

NUCLEAR MAGNETIC RESONANCE SPECTROSCOPY (NMR)

^{1}H NMR spectroscopy to determine inclusion complex stoichiometry

^{1}H NMR spectroscopy was used to determine the stoichiometries of the CD inclusion complexes and cocrystals isolated. Single crystals of these products were dissolved in suitable deuterated solvents. ^{1}H NMR experiments were performed at 300 MHz with a Varian-Gemini 300 spectrometer or with a Bruker Avance III spectrometer at 600MHz, at 298 K. Using the program MestReNova,[11] unambiguous peaks of known proton count in the inclusion complex or cocrystal spectrum were integrated and the molar ratios of the organic entities in each multi-component system were thus determined.

Solution ^{1}H NMR spectroscopy

Apparatus

The solution ^{1}H NMR experiments were performed on a Bruker Avance III spectrometer at 500MHz for protons. A Broad Band Observed probe was used, as well as automatic tuning and matching, and the frequency was locked for D_2O. All measurements were performed at 298 K, using a variable temperature unit VT 3000 to control the temperature. The number of spins varied from 36 to 256, depending on the concentration of the sample being measured. The sweep width was 6 ppm (from 2 ppm to 8 ppm) as all the relevant proton signals appeared in this range. The digital resolution was 0.1 Hz. Each sequence was performed with a 30° pulse. The Homonuclear Overhauser effect (NOE) difference experiment was

carried out at 303 K with 16 spins and a sweep width of 8 ppm. The mixing time used was 250 ms. The resulting data were analysed using the program Topspin, version 2.4.

The method of continuous variation (Job Plot)

Solution NMR spectroscopy is also used in host-guest chemistry to determine the association constants (K) of particular host-guest interactions; the extent of a certain intermolecular binding process is thus quantified.

The inclusion of a guest molecule into the cavity of a CD produces changes in the ^{1}H chemical shifts of the protons in the CD cavity, namely H3, H5 and H6. ^{1}H shifts of the guest molecule may also be observed, giving some indication of the mode of inclusion. While being able to observe the chemical shifts of both host and guest, difficulties may arise when the host and guest signals overlap. It is also important to note that the stoichiometry of an inclusion complex may not be the same in solution and in the crystalline state, as the solution state facilitates a more dynamic relationship between host and guest molecules. Nonetheless this method is very useful in the determination of the stoichiometry and association constant of a complex. The process of complexation can be described in the equation

$$a \cdot H + b \cdot G \rightleftharpoons C \tag{1}$$

where a and b are the stoichiometric ratios of each reactant, H is the host, G is the guest and C is the complex formed (also written as $H_a{\cdot}G_b$). The association constant is defined as

$$K = \frac{[C]}{[H]^a[G]^b} \tag{2}$$

where [H], [G] and [C] are the concentrations of the host, guest and complex at equilibrium. By substituting equations (3) and (4) into equation (2) we obtain equation (5), where $[H]_t$ and $[G]_t$ are the total host and guest concentrations, respectively. K, a and b are constants.

$$[G]_t = [G] + b \cdot [C] \tag{3}$$

$$[H]_t = [H] + a \cdot [C] \tag{4}$$

$$K = \frac{[C]}{([H]_t - a \cdot [C])^a([H]_t - b \cdot [C])^b} \tag{5}$$

It is essential when calculating K in equation (5) to first determine the stoichiometric coefficients *a* and *b*. This is easily accomplished using NMR data and Job plot analysis.[12]

To determine the stoichiometry of each complex, a modified Job plot analysis was performed. In order to carry out a Job plot analysis a range of samples is made up of varying proportions of host and guest (where the total concentration is kept constant) and NMR data recorded. Specific attention is given to the changes in chemical shifts which may be observed over the range of samples. The rate of the guest

inclusion/exclusion at the equilibrium of the host-guest complexation is very fast compared to the NMR time scal esuch that the peaks assigned to complexed host and those assigned to the free host are indistinguishable and appear at the weighted average chemical shift of the complexed and free host. As [C] is not directly measurable, a measurable value proportional to [C] is studied. The data obtained (change in chemical shift, Δδ, which is directly proportional to [C]) can be plotted as a function of the concentration of the host and guest at the start of the experiment. The stoichiometry is obtained from the x-coordinate at the maximum of the Job plot curve in which the y-axis is $[H]_t \cdot (\delta_h - \delta_{obs})$ (similarly for the guest) and the x-axis is $[H]_t/([H]_t+[G]_t)$, where δ_h is the free host chemical shift and δ_{obs} is the observed chemical shift (Figure 2.1). This maximum point is equal to a/(a+b) for the host Job plot analysis (similarly for the guest).[13]

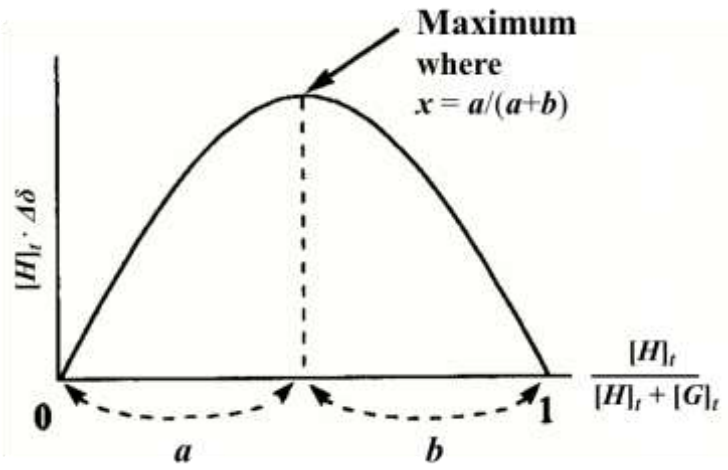

Figure 2.1: Job plot illustrating the relationship between stoichiometry (*a* and *b*) and change in chemical shift (*Δδ*)

Determining the association constant

The determination of the association constant (K) was carried out using a non-linear curve-fitting method, giving values that are the best fit of calculated data to the observed data. This method requires no approximations and allows an almost unrestricted distribution of experimental points. The observed chemical shift value, δ_{obs}, is the weighted average of the chemical shifts of the free host proton, δ_h, and the complexed host proton, δ_c, to give equation (6)

$$\delta_{obs} = \frac{[G] \cdot \delta_f + b \cdot [C] \cdot \delta_c}{[G]_t} \quad (6)$$

which can be written as

$$\delta_{obs} = z \cdot \delta_f + \delta_c \cdot (1 - z) \text{ where } z = \frac{[G]}{[G]_t} \quad (7)$$

When [G] ≈ 0 almost all the guest molecules are complexed, z ≈ 0 and $\delta_{obs} \rightarrow \delta_c$. When [G] = $[G]_t$ or when $[G]_t$ >> [H], z = 1 and $\delta_{obs} \rightarrow \delta_h$. Similar equations can be derived for the host. Noting the observed difference in chemical shift and using the chemical shift difference between the free component and the pure inclusion complex for a given proton, equation (8) can be derived.

$$\delta_{obs}^{(X)} = \frac{[C]}{[X]_t} \cdot \Delta\delta_c^{(X)} \tag{8}$$

where X = H or G. Substituting this equation into (5) gives an equation with the solution

$$[X]_t^2(\Delta\delta_{obs}^{(X)})^2 - [X]_t\Delta\delta_{obs}^{(X)}\Delta\delta_c^{(X)}\left\{[M] + \frac{1}{K}\right\} + [H]_t[G]_t(\Delta\delta_c^{(X)})^2 = 0 \tag{9}$$

where $[M] = [H]_t + [G]_t$.

Solving equation (9) we obtain equation (10)

$$\Delta\delta_{obs}^{(X)} = \frac{\Delta\delta_c^{(X)}}{2[X]_t} \times \left\{[M] + \frac{1}{K} \pm \left[\left([M] + \frac{1}{K}\right)^2 - 4[H]_t[G]_t\right]^{\frac{1}{2}}\right\} \tag{10}$$

Only the negative solution has physical meaning as the ratio $\Delta\delta_{obs}/\Delta\delta_c$ must be less than 1. The correct values of $\Delta\delta_c$ and K are those that afford the best fit of the calculated data to the observed data $\Delta\delta_{obs}$. Equation (10) must be satisfied for each sample studied. The two independent variables ($\Delta\delta_c$ and K) for a given set of samples can be solved using the best fit of the calculated values to the experimental $\Delta\delta_{obs}$ values.[13,14]

The association constants were calculated using a computer program named CONSTEQ.[14] It is written entirely in C++, running under the Windows 95/98/XP operating systems in DOS or Command Prompt. The program evaluates the data by a non-linear least-squares curve-fitting regression analysis, according to equation (10), of the observed chemical shift changes of the guest and CD NMR lines as a function of concentration. No approximations are required and the total concentration of the host and guest molecules with the observed difference in the chemical shift, $\Delta\delta_{obs}$, is correlated. An iterative procedure fits values to specific algorithms in order to fit the experimental values of $\Delta\delta_{obs}$ to the appropriate equation. A quadratic function is set for each step of the iteration in order to determine the direction of search as well as to calculate the error function:

$$E = \sum_{i,j}\left(\Delta\delta_{obs}^{(i,j)} - \Delta\delta_{calc}^{(i,j)}\right)^2 \tag{11}$$

where *i* counts the sample number and *j* the studied proton. The data converge when the difference between two consecutive E values is less than 10^{-6}. One single K value is produced for the entire process together with a set of calculated $\Delta\delta_c$ values. Both the host and guest proton chemical shifts can be included using this program, which allows up to 15 protons to be used in the fitting process.[14] Recently, the program has been improved in order to determine the association constants of complexes with 1:2 or 2:1 stoichiometry.

ISOTHERMAL TITRATION CALORIMETRY (ITC)

The isothermal titration calorimetry (ITC) technique is used to investigate the thermodynamics of the interactions that may occur between molecules. It measures the heat released or absorbed when molecules interact.[15] This technique has become useful in drug design, providing insight into the binding affinity as well as the enthalpy and entropy contributions of the interaction of a drug molecule with binding sites and drug delivery systems.[16]

This technique has been used to investigate the thermodynamic interaction between a guest molecule and CDs. The stoichiometry of the interaction (n), the association constant (K) and the change in enthalpy (ΔH) are determined using ITC and the entropy (S) and Gibbs free energy (G) can be calculated from the ITC data.[16,17]

An ITC experiment is carried out by measuring the changes in the enthalpy of an interactive system during a titration of a solution of one component into a solution of another. The feedback mechanism of the ITC instrument during the experiment results in the plot of heat rate (μcal/sec) versus time (min). These signals are integrated and a plot of the heat per injection (kcal/mol) versus the molar ratio of the injected CD and the total guest concentration ($[CD_i]_{tot}/[G]_{tot}$) is generated. A non-linear least-squares curve-fitting based on the Wiseman Isotherm (equation 12) is applied to the correct interaction model, allowing the thermodynamic parameters to be determined using equations 13 and 14.[18-20] In equation 12, the composition variable is defined as $r = 1/[CD]_T K$, V_0 is the volume of solution in the titration cell and X_R is the ratio of guest to CD i.e. $[G]_T/[CD]_T$.

$$\frac{dq}{d[CD]_T} = \Delta H V_0 \left[\frac{1}{2} + \frac{1 - X_R - r}{2\sqrt{(1 + X_R + r)^2 - 4X_R}}\right] \quad (12)$$

$$\Delta G^\circ = -RT \ln K \quad (13)$$

$$\Delta G^\circ = \Delta H^\circ - T\Delta S^\circ \quad (14)$$

These parameters rely strongly on the concentrations of the components in solution, which often possess low aqueous solubility, and they are therefore often considered unreliable. It has been found that setting one of the parameters to a known value results in lower error values and more reliable

results.[18] Here the value for n was fixed, based on the fit of the non-linear least-squares curve to the recorded data.

Apparatus

ITC was carried out at 298 K using a MicroCal iTC200 Microcalorimeter (MicroCal Inc., Northampton, MA) controlled by MicroCal's VP viewer software version 5.0 (MicroCal Software Inc., Northampton, MA). For each experiment the reaction cell (200 µL) was filled with an aqueous solution of the guest and the titration syringe (40 µL) was filled with an aqueous solution of the host. The host solution was injected into the guest solution in thirty portions of 1.3 µL at 120 s intervals, such that the reaction could reach equilibrium after each addition. The initial delay was 60 s and the feedback was set to high. A stirring speed of 1000 rpm was employed. The first injection (0.4 µL) was discarded to eliminate the effect of the diffusion of the titrant into the cell. The data were converted to binding isotherms after each experiment. The heats of dilution were determined for each host and guest such that the host was titrated against water and water was titrated against the guest. These quantities were found to be negligible.

PHASE SOLUBILITY

CDs are known to have a solubilising effect on many insoluble compounds as the hydrophobic part of the molecule interacts with the relatively hydrophobic cavity of the CD, while the outer part of the CD may interact with water, rendering the unit more hydrophilic. An effective method of measuring the solubility increase induced by CD inclusion complex formation is phase solubility testing. Phase solubility studies were carried according to the method described by Higuchi and Connors.[21] The guests studied were *trans*-resveratrol, caffeic acid, ferulic acid and *p*-coumaric acid.

Selected CDs [β-CD, γ-CD, TRIMEB, DIMEB, HP-β-CD and RAMEB] were dissolved in water over the concentration range 2-12 x 10^{-3} M. An excess amount of the guest compound (1.5 - 2.5 mg) was added to 2 mL of each CD solution and the solutions were allowed to stir at 25 ± 0.5 °C. The quantity S_0 is the intrinsic solubility of the guest compound in water and its value was determined by preparing saturated solutions of each component in water, stirring at 25 ± 0.5 °C. After 48 hours the samples were filtered through 0.45 µm PTFE, 0.45 µm NYLON or 0.22 µm PES syringe filters and diluted appropriately.

The concentration of the guest was determined using UV-vis spectrophotometry as the host molecules are not UV-vis active while the conjugated guest compounds show an absorption peak. The Beer-Lambert law (15) was used to quantify the concentration, where A is the absorbance of the guest, ε_0 is the extinction coefficient, c is the concentration and l is the path length used (1 cm for all experiments).

$$A = \varepsilon_0 cl \quad (15)$$

The wavelength of the absorption peak maximum was selected for each guest compound and the extinction coefficient was determined for these wavelengths by preparing calibration curves of each guest compound in water (Figures are provided in Appendix F). All experiments were performed in triplicate.

The experimental results were compiled such that the concentrations (and hence solubilities) of the respective guest compounds were plotted against the corresponding concentrations of the CD used. These phase solubility diagrams can be classified as being of type A or type B. A-type curves result from an increase in the solubility of the drug as the concentration of the CD is increased, forming soluble complexes. These curves can be described as increasing the solubility linearly (A_L) or increasing it with a positive or negative deviation due to a change in the physical properties of the solution as the CD concentration increases (A_P or A_N). A_P-type phase-solubility diagrams indicate the formation of a higher-order complex with respect to CD, while a negative deviation (A_N) is due to CD aggregation as the CD concentration increases. B-type curves indicate the formation of an insoluble complex, where B_S suggests the formation of a complex with limited solubility while B_I is associated with the formation of an insoluble complex. Figure 2.2 illustrates these phase solubility profiles.[21,22]

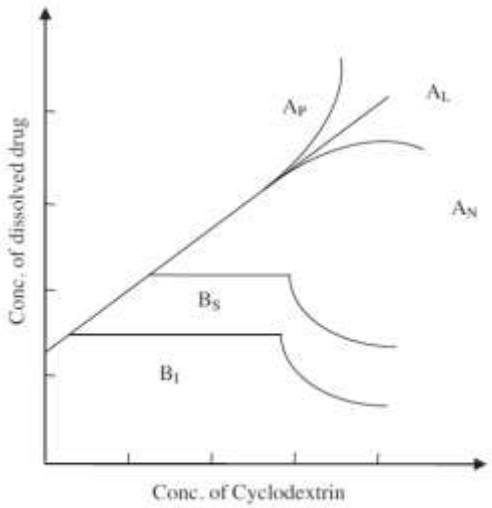

Figure 2.2: The typology of the phase solubility diagrams according to Higuchi and Connors.[21]

The approximate stability constants, K_C, were calculated according to the Higuchi-Connors equation (16) using the phase solubility diagrams obtained, assuming a 1:1 host to guest interaction.[21]

$$K_C = \frac{slope}{S_0(1 - slope)} \quad (16)$$

As defined earlier, S_0 is the intrinsic solubility of the guest compound and the slope, which must be less than unity, is obtained from the phase solubility diagram.

The UV spectra were recorded on a GCB Cintra 20 UV-Visible Spectrometer and analysed using GBC Spectral software over a wavelength range of 200 nm to 500 nm at a scanning rate of 200 nm min^{-1}.[23] The parameters used to calculate the concentration of each respective guest compound at each respective host concentration are listed in Table A, Appendix F.

ADDITIONAL RESOURCES

For each crystal structure determined in the study, program LAZY PULVERIX[24] was used to generate the idealized X-ray powder pattern.

Program LAYER[25] was used to display the intensity data graphically as simulated precession photographs.

The program PLATON[26] was used to calculate all molecular geometrical parameters and non-bonded interactions.

All molecular and packing diagrams were produced using POV-Ray for Windows.[27]

CS ChemDraw Pro[28] was used for molecule line drawing diagrams.

The Cambridge Structural Database (CSD)[29] was accessed to obtain structural data of isostructural cyclodextrin complexes as well as average geometrical parameters.

The IUCr online version of the program CheckCIF was used to validate all aspects of the solution and refinement of each crystal structure reported.[30]

Literature searching and retrieval were carried out using resources provided by the University of Cape Town.

REFERENCES

1. TA instruments, Universal Analysis 2000 for Windows. Version 4.7A, TA Instruments – Waters LLC, Delaware, © 1998-2009.
2. Soft Imaging System GmbH, Digital Solutions for Imaging and Microscopy, Version 3.1 for Windows, © 1987-2000.
3. M. R. Caira, *Rev. Roum. Chim.*, 2001, **46**, 371-386.
4. G. M. Sheldrick, *SADABS,* University of Göttingen, Germany, 1996.
5. International Tables for Crystallography, Vol II: Mathematical Tables, J.S. Kasper and K. Lonsdale (eds.), Kynoch Press, Birmingham, England, 1967, 291.
6. XPREP, Data Preparation & Reciprocal Space Group Exploration, Version 5.1/NT, Bruker Analytical X-ray Systems, © 1997.
7. G. M. Sheldrick, *Direct Methods for Solving Macromolecular Structures*, Kluwer Acedemic Publishers, Dordrecht, 1998.
8. G. M. Sheldrick and T. R. Schneider, *Macromol. Crystallogr*., 1997, **B277**, 319-343.
9. L. J. Barbour, *J. Supramol. Chem.*, 2001, **1**, 189-191.
10. G. M. Sheldrick, *Acta Cryst.*, 2015, **C71**, 3-8.
11. MestreNova V5.1.1-3092, Mestrelab Research S.L., © 2007.
12. P. Job, *Ann. Chim. Phys.*, 1928, **9**, 113-203.
13. K. Hirose, *J. Incl. Phenom. Macrocycl. Chem.*, 2001, **39**, 193-209.
14. C. Floare, F. Balibanu, M. Bogdan, *Studia Universitatis Babes-Bolyai, Physica, Special Issue*, 2005, 451-454.
15. K. Bouchemal and S. Mazzaferro, *Drug Discov. Today*, 2012, **17**, 623-629.
16. F. P. Schmidtchen, *Analytical Methods in Supramolecular Chemistry*, ed. C. A. Schalley, Wiley-VCH, Weinheim, 2007, 55-78.
17. K. Bouchemal, *Drug Discov. Today*, 2012, **13**, 960-972.
18. W. B. Turnbull and A. H. Daranas, *J. Am. Chem. Soc.*, 2003, **125**, 14859-14866.
19. T. Wiseman, S. Williston, J. F. Brandts and L. N. Lin, *Anal. Biochem.*, 1989, **179**, 131-137.
20. L. Indyk and H. F. Fisher, *Methods Enzymol.*, 1998, **295**, 350-364.
21. T. Higuchi and K. Connors, *Adv. Anal. Chem. Instrum.*, 1965, **7**, 117-212.
22. S. Massaferro, K. Bouchemal, J. F. Gallard, B. Iorga, M. Cheron, C. Gueutin, C. Steinmesse, G. Ponchel, *Int. J. Pharm.*, 2011, **416**, 171-180.
23. GBC Spectral, LabControl® GmbH, © 1993-1998.
24. K. Yvon, W. Jeitschko and E. Parthé, *J. Appl. Crystallogr*., 1977, **10**, 73-74.
25. L. J. Barbour, *J. Appl. Cryst*., 1999, **32**, 351-352.
26. A. L. Spek, PLATON, A Multipurpose Crystallographic Tool, Version 20604, © 1980-2004.

27. POV-Ray for Windows, Version 3.1e, The persistence of vision team, © 1991-1999.
28. S. Rubenstein, CS ChemDraw Pro^{TM}, Version 4.0.1, CambridgeSoft Corporation, Massachusetts, © 1985-1997.
29. Cambridge Structural Database and Cambridge Structural Database System, Version 5.37, May 2016, Cambridge Crystallographic Data Centre, University Chemical Laboratory, 12 Union Road, Cambridge, England.
30. http://checkcif.iucr.org/ (accessed 2012-2016).

Chapter 3: Inclusion of *trans*-resveratrol in methylated cyclodextrins

The solid state inclusion complex formation of *trans*-resveratrol with three derivatised cyclodextrins (CDs) is reported in this chapter. The CDs are heptakis(2,3,6-tri-O-methyl)-β-CD (TRIMEB or TMB), hexakis(2,3,6-tri-O-methyl)-α-CD (TRIMEA or TMA) and heptakis(2,6-di-O-methyl)-β-CD (DIMEB or DMB). Single crystals were obtained and analysed using single crystal X-ray diffraction, powder X-ray diffraction, thermal analysis and proton nuclear magnetic resonance spectroscopy. The solubilising effect of the CDs on *trans*-resveratrol was studied using the phase solubility technique, where UV-Vis spectrophotometry was used to quantify the results.

Preparation of inclusion complex crystals

trans-Resveratrol (20 mg) was dissolved in 0.5 ml of EtOH and the resulting solution was added to an equimolar amount of CD dissolved in water, according to Table 3.1. If the solution became turbid, EtOH was added dropwise until the solution cleared. The solution was then filtered into a new vial, closed with a punctured poly-top lid and allowed to evaporate slowly on the benchtop or in an oven. The vial was sealed after crystals appeared. The complexes obtained are named TMA·RES, TMB·RES and DMB·RES.

Table 3.1: The amounts of each CD added to the *trans*-resveratrol solution, the volume of water added and the temperature at which the complex crystals were obtained.

	Mass (mg)	Volume (ml)	Temperature (° C)
TRIMEA	107.34	1	20
TRIMEB	125.22	3	60
DIMEB	116.63	3	60

Data-collection and space group determination

The intensity data for all three complex single crystals were collected on a Bruker KAPPA APEX II DUO diffractometer. In each case a single crystal was surface-dried and coated in Paratone N oil.[1] The crystal systems and space groups for the CD complexes were determined using LAYER.[2] The Laue symmetry was found to be 2/*m* for TMA·RES and TMB·RES indicating the monoclinic system. DMB·RES crystallises in the orthorhombic system as the Laue symmetry was *mmm*. The respective space groups were determined from systematically absent reflections.

TRIMEB INCLUSION COMPLEX WITH *trans*-RESVERATROL (TMB·RES)

Thermal analysis

Figures 3.1 and 3.2 illustrate the TGA and DSC traces and the HSM photographs. The TGA trace of the complex TMB·RES shows an initial mass loss of 5.3 ± 0.1 % (n = 2) which is equivalent to 5.1 ± 0.1 water molecules per 1:1 complex unit. The endotherm seen in the DSC recorded over the range 30 - 120 °C appears sharper than expected for the solvent loss process, suggesting concurrent melting of the complex. The HSM photographs confirm that complex dehydration (indicated by bubbling) is accompanied by a melt. The TGA trace suggests that decomposition occurs at different rates; it may be that guest loss occurs concurrently with host decomposition, beginning at *ca*. 280 °C.

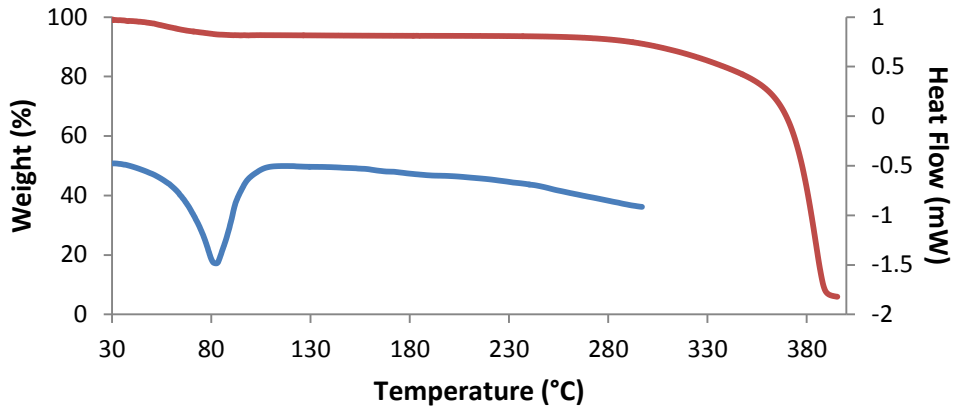

Figure 3.1: TGA (red) and DSC (blue) traces for the TMB·RES complex.

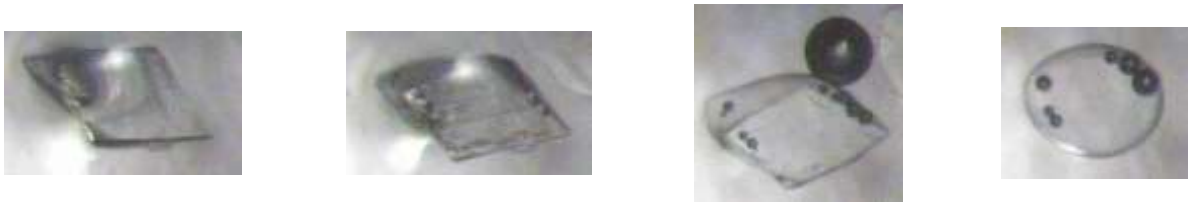

30 °C 90 °C 96 °C 120 °C

Figure 3.2: HSM photographs of the complex TMB·RES at various temperatures.

Confirmation of stoichiometry

Proton nuclear magnetic resonance spectroscopy (^{1}H NMR) was used to determine the stoichiometry of TMB·RES. Selected crystals were dissolved in acetone-d_6 and the ^{1}H NMR spectrum was recorded. Integration of the clearly separated proton peaks revealed a 1:1 host to guest ratio for the TMB·RES complex (Table 3.2).

Table 3.2: Integrals of the guest and host protons for TMB·RES.

Guest proton	δ (ppm)	Multiplicity	J (Hz)	Integration	Experimental/ Theoretical	
2 x C-$\underline{H}_B$	7.435	d	^{3}J = 8.73	1.98	0.99	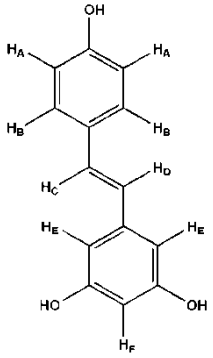
C-$\underline{H}_C$ + C-$\underline{H}_D$	6.965	d of d	^{4}J = 16.34	3.80	0.95	
2 x C-$\underline{H}_A$	6.859	d	^{3}J = 8.65		0.95	
2 x C-$\underline{H}_E$	6.557	d	^{3}J = 2.15	2.00 *	1.00	
C-$\underline{H}_F$	6.288	t	^{4}J = 2.17	0.92	0.92	
Host proton	**δ (ppm)**	**Multiplicity**	**J (Hz)**	**Integration**	**Experimental/ Theoretical**	
7 x C-$\underline{H}_1$	5.148	d	^{3}J = 3.68	7.22	1.03	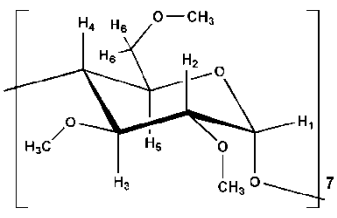
7 x O-C$\underline{H}_3$	3.352	s		20.90	1.00	
7 x C-$\underline{H}_5$	3.111	d of d	^{4}J = 3.67	7.38	1.05	

*Reference integral

Crystal structure solution and refinement

Refinement parameters and crystal data are reported in Table 3.3. The structure was solved by direct methods using the program SHELXD,[3] as none of the isostructural series matched the unit cell parameters accurately enough.[4] SHELXD provided a structure solution (CC = 87.11) and all the non-hydrogen atoms were assigned and refined isotropically. The glucopyranose units were labelled G1-G7 and any disordered atoms were labelled by parts. The structure was refined using SHELXH-97.[5] The primary methoxy fragment on glucopyranose unit G1 was found to be disordered over two positions and the two components were refined with partial site occupancy factors (s.o.f.s) of x and 1 – x respectively. The s.o.f. of the major component C611-O611-C911 refined to 0.65. The ordered non-hydrogen atoms displayed reasonable isotropic thermal displacement parameters (U_{iso}) and were subsequently allowed to refine anisotropically. Many of the hydrogen atoms appeared in the difference Fourier map; however, all were placed in idealised positions using a riding model with a U_{iso} magnitude of 1.2 times that of the parent atoms except for the methyl hydrogen atoms which were assigned U_{iso} values of 1.5 times that of the parent atoms.

Table 3.3: Crystal structure and data-collection parameters for TMB·RES.

Complex Formula	**$C_{63}H_{112}O_{35}\cdot C_{14}H_{12}O_3\cdot 5.6H_2O$**
Formula weight / g mol^{-1}	1758.73
Crystal system	Monoclinic
Space group	$P2_1$
a / Å	10.2142(5)
b / Å	15.2465(8)
c / Å	29.2092(16)
β / °	97.176(1)
Volume / $Å^3$	4513.1(4)
Z	2
Calculated density / g cm^{-3}	1.292
μ (MoKα) / mm^{-1}	0.106
F (000)	1886
Temperature of data collection / K	173(2)
Crystal size / mm^3	0.24 x 0.32 x 0.59
Theta ranges scanned / °	1.9 ≤ θ ≤ 27.1
Index ranges	h: -13: 13; k: -19: 19; l: -37: 37
Total number of reflections	60403
No. of independent reflections	10306
No. of reflections with I > 2σ(I)	9131
No. of parameters	1102
R_{int}	0.037
S	0.972
R_1 (I > 2σ(I))	0.0399
No. of reflections omitted	17
wR_2	0.1068
Weighting scheme parameters *a* and *b* ($w = 1/[\sigma^2(Fo^2) + (aP)^2 + (bP)]$)	a = 0.0640, b = 1.4136
$(\Delta/\sigma)_{mean}$	0.00, 0.00
Δρ excursions / e $Å^{-3}$	-0.31, 0.54

Electron density peaks not associated with either the host or guest molecules were assigned as oxygen atoms of water molecules, provided that they satisfied hydrogen bonding criteria and their numbers were consistent with the TGA results. Atoms O4W and O5W were found to be disordered over two positions. The U_{iso} values of O6W and O7W were very high indicating partial occupancy. An average U_{iso} was applied to these water molecules and their s.o.f.s were allowed to refine freely. Once the s.o.f.s had settled, these were fixed and the U_{iso} values were allowed to refine freely. Electron density peaks corresponding to the expected positions of the hydrogen atoms of the water molecules were identified and assigned for atoms O1W, O2W, O3W and O4W. The positions of the hydrogen atoms were fixed using the DANG and DFIX commands. A total of 5.6 water molecules were assigned over 9 sites (Table 3.4 lists the atom names and s.o.f.s). This is in reasonable agreement with the TGA result of 5.1 ± 0.1.

Table 3.4: The site occupancy factors attributed to each water oxygen atom.

Atom	S.o.f.	Atom	S.o.f.
O1W	1.00	O5W1	0.50
O2W	1.00	O5W2	0.50
O3W	1.00	O6W	0.31
O4W1	0.73	O7W	0.29
O4W2	0.27		

Modelling of the *trans*-resveratrol guest

After careful examination of the difference map the highest peaks found within the CD cavity were assigned as a phenyl ring which was identified by its hexagonal shape. Subsequent refinements revealed the remainder of the guest molecule. Further refinements revealed that the guest was disordered over two positions with the disorder occurring as a result of rotation about the C4-C7 and C8-C9 bonds, such that the double bonds intersect while the phenolic groups maintain the same orientation. The site occupancy of the major disordered component (labelled A) was refined as x while the minor disordered component (labelled B) was refined as 1-x. The final s.o.f. of A was 0.73. Component A was allowed to refine anisotropically. The AFIX 66 command was applied to the phenyl rings such that they were constrained as rigid hexagons. The aromatic hydrogen atoms were added in idealised positions in a riding model. The hydroxyl hydrogen atoms were placed using a hydrogen bond searching model. Hydrogen atoms were assigned U_{iso} values 1.2 – 1.5 times those of their parent atoms. Figure 3.3 shows the disordered model with atom labels.

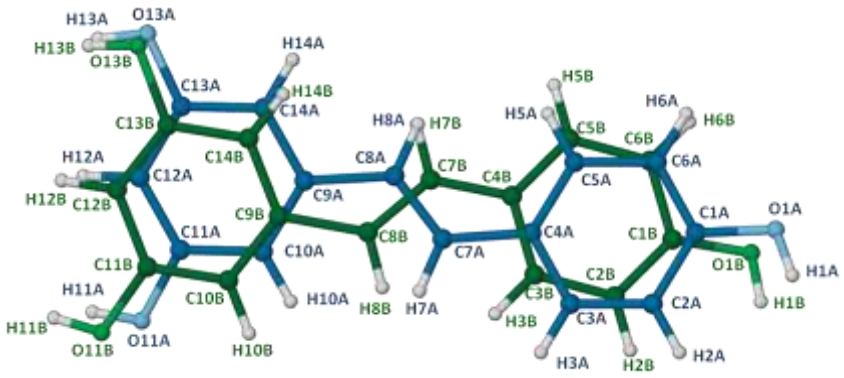

Figure 3.3: Labelling of the disordered *trans*-resveratrol guest molecule. A is shown in blue while B is shown in green.

Molecular structure

The asymmetric unit (ASU) consists of one RES molecule, one TRIMEB molecule and 5.6 water molecules (Figure 3.4). The 4-hydroxyphenyl ring of RES is inserted into the CD cavity from the secondary rim of the CD. The 1,3-benzenediol ring exists in the interstitial space between complex units. The atom labels of the host molecule are shown in Figure 3.5.

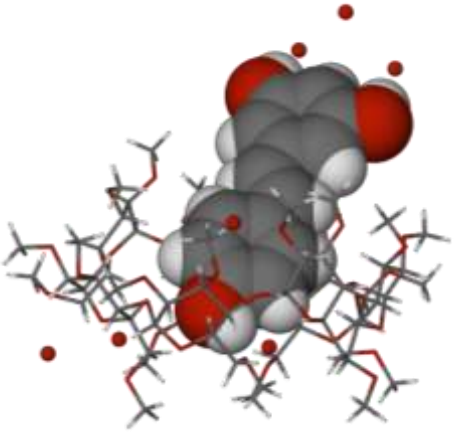

Figure 3.4: The ASU of TMB·RES illustrating how the guest is included in the CD cavity.

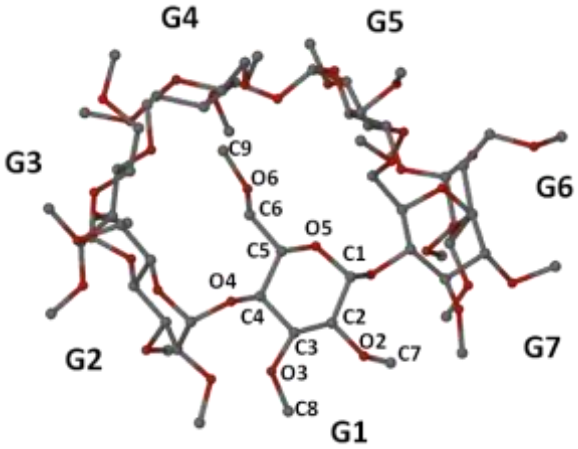

Figure 3.5: Labelling of the glucopyranose units of the macrocycle.

Geometrical analysis

Host geometry

The host molecule is distorted upon complex formation with the guest. The geometric parameters, which are described in Chapter 1, are listed in Table 3.5. The symmetry of the host molecule is described by the radii (*r*) and the glycosidic distance (*D*) and angle (*a*). These values illustrate that the macrocycle is elliptical in shape. The O4 heptagon has a saddle shape when viewed side-on as shown in Figure 3.6. The degree of the curvature is described by the torsion angle (*d*) and the deviation of the O4 atoms from the least-squares O4 plane (α). The tilt angles (τ_1 and τ_2) are positive for each complex indicating that the methylglucose units are tilted such that the primary face is “closed”.

Table 3.5: Geometric parameters of the TRIMEB molecule in the complex TMB·RES.

Residue	*r* (Å)	*D* (Å)	*a* (°)	*d* (°)	*φ* (°)	D_3 (Å)	*α* (Å)	τ_1 (°)	τ_2 (°)
G1	4.790	4.461	134.3	-12.33	116.5(2)	3.385	0.082(1)	32.37(7)	37.9(1)
G2	5.045	4.483	124.0	22.32	118.5(2)	3.300	0.626(1)	9.71(7)	11.1(1)
G3	5.178	4.412	126.4	9.09	116.5(2)	3.465	-0.330(1)	19.94(5)	20.1(2)
G4	5.145	4.475	119.8	-44.02	118.2(2)	3.473	-0.586(1)	44.08(5)	46.4(1)
G5	4.617	4.313	134.8	23.88	114.9(2)	3.560	0.735(1)	33.26(7)	44.2(1)
G6	5.139	4.350	123.1	19.16	118.3(2)	4.097	0.183(1)	15.40(6)	19.3(1)
G7	5.169	4.387	121.9	-21.35	117.5(2)	3.889	-0.709(1)	49.81(7)	47.5(1)

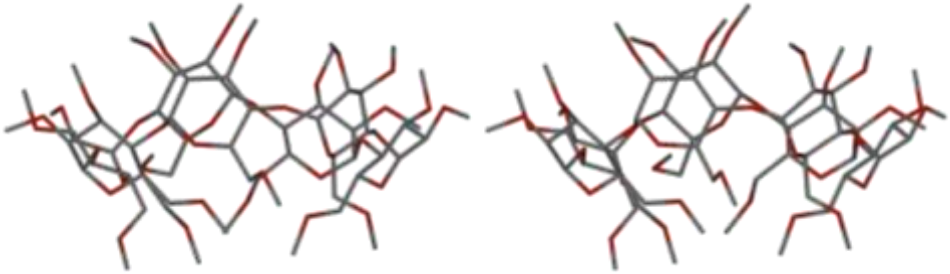

Figure 3.6: Stereoview of the TRIMEB molecule illustrating the saddle-like shape of the molecule. Only the major components of the disordered atoms are included in the figure and hydrogen atoms are omitted for clarity.

The torsion angle O5-C5-C6-O6 (*ω*) describes the orientation of the C6-O6 bond. The major disorder component of the glucose unit G1 and the fully-occupied glucose unit G4 have positive ω torsion angles, indicating a (+)-*gauche* conformation. The torsion angles of the remaining C6-O6 bonds have (-)-*gauche* orientations on residues G2, G3, G5, G6 and G7. All O6-C9 bonds are *trans* to the corresponding C5-C6 bonds, except in residue G6 where the bond lies *anticlinal*.

Guest inclusion

Both the major and minor disordered components of the guest molecule are inserted into the CD cavity from the 4-hydroxyphenyl end, with the 1,3-benzenediol end protruding from the cavity into the interstitial space between the complex units. The angle between the mean O4 plane of the CD and the mean plane through the RES molecule is 44.5(5)°. Figures 3.7 and 3.8 show the space-filling diagrams of the TMB·RES complex. The components of the disordered RES molecule deviate slightly from planarity. The interplanar angles between the phenyl rings are 17.7(1)° and 23.9(3)° for the major and minor components, respectively. The C3-C4-C7-C8, C4-C7-C8-C9 and C7-C8-C9-C14 torsion angles are 166.1(1)°, 179.4(1)° and 176.0(1)° for component A and the torsion angles C5-C4-C7-C8, C4-C7-C8-C9 and C7-C8-C9-C10 are 163.1(3)°, 179.3(2)° and 169.2(4)° for component B.

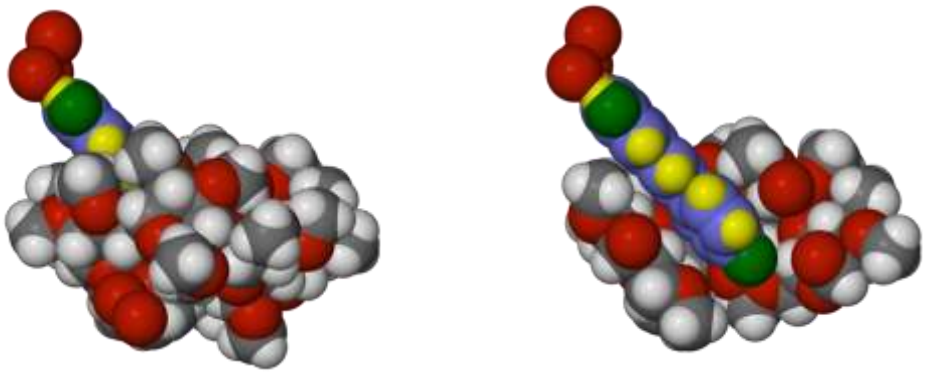

Figure 3.7: A space-filling diagram of TMB·RES viewed side-on (left) and a cutaway image of TMB·RES (right). For clarity only the major component of the disordered RES molecule is shown and the hydrogen atoms of the water molecules are omitted.

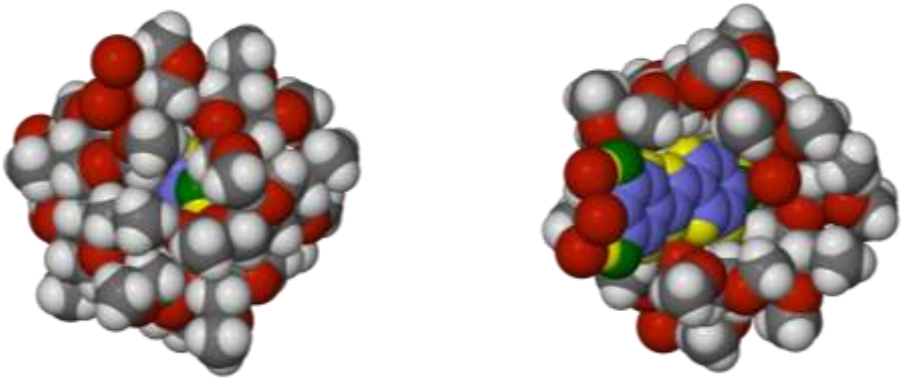

Figure 3.8: Space-filling diagrams of TMB·RES viewed from the primary (left) and secondary (right) rims. For clarity only the major component of the disordered RES molecule is shown and the hydrogen atoms of the water molecules are omitted.

Hydrogen bonding interactions

Host-guest intermolecular interactions

A relatively strong hydrogen bond exists between the 4-hydroxyl group of RES and an O6 atom on TRIMEB. The major component of the guest exhibits a more favourable interaction such that O1A-H1A···O611 has a O···H distance of 1.947(5) Å, an O···O distance of 2.732(5) Å and a bond angle of 155°. The minor component interaction is such that O1B-H1B···O611 has a O···H distance of 2.334(1) Å, an O···O distance of 2.953(13) Å and a bond angle of 130°. A third, weak interaction can be identified: C5G1-H5G1···O1A, which has a O···H distance of 2.559(2) Å, a C···O distance of 3.440(4) Å and a bond angle of 147°.

Host-host interactions

The crystal structure is stabilised by four intermolecular host-host hydrogen bonding interactions listed in Table 3.6. These interactions exist between symmetry-generated TRIMEB molecules where no interstitial water molecules are present.

Table 3.6: Hydrogen bond parameters for the host-host interactions in TMB·RES.

D-H···A	D-H (Å)	H···A (Å)	D···A (Å)	D-Ĥ···A (°)	Symmetry Operation
C1G1-H1G1···O6G6*	1.00	2.57	3.541(3)	165	-x,-1/2+y,-z
C8G4-H8G5···O3G3*	0.98	2.52	3.451(4)	159	-x,1/2+y,1-z
C2G5-H2G5···O6G2*	1.00	2.43	3.418(4)	171	x,1+y,z
C9G6- H9G5···O6G7*	0.98	2.49	3.411(5)	156	-x,1/2+y,-z

*Atom to which the symmetry operation applies.

Weak host intramolecular close contacts

The weak intramolecular close contacts of the form C-H···O present in the TMB·RES complex are tabulated in Appendix E. These close contacts have reasonable hydrogen bond distances between donors and acceptors but typically less than ideal bond angles (100.0° ≤ D-H···A ≤ 130.0°). The cumulative effect of these interactions contributes to the shape and stability of the macrocycle.

Water interactions

The water molecules in the structure interact with both host and guest, as well as with neighbouring water molecules. The hydrogen bonds found between the host and the water molecules are listed in Table 3.7. Six of the interactions occur between O-H donors and host O acceptors, while five are considered to be O···O close contacts as the water hydrogen atoms could not be modelled. Finally, a C-H···O bond exists between the disordered atom C912 and O6W.

Table 3.7: Hydrogen bond parameters for the interactions involving water in TMB·RES.

D-H···A	D-H (Å)	H···A (Å)	D···A (Å)	D-Ĥ···A (°)	Symmetry Operation
O1W-H1WA···O3G4*	0.85	1.89	2.74(1)	174	-1+x,y,z
O1W-H1WB···O2G3*	0.85	2.09	2.94(1)	173	-1-x,1/2+y,1-z
O3W-H3WA···O5G2*	0.86	2.05	2.88(1)	163	x,1+y,z
O3W-H3WB···O6G5	0.85	2.02	2.84(1)	166	-
O4W1-H4WA···O5G3*	0.86	2.34	3.03(1)	137	-x,1/2+y,1-z
O4W1-H4WA···O6G3*	0.86	2.40	3.09(1)	137	-x,1/2+y,1-z
O5W1···O3G7	-	-	2.97	-	-
O5W2···O3G7	-	-	3.00	-	-
O7W···O612	-	-	2.65	-	-
O7W···O6G4	-	-	3.13	-	-
O6W···O2G2	-	-	2.96	-	-
C912-H91E···O6W	0.98	2.457	2.90	107	-

*Atom to which the symmetry operation applies.

The hydrogen bonding interactions between the RES molecule and the water molecules are unique. Three water molecules form a chain of hydrogen bonds and the terminal water oxygen atoms are H-bond acceptors from the hydroxyl groups on the 1,3-benzenediol moiety of RES, creating a “crown” on the RES guest molecule (Figure 3.9).

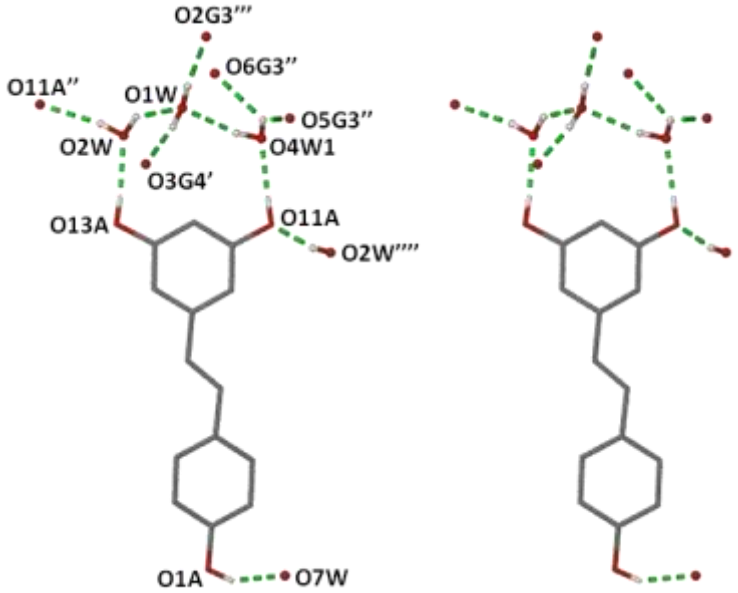

Figure 3.9: Stereoview of the hydrogen bonding present in TMB·RES including water-water interactions, water-host interactions and water-guest interactions. The hydrogen atoms not included in these interactions are omitted for clarity. The superscript symbols in the atom labels indicate symmetry-generated atoms having symmetry operations listed in Table3.7.

Further water-water close contacts indicate hydrogen bond interactions, which add stability to the structure. The hydrogen bonding interactions between the guest and the water molecules are listed in Table 3.8.

Table 3.8: Hydrogen bond parameters for the water-guest interactions in TMB·RES.

D-H···A	D-H (Å)	H···A (Å)	D···A (Å)	D-Ĥ···A (°)	Symmetry Operation
O11A-H11A···O4W1	0.84	1.88	2.71(1)	170	-
O13A-H13A···O2W	0.84	1.93	2.76(1)	173	-
O2W-H2WB···O11A*	0.84	2.09	2.93(1)	171	-1-x,1/2+y,1-z
O1A-H1A···O7W	0.84	1.84	2.60	149	-
O1B-H1B···O7W	0.84	2.11	2.78	137	-
O2W-H2WA···O1W	0.85	2.20	2.94(1)	144	-
O4W1-H4WB···O1W	0.86	2.09	2.94(1)	168	-
O5W1···O3W	-	-	2.83(1)	-	-
O5W2···O3W	-	-	2.88(1)	-	-

*Atom to which the symmetry operation applies.

Crystal packing

The complex units stack in columns parallel to the *a*-axis in a head-to-tail fashion. Adjacent columns are related by a two-fold screw axis. Figure 3.10 illustrates the anti-parallel columns and the translational relationship between symmetry-generated complex units.

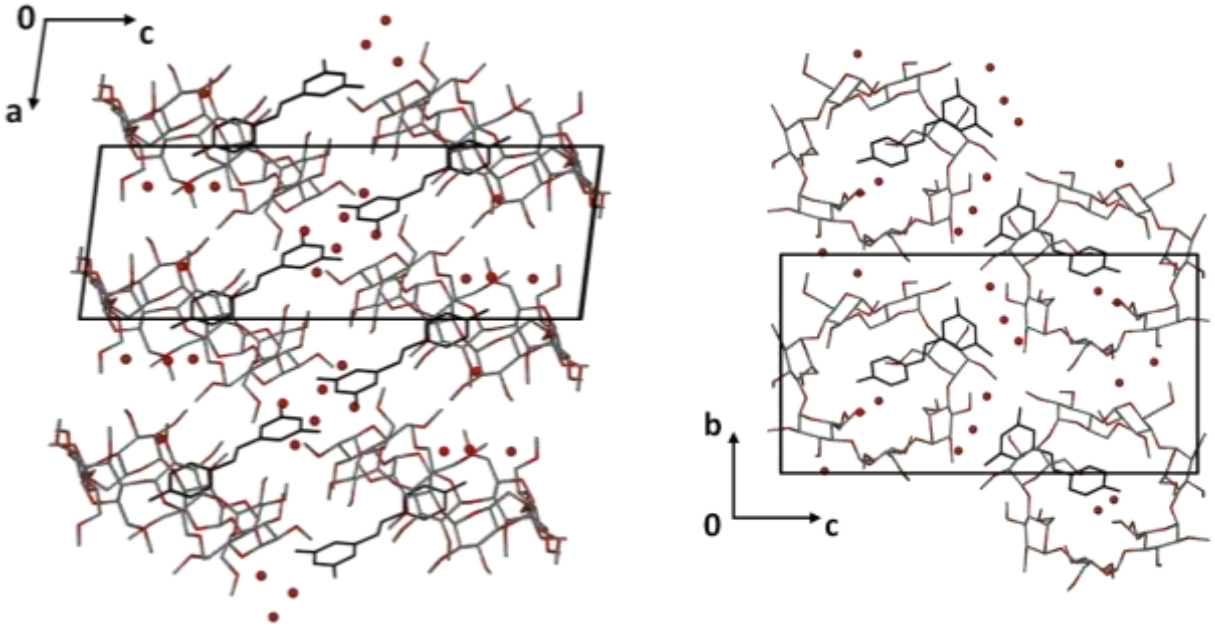

(a) (b)

Figure 3.10: Packing diagrams of the TMB·RES complex as viewed down (a) [010] and (b) [100]. Hydrogen atoms are omitted for clarity, water oxygen atoms are shown as red dots.

Comparative PXRD analysis

The calculated and experimental PXRD patterns shown in Figure 3.11 correlate well, indicating that the bulk material is the same as the single crystal used for X-ray analysis. The close match between the peak positions (2θ) is evidence of a pure product. Differences in the relative intensities between the two patterns are attributed to preferred orientation.

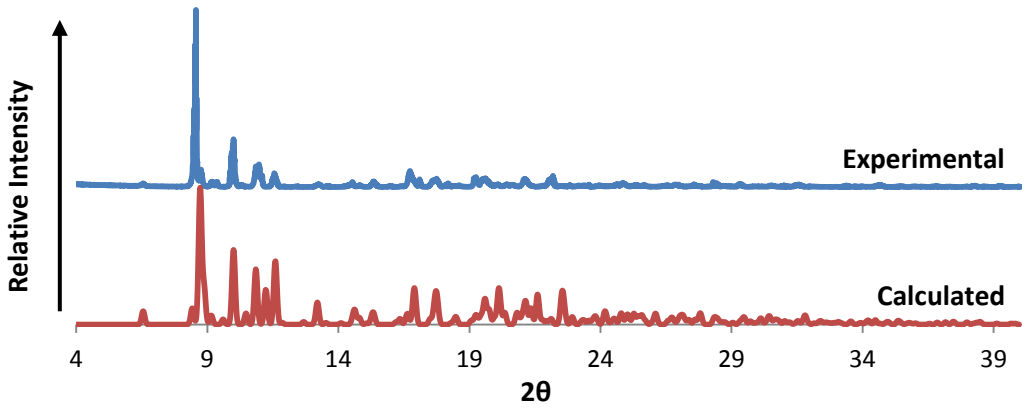

Figure 3.11: The PXRD trace of the experimental product and the pattern calculated from the structure of TMB·RES.

DIMEB INCLUSION COMPLEX WITH *trans*-RESVERATROL (DMB·RES)

Thermal analysis

Figure 3.12 shows the TGA and DSC curves for the complex DMB·RES. The TGA trace shows an initial mass loss of 4.4 ± 0.2 % (n = 3) over the range 30 - 110 °C, equalling 4.0 ± 0.2 water molecules per complex unit. This corresponds to the broad endotherm recorded in the DSC over the same temperature range and is physically observed in the HSM images by fracturing of the crystal at 130 °C (Figure 3.13). The crystal appears to undergo more than one phase transformation over the range 150 to 200 °C, recorded both in the DSC trace and HSM photographs, where the crystal is seen to change in opacity. A second mass loss appears in the TGA corresponding to partial guest loss and the DSC shows a sharp but small melting endotherm at *ca*. 233 °C. The remaining sample decomposes soon after, at *ca*. 320 °C.

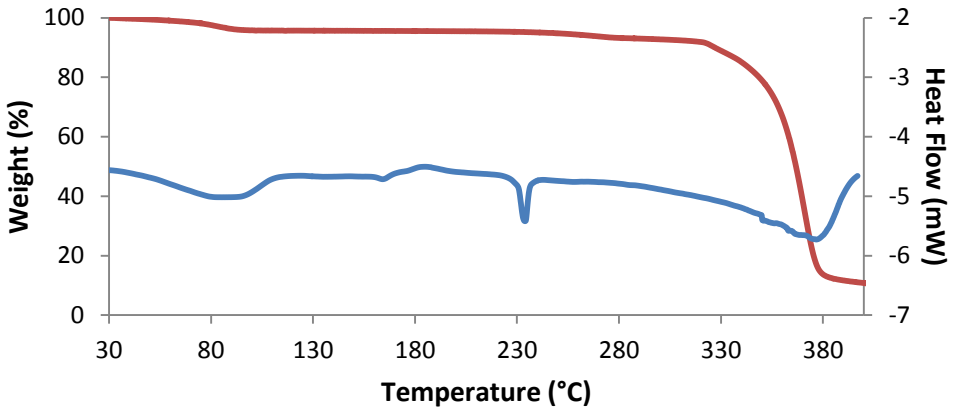

Figure 3.12: TGA (red) and DSC (blue) traces for the complex DMB·RES.

Figure 3.13: HSM photographs of DMB·RES at various temperatures.

Confirmation of complex stoichiometry

Crystals of DMB·RES were dissolved in DMSO-d_6 and the sample was analysed. A 1:1 host-guest stoichiometry was found using ^{1}H NMR spectroscopy by the integration of clearly separated host and proton signals (Table 3.9).

Table 3.9: Integrals of the host and guest protons of DMB·RES.

Guest proton	δ (ppm)	Multiplicity	J (Hz)	Integration	Experimental/ Theoretical	
p-OH	9.515	s		0.96	0.96	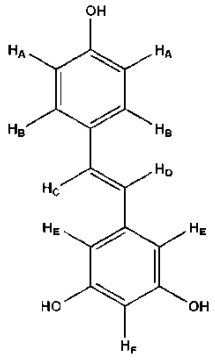
2 x m-OH	9.159	s		2.00	1.00	
2 x C-$\underline{H}_B$	7.399	d	^3J = 8.62	2.02	1.01	
C-$\underline{H}_C$ + C-$\underline{H}_D$	6.873	d of d	^4J = 16.32	1.93	0.97	
2 x C-$\underline{H}_A$	6.763	d	^3J = 8.64	2.06	1.03	
2 x C-$\underline{H}_E$	6.387	d	^3J = 2.13	2.05	1.02	
C-$\underline{H}_F$	6.124	t	^4J = 2.13	1.00 *	1.00	
Host proton	**δ (ppm)**	**Multiplicity**	**J (Hz)**	**Integration**	**Experimental/ Theoretical**	
7 x C-$\underline{H}_1$	4.982	d	^3J = 3.68	14.72	1.05	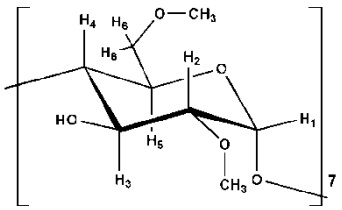
7 x C-O$\underline{H}$	4.958	s			1.05	
14 x C-$\underline{H}_6$	3.582	d	^3J = 3.14	14.75	1.05	
7 x O-C$\underline{H}_3$	3.519	s		22.47	1.07	
7 x O-C$\underline{H}_3$	3.269	s		22.65	1.08	
C-$\underline{H}_5$	3.218	d of d	^3J = 3.58	7.61	1.08	

*Reference integral

Crystal structure solution and refinement

The crystallographic data and data-collection conditions for DMB·RES are shown in Table 3.10. No isostructural complex was available at the time of data-collection and the structure was solved by direct methods using the program SHELXD.[3] A final correlation coefficient of 89.8 was achieved, the resulting E-map revealing many of the non-hydrogen atoms of both the host and guest. Refinement was performed using the full-matrix least-squares technique implemented in SHELXH-97.[5] Successive difference Fourier maps revealed the remaining non-hydrogen atoms and they were appropriately assigned. Neither of the guest phenol rings required restraints of any kind. The glucopyranose units were labelled G1-G7 and any disordered atoms were labelled by parts. The methyl carbon on the O6 methoxy group of glucopyranose unit G2 experienced large thermal motion and was found to be disordered over two positions. The major component refined with an s.o.f. of 0.55 and the minor component with an s.o.f. of 0.45. The bond lengths of the disordered methyl groups O6G2-C821 and O6G2-O822 were restrained to a length of 1.40(2) Å.

The hydrogen atoms of the host were placed in idealised positions using a riding model, except for the hydroxyl hydrogen atom H3G3, which was assigned from the electron density map and restrained to 0.84(2) Å to obtain the correct directionality of the hydrogen bond interaction with the adjacent oxygen atom. The tertiary and secondary hydrogen atoms were assigned U_{iso} values 1.2 times that of the host parent atom and the methyl hydrogen atoms were assigned U_{iso} values 1.5 times that of the host parent

atom. Examination of the electron density map revealed the guest hydrogen atoms, which were placed in idealised positions in a riding model. The hydroxyl hydrogen atoms were placed using the AFIX 147 command which searches for the highest electron density. This resulted in H-atom positions satisfying hydrogen bonding requirements.

Four water molecules were identified and assigned. This correlates well with the TGA results. The water hydrogen atoms were placed and constrained using the DANG and DFIX commands.

Table 3.10: Data-collection and refinement parameters for DMB·RES.

Complex Formula	**$C_{56}H_{98}O_{35}\cdot C_{14}H_{12}O_3\cdot 4H_2O$**
Formula weight / g mol^{-1}	1631.71
Crystal system	Orthorhombic
Space group	$P2_12_12_1$
a / Å	10.6132(5)
b / Å	15.1612(7)
c / Å	51.066(2)
Volume / $Å^3$	8216.9(7)
Z	4
Calculated density / g cm^{-3}	1.319
μ (MoKα) / mm^{-1}	0.109
F (000)	3496
Temperature of data collection / K	173(2)
Crystal size / mm^3	0.19 x 0.31 x 0.37
Theta ranges scanned / °	1.8 ≤ θ ≤ 26.0
Index ranges	h: -13: 6; k: -18: 18; l: -28: 62
Total number of reflections	39193
No. of independent reflections	8924
No. of reflections with I > 2σ(I)	7413
No. of parameters	1063
R_{int}	0.047
S	1.022
R_1 (I > 2σ(I))	0.0386
No. of reflections omitted	9
wR_2	0.0887
Weighting scheme parameters *a* and *b* ($w = 1/[\sigma^2(Fo^2) + (aP)^2 + (bP)]$)	a = 0.0439, b = 1.5448
$(\Delta/\sigma)_{mean}$	0.00, 0.00
Δρ excursions / e $Å^{-3}$	-0.25, 0.32

Molecular structure

The asymmetric unit consists of one RES molecule, one DIMEB molecule and 4 water molecules (Figure 3.14a and b). The RES molecule is included in the CD cavity at the 4-hydroxyphenyl ring end with the di-substituted phenol ring protruding from the secondary rim. The atom labels of the host and guest molecules are shown in Figure 3.14c.

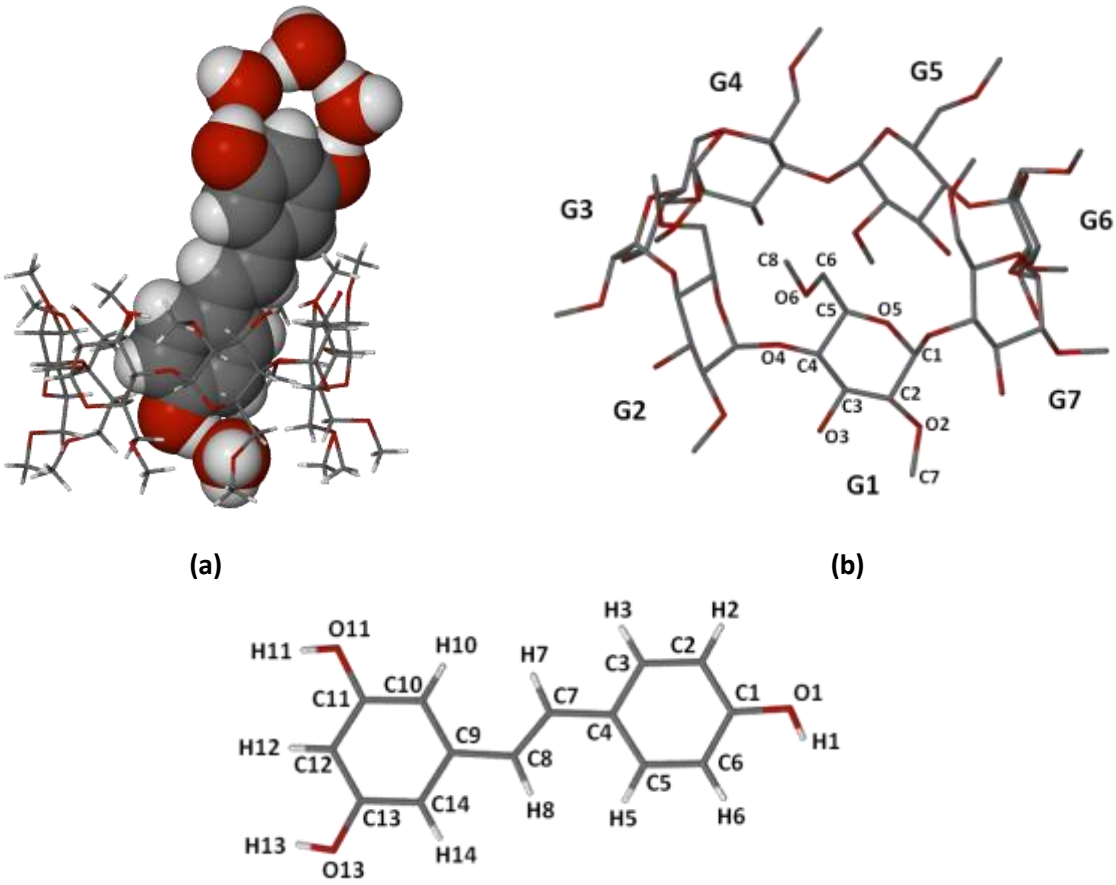

(a) **(b)**

(c)

Figure 3.14: (a) The asymmetric unit of DMB·RES, (b) the labelling of the glucopyranose unit of the host molecule (hydrogen atoms are omitted for clarity) and (c) the labelling of the guest molecule.

Geometrical analysis

Host geometry

The geometric parameters of the O4 heptagon of the DMB·RES structure are listed in Table 3.11. The radii (*r*), the O4(n)···O4(n+1) distance (*D*) and angle (*a*), the O4(n-1)···O4(n)···O4(n+1) ···O4(n+2) torsion angle (*d*), the intersaccharidic bond angle O4(n)···C4(n)···C1(n+1) (*φ*), the inter-ring O2(n)···O3(n-1) distance (D_3), the deviation of the O4 atoms from the mean O4-plane (*α*) and the tilt angles τ_1 and τ_2 describe the shape of the host molecule. The DIMEB molecule is round and somewhat symmetrical. The D_3 values (average 2.83 Å) indicate that the hydroxyl group O3-H of each glucose ring is the donor in a hydrogen bond to the O2 atom of the adjacent glucose ring, resulting in the formation of a 'belt' of intramolecular O2(n)···H-O3(n-1) bonds. These hydrogen bonding interactions contribute to the symmetry and stability of the host skeleton. The tilt angles show larger tilting to the extremities of the host curvature but allow both primary and secondary ends of the host to be relatively open.

Table 3.11: Geometric parameters of the DIMEB molecule in the complex DMB·RES.

Residue	*r* (Å)	*D* (Å)	*a* (°)	*d* (°)	*φ* (°)	D_3 (Å)	*α* (Å)	τ_1 (°)	τ_2 (°)
G1	4.974	4.439	129.50	13.65	117.7	2.796	-0.287(2)	6.27	8.92
G2	5.151	4.306	125.36	0.84	119.2	2.894	0.155(2)	9.25	9.49
G3	5.031	4.412	128.62	-13.45	117.8	2.909	0.187(2)	23.93	24.89
G4	4.920	4.403	130.69	7.47	117.7	2.788	-0.246(2)	11.64	15.42
G5	5.103	4.312	125.87	5.16	120.0	2.822	-0.044(2)	2.34	2.98
G6	5.038	4.333	129.33	-3.14	117.5	2.734	0.210(1)	10.72	12.26
G7	4.993	4.404	128.49	-10.96	118.1	2.877	0.025(1)	20.58	22.22

The C6-O6 bonds are (-)-*gauche* for residues G1, G2, G4, G5 and G6, while those of the other two, G3 and G7, are (+)-*gauche*. All of the O6-C8 bonds are *trans* with respect to the C5-C6 bonds, except for those on G3 (*synclinal*) and G7 (*anticlinal*). The O6 methoxy moiety of the G3 residue is directed toward the centre of the CD cavity.

Guest inclusion

The inclusion of the guest molecule in the CD cavity occurs from the secondary face of the CD such that the 4-hydroxyphenyl moiety is deeply inserted within the CD cavity and the 1,3-benzenediol moiety protrudes from the CD cavity. The angle between the mean O4 plane of the CD and the mean plane through the RES molecule is 73.2(5)°. Figure 3.15 shows space-filling diagrams of the TMB·RES complex. The RES molecule shows only a small deviation from planarity with the angle between the phenyl rings being 13.6(2)°. The torsion angles around the double bond of RES, namely C3-C4-C7-C8, C4-C7-C8-C9 and C7-C8-C9-C14 are -175.0(3)°, -180.0(3)° and -171.5(3)°, respectively.

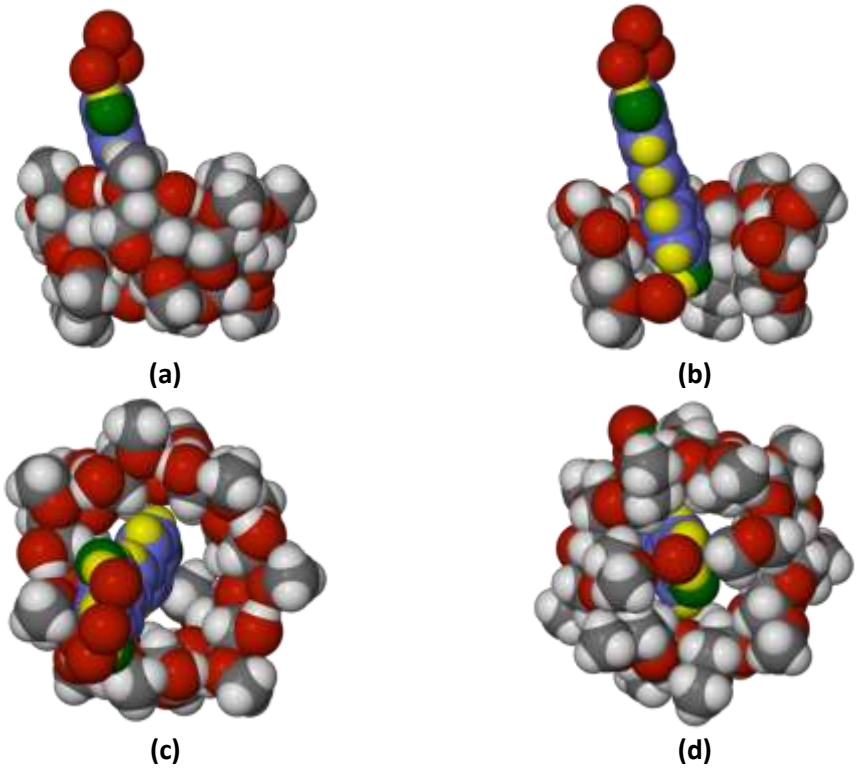

Figure 3.15: Space-filling diagrams of DMB·RES viewed (a) side-on, (b) cutaway, (c) from the secondary rim of the host, and (d) from the primary rim.

Hydrogen bonding interactions

Host-guest intermolecular interactions

The DIMEB host molecule has one weak hydrogen bonding interaction with a symmetry-generated guest molecule at position x,-1+y,z: C7G5-H7G1···O13, for which the O···H distance is 2.466(4) Å, the C···O distance is 3.278(4) Å and the bond angle is 140°.

Host-host interactions

The circular shape of the host molecule is stabilised by seven intramolecular interactions between O2(n) and O3(n-1).[6] These hydrogen bonds have an average O···O bond length of 2.83 Å and the O-H···O bond angle range is 165°-173°. The crystal structure is further stabilised by five intermolecular host-host hydrogen bonding interactions listed in Table 3.12. These interactions exist between symmetry-generated DIMEB molecules where no interstitial water molecules are present.

Table 3.12: Hydrogen bond parameters for host-host interaction in DMB·RES.

D-H···A	D-H (Å)	H···A (Å)	D···A (Å)	D-Ĥ···A (°)	Symmetry Operation*
C2G1-H2G1···O6G5	1.00	2.47	3.363(4)	149	x,1+y,z
C2G5-H2G5···O3G1	1.00	2.56	3.441(3)	146	x,-1+y,z
C1G4-H1G4···O6G3	1.00	2.26	3.258(4)	175	1/2+x,3/2-y,2-z
C7G6-H7G8···O2G7	0.98	2.49	3.461(4)	171	1-x,-1/2+y,3/2-z
C7G1-H7GE···O3G6	0.98	2.39	3.335(5)	161	1-x,1/2+y,3/2-z

*The symmetry operation applies to the acceptor O atom.

Weak host intramolecular close contacts

Appendix E lists the weak C-H···O intramolecular close contacts present in the DMB·RES complex. The hydrogen bond distances of these close contacts are reasonable but typically have less than ideal bond angles (100.0° ≤ D-H···A ≤ 130.0°). Where the bond length is very long, the D-H···A angle is more favourable.

Water interactions

There are five water-host hydrogen bond interactions in the DMB·RES structure. Four of these interactions occur between water and symmetry-generated host molecules while one of the interactions occurs within the same complex unit, anchoring the guest molecule to the host molecule. As with the TMB·RES structure, water molecules form a “crown” of hydrogen bonded water with RES: three water molecules interact with each other and with the two hydroxyl groups of the phenol moiety protruding from the CD cavity (Figure 3.16). The hydrogen bonding interactions involving water are listed in Table 3.13. Figure 3.16 also shows the bridging role of a water molecule that lies near the interface of the two complex units shown.

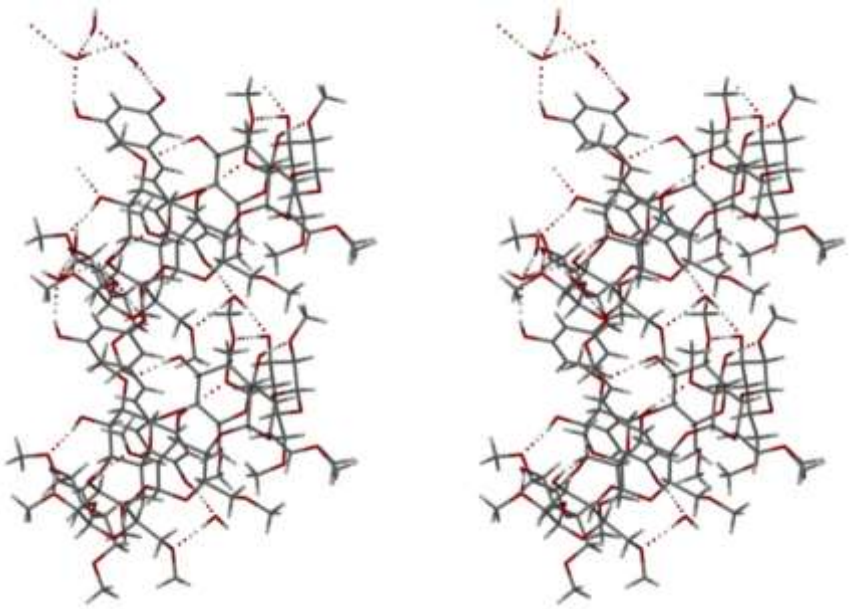

Figure 3.16: A stereodiagram illustrating the hydrogen bonding motif present in the DMB·RES complex. The host hydrogen atoms are omitted for clarity.

Table 3.13: Hydrogen bond parameters for water interactions in DMB·RES.

D-H···A	D-H (Å)	H···A (Å)	D···A (Å)	D-Ĥ···A (°)	Symmetry Operation
Host-Water					
O1W-H1WB···O3G5*	0.85	2.01	2.834(3)	163	2-x,1/2+y,3/2-z
O1W-H1WA···O3G7*	0.85	1.95	2.790(3)	170	1+x,y,z
O2W-H2WA···O6G7	0.86	1.92	2.778(4)	177	-
O2W-H2WB···O3G3*	0.85	2.01	2.857(3)	172	-1+x,y,z
O3W-H3WA···O3G6*	0.86	2.24	3.096(4)	175	2-x,1/2+y,3/2-z
Water-Guest					
O1-H1···O2W	0.84	1.89	2.718(4)	168	-
O11-H1···O1W	0.84	2.06	2.849(3)	155	-
O13-H13···O4W	0.84	1.89	2.714(4)	166	-
O4W-H4WA···O11*	0.85	2.28	3.117(4)	167	2-x,1/2+y,3/2-z
Water-Water					
O3W-H3WB···O1W	0.86	2.08	2.923(4)	166	-
O4W-H4WB···O3W	0.85	2.01	2.847(4)	170	-

*Atom to which the symmetry operation applies.

Crystal packing

The complex units stack in columns parallel to the *a*-axis in a head-to-tail fashion. Adjacent columns are related by a two-fold screw axis. Figure 3.17 shows the packing arrangement in DMB·RES and Figure 3.18 illustrates the modified herringbone type packing. The host molecules self-include such that two primary methoxyl groups interact with the cavity of a symmetry-generated neighbouring CD.

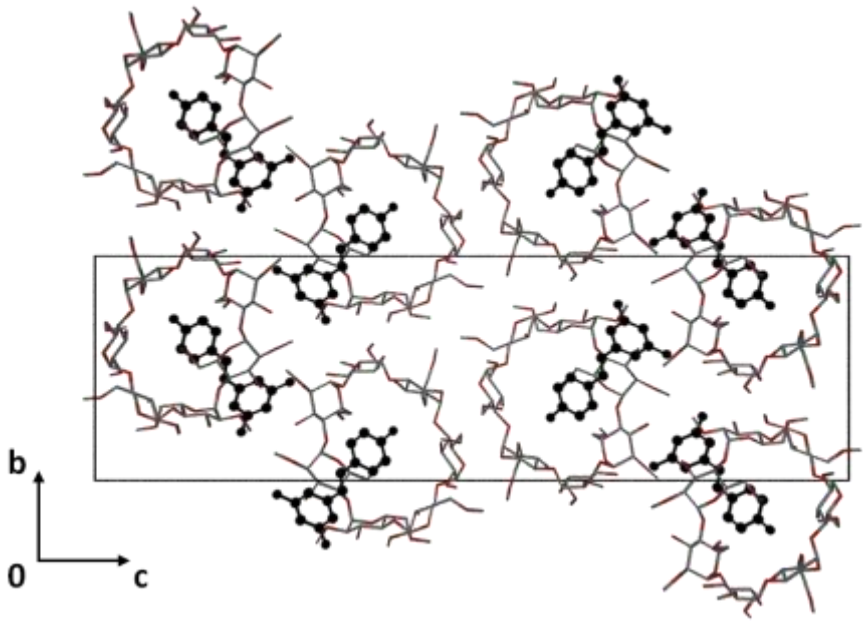

Figure 3.17: The packing arrangement in DMB·RES viewed along the [1 0 0] direction. Hydrogen atoms are omitted for clarity.

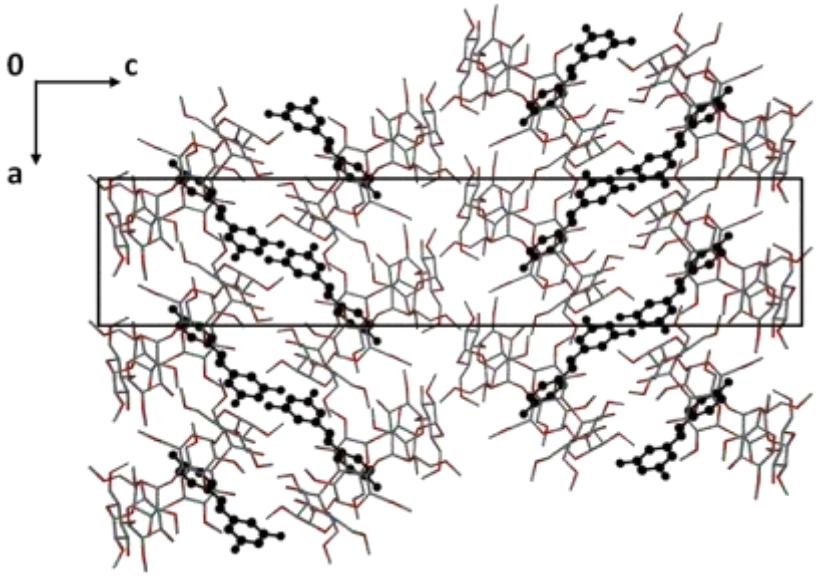

Figure 3.18: The packing arrangement in DMB·RES viewed down the line [0 1 0], illustrating the modified herringbone type packing. Hydrogen atoms are omitted for clarity.

Comparative PXRD analysis

Figure 3.19 shows the calculated and experimental PXRD traces of the DMB·RES complex. There is good agreement between the two indicating that the single crystal used for X-ray analysis is representative of the bulk material. The product is pure and differences in the relative intensities between the two patterns are attributed to preferred orientation.

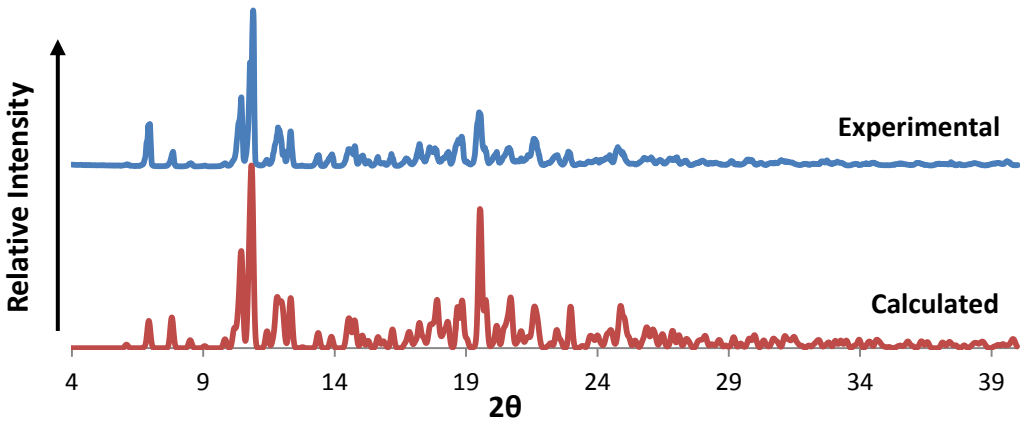

Figure 3.19: Comparison of the experimental and calculated PXRD traces for DMB·RES.

TRIMEA INCLUSION COMPLEX WITH *trans*-RESVERATROL (TMA·RES)

Thermal analysis

The TGA and DSC curves are shown in Figure 3.20. Over the temperature range 30 – 100 °C a mass loss of 7.5 ± 1.3 % (n = 3) is observed, which corresponds to 6.6 ± 1.2 water molecules per 1:1 complex unit. This water loss is physically observed in the HSM photographs by bubbling that begins at 112 °C (Figure 3.21). The initial broad endotherm over the range 30 – 130 °C in the DSC curve corresponds to this water mass loss. The development of a sharp endotherm which overlaps the broad endotherm at 110 °C indicates complex fusion which occurs with the dehydration process. The small, sharp endotherm at 150 °C is evidence of a melt of a new phase. The HSM photographs appear to support this: at 120 °C melting is observed. A phase change accompanies the melt and at 136 °C the sample appears to be both liquid and microcrystalline. At 177 °C the sample has melted completely. The TGA indicates that complex decomposition begins at an onset of *ca*. 280 °C.

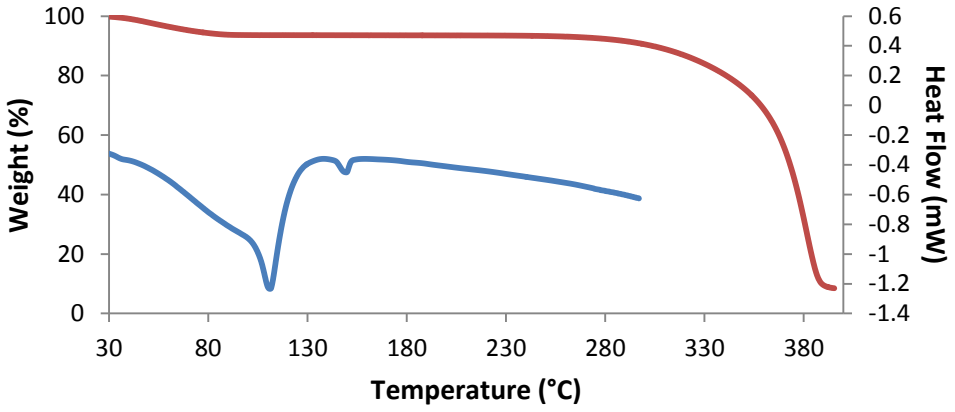

Figure 3.20:TGA and DSC thermograms for TMA·RES.

30 °C 112 °C 120 °C 136 °C 177 °C

Figure 3.21: Representative HSM photographs of TMA·RES at various temperatures.

Confirmation of complex stoichiometry

The stoichiometry of the complex TMA·RES was found by dissolving the complex crystals in acetone-d_6 and analysing the solution using ^{1}H NMR spectroscopy. The resulting host and guest signals in the ^{1}H NMR spectrum were integrated, giving a quantification of the host and guest molecules present in the sample (Table 3.14). A 1:1 host-guest ratio was established.

Table 3.14: Integrals of the host and guest protons in TMA·RES.

Guest proton	δ (ppm)	Multiplicity	J (Hz)	Integration	Experimental/ Theoretical	
2 x C-$\underline{H}_B$	7.435	d	^{3}J = 8.33	2.00	1.00	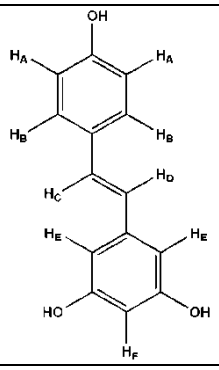
C-$\underline{H}_C$ + C-$\underline{H}_D$	6.965	d of d	^{4}J = 16.29	3.88	0.97	
2 x C-$\underline{H}_A$	6.859	d	^{3}J = 8.65		0.97	
2 x C-$\underline{H}_E$	6.557	d	^{3}J = 2.15	2.00 *	1.00	
C-$\underline{H}_F$	6.288	t	^{4}J = 2.17	0.92	0.92	
Host proton	**δ (ppm)**	**Multiplicity**	**J (Hz)**	**Integration**	**Experimental/ Theoretical**	
6 x C-$\underline{H}_1$	5.036	d	^{3}J = 3.45	6.14	1.02	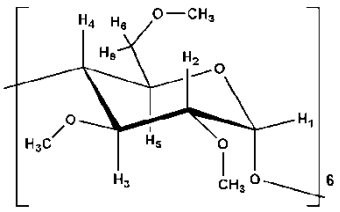
6 x O-C$\underline{H}_3$	3.613	s		18.52	1.02	
6 x O-C$\underline{H}_3$	3.355	s		18.46	1.02	
6 x C-$\underline{H}_5$	3.069	d of d	^{4}J = 3.43	6.26	1.04	

*Reference integral

Crystal structure solution and refinement

The structure was originally solved using program SHELXD[3] (CC = 77.32) from data collected at 173 K. While the host structure was well-defined, some of the guest atoms appeared to be severely disordered. In an effort to improve the result, intensity data from a fresh crystal were collected at a lower temperature (133 K). Isomorphous replacement using the host molecule coordinates as a trial model with the new intensity data led to a significantly improved model for the guest atoms. The refinement parameters and crystal data are reported in Table 3.15.

Table 3.15: Crystal structure and data-collection parameters for TMA·RES.

Complex Formula	**$C_{54}H_{96}O_{30}·C_{14}H_{12}O_3·6.25H_2O$**
Formula weight / g mol^{-1}	1566.14
Crystal system	Monoclinic
Space group	$P2_1$
a / Å	18.690(9)
b / Å	21.244(8)
c / Å	20.528(10)
β / °	94.604(16)
Volume / $Å^3$	8125(6)
Z	4
Calculated density / g cm^{-3}	1.280
μ (MoKα) / mm^{-1}	0.105
F (000)	3370
Temperature of data collection / K	133(2)
Crystal size / mm^3	0.37 x 0.58 x 0.60
Theta ranges scanned / °	1.7 ≤ θ ≤ 26.4
Index ranges	h: -23: 15; k: -26: 26; l: -25: 25
Total number of reflections	72298
No. of independent reflections	17061
No. of reflections with I > 2σ(I)	13939
No. of parameters	1853
R_{int}	0.040
S	1.026
R_1 (I > 2σ(I))	0.0677
No. of reflections omitted	32
wR_2	0.1945
Weighting scheme parameters *a* and *b* ($w = 1/[\sigma^2(Fo^2) + (aP)^2 + (bP)]$)	a = 0.0977, b = 8.0492
$(\Delta/\sigma)_{mean}$	0.00, 0.00
Δρ excursions / e $Å^{-3}$	-0.48, 0.76

The asymmetric unit was found to contain two TRIMEA molecules and two RES molecules as well as several water molecules. The glucopyranose units of the respective host molecules were labelled An and Bn (n = 1-6). Several atoms of the host molecule B were found to be disordered and these were assigned s.o.f.s of x and 1-x, where x is variable. Table 3.16 shows the disordered pairs and their s.o.f.s.

Table 3.16: Parameters for the disordered atoms on the TRIMEA host molecule B.

Atom	**s.o.f.**	**Atom**	**s.o.f.**	**Atom**	**s.o.f.**
C721/C722	0.4155/0.5845	C631/C632 O631/O632 C931/C932	0.4937/0.5063	O561/O562 C561/C562 C661/C662 O661/O662 C961/C962	0.5525/0.4475
C751/C752	0.5744/0.4256				
C761/C762	0.5496/0.4504				
O651/O652 C951/C952	0.8295/0.1705				

The remaining isolated electron density peaks were assigned as water molecules, a total of 12.5 being assigned. This correlates well with the TGA results, which revealed a loss of 13.2 ± 2.4 water molecules per asymmetric unit. These were assigned over 20 sites, eight of which were fully occupied (s.o.f. = 1.0)

while 12 sites were partially occupied. The U_{iso} values of the water oxygen atoms settled between 0.04 and 0.11 Å^2, with a mean value of 0.06 Å^2. The hydrogen atoms of the water molecules were not located.

The non-hydrogen atoms assigned full s.o.f.s were refined anisotropically; all disordered non-hydrogen atoms were refined isotropically. A number of bond lengths involving the disordered atoms in the host were constrained to the range 1.40(2) Å - 1.50(2) Å.[7]

All of the host tertiary, secondary and methyl hydrogen atoms were placed in idealised positions in a riding model. The hydrogen atoms were assigned U_{iso} values 1.2 times those of their parent atoms, except for the methyl hydrogen atoms which were assigned U_{iso} values 1.5 times those of their parent atoms.

Modelling the *trans*-resveratrol guest

Difference electron density peaks found within the host molecule A were assigned as the non-hydrogen atoms of guest molecule A. No disorder was evident and following isotropic refinement, the U_{iso} values were found to be stable. The non-hydrogen atoms were refined anisotropically. The guest molecule inserted in CD host molecule B was found to be disordered over two positions. After some effort, the disordered components were successfully modelled and labelled B and C, respectively. The phenol rings of the disordered components B and C were constrained as rigid hexagons using the AFIX 66 command. The refined s.o.f.s of the disordered components were 0.56 for component B and 0.44 for component C. The aromatic hydrogen atoms were placed in idealised positions using the AFIX 43 command. The hydroxyl hydrogen atoms were placed in idealised positions using the commands AFIX 83 and AFIX 147. The former uses the hydrogen bond searching model while the latter identifies the idealised position by the highest electron density using a rotating group model. Reasonable hydrogen bonding positions were thus achieved for the hydroxyl hydrogen atoms.

Molecular structure

The asymmetric unit consists of two RES molecules, two TRIMEA molecules and 12.5 water molecules (Figure 3.22). The 4-hydroxyphenyl residue of the RES molecule is included in the CD cavity and the 1,3-benzenediol moiety extends into the interstitial space from the secondary side of the host. The hydroxyl groups of the 1,3-benzenediol moiety form hydrogen bond interactions with water molecules. The atom labels of the host molecule A are shown in figure 3.23, the atom labels for host molecule B following the same trend, with the disordered atoms labelled by parts. The labelling of the guest molecules is illustrated in Figure 3.24. The guest molecule included in CD molecule A was labelled A, while the disordered guest in CD molecule B is labelled B for the major part and C for the minor part.

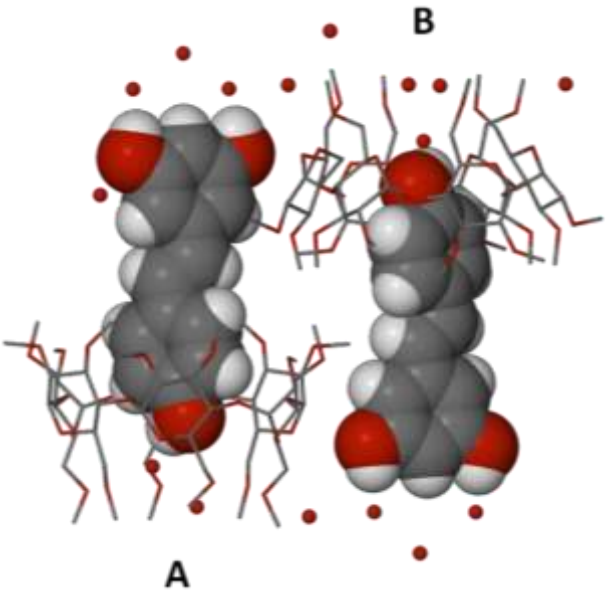

Figure 3.22: The asymmetric unit of the complex TMA·RES. Only the major components of disorder are shown and the hydrogen atoms are omitted for clarity.

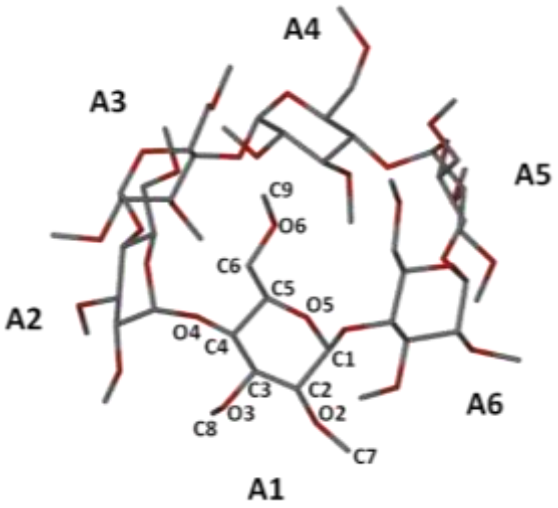

Figure 3.23: Labelling of the glucopyranose units of the host molecule A (similarly for B).

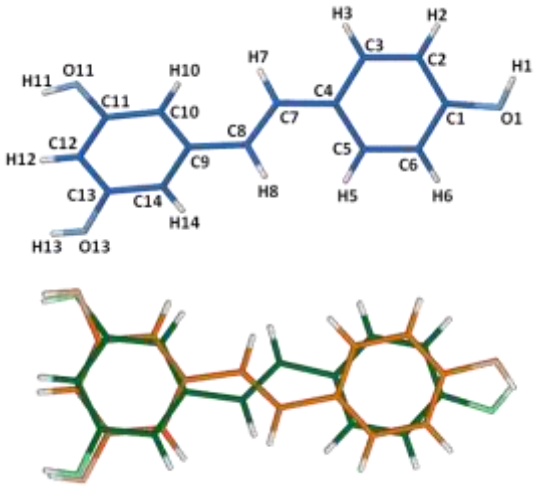

Figure 3.24: The labelling of the guest molecule A (shown in blue) and the orientation of the disordered guests B and C where B is shown in orange and C is shown in green.

Geometrical analysis

Host geometry

Table 3.17 lists the geometrical parameters used to describe the structures of the two TRIMEA host molecules. These parameters are defined in Chapter 1 and illustrate how the two host molecules have different conformations due to the different guest conformations. Both of the host molecules have a slightly elliptical shape, indicated by the variations in the values for *r*, *D* and *a*. The primary face of host molecule A is relatively open, having small τ_1 and τ_2 torsion angles. The primary face of host molecule B is slightly more closed as indicated by the larger τ_1 and τ_2 torsion angles and the orientation of the O6 methoxy groups.

Table 3.17: Geometrical parameters of the TRIMEA molecules in the complex TMA·RES.

Residue	*r* (Å)	*D* (Å)	*α* (°)	*d* (°)	*φ* (°)	D_3 (Å)	*α* (Å)*	τ_1 (°)	τ_2 (°)
A1	4.513	4.032	114.77	-2.17	118.2(4)	3.154	-0.0515	14.90(13)	3.24(3)
A2	4.485	4.502	115.59	-0.02	119.1(4)	3.287	0.0308	19.34(13)	5.83(4)
A3	3.929	4.395	128.97	2.85	118.6(4)	3.493	0.0248	12.77(13)	5.29(5)
A4	4.498	4.059	115.67	-2.81	117.4(4)	3.222	-0.0594	16.84(13)	3.66(3)
A5	4.503	4.469	114.55	0.71	119.4(4)	3.284	0.0383	19.62(12)	6.44(5)
A6	3.893	4.399	130.35	2.10	118.0(4)	3.473	0.0169	11.68(12)	5.12(6)
*Average e.s.d. = 0.0027 Å									
B1	4.610	4.361	112.04	11.47	118.9(4)	3.222	-0.1945	6.98(14)	9.04(7)
B2	4.251	4.387	121.25	-7.22	118.9(4)	3.591	0.2032	23.26(14)	6.22(6)
B3	4.111	4.295	126.93	-4.33	116.4(5)	3.387	-0.0157	27.21(16)	10.32(9)
B4	4.643	4.320	110.43	10.63	119.5(5)	3.229	-0.1841	5.73(17)	7.49(8)
B5	4.219	4.448	122.93	-6.33	118.2(5)	3.631	0.1948	25.34(15)	5.72(4)
B6	4.164	4.264	124.88	-5.37	116.9(5)	3.332	-0.0037	18.50(26)	9.68(8)
*Average e.s.d. = 0.0033 Å									

The torsion angles O5-C5-C6-O6 are (+)-*gauche* for A1, A2, A3, A5 and A6, and (-)-*gauche* for A4. These torsion angles are (+)-*gauche* for B1, B4 and both disordered components of each of B3 and B6. The torsion angles are (-)-*gauche* for residues B2 and the major component of B5. The minor component of B5 is (+)-*syn*. The O6-C9 bonds are *trans* with respect to the C5-C6 bonds, except for those on residue A4, both disordered components on residue B3, and the minor component on the residue B5, which are all *anticlinal*.

Guest inclusion

The 4-hydroxyphenyl residue of the RES molecule is included in the CD cavity and the 1,3-benzenediol moiety extends from the secondary side of the host into the interstitial space between the complex units. The guest molecules include such that the angles between the mean plane through the RES molecules and the mean O4-planes of the respective host molecules are virtually the same, being 85.6° for complex unit A and 86.8° for complex unit B (using the mean plane through the major disorder component molecule B). Figures 3.25 to 3.28 show space-filled diagrams of each guest within its respective host molecule, illustrating the modes of guest inclusion.

The guest molecules deviate from planarity, with the angle between the phenyl groups of molecule A being 51.6(3)° and that of the disorder guest component B being 23.5(4)°. Table 3.18 lists the torsion angles describing the distortion around the double bond.

Table 3.18: Torsion angle parameters (°) for each guest A, B and C

Guest A		Guest B		Guest C	
C5A-C4A-C7A-C8A	-154.0(6)	C3B-C4B-C7B-C8B	-162.3(7)	C5C-C4C-C7C-C8C	-161.2(7)
C4A-C7A-C8A-9A	-175.1(5)	C4B-C7B-C8B-C9B	-173.7(7)	C4C-C7C-C8C-C9C	-171.5(9)
C7A-C8A-C9A-C10A	-159.9(6)	C7B-C8B-C9B-C10B	-177.1(5)	C7C-C8C-C9C-C14C	-170.8(5)

Complex A **Complex B**

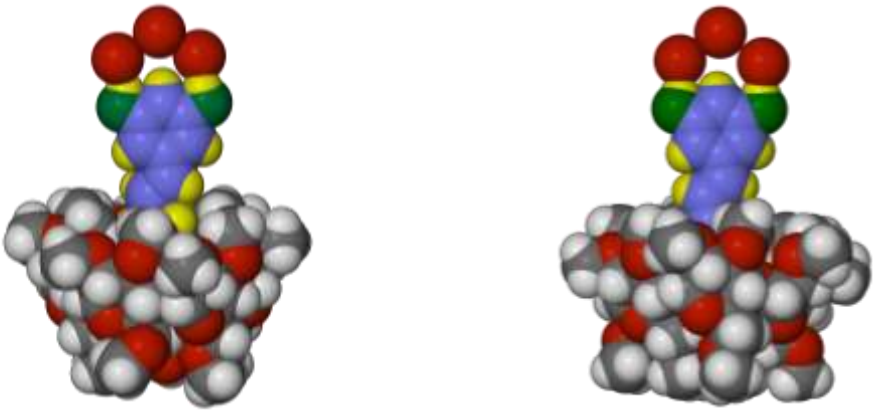

Figure 3.25: Space-filling diagrams of the structures viewed from the side.

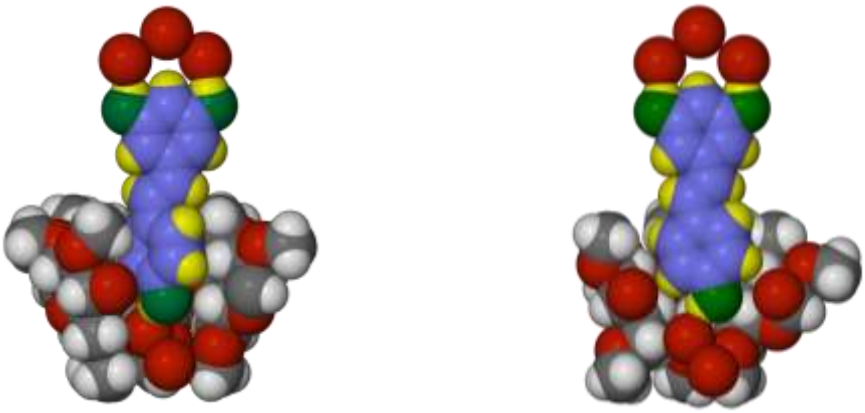

Figure 3.26: Sectioned space-filling diagrams of the structures viewed from the side.

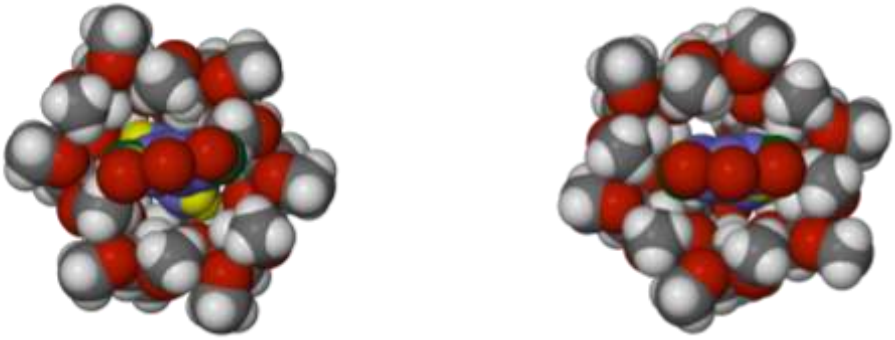

Figure 3.27: Space-filling diagrams of the structures viewed from the secondary rim.

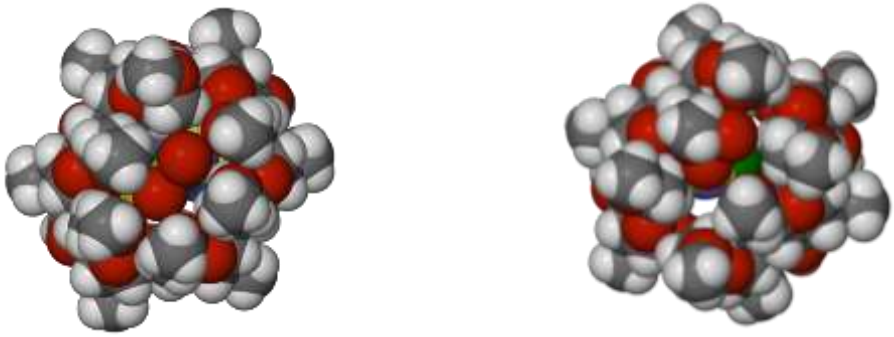

Figure 3.28: Space-filling diagrams of the structures viewed from the primary rim.
For clarity, only the major component of the disordered RES molecule in complex B is shown.

Hydrogen bonding interactions

Host-guest intermolecular interactions

There are seven host-guest intermolecular hydrogen bonds in the TMA·RES structure, all of which are of the type C-H···O and are listed in Table 3.19. Due to the disorder of the guest some measurements were performed manually and do not have an e.s.d.

Table 3.19: Host-guest hydrogen bond parameters in TMA·RES

D-H···A	D-H (Å)	H···A (Å)	D···A (Å)	D-Ĥ···A (°)	Symmetry Operation
C4A1-H4A1···O11A*	1.00	2.57	3.568(7)	172	2-x,-1/2+y,1-z
C4A2-H4A2···O11B*	1.00	2.52	3.47(1)	159	x,y,-1+z
C4A5-H4A5···O13B	1.00	2.45	3.40(1)	158	-
C4A2-H4A2···O11C*	1.00	2.40	3.357	161	x,y,-1+z
C4A5-H4A5···O13C	1.00	2.42	3.386	162	-
C10A-H10A···O3B6	0.95	2.59	3.440(8)	148	-

*Atom to which the symmetry operation applies.

Host-host interactions

A number of C-H···O interactions stabilise the crystal structure. There are ten C6-H···O5(n+1) intramolecular interactions with an average C···O distance of 3.30 Å and an average C-H···O angle of 146°. A further nine intramolecular interactions are of the type C8-H···O2, C8-H···O2(n+1), C9-H···O5, C4-H···O6 and C5-H···O4(n-1). Table 3.20 shows the intermolecular interactions which occur between hydrogen bond donors on host molecule A and the oxygen atoms of host molecule B and vice versa.

Table 3.20: Hydrogen bond parameters for host-host interactions in the TMA·RES structure.

D-H···A	D-H (Å)	H···A (Å)	D···A (Å)	D-Ĥ···A (°)	Symmetry Operation*
C2A6-H2A6···O6B2	1.00	2.58	3.557(7)	169	2-x,-1/2+y,2-z
C2A3-H2A3···O651	1.00	2.49	3.477(7)	168	1-x,-1/2+y,1-z
C2A5-H2A5···O5B4	1.00	2.54	3.509(7)	164	1-x,-1/2+y,2-z
C2A2-H2A2···O5B1	1.00	2.40	3.335(7)	155	2-x,-1/2+y,1-z
C6A3-H6A6···O3B5	0.99	2.50	3.414(8)	152	1-x,-1/2+y,1-z
C2B5-H2B5···O5A3	1.00	2.55	3.457(7)	151	1-x,1/2+y,1-z
C2B2-H2B2···O5A6	1.00	2.47	3.369(7)	149	2-x, ½+y, 2-z
C9B2-H9B5···O3A6	0.98	2.54	3.401(10)	147	2-x, ½+y, 2-z
C951-H95B···O3A3	0.98	2.54	3.363(13)	142	1-x,1/2+y,1-z

*The symmetry operation applies to the acceptor O atom.

Water interactions

There are 12.5 water molecules in the asymmetric unit. The water molecules interact with at least one other water, host or guest molecule. The water O···O close contacts have an average distance of ~2.77 Å. A large number of O···O close contacts exist between the oxygen atoms of the water and host molecules

with an average distance of ~2.85 Å and there are four C-H···O hydrogen bonding interactions from 3.25 Å to 3.50 Å for C···O.

As with the TMB·RES and DMB·RES complexes the water molecules interact with the guest and other water molecules to form a hydrogen bond network which "crowns" the 1,3-benzenediol end of the RES molecule that is located in the interstitial space. Further water-water, host-water and guest-water interactions hold the 4-hydroxyphenyl end of the RES molecule firmly in the CD cavity. This is illustrated in Figure 3.29.

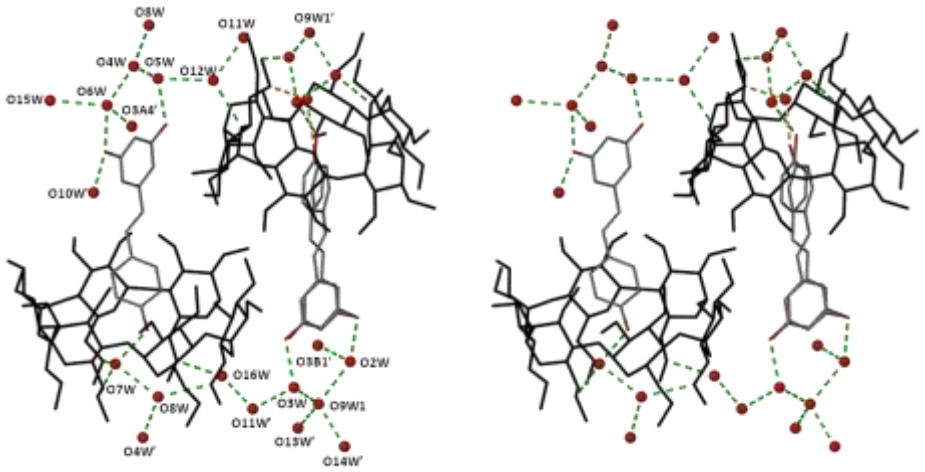

Figure 3.29: Stereodiagram illustrating the hydrogen bonding motifs in the structure of TMA·RES. The orange broken lines indicate hydrogen bonding of the minor disorder component, which has a different orientation from that of the major disordered component.

Crystal packing

The complex units pack in a head-to-tail manner in columns parallel to the *b*-axis (Figure 3.30). The columns of each host A and B form layers parallel to the *yz*-plane. Adjacent columns in a layer are related by a two-fold screw axis (Figure 3.31). The vertical shift between the complex units in a column is equal to one unit along the *b*-axis.

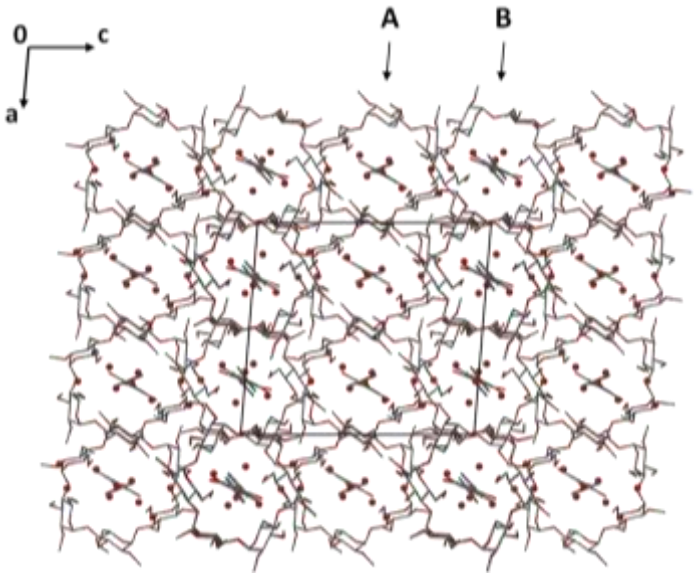

Figure 3.30: Packing diagram of TMA·RES viewed down [0 1 0]. Hydrogen atoms are omitted for clarity.

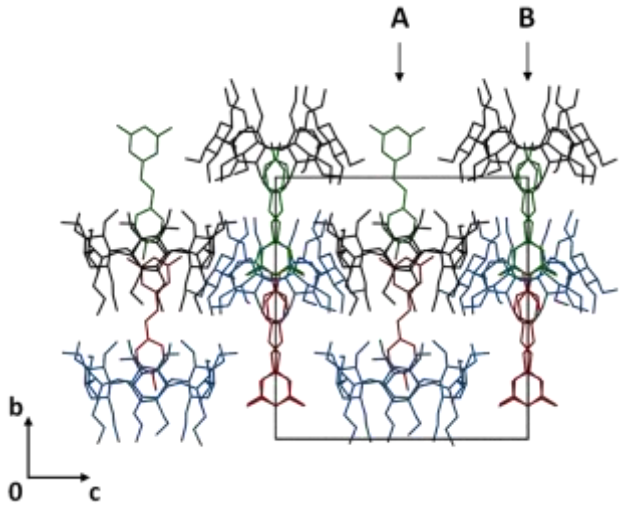

Figure 3.31: Packing diagram of TMA·RES viewed down [1 0 0]. Red guest molecules are included in blue host molecules and green guest molecules are included in black host molecules. Hydrogen atoms and water oxygen atoms are omitted for clarity.

Comparative PXRD analysis

The calculated and experimental PXRD traces of the TMA·RES complex were compared to determine whether the single crystal used for X-ray analysis is representative of the bulk material (Figure 3.32). There is good agreement between the two and the product appears to be pure. Differences in the relative intensities between the two patterns are due to preferred orientation.

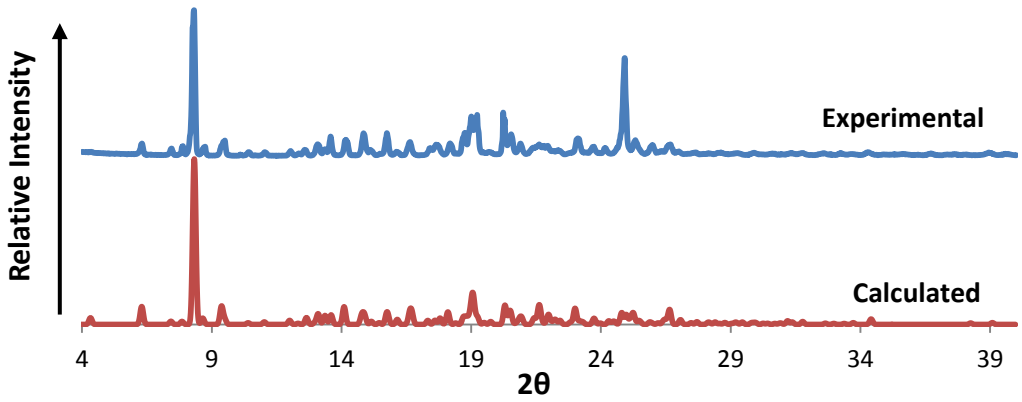

Figure 3.32: The PXRD trace of the experimental product and the pattern calculated from the single crystal X-ray structure of TMA·RES.

PHASE SOLUBILITY STUDIES AND DETERMINATION OF COMPLEX ASSOCIATION CONSTANTS

Phase solubility studies were carried out according to the method described by Higuchi and Connors, discussed in Chapter 2.[8] The S_0 value is the intrinsic solubility of the guest compound in water and was determined for *trans*-resveratrol by preparing a solution of an excess of guest in water, stirring at 25 °C. The solution was filtered to remove the excess RES and analysed using UV-Vis. The S_0 value was found to be 9.77 x 10^{-5} M. Selected CDs were dissolved in water over the concentration range 2-12 x 10^{-3} M and an excess amount of *trans*-resveratrol was added to each solution. Each solution was allowed to stir for 48 hours at 25 °C, filtered and the concentration of the guest was determined using UV-Vis spectrophotometry. This concentration was plotted against the corresponding concentrations of the CD used and a phase solubility profile determined for each CD with *trans*-resveratrol. The complex association constants (K_c) were calculated as described below.

Figure 3.33 shows the phase solubility analysis of *trans*-resveratrol and the native CDs β- and γ-CD. β-CD affords the greater solubility enhancement (26-fold at the highest concentration of this host employed) with a phase-solubility profile A_L, where the solubility of the drug increases linearly with the concentration of the CD. The results for the phase solubility experiments with γ-CD were limited by inefficient filtration through the filter membrane used to a maximum CD concentration of 6 mM. The precipitation of complex or aggregated CD particulates was physically observed during sample preparation. Over this range the solubility plot appears to increase to a plateau, indicating an A_N solubility profile where the solubility increase has a negative deviation, possibly due to changes in the solubility of the complex or aggregation of the CD molecules. The solubility enhancement of *trans*-resveratrol with γ-CD is 3.4 times at the highest concentration examined for this host.

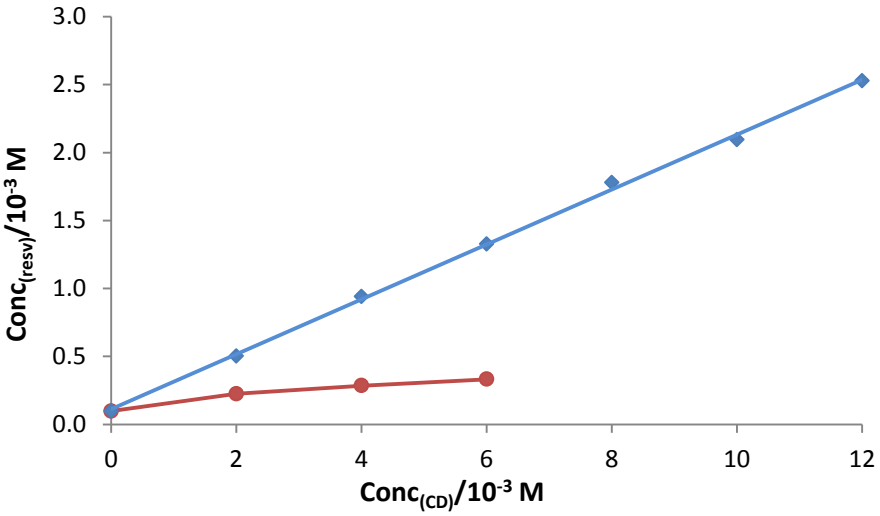

Figure 3.33: Solubility of *trans*-resveratrol as a function of β-CD (♦) and γ-CD (●) at T = 298 K.

The presence of derivatised CDs also effects significant solubility enhancement of *trans*-resveratrol (see Figure 3.34). With TRIMEB, an A_L-type profile is observed with a solubility enhancement of 36 times that of the intrinsic solubility of the guest. The remaining derivatised CDs show two different solubility profiles over the studied concentration range.

HP-β-CD and RAMEB show a small solubility increase at the CD concentrations 2 mM to 4 mM. From CD concentration 6 mM to 12 mM the solubility enhancement increases significantly, following an A_L-type solubility profile. This may indicate that there is an increase in the complex order with respect to *trans*-resveratrol. The solubility enhancement at the highest CD concentration is 44 times for HP-β-CD and 63 times for RAMEB.

The phase solubility results with DIMEB follow the opposite trend, with the solubility of the guest increasing linearly from 0 mM to 8 mM. At 10 mM to 12 mM CD concentration the solubility of the guest decreases, possibly due to the formation of an insoluble complex product which removes *trans*-resveratrol from the solution. This may be an A_N profile or a B_S profile, where the solubility is limited in water. The maximum solubility enhancement which occurs at 8 mM CD concentration is 45 times the intrinsic solubility of the guest.

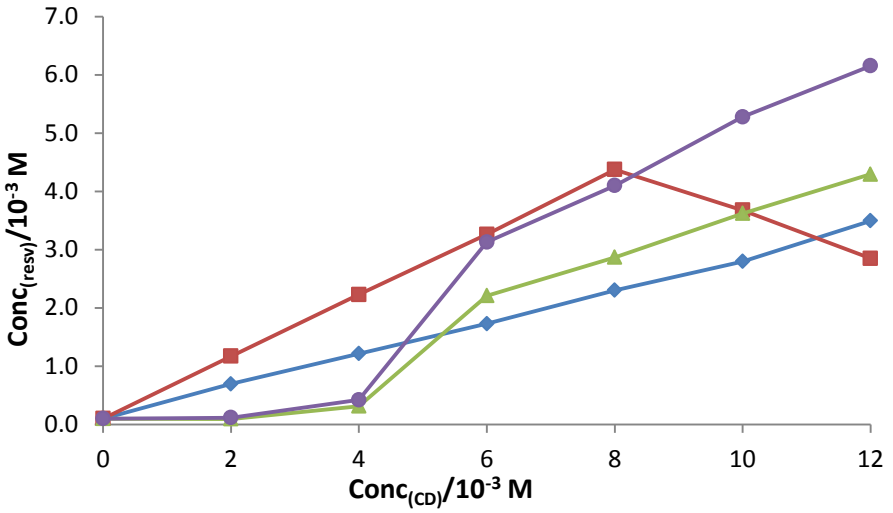

Figure 3.34: Solubility of *trans*-resveratrol as a function of TRIMEB (♦), DIMEB (■), HP-β-CD (▲) and RAMEB (●) at T = 298 K.

The stability constants (K_C) were calculated according to the Higuchi-Connors equation using the phase solubility diagrams obtained, assuming a 1:1 host-guest interaction.[8]

$$K_C = \frac{slope}{S_0(1 - slope)}$$

Table 3.21 shows the estimated stability constants for complexation between *trans*-resveratrol and each of the CDs. Only the initial slopes were used to calculate K_C (up to 6 mM for γ-CD, 8 mM for DMB and 4 mM for HP-β-CD and RAMEB).

Table 3.21: The apparent stability constants (K_C) for 1:1complex formation between RES and various CDs

Cyclodextrin	K_C
β-CD	2600
γ-CD	410
TRIMEB	3900
DIMEB	11600
HP-β-CD	580
RAMEB	890

The values obtained indicate relatively weak interactions between the guest and γ-CD, initially weak interaction with HP-β-CD and RAMEB, fairly strong binding with β-CD and TRIMEB, and the formation of a very stable complex between *trans*-resveratrol and DIMEB up to the CD concentration of 8 mM.

Lu *et al.* found a linear relationship between the concentration of *trans*-resveratrol and the concentrations of β-CD and HP-β-CD, respectively.[9] The stability constants associated with the linear phase solubility diagrams were 6778 M^{-1} for HP-β-CD·RES and 1815 M^{-1} for β-CD·RES. However, the conditions under which these experiments were carried out were slightly different: an excess of *trans*-resveratrol was added to 5 mL of CD solution; the solutions were shaken for 24 hours and the suspensions were filtered with cellulose acetate. The results obtained here for the phase solubility of

trans-resveratrol with β-CD are comparable to those obtained by Lu *et al.*[9] The results obtained with HP-β-CD are quite different, however, perhaps due to the different preparation methods used. However a comparison with the derivatised CDs TRIMEB and DIMEB show a similarly strong interaction to that obtained by Lu *et al*. with HP-β-CD.

The results obtained in this study show that greater solubility enhancement of *trans*-resveratrol may be achieved in the presence of derivatised CDs rather than the native CDs. This has been noted before[9] as the derivatised CDs possess higher aqueous solubility and generally impart that property to an insoluble guest upon inclusion.

It is worth noting that the choice of filtration membrane in these studies can greatly affect the outcome of the experiment. In this study it was found that nylon filters remove *trans*-resveratrol from the aqueous solution completely – only allowing some of the molecules which are protected by the CD to pass through the filter membrane. It was found that PTFE filters gave the most consistent results of all the membranes tested, although cellulose acetate was not tested.

PREVIOUS WORK ON *trans*-RESVERATROL

The current work is a continuation of a Chemistry Honours project conducted in 2009. During this previous work the author of the present thesis obtained two novel CD complexes with RES.

The first was a complex formed between RES and γ-CD. Single crystals were obtained by co-precipitation from water. Single crystal X-ray diffraction revealed that the complex could be classified as belonging to the isostructural series G1, for which the crystal system is tetragonal and the space group is $P42_12$.[10] The unit cell parameters were a = b = 23.759(1) Å and c = 22.929(1) Å with a unit cell volume of 12942.8(1) $Å^3$. The asymmetric unit contains six symmetry-independent glucose residues totalling ¾ of a γ-CD molecule. Due to the four-fold symmetry of the γ-CD molecule, it was not possible to model the disordered guest molecule. Water molecules found in the interstitial spaces were found to total 16 per γ-CD. TGA confirmed the number of water molecules, with the initial mass loss corresponding to 17.7 water molecules per CD. DSC and HSM also confirmed complex formation and the presence of water. ^{1}H NMR spectroscopy and UV-Vis spectrophotometry were used to determine the stoichiometry of the complex. Both methods revealed a host to guest ratio of 3:1.

The second inclusion complex was formed between RES and permethylated α-CD (TRIMEA). Brown single crystals were obtained after incubation of the dissolved mixture of host and guest in a water/EtOH solution at 60 °C. After some difficulty solving the structure, the single crystal X-ray diffraction analysis revealed a unique triclinic crystal structure in the space group P1. Four complex units were found in the asymmetric unit and the unit cell parameters were a = 14.123(2) Å, b = 20.394(2) Å, c = 28.079(3) Å, α =

93.503(5)°, β = 98.875(5)° and γ = 92.542(7)° with a unit cell volume of 7963.8(2) Å^3. Examination of the reciprocal lattice level images hk0 and hk1 revealed pseudosymmetry between the complex units between z = 0 - 0.5 and z = 0.5 – 1, any differences being manifested by the weak intensity levels with l = 2n + 1. It was found that cooling the crystal to 173 K (the temperature at which the single crystal X-ray diffraction data were collected) caused a doubling in the *c*-axis compared to the unit cell parameters determined at room temperature (c ≈ 14 Å). The number of water molecules present in the crystal was determined by TGA, with a mass loss in the range 30 - 100 °C corresponding to 3.3 water molecules per CD. This did not match the 7.7 water molecules found per CD in the structure; however, the discrepancy may be due to water being lost during the preparative process. DSC and HSM confirmed complex formation and the presence of water. UV-Vis spectrophotometry was used to verify a 1:1 host to guest ratio. This inclusion complex is a second form of a TMA·RES complex and is not further described as the results were not reproducible.

Solubility experiments were prepared by allowing a known amount of *trans*-resveratrol to dissolve in an unsaturated CD solution at 25 °C. Due to the paucity of the compound *trans*-resveratrol, which is expensive, saturation was not attained in the solubility measurements. UV-Vis spectrophotometry was used to determine the minimum solubility increase obtained in each case, the results are listed in Table 3.22.

Table 3.22: Solubility enhancement of *trans*-resveratrol by CD inclusion at 25 ˚C.

	Solubility of *trans*-resveratrol in aqueous CD (mg L^{-1})	Solubility enhancement (minimum)
γ-CD	225	12 x
RAMEB	644	35 x
HP-β-CD	349	18 x

DISCUSSION

Derivatised CDs are often used to improve the physical properties of APIs and nutraceuticals. The CSD[11] holds structural information for inclusion complexes of TRIMEA, TRIMEB and DIMEB. Sixteen TRIMEA structures are reported on the CSD, one of which is the anhydrous form of this host and the remaining 15 are inclusion complexes. There are 32 TRIMEB structures comprising one anhydrous form, two hydrated forms and 29 inclusion complexes. Of the 23 DIMEB structures one is anhydrous, three are hydrates and 19 are inclusion complexes. Tables 3.23 - 3.25 list these structures including the space group, unit cell parameters and the guests included in the complex for each of the hosts TRIMEB, TRIMEA and DIMEB.

Table 3.23: TRIMEB structures from the CSD including structural parameters.

Refcode	H:G:W	Space group	a (Å)	b (Å)	c (Å)	α (°)	β (°)	γ (°)	Guest	Ref.
ASIQOI	1:1:2	$P2_1$	11.680	15.020	28.230	90	90	112.63	2,4-dichlorophenoxyacetic acid	27
ASIQUO	1:1:0.37	$P2_1$	11.411	15.069	28.629	90	90	111.91	indole-3-butyric acid	27
BIFGON	1:1:0.5	$P2_1$	11.553	14.605	27.715	90	90	109.39	(E)-ajoene	28
EKOGUG	1:1:1	$P2_1$	10.563	14.731	27.355	90	98.46	90	(R)-1-(p-bromophenyl)ethanol	29-30
EZAVOQ	1:1:0.36	$P2_1$	10.891	14.858	27.583	90	99.62	90	4-aminobenzoic acid n-butyl ester	31
FEXBUG	1:1:2	$P2_1$	10.926	25.284	29.954	90	92.86	90	4-chlorophenoxyacetic acid	32
AZOYOD	1:1:0	$P2_12_12_1$	11.188	25.291	29.152	90	90	90	endo-8-azibicyclo(3.2.1)octan-3-ol	33
BIFGIH	1:1:1	$P2_12_12_1$	10.945	25.652	29.939	90	90	90	Psoralen	34
XAQJII	1:1:0	$P2_12_12_1$	11.149	25.664	29.427	90	90	90		35-36
MODHUI	1:1:0	$P2_12_12_1$	11.190	26.080	29.185	90	90	90	(R)-5-ethyl-1,3,5-trimethylhydantoin	36
NIZHAF	1:1:2	$P2_12_12_1$	11.060	26.138	29.669	90	90	90	(L)-Menthol	37
BIFGUT	1:1:0	$P2_12_12_1$	15.102	21.520	27.313	90	90	90	(Z)-ajoene	28
CAMPIP	1:1:4	$P2_12_12_1$	14.997	21.368	28.205	90	90	90	p-iodophenol	38
CETKUI	1:1:0	$P2_12_12_1$	14.854	21.383	28.509	90	90	90	(-)-(R)-5-methyl-5-(p-tolyl) hydantoin	39
COYXAP	1:1:1	$P2_12_12_1$	15.092	21.714	28.269	90	90	90	(R)-(-)-flurbiprofen	40-41
COYXET	1:1:0	$P2_12_12_1$	15.271	21.451	27.895	90	90	90	(S)-(+)-flurbiprofen	40-42
DORLEC	1:1:6	$P2_12_12_1$	14.845	22.171	27.544	90	90	90	4-hydroxyazobenzene	43
WEZSOK	1:1:0	$P2_12_12_1$	15.389	21.051	27.027	90	90	90	suprofen	44
DORLIG	1:1:1	$P2_12_12_1$	10.699	27.363	29.167	90	90	90	4-aminoazobenzene	45
EKOGOA	1:1:0	$P2_12_12_1$	15.113	15.223	35.876	90	90	90	(S)-1-(p-bromophenyl)ethanol	29-30
GELKEN	1:1:0	$P2_12_12_1$	15.669	20.798	25.486	90	90	90	m-iodophenol	45-46
HEZWAK	1:0:1	$P2_12_12_1$	14.818	19.362	26.510	90	90	90	monohydrate	47-48
OYAPIO	1:1:0.91	$P2_12_12_1$	14.887	21.244	27.933	90	90	90	cycluron	21
PAFSOE	1:1:1	$P2_12_12_1$	14.890	21.407	28.540	90	90	90	4-biphenylacetic acid	46
PINMAA	1:1:1.92	$P2_12_12_1$	14.796	22.444	27.720	90	90	90	ethyl laurate	49
RONWOG	1:1:0	$P2_12_12_1$	15.232	21.327	27.597	90	90	90	(S)-ibuprofen	50
SIBSIG	1:1:0	$P2_12_12_1$	14.775	21.333	27.872	90	90	90	(S)-p-methoxyphenyl propylthiosulfinate	51
HUPSAN	1:1:0	$P2_12_12_1$	15.159	21.128	27.558	90	90	90	fenitrothion	20
WAGLOG	1:0:3	$P2_12_12_1$	16.205	16.287	30.099	90	90	90	trihydrate	52
WAGLUM	1:0:0	$P2_12_12_1$	15.951	16.577	28.941	90	90	90		52
ZIFQOU	1:1:0	$P2_12_12_1$	15.179	21.407	27.670	90	90	90	(S)-Naproxen	53
QOYLIZ	1:1:0.57	$P2_12_12_1$	10.936	25.530	29.640	90	90	90	(S)-1,7-dioxaspiro(5.5) undecane	22

Table 3.24: TRIMEA structures from the CSD including structural parameters.

Refcode	H:G:W	Space group	a (Å)	b (Å)	c (Å)	α (°)	β (°)	γ (°)	Guest	Ref.
BEYLOG	1:1:1	$P2_1$	11.440	13.531	23.674	90	90	91.90	p-iodoaniline	12
BOHWUQ	1:1:0	$P2_1$	11.604	13.593	23.832	90	90	106.11	benzaldehyde	13
BUPDIZ	1:1:1	$P2_1$	11.590	13.901	23.285	90	90	106.98	iodoacetic acid	14
CECMEC	1:1:2	$P2_1$	11.624	13.786	23.739	90	90	106.56	D-mandelic acid	15-16
JEJWOK	1:1:0	$P2_1$	11.604	13.824	23.669	90	90	106.72	(R)-1-phenylethanol	17
JEJXAX	1:1:1	$P2_1$	11.586	13.762	23.641	90	90	106.45	(S)-1-phenylethanol	17
YIRZOP	1:1:0	$P2_1$	11.567	13.668	23.725	90	90	106.37	(S)-1-phenylethanol	18
BUDKEQ	1:1:1	$P2_1$	11.307	14.578	22.118	90	93.62	90	p-nitrophenol	19
CECMAY	1:1:3	$P2_1$	13.113	13.123	23.187	90	90	107.19	L-mandelic acid	17-18
HUPRUG	1:1:0	$P2_12_12_1$	15.097	24.278	38.385	90	90	90	fenitrothion	20
OYAPEK	1:1:3.5	$P2_12_12_1$	17.140	28.288	30.048	90	90	90	cycluron	21
QOYLEV	1:1:5.1	$P2_12_12_1$	14.636	21.637	23.450	90	90	90	(R)-1,7-dioxaspiro(5.5)undecane	22
TEVCEC	1:0:0	$P2_12_12_1$	15.424	18.167	23.128	90	90	90		23
CECMAY11	1:1:3	$C222_1$	13.118	13.118	23.187	90	90	107.19	(S)-mandelic acid	24
RACVIA	1:1:4	$C222_1$	14.102	14.102	21.792	90	90	116.64	1,7-dioxaspiro(5.5)undecane	25-26

Table 3.25: DIMEB structures from the CSD including structural parameters.

Refcode	H:G:W	Space group	a (Å)	b (Å)	c (Å)	α (°)	β (°)	γ (°)	Guest	Ref.
QAZYIZ	1:1:7	$P2_1$	9.669	15.603	29.036	90	90	99.39	isobornylacrylate	54
NITSIS	2:1:3	$P2_1$	10.613	15.165	23.188	102.02	90	90	acetic acid	55
CEQCUW	1:0:2	$P2_1$	10.639	15.242	23.324	101.80	90	90	dihydrate	56
SAJPOI	1:1:3	$P2_1$	15.697	15.947	18.533	90	90	106.64	carmofur	57
ZEVLOD	1:1:0	$P2_1$	15.049	19.626	26.854	96	90	90	fenitrothion	58
OYAPAG	1:1:2.9	$P2_12_12_1$	10.387	15.092	51.862	90	90	90	cycluron	21
VOFJUW	1:1:3.7	$P2_12_12_1$	10.601	15.476	48.244	90	90	90	methyl paraben	59
VOFKAD	1:1:4	$P2_12_12_1$	10.656	15.307	49.042	90	90	90	ethyl paraben	59
COFLOY	1:1:0	$P2_12_12_1$	11.080	14.932	44.906	90	90	90	m-cresol-acetate	60
XIXKUL	1:1:0	$P2_12_12_1$	11.321	14.910	45.190	90	90	90	2,2'-bithiophene	61
QIYKEO	1:0:1.08	$P2_12_12_1$	13.328	17.410	29.760	90	90	90	hydrate	60,62-63
ZULQAY	1:0:0	$P2_12_12_1$	13.821	17.424	29.610	90	90	90		64
BOYGAX	1:1:0	$P2_12_12_1$	14.163	23.096	27.641	90	90	90	prostaglandin	65
BOYFOK	1:1:15	$P2_12_12_1$	14.163	20.828	29.261	90	90	90	pentadecahydrate	60,62, 63,65
DEZMIE	1:1:3	$P2_12_12_1$	14.779	18.965	28.741	90	90	90	p-nitrophenol	66-67
DEZMOK	1:1:3	$P2_12_12_1$	14.796	18.853	28.989	90	90	90	p-iodophenol	66-67
PABNEM	1:1:0.31	$P2_12_12_1$	14.886	18.980	28.515	90	90	90	2,4-dichlorophenoxyacetic acid	68
VOFKEH	1:1:3.9	$P2_12_12_1$	15.140	18.894	28.401	90	90	90	n-propyl paraben	59
VOFKIL	1:1:3.7	$P2_12_12_1$	15.374	18.811	28.399	90	90	90	n-butyl paraben	59
WAGHAN	1:1:3	$P2_12_12_1$	15.463	18.922	27.852	90	90	90	2-naphthoic acid	69-70
BEFJOL	1:1:12	$P2_12_12_1$	18.266	19.333	24.210	90	90	90	adamantanol	6
ZEFCIY	1:1:1	$P2_12_12_1$	20.352	26.907	29.784	90	90	90	β-endosulfan	71
QAZYEV	1:1:1	$P2_12_12_1$	10.776	15.108	49.029	90	90	90	n-butylacrylate	60

Summary of *trans*-resveratrol inclusion complexes and their comparison with previously published data

Inclusion complexes of *trans*-resveratrol with each of the CDs TRIMEA, TRIMEB and DIMEB, respectively, are presented in this study and the details of their structural parameters are summarised in Table 3.26.

Table 3.26: Summary of the structural parameters of TMA·RES, TMB·RES and DMB·RES.

Complex	Space group	Z	a (Å)	b (Å)	c (Å)	β (°)	Water molecules per complex unit
TMA·RES	$P2_1$	4	18.69	21.24	20.93	94.60	6.25
TMB·RES	$P2_1$	2	10.214	15.246	29.209	97.17	5.6
DMB·RES	$P2_12_12_1$	4	10.613	15.161	51.066		4

The structure of the inclusion complex TMA·RES was solved using direct methods as the unit cell parameters did not match any of the previously published inclusion complex structures. It was found to crystallise with a host to guest ratio of 1:1. The complex units pack in a channel-like fashion. The guest molecule was found to be disordered over two positions and a number of water molecules were assigned as disordered with partial occupancy.

Isomorphous replacement was attempted to solve the structure of TMB·RES using the isomorphous complexes EKOGUG[29-30] and EZAVOQ;[31] however, the unit cell parameters did not match closely enough to obtain a solution using this method. The structure was solved using direct methods. The channel-like packing observed in this structure resembles the packing seen in EKOGUG[29-30] and EZAVOQ[31]. The stoichiometry of the inclusion complex was found to be 1:1. The guest molecule was disordered over two positions and a total of 5.6 water molecules were assigned over nine sites.

The DMB·RES structure is isostructural with OYAPAG;[21] however, these data were not available at the time of structure solution and the structure was solved independently using direct methods. The packing of the inclusion complex units is analogous to the modified herringbone pattern seen in OYAPAG.[21] Four water molecules were assigned including the hydrogen atoms, which were fixed using the DANG and DFIX commands.

The geometrical parameters of the heptagonal and hexagonal rings (*r*, *D*, *a*) of DIMEB and TRIMEA respectively indicate a round shape. The deviation of the O4 atoms from the mean O4-plane (*d*) and the tilt angles associated with the glucose rings are small, suggesting a symmetrical shape of the truncated cone. This consistency with the regular CD shape is due to the O2n-H···O3(n-1) hydrogen bond interactions present in DIMEB. The geometric parameters of the host molecule in TMB·RES indicate that the CD is elliptical in shape with significant curvature when viewed side-on, such that the primary end of the CD is open and the secondary end is relatively closed.

The 4-hydroxyphenyl rings of the symmetry-independent guest molecules are inserted into each of the respective CD cavities. In each case the insertion of the guest is assisted by one or more water molecules found within the primary end of the CDs. The guest lies nearly parallel to the mean O4-plane for the complex TMB·RES while the guest molecules in the complexes TMA·RES and DMB·RES are more steeply inclined to their respective O4-planes. The 1,3-benzenediol rings of the guest molecules are found in the interstitial space between the complex units for each of the structures TMA·RES, TMB·RES and DMB·RES. The guest molecules deviate from planarity by varying degrees as a result of their inclusion in the different host molecules; the largest interplanar angle between the two phenyl rings is 51.6(3)° for the RES molecule included in the host TRIMEA (molecule A), while the smallest angle is 13.6(2)° for the RES molecule included in host molecule DIMEB.

The conformations of both the host and guest molecules in each complex illustrate the phenomenon of "mutual induced fit" whereby the conformation of each component is dependent on the other.[72]

Hydrogen bonding is a prominent feature in all three structures. A hydrogen bond of the type (guest)O4-H···O6(host) holds the RES molecule within the TMB cavity. A similar interaction is mediated by a water molecule in the DMB·RES and TMA·RES complexes such that the H-bond RES(4-OH)···O(water)···O6(primary methoxy) is formed. There is a weak C-H···O hydrogen bond between the host and guest in each complex. A number of water hydrogen bonding interactions exist between water, host and guest molecules. The hydrogen bonding observed between 1,3-benzenediol moieties and water is analogous in all three of the structures, such that a "crown" of water molecules is formed on the 1,3-benzenediol ring. This hydrogen bonding motif is unique to the *trans*-resveratrol inclusion complexes formed with the CDs studied as no similar motifs were found on searching the CSD.[11] Both inter- and intramolecular host interactions of the type C-H···O are prominent.

Chapter 4 describes the cyclodextrin inclusion of hydroxycinnamic acids with the native CDs β- and γ-CD, as well as the derivatised CDs TRIMEA, TRIMEB and DIMEB.

REFERENCES

1. Paratone N oil (Exxon Chemical Co., TX, USA).
2. L. J. Barbour, *J. Appl. Cryst*., 1999, **32**, 351-352.
3. G. M. Sheldrick, *Acta Crystallogr*., 2008, **A64**, 112-122.
4. M. R. Caira, *Roum. Chim. Rev*., 2001, **46**, 371-386.
5. G. M. Sheldrick, *Direct Methods for Solving Macromolecular Structures*, Kluwer Academic Publishers, Dordrecht, 1998.
6. M. Czugler, E. Eckle and J. J. Stezowski, *J. Chem. Soc., Chem. Commun.*, 1981, 1291–1292.
7. F. H. Allen, O. Kennard, D. G. Watson, L. Brammer, A. G. Orpen and R. Taylor, *J. Chem. Soc. Perkin Trans. II*, 1987, 1-19.
8. T. Higuchi and K. Connors, *Adv. Anal. Chem. Instrum.*, 1965, **7**, 117-212.
9. Z. Lu, B. Cheng, Y. Hu, Y. Zhang and G. Zou, *Food Chemistry*, 2009, **113**, 17-20.
10. T. Steiner and W. Saenger, *Acta Crystallogr. Sect. B*, 1998, **54**, 450-455.
11. Cambridge Structural Database and Cambridge Structural Database system, Version 5.36, Cambridge Crystallographic Data Centre, University Chemical Laboratory, Cambridge England, 2015.
12. K. Harata, K. Uekama, M. Otagiri, F. Hirayama, *Bull. Chem. Soc. Jpn.*, 1982, **55**, 407-410.
13. K. Harata, K. Uekama, M. Otagiri, F. Hirayama, Y. Sugiyama, *Bull. Chem. Soc. Jpn.*, 1982, **55**, 3386-3389.
14. K. Harata, K. Uekama, M. Otagiri, F. Hirayama, *J. Chem. Soc. Jpn.*, 1983, 173-180.
15. K. Harata, K. Uekama, M. Otagiri, F. Hirayama, *Chem.Lett.*, 1983, 1807-1810.
16. K. Harata, K. Uekama, M. Otagiri, F. Hirayama, *Bull. Chem. Soc. Jpn.*, 1987, **60**, 497-502.
17. K. Harata, *J. Chem. Soc., Perkin Trans. 2*, 1990, 799-804.
18. A. Grandeury, L. Renou, F. Dufour, S. Petit, G. Gouhier, G. Coquerel, *J. Therm. Anal. Calorim.*, 2004, **77**, 377-390.
19. K. Harata, K. Uekama, M. Otagiri and F. Hirayama, *Bull. Chem. Soc. Jpn.*, 1982, **55**, 3904-3910.
20. D. Cruickshank, N. M. Rougier, R. V. Vico, R. H. de Rossi, E. I. Bujan, S. A. Bourne and M. R. Caira, *Carbohydr. Res.*, 2010, **345**, 141-147.
21. D. L. Cruickshank, S. A. Bourne and M. R. Caira, *ARKIVOC*, 2011, **12**, 103-107.
22. S. Makedonopoulou, K. Yannakopoulou, D. Mentzafos, V. Lamzin, A. Popov and I. M. Mavridis, *Acta Crystallogr., Sect. B: Struct. Sci.*, 2001, **57**, 399-409.
23. T. Steiner and W. Saenger, *Carbohydr. Res.*, 1996, **282**, 53-63.
24. R. E. Marsh, M. Kapon, Shengzhi Hu and F. H. Herbstein, *Acta Crystallogr., Sect. B: Struct. Sci.*, 2002, **58**, 62-77.

25. K. Yannakopoulou, D. Mentzafos, I. M. Mavridis and K. Dandika, *Angew. Chem., Int. Ed.*, 1996, **35**, 2480-2482.
26. D. Mentzafos, I. M. Mavridis and K. Yannakopoulou, *J. Inclusion Phenom. Macrocyclic Chem.*, 1999, **33**, 321-330.
27. F. Tsorteki, K. Bethanis and D. Mentzafos, *Carbohydr.Res.*, 2004, **339**, 233-240.
28. M. R. Caira, R. Hunter, S. A. Bourne and V. J. Smith, *Supramol. Chem.*, 2004, **16**, 395-403.
29. A. Grandeury, S. Petit, G. Gouhier, V. Agasse and G. Coquerel, *Tetrahedron: Asymmetry*, 2003, **14**, 2143-2152.
30. Y. Amharar, A. Grandeury, M. Sanselme, S. Petit and G. Coquerel, *Ann. Pharm. Fr.*, 2010, **68**, 212-217.
31. M. R. Caira, S. A. Bourne, S. L. Vilakazi and L. Reddy, *Supramol. Chem.*, 2004, **16**, 279-285.
32. F. Tsorteki, K. Bethanis, N. Pinotsis, P. Giastas and D. Mentzafos, *Acta Crystallogr., Sect. B: Struct. Sci.*, 2005, **61**, 207-217.
33. J. -L. Mieusset, D. Krois, M. Pacar, L. Brecker, G. Giester and U. H. Brinker, *Org. Lett.*, 2004, **6**, 1967-1970.
34. M. R. Caira, F. Giordano and S. L. Vilakazi, *Supramol. Chem.*, 2004, **16**, 389-393.
35. A. Rontoyianni, I. M. Mavridis, R. Israel and G. Beurskens, *J. Inclusion Phenom. Mol. Recog. Chem.*, 1998, **32**, 415-428.
36. P. Cardinael, V. Peulon, G. Perez, G. Coquerel and L. Toupet, *J. Inclusion Phenom. Macrocyclic Chem.*, 2001, **39**, 159-167.
37. M. R. Caira, V. J. Griffith, L. R. Nassimbeni and B. van Oudtshoorn, *Supramol. Chem.*, 1996, **7**, 119-124.
38. K. Harata, K. Uekama, M. Otagiri and F. Hirayama, *Bull. Chem. Soc. Jpn.*, 1983, **56**, 1732-1736.
39. L. Ferron, F. Guillen, S. Coste, G. Coquerel and J. -C. Plaquevent, *Chirality*, 2006, **18**, 662-666.
40. K. Harata, F. Hirayama, T. Imai, K. Uekama and M. Otagiri, *Chem. Lett.*, 1984, 1549-1552.
41. K. Harata, K. Uekama, T. Imai, F. Hirayama and M. Otagiri, *J. Inclusion Phenom. Mol. Recog. Chem.*, 1988, **6**, 443-460.
42. K. Harata, K. Uekama, M. Otagiri and F. Hirayama, *J. Inclusion Phenom. Mol. Recog. Chem.*, 1984, **1**, 279-293.
43. J. Shi, D. –S. Guo, F. Ding and Y. Liu, *Eur. J. Org. Chem.*, 2009, 923-931.
44. P. M. Dean, *Aust. J. Chem.*, 2007, **60**, 133-138.
45. K. Harata, *Chem. Commun.*, 1988, 928-929.
46. K. Harata, F. Hirayama, H. Arima, K. Uekama and T. Miyaji, *J. Chem. Soc., Perkin Trans. 2*, 1992, 1159-1166.
47. M. R. Caira, V. J. Griffith, L. R. Nassimbeni and B. van Oudtshoorn, *J. Chem. Soc., Perkin Trans. 2*, 1994, 2071-2072.

48. T. Steiner and W. Saenger, *Angew. Chem., Int. Ed.*, 1998, **37**, 3404-3407.
49. D. Mentzafos, I. M. Mavridis and H. Schenk, *Carbohydr. Res.*, 1994, **253**, 39-50.
50. G. R. Brown, M. R. Caira, L. R. Nassimbeni and B. van Oudtshoorn, *J. Inclusion Phenom. Mol. Recog. Chem.*, 1996, **26**, 281-294.
51. N. Stellenboom, R. Hunter, M. R. Caira, S. A. Bourne, K. Cele, T. Qwebani and T. le Roex, *ARKIVOC*, 2007, **8**, 53-9
52. M. R. Caira, S. A. Bourne, W. T. Mhlongo and P. M. Dean, *Chem. Commun.*, 2004, 2216-2217.
53. M. R. Caira, V. J. Griffith, L. R. Nassimbeni and B. Van Oudtshoorn, *J. Inclusion Phenom. Mol. Recognit. Chem.*, 1995, **20**, 277-290.
54. P. Glockner, H. Ritter, D. Schollmeyer, CCDC 153137: Experimental Crystal Structure Determination, 2000, DOI:10.5517/cc54bxj.
55. M. Selkti, A. Navaza, F. Villain, P. Charpin and C. De Rango, *J. Inclusion Phenom. Mol. Recognit. Chem.*, 1997, **27**, 1-12.
56. T. Aree, W. Saenger, P. Leibnitz and H. Hoier, *Carbohydr. Res.*, 1999, **315**, 199-205.
57. K. Harata, F. Hiryama, K. Uekama and G. Tsoucaris, *Chem. Lett.*, 1988, 1585-1588.
58. D. L. Cruickshank, N. M. Rougier, R. V. Vico, S. A. Bourne, E. I. Bujan, M. R. Caira and R. H. de Rossi, *Beilstein J. Org.Chem.*, 2013, **9**, 106-117.
59. E. J. C. de Vries and M. R. Caira, *Carbohydr. Res.*, 2008, **343**, 2433-2438.
60. H. Pohlmann, M. Gdaniec, E. Eckle, G. Geiger and J. J. Stezowski, *Acta Crystallogr., Sect. A: Found. Crystallogr.*, 1984, **40**, C276.
61. Y. Takashima, K. Sakamoto, Y. Oizumi, H. Yamaguchi, S. Kamitori and A. Harada, *J. Inclusion Phenom. Macrocyclic Chem.*, 2006, **56**, 45-53.
62. J. J. Stezowski, W. Parker, S. Hilgenkamp and M. Gdaniec, *J. Am. Chem. Soc.*, 2001, **123**, 3919-3926.
63. J. J. Stezowski, M. Czugler and E. Eckle, *Proc. I. S. Cyclodextrins*, 1981, 151.
64. T. Steiner and W. Saenger, *Carbohydr. Res.*, 1995, **275**, 73-82.
65. T. Aree, H. Hoier, B. Schulz, G .Reck and W. Saenger, *Angew. Chem., Int. Ed.*, 2000, **39**, 897-899.
66. K. Harata, *Chem. Lett.*, 1984, 1641-1644.
67. K. Harata, *Bull. Chem. Soc. Jpn.*, 1988, **61**, 1939-1944.
68. F. Tsorteki and D. Mentzafos, *Carbohydr. Res.*, 2002, **337**, 1229-1233.
69. K. Harata, *Chem. Commun.*, 1993, 546-547.
70. K. Harata, *Chem. Commun.*, 1999, 191-192.
71. D. L. Cruickshank, S. A. Bourne and M. R. Caira, *New J. Chem.*, 2012, **36**, 2007-2013.
72. A. Cooper, M. Nutley, E. J. MacLean, K. Cameron, L. Fielding, J. Mestres and R. Palin, *Org. Biomol. Chem.*, 2005, **3**, 1863–1871.

Chapter 4: Cyclodextrin inclusion of Caffeic Acid and its analogues

The solid inclusion complexes formed from a series of hydroxycinnamic acids, namely 3,4-dihydroxycinnamic acid (caffeic acid, CAF), 3-methoxy-4-hydroxycinnamic acid (ferulic acid, FA), 4-hydroxycinnamic acid (*p*-coumaric acid, PCA), 3,5-dimethoxy-4-hydroxycinnamic acid (sinapic acid, SA), 3,4-dihydroxyhydrocinnamic acid (hydrocaffeic acid, HCA) and 3-methoxy-4-hydroxyhydrocinnamic acid (hydroferulic acid, HFA) and the native cyclodextrins (CDs) β- and γ-CD are reported in this chapter. The chemical structures of the six guest compounds are shown in Chapter 1 (p. 7). To complement this study the interactions between each guest and each host were also studied in solution using isothermal titration calorimetry (ITC). The inclusion complexes formed between the guests and derivatised CDs were also investigated using heptakis(2,3,6-tri-*O*-methyl)-β-CD (TRIMEB or TMB), hexakis(2,3,6-tri-*O*-methyl)-α-CD (TRIMEA or TMA) and heptakis(2,6-di-*O*-methyl)-β-CD (DIMEB or DMB). Crystalline products were obtained and analysed using single crystal X-ray diffraction, powder X-ray diffraction (PXRD), thermal analysis and ^{1}H NMR spectroscopy. The solubility enhancement of CAF, FA and PCA were investigated with β-CD, hydroxypropyl-β-CD (HP-β-CD) and randomly methylated β-CD (RAMEB).

HYDROXYCINNAMIC ACIDS: INCLUSION COMPLEXATION WITH γ-CD

Preparation by kneading experiments

Kneading experiments were carried out in order to form inclusion complexes of each hydroxycinnamic acid guest and the native γ-CD. Each guest (20 mg) was added to an equimolar amount of γ-CD. The host and guest materials were kneaded together for a minimum of 10 minutes in a mortar. Water was added dropwise such that a paste-like consistency was maintained. The kneaded product was allowed to dry and analysed using powder X-ray diffraction (PXRD).

The PXRD patterns of the kneaded products were compared to those of the known isostructural series.[1] Due to expected differences in the prepared powders and the single crystals used for comparison in the isostructural series (water content, guest size, temperature of data collection), the 2θ values or relative peak intensities of the experimental patterns may vary slightly in comparison to those of the isostructural series. Complexation was confirmed for all of the host-guest combinations.

Complex formation with γ-CD

The six kneaded products were found to be isostructural. The peak positions in the experimental PXRD patterns matched the 2θ values of the reference trace for inclusion complexes with γ-CD.[1] The inclusion complexes crystallise in the tetragonal space group $P42_12$ with unit cell dimensions $a = b \approx 23.8$ Å and $c \approx 23.2$ Å.[2]

The crystal structures of the inclusion complexes are characterised by three independent γ-CD molecules which are located on a four-fold axis (Figure 4.1). The asymmetric unit contains six symmetry-independent glucose residues amounting to ¾ of a γ-CD molecule. The CDs pack in columns which form infinite channels parallel to the *c*-axis where the guest molecules exist within the channel, often disordered due to the requirement of four-fold symmetry and the host-guest stoichiometry usually differs from 1:1. Hydrogen bonds of type O-H···O between the faces of the γ-CD molecules occur such that connections form in a head-to-tail (A-C), head-to-head (B-C) and tail-to-tail (A-B) fashion (Figure 4.2). Water molecules are distributed in the interstitial spaces.[2]

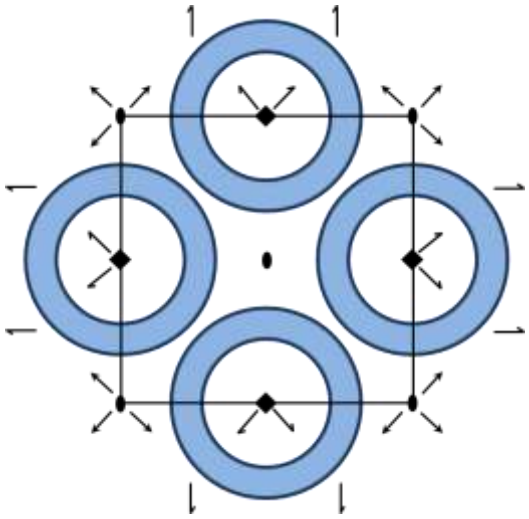

Figure 4.1: The crystal packing arrangement viewed down the *c*-axis. Symmetry elements are shown.

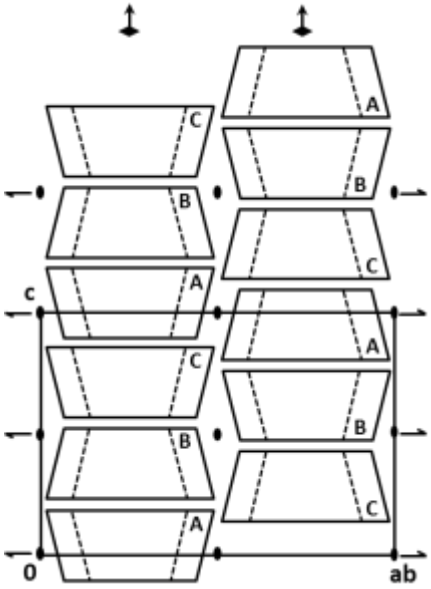

Figure 4.2: The columns present in the $P42_12$ complex structure, projected onto the diagonal plane (110) of the unit cell.

The result of these common crystallographic features is isostructurality between the inclusion complexes of γ-CD with different guest molecules. The PXRD patterns will therefore match in the 2θ values, making it easy to identify the formation of an inclusion complex with γ-CD (Figure 4.3).

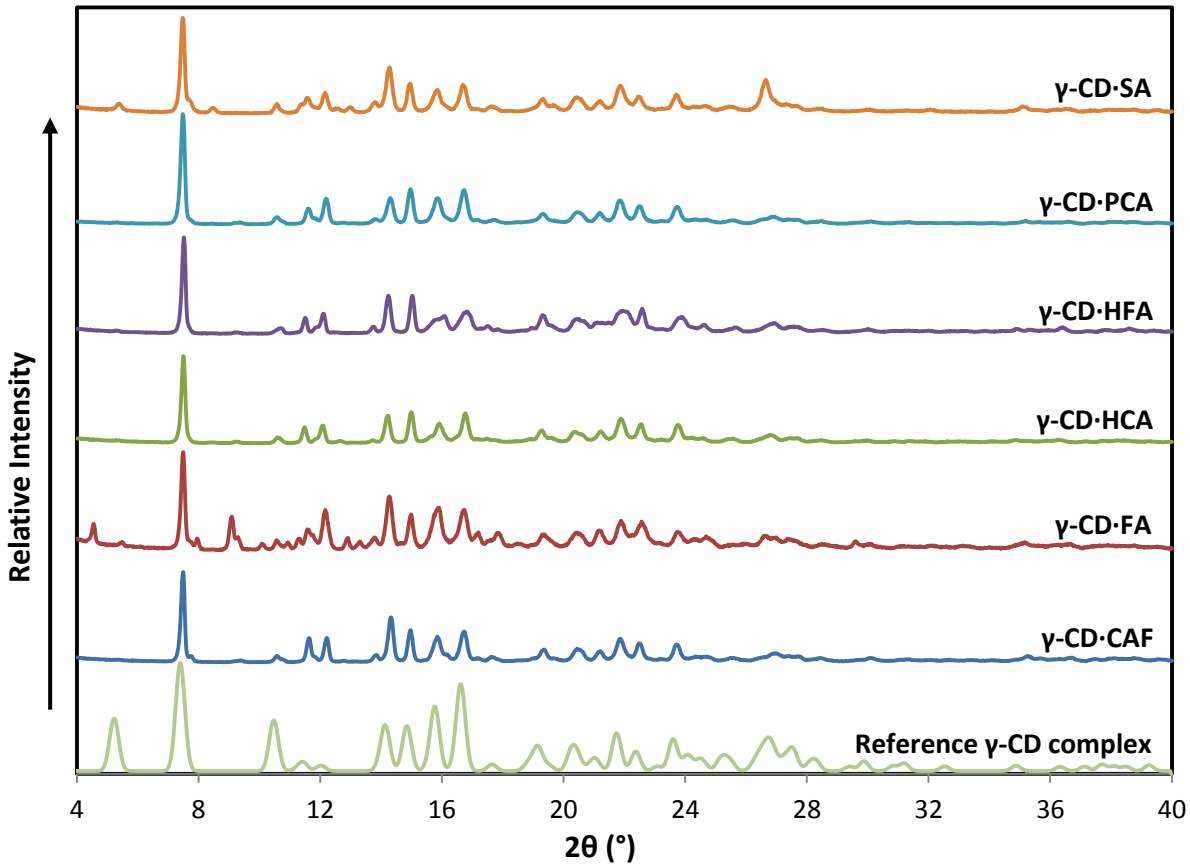

Figure 4.3: Experimental PXRD patterns of the kneaded product of each hydroxycinnamic acid guest with γ-CD and reference PXRD pattern to determine complex formation.

Preparation of inclusion complex crystals

Solutions of the guest with γ-CD were prepared in an equimolar ratio (mmol guest: CAF 0.111, HCA 0.1098, FA 0.1030, HFA 0.1019, PCA 0.1218, SA 0.0892). The host was dissolved in at least 2 ml of distilled water. When the solution cleared, the guest was added. The resulting suspension was stirred and where necessary the sample was heated to 60 °C to aid dissolution. Once clear, the solution was filtered into a new vial, covered with parafilm and left to evaporate slowly in a dark room. Crystals of the inclusion complexes tentatively designated γ-CD·CAF, γ-CD·HCA and γ-CD·PCA were isolated in this way while crystals of γ-CD·FA and γ-CD·HFA were obtained by slow cooling. In the latter case, after the solutions were prepared as above the vials were submerged in hot water in a Dewar flask and allowed to cool over two days. The crystals were confirmed to be inclusion complexes using single crystal X-ray diffraction. However, the solution containing SA and γ-CD produced a yellow precipitate which proved to be crystals of SA alone.

As for the kneading experiments, the crystallographic parameters of the inclusion complexes formed between each guest and γ-CD conform to the known isostructural series where the inclusion complexes have unit cell dimensions $a = b \approx 23.8$ Å and $c \approx 23.2$ Å in the space group $P42_12$.[3] All inclusion complexes were analysed using thermal analysis, PXRD and ^{1}H nuclear magnetic resonance spectroscopy (data provided in Appendix B and C).

Thermal analysis

Inspection of the TGA traces of each of the γ-CD inclusion complex crystals reveals a mass loss between 25 °C and 150 °C coinciding with water loss. This event is echoed in the DSC traces by the presence of a broad endotherm over the same temperature range. A second mass loss is evident in the TGA traces where the guest is unsaturated (CAF, FA and PCA), corresponding to the loss of the guest molecule over the range 150 °C to 275 °C leading to decomposition. This mass loss is not seen for the saturated guests (HCA and HFA), however a small exotherm in the DSC traces indicates a phase transformation event at 245 °C for γ-CD·HCA and 225 °C for γ-CD·HFA. Decomposition begins at 280 °C. Table 4.1 lists the results of the thermal analysis of the γ-CD inclusion complexes as well as the complex stoichiometries determined from ^{1}H NMR spectroscopy of dissolved complex crystals. The inclusion complexes are named by their abbreviated complex formulae, for example γ-CD·CAF, for ease of legibility.

Table 4.1: Percentage mass losses and quantitative results of thermal analysis and ^{1}H NMR spectroscopy of the γ-CD inclusion complexes of the hydroxycinnamic acids and their derivatives.

	CAF	HCA	FA	HFA	PCA
No. of replicates	2	3	2	2	2
Water % mass loss	15.5 ± 0.3	17.0 ± 0.5	15.5 ± 0.1	14.7 ± 0.5	15.4 ± 0.1
No. of water molecules per CD molecule	13.9 ± 0.3	16.8 ± 0.6	14.2 ± 0.1	14.3 ± 0.5	14.7 ± 0.1
Guest % mass loss	4.1 ± 0.2	-	6.5 ± 0.1	-	5.7 ± 0.2
No. of guest molecules per CD molecule	0.4 ± 0.1	-	0.5 ± 0.1	-	0.6 ± 0.1
^{1}H NMR H:G	1.3:1	1:1	2:1	1:1	1:1
Proposed ratio in complex formula H:G:H_2O	1.3:1:14	1:1:17	1:0.5:14	1:1:14	1:1:15

The physical changes to the complex crystals with increasing temperature were observed using hot stage microscopy (HSM) with samples immersed in silicone oil (Figures 4.4 to 4.8). The crystals are clear at room temperature. In general, bubbling occurs due to the loss of water from the system, accompanied with crystal fracturing, at the same temperatures seen in the TGA traces. The microcrystals present in the sample of γ-CD·HFA appear to undergo a phase transformation at 220 °C. Decomposition is indicated by the browning of the crystals.

30 °C **130 °C** **215 °C** **320 °C**

Figure 4.4: HSM photographs of γ-CD·CAF.

30 °C **110 °C** **140 °C** **240 °C** **300 °C**

Figure 4.5: HSM photographs of γ-CD·HCA.

30 °C **120 °C** **270 °C** **320 °C**

Figure 4.6: HSM photographs of γ-CD·FA.

30 °C **220 °C** **265 °C** **300 °C**

Figure 4.7: HSM photographs of γ-CD·HFA.

40 °C **100 °C** **135 °C** **270 °C** **340 °C**

Figure 4.8: HSM photographs of γ-CD·PCA.

INCLUSION COMPLEXATION BETWEEN HYDROXYCINNAMIC ACIDS AND β-CD

Preparation by kneading experiments

Each guest (20 mg) was added to an equimolar amount of β-CD. Both the host and guest materials were placed in a mortar, water was added dropwise such that a paste-like consistency was maintained and the two compounds were kneaded together for a minimum of 10 minutes. The kneaded product was allowed to dry and analysed using powder X-ray diffraction (PXRD).

The PXRD patterns of the kneaded products were compared with those of the known isostructural series[1] and complexation was confirmed for β-CD·HCA, β-CD·HFA and β-CD·PCA (tentative complex designations in the absence of stoichiometric data initially).

Complex formation with β-CD

Figure 4.9 shows the experimental PXRD patterns and the matching isostructural series patterns. The PXRD patterns of β-CD·CAF, β-CD·FA and β-CD·SA appeared to match the reference pattern for uncomplexed β-CD, indicating that the formation of an inclusion complex did not occur. β-CD·HCA and β-CD·HFA were found to be isostructural, matching the reference traces for the P1 (triclinic) and C2 (monoclinic) channel type structures, which are very similar. The P1 and C2 structures are related by a metric transformation: applying the transformation $a' = a + b$, $b' = b - a$, $c' = c$ to the parameters of the triclinic structure results in cell parameters similar to those of the C2 structure, a well-documented phenomenon.[6] The *c*-axis is common in both structures with the cyclodextrin dimers in the same orientation, resulting in the two effectively indistinguishable reference patterns. Determining which inclusion complexes has been generated by kneading is not possible from attempted matching of PXRD patterns; however, the procedure does confirm that inclusion complexes were formed. Obtaining the unit cell parameters by single crystal X-ray diffraction may be used to differentiate between the two forms.

The experimental PXRD pattern of β-CD·PCA appears to most closely match the reference trace for β-CD complexes crystallising in the space group $C222_1$.

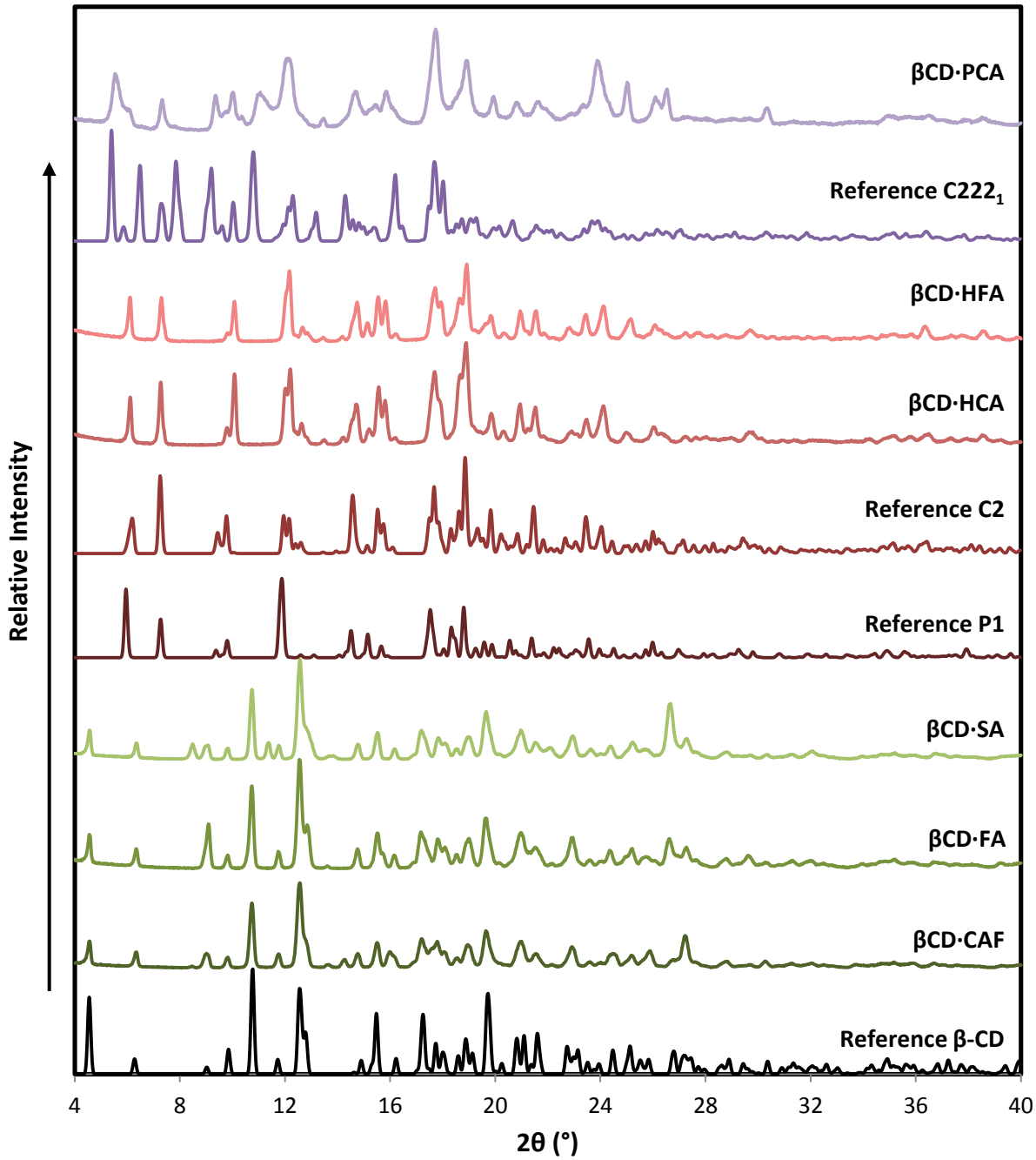

Figure 4.9: Experimental PXRD patterns of the kneaded product of each hydroxycinnamic acid guest with β-CD and reference PXRD patterns to determine complex formation.

Preparation of inclusion complex crystals

The host β-CD was dissolved in 7 ml of distilled water and an equimolar amount of the guest (20 mg) was added once the host solution had cleared. The solution was stirred and heated to 60 °C to aid dissolution. The solution was filtered into a new vial, covered with parafilm and left to evaporate slowly in a dark room. Crystals were obtained for β-CD·FA and β-CD·HFA. The method of slow cooling was employed to obtain crystals of β-CD·PCA. The complexes were analysed using single crystal X-ray diffraction, TGA, DSC, HSM and PXRD. The paucity of these crystals presented difficulty in the full analysis of the complexes.

Thermal analysis

The TGA traces of the β-CD inclusion complex crystals show mass losses between 25 °C and 150 °C corresponding with water loss. A broad endotherm in the DSC traces over the same range underpins this conclusion. The guest molecule is released from the crystals over the temperature range 150 °C to 275 °C, evident by a second mass loss in the TGA traces. This is followed by decomposition. A small exotherm can be seen in the DSC trace of β-CD·PCA, possibly due to a phase transformation event at 230 °C. Decomposition begins at *ca*. 300 °C. Table 4.4 lists the results of the thermal analysis for the β-CD inclusion complexes.

Table 4.4: Percentage mass losses and quantitative results of thermal analysis of β-CD·FA, β-CD·HFA and β-CD·PCA.

	FA	HFA	PCA
No. of replicates	2	2	2
Water % mass loss	16.9 ± 2.9	10.1 ± 1.2	20.8 ± 2.0
No. of water molecules per CD molecule	15.0 ± 3.0	8.3 ± 1.1	17.8 ± 2.2
Guest % mass loss	8.0 ± 0.2	11.2 ± 0.3	6.1 ± 1.2
No. of guest molecules per CD molecule	0.6 ± 0.1	0.8 ± 0.1	0.6 ± 0.1
Proposed ratio in complex formula H:G:H_2O	1:0.6:15	1:0.8:9	1:0.5:18

The physical changes to the complex crystals with increasing temperature were observed using HSM (Figures 4.10 and 4.11). The crystals are clear at room temperature and begin to fracture as they are heated. As water loss takes place, the crystal turns opaque. At 260 °C to 270 °C the crystals begin to decompose as indicated by the darkening of the microcrystalline material.

30 °C **60 °C** **100 °C** **260 °C** **300 °C**

Figure 4.10: HSM photographs of β-CD·FA.

30 °C **60 °C** **270 °C** **300 °C**

Figure 4.11: HSM photographs of β-CD·HFA.

Data collection and space group determination

Intensity data for β-CD·FA, β-CD·HFA and β-CD·PCA were collected on a Bruker KAPPA APEX II DUO diffractometer. Crystals of each complex were surface dried, covered in Paratone N oil and mounted onto a cryoloop.[7] The crystal systems were found to be monoclinic for β-CD·FA and β-CD·HFA having

Laue symmetry 2/*m* and orthorhombic for β-CD·PCA (Laue class–*mmm*).[3] All three crystals displayed C-centring (from systematic absences *hkl*: *h + k = 2n + 1*), β-CD·PCA showing in addition the condition *00l*: *l = 2n + 1,* indicating a twofold screw axis parallel to *c*. For β-CD·FA and β-CD·HFA, the only space group possibility was C2 since the host molecule is chiral, while the space group $C222_1$ for β-CD·PCA was unequivocally indicated by the systematic absences. These space group assignments were consistent with those predicted using PXRD patterns.

Crystal structure solution and refinement

Isomorphous replacement was used to solve each of the structures after preparing the relevant files using XPREP.[8] The host molecule atom coordinates (without moveable OH groups) of the .res file for the complex with CSD refcode AJUVEG were used to solve the structures of β-CD·FA and β-CD·HFA while the host atom coordinates for KOFJEU were similarly used to solve β-CD·PCA.[6,9] All non-hydrogen atoms were refined isotropically and SHELXL was used to refine the structures.[5] After assigning the remaining non-hydrogen atoms the glucopyranose units were labelled G1 to G7 with the carbon atoms labelled C1 to C6 and the O atoms according to the corresponding C atoms (Figure 4.12). The disordered atoms were assigned with partial site-occupancy factors (s.o.f.s) of x for the major component and 1-x for the minor component and labelled by parts. The disordered host atoms are listed in Table 4.5. The U_{iso} values of the ordered host non-hydrogen atoms were found to be thermally stable and these atoms were subsequently refined anisotropically. Hydrogen atoms were placed on the host carbon atoms using a riding model and hydroxyl hydrogen atoms were added using the AFIX 147 command for β-CD·FA and β-CD·HFA and AFIX 83 for β-CD·PCA. All hydrogen atoms were refined with U_{iso} values 1.2 times those of the parent atoms.

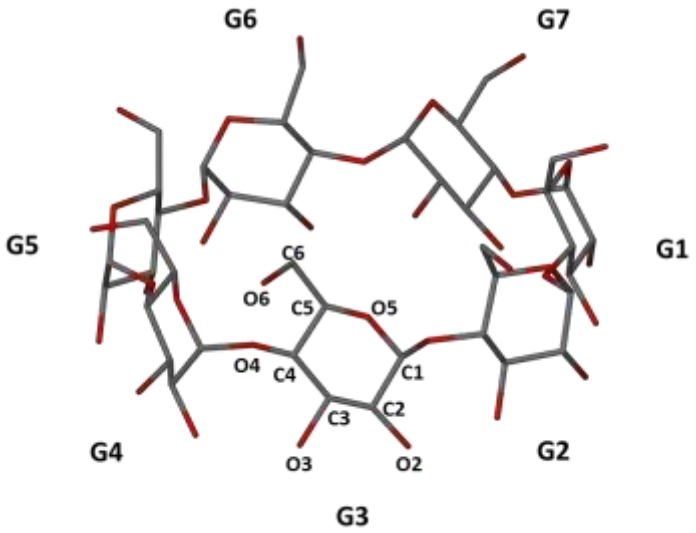

Figure 4.12: The host atom labels used for β-CD·PCA. The host atoms for β-CD·FA and β-CD·HFA are labelled similarly.

Table 4.5: Site-occupancy factors for the disordered atoms in β-CD·FA, β-CD·HFA and β-CD·PCA

Complex	Atom 1	x	Atom 2	1 - x
β-CD·FA	C621/O621	0.67(3)	C622/O622	0.33
	C641/O641	0.64(2)	C642/O642	0.36
	C671/O671	0.56(4)	C672/O672	0.44
	O5W1	0.61(4)	O5W2	0.39
	O6W1	0.67(3)	O6W2	0.33
	O9W1	0.59(4)	O9W2	0.41
β-CD·HFA	C641/O641	0.66(2)	C642/O642	0.34
	C671/O671	0.54(2)	C672/O672	0.46
	O4W1	0.74(2)	O4W2	0.26
	O5W1	0.70(3)	O5W2	0.30
	O7W1	0.63(3)	O7W2	0.37
β-CD·PCA	C671/O671	0.76(2)	C672/O672	0.24
	O2W1	0.68(5)	O2W2	0.32
	O4W1	0.68(3)	O4W2	0.32
	O5W1	0.66(4)	O5W2	0.34
	O6W1	0.56(6)	O6W2	0.44
	O8W1	0.52(3)	O8W2	0.48

The guest molecule in the crystal of β-CD·FA was highly disordered within the CD cavity and could not be modelled. The guest molecules were modelled for the structures β-CD·HFA and β-CD·PCA. The HFA molecule was found to be disordered over two positions, except for the carboxylic acid group which has an s.o.f. of 1. The PCA molecule has an s.o.f. value of 0.5, resulting in two partial PCA molecules existing within the CD dimer generated by symmetry. The AFIX 66 command was used to maintain the geometry of the aromatic ring. The guest molecules were refined isotropically due to high U_{iso} values of some atoms and hydrogen atoms were added using a riding model with U_{iso} values 1.2 to 1.5 times those of the parent atoms. The labels of the guest molecules HFA and PCA are shown in Figure 4.13. Table 4.6 lists the refinement parameters and crystal data for the three structures.

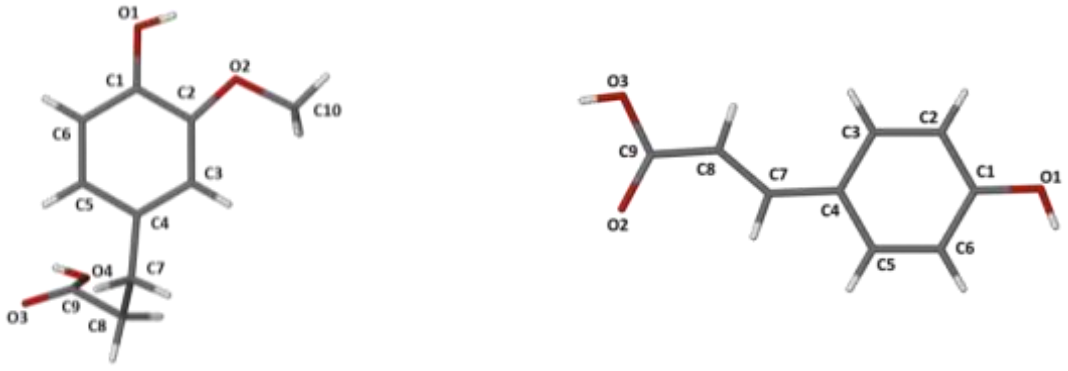

Figure 4.13: The guest non-hydrogen atom labels used for β-CD·HFA (left) and β-CD·PCA (right).

Table 4.6: Crystallographic data for the complexes β-CD·FA, β-CD·HFA and β-CD·PCA.

Name	**β-CD·FA**	**β-CD·HFA**	**β-CD·PCA**
Complex Formula	$C_{42}H_{70}O_{35}\cdot(C_{10}H_{10}O_4)_{0.5}$ $\cdot 10.4H_2O$	$C_{42}H_{70}O_{35}\cdot C_{10}H_{12}O_4$ $\cdot 8.6H_2O$	$(C_{42}H_{70}O_{35})_2\cdot C_9H_8O_3$ $\cdot 31.6H_2O$
Formula weight / g mol^{-1}	1420.3	1486.1	3003.4
Crystal system	Monoclinic	Monoclinic	Orthorhombic
Space group	C2	C2	$C222_1$
a / Å	19.321(1)	18.870(2)	19.224(2)
b / Å	24.487(2)	24.383(2)	24.134(3)
c / Å	15.908(1)	15.448(1)	32.804(3)
β / °	109.598(1)	109.989(2)	90
Volume / $Å^3$	7090(2)	6680(1)	15219(3)
Z	4	4	4
Calculated density / g cm^{-3}	1.331	1.478	1.311
μ (MoKα) / mm^{-1}	0.121	0.132	0.121
F (000)	3030	3168	6424
Temperature / K	173(2)	142(2)	173(2)
Crystal size / mm^3	0.18 x 0.12 x 0.09	0.14 x 0.16 x 0.25	0.30 x 0.27 x 0.22
Theta range scanned / °	1.4 < θ < 27.2	1.4 < θ < 26.5	2.3 < θ < 26.3
Index ranges	h: -21: 24; k: -33: 32; l: -20: 20	h: -23: 23; k: -30: 30; l: -19: 14	h: -23: 23; k: -30: 30; l: -35: 40
Total number of reflections	26665	21301	57727
No. of independent reflections	15597	13595	15398
No. of reflections with I > 2σ(I)	12195	9202	12888
No. of parameters	772	829	857
R_{int}	0.021	0.025	0.025
R_1 (I > 2σ(I))	0.1099	0.0878	0.0831
wR_2(I > 2σ(I))	0.3045	0.2392	0.2366
S	1.350	1.048	1.039
Coefficients in weighting scheme	a = 0.2000, b = 0.000	a = 0.1635, b = 8.0738	a = 0.1779, b = 20.9083
Δρ excursions / e $Å^{-3}$	-0.54, 1.07	-0.59, 0.86	-0.53, 0.77

Any electron density peaks not associated with either host or guest molecules were assigned as water oxygen atoms, provided that they satisfied hydrogen bond criteria. Where these oxygen atoms had high U_{iso} values they were assigned partial s.o.f.s. Water hydrogen atoms were not found in difference Fourier syntheses. The total s.o.f.s values of the water O atoms in each structure were within range of water molecules estimated from the TGA of the respective complex except those of β-CD·HFA, where disorder within the host cavity prevented accurate water O atom placement.

Geometrical analysis

Host Geometry

Tables 4.7 to 4.9 list the geometrical parameters (discussed previously) of the macrocycles of β-CD·FA, β-CD·HFA and β-CD·PCA, respectively. All of the glucopyranose units are in the $^4C_1$ chair conformation.

Table 4.7: Geometric parameters of the β-CD molecule in the complex β-CD·FA.

Residue	*r* (Å)	*D* (Å)	*a* (°)	*φ* (°)	*d* (°)	D_3 (Å)	*α* (Å)	τ_1 (°)	τ_2 (°)
G1	5.121	4.402	126.5	118.4(7)	1.1	2.835(9)	-0.529(3)	11.4(2)	14.3(3)
G2	5.092	4.324	127.9	117.9(6)	-0.7	2.898(9)	-0.204(3)	11.0(2)	12.1(3)
G3	4.970	4.442	130.0	117.7(5)	1.1	2.768(7)	0.624(3)	5.4(2)	6.7(2)
G4	5.003	4.390	129.4	117.8(5)	-1.9	2.785(7)	-0.160(3)	9.8(2)	11.1(1)
G5	5.159	4.277	126.1	118.0(6)	1.7	2.855(7)	-0.409(3)	12.6(2)	12.9(1)
G6	5.021	4.483	129.1	117.1(7)	-0.2	2.865(7)	0.245(3)	6.5(2)	8.5(1)
G7	4.935	4.319	131.0	117.0(8)	-1.2	2.860(9)	0.434(3)	16.4(3)	16.0(1)
Mean	**5.04**	**4.38**	**128.6**	**117.7**	**1.2**	**2.84**	**0.406**	**10.4**	**11.7**

Table 4.8: Geometric parameters of the β-CD molecule in the complex β-CD·HFA.

Residue	*r* (Å)	*D* (Å)	*a* (°)	*φ* (°)	*d* (°)	D_3 (Å)	*α* (Å)	τ_1 (°)	τ_2 (°)
G1	5.178	4.296	125.6	117.8(7)	2.74	2.759(11)	0.104(4)	7.3(2)	8.4(3)
G2	4.837	4.561	133.1	117.8(7)	3.77	2.759(8)	-0.008(4)	2.4(2)	3.7(1)
G3	5.010	4.292	129.5	118.6(6)	-5.83	2.765(11)	-0.118(4)	10.4(2)	10.9(1)
G4	5.307	4.368	122.5	118.9(7)	0.69	2.795(9)	0.078(4)	12.0(2)	14.4(1)
G5	4.954	4.455	131.5	116.7(6)	4.42	2.967(9)	0.064(4)	7.4(2)	9.1(1)
G6	4.893	4.394	131.0	118.1(6)	-1.87	2.838(9)	-0.093(4)	10.4(2)	11.5(1)
G7	5.160	4.323	126.5	119.1(7)	-3.33	2.781(11)	-0.028(4)	10.7(2)	12.8(3)
Mean	**5.05**	**4.38**	**128.5**	**118.1**	**3.6**	**2.81**	**0.080**	**8.7**	**10.1**

Table 4.9: Geometric parameters of the β-CD molecule in the complex β-CD·PCA.

Residue	*r* (Å)	*D* (Å)	*a* (°)	*φ* (°)	*d* (°)	D_3 (Å)	*α* (Å)	τ_1 (°)	τ_2 (°)
G1	5.035	4.411	129.6	117.8(4)	0.2	2.727(6)	0.012(3)	2.6 (1)	3.7(1)
G2	5.201	4.299	124.8	119.3(4)	0.5	2.816(6)	-0.002(3)	10.5(1)	10.8(2)
G3	4.975	4.502	130.5	117.9(5)	-0.8	2.805(6)	-0.016(3)	4.4(1)	6.8(2)
G4	4.952	4.322	131.0	116.5(4)	0.0	2.849(7)	0.011(3)	11.0(2)	11.8(1)
G5	5.190	4.373	124.9	119.7(4)	1.0	2.775(8)	0.011(3)	7.5(2)	9.6(1)
G6	5.039	4.383	129.8	117.2(4)	-0.9	2.856(7)	-0.020(3)	8.6(1)	9.3(1)
G7	4.973	4.406	129.4	118.0(4)	0.0	2.765(6)	-0.003(3)	5.9(1)	7.4(1)
Mean	**5.05**	**4.39**	**128.6**	**118.1**	**0.6**	**2.80**	**0.012**	**7.2**	**8.5**

The host molecules are symmetrical in shape as the *r*, *D* and *a* values do not deviate significantly from the literature values for β-CD parameters.[6] The molecule does not curve significantly, as indicated by the small deviation of O4 atoms (*α*) from the mean O4 plane, as well as the small degree of deviation in the torsion angle between four consecutive O4 atoms (d). The positive tilt angles (τ_1 and τ_2) indicate that the secondary rim of each host molecule is wider than the primary rim.

Six of the seven glucopyranose units of β-CD·FA display negative O5-C5-C6-O6 torsion angles (*ω*) indicating the (-)-*gauche* conformation, including both the major and minor disordered components on unit G2, the major component on G5 and the minor component of G7. The major component on G7 and the minor component of G5 are (+)-*gauche*. The torsion angles (*ω*) for the host molecule in β-CD·PCA indicate a (-)-*gauche* conformation for all glucopyranose units, except for the minor disordered component on G7.

Hydrogen bonding interactions

In the three structures the CD molecules are kept rigid and round by the 'flip-flop' hydrogen bonds O(3n)-H···O[2(n+1)] which fall within a narrow range and the average O(3n)···O[2(n+1)] distances were 2.84 Å, 2.81 Å and 2.80 Å for β-CD·FA, β-CD·HFA and β-CD·PCA, respectively.[10] The host molecules form head-to-head dimers through the interaction of the O(3) atoms of adjacent CDs related by a crystallographic twofold axis. O6-H hydroxyl groups link contiguous dimers adding stability to the crystal structure.

There is one hydrogen bond interaction between the guest HFA and the O6G1 atom of a symmetry-related host molecule (1-x, y, -z) such that O4-H4···O6G1' has a O4···O6G1 distance of 2.60(2) Å and O-H···O angle of 174°. Both disordered guest components possess an intramolecular hydrogen bond between the *p*-hydroxyl and *O*-methyl groups (O1A-H1A···O2A: O1A···O2A = 2.65(3) Å and bond angle = 113°; O1B-H1B···O2B: O1B···O2B = 2.45(3) Å and bond angle = 114°). The guest molecules do not interact with the water molecules, which exist only in the interstitial spaces between β-CD dimers.

The guest molecule PCA does not interact with the host by hydrogen bonding but is held in the CD cavity by van der Waals and hydrophobic interactions. The hydroxyl and carboxylic acid groups form hydrogen bonds with water O atoms within the CD cavity. Water O···O close contacts form an extended network and interact with both the host and guest.

Guest inclusion

The ASU of β-CD·HFA includes one β-CD molecule, two disorder components of HFA each with s.o.f = 0.5 and 8.6 water molecules. The HFA molecule is disordered over two positions and lies within the dimer such that part A pairs with part B' and part B pairs with part A' (Figure 4.14). The aliphatic tail curls under the aromatic ring such that the torsion angle C4-C7-C8-C9 is 71(3)° for part A and -50(8)° for part B. The guest inclusion appears to be driven predominantly by hydrophobic interactions while the O4-H4···O6G1' guest-host interaction maintains the dimeric channels.

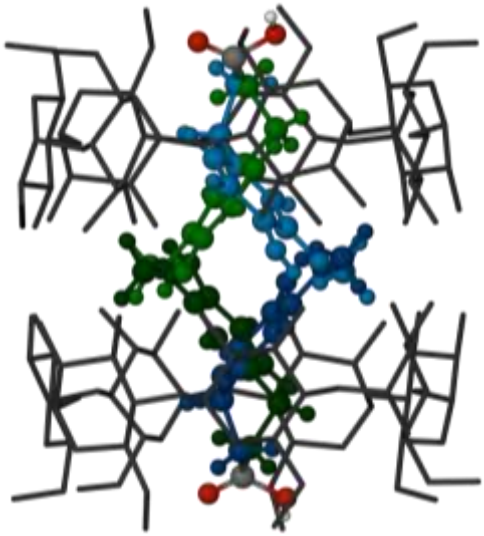

Figure 4.14: The β-CD dimer with two disordered guest molecules included within the cavity. Part A of the HFA molecule is shown in green and part B shown in blue. Host hydrogen atoms are omitted for clarity.

The ASU of β-CD·PCA includes one β-CD molecule, a PCA molecule of half occupancy and 31.6 water molecules. The guest is included such that when the dimer is formed through the twofold symmetry, two half occupancy PCA molecules exist within the dimer (Figure 4.15a). The PCA molecules are planar and lie antiparallel with an angle of 18.5(5)° between the planes through the carbon atoms of the molecules (Figure 4.15b). The driving force of the interaction is primarily hydrophobic as no hydrogen bonds occur between the host and guest molecules.

(a)

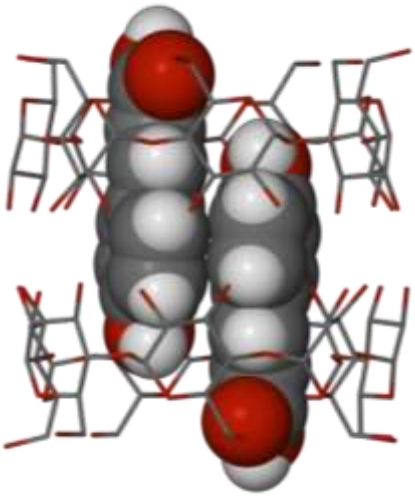

(b)

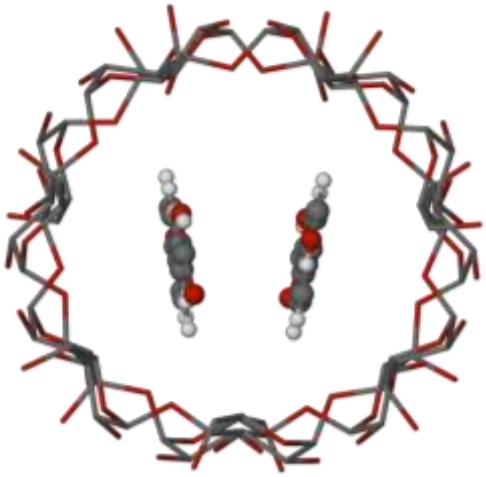

Figure 4.15: The β-CD dimer with two partially occupied guest PCA molecules within the cavity, viewed side-on (a) and from above (b). The host hydrogen atoms are omitted for clarity.

Crystal packing

The head-to-head β-CD dimers stack parallel to the *c*-axis in all three structures. The dimers in the C2 structures β-CD·FA and β-CD·HFA form infinite channels in the *z*-direction (CH packing) while the dimers of the $C222_1$ structure β-CD·PCA form layers in the *ab*-plane and are shifted such that cages are formed, an arrangement known as chessboard packing (CB)(Figure 4.16).[6]

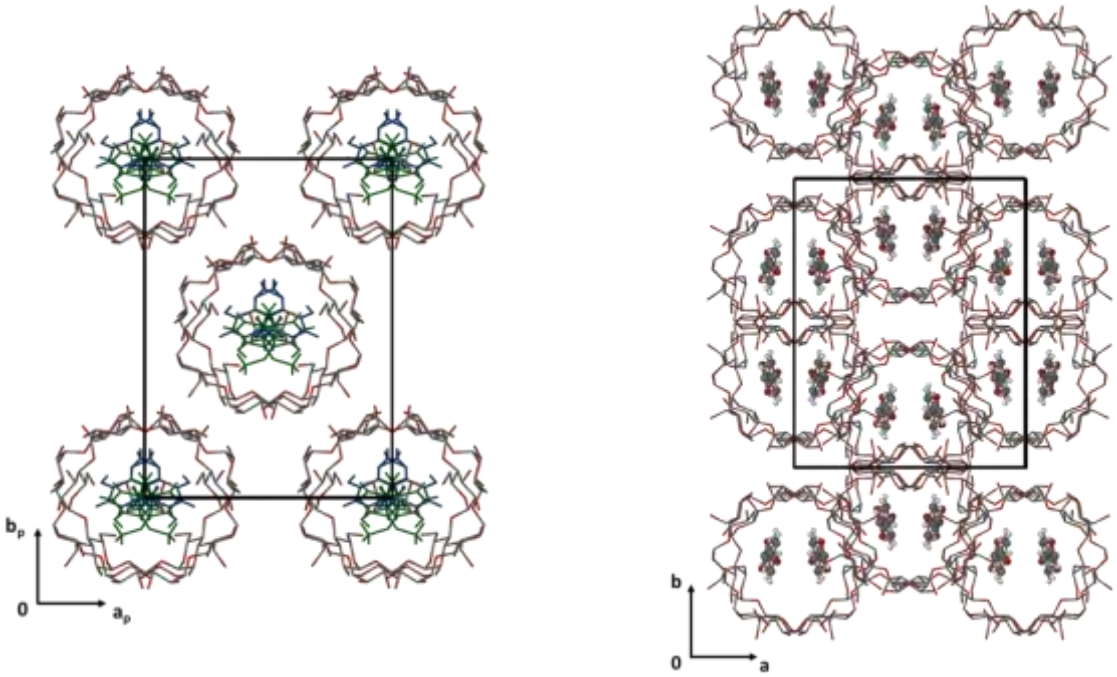

Figure 4.16: Packing diagrams of the complexes β-CD·HFA (left) and β-CD·PCA (right). The disordered components A and B of HFA are shown in green and blue, respectively. The host hydrogen atoms are omitted for clarity.

PHASE SOLUBILITY STUDIES AND DETERMINATION OF COMPLEX ASSOCIATION CONSTANTS

Phase solubility studies were carried out for CAF, FA and PCA with the native CDs β- and γ-CD as well as the derivatised CDs TMB, TMA and DMB, according to the Higuchi and Connors method discussed in Chapter 2.[11] The intrinsic solubility (S_0) of each guest compound was determined by adding an excess of guest in water, stirring at 25 °C for 24 hours. The solution was filtered and analysed using UV-Vis spectrophotometry. The S_0 value was found to be 2.91 x 10^{-3} M for CAF, 3.48 x 10^{-3} M for FA and 9.31 x 10^{-3} M for PCA (see Chapter 2 for the relevant calibration curves).

The host CDs β-CD, HP-β-CD and RAMEB were used to increase the solubility of each guest in water. γ-CD did not increase the solubility of the guests but rather precipitated out of the solution. Due to the limited availability of the derivatised CDs TMB, TMA and DMB at the time of experimentation, these were not used. The concentration of each CD in water spanned a range of 5 to 20 x 10^{-3} M and an excess of each respective guest was added to each CD solution. After allowing each solution to stir for 48 hours at 25 °C, it was filtered and the concentration of the guest was determined using UV-Vis spectrophotometry. A plot of the concentration of each guest versus the corresponding concentration of each host was prepared to determine a phase solubility profile for each host and guest combination. The complex association constants (K_c) were calculated as described below.

Figure 4.17 shows the phase solubility analysis of CAF, FA and PCA with each of the CDs β-CD, HP-β-CD and RAMEB.

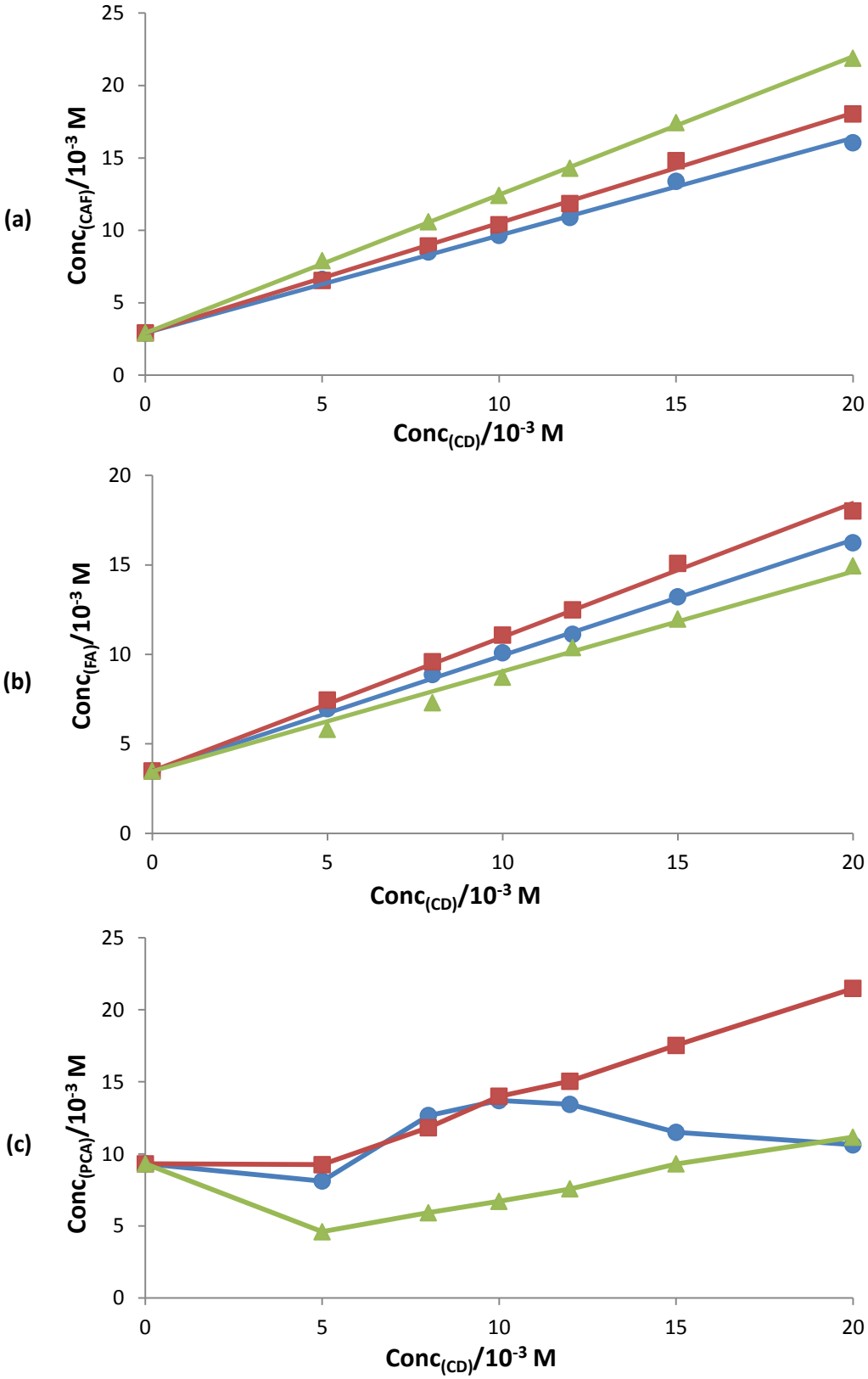

Figure 4.17: Solubility of (a) CAF, (b) FA and (c) PCA as a function of β-CD (●), HP-β-CD (■) and RAMEB (▲) concentrations at T = 298 K.

When studying CAF an increase in solubility is observed when in combination with all three CDs, with phase-solubility profiles A_L such that the solubility of the drug increases linearly with the concentration

of the CD. RAMEB affords the greatest solubility enhancement (a 7.5-fold increase at the highest concentration of this host employed).

The phase solubility profiles for FA combined with the host molecules indicate that the concentration of FA increases as the concentration of the host increases (A_L-type profile). HP-β-CD gives the largest solubility enhancement of 5.2-fold at the highest concentration of CD studied.

The phase solubility profiles for PCA with each CD studied do not follow the linear profile. The greatest solubility increase is seen with HP-β-CD although it does not increase linearly initially, following an A_L-type profile from 5 mM onwards. β-CD follows an A_N or B_S profile as both are affected by limited solubility in water. From 5 mM onwards a maximum solubility increase of 1.5 times is observed at 10 mM CD concentration. RAMEB produces a negative effect on the solubility of the guest initially followed by an increase in solubility at a host concentration of 5 mM. Overall there is no solubility enhancing effect over the range studied. The atypical results obtained for PCA with each host CD are possibly due to changes in the solubility of the complex or aggregation of the CD molecules, followed by an increase in the complex order.

The stability constants (K_C) were calculated as in Chapter 3 using the Higuchi-Connors equation assuming a 1:1 complex formation.[11]

$$K_C = \frac{slope}{S_0(1 - slope)}$$

Table 4.10 shows the estimated stability constants for complexation between the guests CAF, FA and PCA with each of the CDs, respectively. Only the initial slopes were used to calculate K_C (up to 5 mM for HP-β-CD).

Table 4.10: The apparent stability constants (K_C) for 1:1 complex formation between each guest CAF, FA and PCA and various CDs, respectively.

Cyclodextrin	CAF	FA	PCA
β-CD	660	500	-
HP-β-CD	1140	800	-
RAMEB	6290	410	90

These values indicate relatively weak interactions between the guests and β-CD, fairly strong binding with HP-β-CD for CAF and FA, and a very stable complex formation between CAF and RAMEB. FA interacts weakly with RAMEB and PCA does not interact with the host molecules at low host concentration.

Zhang *et al*. found A_L-type phase solubility profiles for CAF and FA with both β-CD and HP-β-CD.[12] Kfoury *et al.* reported that the solubility of CAF, FA and PCA increased linearly (A_L-type), having a 1:1 host-guest ratio over the host concentration range studied (0 to 10 mM).[13] This correlates with results of this study

except for those of PCA, likely due to differences in the determination of S_0 for this guest (Kfoury obtained a smaller S_0 value). Kfoury *et al*. calculated the K_c values of complex formation using the slope and S_0 values obtained; these are compared with those found in the current study in Table 4.11. In general the stability constant increases when using derivatised CDs, with β-CD showing the lowest stability constant and RAMEB proving to form the most stable complexes with the guests studied.

Table 4.11: Stability constants for CD complexes formed in solution.

	β-CD		HP-β-CD		RAMEB	
	Present study	Kfoury, *et al.*	Present study	Kfoury, *et al.*	Present study	Kfoury, *et al.*
CAF	660	425	1140	534	6290	825
FA	500	326	800	833	410	1045
PCA	-	306	-	1099	90	1228

ISOTHERMAL TITRATION CALORIMETRY (ITC) INVESTIGATIONS OF THE INTERACTIONS BETWEEN HYDROXYCINNAMIC ACID DERIVATIVES AND THE NATIVE CDs β- and γ-CD

ITC was used to determine the thermodynamic parameters for the inclusion of the guest molecules caffeic acid (CAF), *p*-coumaric acid (PCA), ferulic acid (FA), sinapic acid (SA), hydrocaffeic acid (HCA) and hydroferulic acid (HFA) (Figure 4.18), in the native CDs, β- and γ-CD.

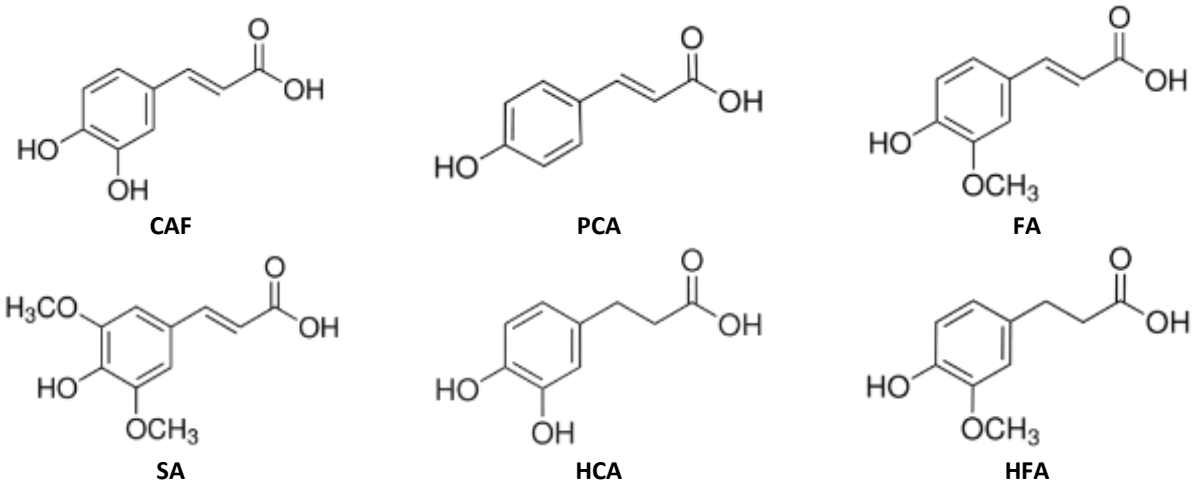

Figure 4.18: The chemical structures of the guest molecules.

This involved measuring the heat generated upon the incremental injection of the aqueous CD solution into a reaction vessel containing the guest in aqueous solution. The results of the ITC experiments are represented as plots showing the heat rate (μcal/sec) versus time (min) and the heat per injection (kcal/mol) versus the molar ratio of the injected CD and the total guest concentration ($[CD_i]_{tot}/[G]_{tot}$). A binding model was applied to fit the binding isotherm. The binding models tested were the "one set of sites model" and the "sequential binding model" corresponding to the reactions:

$$G + nCD \rightleftharpoons G(CD)_n \quad (1)$$

$$G + CD \overset{K_1}{\rightleftharpoons} G{\cdot}CD \overset{K_2}{\rightleftharpoons} G(CD)_2 \quad (2)$$

where G represents the guest molecule.

The data for all of the experiments showed the best fit to a model of one set of sites, with n = 1 or 2. The heats of dilution were measured for the host and the guest, respectively, by titrating the host against water and water against the guest. These quantities were found to be negligible (on average, ≈ 3% of the experimental signal changes obtained for β- and γ-CD reactions were due to the heats of dilution, which were not reproducible). All experiments were performed in duplicate or triplicate such that reproducible results were obtained and the error in any thermodynamic quantity was calculated between replicates. TGA was used to determine the water content of each host (10 water molecules per β-CD molecule, 7 water molecules per γ-CD molecule) in order to determine the molar masses of the hydrated hosts for preparation of solutions of accurate concentration. The results are reported in order of decreasing hydrophobicity of the unsaturated guest molecules (CAF > PCA > FA > SA), followed by the saturated, hydrophilic guests HCA and HFA.

The concentration of β-CD was 12.0 mM and the guest concentrations were 1.25 mM for CAF, 1.23 mM for PCA, 1.18 mM for FA, 1.29 mM for SA, 1.21 mM for HCA and 1.24 mM for HFA. Figure 4.19 shows the ITC results obtained for the reactions between β-CD and each of the six guest molecules.

Table 4.12 shows a summary of the data obtained. The value for n was set to 1 corresponding to a host to guest ratio of 1:1 (for β-CD·CAF this is supported by Chao *et. al*[14] who reported a 1:1 stoichiometric ratio obtained by Job plot analysis of NMR titration data[15]). All of the titration curves obtained fit well to the model of one set of sites with n = 1. The ΔG° values obtained indicate that complex formation between all six guest molecules and β-CD is spontaneous at 298 K.[16] All six complexes show negative standard formation enthalpies indicating an exothermic reaction (this is supported by the raw data signals obtained from the feedback mechanism of the ITC apparatus during the experiment). CAF, HCA and HFA exhibit negative values for the TΔS term while the values for PCA, FA and SA are positive. For all of the guest molecules, except SA, the magnitudes of the TΔS term are smaller than the values reported for the enthalpy values and the complex formation reaction in solution is thus mostly enthalpy-driven. The ΔH and TΔS values for the formation of the β-CD·SA complex appear to differ by only a small amount, indicating that enthalpy and entropy contribute to the Gibbs energy to a similar degree.

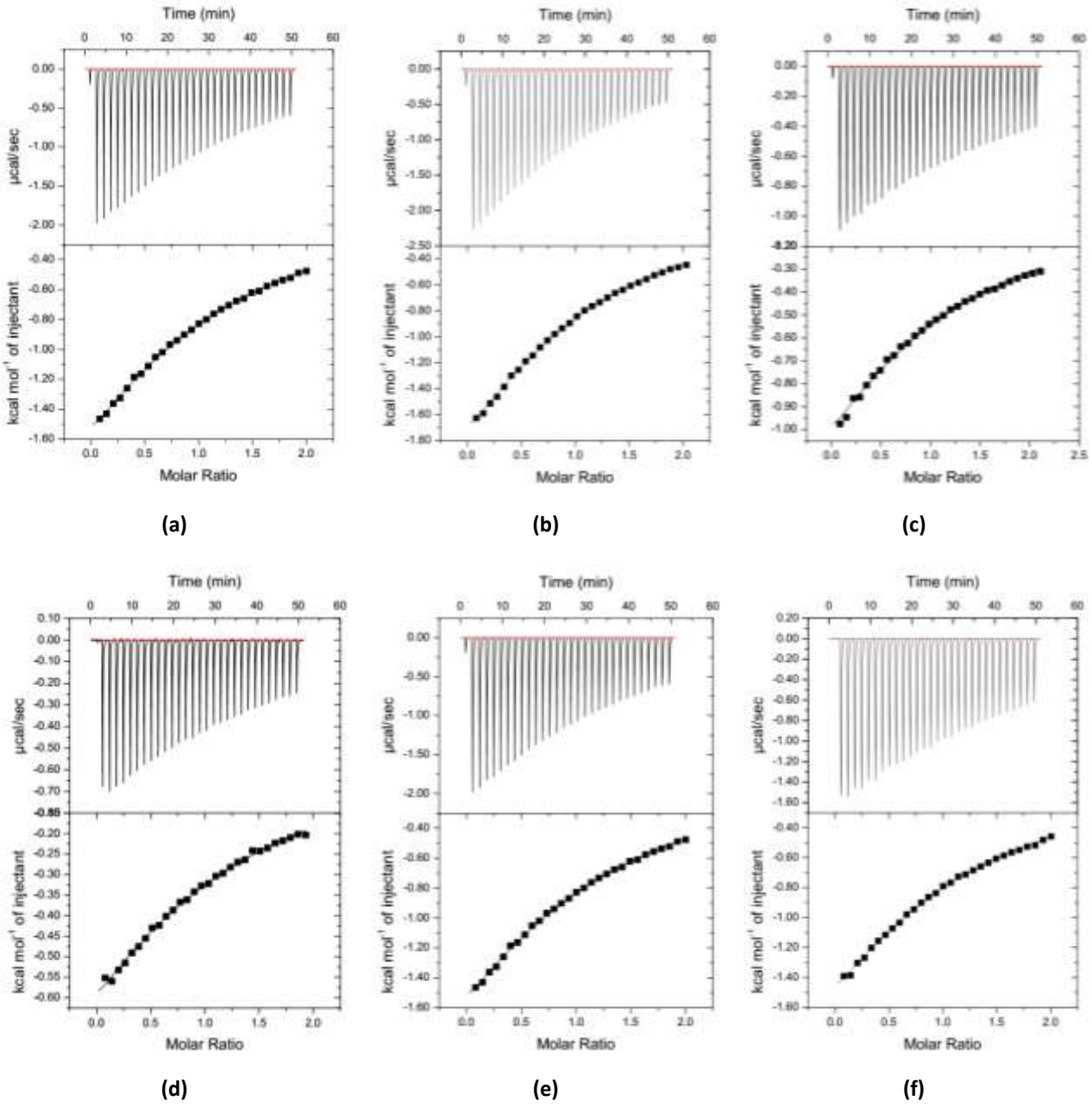

Figure 4.19: Calorimetric titration of β-CD with the guest molecules (a) CAF, (b) PCA, (c) FA, (d) SA, (e) HCA and (f) HFA. Top: Raw data for 30 sequential injections (3 µL per injection) of the CD solution into the guest solution. Bottom: Heat isotherms obtained from the integration of the calorimetric curves.

Table 4.12: Association constant (*K*) and the thermodynamic parameters (*ΔH°*, *TΔS°* and *ΔG°*)* for the complexation of the hydroxycinnamic acids with β-CD at 298 K.

	K (M^{-1})	*ΔH°* (kJ mol^{-1})	*TΔS°* (kJ mol^{-1})	*ΔG°* (kJ mol^{-1})
CAF	478.5 ± 10.3	-16.97 ± 0.11	-1.67 ± 0.14	-15.30 ± 0.05
PCA	774.5 ± 0.7	-14.42 ± 0.01	2.07 ± 0.01	-16.49 ± 0.01
FA	502.5 ± 3.5	-10.96 ± 0.02	4.45 ± 0.00	-15.42 ± 0.02
SA	452.3 ± 24.0	-6.72 ± 0.32	8.43 ± 0.45	-15.15 ± 0.13
HCA	246.7 ± 15.9	-14.98 ± 0.54	-1.33 ± 0.69	-13.65 ± 0.15
HFA	457.6 ± 9.5	-16.78 ± 0.19	-1.60 ± 0.24	-15.19 ± 0.05

*Note: While Figure 5.2.1 shows enthalpy values in kcal mol^{-1}, the table lists all data in SI units.

Similar experiments were carried out with γ-CD as the host compound, using γ-CD at a concentration of 28.0 mM while the guest concentrations were 1.17 mM for CAF, 1.25 mM for PCA, 1.28 mM for FA, 1.24 mM for SA, 1.17 mM for HCA and 1.22 mM for HFA. Figure 4.20 shows the results obtained from the ITC experiments with γ-CD as host.

HCA and HFA did not appear to interact significantly with γ-CD. The data points of the binding isotherms showed significant scatter and the temperature change observed upon each injection was comparable to the changes in temperature observed when the heats of dilution of the host and guests were measured. Hence, no data for complexation with these guests are reported.

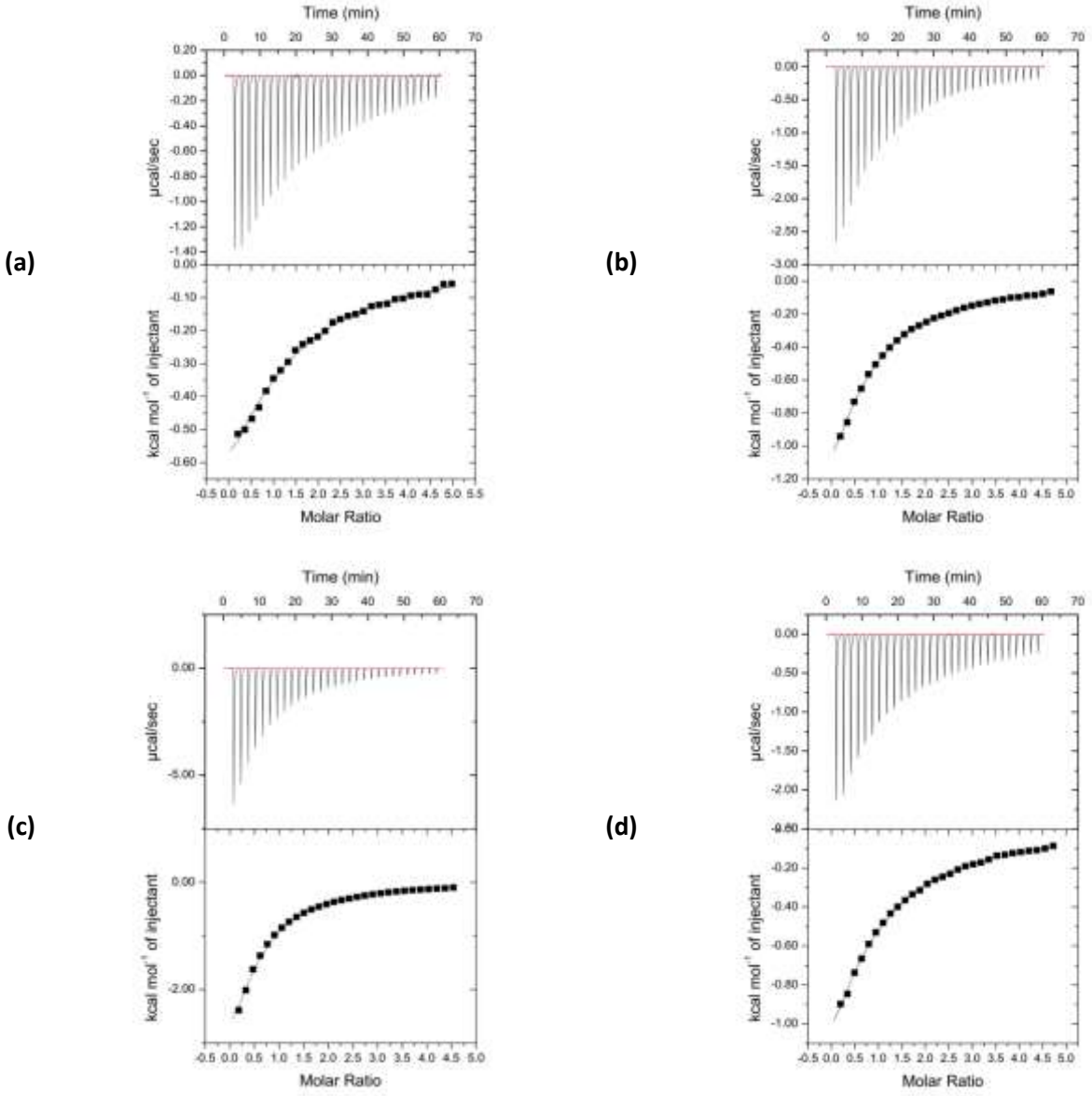

Figure 4.20: Calorimetric titration of γ-CD with the guest molecules (a) CAF, (b) PCA, (c) FA and (d) SA. Top: Raw data for 30 sequential injections (3 µL per injection) of the CD solution into the guest solution. Bottom: Heat isotherms obtained from the integration of the calorimetric curves.

The results for the ITC experiments of each of the hydroxycinnamic acid guests with γ-CD are listed in Table 4.13. The binding isotherm of γ-CD·CAF fit best with the one set of sites model with n = 1, indicating a 1:1 host to guest ratio in solution. Zhao *et al*. reported the formation of a 1:1 host to guest complex of γ-CD·CAF in solution using fluorescence measurements.[17] The binding isotherms of the inclusion complexes γ-CD·PCA, γ-CD·FA and γ-CD·FA were found to fit a one set of sites binding model with n = 2. This indicates either that complex formation is bimodal in solution or that the CD aggregates in solution such that two CD molecules interact with one guest molecule.

The ΔG° value for each binding step indicates that complex formation is spontaneous in solution at 298 K.[16] The ΔH° values are negative for each guest while the ΔS° values are positive. For γ-CD·CAF enthalpy and entropy contribute to ΔG° to a similar extent. The formation of γ-CD·PCA is predominantly enthalpy-driven when n = 2. Formation of the complex γ-CD·FA is associated with a large negative ΔH° value and a smaller positive ΔS° value and the reaction is primarily enthalpy-driven. γ-CD·SA exhibits the same trend when n = 2.

Table 4.13: Association constant (*K*) and the thermodynamic parameters (*ΔH°*, *TΔS°* and *ΔG°*) for the complexation of the hydroxycinnamic acids with γ-CD at 298 K.

	K **(M^{-1})**	***ΔH°*** **(kJ mol^{-1})**	***TΔS°*** **(kJ mol^{-1})**	***ΔG°*** **(kJ mol^{-1})**
CAF	475.3 ± 8.8	-6.75 ± 0.08	8.52 ± 0.12	-15.27 ± 0.05
PCA	302.7 ± 1.5[a]	-7.82 ± 0.32	6.34 ± 0.33	-14.16 ± 0.01
FA	543.0 ± 21.2[a]	-12.67 ± 0.61	2.94 ± 0.50	-15.60 ± 0.10
SA	228.0 ± 2.7[a]	-9.64 ± 0.19	3.82 ± 0.18	-13.46 ± 0.03

[a] Data fit to a one set of sites model with n = 2

Some considerations

The reversible formation and cleavage of non-covalent interactions as well as the reorganization of the solvent molecules around each component leads to a thermodynamic response. This response is measured using ITC. The mechanisms of such interactions are not directly observable and are largely open to interpretation. Careful optimisation of the experimental conditions is necessary. The binding isotherms obtained for the experiments with β-CD do not show an inflection point, which affects the accuracy of the n-value, and the gradualness of the curve may lead to a bad estimation of the error minimum. There are no guarantees that the minimum achieved by the computer software used to fit the data to a model is the global minimum.[18]

Discussion

The K values obtained for the interaction of both β- and γ-CD with the respective guest molecules are of the same order of magnitude. The magnitudes vary with the guest molecules used (246-774 M^{-1} for β-CD, n = 1, and 228-543 M^{-1} for γ-CD, n = 1 or 2). These values indicate a weak to moderate binding between

host and guest and are comparable with results found using similar small molecules.[19,20] The differences in the binding constants may be attributed to the differences in hydrophobicity and size of the guests and how these differences affect the interaction of the guest with the cavity of each host.[21] Formation constants were evaluated for β-CD·CAF over the pH range 3.05 to 12.5 by Chao *et al*.[14] using the fluorescence technique. The results were found to be 253 M^{-1} at pH 7.5, which is of the same order of magnitude as that found in this study at approximately neutral pH.

In all cases the ΔG° value is negative (ranging from -13.46 to -16.49 kJ/mol) indicating that the reaction between the host and guest molecules in solution is thermodynamically spontaneous. The different degrees to which ΔH° and ΔS° affect ΔG° reflect the differences between these host-guest interactions. The thermodynamic parameters obtained as a result of each guest interacting with β-CD are shown in Figure 4.21 and with γ-CD in Figure 4.22.

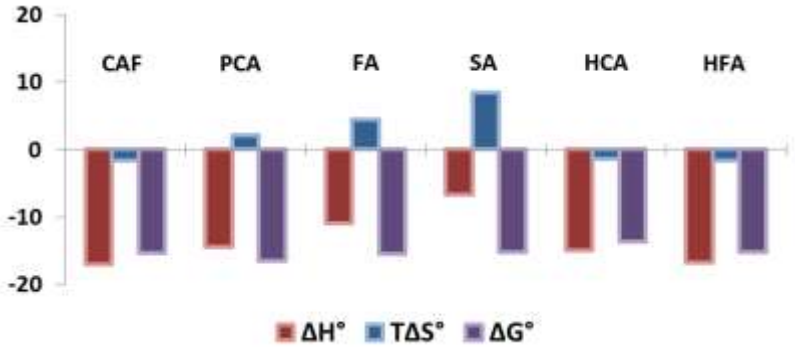

Figure 4.21: A graphical comparison of the thermodynamic parameters obtained for complexation between each guest and β-CD.

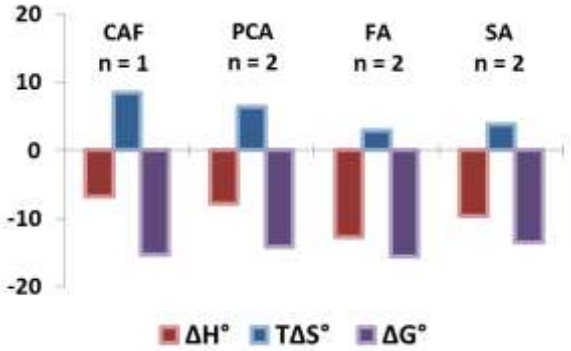

Figure 4.22: A graphical comparison of the thermodynamic parameters obtained for complexation between each guest and γ-CD.

The enthalpy term is increased by van der Waals interaction between host and guest,[22] possible hydrogen bond interactions and the reformation of hydrogen bonds in the bulk water after the guest solvation shell collapses and the exclusion of water molecules from the cavity. It is decreased when the hydrogen bonds between the CD and water in the CD cavity are broken.

For a favourable van der Waals interaction between the host and guest, where the guest is deeply inserted into the CD cavity - such as in β-CD·CAF, ΔH° is large. As the molecule becomes more hydrophobic (favouring a hydrophobic interaction over a van der Waals interaction) and the substituents on the phenol ring become more bulky, it is probable that the fit of guest to host cavity is enthalpically unfavourable, resulting in shallow insertion of the guest into the cavity. More water is retained in the cavity and overall, the ΔH contribution is smaller, such as for that of β-CD·SA.

The hydrophobic effect of the non-polar portions of the guests interacting with the CD cavity increases ΔS°.[23] This increases as the hydrophobicity of the guest increases. This is evident in Figure 4.21: as the hydrophobicity of the first four guest molecules increases, the ΔH° decreases in magnitude and the ΔS° increases, leaving ΔG° relatively unchanged. This demonstrates the enthalpy-entropy compensation effect.[24] A large contribution to the entropy change is also due to the reorganisation of the bulk water molecules, making the system more ordered.

Entropy is reduced by the restriction of the degrees of freedom when the guest and the host molecules interact.[22] The guest molecules CAF and PCA are relatively rigid and therefore this contribution is likely to be small. FA and SA may have some contribution due to the free rotation of the *O*-methyl groups. The largest loss of degrees of freedom upon complexation may be experienced by HCA and HFA, as the chain bearing the carboxylic acid has significant torsional freedom.

The size and nature of the host molecule affect the thermodynamics of inclusion complex formation. The respective volumes of the CD cavity for β- and γ-CD are 262 $Å^3$ and 427 $Å^3$. Assuming that the volume of a water molecule is ≈ 30 $Å^3$, the β- and γ-CD cavities can accommodate 9 and 14 water molecules, respectively.[25] The results show that the binding of CAF to β-CD is enthalpy-driven while the binding to γ-CD is predominantly entropy-driven. The aromatic portion of the CAF molecule fits well into the cavity of β-CD by van der Waals interactions and the exclusion of water molecules (and subsequent reformation of hydrogen bonds in the bulk water), leading to a large favourable ΔH° contribution. The entropic contribution is small and negative for the complex formation between CAF and β-CD. This is not observed for the γ-CD interaction with CAF: here the cavity of the CD is much larger, allowing the CAF to bind more loosely to the CD. Some water is retained within the cavity while only the loosely-bound water molecules are excluded and the bulk water does not require substantial reorganisation upon inclusion of the guest into the CD cavity. A large entropic contribution may be due to the conformational freedom of the CD because of the loose fit of host and guest.[26] Thermodynamic results for the formation of the complex γ-CD·CAF were reported by Zhao *et al.* using UV-vis spectrophotometry, but unfortunately no units were reported for these properties, making it impossible to compare them with the results obtained in this study.[17]

Figure 4.22 refers to complexes formed between the guest molecules CAF, PCA, FA, SA and two γ-CD molecules, resulting in 2:1 host to guest complexes in solution. The model used to fit the data to an isotherm was a one set of sites model, indicating that the CDs formed dimers in solution before including the guest molecule. A 'two sets of sites' model or a sequential binding model would allow one CD to interact with the guest before forming a dimer with a free CD. This aggregation is a well-known result of hydrogen bonding between the hydroxyl groups on the CDs.[27] The ΔH° and ΔS° values for the formation of each complex compensate for each other in such a way that the ΔG° value in each case is of the same order of magnitude and negative (ranging from -13.46 to -15.60 kJ/mol). A ^{1}H NMR spectroscopic study by Anselmi *et al.* demonstrated that the hydrophobic portion of FA is included within the γ-CD cavity in solution.[28] The protons of the aromatic moiety experienced a shift in the presence of the CD. An upfield shift of the host protons located within the CD cavity support inclusion; however, downfield shifts of the protons on the exterior of the CD molecule of the same absolute magnitude indicate significant interaction between the guest and the outside of the CD.

INCLUSION COMPLEX FORMATION BETWEEN HYDROXYCINNAMIC ACIDS AND DERIVATISED CDs

Preparation of single crystals

Inclusion complex crystals were obtained by dissolving the host (0.103 mmol) in cold distilled de-ionised water (2-3 mL) at low temperature (*ca* 4°C). Once the solution cleared, an equimolar amount of the guest was added to the solution and it was allowed to stir vigorously at the same low temperature for three days. The solution was filtered, sealed in a vial and placed in an oven at 50 °C to crystallise. Table 4.14 indicates the inclusion complexes obtained and the masses used to obtain crystals.

Table 4.14: Masses and temperature conditions used to obtain complex crystals.

Guest	CAF	FA	FA	HFA	HFA	PCA	PCA	PCA
Host	DMB	TMA	DMB	TMB	DMB	TMA	TMB	DMB
m_{guest} (mg)	20	20	20	20	20	20	20	20
m_{host} (mg)	148	126	137	142	136	149	169	162

TRIMEB INCLUSION COMPLEXES WITH HYDROFERULIC ACID AND *p*-COUMARIC ACID (TMB·HFA AND TMB·PCA)

Thermal Analysis

The TGA and DSC traces for the inclusion complexes TMB·HFA and TMB·PCA are shown in Figures 4.23 and 4.24. The TGA traces show a small mass loss over the range 30 °C to 100 °C corresponding to water loss. These events are observed in the same temperature range in the DSC results as a single broad endotherm in TMB·HFA and as two overlapping endotherms in TMB·PCA, indicating multiple hydrogen bonding water sites. The percentage mass losses are 1.4 ± 0.2 for TMB·HFA and 8.2 ± 2.2 for TMB·PCA. The recorded water loss yielded the number of water molecules per CD molecule as 1.2 ± 0.2 (n = 2) for

TMB·HFA and 7.7 ± 2.3 (n = 2) for TMB·PCA. DSC analysis showed a sharp endotherm at 136 ˚C for TMB·HFA and at 179 ˚C for TMB·PCA representing fusion of the complex. The guest molecules are expelled from the respective complexes such that the percentage mass losses are 12.0 ± 0.2 for TMB·HFA over the temperature range 150 °C to 275 °C and 8.2 ± 2.2 for TMB·PCA over the range 175 °C to 300 °C. The loss was calculated to be 0.9 ± 0.1 (n = 2) guest molecules for both TMB·HFA and TMB·PCA per complex unit. The decomposition of the remaining residues starts at *ca*. 320 °C.

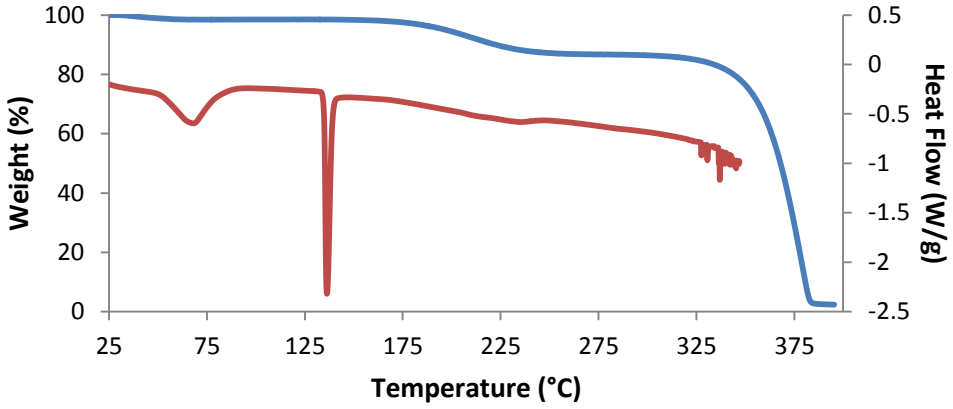

Figure 4.23: DSC (red) and TGA (blue) curves of TMB·HFA.

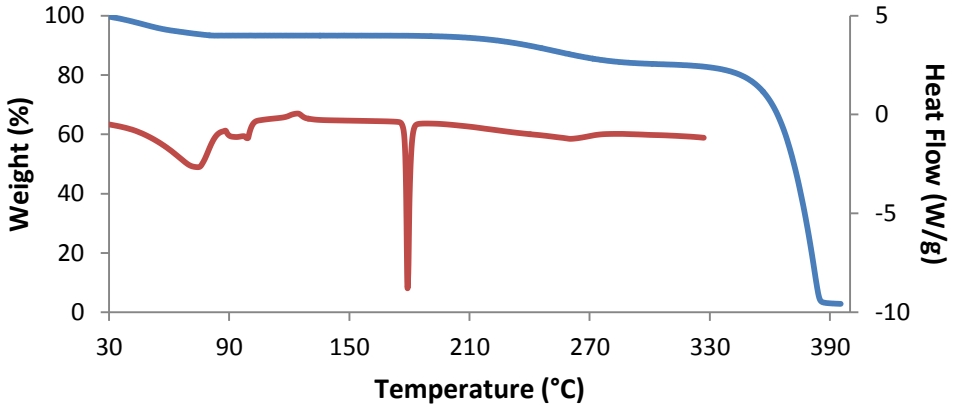

Figure 4.24: DSC (red) and TGA (blue) curves of TMB·PCA.

HSM was used to physically observe the thermal events which occur as the crystals, immersed in silicone oil, are heated. Figure 4.25 shows a crystal of TMB·HFA which is clear at room temperature. Cracking occurs as the crystal is heated and at 100 °C bubbles appear, indicating the release of water from the crystal. The crystal begins to melt at 140 °C. Decomposition begins at *ca*. 300 °C.

30 °C **70 °C** **100 °C** **140 °C** **141 °C**

Figure 4.25: HSM photographs of the complexes TMB·HFA.

A colourless crystal of TMB·PCA is shown in Figure 4.26. The crystal appears to fracture as it is heated and turns opaque. The crystal begins to melt at 184 °C and decomposition begins at 300 °C.

30 °C **85 °C** **95 °C** **130 °C** **184 °C**

Figure 4.26: HSM photographs of the complexes TMB·PCA.

Single crystal X-ray analysis of the complexes TMB·HFA and TMB·PCA

The crystallographic data and refinement parameters for each structure are listed in Table 4.15.

Table 4.15: Crystallographic data for the complexes TMB·HFA and TMB·PCA.

	TMB·HFA	**TMB·PCA**
Complex Formula	**$C_{63}H_{112}O_{35}\cdot C_{10}H_{12}O_4\cdot 1.3H_2O$**	**$C_{63}H_{112}O_{35}\cdot C_9H_8O_3\cdot 7H_2O$**
Formula weight	1649.14	1719.78
Crystal system	Orthorhombic	Orthorhombic
Space group	$P2_12_12_1$ (no. 19)	$P2_12_12_1$ (no. 19)
a / Å	14.657(2)	14.778(3)
b / Å	22.774(3)	22.231(4)
c / Å	26.124(4)	27.728(6)
Volume / $Å^3$	8720(2)	9110(3)
Z	4	4
Calculated density / g cm^{-3}	1.254	1.244
μ (MoKα) / mm^{-1}	0.102	0.104
F (000)	3548	3648
Temperature / K	173(2)	173(2)
Crystal size / mm^3	0.25 x 0.36 x 0.48	0.18 x 0.20 x 0.40
Theta range scanned / °	1.6 < θ < 27.2	1.8 < θ < 26.4
Index ranges	h: -18: 18; k: -29: 28; l: -33: 32	h: -11: 20; k: -19: 24; l: -27: 32
Total number of reflections	57888	97292
No. of independent reflections	19215	18599
No. of reflections with I > 2σ(I)	14183	15850
No. of parameters	1068	969
R_{int}	0.045	0.032
$R_1(I > 2\sigma(I))$	0.0697	0.0663
$wR_2(I > 2\sigma(I))$	0.2011	0.1912
S	1.028	1.035
Coefficients in weighting scheme	a = 0.0992, b = 6.7909	a = 0.1113, b = 6.7606
Δρ excursions / e $Å^{-3}$	-0.62, 0.78	-0.52, 0.82

Data collection and space group determination

The intensity data for TMB·HFA were collected on a Bruker Kappa Apex II Duo diffractometer and those for TMB·PCA on a Nonius Kappa CCD diffractometer. In each case the crystal systems and space groups were determined using LAYER.[3] The Laue symmetry was found to be *mmm* indicating the orthorhombic system. The common space group was determined from the systematically absent reflections.

Structure solution and refinement

Both structures were solved by direct methods using the program SHELXD,[29] as the unit cell parameters did not match any of a known isostructural series closely enough.[1] SHELXD provided a structure solution and all the non-hydrogen atoms were assigned. Full-matrix least-squares methods were used to refine the model using SHELXL.[5] Initially all atoms were refined isotropically.

The glucose units of the host atoms were labelled G1 - G7, as shown in Figure 4.27. Disordered atoms were labelled by parts and are listed in Table 4.16. The disorder occurs on the C6-O6-C9 moiety of G1, G3 and G4 of TMB·HFA and of G1 of TMB·PCA, as well as on the O2 methyl moiety of G1 of TMB·HFA. The ordered non-hydrogen atoms of the host were allowed to refine anisotropically after they were determined to have stable U_{iso} values. Hydrogen atoms were placed in idealised positions using a riding model having U_{iso} values 1.2 times and 1.5 times those of their parent atoms.

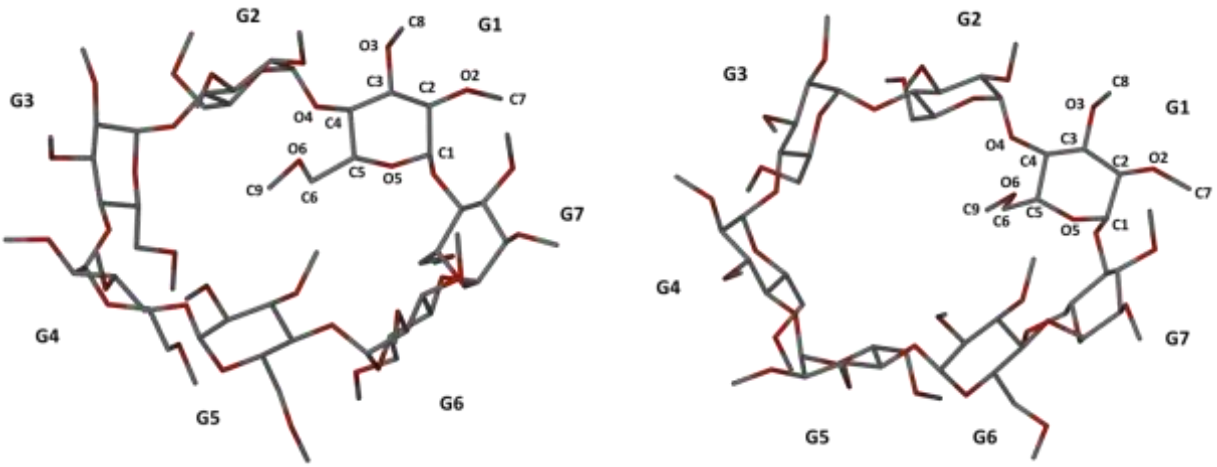

Figure 4.27: The host atom labels used for TMB·HFA (left) and TMB·PCA (right).

Table 4.16: The site-occupancy factors attributed to each disordered host atom in TMB·HFA and TMB·PCA.

Complex	Atom 1	x	Atom 2	1 – x
TMB·HFA	C611/O611/C911	0.60(1)	C612/O612/C912	0.40
	C631/O631/C931	0.87(1)	C632/O632/C932	0.13
	C641/O641/C941	0.72(1)	C642/O642/C942	0.28
	O211/C711	0.58(4)	O212/C712	0.42
TMB·PCA	C611/O611/C911	0.58(1)	C612/O612/C912	0.42

The guest molecules were assigned after further examination of the difference electron density maps. No disorder was evident and the non-hydrogen atoms were allowed to refine anisotropically. The labels of the non-hydrogen atoms are shown in Figure 4.28. Hydrogen atoms were placed using an AFIX 137 command for methyl hydrogen atoms, AFIX 43 for phenyl hydrogen atoms and AFIX 147 or AFIX 83 for hydroxyl hydrogen atoms, the latter using the highest electron density to determine the orientation of the O-H bond and place the hydrogen atom while the former places the hydrogen atom in a position that corresponds to the best hydrogen bond interaction.

Figure 4.28: The guest atom labels used for TMB·HFA (left) and TMB·PCA (right).

Water oxygen atoms were assigned after electron density peaks appeared on the difference map that did not belong to either host or guest. Three were found in TMB·HFA and the O atoms were assigned partial occupancy, such that the total number of water molecules per CD was consistent with that of the TG results. O1W was assigned an s.o.f. of 0.75, O2W of 0.30 and O3W of 0.25. Seven water O atoms were found in TMB·PCA, all having full occupancy. Due to disorder of the hydrogen atoms on the water O atoms they were not assigned.

The ASU of TMB·HFA consists of one TRIMEB molecule, one HFA molecule and 1.3 water molecules and that of TMB·PCA consists of one TRIMEB molecule, one PCA molecule and 7 water molecules (Figure 4.29).

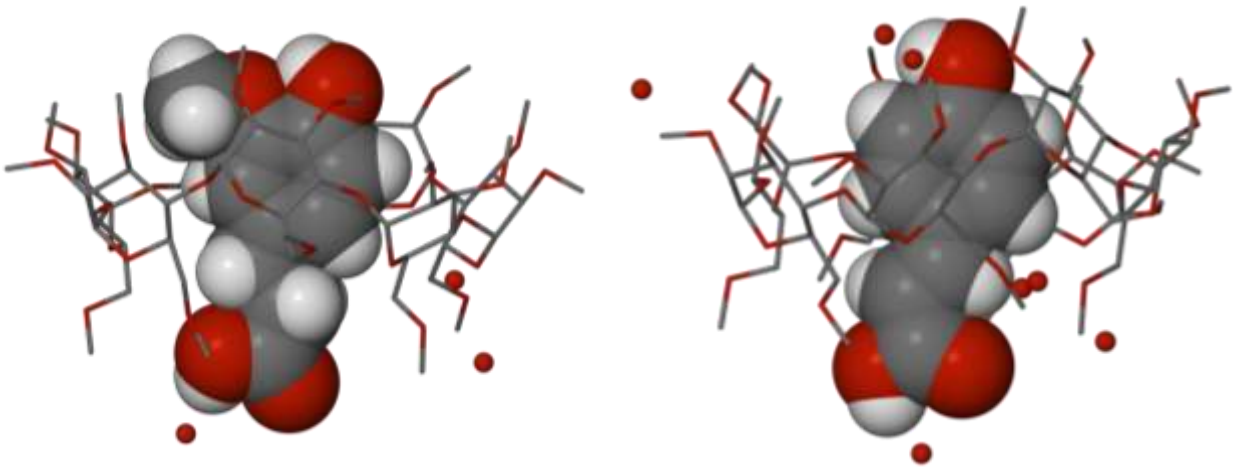

Figure 4.29: The ASU of TMB·HFA (left) and TMB·PCA (right) illustrating the guest included in the CD cavity.

Geometrical analysis

Host Geometry

Tables 4.17 and 4.18 list the geometrical parameters of the macrocycles of TMB·HFA and TMB·PCA, respectively.

Table 4.17: Geometric parameters of the TRIMEB molecule in the complex TMB·HFA.

Residue	*r* (Å)	*D* (Å)	*a* (°)	*φ* (°)	*d* (°)	D_3 (Å)	*α* (Å)	τ_1 (°)	τ_2 (°)
G1	4.322	4.560	141.9	115.0(5)	16.1	3.731	-0.529(3)	44.9(3)	25.0(2)
G2	4.806	4.185	129.7	118.3(4)	21.5	3.889	-0.204(3)	13.0(1)	25.6(2)
G3	5.496	4.195	113.9	118.6(3)	-23.2	3.355	0.624(3)	19.1(1)	39.0(1)
G4	4.871	4.597	131.7	115.9(3)	-3.0	3.432	-0.160(3)	13.5(1)	27.6(1)
G5	4.585	4.494	133.9	116.5(3)	15.1	3.261	-0.409(3)	17.8(1)	2.5(1)
G6	5.239	4.250	124.1	118.1(4)	7.4	3.096	0.245(3)	6.0(1)	16.1(1)
G7	5.416	4.218	114.5	119.2(4)	-33.7	3.366	0.434(3)	16.3(1)	27.9(1)
Mean	**4.96**	**4.36**	**127.1**	**117.4**	**19.6**	**3.45**	**0.406**	**18.7**	**23.4**

Table 4.18: Geometric parameters of the TRIMEB molecule in the complex TMB·PCA.

Residue	*r* (Å)	*D* (Å)	*a* (°)	*φ* (°)	*d* (°)	D_3 (Å)	*α* (Å)	τ_1 (°)	τ_2 (°)
G1	4.551	4.607	140.8	115.8(3)	-9.0	3.374	0.032(2)	24.9(1)	36.9(1)
G2	4.823	4.271	128.2	117.4(3)	14.6	3.212	0.517(3)	19.1(1)	10.1(1)
G3	5.339	4.409	122.6	118.9(4)	11.8	3.241	-0.158(3)	7.6(1)	8.3(1)
G4	5.204	4.353	119.1	118.9(3)	-34.0	3.489	-0.573(2)	19.8(1)	32.8(1)
G5	4.412	4.498	140.5	114.5(3)	7.4	3.833	0.473(2)	43.9(2)	36.6(1)
G6	5.069	4.311	125.2	117.6(3)	22.1	3.725	0.377(2)	15.8(1)	15.1(1)
G7	5.506	4.256	112.1	120.1(3)	-21.5	3.450	-0.668(2)	20.7(1)	32.8(1)
Mean	**4.99**	**4.39**	**126.9**	**117.6**	**19.3**	**3.47**	**0.453**	**21.7**	**24.7**

The host molecules are elliptical in shape as the *r*, *D* and *a* values deviate significantly from the respective average values. The *α* deviations show that the CD molecules have a saddle-like curvature when viewed side-on. The torsion angles τ_1 and τ_2 indicate that the secondary rims are wider than the primary rims, with much variation in the inclinations of the individual glucopyranose rings.

The O5-C5-C6-O6 torsion angles (*ω*) of methyl glucose units G1 (major component), G2, G5 and G7 of TMB·HFA are negative indicating a (-)-*gauche* conformation. The torsion angles of G3, G4, and G6 indicate a (+)-*gauche* conformation for TMB·HFA. These torsion angles in the complex TMB·PCA are all (-)-*gauche* (including the major component of G3), with the exception of the *O*-methyl on G7 which is (+)-*gauche*. In both structures the C6-O6 bonds are directed away from the cavity, allowing the acid moiety of the guests to be located at the primary rim of the CDs.

Guest inclusion

As is evident from Figure 4.29 above, the guest molecules are positioned in the TMB host cavities such that the hydrophobic substituted phenyl ring moiety is included close to the secondary rim while the

carboxylic acid moiety protrudes from the primary rim of the CD. Figures 4.30 to 4.33 are space-filling diagrams presenting different views of the TMB·HFA and TMB·PCA complexes. Only the water O atoms interacting with the guest are shown.

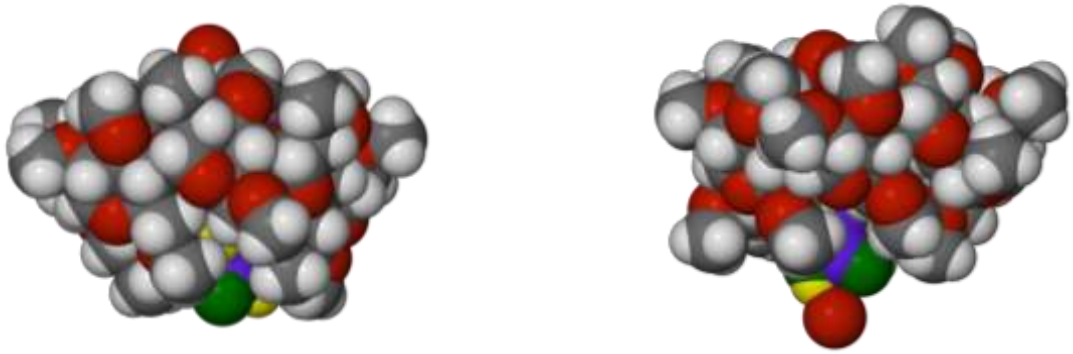

Figure 4.30: A space-filling diagram of TMB·HFA (left) and TMB·PCA (right) viewed side-on. For clarity only the hydrogen atoms of the water molecules are omitted.

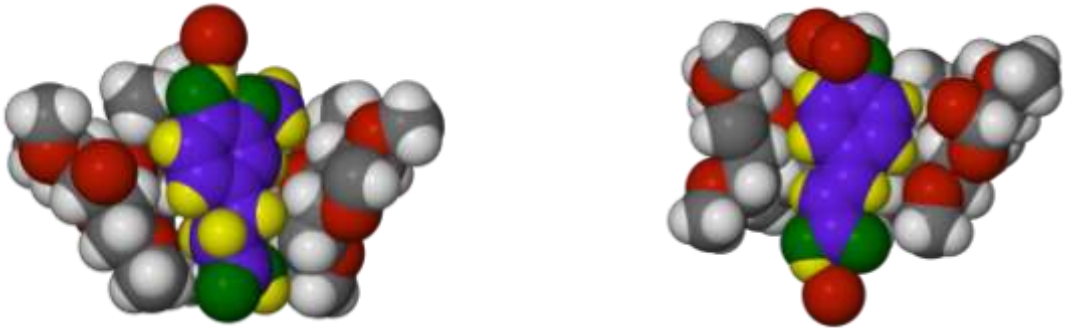

Figure 4.31: A space-filling diagram of TMB·HFA (left) and TMB·PCA (right) cutaway side-on images.

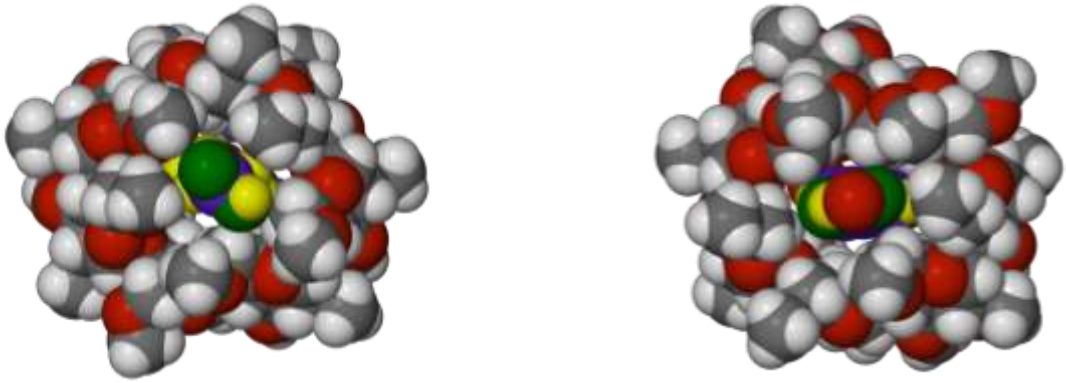

Figure 4.32: A space-filling diagram of TMB·HFA (left) and TMB·PCA (right) viewed from the CD primary end.

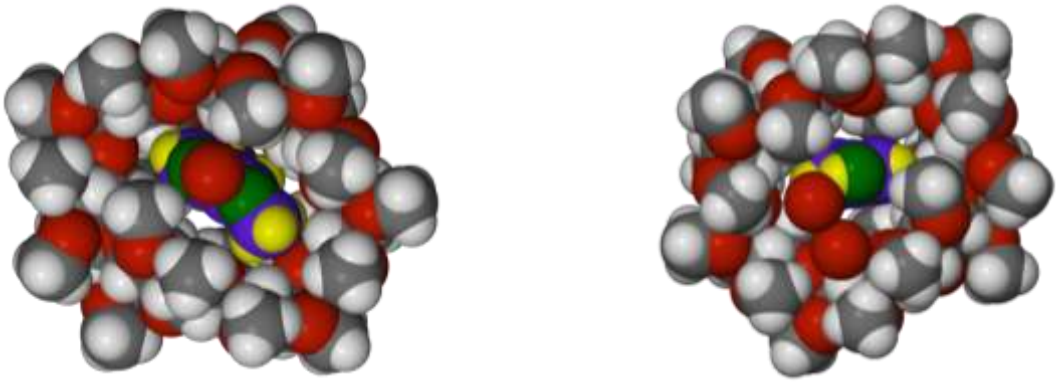

Figure 4.33: A space-filling diagram of TMB·HFA (left) and TMB·PCA (right) viewed from the CD secondary end.

Hydrogen bonding interactions

Host intramolecular interactions

The conformations of the host molecules in TMB·HFA and TMB·PCA are distorted, due in part to a number of weak C-H···O intramolecular hydrogen bonds which are listed in Tables 4.19 and 4.20.[30] The C6-H···O5' interactions contribute towards the large tilt angles observed in TRIMEB molecules.[31]

Table 4.19: Intramolecular host hydrogen bond parameters in TMB·HFA.

D-H···A	D-H (Å)	H···A (Å)	D···A (Å)	D-H···A (°)
C1G2-H1G2···O3G1	1.00	2.36	3.066(7)	127
C1G3-H1G3···O6G2	1.00	2.22	3.126(7)	149
C4G7-H4G7···O6G7	1.00	2.46	2.840(6)	102
C5G1-H5G1···O4G7	1.00	2.31	2.789(9)	108
C5G2-H5G2···O4G1	1.00	2.47	2.849(7)	102
C5G5-H5G5···O4G4	1.00	2.52	2.876(6)	100
C5G7-H5G7···O4G6	1.00	2.39	2.777(6)	102
C6G2-H7···O5G3	0.99	2.59	3.348(8)	133
C631-H6G7···O5G4	0.99	2.41	3.322(9)	153
C641-H6G9···O5G5	0.99	2.53	3.387(10)	144
C6G5-H6G2···O5G6	0.99	2.44	3.176(6)	130
C6G5-H6G2···O6G6	0.99	2.59	3.536(7)	159
C6G6-H6G3···O5G7	0.99	2.44	3.339(6)	150
C6G7-H6G6···O5G1	0.99	2.51	3.223(8)	129
C7G2-H7GZ···O3G2	0.98	2.47	3.095(11)	121
C8G1-H8GZ···O2G1	0.98	2.57	3.151(8)	118
C8G2-H8GA···O4G2	0.98	2.45	3.081(9)	121
C8G3-H8GI···O2G3	0.98	2.59	3.190(11)	120
C8G4-H8G6···O2G4	0.98	2.42	2.999(7)	117
C9G2-H9GX···O5G2	0.98	2.44	3.017(13)	117

Table 4.20: Hydrogen bond parameters for the host-host intramolecular interactions in TMB·PCA.

D-H···A	D-H (Å)	H···A (Å)	D···A (Å)	D-H···A (°)
C1G2-H1G2···O3G1	1.00	2.53	3.128(6)	118
C1G6-H1G6···O3G5	1.00	2.39	3.093(5)	127
C1G7-H1G7···O6G6	1.00	2.42	3.143(5)	129
C5G1-H5G1···O4G7	1.00	2.40	2.773(5)	101
C5G3-H5G3···O4G2	1.00	2.37	2.800(6)	105
C5G4-H5G4···O4G3	1.00	2.38	2.784(6)	103
C5G5-H5G5···O4G4	1.00	2.39	2.782(5)	102
C5G6-H5G6···O4G5	1.00	2.47	2.852(5)	102
C6G2-H6G4···O5G3	0.99	2.56	3.292(6)	131
C631-H63B···O5G4	0.99	2.48	3.291(8)	138
C6G4-H6GZ···O5G5	0.99	2.43	3.112(7)	125
C6G6-H6GX···O5G7	0.99	2.41	3.131(5)	130
C6G7-H6G1···O5G1	0.99	2.30	3.223(5)	155
C8G1-H8G9···O2G1	0.98	2.42	3.028(6)	119

Host intermolecular interactions

A number of C-H···O hydrogen bonds exist between symmetry-related TMB molecules in each structure, lending to the stability of the crystals. These hydrogen bonds are listed in Tables 4.21 and 4.22.

Table 4.21: Hydrogen bond parameters for the host-host interactions in TMB·HFA.

D-H···A	D-H (Å)	H···A (Å)	D···A (Å)	D-H···A (°)	Symmetry Operation
C1G4-H1G4···O6G2	1.00	2.46	3.429(8)	162	-½+x, 3/2-y, 1-z
C2G1-H2G1···O6G5	1.00	2.53	3.487(8)	161	1+x, y, z
C9G7-H9G5···O3G6	0.98	2.52	3.480(9)	168	½+x, 3/2-y, -z

* The symmetry operation applies to the acceptor oxygen atom.

Table 4.22: Hydrogen bond parameters for the host-host interactions in TMB·PCA.

D-H···A	D-H (Å)	H···A (Å)	D···A (Å)	D-H···A (°)	Symmetry Operation
C1G4-H1G4···O6G6	1.00	2.48	3.319(6)	141	3/2-x,1-y,1/2+z
C2G4-H2G4···O5G7	1.00	2.53	3.459(5)	154	3/2-x,1-y,1/2+z
C2G7-H2G7···O6G4	1.00	2.36	3.362(6)	175	3/2-x,1-y,-1/2+z
C2G5-H2G5···O6G2	1.00	2.52	3.514(6)	171	1+x,y,z
C6G7-H6G2···O3G4	0.99	2.48	3.444(6)	165	3/2-x,1-y,-1/2+z
C9G6-H9G1···O3G1	0.98	2.58	3.000(7)	106	1+x,y,z
C9G6-H9G2···O631	0.98	2.54	3.486(8)	161	3/2-x,1-y,-1/2+z

* The symmetry operation applies to the acceptor oxygen atom.

Guest-guest and host-guest interactions

The guest molecule in TMB·HFA contains one intramolecular hydrogen bond and one intermolecular hydrogen bond (Figure 4.34), namely O1-H1···O2 (O-H = 0.84 Å, H···O = 2.20 Å, O···O = 2.657(8) Å and O-H···O = 114°) and O1-H1···O3[a] (O-H = 0.84 Å, H···O = 2.12 Å, O···O = 2.753(6) Å and O-H···O = 132 °, a = 2-x, -½+y, ½-z), respectively. One hydrogen bond exists between the host and guest molecules, namely C8G2-H8GC···O1 which has an O···H distance of 2.51 Å, a C···O distance of 3.370(13) Å and a bond angle of 147°. There is one intramolecular hydrogen bond in the guest molecule of TMB·PCA (C7-H7···O3) with an O···H distance of 2.55 Å, a C···O distance of 2.973(16) Å and a bond angle of 107°.

Water hydrogen bonding interactions

There are three partially occupied water O atoms in the structure of TMB·HFA. O1W acts as an acceptor for the hydrogen bond involving guest atom O4 and is a donor for the interaction with guest atom O1 and host atom O2G5, respectively. These interactions (listed in Table 4.23) connect the guest molecules in consecutive complex units and the guest to the host molecule by using O1W as a bridging atom (Figure 4.34). The remaining two water O atoms interact with the exterior of the host molecule as well as with each other.

Table 4.23: Hydrogen bond parameters for the interactions involving water in TMB·HFA.

D-H···A	D-H (Å)	H···A (Å)	D···A (Å)	D-H···A (°)	Symmetry Operation
O4-H4···O1W	0.84	1.92	2.692(7)	152	-
O1···O1W*	-	-	2.696(7)	-	2-x, ½+y, ½-z
O1W···O2G5*	-	-	2.793(6)	-	2-x, ½+y, ½-z
O2W···O5G5	-	-	2.802(12)	-	-
O2W···O611	-	-	2.835(17)	-	x-1, y, z
O3W···O3G3*	-	-	2.815(17)	-	x-½, 3/2-y, 1-z
O2W···O3W*	-	-	2.842(8)	-	-

* The acceptor oxygen atom to which the symmetry operation applies.

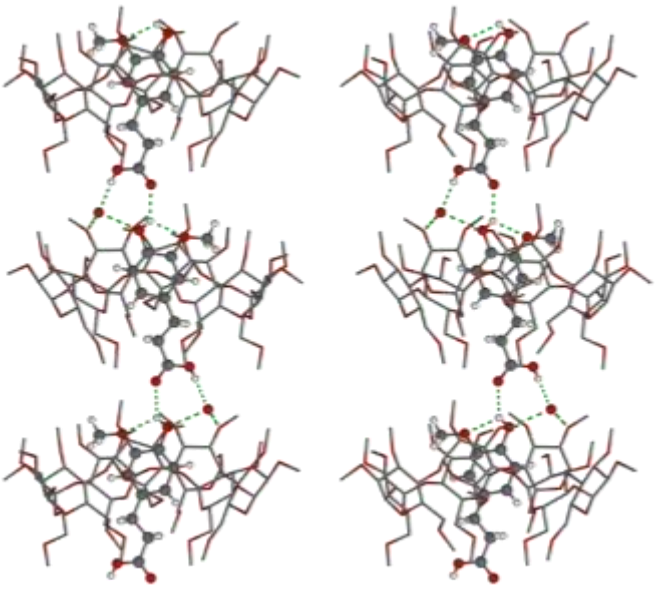

Figure 4.34: A stereodiagram illustrating the guest intramolecular interaction, the water-guest interactions and the water-host interactions within the TMB·HFA complex columns. Successive complex units are related by a 2_1-axis parallel to the *b*-axis.

The interactions between the water O atoms and the host and guest molecules in the complex TMB·PCA are listed in Table 4.24. The water molecule O4W is an acceptor in the interaction with the hydroxyl group on the guest (O1-H1) while O7W is an acceptor in the interaction with the acid hydroxyl group (O2-H2A). Atom O7W also interacts with the O3 and 2_1-related O1 guest atoms as a donor. The guest molecule does not interact directly with the host molecule; however, the interaction is bridged through a hydrogen bond network of water molecules (Figure 4.35). For clarity a labelled diagram follows in Figure 4.36. An interaction through atom O7W binds the guest acid group to atom O2G2 of a 2_1-related host molecule. At the phenolic terminus, a hydrogen bonding network is formed such that O1 bonds to O4W which in turn forms close H-bonding contacts with O3W···O2W···O5W. All water O atoms interact with an *O*-methyl oxygen atom of a host molecule, except for O4W.

Table 4.24: Hydrogen bond parameters for the interactions involving water in TMB·PCA.

D-H···A	D-H (Å)	H···A (Å)	D···A (Å)	D-H···A (°)	Symmetry Operation
O1-H1···O4W	0.84	1.92	2.660(11)	146	-
O2-H2A···O7W	0.84	1.93	2.710(15)	153	-
O1···O7W*	-	-	2.979(10)	-	1-x, ½+y, ½-z
O3···O7W	-	-	2.788(15)	-	-
O1W···O5G2*	-	-	2.858(5)	-	1+x, y, z
O1W···O6G5	-	-	2.821(5)	-	-
O1W···O6W*	-	-	2.752(6)	-	x-1, y, z
O2W···O3W*	-	-	2.819(6)	-	½+x, 3/2-y, 1-z
O2W···O5W*	-	-	2.892(6)	-	½-x, 1-y, ½+z
O2W···O3G3	-	-	2.788(6)	-	-
O3W···O4W	-	-	2.796(9)	-	-
O3W···O2G6	-	-	3.000(6)	-	-
O4W···O5W*	-	-	2.901(8)	-	1-x, ½+y, ½-z
O5W···O5G1	-	-	2.997(6)	-	-
O6W···O6G1	-	-	2.813(6)	-	-
O7W···O2G2*	-	-	2.865(8)	-	1-x, y-½, ½-z

*The atom to which the symmetry operation applies.

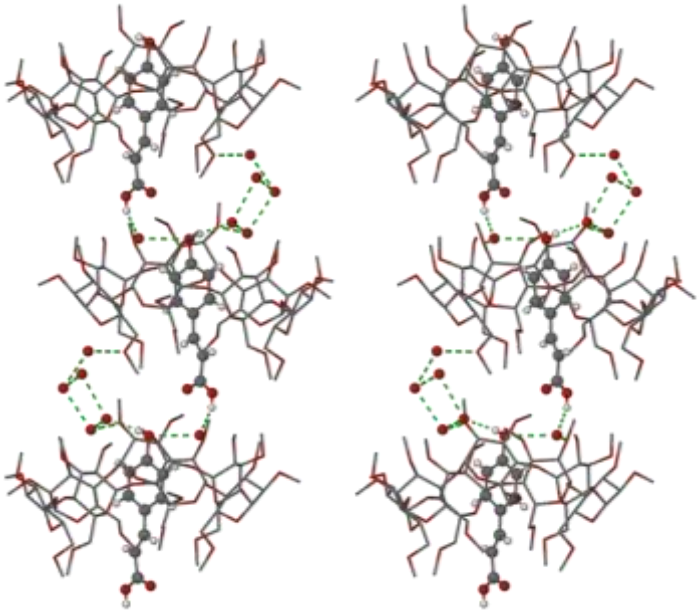

Figure 4.35: A stereodiagram illustrating the interactions of water and the water-host/water-guest interactions within the TMB·PCA complex columns. Successive complex units are related by a 2_1-axis parallel to the *b*-axis.

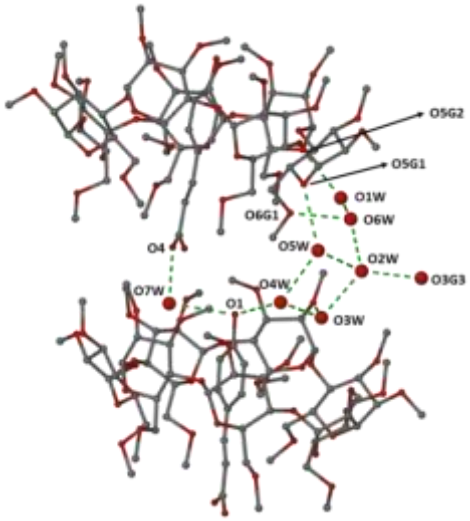

Figure 4.36: Water hydrogen bond interactions including labels of donors and acceptors.

Crystal packing

The host molecules of TMB·HFA and TMB·PCA pack in a head-to-tail fashion, forming regular columns along the axial direction of the CD cavity in TMB·HFA (Figure 4.37). The TMB·PCA host molecules are slightly offset in the columns (compared to those of TMB·HFA) due the extra water molecules in the structure (Figure 4.38). The columns lie parallel to the *b*-axis (Figure 4.39).

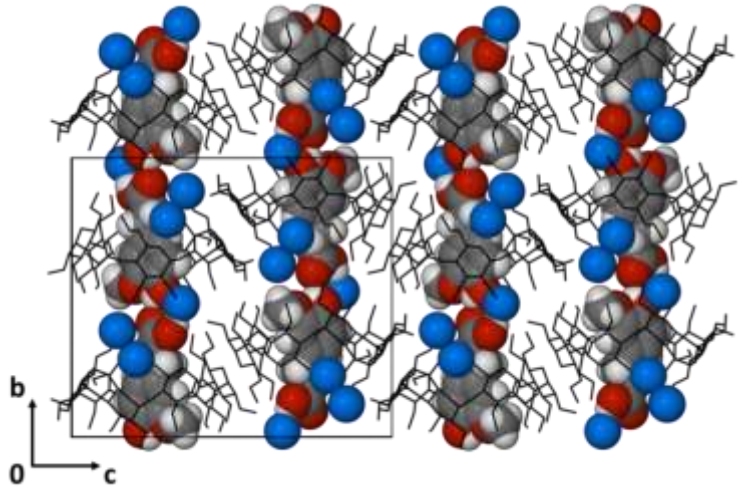

Figure 4.37: Packing diagram of the TMB·HFA complex as viewed down the *a*-axis.
Host hydrogen atoms are omitted for clarity and water oxygen atoms are shown as blue spheres.

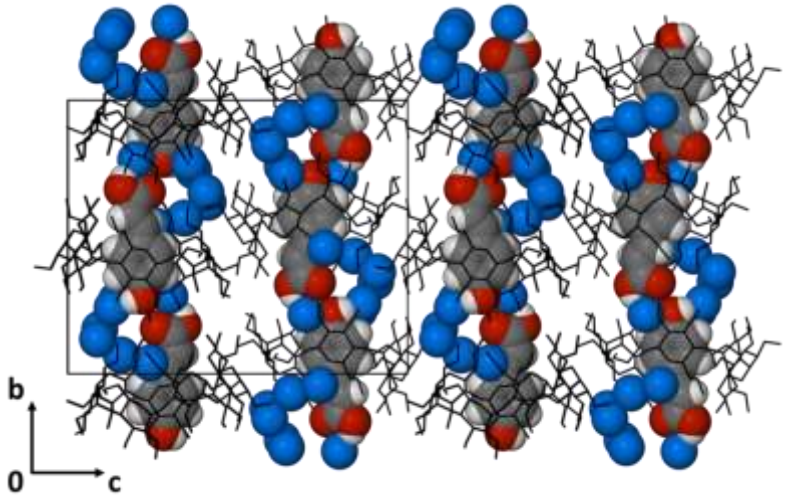

Figure 4.38: Packing diagram of the TMB·PCA complex as viewed down the *a*-axis.
Host hydrogen atoms are omitted for clarity and water oxygen atoms are shown as blue spheres.

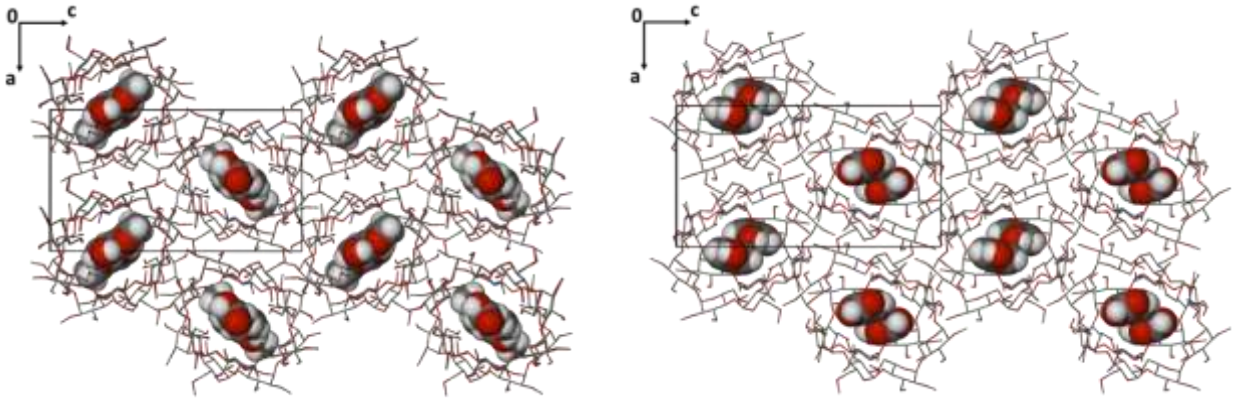

Figure 4.39: Packing diagrams of TMB·HFA (left) and TMB·PCA (right) viewed down the *b*-axis.
Host hydrogen atoms and water oxygen atoms are omitted for clarity.

Comparative PXRD

The experimental and calculated PXRD patterns are in good agreement confirming that the TMB·HFA and TMB·PCA crystals were homogeneous (Figures 4.40 and 4.41). Differences in the relative intensities of the peaks are attributed to some degree of preferred orientation of the sample.

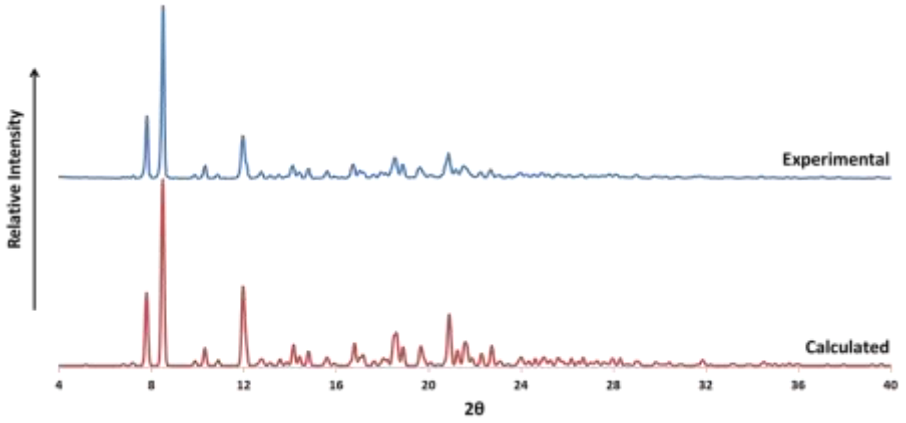

Figure 4.40: The PXRD trace of the experimental product and the pattern calculated from the X-ray structure of TMB·HFA.

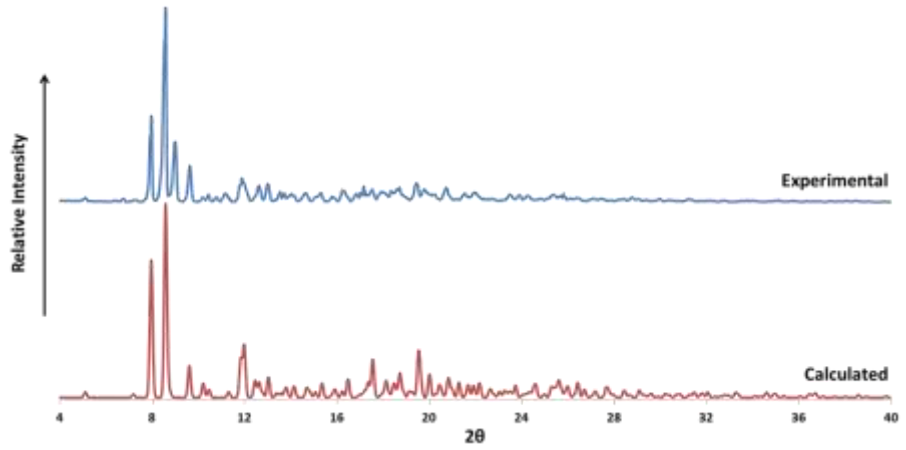

Figure 4.41: The PXRD trace of the experimental product and the pattern calculated from the X-ray structure of TMB·PCA.

DIMEB INCLUSION COMPLEXES WITH CAFFEIC ACID AND FERULIC ACID (DMB·CAF and DMB·FA)

Thermal analysis

Figures 4.42 and 4.43 illustrate the TGA and DSC traces of DMB·CAF and DMB·FA. The TGA traces show initial mass losses of 8.9 ± 3.4 % (n = 2) and 6.5 ± 1.1 % (n = 2) for DMB·CAF and DMB·FA, respectively, which is equivalent to 15.4 ± 6.4 and 11.0 ± 2.1 water molecules per 2:1 complex unit. The broad endotherm seen in each of the DSC traces over the range 30 - 120 °C corresponds to the loss of water. A small exothermic event occurs at 160 °C in the DSC of DMB·CAF. This may be evidence for a phase transformation, but its investigation was not pursued. The guest molecules begin to be lost at 180 °C for DMB·CAF and 130 °C for DMB·FA. These mass losses are 5.0 ± 0.4 % and 6.0 ± 0.2 % for DMB·CAF and DMB·FA, respectively, corresponding to 0.9 ± 0.1 per 2:1 complex unit for both complexes. A shallow,

broad endotherm appears in the DSC of both complexes over the same ranges within which guest mass loss occurs in the TGA. The TGA and DSC traces suggest that decomposition occurs at *ca*. 350 °C.

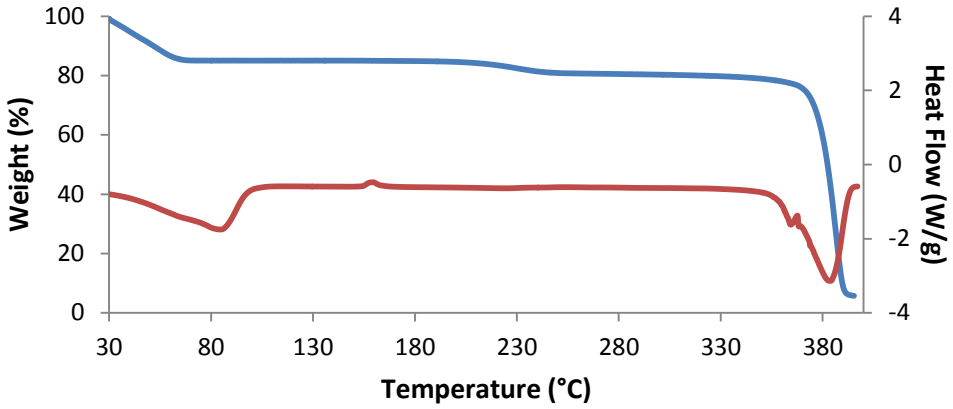

Figure 4.42: DSC (red) and TGA (blue) curves of DMB·CAF.

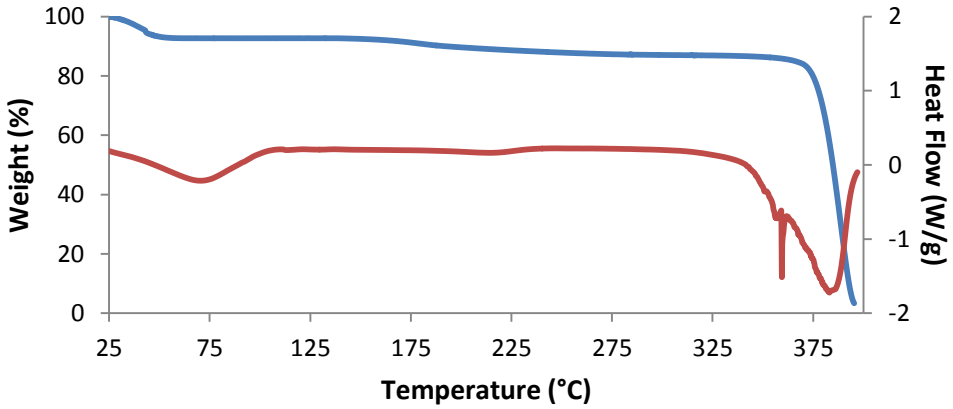

Figure 4.43: DSC (red) and TGA (blue) curves of DMB·FA.

Both crystals are clear at room temperature, as shown in Figures 4.44 and 4.45. As the DMB·CAF crystal is heated it appears to fracture, likely due to dehydration. At 160 °C the crystal turns opaque indicating a possible phase transformation. Decomposition begins at ca. 220 °C, indicated by discolouration of the crystal. For the DMB·FA complex, bubbles of water vapour are released at 100 °C and the crystal turns opaque. Decomposition begins at ca. 280 °C, indicated by discolouration of the crystal and bubbling as the decomposition products are released.

30 °C **100 °C** **150 °C** **240 °C** **345 °C**

Figure 4.44: HSM photographs of the complexes DMB·CAF.

30 °C **100 °C** **120 °C** **280 °C** **345 °C**

Figure 4.45: HSM photographs of the complexes DMB·FA.

Single crystal X-ray analysis of the complexes DMB·CAF and DMB·FA

The crystallographic data and refinement parameters for each structure are listed in Table 4.25.

Table 4.25: Crystallographic data for the complexes DMB·CAF and DMB·FA.

	DMB·CAF	**DMB·FA**
Complex Formula	**$(C_{56}H_{98}O_{35})_2 \cdot C_9H_8O_4 \cdot 12.6H_2O$**	**$(C_{56}H_{98}O_{35})_2 \cdot C_{10}H_{10}O_4 \cdot 11.2H_2O$**
Formula weight	3069.83	3058.63
Crystal system	Monoclinic	Monoclinic
Space group	$P2_1$ (No. 4)	$P2_1$ (No. 4)
a / Å	17.550(2)	17.567(4)
b / Å	25.851(2)	25.757(5)
c / Å	17.787(2)	17.847(4)
β / °	101.50(1)	100.97(2)
Volume / $Å^3$	7907(2)	7928(3)
Z	2	2
Calculated density / g cm^{-3}	1.289	1.272
μ (MoKα) / mm^{-1}	0.110	0.109
F (000)	3296	3284
Temperature / K	173(2)	173(2)
Crystal size / mm^3	0.20 x 0.22 x 0.51	0.18 x 0.25 x 0.45
Theta range scanned / °	1.4 < θ < 22.8	2.8 < θ < 26.4
Index ranges	h: -19: 19; k: -28: 28; l: -19: 19	h: -21: 21; k: -32: 32; l: -22: 22
Total number of reflections	51904	121634
No. of independent reflections	21330	32264
No. of reflections with I > 2σ(I)	18874	27296
No. of parameters	1818	1866
R_{int}	0.027	0.035
$R_1(I > 2\sigma(I))$	0.0559	0.0615
$wR_2(I > 2\sigma(I))$	0.1533	0.1784
S	1.028	1.021
Coefficients in weighting scheme	a = 0.0922, b = 5.2881	a = 0.1132, b = 3.3305
Δρ excursions / e $Å^{-3}$	-0.52, 0.73	-0.48, 1.08

Data collection and space group determination

A Bruker Kappa Apex II Duo diffractometer was used to collect intensity data for DMB·CAF, while a Nonius Kappa CCD diffractometer was used for the complex DMB·FA. The intensity data for both complexes belong to the Laue class *2/m* indicating the monoclinic crystal system.[3] Two space groups ($P2_1$ and $P2_1/m$) were indicated by the reflection conditions *hkl: none, h0l: none, 0k0: k = 2n* and the latter was chosen as the host molecules are chiral. It was evident from the common space group and very similar unit cell dimensions that the two inclusion complexes are isostructural.

Structure solution and refinement

The unit cell parameters of DMB·CAF did not match any of a known isostructural series[1] closely enough and the structure was solved by direct methods using the program SHELXD.[29] A solution was obtained with a final CC value of 85.91 and all the non-hydrogen atoms were assigned and the model was refined using SHELXL.[5] Initially all atoms were refined isotropically and all the non-hydrogen host and guest atoms were located in successive difference Fourier maps. Counter-intuitively, the guest molecule was found to be located outside the CD cavities, forming an 'exclusion complex'. The glucose units were labelled A1 - A7 and B1 - B7 for the two independent DIMEB molecules (Figure 4.46). After the isotropic thermal parameters of the atoms were verified to be stable the atoms were allowed to refine anisotropically, except for two disordered host atoms which were refined isotropically. The s.o.f.s of the major components of the disordered atoms were set to x and the minor parts were set to 1-x. The values of x subsequently refined to 0.46(2) for C741 and 0.70(3) for C841. The guest was found to be disordered over two positions, the s.o.f. of the major component refining to 0.55(1). The guest atoms were refined isotropically. All hydrogen atoms were geometrically constrained to their parent atoms and refined with linked temperature factors.

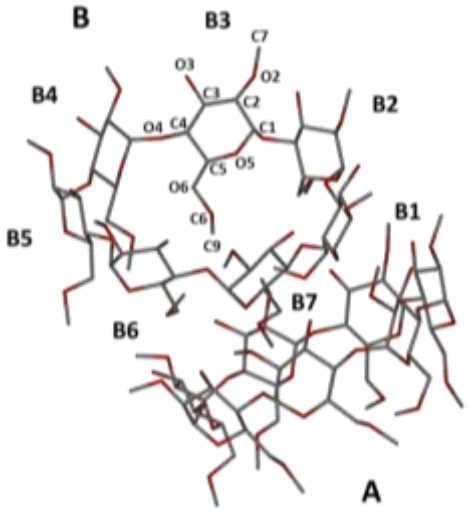

Figure 4.46: Host molecule and guest atom labels of DMB·FA; DMB·CAF host molecules and guest atoms are labelled similarly. Hydrogen atoms are omitted for clarity.

A number of remaining electron density peaks were assigned as water oxygen atoms, based on their peak heights and favourable locations for engagement in H-bonding interactions. The s.o.f.s of these atoms were later adjusted accordingly to match the number of water molecules obtained by TGA, while satisfying the requirement that their thermal displacement parameters should have physically acceptable values. Six water O atoms were refined with full s.o.f.s (O1W, O3W, O5W, O6W, O11W and O14W) while three O atoms were each disordered over two positions (s.o.f.s of their major components refining to 0.54(2) for O4W1, 0.75(2) for O7W1 and 0.69(3) for O8W1). The remaining water O atoms were assigned the partial s.o.f.s listed in Table 4.26. Altogether, 11.9 water O atoms were assigned over 16 sites located in the interstitial spaces between the CD molecules.

Table 4.26: The site-occupancy factors attributed to each water oxygen atom.

Atom	s.o.f.	Atom	s.o.f.	Atom	s.o.f.
O2W1	0.40	O9W1	0.40	O12W	0.50
O2W2	0.30	O9W2	0.40	O13W	0.70
		O9W3	0.20		

The structure of DMB·FA was solved using isomorphous replacement, the coordinates of the host skeletons of the structure obtained for DMB·CAF being used as a trial model. Successive refinement cycles revealed the hydroxyl and methoxyl groups of the host molecules. The glucose rings were labelled as for DMB·CAF. Three atoms on host molecule B were disordered over two positions (C741: s.o.f. 0.43(2), O671 and C871: s.o.f. 0.81(1)). The non-hydrogen atoms of the guest were identified and assigned, also located outside the CD cavities. All atoms were refined anisotropically except for the disordered host atoms, C8A1 and C8A5 of host molecule A and C10 of the guest molecule. Hydrogen atoms were placed as for DMB·CAF.

Fourteen sites were revealed to be populated by water O atoms from the electron density map. Four were found to have full s.o.f.s (O1W, O2W, O3W and O4W). Three atoms were found to be disordered over two positions; the s.o.f. of the major component was set to x and the minor to 1-x. The major components are O5W1 (s.o.f. = 0.67(3)), O6W1 (s.o.f. = 0.57(3)) and O7W1 (s.o.f. = 0.64(2)). A further seven atoms were identified as partially occupied water oxygens with a total s.o.f. of 4.2. A total of 11.2 water O atoms were assigned over 14 sites located only in the interstitial spaces between the host molecules.

The ASU of DMB·CAF consists of two DIMEB molecule, one CAF molecule and 11.9 water molecules and that of DMB·FA consists of two DIMEB molecule, one FA molecule and 11.2 water molecules (Figure 4.47).

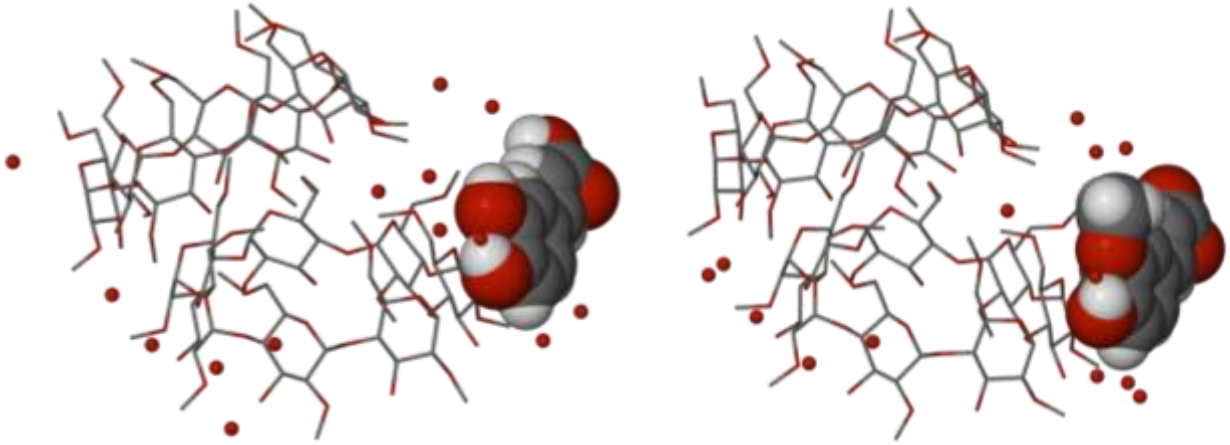

Figure 4.47: The ASU of DMB·CAF (left) and DMB·FA (right) illustrating the guest positioned in the intermolecular space. Host hydrogen atoms are omitted for clarity. Small red spheres represent water oxygen atoms.

Geometrical analysis

Host geometry

The geometric parameters of the O4 heptagon, including deviations of the O4 atoms from the mean O4 plane, the O2n···O3(n-1) distances and the tilt angles τ_1 and τ_2 for the complexes DMB·CAF and DMB·FA are listed in Tables 4.27 and 4.28, respectively.

Table 4.27: Geometric parameters of the DIMEB molecule in the complex DMB·CAF.

Residue	*r* (Å)	*D* (Å)	*α* (°)	*φ* (°)	*d* (°)	D_3 (Å)	*α* (Å)	τ_1 (°)	τ_2 (°)
A1	5.092	4.457	128.8	117.9(5)	1.8	2.860	-0.012(3)	10.5(1)	11.8(3)
A2	5.058	4.411	128.5	119.8(4)	-1.4	2.826	0.035(3)	18.3(1)	18.6(3)
A3	5.057	4.378	130.0	116.4(4)	-1.1	2.941	-0.013(3)	11.8(1)	12.6(3)
A4	5.155	4.457	126.6	117.4(5)	3.3	3.255	-0.037(3)	17.5(1)	18.8(3)
A5	5.065	4.389	129.0	118.3(5)	-3.2	2.846	0.052(3)	18.5(2)	19.0(2)
A6	5.035	4.445	129.8	118.1(5)	1.6	2.844	-0.019(3)	11.5(2)	12.6(3)
A7	5.133	4.355	127.3	118.8(5)	-1.1	2.826	-0.006(3)	15.8(2)	15.9(2)
Mean	**5.09**	**4.41**	**128.6**	**118.1**	**2.1**	**2.91**	**0.029**	**14.8**	**15.6**
B1	5.009	4.438	130.2	119.0(5)	4.5	2.792	-0.120(3)	15.6(1)	17.3(4)
B2	4.978	4.351	129.8	117.1(5)	1.9	2.880	0.007(3)	4.1(1)	3.9(3)
B3	5.093	4.459	128.4	118.2(4)	-3.4	2.987	0.096(3)	20.9(1)	21.6(2)
B4	5.187	4.285	125.4	119.1(4)	-1.1	2.875	-0.037(3)	15.6(1)	16.8(2)
B5	4.951	4.548	131.4	117.0(4)	3.6	2.810	-0.077(3)	9.3(1)	11.0(2)
B6	5.013	4.310	129.6	117.7(5)	0.9	2.877	0.062(3)	14.6(2)	14.5(2)
B7	5.214	4.382	124.9	119.5(5)	-6.1	2.850	0.069(3)	14.7(1)	16.2(3)
Mean	**5.06**	**4.40**	**128.5**	**118.2**	**3.5**	**2.87**	**0.075**	**13.5**	**14.5**

*Average e.s.d. = 0.007 Å

Table 4.28: Geometric parameters of the DIMEB molecule in the complex DMB·FA.

Residue	*r* (Å)	*D* (Å)	*a* (°)	*φ* (°)	*d* (°)	D_3 (Å)*	*α* (Å)	τ_1 (°)	τ_2 (°)
A1	5.057	4.470	129.6	117.8(4)	1.2	2.833	-0.013(2)	10.6(1)	12.5(2)
A2	5.082	4.388	128.2	118.9(4)	0.0	2.873	0.031(2)	18.8(1)	19.0(3)
A3	5.096	4.390	129.0	116.7(3)	-3.0	2.829	0.009(2)	11.5(1)	12.5(1)
A4	5.109	4.493	127.7	117.8(3)	4.5	2.930	-0.061(2)	17.9(1)	18.9(2)
A5	5.074	4.356	128.6	118.2(4)	-3.1	3.291	0.056(2)	18.7(1)	19.7(2)
A6	5.065	4.445	129.5	118.0(4)	0.9	2.846	-0.007(3)	10.1(1)	11.9(2)
A7	5.126	4.362	127.3	118.3(4)	-0.6	2.825	-0.015(2)	16.2(1)	16.3(1)
Mean	**5.09**	**4.41**	**128.6**	**118.0**	**2.4**	**2.92**	**0.035**	**14.8**	**15.8**
B1	5.050	4.417	129.3	118.1(3)	4.8	2.769	-0.109(2)	16.2(1)	17.5(3)
B2	4.951	4.361	130.4	116.7(3)	0.6	2.830	0.018(2)	3.6(1)	3.4(2)
B3	5.058	4.466	129.2	117.9(4)	-2.1	2.970	0.070(2)	19.3(1)	20.2(2)
B4	5.230	4.281	124.4	119.0(3)	-1.2	2.889	-0.026(2)	15.9(1)	17.0(2)
B5	4.973	4.553	131.1	117.2(3)	2.9	2.825	-0.065(2)	10.1(1)	11.9(2)
B6	4.974	4.333	130.5	117.7(4)	1.1	2.875	0.049(2)	16.0(1)	15.7(1)
B7	5.215	4.367	124.8	119.0(4)	-5.8	2.844	0.063(2)	14.1(1)	15.8(2)
Mean	**5.06**	**4.40**	**128.5**	**117.9**	**3.2**	**2.86**	**0.064**	**13.6**	**14.5**

*Average e.s.d. = 0.005 Å

The DIMEB molecules are symmetrical and round for both complexes as can be seen from the narrow ranges in the *r*, *D* and *a* parameters. The round shape of DIMEB molecules is usually attributed to the well-known intramolecular O2n···H-O3(n-1) hydrogen bonds linking neighbouring methylglucose residues. However, in DMB·CAF and DMB·FA the host molecules self-include to form interactions between molecule A and molecule B, disrupting the O2n···H-O3(n-1) hydrogen bonds. The deviations of the O4 atoms from the mean O4 plane (*α*) are small indicating little curvature in the hosts. The tilt angles are positive, making the secondary rim wider than the primary rim.

The primary hydroxyl torsion angle O5-C5-C6-O6 describes the orientation of the C6-O6 bond relative to the CD cavity. The C6-O6 bonds in both the host molecules A and B in CAF·DMB and FA·DMB are similarly orientated. For molecule A, in both cases four of the seven primary methoxyl groups are rotated towards the CD cavity having a (+)-*gauche* conformation. The remaining three O5-C5-C6-O6 torsion angles on residues A3, A4 and A6 are (-)-*gauche*. The torsion angles for molecule B in each structure are (+)-*gauche* on five of the glucose residues and (-)-*gauche* on residues B2 and B5, directed away from the CD cavity. In both CAF·DMB and FA·DMB the primary methoxyl group on residue B7 is included into the CD cavity of host molecule A while the methoxyl group on residue A1 is included into the CD cavity of host molecule B.

The angle between the mean O4 planes of host molecules A and B is 34.4(5)° in CAF·DMB and 34.6(5)° in FA·DMB. The overall geometries of the two independent host molecules in each structure CAF·DMB and FA·DMB are not significantly different. The mean values of each geometrical parameter for the host molecules are also very similar for the two complexes.

Guest exclusion

In each of the structures the guest molecule lies in the interstitial columns between the CD molecules and is flanked by host molecule B as well as host molecules related by unit translations (A' at 1 + x, y, 1 + z; A" at 1 + x, y, z; B' at x, y, 1 + z). The guest molecule is disordered over two positions in DMB·CAF with the major part having a s.o.f. of 0.55(1) while the atoms of the guest molecule in DMB·FA have full occupancy (see Figure 4.48 for non-hydrogen atom labels). In both structures the aromatic rings of the guest molecules are planar and the acrylic functional groups are rotated slightly such that the C4-C7-C8-C9 torsion angle is 178(1)° for the major part of CAF in the structure DMB·CAF and -176(1)° for FA in DMB·FA. The *syn*-conformation of the acid group in CAF is associated with the hydrogen bond O12-H···O2W1.

Figure 4.48: Atom labelling of the guest molecules CAF (left) and FA (right).

Hydrogen bonding interactions

Host-host interactions

The round shape of the host molecules is maintained by the O2(n)-H···O3(n-1) hydrogen bonds. In both structures seven O2(n)-H···O3(n-1) hydrogen bonds exist in host molecule B, however only six interactions exist in host molecule A. These hydrogen bonds are further stabilised by weak O3(n)-H···O4(n) hydrogen bonds and are listed in Tables 4.29 and 4.30. The seventh interaction is a hydrogen bond O3A4-H3A4···O6B6 with an O···H distance of 1.88 Å, a O···O distance of 2.707(7) Å and a bond angle of 168° in DMB·CAF. An analogous bond occurs in DMB·FA with O···H and O···O distances of 1.85 Å and 2.675(5) Å, respectively, and a bond angle of 169° (Figure 4.49).

Two intermolecular interactions occur between the host molecules in DMB·CAF, namely hydrogen bonds O3A4-H3A4···O6B6 and O3B3-H3B3···O6A7 with D···A distances of 2.707(7) Å and 2.999(8) Å, respectively, and D-Ĥ···A angles of 168° and 116°, respectively, where atom O6A7 is at symmetry position 1-x,-1/2+y,-z.

Table 4.29: Parameters for intramolecular host hydrogen bonds in DMB·CAF.

D-H···A	D-H (Å)	H···A (Å)	D···A (Å)	D-H···A (°)
O3A1-H3A1···O2A2	0.84	2.08	2.860(7)	155
O3A2-H3A2···O2A3	0.84	2.01	2.826(6)	162
O3A3-H3A3···O2A4	0.84	2.12	2.941(7)	164
O3A5-H3A5···O2A6	0.84	2.02	2.846(7)	169
O3A6-H3A6···O2A7	0.84	2.01	2.844(8)	170
O3A7-H3A7···O2A1	0.84	2.00	2.826(8)	168
O3B1-H3B1···O2B2	0.84	1.96	2.792(7)	174
O3B2-H3B2···O2B3	0.84	2.08	2.880(7)	159
O3B3-H3B3···O2B4	0.84	2.24	2.987(7)	149
O3B4-H3B4···O2B5	0.84	2.09	2.875(5)	157
O3B5-H3B5···O2B6	0.84	2.00	2.810(7)	162
O3B6-H3B6···O2B7	0.84	2.06	2.877(6)	163
O3B7-H3B7···O2B1	0.84	2.03	2.850(7)	165

Table 4.30: Parameters for intramolecular host hydrogen bonds in DMB·FA.

D-H···A	D-H (Å)	H···A (Å)	D···A (Å)	D-H···A (°)
O3A1-H3A1···O2A2	0.84	2.12	2.883(5)	150
O3A2-H3A2···O2A3	0.84	2.00	2.833(5)	172
O3A3-H3A3···O2A4	0.84	2.10	2.929(5)	168
O3A5-H3A5···O2A6	0.84	2.03	2.848(6)	164
O3A6-H3A6···O2A7	0.84	1.99	2.825(6)	175
O3A7-H3A7···O2A1	0.84	1.99	2.832(5)	174
O3B1-H3B1···O2B2	0.84	1.94	2.779(5)	174
O3B2-H3B2···O2B3	0.84	2.01	2.829(5)	164
O3B3-H3B3···O2B4	0.84	2.59	2.972(5)	109
O3B4-H3B4···O2B5	0.84	2.05	2.887(5)	174
O3B5-H3B5···O2B6	0.84	1.99	2.826(5)	174
O3B6-H3B6···O2B7	0.84	2.11	2.886(5)	153
O3B7-H3B7···O2B1	0.84	2.01	2.845(5)	173

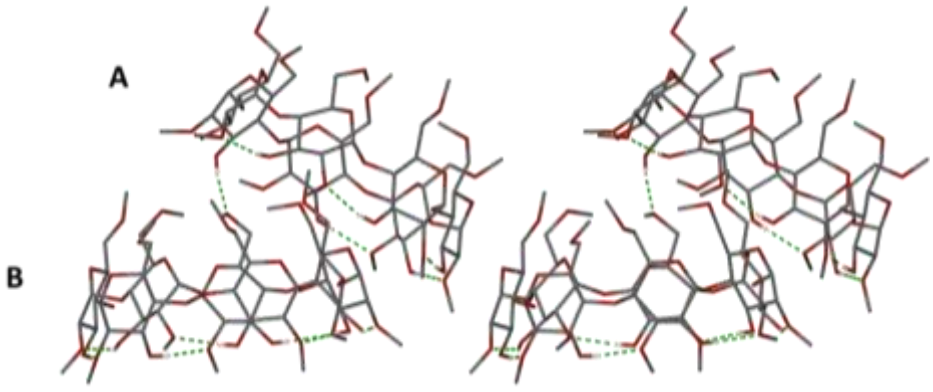

Figure 4.49: A stereodiagram illustrating both the intramolecular hydrogen bonds in the independent host molecules in DMB·FA and that between the two host molecules. The hydrogen atoms not involved in hydrogen bonding are omitted for clarity.

Further weak interactions of the type C-H···O provide cumulative strength to the crystal. These interactions are both intramolecular and intermolecular; the parameters of the latter are listed in Tables 4.31 and 4.32. The intramolecular interactions span a D···A range of 2.770(5) Å to 3.491(6) Å and a D-Ĥ···A range of 100° to 162° in the complex DMB·CAF and, similarly in the complex DMB·FA, a D···A range of 2.776(6) Å to 3.430(9) Å and a D-Ĥ···A range of 100° to 155°.

Table 4.31: Parameters for intermolecular host-host hydrogen bonds in DMB·CAF.

D-H···A	D-H (Å)	H···A (Å)	D···A (Å)	D-H···A (°)	Symmetry Operation
C8A3-H8A2···O5B4*	0.98	2.40	3.351(8)	165	1-x,1/2+y,1-z
C2B7-H2B7···O3A6	1.00	2.54	3.502(9)	162	-
C6B6-H6B4···O2A5	0.99	2.26	3.170(10)	153	-
C1A4-H1A4···O3B4*	1.00	2.44	3.351(7)	152	1-x,1/2+y,1-z
C7A5-H7AI···O6B2*	0.98	2.51	3.394(12)	149	-1+x,y,z
C6A7-H6AB···O2B4*	0.99	2.47	3.352(10)	147	1-x,1/2+y,-z
C1A2-H1A2···O3B6*	1.00	2.47	3.247(9)	134	1-x,1/2+y,-z

*The atom to which the symmetry operation applies.

Table 4.32: Parameters for intermolecular host-host hydrogen bonds in DMB·FA.

D-H···A	D-H (Å)	H···A (Å)	D···A (Å)	D-H···A (°)	Symmetry Operation
C8A3-H8A2···O5B4*	0.98	2.42	3.368(6)	163	1-x,1/2+y,1-z
C2B7-H2B7···O3A6	1.00	2.59	3.563(6)	163	-
C8A3-H8A1···O3B1*	0.98	2.56	3.498(6)	160	1-x,1/2+y,-z
C4B4-H4B4···O6A3*	1.00	2.57	3.526(5)	160	1-x,-1/2+y,1-z
C6B6-H6B8···O2A5	0.99	2.24	3.188(8)	160	-
C1A4-H1A4···O3B4*	1.00	2.50	3.430(6)	154	1-x,1/2+y,1-z
C7A5-H7AF···O6B2*	0.98	2.52	3.431(10)	154	-1+x,y,z
C6A7-H6AX···O2B4*	0.99	2.45	3.315(8)	145	1-x,1/2+y,-z
C1A2-H1A2···O3B6*	1.00	2.46	3.249(6)	136	1-x,1/2+y,-z

*The atom to which the symmetry operation applies.

Guest intramolecular interactions and host-guest interactions

Two relevant intramolecular hydrogen bonds are O10-H10···O11 (O···O = 2.579(2) Å, O-Ĥ···O = 118° in DMB·CAF and O1-H1···O2 (D···A = 2.695(9) Å, D-Ĥ···A = 112°) in DMB·FA. A host-guest interaction occurs between the FA molecule in DMB·FA and a DMB molecule A (1+x,y,z) with a O···O distances of 2.636(6) Å and a O-Ĥ···O angle of 166°.

Water Interactions

The guest molecule in DMB·FA interacts with a neighbouring water O atom to form the hydrogen bond O1-H1···O9W (D···A = 2.939(9) Å and D-Ĥ···A = 159°). Also, within this complex the host molecule interacts with a water O atom to form a hydrogen bond O3B3-H3B3···O11W with a D···A distance of 2.739(8) Å and a D-Ĥ···A angle of 106°. The remaining hydrogen bonds can be inferred by the presence of O···O close contacts, where the D···A distance is within hydrogen bonding range; however, the hydrogen atoms involved in the hydrogen bond are not modelled. These close contacts are listed in Tables 4.33 and 4.34 and illustrated in Figures 4.50 and 4.51.

Table 4.33: Parameters for hydrogen bonds involving water in DMB·CAF.

D-H···A	D···A (Å)	Symmetry Operation	D-H···A	D···A (Å)	Symmetry Operation
O1W···O4W2	2.828(17)	-	O3A5···O3W	2.788(7)	-
O1W···O4W1	2.824(15)	-	O3A6···O9W3*	2.96(3)	-1+x,y,-1+z
O14W···O4W2	2.814(17)	-	O5A6···O6W	2.923(9)	-
O14W···O4W1	2.799(14)	-	O6A4···O2W2*	2.684(19)	-1+x,y,z
O11W···O9W1*	2.857(19)	-1+x,y,-1+z	O6A6···O6W	3.040(9)	-
O11W···O9W3*	2.54(3)	-1+x,y,-1+z	O3B1···O13W*	3.085(12)	x,y,-1+z
O5W···O2W1	2.892(19)	-	O3W···O3B2*	2.947(8)	-x,1/2+y,-z
O5W···O2W2	2.728(19)	-	O3B3···O8W1	2.765(10)	-
O6W···O7W1*	2.947(13)	-1+x,y,z	O3B3···O8W2	3.09(2)	-
O12A···O2W1	3.03(3)	-	O3B5···O14W	2.822(8)	-
O12A···O2W2	2.94(3)	-	O3B7···O11W	2.771(7)	-
O12W···O12B	2.89(4)	-	O5B4···O12W	3.079(13)	-
O6W···O11A*	2.519(17)	-1+x,y,-1+z	O5B5···O1W	3.032(7)	-
O3A1···O7W1	2.917(10)	-	O6B3···O10W	2.773(12)	-
O3A1···O7W2	2.99(2)	-	O6B4···O12W	3.084(15)	-
O3A2···O5W	2.844(8)	-	O6B5···O1W	3.190(7)	-

*The atom to which the symmetry operation applies.

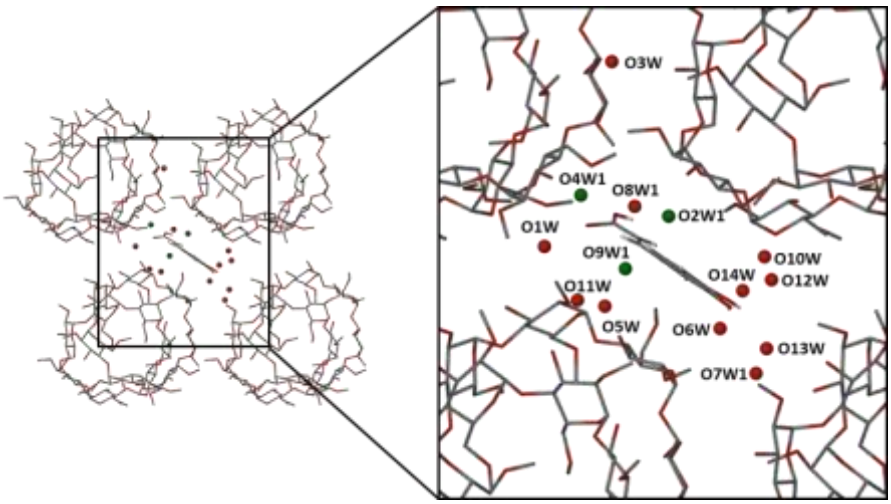

Figure 4.50: A random view (minimising molecule overlap) of the interstitial water molecules in DMB·CAF with their respective labels. Atoms shown in green are not directly bonded to the CD.

Table 4.34: Parameters for hydrogen bonds involving water in DMB·FA.

D-H···A	D···A (Å)	Symmetry Operation	D-H···A	D···A (Å)	Symmetry Operation
O1W···O3W*	2.756(7)	1-x,-1/2+y,-z	O3A1···O6W	2.985(10)	-
O1W···O14W	2.733(14)	-	O3A1···O6W2	2.958(17)	-
O2W···O7W1	2.838(12)	-	O3A2···O3W	2.854(6)	-
O2W···O7W2	2.91(2)	-	O6A4···O10W*	2.867(11)	1-x,-1/2+y,1-z
O3W···O5W1	2.816(12)	-	O3A5···O4W	2.789(7)	-
O8W···O12W	2.774	-	O3B1···O9W*	3.100(8)	x,y,-1+z
O4W1···O10W	2.755	-	O3A6···O14W	2.870(13)	-
O6W1···O9W*	2.858	x, y, z-1	O3B2···O4W*	2.982(6)	1+x,y,z
O1W···O2W*	2.782	x, y, z-1	O3B5···O8W*	2.848(9)	1-x,1/2+y,1-z
O7W1···O5W2*	2.706	1-x, y-1/2, 1-z	O3B7···O1W	2.722(6)	-
O7W1···O11W*	2.871	x-1, y, z	O5B5···O2W	2.996(6)	-
O7W2···O11W*	2.748	x-1, y, z	O6B5···O2W	3.209(7)	-
O4W1···O5W1*	2.821	2-x, ½+y, 1-z	O1···O10W	2.680(11)	-
O9W1···O6W1*	2.858	x, y, 1+z	O2···O9W	2.976(11)	-
O8W···O7W1*	2.777	1-x, ½+y, 1-z	O3···O5W1	2.905(12)	-
O4W1···O14W*	2.671	x-1, y, z-1	O3···O5W2	3.12(2)	-

*The atom to which the symmetry operation applies.

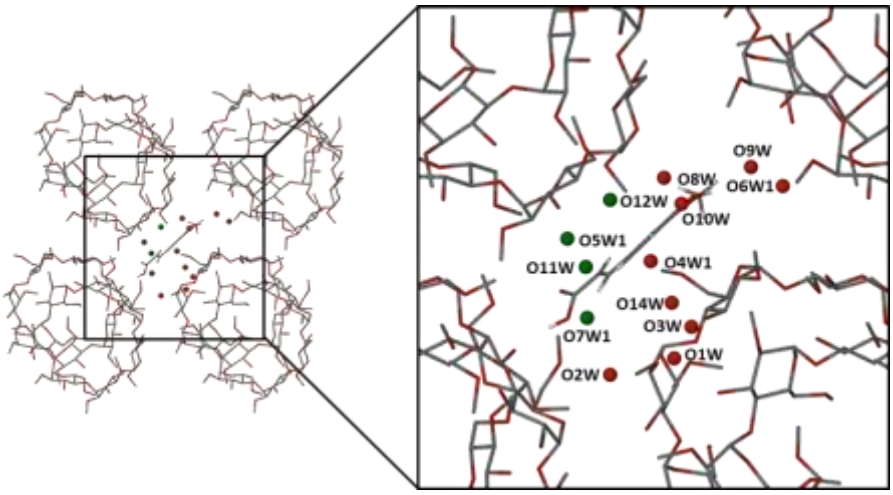

Figure 4.51: A random view (minimising molecule overlap) of the interstitial water molecules in DMB·FA with their respective labels. Atoms shown in green are not directly bonded to the CD.

Crystal packing

The crystallographically independent DMB molecules A and B pack in spiralling columns parallel to the *b*-axis as shown in Figure 4.52. The guest molecules and water O atoms are located in interstitial columns also parallel to the *b*-axis (Figure 4.53).

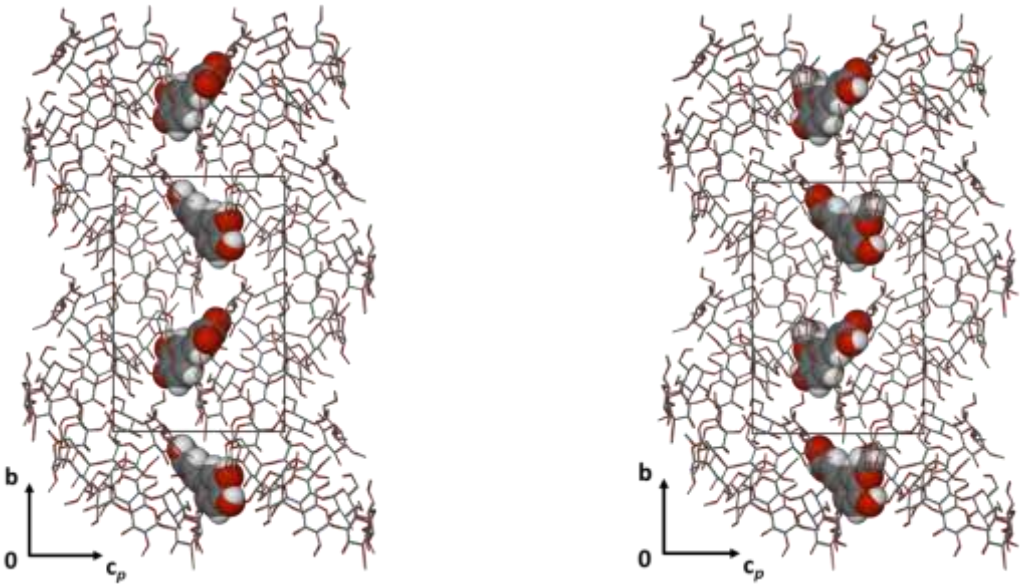

Figure 4.52: The packing arrangement in DMB·CAF (left) and DMB·FA (right) viewed down the *a*-axis. Host hydrogen atoms are omitted for clarity.

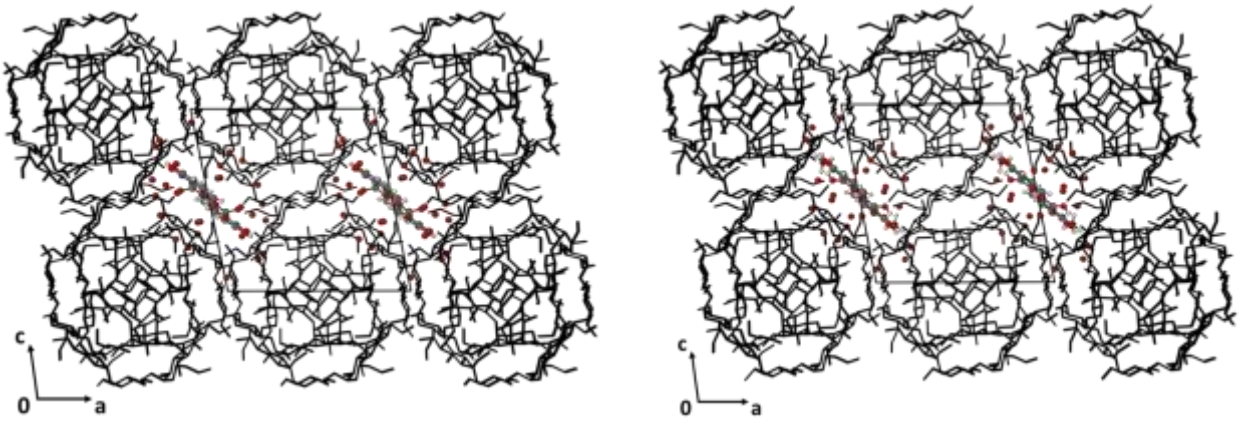

Figure 4.53: The packing arrangement in DMB·CAF (left) and DMB·FA (right) viewed down the *b*-axis. Water molecules are illustrated as red dots. Host molecules are shown in black and hydrogen atoms are omitted for clarity.

Comparative PXRD

The experimental and calculated PXRD patterns for both DMB·CAF and DMB·FA were compared to confirm that the respective crystals chosen for single crystal X-ray diffraction were representative of the bulk products. The correlation of the peaks indicates that the samples used for diffraction are the same crystalline phase as the bulk coprecipitation material (Figures 4.54 and 4.55). Comparing the PXRD patterns of the two complexes confirms that they are isostructural. The relative intensities of the peaks differ, particularly for the DMB·FA complex, and this is attributed to preferred orientation of the sample during PXRD analysis.

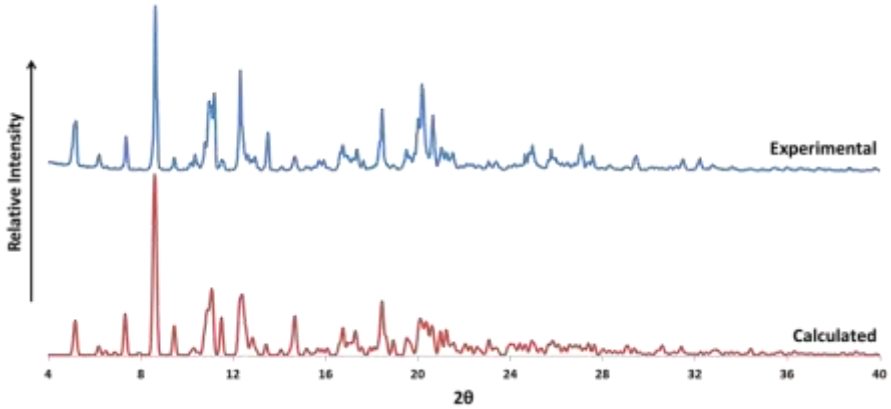

Figure 4.54: Comparison of the experimental and calculated PXRD traces for DMB·CAF.

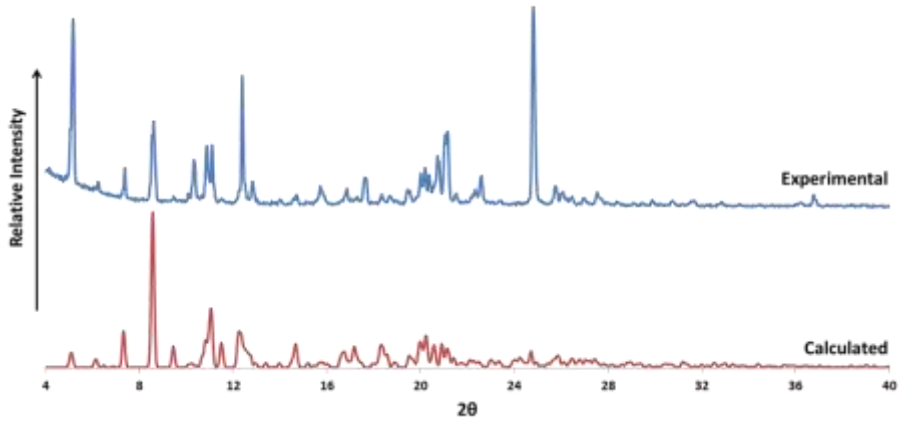

Figure 4.55: Comparison of the experimental and calculated PXRD traces for DMB·FA.

DIMEB INCLUSION COMPLEXES WITH HYDROFERULIC ACID AND *p*-COUMARIC ACID (DMB·HFA and DMB·PCA)

Thermal analysis

TGA reveals that for both samples there is a mass loss in the range 25 °C to 100 °C of 4.2 ± 0.2 % for DMB·HFA and 3.9 ± 0.7 % for DMB·PCA (Figures 4.56 and 4.57). These values equate to the loss of 3.7 ± 0.2 and 3.4 ± 0.6 water molecules per complex unit for DMB·HFA and DMB·PCA, respectively. This is followed by a two-step mass loss from 100 °C to 300 °C for DMB·HFA and single-step mass loss from 180°C to 300 °C for DMB·PCA, corresponding to the loss of the respective guest molecules from the complexes. The guest loss was determined as 1.1 ± 0.1 for DMB·HFA and 1.0 ± 0.1 for DMB·PCA per complex unit (13.2 ± 0.3 % and 10.5 ± 0.2 %, respectively). The DSC traces show broad endotherms from 25 °C to 100 °C corresponding to the water loss event. A number of small, sharp endotherms follow, occurring at 134 °C and 180 °C for DMB·HFA and at 158 °C and 282 °C for DMB·PCA. The former in each case may be due to phase transformations which occur as the crystals are heated, while the latter occurs with guest loss. The DSC trace of DMB·HFA also shows a very broad endotherm over the range 225 °C to 325 °C, which corresponds to the second mass loss step in the TGA.

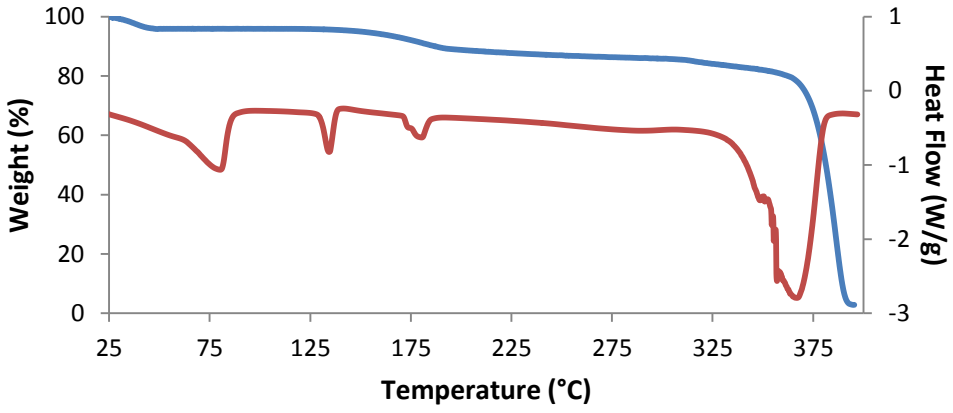

Figure 4.56: DSC (red) and TGA (blue) curves of DMB·HFA.

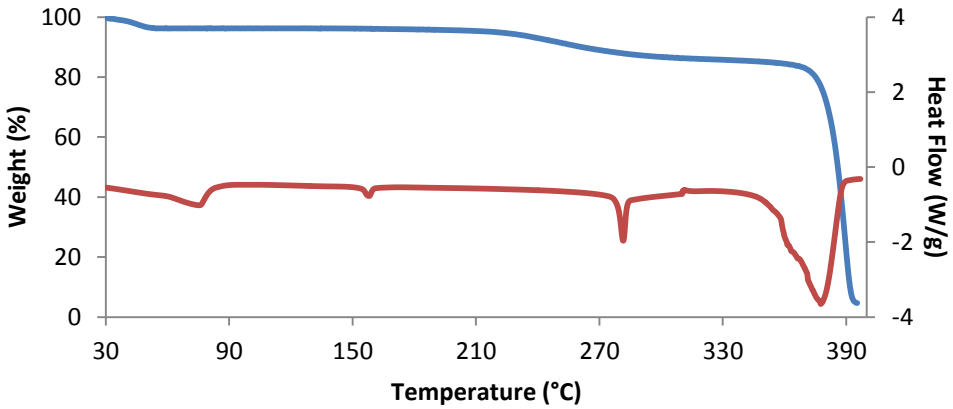

Figure 4.57: DSC (red) and TGA (blue) curves of DMB·PCA.

Figure 4.58 shows HSM photographs of the complex DMB·HFA immersed in silicone oil. From 100 °C bubbles of water vapour are released from the crystal and it turns opaque as it is heated further, possibly due to a phase transformation (the first sharp endotherm seen in the DSC). As the crystal is heated to 190 °C it appears to become more transparent, possibly due to another phase transformation (the second small endotherm seen in the DSC). Decomposition begins at ca. 330 °C, indicated by discolouration of the crystal and bubbling as the decomposition products are released.

30 °C **110 °C** **130 °C** **190 °C** **290 °C**

Figure 4.58: HSM photographs of the complexes DMB·HFA.

The crystal of DMC·PCA is clear at room temperature (Figure 4.59). As the crystal is heated it appears to fracture and become opaque. At 100 °C bubbling begins as water vapour is expelled from the complex. At 160 °C the crystal appears to expand slightly due to a possible phase transformation. Bubbles are released from the crystal again at 220 °C as the guest is released in gaseous form and decomposition begins at ca. 330 °C, indicated by discolouration of the crystal.

30 °C **70 °C** **120 °C** **220 °C** **287 °C** **353 °C**

Figure 4.59: HSM photographs of the complexes DMB·PCA.

Single crystal X-ray analysis of the complexes DMB·HFA and DMB·PCA

Data collection and space group determination

The crystallographic data and refinement parameters for each structure are listed in Table 4.35.

Table 4.35: Crystallographic data for the complexes DMB·HFA and DMB·PCA.

	DMB·HFA	**DMB·PCA**
Complex Formula	**$C_{56}H_{98}O_{35}\cdot C_{10}H_{12}O_4\cdot 3.85H_2O$**	**$C_{56}H_{98}O_{35}\cdot C_9H_8O_3\cdot 3.2H_2O$**
Formula weight	1596.89	1553.14
Crystal system	Orthorhombic	Orthorhombic
Space group	$P2_12_12_1$ (No. 19)	$P2_12_12_1$ (No. 19)
a / Å	14.732(1)	15.006(3)
b / Å	18.840(1)	19.033(4)
c / Å	29.205(2)	27.615(6)
Volume / $Å^3$	8106(1)	7887(3)
Z	4	4
Calculated density / g cm^{-3}	1.309	1.308
μ (MoKα) / mm^{-1}	0.110	0.109
F (000)	3426	3328
Temperature / K	173(2)	173(2)
Crystal size / mm^3	0.34 x 0.36 x 0.42	0.34 x 0.36 x 0.42
Theta ranges scanned / ˚	1.4 < θ < 28.4	2.8 < θ < 26.4
Index ranges	h: -19: 19; k: -25: 25; l: -39: 38	h: -18: 18; k: -23: 23; l: -34: 34
Total number of reflections	60872	103377
No. of independent reflections	20262	16089
No. of reflections with I > 2σ(I)	16933	13862
No. of parameters	1035	955
R_{int}	0.033	0.034
$R_1(I > 2\sigma(I))$	0.0499	0.0609
$wR_2(I > 2\sigma(I))$	0.1358	0.1698
S	1.010	1.038
Coefficients in weighting scheme	a = 0.0726, b = 3.0041	a = 0.0918, b = 5.9490
Δρ excursions / e $Å^{-3}$	-0.43, 0.59	-0.60, 0.82

Intensity data for DMB·HFA were collected on a Bruker KAPPA APEX II DUO diffractometer and for DMB·PCA on a Nonius KappaCCD diffractometer. For both complexes, the Laue group was found to be *mmm* indicating the orthorhombic crystal system and systematic absences confirmed the space group $P2_12_12_1$.[3]

Structure solution and refinement

The two structures were solved by direct methods using SHELXD.[29] While the cell parameters of the structures nearly match those of an isostructural series, they did not match closely enough to use isomorphous replacement to solve the structures.[1] Many of the non-hydrogen host and guest atoms were assigned and the partial structure was refined with isotropic thermal parameters using the full-matrix least-squares technique carried out using SHELXL.[5]

The remaining non-hydrogen atoms were revealed by successive Fourier maps and assigned appropriately. The host glucopyranose rings were labelled G1 to G7 and disordered atoms were labelled by parts (see Figure 4.60 for host atom labels and Figure 4.61 for guest atom labels.). After the U_{iso} values were found to be stable upon refinement the non-hydrogen atoms were refined anisotropically, except for disordered atoms. Disorder was identified and major components were assigned s.o.f. values of x while the minor components were assigned s.o.f. values of 1-x. The disordered atoms comprise the chain C641-O641-C841 (s.o.f. = 0.71(1)) for the host molecule of DMB·HFA, C10A (s.o.f. = 0.57(2)) for the guest molecule of DMB·HFA and the chain of atoms C661-O661-C861 (s.o.f. = 0.54(1)) for the host molecule of DMB·PCA. The bond lengths were constrained to chemically reasonable values to maintain the fragment geometries. Hydrogen atoms were placed in idealised positions using a riding model and assigned U_{iso} values 1.2 times and 1.5 times those of their parent atoms. The hydroxyl hydrogen atoms of the host molecules were placed using the electron density searching model (AFIX 147). While the hydrogen atoms of the guest molecules appeared on the difference Fourier map, they were placed in idealised positions using the AFIX 147 command. The aromatic rings of the respective guest molecules were not restrained.

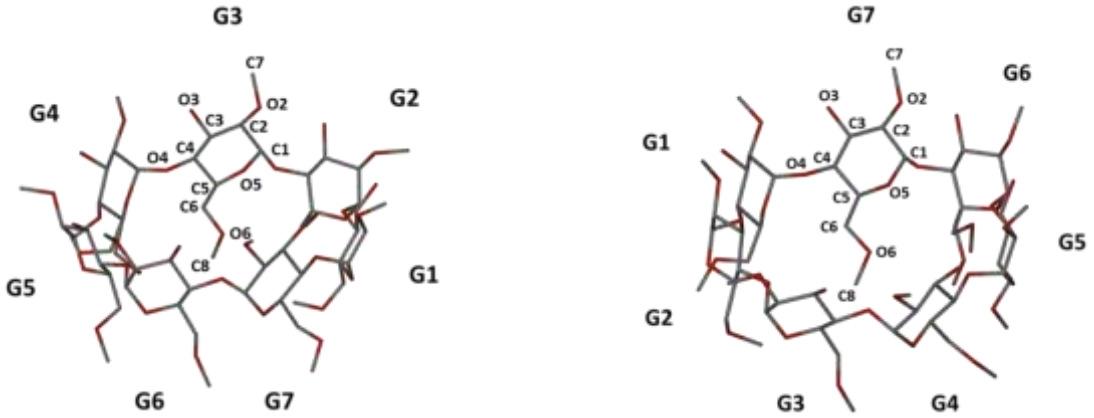

Figure 4.60: Labelling of the glucopyranose units of the macrocycles in DMB·HFA (left) and DMB·PCA (right).

Figure 4.61: Labelling of the guest molecules in DMB·HFA (left) and DMB·PCA (right).

Electron density peaks found not to be part of the host or guest molecules were assigned as water oxygen atoms, provided that they engaged in at least one hydrogen bond interaction in the structures. In DMB·HFA five water oxygen atom sites were identified and assigned, totalling 3.7 water molecules per asymmetric unit (ASU). In DMB·PCA six water oxygen atom sites were identified and assigned, totalling 3.85 water molecules. Hydrogen atoms were assigned from the difference Fourier map on water oxygen atoms O1W, O2W, O3W and O4W only in DMB·PCA, using a DFIX constraint (O-H = 0.84 Å) to set the bond lengths and the DANG command (H···H = 1.34 Å) to set the bond angle H-Ô-H.

The ASU of DMB·HFA consists of one DIMEB molecule, one HFA molecule and 3.7 water molecules and that of DMB·PCA consists of one DIMEB molecule, one PCA molecule and 3.8 water molecules (Figure 4.62).

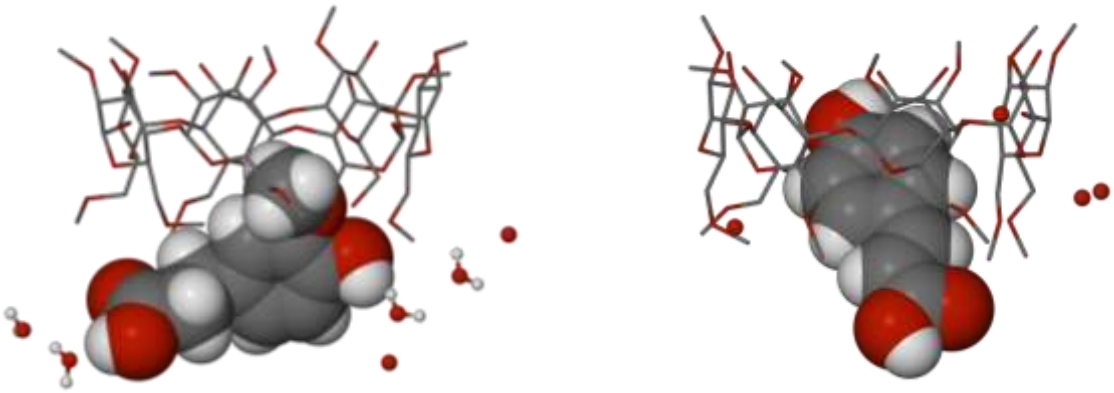

Figure 4.62: The asymmetric units of DMB·HFA (left) and DMB·PCA (right).

Geometrical analysis

Host Geometry

The geometrical parameters (defined and discussed in Chapter 1) of the host molecules of DMB·HFA and DMB·PCA are listed in Tables 4.36 and 4.37, respectively.

Table 4.36: Geometric parameters of the DIMEB molecule in the complex DMB·HFA.

Residue	*r* (Å)	*D* (Å)	*a* (°)	*φ* (°)	*d* (°)	D_3 (Å)	*α* (Å)	τ_1 (°)	τ_2 (°)
G1	5.304	4.181	120.3	119.7(2)	-14.5	2.796(3)	-0.284(2)	17.3(1)	16.7(1)
G2	4.768	4.618	135.0	116.4(2)	2.3	2.868(4)	0.158(2)	13.3(1)	18.0(2)
G3	4.899	4.265	130.6	117.7(2)	8.3	2.865(3)	0.164(2)	4.0(1)	4.5(2)
G4	5.324	4.291	121.4	118.5(2)	-2.0	2.898(4)	-0.183(2)	12.4(1)	12.6(1)
G5	4.980	4.477	131.0	117.3(2)	-8.1	2.942(3)	-0.097(2)	19.8(1)	20.6(1)
G6	4.845	4.377	130.3	118.1(2)	3.4	2.787(3)	0.206(2)	9.9(1)	12.0(1)
G7	5.042	4.373	129.6	117.1(2)	10.1	2.843(3)	0.035(2)	3.8(1)	5.0(1)
Mean	**5.00**	**4.37**	**128.3**	**117.8**	**8.2**	**2.86**	**0.177**	**11.5**	**12.8**

Table 4.37: Geometric parameters of the DIMEB molecule in the complex DMB·PCA.

Residue	*r* (Å)	*D* (Å)	*α* (°)	*φ* (°)	*d* (°)	D_3 (Å)	*α* (Å)	τ_1 (°)	τ_2 (°)
G1	5.116	4.384	128.4	118.3(3)	3.2	2.776(5)	0.162(3)	12.9(1)	13.9(2)
G2	4.978	4.410	129.2	118.9(3)	7.1	2.826(6)	0.099(2)	8.6(1)	3.9(2)
G3	4.950	4.411	130.2	117.8(3)	-4.0	2.975(5)	-0.172(2)	20.1(1)	4.3(1)
G4	5.146	4.330	127.4	118.4(3)	-5.0	2.833(5)	-0.035(2)	18.4(1)	6.9(2)
G5	5.175	4.413	124.7	119.3(3)	4.4	2.816(5)	0.176(2)	5.8(1)	8.0(2)
G6	4.835	4.527	134.3	116.8(3)	6.5	2.894(5)	0.022(2)	12.0(1)	1.6(1)
G7	5.137	4.226	124.8	119.9(3)	-11.4	2.812(5)	-0.208(2)	19.6(1)	7.2(2)
Mean	**5.05**	**4.39**	**128.4**	**118.5**	**6.5**	**2.85**	**0.142**	**13.9**	**6.5**

The tables show that the parameter values deviate significantly from the respective average values and the host molecule is slightly elliptical in shape. The D_3 values indicate that hydrogen bond interactions are possible between O3-H and the O2 atom of the adjacent glucose rings. The tilt angles (τ_1 and τ_2) are all positive indicating that the primary rims of the glucose rings are tilted towards the CD cavities. The primary sides of the CDs are narrower than the secondary sides, but both sides of the host molecules remain open.

The rotation of the C6-O6 bond relative to the CD cavity is described by the torsion angle O5-C5-C6-O6 (ω). The torsion angles ω indicating a (-)-*gauche* conformation reflect that the C6-O6 bonds are directed away from the CD cavity while the torsion angles indicating (+)-*gauche* conformation refer to C6-O6 bonds that are directed towards the CD cavity. The torsion angles of DMB·HFA on glucose residues G2, G4 (major component), G5, G6 and G7 are (-)-*gauche* while those on residues G1 and G3 are (+)-*gauche*. The (-)-*gauche* torsion angle of the *O*-methyl moiety on G2 facilitates the inclusion of this methyl group into the CD cavity of an adjacent CD molecule at the secondary side. Similarly, the torsion angles ω in the complex DMB·PCA on residues G1, G3, G4 and G6 are (-)-*gauche* and those on residues G2, G5 and G7 are (+)-*gauche*. The *O*-methyl group on residue G1 is included into an adjacent CD cavity at the secondary side.

Guest inclusion

Space-filling diagrams are shown in Figures 4.63 to 4.66 and illustrate the modes of inclusion of the guest molecules in DMB·HFA and DMB·PCA. The guest molecule in DMB·HFA protrudes into the interstitial space while the *O*-methyl substituent on the aromatic ring lies within the primary ethyl skirt of the CD, bound by van der Waals interactions. The aromatic ring of the PCA molecule in DMB·PCA is included into the CD cavity while the acid tail protrudes from the primary end into the interstitial space.

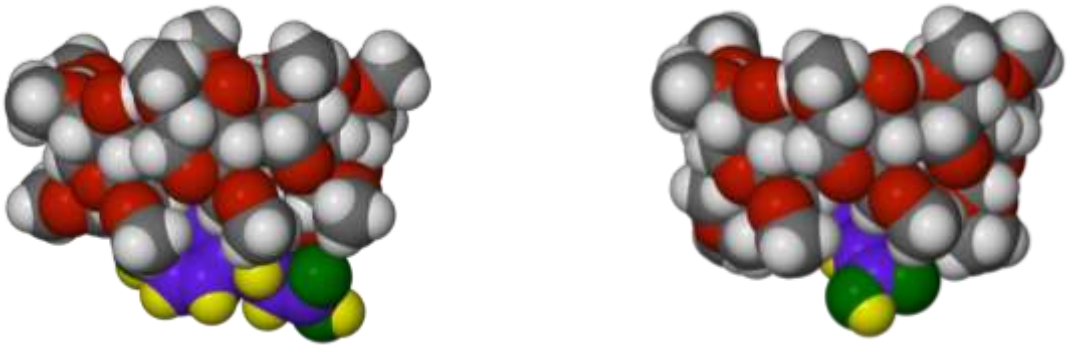

Figure 4.63: CPK diagrams of DMB·HFA (left) and DMB·PCA (right) viewed side-on.

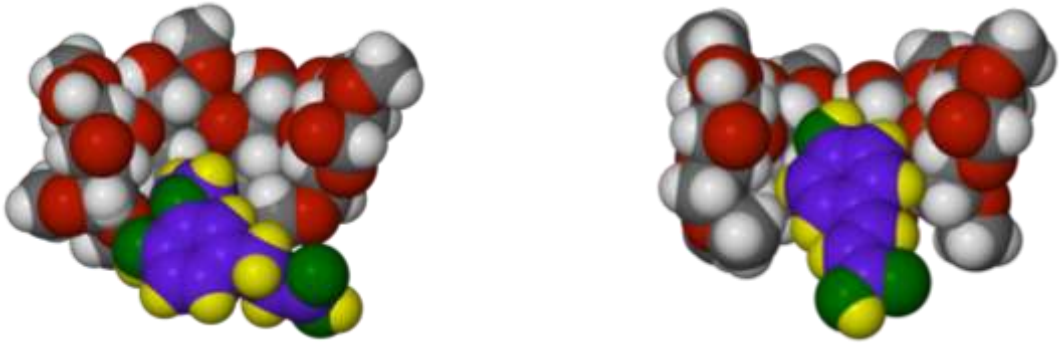

Figure 4.64: CPK diagrams of DMB·HFA (left) and DMB·PCA (right): cutaway side-on images.

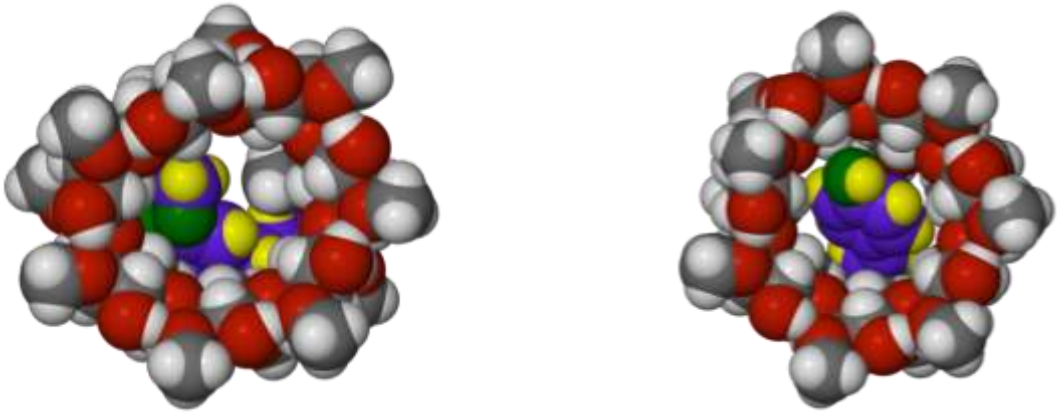

Figure 4.65: CPK diagrams of DMB·HFA (left) and DMB·PCA (right) viewed from the CD secondary end.

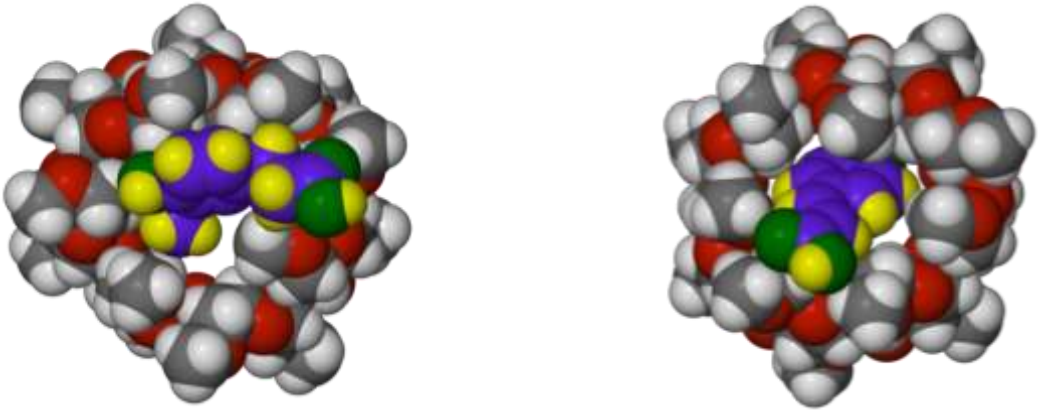

Figure 4.66: CPK diagrams of DMB·HFA (left) and DMB·PCA (right) viewed from the CD primary end.

Hydrogen bonding interactions

Intramolecular host interactions

The O2n···H-O3(n-1) interactions which exist between glucopyranose units are common to both the DMB·HFA and PCA·DMB complexes (Tables 4.38 and 4.39), and are typical of the majority of DIMEB structures. These hydrogen bonds are reinforced by the weaker O3(n)-H···O4(n) interactions.

Table 4.38: Parameters for intramolecular host-host hydrogen bonds in DMB·HFA.

D-H···A	D-H (Å)	H···A (Å)	D···A (Å)	D-H···A (°)
O3G1-H3G1···O2G2	0.84	2.06	2.868(4)	161
O3G2-H3G2···O2G3	0.84	2.04	2.865(3)	167
O3G3-H3G3···O2G4	0.84	2.08	2.898(4)	163
O3G4-H3G4···O2G5	0.84	2.18	2.942(3)	151
O3G5-H3G5···O2G6	0.84	1.96	2.787(3)	169
O3G6-H3G6···O2G7	0.84	2.02	2.843(3)	165
O3G7-H3G7···O2G1	0.84	1.99	2.796(3)	160

Table 4.39: Parameters for intramolecular host-host hydrogen bonds in DMB·PCA.

D-H···A	D-H (Å)	H···A (Å)	D···A (Å)	D-H···A (°)
O3G1-H3G1···O2G2	0.84	2.01	2.826(6)	162
O3G2-H3G2···O2G3	0.84	2.15	2.975(5)	168
O3G3-H3G3···O2G4	0.84	2.04	2.833(5)	157
O3G4-H3G4···O2G5	0.84	1.99	2.816(5)	166
O3G5-H3G5···O2G6	0.84	2.06	2.894(5)	172
O3G6-H3G6···O2G7	0.84	2.00	2.812(5)	162
O3G7-H3G7···O2G1	0.84	1.94	2.776(5)	171

A number of weak C-H···O hydrogen bonding interactions exist in both structures, having D···A distances in the range 2.839(3) Å to 3.511(5) Å and bond angles of 100°to 158° for DMB·HFA and, similarly for DMB·PCA, D···A distances of 2.898(6) Å to 3.354(7) Å with bond angles of 101° to 155°.

Host-guest interaction

One host-guest interaction exists in the complex DMB·PCA: the *p*-hydroxyl group forms a hydrogen bond with atom O6G2 of the host (O1-H···O6G2) with hydrogen bond parameters H···A = 1.93 Å, D···A = 2.718(4) Å and D-Ĥ···A = 157°.

Water-water, host-water and guest-water interactions

The water molecules are confined to discrete interstitial “pockets” formed between host molecules and form various hydrogen bonding interactions with host and guest molecules (Tables 4.40 and 4.41). These interactions add stability to the crystal structure. Figure 4.67 shows the relevant interactions with labels while Figures 4.68 and 4.69 show the interactions as stereodiagrams.

Table 4.40: Parameters for hydrogen bonds involving water in DMB·HFA.

Type	D-H···A	D-H (Å)	H···A (Å)	D···A (Å)	D-H···A (°)	Symmetry Operation
Guest-water	O1-H1A···O4W	0.84	1.89	2.671(6)	154	-
Guest-water	O4-H4···O1W	0.84	1.84	2.674(4)	170	-
Water-water	O1W-H1W2···O3W	0.84(4)	1.88(4)	2.700(5)	166(5)	-
Water-host	O1W-H1W1···O6G5	0.83(4)	2.09(5)	2.873(3)	155(5)	-1/2+x,1/2-y,-z
Water-host	O2W-H2W2···O3G7	0.83(3)	2.18(5)	2.853(4)	138(6)	1/2-x,1-y,1/2+z
Water-host	O3W-H3W2···O3G5	0.82(6)	2.24(5)	2.966(4)	148(6)	-1/2+x,1/2-y,-z
Water-host	O3W-H3W1···O3G4	0.84(6)	2.00(6)	2.795(5)	159(5)	1/2-x,1-y,-1/2+z
Guest-water	O4W-H4W1···O1	0.82(8)	2.07(8)	2.671(6)	130(7)	-
Water-host	O2W···O641	-	-	2.869(18)	-	-
Water-host	O4W···O3G2	-	-	2.885(5)	-	x-1/2, 3/2-y, -z
Water-water	O4W···O6W	-	-	2.708(30)	-	-
Water-water	O4W···O2W	-	-	2.793(5)	-	-
Water-water	O2W···O5W	-	-	2.826(5)	-	-
Water-host	O5W···O3G1	-	-	2.831(18)	-	x-1/2, 3/2-y, -z

*The atom to which the symmetry operation applies.

Table 4.41: Parameters for hydrogen bonds involving water in DMB·PCA.

Type	D-H···A	D-H (Å)	H···A (Å)	D···A (Å)	D-H···A (°)	Symmetry Operation
Guest-water	O11-H11···O1W*	0.84	1.84	2.635(6)	159	1/2+x,1/2-y,2-z
Water-water	O1W···O4W*	-	-	2.856(6)	-	1/2-x, 1-y, 1/2+z
Water-host	O5G6···O1W	-	-	2.973(5)	-	-
Water-host	O661···O1W	-	-	2.910(7)	-	-
Water-host	O4W···O6G3	-	-	2.827(6)	-	-
Water-host	O4W···O3G7*	-	-	2.838(6)	-	-x, y-1/2, 5/2-z
Water-water	O2W···O3W	-	-	2.719(5)	-	-
Water-host	O2W···O3G3*	-	-	2.834(8)	-	-x,-1/2+y,3/2-z
Water-water	O3W···O6W	-	-	2.985(30)	-	-
Water-host	O3W···O6G4*	-	-	2.735(12)	-	1/2-x,1-y,1/2+z
Water-host	O6W···O5G5	-	-	2.885(30)	-	-

*The atom to which the symmetry operation applies.

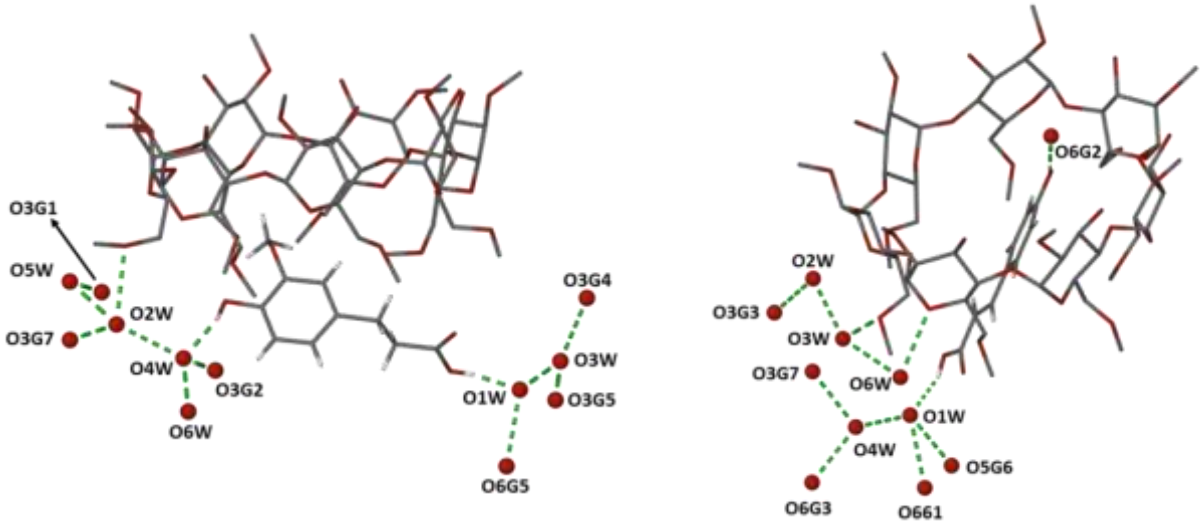

Figure 4.67: Hydrogen bonding interactions between the host and water molecules as well as the guest and water molecules, including water O atom labels, for DMB·HFA (left) and DMB·PCA (right). The host hydrogen atoms are omitted for clarity.

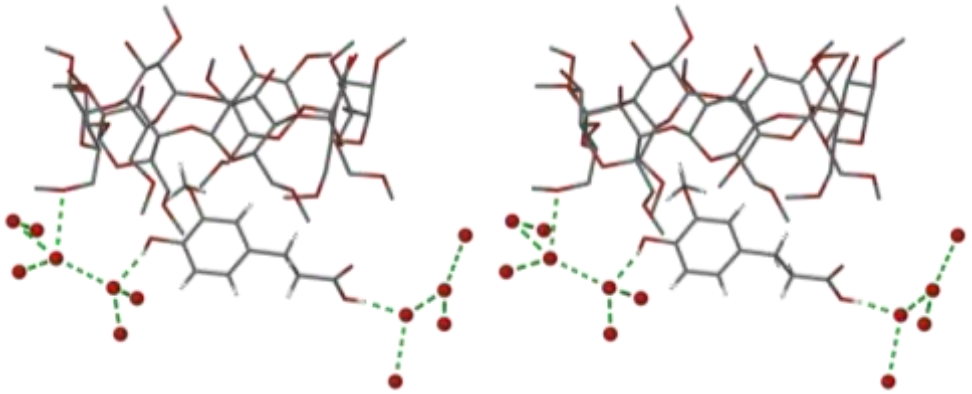

Figure 4.68: A stereodiagram illustrating the hydrogen bonding motif present in the DMB·HFA complex.

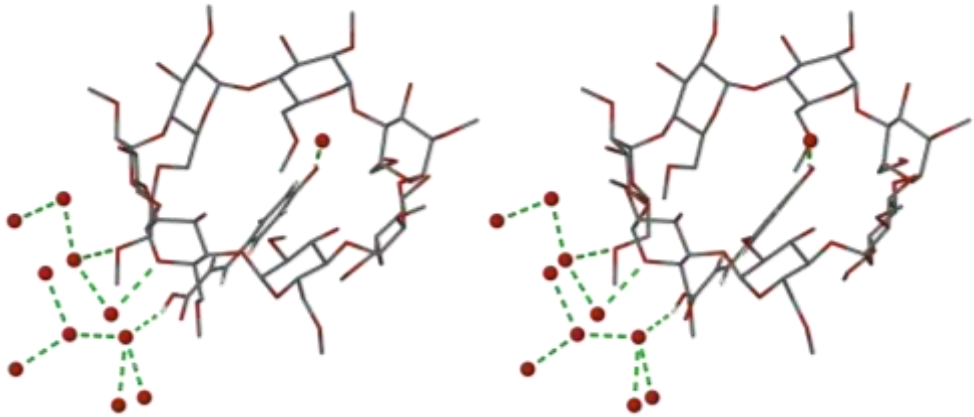

Figure 4.69: A stereodiagram illustrating the hydrogen bonding motif present in the DMB·PCA complex.

Intermolecular interactions

A number of C-H···O intermolecular hydrogen bonds exist between host molecules and symmetry-related host molecules, guest molecules and water O atoms. These interactions have a cumulatively stabilising effect on the structure and are listed in Tables 4.42 and 4.43.

Table 4.42: Parameters for host-host hydrogen bonds in DMB·HFA.

D-H···A	D-H (Å)	H···A (Å)	D···A (Å)	D-H···A (°)	Symmetry Operation
C2G2-H2G2···O3G5*	1.00	2.50	3.471(4)	164	-1/2+x,3/2-y,-z
C2G1-H2G1···O6G5*	1.00	2.48	3.470(4)	170	1/2-x,1-y,-1/2+z
C8G7-H8G9···O3	0.98	2.55	3.514(6)	167	-
C6G5 H6G5···O1	0.99	2.58	3.545(5)	166	-
C2G6-H2G6···O3*	1.00	2.53	3.279(4)	131	1/2+x,1/2-y,-z
C8-H8A···O6G6*	0.99	2.49	3.384(4)	150	-1/2+x,1/2-y,-z
C7G2-H7GY···O2W*	0.98	2.59	3.394(5)	139	1/2+x,3/2-y,-z

*The atom to which the symmetry operation applies.

Table 4.43: Parameters for host-host hydrogen bonds in DMB·PCA.

D-H···A	D-H (Å)	H···A (Å)	D···A (Å)	D-H···A (°)	Symmetry Operation
C861-H96B···O3G3*	0.98	2.59	3.403(12)	141	1/2-x,1-y,1/2+z
C7G2-H7G4···O3G5*	0.98	2.52	3.335(7)	140	1/2+x,3/2-y,2-z
C7G5-H7GB···O3G1*	0.98	2.55	3.266(7)	130	-1/2+x,3/2-y,2-z
C2G7-H2G7···O6G4*	1.00	2.56	3.497(6)	155	1/2-x,1-y,1/2+z
C8G5-H8G8···O12	0.98	2.54	3.466(11)	158	-
C1G6-H1G6···O12*	1.00	2.38	3.308(9)	154	-1/2+x,1/2-y,2-z
C5G1-H5G1···O10	1.00	2.56	3.517(6)	160	-
C4G4-H4G4···O2W	1.00	2.53	3.376(9)	142	-
C1G1-H1G1···O3W	1.00	2.42	3.417(12)	176	-
C8G4-H8GE···O3W*	0.98	2.56	2.917(15)	101	1/2-x,1-y,-1/2+z
C7G7-H7GZ···O4W*	0.98	2.55	3.365(10)	141	-1/2+x,3/2-y,2-z
C7G4-H7G8···O3W*	0.98	2.49	3.462(13)	172	-1/2+x,3/2-y,2-z

*The atom to which the symmetry operation applies.

Crystal packing

The DIMEB molecules stack along the *a*-axis in a zig-zag fashion. The host molecules are related by a two-fold screw axis forming columns parallel to the *a*-axis (Figure 4.70). The secondary side of the CD is blocked by the primary end of an adjacent CD molecule such that the *O*-methyl group O6G1-C8G1 of the latter host molecule includes into cavity of the former host molecule. The consecutive columns lie antiparallel, propagating in the *b*-direction (Figure 4.71). Figure 4.72 illustrates the different modes of inclusion of the guest molecules in each complex.

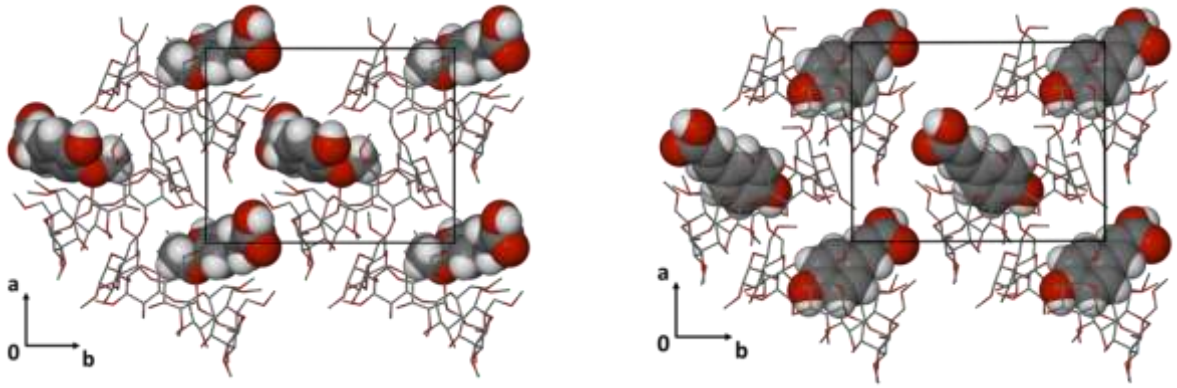

Figure 4.70: The packing arrangement in DMB·HFA (left) and DMB·PCA (right) viewed along the [0 0 1] direction. Host hydrogen atoms are omitted for clarity.

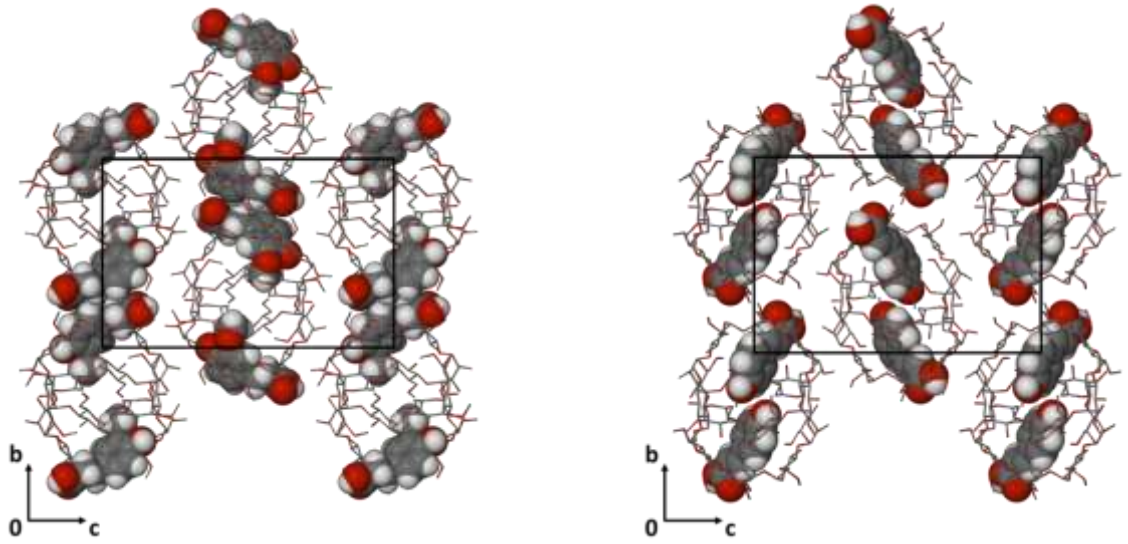

Figure 4.71: The packing arrangement in DMB·HFA (left) and DMB·PCA (right) viewed along the [1 0 0] direction. Host hydrogen atoms are omitted for clarity.

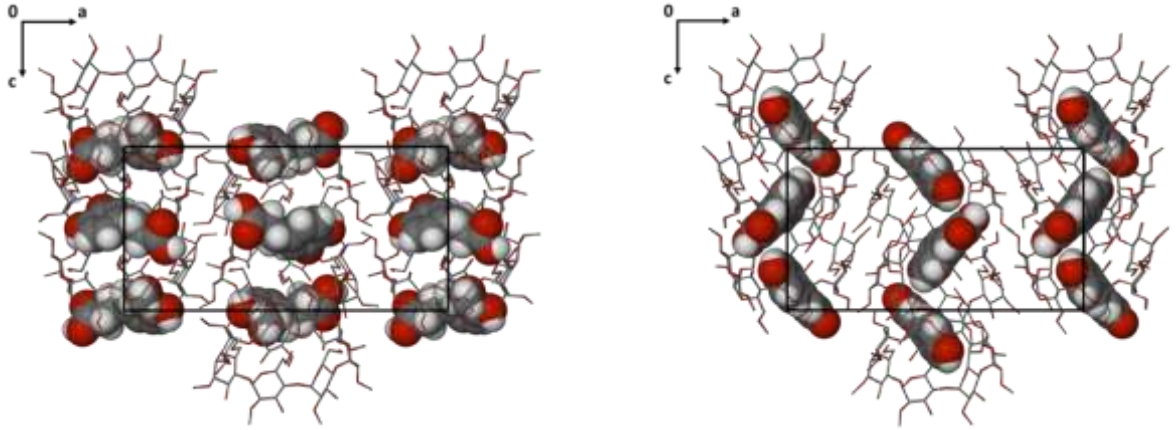

Figure 4.72: The packing arrangement in DMB·HFA (left) and DMB·PCA (right) viewed along the [0 1 0] direction. Host hydrogen atoms are omitted for clarity.

Comparative PXRD

The PXRD patterns calculated from the single crystal X-ray structures were compared with the respective experimental patterns (Figures 4.73 and 4.74). The calculated patterns were in good agreement with the experimental patterns for both DMB·HFA and DMB·PCA. When comparing the PXRD pattern of one structure with that of the other it is clear that there are some similarities involving a number of peaks matching in their 2θ values. However, while the host assemblies of the two complexes are nearly isostructural, the molecular structures and the locations of the guest molecules differ significantly, with the result that the two complexes present different overall PXRD profiles.

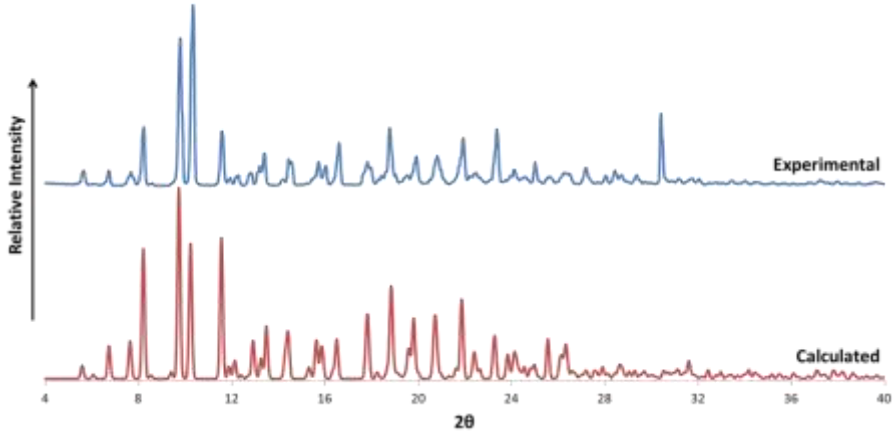

Figure 4.73: Comparison of the experimental and calculated PXRD traces for DMB·HFA.

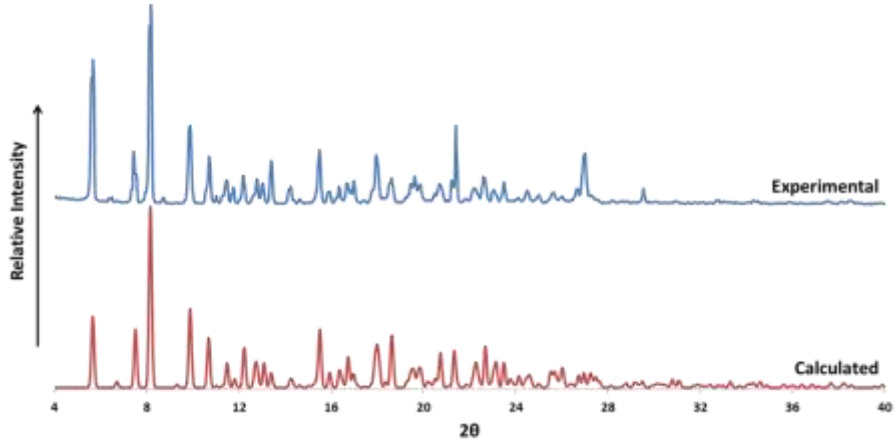

Figure 4.74: Comparison of the experimental and calculated PXRD traces for DMB·PCA.

TRIMEA INCLUSION COMPLEX WITH FERULIC ACID (TMA·FA)

Thermal analysis

TGA, DSC and HSM were used to determine the thermal behaviour of TMA·FA (Figures 4.75 and 4.76). The TGA analysis shows a mass loss of 1.3 ± 0.2 % (n = 3) over the temperature range 30 °C to 150 °C. This equates to 1.3 ± 0.1 water molecules per complex unit. The mass loss corresponds to the broad endotherm observed in the DSC curves over the same range. A phase transformation is evident in the DSC trace at 160 °C, and can be physically observed in the HSM photographs. The complex melts, as indicated by the sharp endotherm in the DSC trace at 185 °C and shown in the HSM photographs at 190°C. The melt is followed by a broad endotherm over the range 175 °C to 300 °C, seen concurrently as a mass loss of 13.8 ± 0.2 % (n = 3) in the TGA trace, which equates to a guest loss of 1.0 ± 0.1 per complex unit. Decomposition occurs above 330 °C.

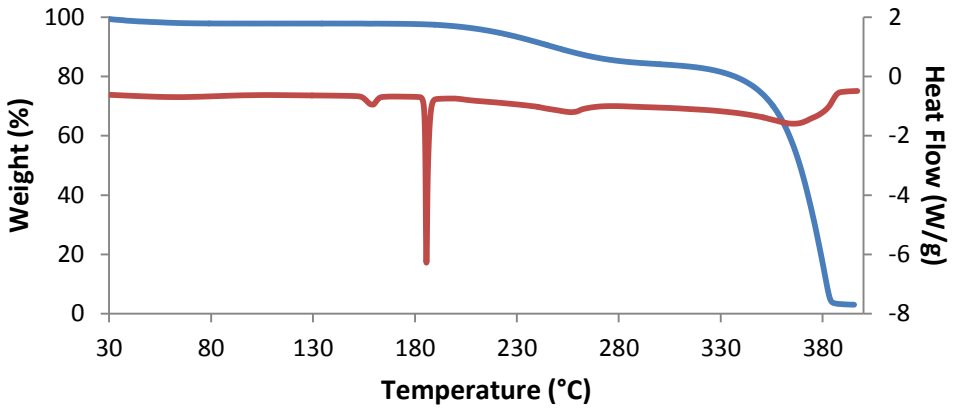

Figure 4.75: DSC (red) and TGA (blue) curves of TMA·FA.

30 °C **100 °C** **160 °C** **190 °C**

Figure 4.76: HSM photographs of the complex TMA·FA.

Single crystal X-ray analysis of the complex TMA·FA

Data collection and space group determination

The single crystal X-ray diffraction data were collected on a Nonius KappaCCD diffractometer. Using the program LAYER to inspect the reciprocal lattice layers the Laue symmetry was found to be 2/*m*, indicating the monoclinic crystal system.[3] Due to the chiral nature of the host molecule and the conditions limiting the reflections (*hkl: none, h0l: none, 0k0: k = 2n*) the space group $P2_1$ was identified as the correct one. The crystallographic data and refinement parameters for the structure are listed in Table 4.44.

Structure solution and refinement

The structure of TMA·FA was solved using direct methods implemented in program SHELXD.[29] The solution obtained had a final correlation coefficient (CC) of 85.9 and revealed most of the non-hydrogen host and guest atoms (Figures 4.77 and 4.78 show the atom labels for the host and guest molecule). The remaining atoms were located after successive full-matrix least-squares refinements using SHELXL.[5] The glucose units were labelled G1 – G7 and disordered atoms were labelled by parts. All atoms were allowed to refine anisotropically except for the disordered atoms O641-C941/O642-C942 and the methyl carbon atoms C9G1, C7G3 and C7G1. Hydrogen atoms were placed in geometrically constrained positions in a riding model with U_{iso} values 1.2 times and 1.5 times those of their parent atoms. Hydroxyl hydrogen atoms were modelled using the AFIX 147 command.

Table 4.44: Crystallographic data for the complex TMA·FA.

	TMA·FA
Complex Formula	**$C_{54}H_{96}O_{30}·C_{10}H_{10}O_4·1.25H_2O$**
Formula weight	1442.00
Crystal system	Monoclinic
Space group	$P2_1$ (No. 4)
a / Å	11.123(2)
b / Å	23.701(5)
c / Å	14.310(3)
β / °	103.02(3)
Volume / $Å^3$	3675(2)
Z	2
Calculated density / g cm^{-3}	1.303
μ (MoKα) / mm^{-1}	0.106
F (000)	1549
Temperature / K	173(2)
Crystal size / mm^3	0.10 x 0.22 x 0.41
Theta range scanned / °	2.5 < θ < 26.4
Index ranges	h: -13: 13; k: -29: 29; l: -17: 17
Total number of reflections	58828
No. of independent reflections	14934
No. of reflections with I > 2σ(I)	13151
No. of parameters	923
R_{int}	0.036
$R_1(I > 2σ(I))$	0.0421
$wR_2(I > 2σ(I))$	0.1032
S	1.028
Coefficients in weighting scheme	a = 0.0488, b = 1.2570
Δρ excursions / e $Å^{-3}$	-0.40, 0.62

Two electron density peaks in the difference Fourier map were identified as not being part of either the host or the guest and were assigned as water oxygen atoms. One site was fully occupied while the water oxygen atom at the second was assigned an s.o.f. of 0.25 based on the abnormally high thermal parameter obtained when it was treated as a full atom. The total water content modelled (1.25 molecules per complex unit) is in good agreement with the estimate from TGA (1.3 ± 0.1). Hydrogen atoms were added to O1W from the difference Fourier map ensuring that appropriate hydrogen bonding interactions were formed with the host molecule. The O-H bond lengths were fixed at 0.84(1) Å and a DANG command was used to fix the H-Ô-H bond (H···H distance = 1.34(4) Å).

The asymmetric unit of TMA·FA consists of one TMA molecule, one FA molecule and 1.25 water molecules (Figure 4.79).

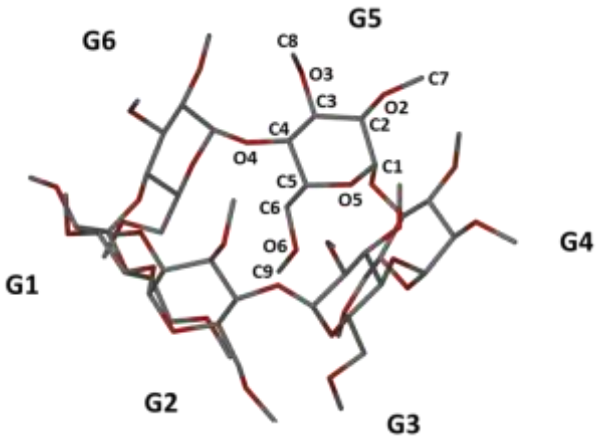

Figure 4.77: Labelling of the glucopyranose units of the host molecule.

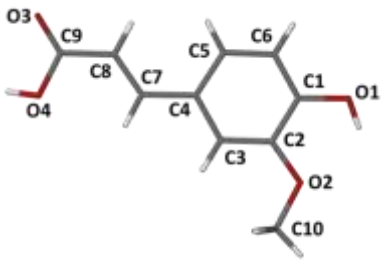

Figure 4.78: The conformation and atom labelling of the guest molecule.

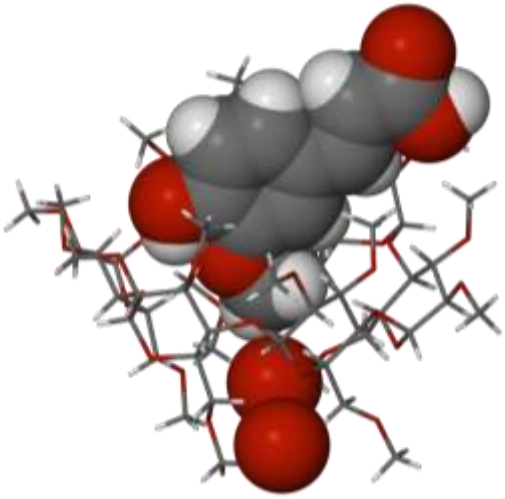

Figure 4.79: The asymmetric unit of the complex TMA·FA. Host hydrogen atoms are omitted for clarity and water O atoms are shown as red spheres.

Geometrical analysis

Host geometry

The conformations indicated by the primary methoxyl torsion angles (ω) for the TMA molecule are listed in Table 4.45. These angles are described as being (+)- or (-)-*gauche* such that (+)-*gauche* indicates that the C6-O6 bond is directed towards the CD cavity while the (-)-*gauche* designation indicates that it is directed away from the cavity.

Table 4.45: O5-C5-C6-O6 Torsion angles (ω) in the complex TMA·FA.

Residue	ω (°)	Conformation
G1	82.1(3)	(+)-gauche
G2	-80.9(3)	(-)-gauche
G3	69.0(4)	(+)-gauche
G4 major part	61.5(5)	(+)-gauche
G5	71.3(3)	(+)-gauche
G6	-71.9(3)	(-)-gauche

The geometrical parameters described previously in Chapter 1 are listed in Table 4.46. The parameters *r*, *D* and *a* indicate that the host molecule is slightly elliptical in shape. The tilt angles τ_1 and τ_2 are positive indicating that the primary rims of the glucopyranose rings are inclined towards the CD cavity. The largest tilts of the glucopyranose residues occur at the extremities of the major axis of the ellipse. The very significant extents of tilt of residues G1 and G4 coupled with the (+)-*gauche* conformation of their O6 methoxyl groups result in closure of the primary side of the TMA molecule (Figure 4.80).

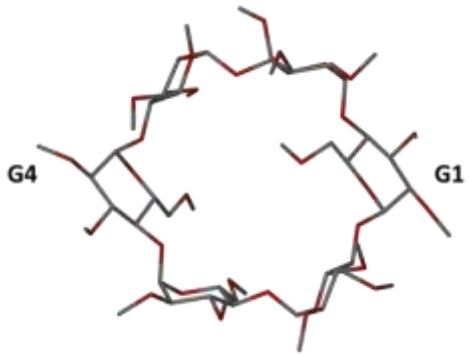

Figure 4.80: The host CD viewed from the secondary end illustrating its elliptical shape.

Table 4.46: Geometric parameters of the TRIMEA molecule in the complex TMA·FA.

Residue	*r* (Å)	*D* (Å)	*a* (°)	φ (°)	*d* (°)	D_3 (Å)*	α (Å)	τ_1 (°)	τ_2 (°)
G1	4.239	4.324	119.9	118.3(2)	-13.3	3.508	0.084(1)	40.1(1)	41.1(1)
G2	4.133	4.396	122.2	118.1(2)	17.7	3.536	-0.336(2)	3.5(1)	7.7(1)
G3	4.457	4.093	113.0	119.6(2)	-5.0	3.299	0.253(2)	9.2(8)	11.8(1)
G4	4.142	4.379	124.4	115.7(2)	-12.3	3.612	0.070(1)	35.8(1)	38.2(1)
G5	4.192	4.239	119.0	118.4(2)	17.2	3.456	-0.324(1)	6.8(1)	10.4(1)
G6	4.340	4.162	117.8	118.3(2)	-5.0	3.244	0.253(1)	4.9(1)	8.7(1)
Mean	**4.25**	**4.27**	**119.4**	**118.1**	**11.9**	**3.44**	**0.226**	**16.7**	**19.7**

*Average e.s.d. = 0.003 Å

Guest inclusion

The guest molecule is not deeply inserted into the cavity of the CD; only the *O*-methyl moiety is included at the secondary side by hydrophobic interactions (Figure 4.81). A hydrogen bond between the guest *p*-OH group and the glycosidic host atom O4G4 contributes significantly to complex formation. The acid tail of the FA molecule protrudes into the intermolecular space.

The angle between the O4 mean plane of TMA and the mean plane through the aromatic ring of FA is 85.1(5)° and the distance of the *O*-methyl carbon atom to the O4 mean plane is 0.31(5) Å. The guest

molecule is planar, as indicated by the torsion angles C3-C2-O2-C10 = -3.0(5)°, C5-C4-C7-C8 = 1.4(5)° and C7-C8-C9-O4 = -6.3(4)°.

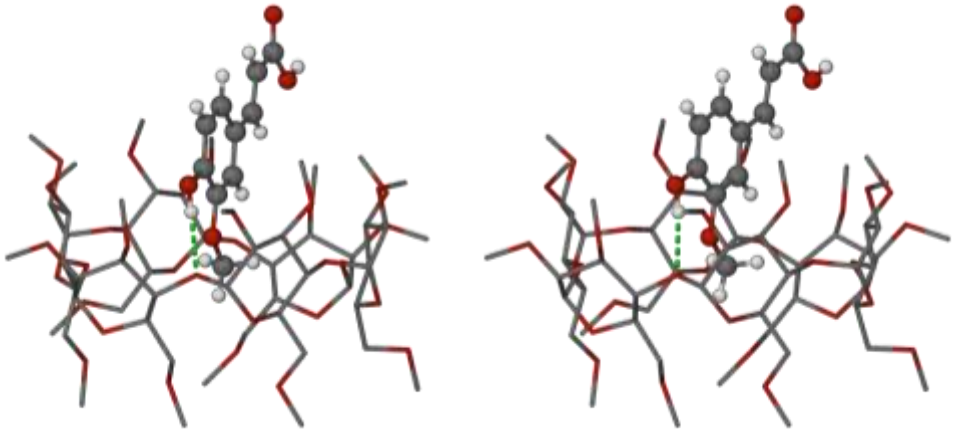

Figure 4.81: A stereodiagram illustrating the position of the guest within the host cavity.

Hydrogen bonding interactions

Strong host-guest, guest-guest and water interactions

Figure 4.82 illustrates the host-guest, guest-guest and water interactions as a stereodiagram. An intramolecular hydrogen bond exists between the O1-H and O2 atoms of the guest molecule (D···A = 2.654(3) Å, D-Ĥ···A = 114°). The O1-H group also interacts with the host O atom O4G4 (D···A = 3.031 (3) Å, D-Ĥ···A = 149°). The guest molecule further interacts with a symmetry-related host molecule through O4-H···O3G5[a] (D···A = 2.748(3) Å, D-Ĥ···A = 170°, a = -x, -1/2+y, -z). Water molecule O1W forms hydrogen bonds O1W-H1W1···O5G6 (D···A = 2.890(4) Å, D-Ĥ···A = 130(5)°) and O1W-H1W1···O5G6[b] (D···A = 2.815(4) Å, D-Ĥ···A = 164(5)°, b = 1-x, ½+y, -z). A close contact exists between the partially occupied O2W (s.o.f. = 0.25) and O6G5 with a D···A distance of 2.758(12) Å, consistent with hydrogen bonding.

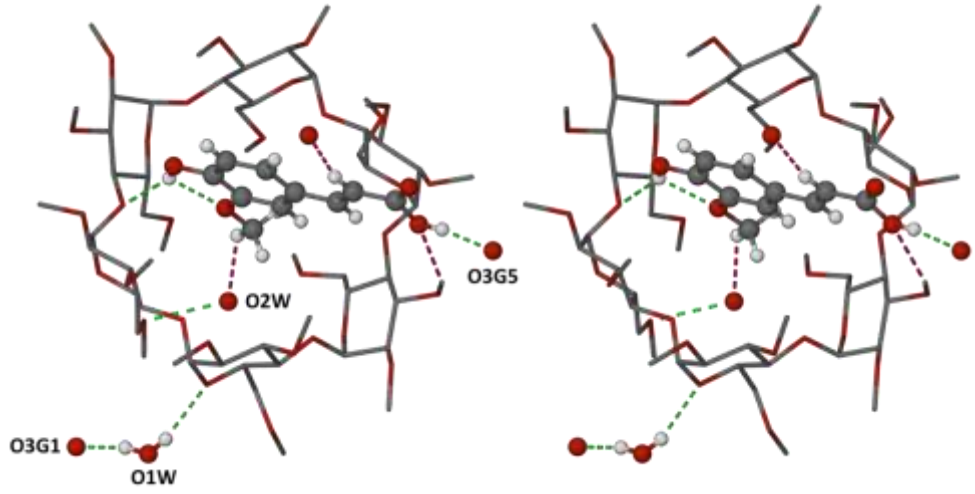

Figure 4.82: A stereodiagram illustrating the hydrogen bonding motifs in the structure of TMA·FA. The green broken lines indicate O-H···O hydrogen bonds while the purple broken lines indicate C-H···O hydrogen bonds.

Weak interactions

There are six C-H···O hydrogen bonds of the type C6G(n)-H···O5G(n-1) having an average D···A distance of 3.318(4) Å and an average D-Ĥ···A of 144°, which support the positive tilt angles. The structure is stabilised by the weak C-H···O interactions listed in Table 4.47, namely one host-host intermolecular interaction, one guest intramolecular interaction, three host-guest interactions, one host-water interaction and one guest-water interaction.

Table 4.47: Parameters for hydrogen bonds involving water in TMA·FA.

D-H···A	D-H (Å)	H···A (Å)	D···A (Å)	D-H···A (°)	Symmetry Operation
C7G6-H7G6···O3G3*	0.98	2.40	3.335(5)	160	x,y,-1+z
C7-H7···O4	0.95	2.49	2.811(4)	100	-
C8-H8···O5G1*	0.95	2.46	3.371(4)	162	-1+x,y,z
C4G5-H4G5···O3*	1.00	2.40	3.300(4)	149	-x,1/2+y,-z
C8G1-H8G4···O4	0.98	2.50	3.130(4)	122	-
C1G4-H1G4···O1W*	1.00	2.36	3.328(4)	163	x,y,1+z
O2W···C10	-	-	3.307(13)	-	-

*The atom to which the symmetry operation applies.

The structure is further stabilised by host C-H···O intramolecular interactions with a D···A distance range of 2.781(4) Å to 3.420(5) Å and a D-Ĥ···A angle range of 100° to 159°.

Crystal packing

The TMA molecules pack in a head-to-tail fashion forming columns parallel to the *b*-axis (Figure 4.83). The columns propagate in the *c*-direction to form layers (Figure 4.84). Figure 4.85 shows the adjacent layers of columns which lie anti-parallel, being related by a two-fold screw axis.

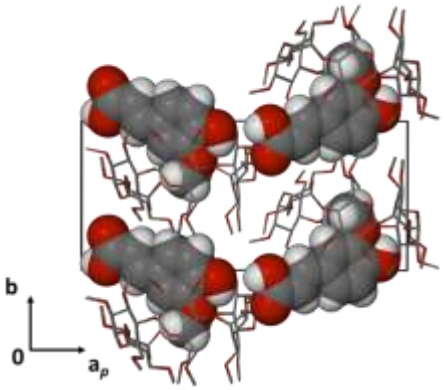

Figure 4.83: Packing diagram of TMA·FA viewed down the *c*-axis. Host hydrogen atoms are omitted for clarity.

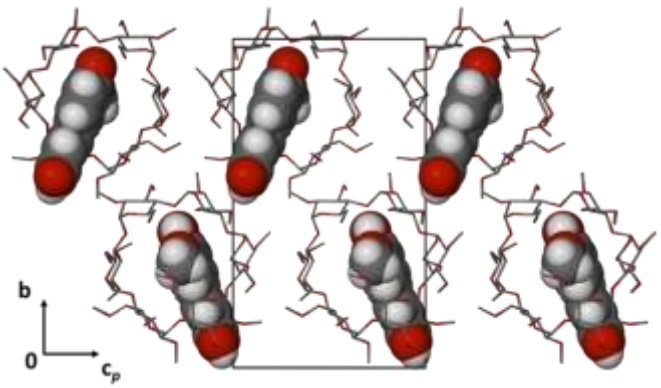

Figure 4.84: Packing diagram of TMA·FA viewed down the *a*-axis illustrating the columns formed parallel to the *a*-axis. Host hydrogen atoms are omitted for clarity.

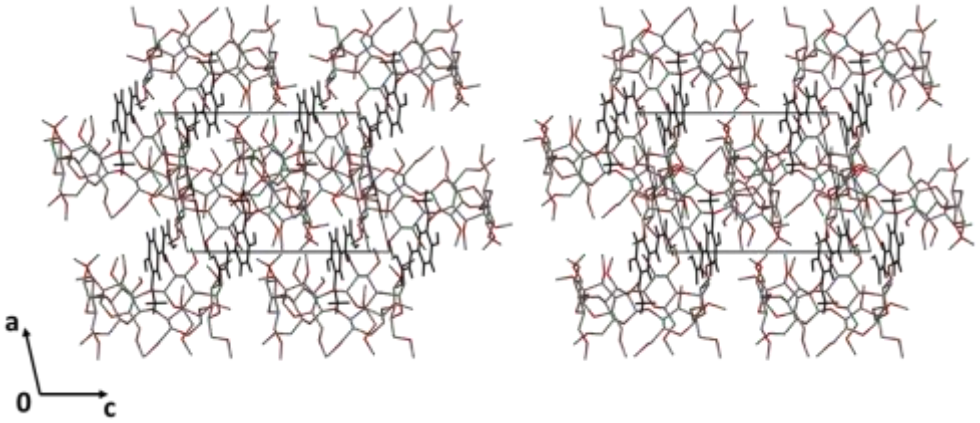

Figure 4.85: A stereodiagram of the packing arrangement of the TMA·FA complex units viewed down [0 1 0]. Host hydrogen atoms are omitted for clarity.

Comparative PXRD

Good agreement was found between the experimental and calculated PXRD patterns of TMA·FA, confirming that the crystal used for single crystal X-ray diffraction data collection was representative of the bulk product (Figure 4.86). Discrepancies in peak positions and relative intensities are due to the different temperatures to which the PXRD traces refer (experimental 294 K, calculated 173 K) and preferred orientation of crystallites in the experimental sample.

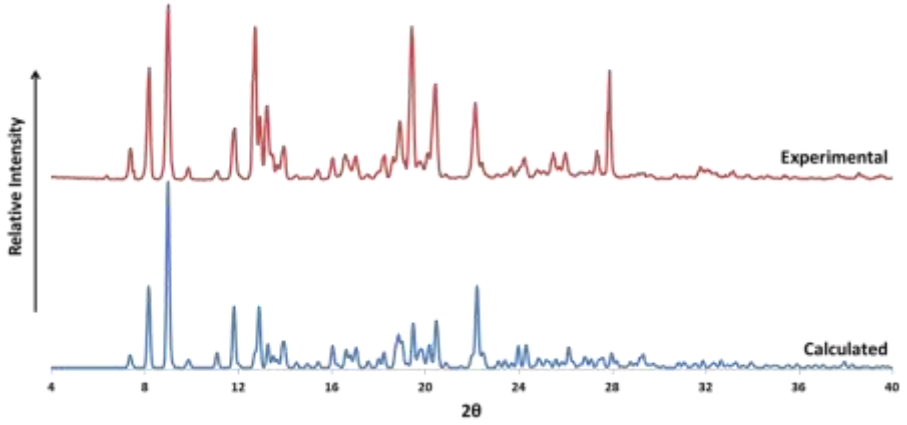

Figure 4.86: Comparison of the experimental and calculated PXRD traces for TMA·FA.

TRIMEA INCLUSION COMPLEX WITH *p*-COUMARIC ACID (TMA·PCA)

Thermal analysis

TGA, DSC and HSM were used to determine the thermal behaviour of TMA·PCA (Figures 4.87 and 4.88). TGA analysis shows a mass loss of 3.2 ± 1.8 % (n = 2) over the temperature range 30 °C to 150 °C. The mass loss corresponds to 2.5 ± 1.5 water molecules per complex unit and is reflected in the DSC curve by the presence of a broad endotherm observed over the same range. A second mass loss step is observed as the sample melts at 200 °C, indicated by a sharp endotherm in the DSC trace and shown in the HSM

photographs. The second mass loss is 11.6 ± 0.3 % (n = 2) accounting for 1.0 ± 0.1 guest molecules per complex unit. Decomposition occurs above 330 °C.

The HSM photographs (Figure 4.88) show the TMA·PCA crystals as the temperature was increased at a rate of 10 °C/min. At 30 °C the crystal is clear and fractures become evident as the sample is heated. The crystal appears to start melting at 194 °C.

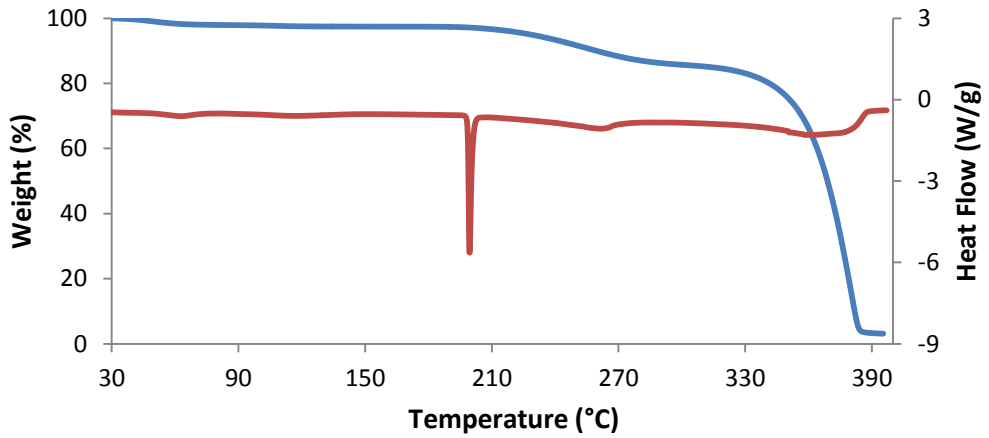

Figure 4.87: DSC (red) and TGA (blue) curves of TMA·PCA.

30 °C **130 °C** **194 °C** **207 °C**

Figure 4.88: HSM photographs of the complex TMA·PCA.

Single crystal X-ray analysis of the complex TMA·PCA

Data collection and space group determination

Intensity data-collection for TMA·PCA was performed on a Bruker KAPPA APEX II DUO diffractometer. The reciprocal lattice layers indicate Laue symmetry *mmm*, corresponding to the orthorhombic crystal system.[3] Systematic absences indicated the space group $P2_12_12_1$. The crystallographic data and refinement parameters for the structure are listed in Table 4.48.

Structure solution and refinement

The crystal structure of TMA·PCA was solved by direct methods using SHELXD as no isostructural series was found matching the unit cell parameters.[29] Most of the host and guest non-hydrogen atoms were revealed in the E-map after a solution (CC = 82.5) was obtained. The respective atoms were assigned and allowed to refine with isotropic thermal parameters using SHELXL.[5] Successive full-matrix least-squares

refinements revealed the remaining non-hydrogen atoms. The host glucopyranose residues were labelled G1-G6 and disordered atoms were labelled PART 1 and PART 2 (Figure 4.89).

Table 4.48: Crystallographic data for the complexes TMA·PCA.

	TMA·PCA
Complex Formula	**$C_{54}H_{96}O_{30}·C_9H_8O_3·4.5H_2O$**
Formula weight	1470.53
Crystal system	Orthorhombic
Space group	$P2_12_12_1$ (No. 19)
a / Å	15.952(2)
b / Å	18.792(2)
c / Å	25.491(3)
Volume / $Å^3$	7642(1)
Z	4
Calculated density / g cm^{-3}	1.278
μ (MoKα) / mm^{-1}	0.105
F (000)	3164
Temperature / K	173(2)
Crystal size / mm^3	0.28 x 0.32 x 0.45
Theta range scanned / ˚	1.9 < θ < 27.3
Index ranges	h: -11: 20; k: -19: 24; l: -27: 32
Total number of reflections	29033
No. of independent reflections	16977
No. of reflections with I > 2σ(I)	10586
No. of parameters	915
R_{int}	0.035
$R_1(I > 2σ(I))$	0.0751
$wR_2(I > 2σ(I))$	0.2139
S	1.022
Coefficients in weighting scheme	a = 0.1135, b = 3.4339
Δρ excursions / e $Å^{-3}$	-0.39, 0.66

Disorder was identified on the *O*-methyl groups of residues G1 and G3 (C911/C912 and C931/C932). The guest molecule was also found to be disordered over two positions, except for the common acid group. (Further details of guest disorder are provided below). The host atoms were refined anisotropically once it was found that the isotropic thermal parameters of the atoms were stable. Hydrogen atoms were placed in idealised positions and added in a riding model with U_{iso} values 1.2 times and 1.5 times those of their parent atoms. Hydroxyl hydrogen atoms on the guest were placed using a rotating model except for the acid group where partial hydrogen atoms were found from Fourier maps to be present on each of the components of guest disorder.

Electron density peaks on the difference Fourier map not associated with either the host or guest but within hydrogen bonding distances to appropriate donor or acceptor atoms were assigned as oxygen atoms of water molecules. Eight peaks were assigned as water O atoms, the sum of the s.o.f.s totalling 4.5. The individual s.o.f.s are listed in Table 4.49. The sum of the s.o.f.s matches the value found by TGA (2.5 ± 1.5) to within two times the e.s.d. Hydrogen atoms of the partial (disordered) water molecules were not located.

Table 4.49: Site-occupancy factors of the water molecules in the complex TMA·PCA.

Molecule	S.o.f.	Molecule	S.o.f.
O1W	0.65	O5W1/O5W2	0.55/0.45
O2W	0.65	O6W	0.55
O3W	0.60	O7W	0.25
O4W	0.60	O8W	0.20

The asymmetric unit of PCA·TMA contains one TRIMEA molecule, one PCA molecule disordered over two positions with site-occupancies and 4.5 water molecules (Figure 4.90).

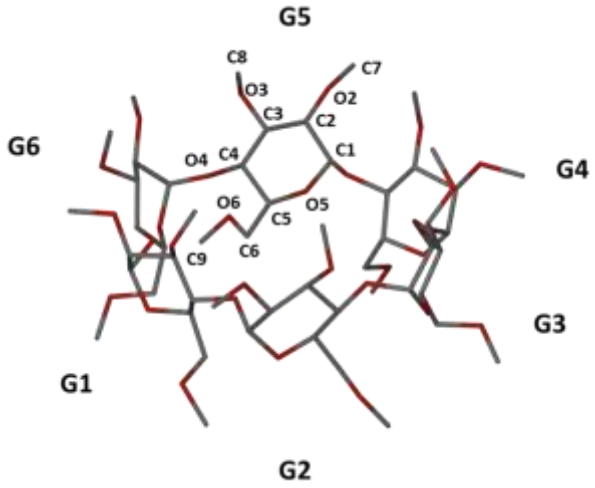

Figure 4.89: The labels used to identify host glucopyranose units and atoms in TMA·PCA. Hydrogen atoms and disordered atoms are omitted for clarity.

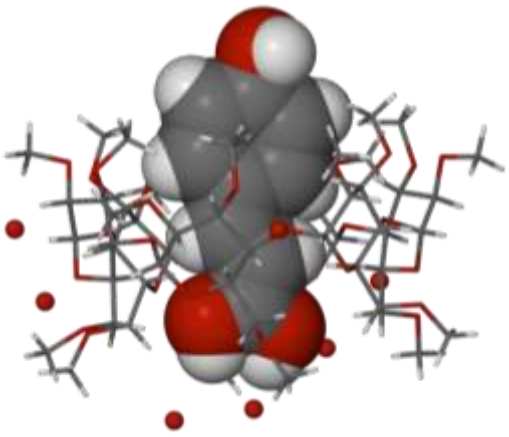

Figure 4.90: The ASU of TMA·PCA illustrating the position of the guest included in the CD cavity. Only the major component of PCA is shown.

Geometrical analysis

Host geometry

The rotation of the C6-O6 bond relative to the CD cavity is described by the O5-C5-C6-O6 torsion angle (*ω*). In the TMA·PCA complex all of the *ω* angles are negative signifying a (-)-gauche conformation and the C6-O6 bonds are directed away from the CD cavity. The primary end of the CD is therefore open.

The parameters of the O4-hexagon are listed in Table 4.50. These parameters show that the CD is slightly distorted from the ideal 'round' shape in the direction of the axis of the guest phenol ring (parameters *r*, *D* and *a*). The O4 atoms do not deviate significantly from the mean O4 plane (*α* has a maximum deviation

of 0.19 Å). The tilt angles τ_1 and τ_2 are positive, indicating that the primary sides of the glucopyranose rings tilt toward the cavity.

Table 4.50: Geometric parameters of the TRIMEA molecule in the complex TMA·PCA.

Residue	*r* (Å)	*D* (Å)	*α* (°)	*φ* (°)	*d* (°)	D_3 (Å)	*α* (Å)	τ_1 (°)	τ_2 (°)
G1	4.097	4.230	123.6	117.1(4)	-11.6	3.353	0.133(3)	15.5(2)	5.7(1)
G2	4.345	4.206	117.7	117.9(4)	10.0	3.114	-0.192(3)	17.4(1)	14.4(1)
G3	4.341	4.253	117.4	118.3(5)	-3.1	3.296	0.101(3)	5.4(1)	5.3(1)
G4	4.060	4.387	125.3	116.3(4)	-3.3	3.478	0.044(3)	30.8(1)	9.9(1)
G5	4.385	4.078	116.6	117.6(5)	2.3	3.313	-0.104(3)	9.8(1)	7.0(1)
G6	4.338	4.439	118.3	117.7(4)	5.1	3.408	0.018(3)	18.6(2)	3.5(1)
Mean	**4.26**	**4.27**	**119.8**	**117.5**	**6.4**	**3.33**	**0.105**	**16.3**	**7.6**

Guest inclusion

The guest molecule is deeply inserted into the CD cavity such that the acid tail extends to the primary end of the CD and the phenol ring protrudes from the secondary end. The angle between the planes through the respective phenol rings of guest components A and B is 34.3(5)°. The angle between the plane through the phenol ring of each disorder component of the guest molecule and the mean O4 plane of the host is 85.2(5)° for A and 83.3(3)° for B. The major part of the guest molecule is planar (Figure 4.91).

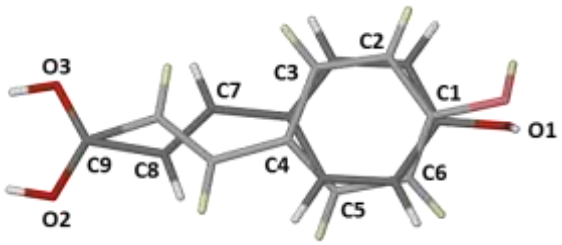

O1A-C1A-C2A-C3A = 175.7(13)°
C4A-C7A-C8A-C9 = -178.4(9)°
O3-C9-C8A-C7A = 167.3(9)°

Figure 4.91: The guest non-hydrogen atom labels and torsion angles describing the planarity of the guest molecule A.

Hydrogen bonding interactions

Host-host, host-guest and water interactions

A number of O-H···O hydrogen bonds, implied by close contacts between intramolecular host O atoms with D···A distances ranging between 2.759(6) Å and 3.114(6) Å, stabilise the conformation of the TMA molecule. Close contacts between the water O atoms and host O atoms as well as adjacent water O atoms are listed in Table 4.51. The guest molecule forms a hydrogen bond with the host molecule, namely O1A-H1A···O3G1^{c}, with a D···A distance of 2.898(14) Å and a D-Ĥ···A angle of 132° (where c denotes symmetry operation -1/2+x, 1/2-y, 2-z). The interactions involving water O atoms as well as the O1A-H1A···O3G1 H-bond are shown in Figure 4.92 (which excludes the low s.o.f. water O atoms O7W and O8W).

Table 4.51: Parameters for hydrogen bonds involving water in TMA·PCA.

D···A	D···A (Å)	Symmetry Operation
O3W···O3G4*	2.803(8)	1+x,y,z
O5G1···O8W	2.980(20)	-
O4W···O6G3*	2.828(8)	1/2+x,-1/2-y,2-z
O1W···O5G4*	2.871(8)	1/2+x,-1/2-y,2-z
O6G1···O6W	2.847(11)	-
O2W···O3G2	2.916(9)	-
O7W···O3G4	2.970(30)	-
O6G2···O5W2	2.854(14)	-
O6G2···O5W1	2.736(11)	-
O3G6···O5W2*	2.936(14)	1/2-x,-y,1/2+z
O3G6···O5W1*	2.755(11)	1/2-x,-y,1/2+z
O1W···O8W*	3.130(20)	-1/2+x,-1/2-y,2-z
O4W···O1W	2.657(9)	-
O1W···O6W	2.647(9)	-
O2W···O3W	2.696(8)	-
O2W···O5W1	2.768(7)	-
O2W···O5W2	2.538(8)	-

*The atom to which the symmetry operation applies.

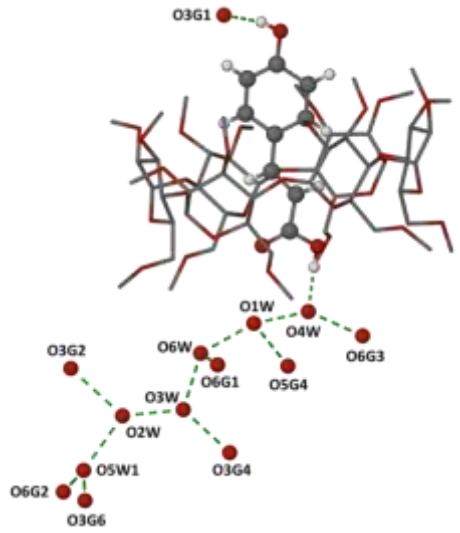

Figure 4.92: The hydrogen bonding interactions between the host (major disorder component only), guest and water molecules.

Weak host-host, host-guest and water interactions

There are five long-range C-H···O attractive interactions (listed in Table 4.52) between the host and guest, host and water and symmetry-related host molecules.

Table 4.52: Parameters for C-H···O hydrogen bonds in TMA·PCA.

D-H···A	D-H (Å)	H···A (Å)	D···A (Å)	D-H···A (°)	Symmetry Operation
C7G4-H7GB···O1A*	0.98	2.59	3.326(13)	132	-1/2+x,1/2-y,2-z
C6G2-H6G5···O1W	0.99	2.49	3.358(9)	147	-
C4G2-H4G2···O2W	1.00	2.50	3.345(9)	142	-
C7G2-H7G6···O6G6*	0.98	2.55	3.429(9)	149	1/2-x,-y,-1/2+z
C7G3-H7G3···O5G5*	0.98	2.46	3.375(9)	156	-1/2-x,-y,-1/2+z

*The atom to which the symmetry operation applies.

A further 14 weak C-H···O intramolecular host interactions add to the cumulative stability of the crystal structure, having an average D···A distance of 3.034 Å over the range 2.776 Å to 3.335 Å and an average D-Ĥ···A angle of 116° over the range 100° to 140°.

Crystal packing

The TMA complex units pack similarly to those of α-CD cage-type structures.[32] The host molecules form layers in the *ac*-plane with adjacent layers being shifted by *b*/2 + *c*/2 to form a brickwork motif (Figure 4.93). The primary face of the CD is blocked by the primary faces of adjacent CDs (not shown), and similarly for the secondary face. A channel of water is formed in the interstitial space at *c*/4 and parallel to the *a*-axis (Figure 4.94).

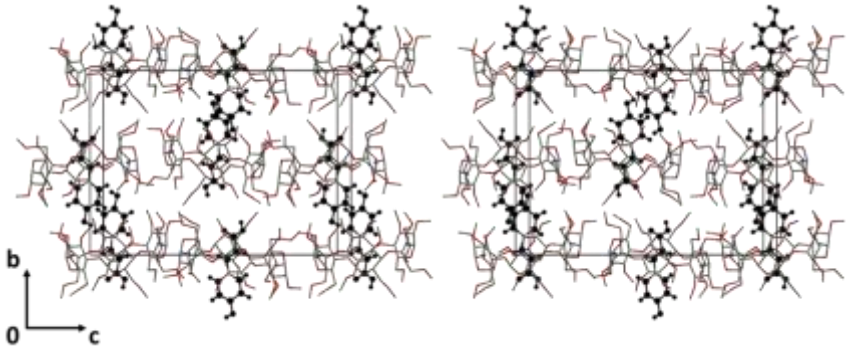

Figure 4.93: A stereodiagram of the packing arrangement of TMA·PCA complex units viewed down [1 0 0]. Host hydrogen atoms are omitted for clarity.

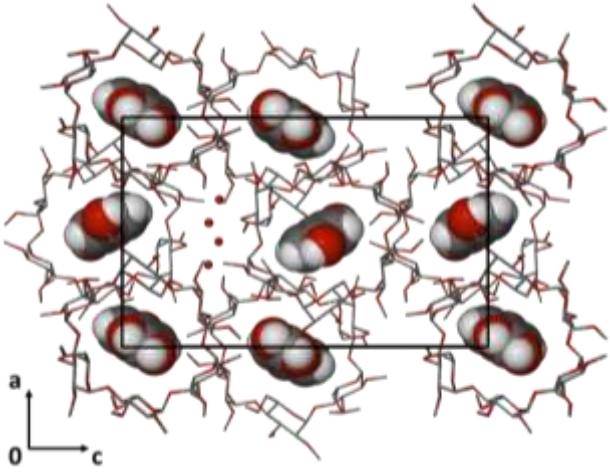

Figure 4.94: Packing diagram of TMA·PCA viewed down the *b*-axis. Host hydrogen atoms are omitted for clarity.

Comparative PXRD

The homogeneity of the bulk sample of the complex was confirmed by comparing its PXRD pattern with the calculated PXRD pattern (Figure 4.95). Differences in peak intensities are due to preferred orientation.

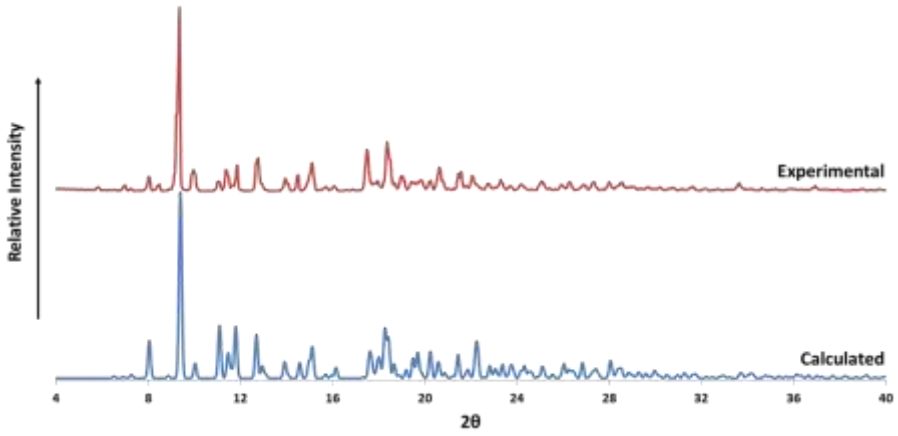

Figure 4.95: Comparison of the experimental and calculated PXRD traces for TMA·PCA.

CONCLUSION

This chapter described the inclusion of hydroxycinnamic acids in a number of CDs, namely β- and γ-CD, and the derivatised CDs TMB, TMA and DMB. Inclusion complex formation with the native CDs was achieved by kneading as well as coprecipitation. Complexes were formed between β-CD and each guest FA, HFA, HCA and PCA, respectively, as well as between γ-CD and each guest CAF, FA, HFA, HCA and PCA, respectively. ITC was used to study the thermodynamics of complex formation in solution with the result that the reactions between all host and guest molecules studied are thermodynamically spontaneous and mostly driven by enthalpy, while instead, reactions between β-CD and SA as well as γ-CD and CAF, are entropy-driven. Phase solubility studies demonstrated significant aqueous solubility enhancements for CAF and FA with β-CD, HP-β-CD and RAMEB, respectively.

Four of the reported complexes formed with derivatised CDs are inclusion complexes, namely TMB·HFA, TMB·PCA, TMA·FA and TMA·PCA. The remaining complexes (DMB·CAF, DMB·FA, DMB·HFA and DMB·PCA) form 'exclusion' or 'partial inclusion' complexes. While uncommon in CD inclusion in general, partial inclusion has been reported for complexes formed with DMB. Harata described the complexation of the small molecules *p*-iodophenol and *p*-nitrophenol with DMB,[33] in both of which the guest molecules interact preferentially with the *O*6-methyl groups on the primary side of DMB rather than within the CD cavity. The guest molecules are located in the zig-zag crevices formed along the *a*-axis. Harata suggested that the presence of the *O*-methyl groups renders the intermolecular space more hydrophobic in nature than the CD cavity such that, given the size and shape of the guest, the guest could be located in the intermolecular space. Expanding on this, it is possible that the close contacts between host molecules and the inclusion of an *O*-methyl group of one CD into the cavity of an adjacent CD (as for DMB·CAF and DMB·FA) play an important role in guest exclusion.

Chapter 5 reports the cocrystallisation results of the hydroxycinnamic acids with the coformers nicotinamide and isonicotinamide.

REFERENCES

1. M. R. Caira, *Rev. Roum. Chim*., 2001, **46**, 371-386.
2. T. Steiner and W. Saenger, *Acta Cryst.*, 1998, **B54**, 450-455.
3. L. J. Barbour, *J. Appl. Cryst.*, 1999, **32**, 351-352.
4. Sheldrick, G. M., *SHELXS-97, Program for Crystal Structure Solution*, Institut für Anorganische Chemie der Universität, Tammanstrasse, D-3400 Göttingen, Germany, 1997.
5. G. M. Sheldrick, *Acta Crystallogr*., 2015, **C71**, 3-8.
6. D. Mentzafos, I. M. Mavridis, G. Le Bas and G. Tsoucaris, *Acta Cryst*., 1991, **B47**, 746-757.
7. Paratone N oil (Exxon Chemical Co., TX, USA).
8. XPREP, *Data Preparation and Reciprocal Space Exploration*, Version 5.1, ©Bruker Analytical X-ray Systems, 1997.
9. **M. R. Caira, E. J. C. de Vries and L. R. Nassimbeni, *Chem. Commun.***, 2003, 2058-2059.
10. W. Saenger and T. Steiner, *Acta Cryst.*, 1998, **A54**, 798-805.
11. T. Higuchi and K. Connors, *Adv. Anal. Chem. Instrum.*, 1965, **7**, 117-212.
12. (a) M. Zhang, J. Li, W. Jia, J. Chao and L. Zhang, *Supramol. Chem*., 2009, **21**, 597-602. (b) M. Zhang, J. Li, L. Zhang and J. Chao, *Spectrochim. Acta Mol. Biomol. Spectrosc*., 2009, **71**, 1891-1895.
13. M. Kfoury, D. Landy, L. Auezova, H. Greige-Gerges and S. Fourmentin, *Beilstein J. Org. Chem*., 2014, **10**, 2322-2331.
14. J.-B. Chao, H.-B. Tong, Y.-F. Li, L.-W. Zhang and B.-T. Zhang, *Supramol. Chem.*, 2008, **20**, 461-466.
15. P. Job, *Ann. Chim.*, 1928, **10**, 113-199.
16. G. A. Holdgate and W. H. J. Ward, *Drug Discov. Today*, 2005, **10**, 1543-1550.
17. W. Zhao, J.-B. Chao, R. Du and S. Huang, *J. Incl. Phenom. Macrocycl. Chem.*, 2011, **71**, 25-34.
18. F. P. Schmidtchen, *Analytical Methods in Supramolecular Chemistry*, ed. C. A. Schalley, Wiley-VCH, Weinheim, 2007**,** 55-78.
19. L. Fielding, S. C. McKellar and A. J. Florence, *Magn. Reson. Chem.*, 2011, **49**, 405-415.
20. M. Rekharsky and Y. Inoue, *J. Am. Chem. Soc.*, 2000, **122**, 4418-4435.
21. J. Szejtli, *Chem. Rev.*, 1998, **98**, 1743.
22. L. Liu and Q.-X. Guo, *J. Incl. Phenom. Macrocycl. Chem.*, 2002, **42**, 1-14.
23. G. A. Holdgate, *BioTechniques*, 2001, **31**, 164-184.
24. A. Cooper, C. M. Johnson, J. H. Lakey and M. Nöllmann, *Biophys. Chem.*, 2001, **93**, 215-230.
25. M. Nilsson, A. J. M. Valente, G. Olofsson, O. Söderman and M. Bonini, *Phys. Chem. B*, 2008, **112**, 11310-11316.
26. N. A. Todorova and F. P. Schwarz, *J. Chem. Thermodyn.*, 2007, **39**, 1038-1048.
27. L. Szente, J. Szejtli and G. L. Kis, *J. Pharm. Sci.*, 1998, **87**, 778-781.

28. C. Anselmi, M. Centini, M. Ricci, A. Buonocore, P. Granata, T. Tsuno and R. M. Facino, *J. Pharm. Biomed. Anal.*, 2006, **40**, 875-881.
29. G. M. Sheldrick, *Acta Crystallogr*., 2008, **A64**, 112-122.
30. G. R. Desiraju, *Acc. Chem. Res.*, 1996, **29**, 441-449.
31. M. R. Caira, V. J. Griffith, L. R. Nassimbeni and B. van Oudtshoorn, *Supramol. Chem*., 1996, **7**, 119-124.
32. K. Harata, *Bull. Chem. Soc. Jpn*., 1977, **50**, 1416-1424.
33. K. Harata, *Bull. Chem. Soc. Jpn.*, 1988, **61**, 1939.

Chapter 5: Cocrystallisation of Caffeic Acid and its analogues

Cocrystallisation experiments were carried out between the hydroxycinnamic acids 3,4-dihydroxycinnamic acid (caffeic acid, CAF), 3-methoxy-4-hydroxycinnamic acid (ferulic acid, FA), 4-hydroxycinnamic acid (*p*-coumaric acid, PCA), 3,5-dimethoxy-4-hydroxycinnamic acid (sinapic acid, SA), 3,4-dihydroxyhydrocinnamic acid (hydrocaffeic acid, HCA) and 3-methoxy-4-hydroxyhydrocinnamic acid (hydroferulic acid, HFA) and the cocrystal coformers nicotinamide (NIC) and isonicotinamide (ISO), respectively. The resulting cocrystals were characterised using single crystal X-ray diffraction, PXRD, thermal analysis and ^{1}H NMR spectroscopy. Solubility experiments were carried out using ^{1}H NMR spectroscopy.

COCRYSTALLISATION OF HYDROXYCINNAMIC ACIDS WITH NICOTINAMIDE AND ISONICOTINAMIDE

INTRODUCTION

Cocrystals have been used to modify the physicochemical properties of a drug, as discussed in chapter 1. Cocrystal screening is often employed to test cocrystal formation; however, this may be very time-consuming with a low hit rate. Therefore it was suggested by Springuel *et al*.[1] that by investigating the large knowledge base available regarding cocrystal formation and the interactions that drive the phenomenon (e.g. highly directional hydrogen bonds), a higher hit rate may be obtained.

Using the Cambridge Structural Database (CSD)[2] to establish the competing intermolecular interactions most appropriate for the hydroxycinnamic acids being studied, a shortlist of potential coformers was produced. The search revealed that the types of interactions that are predominant with phenolic and acid groups are those involving nitrogen-containing functional groups – for example amides, pyridyls and diazines. The acid-acid homosynthons were present to a lesser extent. Etter described this phenomenon as follows: "the best hydrogen-bond donor and the best hydrogen-bond acceptor will preferentially form hydrogen bonds to one another".[3] The preference for the formation of the heterosynthon over the formation of the acid-acid homosynthon is supported by Shattock *et al*.[4] in their study of the hierarchy of these kinds of interactions. Thus, in the present study, GRAS coformers were chosen based on the synthons shown in Scheme 1. Scheme 2 shows the compounds (coformers) chosen for cocrystal screening in the present study, based on the CSD investigation.

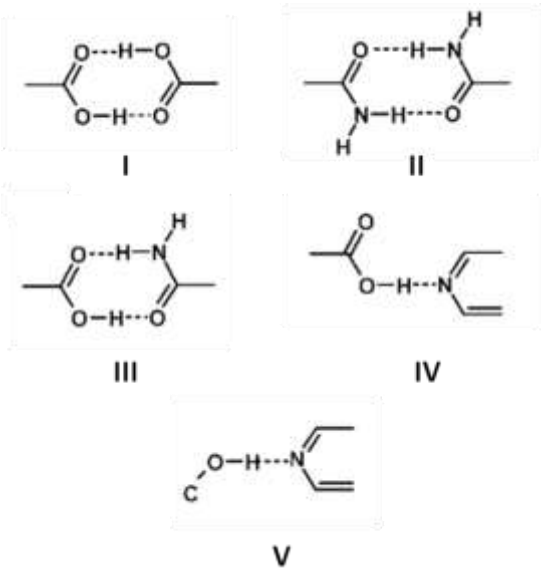

Scheme 1: The supramolecular synthons that may be formed with the hydroxycinnamic acid compounds.

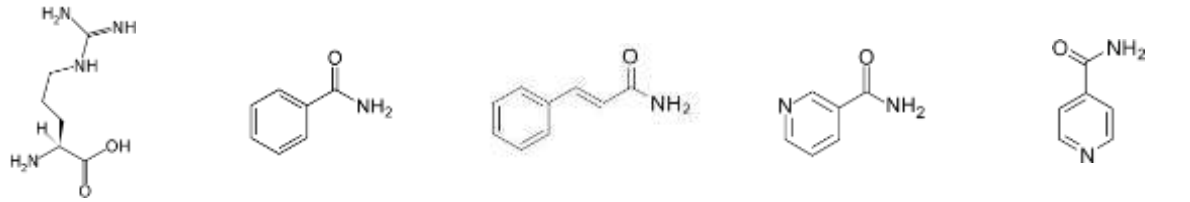

Scheme 2: GRAS coformers used in the present study for cocrystal screening with the hydroxycinnamic acid compounds.

Often in the search for cocrystals other multi-component systems are obtained, such as salts and solvates. In the present study, eight cocrystals were obtained as well as two hydrated cocrystals. The environments in which the water molecules exist are described by the motifs shown in scheme 3.

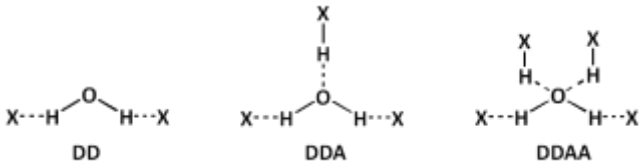

Scheme 3: The potential hydrogen bonding motifs of water (D: donor, A: acceptor).

Graph-set notation[5] was used to classify the basic types of hydrogen bonding interactions observed in the cocrystal structures.

COCRYSTAL SCREENING

In the present study, initial testing for cocrystal formation between the hydroxycinammic acid compounds and the chosen coformers was carried out using the method of dry co-grinding. If full conversion were to take place, then this would be the preferred preparation method as it is simple and "green". Twenty mg of the hydroxycinammic acid and an equimolar amount of each coformer were kneaded together using a pestle and mortar for 20 minutes. The product was then analysed using powder X-ray diffraction (PXRD), the resulting trace being compared with the PXRD traces of the starting materials. The presence of new peaks and disappearance of various peaks of the starting materials in the experimental PXRD pattern indicated the presence of a new crystalline phase. Table 5.1 shows the results of these experiments, the abbreviation PM standing for "physical mixture". A success rate of 22% was achieved.

Table 5.1: Results of the cocrystal screening experiments, determined by PXRD.

Coformer	CAF	FA	SA	PCA	HCA	HFA
Benzamide	PM	PM	PM	PM	PM	PM
Cinnamamide	PM	PM	PM	PM	PM	PM
Isonicotinamide (ISO)	New Form + PM	New Form + PM	PM	New Form + PM	New Form + PM	New Form + PM
L-Arginine	PM	PM	PM	PM	PM	PM
Nicotinamide (NIC)	PM	New Form + PM	New Form + PM	New Form + PM	PM	New Form + PM
Orotic acid	PM	PM	PM	PM	PM	PM
Propionamide	PM	PM	PM	PM	PM	PM
Pyroglutamic acid	PM	PM	PM	PM	PM	PM
Urea	PM	New Form* + PM	PM	New Form* + PM	New Form* + PM	PM

*A cocrystal was obtained by coprecipitation but is not reported in this chapter. There is a lack of data for the cocrystal due to its elusiveness.

Due to time constraints further screening experiments using LAG or different solvent systems were not pursued. This, however, has been shown to be effective in producing results when dry co-grinding does not, as the liquid phase often has a catalytic effect on the cocrystal formation by aiding molecular diffusion.[6]

PREPARATION OF COCRYSTALS

Coprecipitation experiments were carried out by dissolving the starting materials in EtOH or a 1:1 v/v EtOH/H_2O mixture, as listed in Table 5.2. A low heat (temperature 40 °C) was applied to break any pre-existing hydrogen bond interactions and to aid dissolution. The solution was then filtered and sealed with parafilm. A few holes were poked into the parafilm for controlled evaporation at room temperature. Single co-crystals were obtained and analysed using thermal analytical techniques, spectroscopy and X-ray diffraction methods. Where positive results were obtained by dry co-grinding, crystalline materials were obtained and will also be discussed in this chapter.

Table 5.2: Masses and solvents used to obtain cocrystals.

Cocrystal	Mass hydroxycinnamic acid (mg)	Mass coformer (mg)	Solvent
HCA·ISO	20	27	3 mL EtOH
FA·ISO	20	13	2 mL EtOH
FA·NIC	20	13	2 mL EtOH/H_2O
HFA·ISO	20	13	1 mL EtOH
HFA·NIC	20	13	1 mL EtOH
PCA·ISO	20	15	2 mL EtOH
PCA·NIC	20	15	1 mL EtOH
$(PCA)_2$.NIC	20	15	2 mL EtOH/H_2O

PREVIOUSLY PUBLISHED COCRYSTALS CONTAINING HYDROXYCINNAMIC ACIDS

To date, according to a search of the CSD, a number of cocrystals exist with hydroxycinnamic acids. Bevill *et al*.[7] generated three polymorphic 1:1 PCA·NIC cocrystals as well as a 2:1 cocrystal. Forms I and II of the 1:1 cocrystal were obtained by slow evaporation from ethanol and tetrahydrofuran, respectively, although their production is not limited to these conditions and solvents. Form III was obtained from vapour diffusion and the 2:1 cocrystal from various slurry experiments. The polymorphs were found to be energetically similar and nearly equally thermodynamically stable. The compounds PCA, NIC and ISO were used in the present study to generate cocrystals, with PCA·NIC being equivalent to cocrystal Form II and $(PCA)_2$·NIC being the 2:1 cocrystal found by Bevill *et al*. The two cocrystals were isolated experimentally in the present study prior to publication of these phases by other researchers.

Clarke *et al*.[8] obtained the cocrystal hydrates CAF·NIC·1H_2O, FA·ISO·1H_2O and FA·NIC·1H_2O. These were obtained by coprecipitation from EtOH/H_2O (1:1 v/v) for CAF and EtOH for FA. The hydrates were analysed using thermal analysis (TGA and DSC) to determine the influence of the water molecules on the

stability of the crystal. Both FA hydrates were found to have loosely bound water in tunnels having no interaction with other water molecules (dehydration occurs below 100 °C) while the CAF hydrate releases water upon melting as the water molecules hydrogen bond with the CAF molecules as well as other water molecules. They concluded that the formation of hydrated cocrystals may still be seen as unfavourable due to the unpredictable effect of water molecules on crystal stability.

The aim of a study by Aakeröy *et al*.[9] was to generate ternary structures using the principles of hydrogen bond formation hierarchy and the cumulative stabilisation effect of a few well-chosen intermolecular interactions. The result was a 1:1:1 ternary cocrystal of 3,5-dinitrobenzoic acid, ISO and FA crystallised from water.

Structural data for a cocrystal formed between FA and 2,3,5,6-tetramethylpyrazine grown from acetone were published by Tan *et al*.[10] The cocrystal was generated in order to study its pharmacological effects, but further information was not available.

Cocrystals of PCA having different stoichiometries were grown with caffeine and theophylline coformers from various solvents. Schultheiss *et al*.[11] produced cocrystals of PCA and caffeine by coprecipitation from acetonitrile (1:1) and from acetone (1:2), respectively. It was also found that two different solid forms of PCA and theophylline were obtained from an acetone/methanol solvent system and upon further investigation by computational methods, the two forms were deemed energetically equivalent. The structural integrity of the cocrystal products will therefore determine which of the two polymorphs is suitable for pharmaceutical application.

Recently, a study was performed in order to improve the physicochemical properties of the anti-tuberculosis drug isoniazid by the formation of a cocrystal with PCA.[12] Here the nutraceutical coformer adds its antioxidant properties to the drug properties, yielding a product called a “synergistic pharmaceutical cocrystal”. The crystal structure indicates that the dominant intermolecular interactions are O-H_{phenol}···$N_{pyridine}$, N-H···O=C and -COOH···N-H.

HYDROCAFFEIC ACID AND ISONICOTINAMIDE (HCA·ISO)

Thermal analysis

HSM analysis of a single crystal of HCA·ISO (later proven to be a cocrystal) was carried out at a heating rate of 10 °C/minute (Figure 5.9). The crystal starts to melt at 145 °C and is completely melted by 149 °C.

30 °C **103 °C** **145 °C** **147 °C** **149 °C**

Figure 5.9: Representative HSM photographs of HCA·ISO

The DSC analysis (Figure 5.10) shows a small endotherm at *ca*. 100 °C. This endotherm is not an artefact as it is present in repeated experiments. Since there is zero mass loss at this temperature, the endotherm is interpreted as a probable phase transition of HCA·ISO. A sharp endotherm at 140 °C corresponds to the crystal melt. The melting temperature is different from the melting points of the starting materials (HCA: 136-139 °C and ISO: 155-157 °C) confirming the formation of a new phase.

TGA analysis (Figure 5.10) reveals a large mass loss due to decomposition, which has an onset temperature of 188 °C. There is no indication of solvent mass loss.

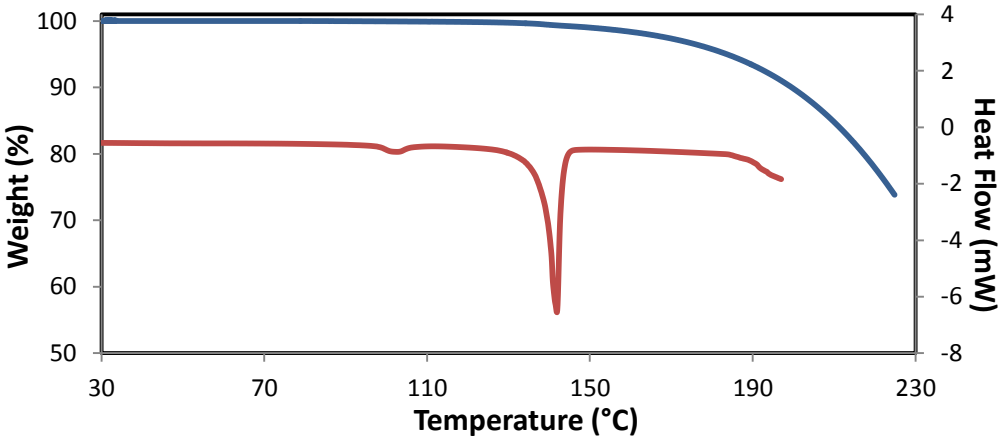

Figure 5.10: TGA (blue) and DSC (red) traces of HCA·ISO

^{1}H Nuclear Magnetic Resonance Spectroscopy

^{1}H NMR spectroscopy was used to determine the stoichiometry of the cocrystal obtained through integration of the signals of HCA and ISO for a sample of the cocrystal dissolved in D_2O (Table 5.5). A stoichiometry of 1:2 was found for HCA·ISO (see Appendix B for full spectrum).

Table 5.5: Integrals of the protons of HCA and ISO used to confirm the stoichiometry of HCA·ISO

Proton	δ (ppm)	Multiplicity	J (Hz)	Integration	Experimental/ Theoretical	
2 x C-$\underline{H}_a$ (ISO)	8.745	d	^{3}J = 5.68	4.103	2	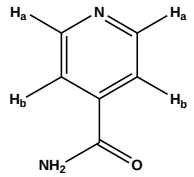
2 x C-$\underline{H}_b$ (ISO)	7.834	d	^{3}J = 6.04	3.893	2	
C-$\underline{H}_C$ (HCA)	6.838	d	^{4}J = 1.64	1.917	2	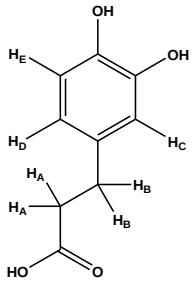
C-$\underline{H}_E$ (HCA)	6.878	d	^{3}J = 8.04			
C-$\underline{H}_D$ (HCA)	6.748	dd	^{3}J = 8.06 ^{4}J = 1.61	1.000*	1	
2 x C-$\underline{H}_A$ (HCA)	2.822	t	^{3}J = 7.52	2.162	1	
2 x C-$\underline{H}_B$ (HCA)	2.590	t	^{3}J = 7.52	2.165	1	

*Reference integral

Single crystal X-ray analysis

A single, colourless crystal was selected from the mother liquor, dried on filter paper and placed in Paratone N oil.[13] Single crystal X-ray intensity data were collected on a Nonius KappaCCD diffractometer. Using the program LAYER it was found that the Laue symmetry was 2/m indicating the monoclinic crystal system.[14] The reflection conditions, namely *hkl: none, h0l: h + l = 2n, 0k0: k = 2n* uniquely identified the space group as $P2_1/n$ (alternative setting of $P2_1/c$) and this was confirmed using XPREP.[15]

Structure solution and refinement

SHELXS-97 was used to solve the structure of HCA·ISO. The ASU was found to consist of one HCA molecule and two ISO molecules (A and B) (Figure 5.11).[16] Non-hydrogen atoms were assigned and refined isotropically on F^2 using SHELXH-97.[17] The atoms were refined anisotropically after the refined isotropic temperature factors were confirmed to be acceptable.

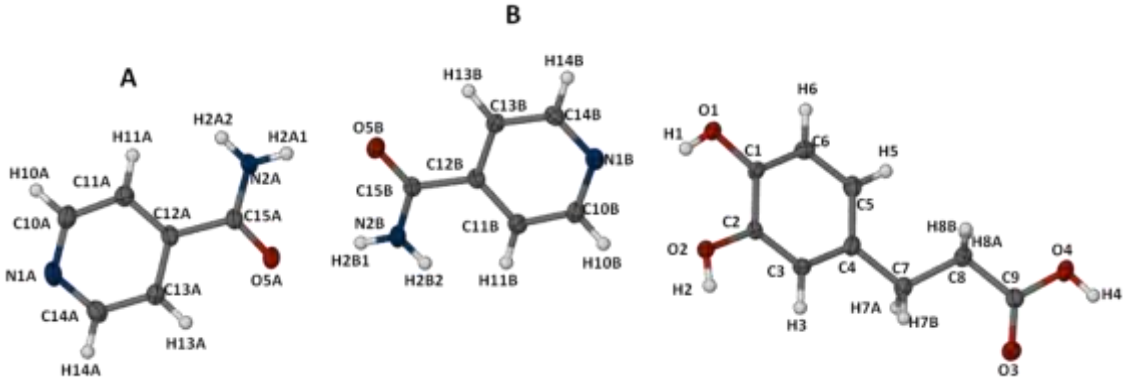

Figure 5.11: The asymmetric unit of HCA·ISO. Thermal ellipsoids are drawn at the 50% probability level, while the hydrogen atoms are shown as spheres of arbitrary radii.

The positions of hydrogen atoms were evident in the difference Fourier synthesis and there was no evidence of proton transfer from either the hydroxyl or acid group of HCA to the pyridyl-N of either ISO

molecule. Further support that a cocrystal had formed rather than a salt is the C10-N1-C14 bond angle which is 117.9(2)° and 116.6(1)° for A and B, respectively. If, instead, a salt had formed, the C-N-C bonds would have been significantly larger (~120°).[18] Aromatic and aliphatic hydrogen atoms were added in idealised positions in a riding model (AFIX 43 and AFIX 23, respectively). The hydroxyl hydrogen atoms were placed using the rotating group method (AFIX 147). The AFIX 93 command was used to place the primary amide hydrogen atoms on both ISO A and ISO B. The temperature factors for the hydrogen atoms were 1.2 times those of the parent atoms.

The crystallographic data and refinement parameters for the structure are listed in Table 5.6.

Table 5.6: Data collection and refinement parameters for HCA·ISO

Chemical Formula	**$C_9H_{10}O_4 \bullet (C_6H_6N_2O)_2$**
Formula weight / g mol^{-1}	426.43
Crystal system	Monoclinic
Space group	$P2_1/n$ (No. 14)
a / Å	12.190(2)
b / Å	11.001(2)
c / Å	15.304(3)
β / °	104.59(3)
Volume / $Å^3$	1986.1(7)
Z	4
Calculated density / g cm^{-3}	1.426
μ (MoKα) / mm^{-1}	0.106
F (000)	896
Temperature of data collection / K	173(2)
Crystal size / mm^3	0.12 x 0.25 x 0.30
Theta range scanned / °	$2.7 \leq \theta \leq 26.4$
Index ranges	h: 0, 15; k: 0, 13; l: -19, 18
Total number of reflections	32632
No. of independent reflections	4060
No. of reflections with $I > 2\sigma(I)$	3142
No. of parameters	280
R_{int}	0.036
R_1 ($I > 2\sigma(I)$)	0.0397
wR_2 ($I > 2\sigma(I)$)	0.1099
S	1.032
Coefficients in weighting scheme	a = 0.0655, b = 0.3130
$(\Delta/\sigma)_{mean}$	< 0.001
Δρ excursions / e $Å^{-3}$	-0.30 and 0.18

Hydrogen bonding

A HCA-ISO-ISO assembly is formed by the homosynthon involving the *syn*-H atom of the amide and the carbonyl-O atoms of the two ISO molecules (A and B) [graph-set designation $R_2^2(8)$] and the heterosynthon formed between the pyridyl-N atom N1A and the acid hydroxyl group of HCA (Figure

5.12). The assemblies are linked by a hydrogen bond between the pyridyl-N atom N1B and the *p*-hydroxyl group of HCA, facilitating the formation of undulating chains. Two hydrogen bonds link the chains together to form a layer in the (3 0 1) plane: these involve the *anti*-H atom of the amide group of ISO A interacting with the *p*-hydroxyl oxygen of an adjacent PCA molecule as well as the *anti*-H atom of the amide group of ISO B and the carbonyl-O of another adjacent HCA molecule. The layers are further stabilised by a number of weak C-H···O hydrogen bonds. An intramolecular hydrogen bond [$S_1^1(5)$] exists between the *m*- and *p*-hydroxyl groups of HCA.

A hydrogen bond between the *m*-hydroxyl of HCA and the carbonyl-O of the ISO molecule in the adjacent layer propagates the crystal in the *a*-direction. Table 5.7 provides parameters of the hydrogen bonds discussed above.

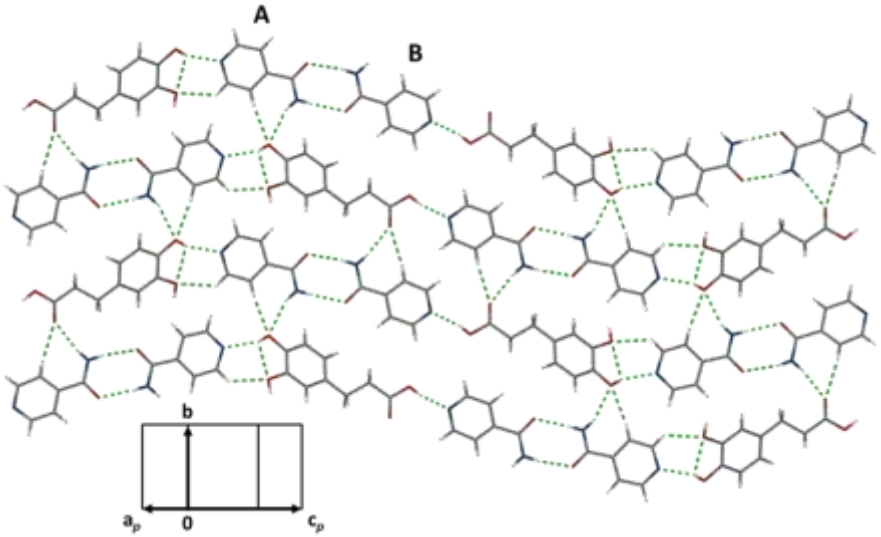

Figure 5.12: A projection onto the (3 0 1) plane illustrating the hydrogen bonding interactions which link the HCA-ISO-ISO fragments to form layers.

Table 5.7: Hydrogen bond parameters for HCA·ISO

D-H···A	D-H (Å)	H···A (Å)	D···A (Å)	D-H···A (°)	Symmetry code
O1-H1···O2	0.84	2.34	2.776(1)	113	-
O1-H1···N1B	0.84	2.07	2.772(2)	141	-
O2-H2···O1A*	0.84	1.94	2.764(2)	165	1/2+x,1/2-y,-1/2+z
O4-H4···N1A*	0.84	1.82	2.647(2)	167	1/2+x,1/2-y,-3/2+z
N2A-H2A1···O5B	0.88	2.12	2.958(2)	159	-
N2A-H2A2···O3*	0.88	2.08	2.954(2)	170	3/2-x,1/2+y,1/2-z
N2B-H2B1···O5A	0.88	2.05	2.913(2)	165	-
N2B-H2B2···O1*	0.88	2.23	3.059(2)	156	3/2-x,-1/2+y,1/2-z
C1B-H1B···O2	0.95	2.44	3.143(2)	131	-
C2A-H2A···O3*	0.95	2.53	3.316(2)	140	3/2-x,1/2+y,1/2-z
C2B-H2B···O1*	0.95	2.47	3.407(2)	170	3/2-x,-1/2+y,1/2-z

*The atom to which the symmetry operation applies.

Additional stabilisation of the structure is provided by face-to-face π-π stacking between two HCA molecules in adjacent layers, the distance between the centroids of their aromatic rings being 3.735 Å.

Figure 5.13 illustrates the formation of discrete π-stacked HCA dimeric motifs, where the different colours represent different layers. Layer A is shown in orange, layer B in green and layer C in blue.

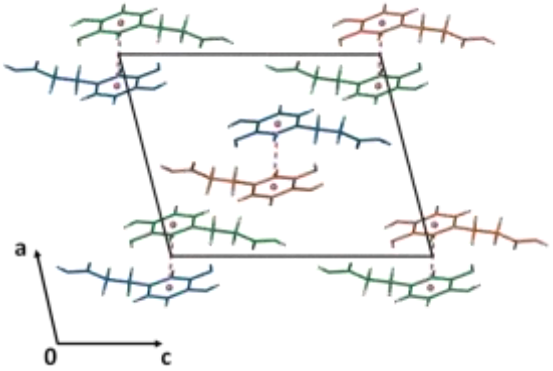

Figure 5.13: π-π stacking in HCA·ISO viewed down the *b*-axis. The molecules are shown in different colours to indicate different layers and the stacking that occurs between the layers.

Molecular geometry

The free rotation in the aliphatic tail of HCA leads to the torsion angles C5-C4-C7-C8 = 29.3(2)°, C4-C7-C8-C9 = 167.1(1)° and C7-C8-C9-O3 = -9.7(2)° in the HCA molecule. (Figure 5.11 shows the atom labels for HCA and NIC). Some twisting of the amide group out of the aromatic ring plane occurs in the ISO molecules, torsion angle C11-C12-C15-N2 having values of 27.7(2)° and -12.6(2)° for molecules A and B, respectively.

Crystal packing

The molecules in the HCA·ISO cocrystal pack in layers along the *a*-direction. The layers pack in an ABCABC sequence as shown in Figure 5.14. Discrete π-π stacking interactions between two HCA molecules in adjacent layers add stability to the structure. The layers are made up of hydrogen bonded HCA-ISO-ISO chains.

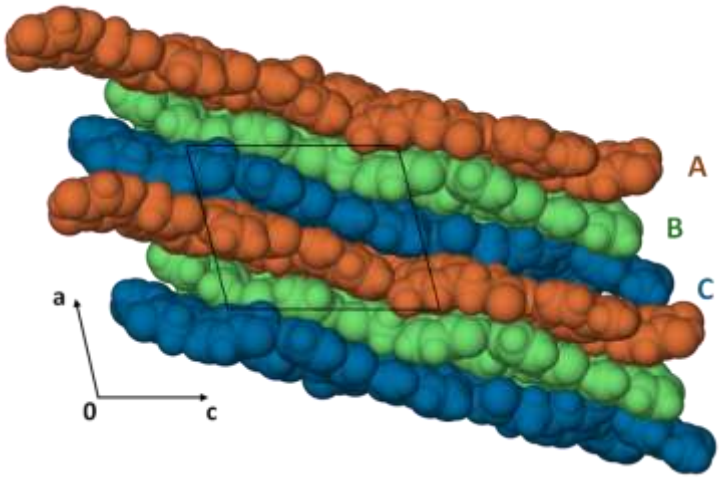

Figure 5.14: Packing of HCA·ISO viewed down the *b*-axis.

Comparative PXRD

PXRD was used to determine that the crystal chosen for single crystal X-ray diffraction was representative of the bulk material. Figure 5.15 shows the experimental PXRD pattern of HCA·ISO as compared with the calculated pattern, determined from the single crystal X-ray diffraction data. A good match was found between the two patterns.

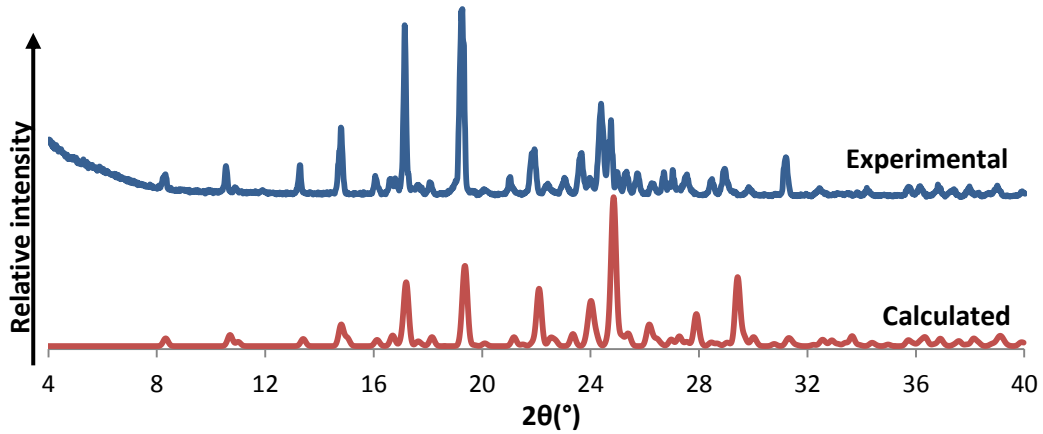

Figure 5.15: PXRD of the cocrystal obtained by coprecipitation as well as the PXRD pattern calculated from the crystal structure.

FERULIC ACID AND ISONICOTINAMIDE (FA·ISO)

Thermal analysis

HSM analysis of a single crystal of FA·ISO was carried out at a heating rate of 10 °C/minute (Figure 5.16). The HSM photographs show that the crystal remains stable until 145 °C when melting begins. After melting the compound decomposes.

30 °C **145 °C** **151 °C**

Figure 5.16: Representative HSM photographs of FA·ISO

The DSC analysis (Figure 5.17) shows a melt at 145 °C as indicated by the sharp endotherm. The melting point differs from those of the starting materials (FA: 168–172 and ISO: 155-157 °C) confirming the formation of a new phase.

The TGA trace is flat until the start of decomposition (onset temperature at *ca.* 160 °C) (Figure 5.17).

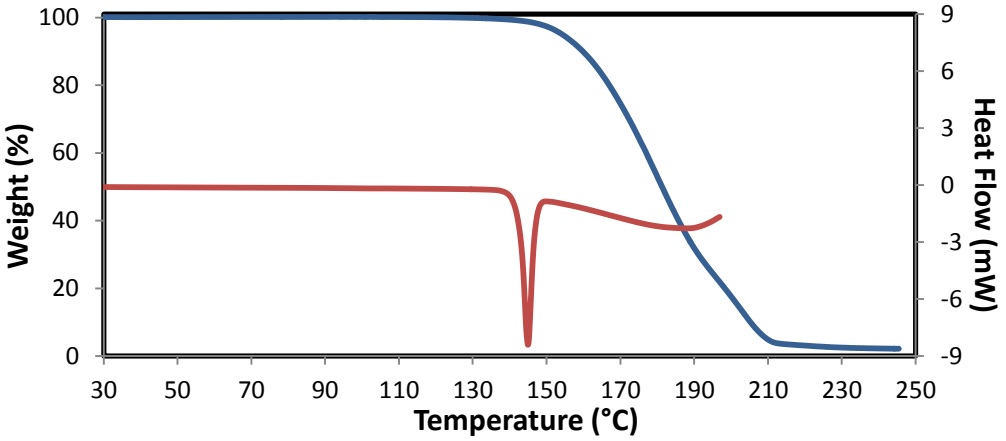

Figure 5.17: TGA (blue) and DSC (red) traces of FA·ISO

^{1}H Nuclear Magnetic Resonance spectroscopy

A stoichiometry of 1:1 was found for FA·ISO using ^{1}H NMR spectroscopy. A sample of the cocrystal was dissolved in DMSO- d_6 and submitted for analysis. The integrations of the signals of FA and ISO are shown in Table 5.8 (see Appendix B for full spectrum).

Table 5.8: Integrals of the protons of FA and ISO used to confirm the stoichiometry of FA·ISO

Proton	δ (ppm)	Multiplicity	J (Hz)	Integration	Experimental/ Theoretical	
2 x C-$\underline{H}_a$ (ISO)	8.726	dd	^{3}J = 4.40 ^{4}J = 1.68	2.011	1	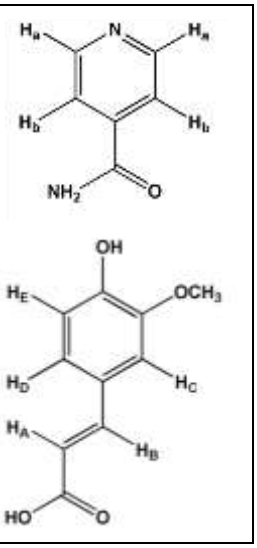
2 x C-$\underline{H}_b$ (ISO)	7.774	dd	^{3}J = 4.38 ^{4}J = 1.66	2.072	1	
C-$\underline{H}_A$ (FA)	6.363	d	^{3}J = 15.77	0.996	1	
C-$\underline{H}_B$ (FA)	7.491	d	^{3}J = 15.77	1.015	1	
C-$\underline{H}_C$ (FA)	7.280	d	^{4}J = 2.00	1.001	1	
C-$\underline{H}_D$ (FA)	7.088	dd	^{3}J = 8.26 ^{4}J = 2.02	0.996	1	
C-$\underline{H}_E$ (FA)	6.802	d	^{3}J = 8.12	1.000*	1	
O-C$\underline{H}_3$ (FA)	3.828	s		3.063	1	

*Reference integral

Single crystal X-ray analysis

Single crystal X-ray intensity data were collected on the Nonius KappaCCD diffractometer. A single, colourless crystal was selected from the mother liquor and dried on filter paper. The crystal was mounted on a nylon loop using Paratone N oil.[13] The crystal system was found to be triclinic using the program LAYER.[14] The space group $P\bar{1}$ was selected as the experimental value for $|E^2 - 1|$ was 0.997 (the theoretical value is 0.968 for centrosymmetric structures and 0.736 for non-centrosymmetric structures).

Structure solution and refinement

The crystallographic data and refinement parameters for the structure are listed in Table 5.9. The positions of the non-hydrogen atoms were determined by direct methods using the program SHELXS-97.[16] The atoms were assigned accordingly and refined isotropically on F^2 using SHELXH-97.[17] The ASU was found to consist of one FA molecule and one ISO molecule (Figure 5.18). After confirming that the refined isotropic thermal parameters were acceptable the atoms were refined anisotropically.

Table 5.9: Data collection and refinement parameters for FA·ISO

Chemical Formula	**$C_{10}H_{10}O_4 \bullet C_6H_6N_2O$**
Formula weight / g mol^{-1}	316.31
Crystal system	Triclinic
Space group	$P\bar{1}$ (No. 2)
a / Å	4.998(1)
b / Å	11.818(1)
c / Å	13.576(1)
α / °	104.420(2)
β / °	94.881(1)
γ / °	101.631(2)
Volume / $Å^3$	752.9(1)
Z	2
Calculated density / g cm^{-3}	1.395
μ (MoKα) / mm^{-1}	0.105
F (000)	332
Temperature of data collection / K	173(2)
Crystal size / mm^3	0.16 x 0.19 x 0.29
Theta range scanned / ˚	$1.6 \leq \theta \leq 28.4$
Index ranges	h: -6, 6; k: -15, 14; l: -12, 18
Total number of reflections	6165
No. of independent reflections	3740
No. of reflections with $I > 2\sigma(I)$	2960
No. of parameters	209
R_{int}	0.022
R_1 ($I > 2\sigma(I)$)	0.0472
wR_2 ($I > 2\sigma(I)$)	0.1316
S	1.043
Coefficients in weighting scheme	a = 0.0663, b = 0.1705
$(\Delta/\sigma)_{mean}$	< 0.001
Δρ excursions / e $Å^{-3}$	-0.37 and 0.28

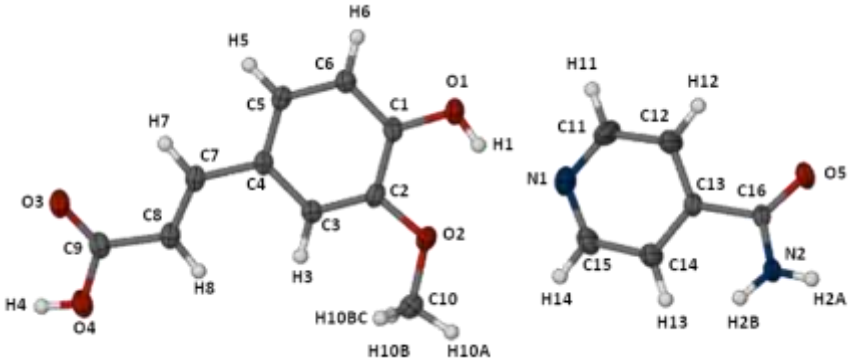

Figure 5.18: The asymmetric unit of FA·ISO. Thermal ellipsoids are drawn at the 50% probability level, while the hydrogen atoms are shown as spheres of arbitrary radii.

The structure was solved using the same strategy as that described for the previous cocrystal. All H atoms were located and their positions were confirmed by examining the lengths between the non-hydrogen atoms and their difference electron density peaks in accordance with known R-H bond lengths.[20] There was no evidence of proton transfer from the hydroxyl group of FA to the pyridyl-*N* of ISO in the difference Fourier map. Hydrogen atoms were added in idealised positions in a riding model (AFIX 43 for aromatic hydrogen atoms and AFIX 137 for methyl hydrogen atoms). The AFIX 93 command was used to place the primary amide hydrogen atoms. The hydroxyl hydrogen atoms were placed using the hydrogen bond searching model (AFIX 83). The temperature factors for the hydrogen atoms were 1.2 times those of their parent atoms (1.5 times for methyl hydrogen atoms).

Hydrogen bonding

One FA and one ISO molecule interact via the heterosynthon formed between the pyridyl-N of ISO and the *p*-hydroxyl group of FA (Figure 5.19). The two-component asymmetric unit forms a centrosymmetric cocrystal unit dimer *via* the homomeric synthon (graph-set designation $R_2^2(8)$) between two ISO molecules. Undulating ribbons are formed due to the interaction of the carboxylic acid groups of two FA molecules ($R_2^2(8)$). The *anti*-H of the amide group and the carbonyl-O of adjacent ISO molecule form a chain (C(4)) parallel to the *a*-axis. This interaction also forms a ring ($R_4^2(8)$) with the hydrogen bond formed between the syn-H and the O of the centrosymmetrically related ISO molecule (Figure 5.20). The layers are linked by a weak C-H···O interaction resulting in a three-dimensional hydrogen bonded network. The conformation of the FA molecule is stabilised by the $S_1^1(5)$ intramolecular interactions between the *p*-hydroxyl group and the oxygen atom of the O-methyl substituent as well as the C-H···O interaction between H7 and the carbonyl oxygen atom. Table 5.10 lists the hydrogen bonding parameters.

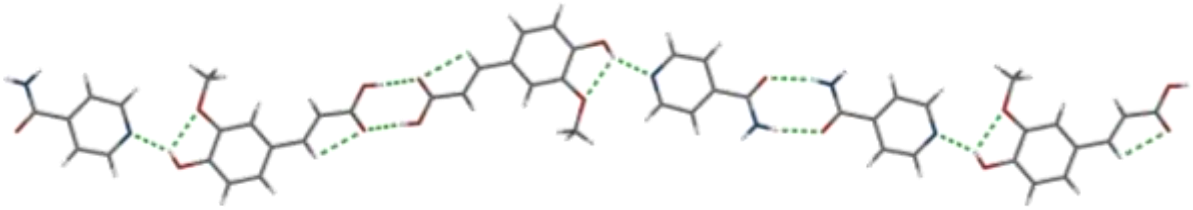

Figure 5.19: The hydrogen bonding chains formed by FA-ISO.

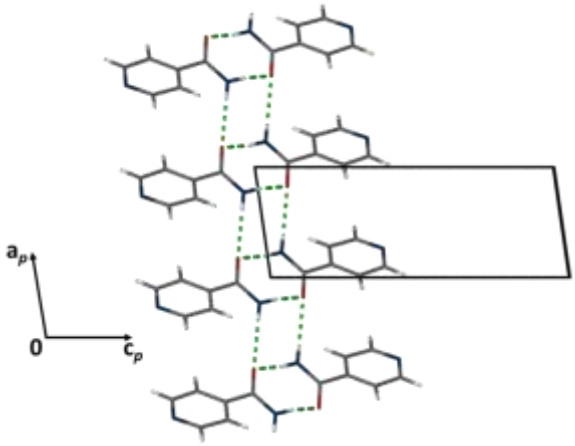

Figure 5.20: The ISO "ladder" viewed down the *b*-axis.

Table 5.10: Hydrogen bonding parameters of FA·ISO

D-H···A	D-H (Å)	H···A (Å)	D···A (Å)	D-H···A (°)	Symmetry code
O1-H1···O2	0.84	2.24	2.694(2)	114	-
O1-H1···N1	0.84	1.95	2.701(2)	148	-
O4-H4···O3*	0.84	1.80	2.640(2)	173	3-x,1-y,2-z
N2-H2A···O5*	0.88	2.12	2.946(2)	156	-x,2-y,-z
N2-H2B···O5*	0.88	2.15	2.929(2)	147	1+x,y,z
C7-H7···O3	0.95	2.50	2.830(2)	101	-
C14-H14···O3*	0.95	2.51	3.368(2)	151	-1+x,y,-1+z

*The atom to which the symmetry operation applies.

Molecular geometry

The FA molecule has a planar aromatic ring but experiences a slight rotation in the acid tail. The torsion angles describing this rotation are C3-C4-C7-C8 = 172.5(2)° and C7-C8-C9-O4 = 177.1(2)° (see Figure 5.18 for atom labels). The pyridyl ring of the ISO molecule is planar while the rotation around the C13-C16 bond leads to the torsion angles C14-C13-C16-N2 = -30.0(2)° and C12-C13-C16-O5 = -29.5(2)°.

Crystal packing

The molecules interact through a number of strong hydrogen bonds. Undulating ribbons are formed by the heteromeric interaction between ISO and FA and the homomeric ISO-ISO and FA-FA interactions. The ribbons are linked by the formation of ISO ladders to make up layers. The layers pack in an ABAB sequence along the *a*-axis and are linked through a C-H···O hydrogen bond (Figures 5.21a,b).

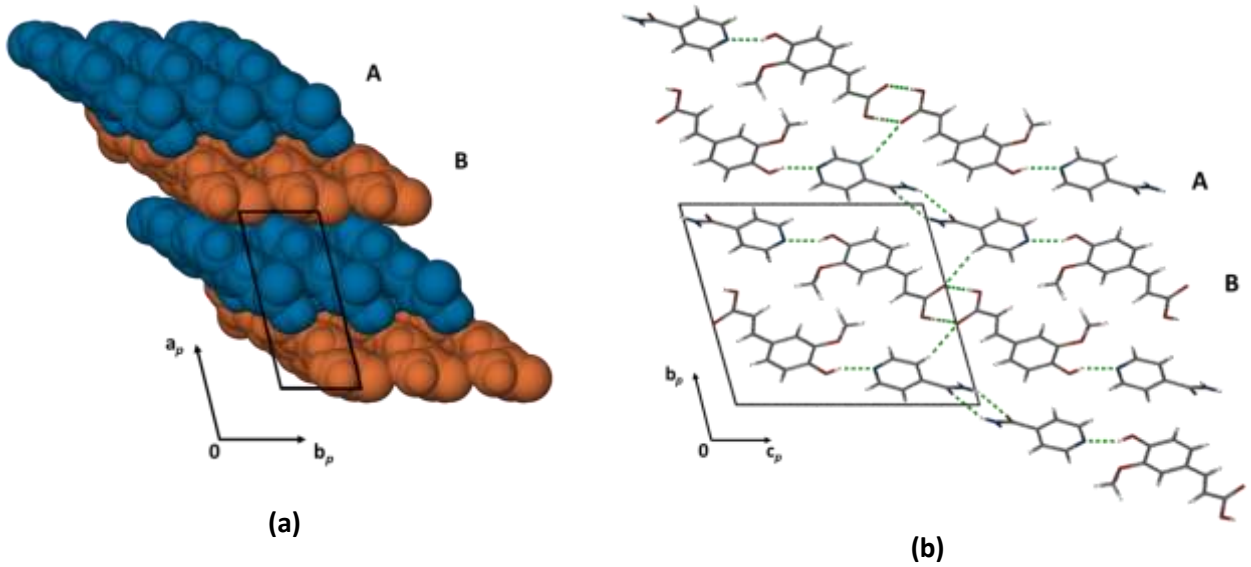

Figure 5.21: (a) A space-filling diagram viewed down the *b*-axis illustrating the layers and (b) a projection down the *a*-axis illustrating the layers (A and B) and the C-H···O hydrogen bonds that link the layers.

Comparative PXRD

Figure 5.22 shows the PXRD pattern of FA·ISO and the calculated pattern from the single crystal X-ray diffraction data. The good match between the two patterns indicates that the single crystal chosen for analysis is representative of the bulk material. The general tendency for peak positions in the experimental pattern (294 K) to occur at lower 2θ values is due to the low temperature of the data collection for the single crystal X-ray analysis (173 K).

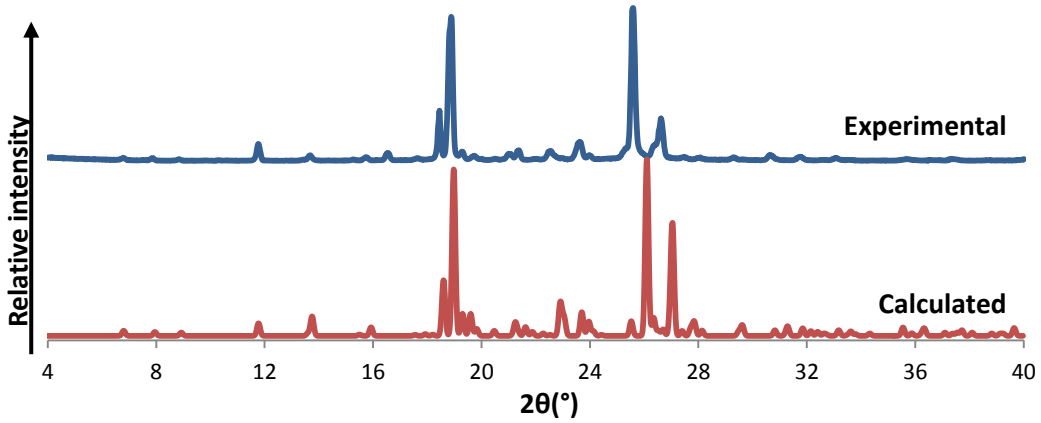

Figure 5.22: PXRD pattern of the cocrystal obtained by coprecipitation and the PXRD pattern calculated from the crystal structure.

FERULIC ACID AND NICOTINAMIDE (FA·NIC)

Thermal analysis

HSM analysis of a single crystal of FA·NIC was carried out at a heating rate of 10 °C/minute (Figure 5.23). The photographs reveal a phase transformation at 90°C, indicated by the crystal changing from colourless to opaque. The sample melts at 129 °C, an event corroborated by the DSC analysis.

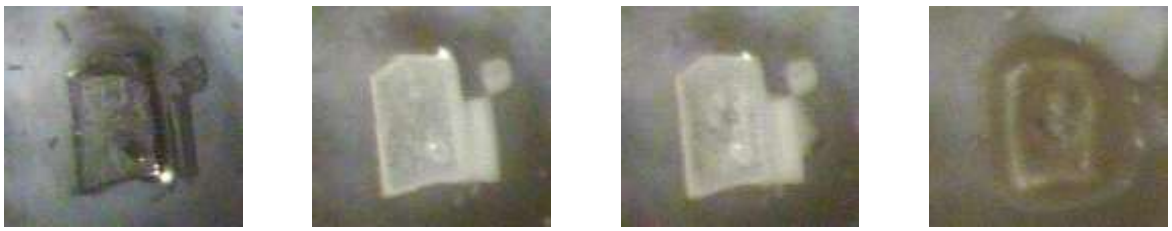

30 °C **90 °C** **111 °C** **129 °C**

Figure 5.23: Representative HSM photographs of FA·NIC

The DSC analysis (Figure 5.24) shows two broad endotherms with a sharp, but small, endotherm overlapping the second broad endotherm. The broad endotherms represent water mass loss, which likely occurs in two steps. The small, sharp endotherm occurring at 95 °C is attributed to a phase transformation following water loss. A sharp endotherm at 126 °C represents the melt, which occurs at a lower temperature than the melting points of the starting components (FA: 168-172; NIC: 128-131 °C), signifying the presence of a new crystal phase. Decomposition begins at *ca.* 160°C. The TGA shows a two-step mass loss between 30 °C and 115 °C. The percentage mass loss is 14.8 ± 1.5 % (n = 3) which corresponds to the loss of 3.0 ± 0.4 water molecules per FA-NIC unit.

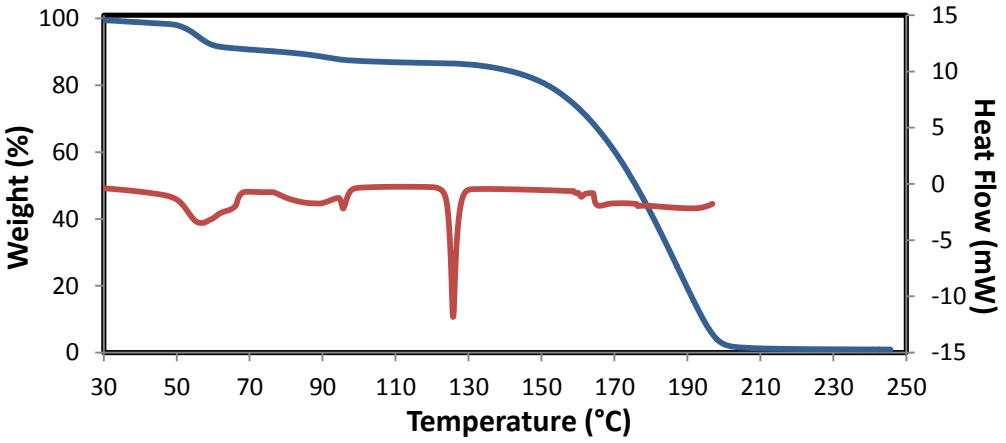

Figure 5.24: TGA (blue) and DSC (red) traces of FA·NIC

^{1}H Nuclear Magnetic Resonance Spectroscopy

A 1:1 stoichiometric ratio was established using ^{1}H NMR spectroscopy through the integration of the respective FA and NIC signals for a sample of the cocrystal dissolved in DMSO-d_6 (Table 5.11) (see Appendix B for full spectrum).

Table 5.11: Integrals of the protons of FA and NIC used to confirm the stoichiometry of FA·NIC

Proton	δ (ppm)	Multiplicity	J (Hz)	Integration	Experimental/ Theoretical	
C-$\underline{H}_a$ (NIC)	8.709	dd	^{3}J = 4.78 ^{4}J = 1.82	0.877	0.9	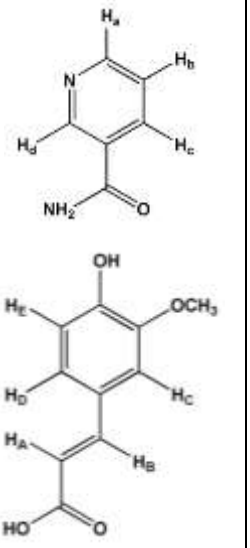
C-$\underline{H}_c$ (NIC)	8.214	ddd	^{3}J = 7.88 ^{4}J = 1.64 ^{4}J = 2.20	1.022	1	
C-$\underline{H}_d$ (NIC)	9.039	dd	^{4}J = 2.20 ^{4}J = 0.92	0.897	0.9	
C-$\underline{H}_A$ (FA)	6.362	d	^{3}J = 15.93	0.996	1	
C-$\underline{H}_C$ (FA)	7.280	d	^{4}J = 2.04	1.000*	1	
C-$\underline{H}_D$ (FA)	7.089	dd	^{3}J = 8.24 ^{4}J = 2.00	1.001	1	
C-$\underline{H}_E$ (FA)	6.801	d	^{3}J = 8.12	0.993		
O-C$\underline{H}_3$ (FA)	3.828	s		3.076	3	

*Reference integral

Single crystal X-ray analysis

A single, colourless crystal was selected from the mother liquor and placed directly into Paratone N oil so as to prevent solvent evaporation.[13] The Bruker APEX DUO II diffractometer was used to collect single crystal X-ray intensity data. The crystal system and space group were determined by examining digital precession photographs using the program LAYER.[14] The Laue symmetry was found to be *mmm* indicating the orthorhombic crystal system. The reflection conditions *hkl: none; 0kl: k = 2n; h0l: l = 2n; hk0: h = 2n* in the reciprocal lattice layers indicated the space group Pbca unequivocally. This assignment was confirmed using program XPREP.[15]

Structure solution and refinement

The collected data were processed using XPREP and the structure was solved using direct methods implemented in the program SHELXS-97.[15,16] The positions of the non-hydrogen atoms were assigned from the E-map and allowed to refine isotropically on F^2 using SHELXH-97.[17] The ASU was found to consist of one FA molecule, one NIC molecule and three water molecules (Figure 5.25). The non-hydrogen atoms were allowed to refine anisotropically once it was established that their refined U_{iso} values were stable.

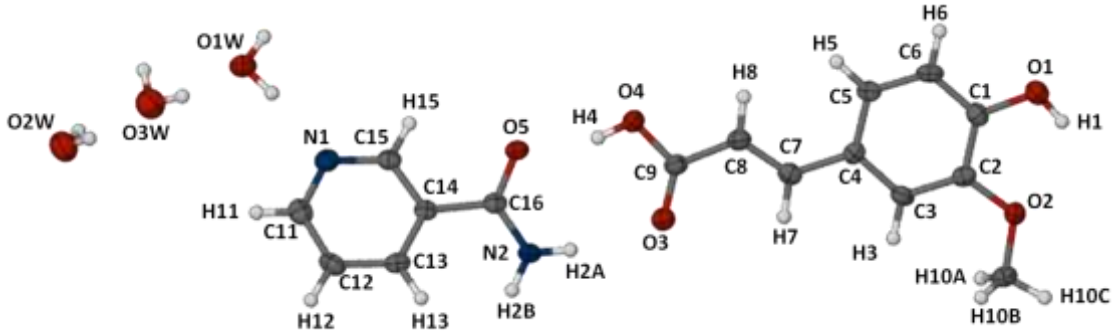

Figure 5.25: The asymmetric unit of FA·NIC. Thermal ellipsoids are drawn at the 50% probability level, while the hydrogen atoms are shown as spheres of arbitrary radii.

The crystallographic data and refinement parameters for the structure are listed in Table 5.12.

Table 5.12: Data collection and refinement parameters for FA·NIC

Chemical Formula	**$C_{10}H_{10}O_4 \bullet C_6H_6N_2O \bullet 3H_2O$**
Formula weight / g mol^{-1}	370.36
Crystal system	Orthorhombic
Space group	Pbca (No. 61)
a / Å	7.147(1)
b / Å	12.235(2)
c / Å	41.011(7)
Volume / $Å^3$	3586(1)
Z	8
Calculated density / g cm^{-3}	1.372
μ (MoKα) / mm^{-1}	0.111
F (000)	1568
Temperature of data collection / K	173(2)
Crystal size / mm^3	0.04 x 0.04 x 0.21
Theta range scanned / °	3.0 ≤ θ ≤ 25.5
Index ranges	h: -8, 5; k: -13, 14; l: -20, 49
Total number of reflections	8045
No. of independent reflections	3300
No. of reflections with I > 2σ(I)	2129
No. of parameters	256
R_{int}	0.044
R_1 (I > 2σ(I))	0.0852
wR_2 (I > 2σ(I))	0.1956
S	1.104
Coefficients in weighting scheme	a = 0.0448, b = 11.1153
$(Δ/σ)_{mean}$	< 0.001
Δρ excursions / e $Å^{-3}$	-0.37 and 0.28

There was no evidence of proton transfer from the hydroxyl group of FA to the pyridyl-N of NIC in the difference Fourier map. Aromatic hydrogen atoms were geometrically placed in a riding model (AFIX 43) while rotating models were used to place the methyl hydrogen atoms and the hydroxyl hydrogen atoms (AFIX 137 and AFIX 147). The primary amide hydrogen atoms were placed using the AFIX 93 command.

Non-hydrogen atoms were initially refined isotropically and subsequently anisotropically. The temperature factors for the hydrogen atoms were 1.2 times those of their parent atoms (1.5 times for methyl hydrogen atoms). The hydrogen atoms belonging to the water molecules were identified on the difference Fourier map and were assigned accordingly. After using the DFIX instruction to fix the O-H bond lengths to 0.85 ± 0.01 Å, the DANG command was added, constraining the bond angles to 100(4)° for O1W, 107(4)° for O2W and 105(4)° for O3W.

Hydrogen bonding

An intramolecular hydrogen bond [graph-set designation $S_1^1(5)$] exists between the *p*-hydroxyl group and the oxygen atom of the O-methyl group of FA. One FA molecule and one NIC molecule hydrogen bond heteromerically to form an acid-amide synthon with the ring designation $R_2^2(8)$. This synthon forms discrete dimers through the homomeric interaction with an inversion-related synthon, such that the hydrogen bond formed between the *anti*-H atom of the amide and the carbonyl-O of adjacent ISO molecule results in a second ring motif $R_4^2(8)$. These heterosynthon dimers form columns parallel to the *b*-axis and the columns are linked by a number of hydrogen bonding interactions with water molecules (Figure 5.26).

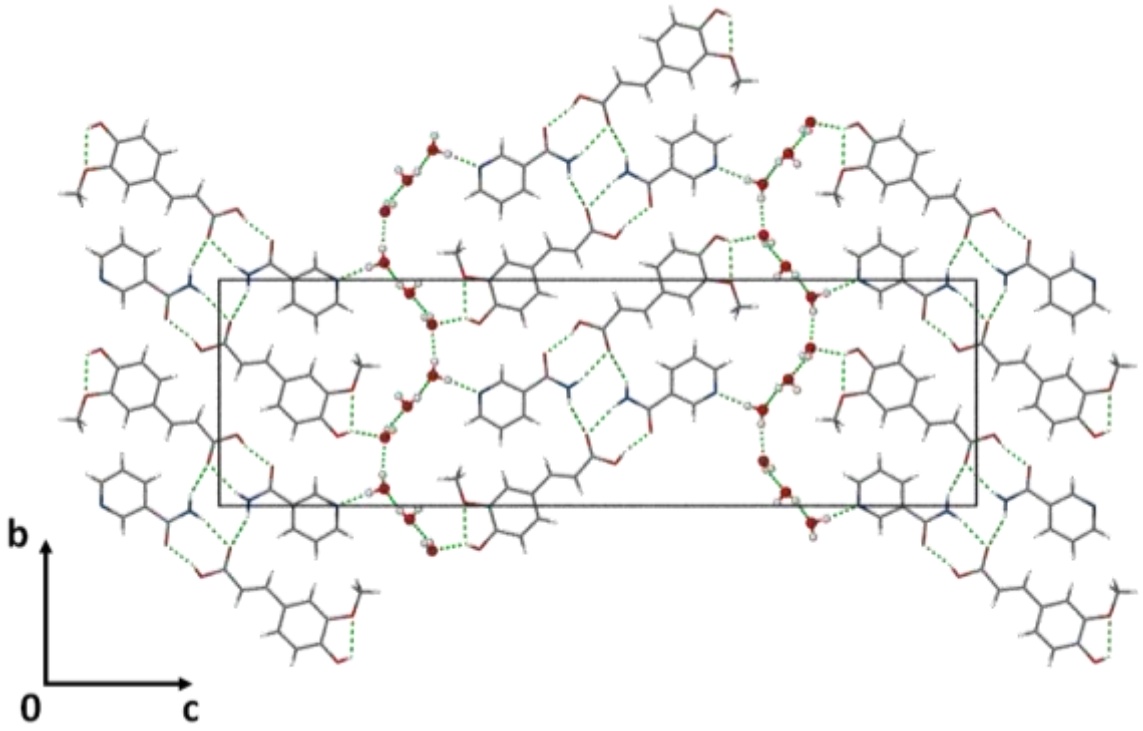

Figure 5.26: The hydrogen bonding arrangement of FA·NIC viewed down the *a*-axis.

O3W hydrogen bonds to two O2W and two O1W molecules in a DDAA (D = donor, A = acceptor) fashion. The O1W and O2W water molecules hydrogen bond to each end of the FA-NIC units such that the pyridyl-N of NIC interacts with the hydrogen atom of O1W and the *p*-hydroxyl of FA interacts with the oxygen atom of O2W (Figure 5.27). O1W and O2W also exist in a DDAA environment.

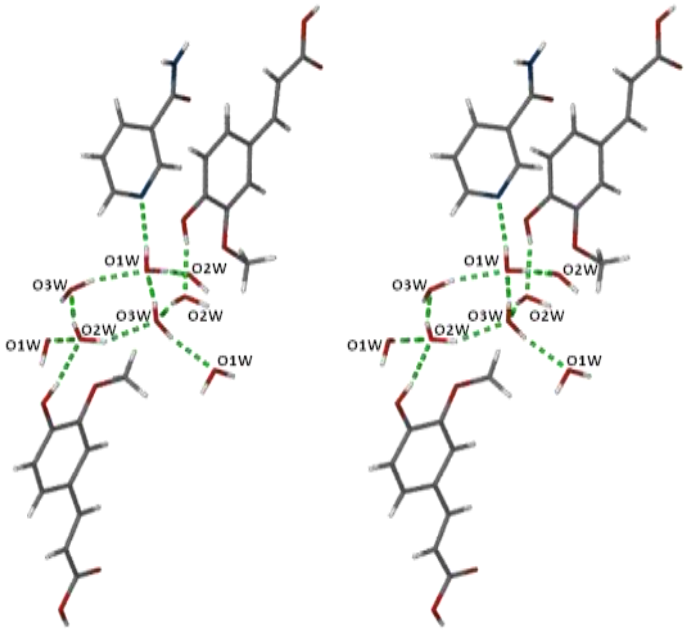

Figure 5.27: A stereodiagram of the three water molecules and their hydrogen bond interactions.

The water molecules form an undulating wall of concatenated rings that is viewed parallel to the *c*-axis in Figure 5.28. The four-membered ring has graph-set designation $R_4^3(8)$ and the six-membered ring a designation $R_6^5(12)$. The hydrogen bonding between the water molecules and the cocrystal units leads to a three-dimensional hydrogen bonded network. Table 5.13 lists the hydrogen bonding parameters.

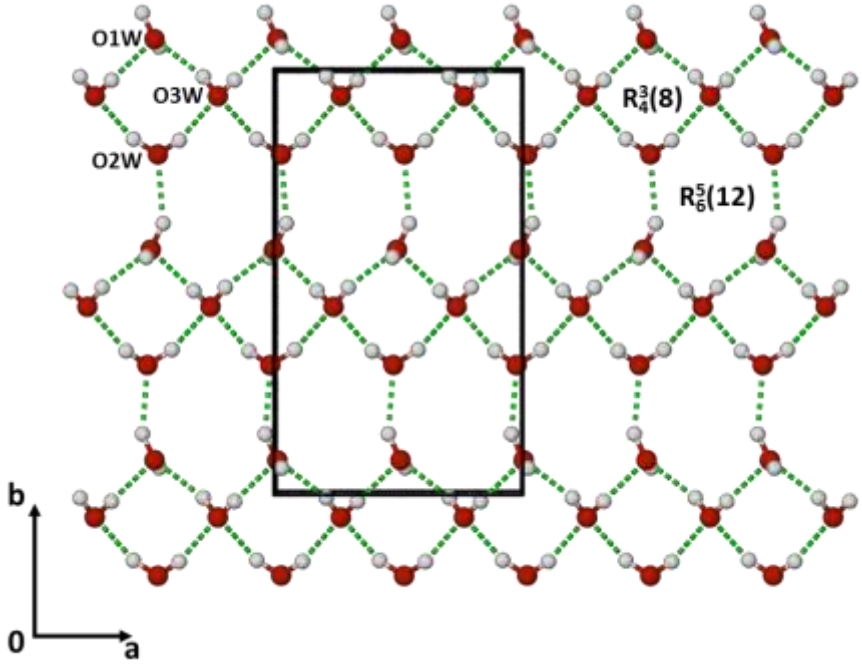

Figure 5.28: A projection down the *c*-axis illustrating the hydrogen bonding involving the three water molecules O1W, O2W and O3W.

Table 5.13: Hydrogen bonding parameters of FA·NIC

D-H···A	D-H (Å)	H···A (Å)	D···A (Å)	D-H···A (°)	Symmetry Operation
O1-H1···O2	0.84	2.25	2.695(4)	113	-
O1-H1···O2W*	0.84	1.95	2.698(5)	148	x,3/2-y,1/2+z
O4-H4···O5	0.84	1.76	2.582(4)	164	-
N2-H2A···O3	0.88	2.12	2.981(5)	166	-
N2-H2B···O3*	0.88	2.25	2.979(5)	140	1-x,1-y,1-z
O1W-H1W1···N1	0.86(2)	1.90(3)	2.757(5)	172(5)	-
O1W-H1W2···O2W*	0.85(3)	2.01(3)	2.773(5)	149(5)	1-x,1/2+y,1/2-z
O2W-H2W1···O3W	0.85(4)	2.00(4)	2.773(6)	152(4)	-
O2W-H2W2···O3W*	0.84(4)	1.95(4)	2.774(6)	167(4)	-1/2+x,y,1/2-z
O3W-H3W1···O1W	0.85(4)	1.93(4)	2.768(6)	168(4)	-
O3W-H3W2···O1W*	0.86(4)	1.94(4)	2.775(6)	163(4)	1/2+x,y,1/2-z

*The atom to which the symmetry operation applies.

The structure is stabilised by two face-to-face π-π stacking interactions between adjacent FA-NIC units which stack parallel to the *a*-axis (Figure 5.29). The distances between the centroids of FA and NIC are shown.

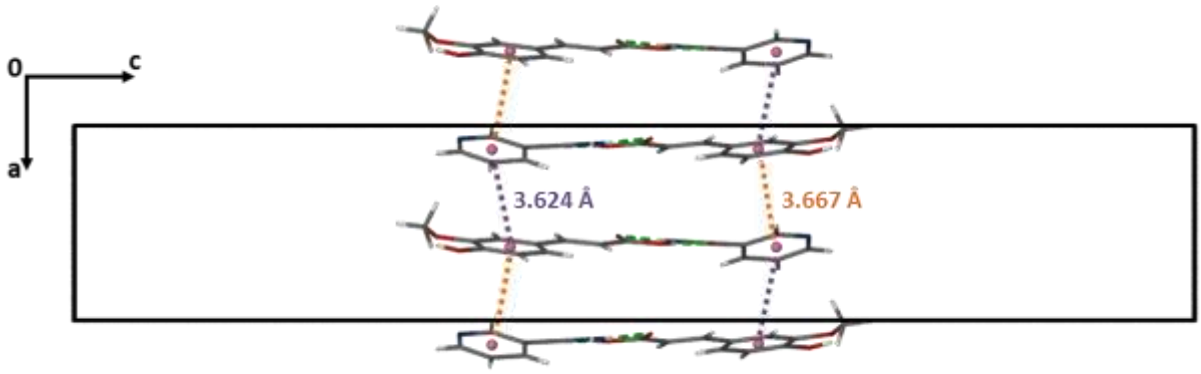

Figure 5.29: π-π stacking interactions in FA·NIC viewed down the *b*-axis.

Molecular geometry

The FA molecule is virtually planar as the torsion angles are in the range of 3.8° to -1.5°. The aromatic ring of NIC is likewise planar but there is significant rotation of the amide group about the C14-C16 bond [C13-C14-C16-N2 = 24.2(6)° and C15-C14-C16-O5 = 20.6(6)°]. Refer to Figure 5.25 for atom numbering.

Crystal packing

Supramolecular tapes are formed between FA-NIC units which dimerise to form centrosymmetrical dimers. The FA-NIC units stack in an anti-parallel manner by π-π stacking interactions parallel to the *a*-axis. The tapes are linked by a number of hydrogen bonding interactions with the water molecules in the columns between the tapes. The columns of water molecules lie parallel to the *a*-axis (Figure 5.30).

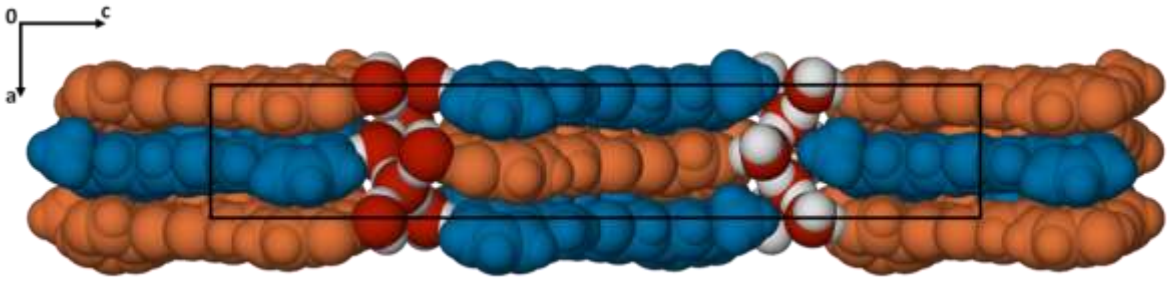

Figure 5.30: Packing of FA·NIC viewed down the *b*-axis.

Comparative PXRD

Figure 5.31 shows the PXRD pattern of the coprecipitation product FA·NIC and the pattern calculated from the single crystal X-ray diffraction data. There is good agreement between the two patterns indicating that the crystal chosen for single crystal X-ray analysis is representative of the bulk material. It is noted, however, that there is a shift to lower 2θ values in the peak positions of the experimental PXRD pattern. This is due to the difference in the temperatures involved: the experimental PXRD was recorded at room temperature (294 K) while the single crystal data were collected at 173 K.

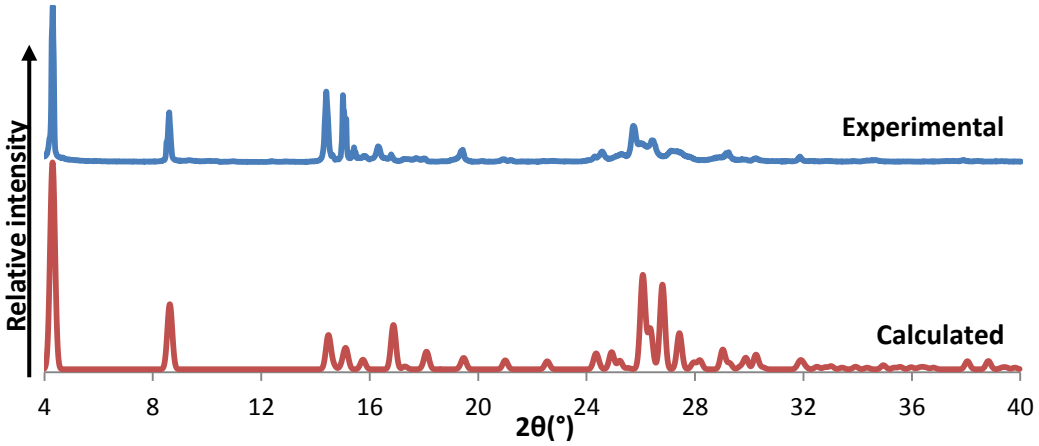

Figure 5.31: PXRD pattern of the cocrystal obtained by coprecipitation and the PXRD pattern calculated from the crystal structure.

HYDROFERULIC ACID AND ISONICOTINAMIDE (HFA·ISO)

Thermal analysis

HSM analysis of a single crystal of HFA·ISO was carried out at a heating rate of 10 °C/minute. The crystal begins to melt at 136 °C (Figure 5.32) and decomposition begins soon after.

30 °C **136 °C** **138 °C**

Figure 5.32: Representative HSM photographs of HFA·ISO

The DSC analysis (Figure 5.33) shows a sharp endotherm representing a melt with an onset temperature of 130 °C and a peak maximum of 132 °C. The melting point is different from those of the starting materials (HFA: 87-93 °C; ISO: 128-131 °C) confirming the formation of a new phase. TG analysis confirms that after the melt, decomposition occurs at *ca*. 160 °C. No solvent/hydroxycinnamic acid loss is observed prior to this event (Figure 5.33).

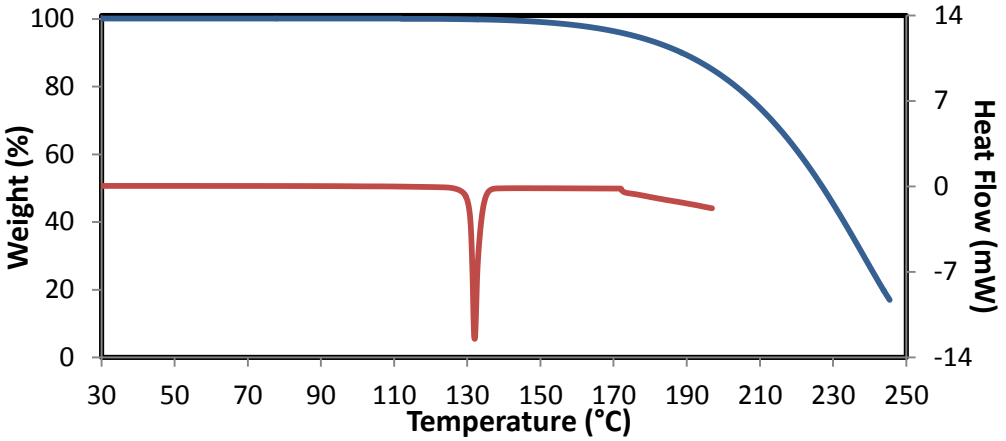

Figure 5.33: TGA (blue) and DSC (red) traces of HFA·ISO

^{1}H Nuclear Magnetic Resonance Spectroscopy

The hydroxycinnamic acid:coformer stoichiometry was determined using ^{1}H NMR spectroscopy by integrating the hydroxycinnamic acid and coformer signals, respectively (see Appendix B for full spectrum). A 1:2 stoichometry was found for a sample of the HFA·ISO cocrystals dissolved in D_2O (Table 5.14).

Table 5.14: Integrals of HFA and ISO protons for HFA·ISO used to confirm the stoichiometry.

Proton	δ (ppm)	Multiplicity	J (Hz)	Integration	Experimental/ Theoretical	
2 x C-$\underline{H}_a$ (ISO)	8.741	d	^{3}J = 5.32	1.509	2	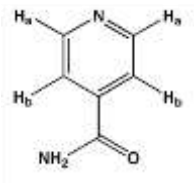
2 x C-$\underline{H}_b$ (ISO)	7.833	d	^{3}J = 5.31	1.464	2	
2 x C-$\underline{H}_A$ (HFA)	2.875	t	^{3}J = 7.51	0.642	1.9	
2 x C-$\underline{H}_B$ (HFA)	2.619	t	^{3}J = 7.51	0.628	1.9	
C-$\underline{H}_C$ (HFA)	6.971	s		0.290	0.9	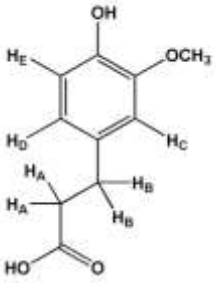
C-$\underline{H}_D$ (HFA) C-$\underline{H}_E$ (HFA)	6.843	dd	^{3}J = 30.65 ^{4}J = 8.07	0.588	1.8	
O-C$\underline{H}_3$ (HFA)	3.879	s		1.000*	3	

*Reference integral

Single crystal X-ray analysis

Single crystal X-ray intensity data were collected on the Bruker APEX DUO II diffractometer. The crystal system (triclinic) was determined using the program LAYER[3] and the space group was determined to be $P\bar{1}$ as the experimental value for $|E^2 - 1|$ was 1.052.

Structure solution and refinement

The collected data were prepared using XPREP and the structure was solved using direct methods with the program SHELXS-97.[16,17] The resulting E-map revealed the positions of the non-hydrogen atoms which were placed accordingly and refined isotropically on F^2 using SHELXH-97.[18] All atoms were later refined anisotropically after it was confirmed that the isotropic temperature factors behaved well upon refinement. The ASU was found to consist of one HFA molecule and two ISO molecules, A and B (Figure 5.34).

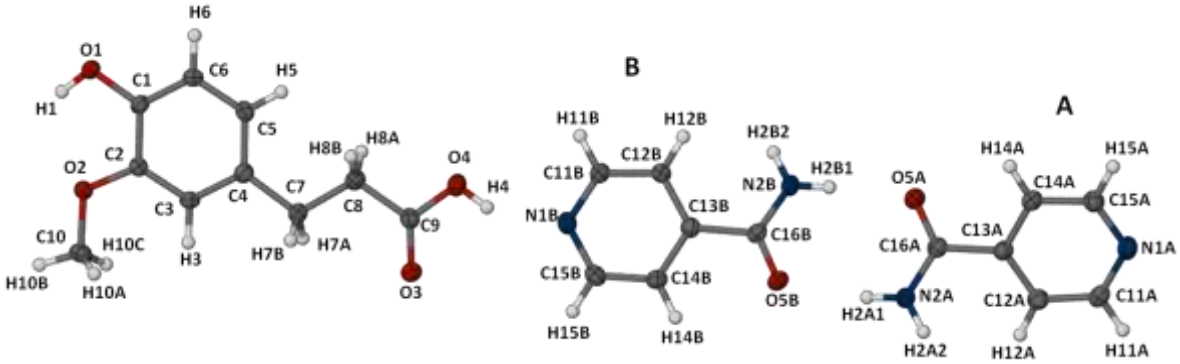

Figure 5.34: The asymmetric unit of HFA·ISO. Thermal ellipsoids are drawn at the 50% probability level, while the hydrogen atoms are shown as spheres of arbitrary radii.

The positions of hydrogen atoms were identified on the difference Fourier map and were placed in idealised positions. There was no evidence of proton transfer from the hydroxyl group of HFA to the

pyridyl-N of ISO in the difference Fourier map. A riding model was used to include the aromatic and aliphatic hydrogen atoms (AFIX 43 and AFIX 23, respectively) and a rotating group model to place the methyl hydrogen atoms (AFIX 137). The hydroxyl hydrogen atoms were placed based on a hydrogen bond searching model (AFIX 83). The temperature factors for the hydrogen atoms were 1.2 times those of the parent atoms (1.5 times for the methyl hydrogen atoms).

The crystallographic data and refinement parameters for the structure are listed in Table 5.15.

Table 5.15: Hydrogen bonding parameters of HFA·ISO

Chemical Formula	**$C_{10}H_{10}O_4 \bullet (C_6H_6N_2O)_2$**
Formula weight / g mol^{-1}	440.45
Crystal system	Triclinic
Space group	$P\bar{1}$ (No. 2)
a / Å	8.945(2)
b / Å	10.127(2)
c / Å	12.803(3)
α / °	96.346(1)
β / °	97.869(1)
γ / °	112.955(1)
Volume / $Å^3$	1040.6(5)
Z	2
Calculated density / g cm^{-3}	1.406
μ (MoKα) / mm^{-1}	0.104
F (000)	464
Temperature of data collection / K	173(2)
Crystal size / mm^3	0.20 x 0.25 x 0.38
Theta range scanned / °	2.5 ≤ θ ≤ 26.4
Index ranges	h: -11, 11; k: -12, 12; l: -15, 15
Total number of reflections	7979
No. of independent reflections	4236
No. of reflections with I > 2σ(I)	3442
No. of parameters	290
R_{int}	0.014
R_1 (I > 2σ(I))	0.0371
wR_2 (I > 2σ(I))	0.1048
S	1.080
Coefficients in weighting scheme	a = 0.0604, b = 0.1147
$(\Delta/\sigma)_{mean}$	< 0.001
Δρ excursions / e $Å^{-3}$	-0.21 and 0.22

Hydrogen bonding

An intramolecular hydrogen bond exists between the *p*-hydroxyl group and the oxygen atom of the *O*-methyl group of HFA [graph-set designation $S_1^1(5)$]. ISO A and ISO B form a homomeric hydrogen bonded ring [$R_2^2(8)$]. HFA forms two heterosynthons with the two ISO molecules: the *p*-hydroxyl OH group of HFA interacts with the pyridyl-N of ISO A and the acid OH of HFA interacts with the pyridyl-N of

ISO B. These interactions result in the formation of molecular chains. The chains are linked by hydrogen bonding between the *anti*-H atoms of the amide groups on ISO A and ISO B and the p-hydroxyl O and acid carbonyl O of HFA, respectively, to form layers. The layers are further stabilised by two C-H···O hydrogen bonds. Figure 5.35 illustrates the hydrogen bonding interactions that exist within a layer.

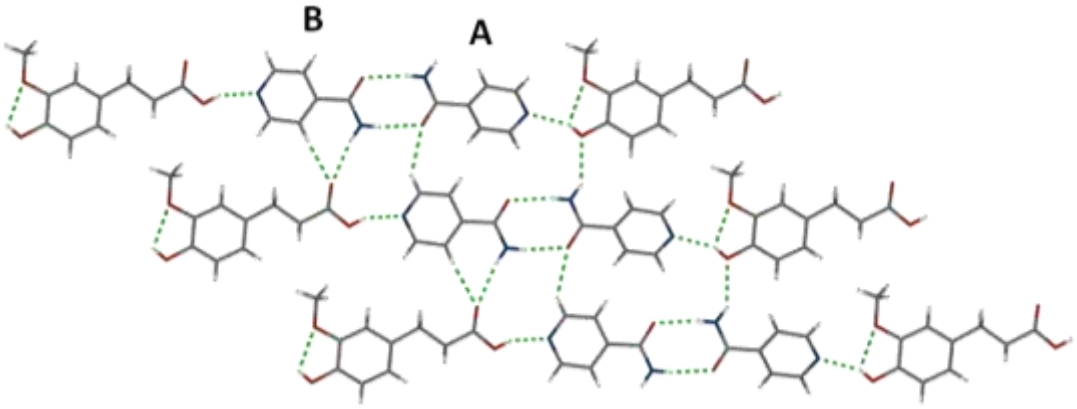

Figure 5.35: Projection onto the (0 2 2) plane illustrating the layer formed by hydrogen bonding interactions in HFA·ISO.

Two layers are linked by a C-H···O hydrogen bond between a hydrogen atom on the methyl group of HFA and the amide oxygen atom of ISO B to form a bilayer. This interaction leads to a column-type packing. Table 5.16 provides parameters of the hydrogen bonds described above.

The structure is further stabilised by three π-π stacking interactions. Within a bilayer two π-π stacking interactions exist, one between an HFA molecule and molecule ISO A (ring centroid···centroid distance CG1···CG2 = 3.845(1) Å) and the other between two centrosymmetrically related ISO B molecules (CG3···CG3 = 3.595(1) Å). A third π-π stacking interaction between two centrosymmetrically related HFA molecules links the bilayers (CG1···CG1 = 3.738(1)) (Figure 5.36).

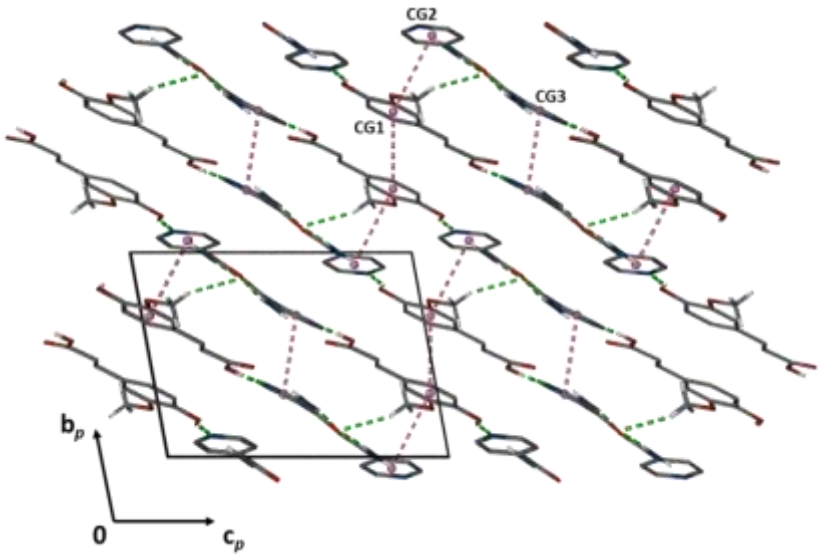

Figure 5.36: A projection down the *a*-axis showing the inter-layer C-H···O hydrogen bonds which form a columnar structure.

Table 5.16: Hydrogen bonding parameters of HFA·ISO.

D-H···A	D-H (Å)	H···A (Å)	D···A (Å)	D-H···A (°)	Symmetry Operation
O1-H1···O2	0.84	2.26	2.709(2)	114	-
O1-H1···N1A*	0.84	2.02	2.780(2)	151	-x,2-y,-z
O4-H4···N1B*	0.84	1.83	2.619(2)	155	2-x,1-y,1-z
N2A-H2A2···O1*	0.88	2.32	3.083(2)	145	1-x,2-y,-z
N2A-H2A1···O5B	0.88	2.04	2.914(2)	171	-
N2B-H2B1···O5A	0.88	2.03	2.897(2)	168	-
N2B-H2B2···O3*	0.88	2.25	3.109(2)	166	1-x,1-y,1-z
C10-H10C···O5B	0.98	2.53	3.357(2)	142	-
C12B-H12B···O3*	0.95	2.38	3.302(2)	165	1-x,1-y,1-z
C15B-H15B···O5A*	0.95	2.43	3.221(2)	140	1+x,y,z

*The atom to which the symmetry operation applies.

Molecular geometry

The HFA molecule is planar (all torsion angles are close to 0° or 180 °) with small deviations in the acid tail [C4-C7-C8-C9 = 177.4(1)° and C7-C8-C9-O3 = -4.1(2)°]. For atom labels refer to Figure 5.34. The aromatic fragment of ISO A is planar as the torsion angle magnitudes are smaller than 1°. The amide group is twisted out of the plane of the aromatic ring [torsion angles C12A-C13A-C16A-N2A = 33.8(2)°, C14A-C13A-C16A-O5A = 30.6(2)°]. Similarly, the aromatic ring of ISO B is planar while the amide group is twisted out of the plane [C14B-C13B-C16B-O5B = -13. 7(2)° and C12B-C13B-C16B-N2B = -14.7(2)°].

Crystal packing

The layers pack in centrosymmetrical pairs to form bilayers, facilitated by a C-H···O hydrogen bond and π-π stacking interactions (HFA···ISO A and ISO B···ISO B). The bilayers pack in an ABAB sequence sustained by a π-π stacking interaction between two HFA molecules related by an inversion centre (Figure 5.37).

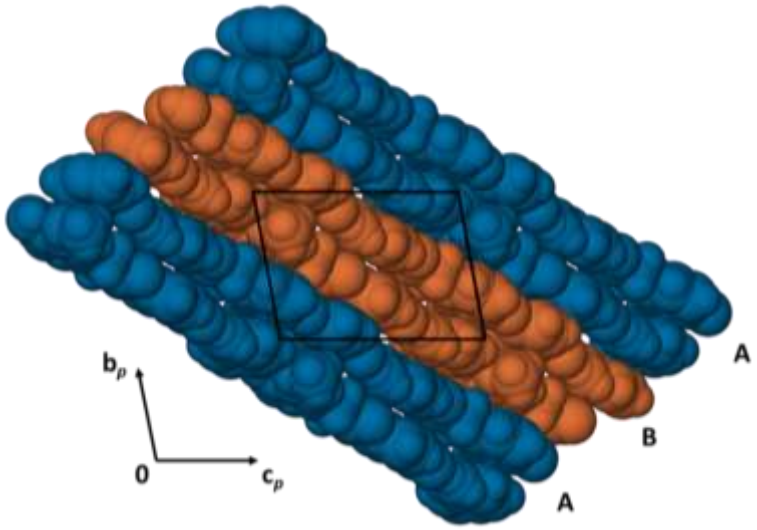

Figure 5.37: Packing of HFA·ISO viewed down the *a*-axis.

Comparative PXRD

Figure 5.38 shows the calculated and experimental traces of HFA·ISO. The peak positions are shifted in 2θ due to the differences in temperature of data collection between the powder sample and the single crystal. Preferred orientation of the experimental sample leads to differences in peak intensities. The comparison the traces demonstrate that the crystal chosen for single crystal X-ray diffraction is representative of the bulk material.

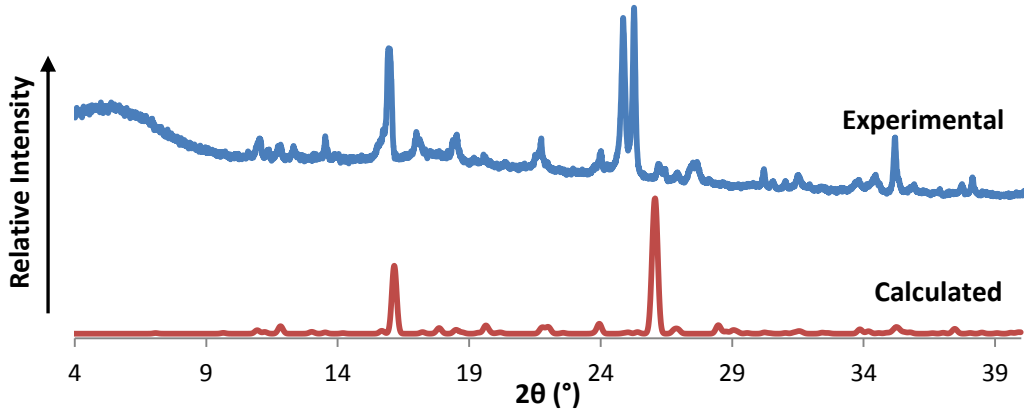

Figure 5.38: PXRD pattern of the cocrystal obtained by coprecipitation and the PXRD pattern calculated from the crystal structure.

HYDROFERULIC ACID AND NICOTINAMIDE (HFA·NIC)

Thermal analysis

HSM analysis of a single crystal of HFA·NIC was carried out at a heating rate of 10 °C/minute. The crystal is stable until 123 °C, at which point melting begins. The crystal is completely melted by 127 °C and decomposition follows after 200 °C (Figure 5.39).

30 °C **123 °C** **125 °C**

Figure 5.39: Representative HSM photographs of HFA·NIC

The DSC analysis (Figure 5.40) shows a sharp endotherm at 120 °C indicating a melt. The melting temperature is different from the melting points of the starting materials (HFA: 87-93 °C; NIC: 128-131 °C) confirming the formation of a new phase. The decomposition event manifests as a broad endotherm starting at *ca*. 170 °C. The TG analysis (Figure 5.40) shows a large mass loss

corresponding to decomposition at *ca*. 170 °C. No solvent/hydroxycinnamic acid loss is observed prior to this event.

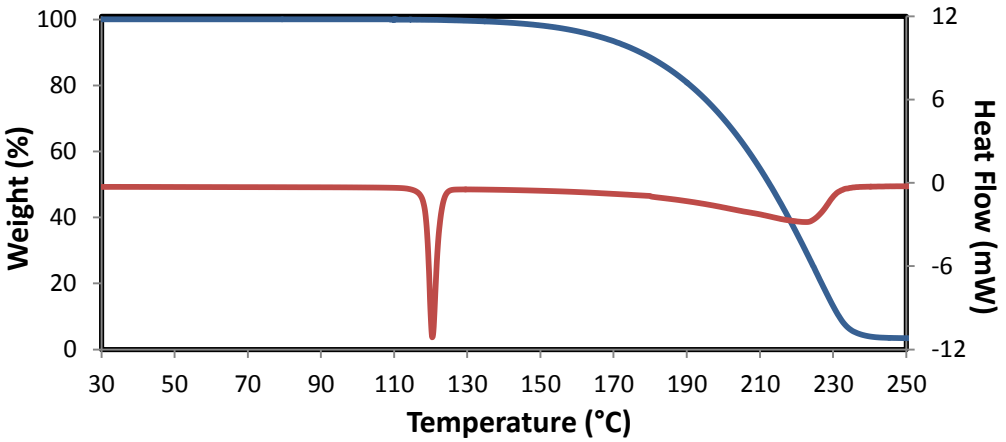

Figure 5.40: TGA (blue) and DSC (red) traces of HFA·NIC

^{1}H Nuclear Magnetic Resonance Spectroscopy

The stoichiometry of the cocrystal HFA·NIC was determined using ^{1}H NMR spectroscopy through integration of the signals of HFA and NIC, respectively, for a sample of the cocrystal dissolved in DMSO-d_6 (Table 5.17). A stoichiometry of 1:2 was found for HFA·NIC (see Appendix B for full spectrum).

Table 5.17: The integrals obtained for the cocrystal HFA·NIC to confirm stoichiometry.

Proton	δ (ppm)	Multiplicity	J (Hz)	Integration	Experimental/ Theoretical	
C-$\underline{H}_a$ (NIC)	8.710	dd	^{3}J = 4.76 ^{4}J = 1.64	1.943	2	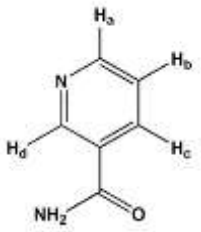
C-$\underline{H}_b$ (NIC)	7.505	ddd	^{3}J = 7.98 ^{3}J = 4.86 ^{5}J = 0.92	2.099	2	
C-$\underline{H}_c$ (NIC)	8.214	ddd	^{3}J = 7.98 ^{4}J = 1.74 ^{4}J = 2.40	2.045	2	
C-$\underline{H}_d$ (NIC)	9.039	dd	^{4}J = 2.20 ^{5}J = 0.92	1.826	1.8	
2 x C-$\underline{H}_A$ (HFA)	2.725	t	^{3}J = 7.70	2.142	1	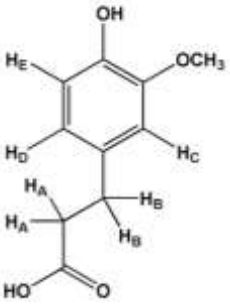
C-$\underline{H}_C$ (HFA)	6.793	d	^{4}J = 2.04	1.000*	1	
C-$\underline{H}_D$ (HFA)	6.670	d	^{3}J = 7.88	0.988	1	
C-$\underline{H}_E$ (HFA)	6.601	dd	^{3}J = 8.06 ^{4}J = 2.02	1.000	1	
O-C$\underline{H}_3$ (HFA)	3.752	s		2.961	1	

*Reference integral

Single crystal X-ray analysis

Using Paratone N oil, a single, colourless and dry crystal was mounted on a nylon loop.[13] X-ray intensity data were collected on the Bruker APEX DUO II diffractometer. Program LAYER indicated that the Laue symmetry of the crystal was 2/*m*, which indicated the monoclinic crystal system.[14] The X-ray diffraction

data were used to determine the unit cell parameters, crystal system and space group. The reflection conditions *hkl*: none; *h0l*: *l* = 2*n*; *0k0*: *k* = 2*n* indicated the space group $P2_1/c$ unequivocally.

The crystallographic data and refinement parameters for the structure are listed in Table 5.18.

Table 5.18: Data collection and refinement parameters for HFA·NIC

Chemical Formula	**$C_{10}H_{12}O_4 \bullet (C_6H_6N_2O)_2$**
Formula weight / g mol^{-1}	440.45
Crystal system	Monoclinic
Space group	$P2_1/c$ (No. 14)
a / Å	20.043(1)
b / Å	15.568(1)
c / Å	6.934(1)
β / °	91.617(2)
Volume / $Å^3$	2162.8(3)
Z	4
Calculated density / g cm^{-3}	1.353
μ (MoKα) / mm^{-1}	0.100
F (000)	928
Temperature of data collection / K	173(2)
Crystal size / mm^3	0.06 x 0.08 x 0.27
Theta range scanned / ˚	1.7 ≤ θ ≤ 25.4
Index ranges	h: -23, 24; k: -18, 18; l: -8, 8
Total number of reflections	10821
No. of independent reflections	3988
No. of reflections with I > 2σ(I)	2914
No. of parameters	290
R_{int}	0.039
R_1 (I > 2σ(I))	0.0411
wR_2 (I > 2σ(I))	0.1060
S	1.025
Coefficients in weighting scheme	a = 0.0519, b = 0.1487
$(\Delta/\sigma)_{mean}$	< 0.001
Δρ excursions / e $Å^{-3}$	-0.22 and 0.16

Structure solution and refinement

The ASU of HFA·NIC includes one HFA molecule and two NIC molecules A and B (Figure 5.41). The program SHELXS-97 was used to solve the structure.[16] Direct methods yielded the positions of the non-hydrogen atoms, which were assigned accordingly and refined isotropically on F^2 using SHELXH-97.[17] The U_{iso} values of the non-hydrogen atoms indicated that the temperature factors were stable and the atoms were allowed to refine anisotropically.

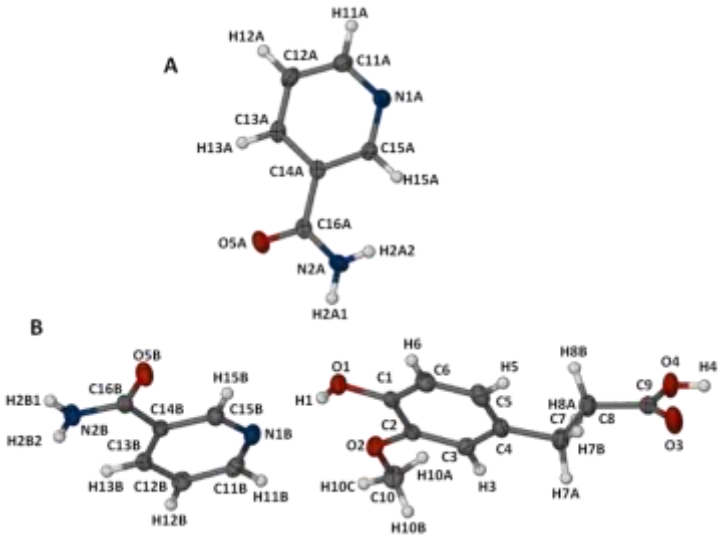

Figure 5.41: The asymmetric unit of HFA·NIC. Thermal ellipsoids are drawn at the 50% probability level, while the hydrogen atoms are shown as spheres of arbitrary radii.

The positions of hydrogen atoms were evident in the difference Fourier map and all hydrogen atoms were attached to their parent atoms in idealised positions. There was no evidence of proton transfer from the hydroxyl group of HFA to the pyridyl-N of NIC. This fact is substantiated by the C5-N1-C1 bond angle which is 118.0(2)° and 117.3(2)° for A and B, respectively. Aromatic and aliphatic hydrogen atoms were placed in a riding model (AFIX 43 and AFIX 23, respectively) while rotating models were used to place the methyl hydrogen atoms (AFIX 137) and the hydroxyl hydrogen atoms were placed using the AFIX 83 instruction (hydrogen bond searching model). The temperature factors for the hydrogen atoms were 1.2 times those of their parent atoms (1.5 times for methyl hydrogen atoms).

Hydrogen bonding

The HFA molecule is linked to two NIC A molecules (stacked anti-parallel), forming hydrogen bonds between the acid group of HFA and the pyridyl-N atom and the *syn*-H atom of the amide group of the respective NIC A molecules. These interactions propagate the crystal in the *c*-direction. The *anti*-H of the amide group of NIC A forms a hydrogen bond with the *p*-hydroxyl group of HFA. The *syn*-H of the amide of NIC B forms a homomeric ring [$R_2^2(8)$] synthon with the amide-O of a centrosymmetrically related NIC B molecule. The *anti*-H of the amide of NIC B forms a hydrogen bond with the amide oxygen of NIC A. Figure 5.42 illustrates the hydrogen bonding motifs described above, such that all interactions can be viewed clearly.

An intramolecular interaction occurs between the *p*-hydroxyl and *O*-methyl oxygen atoms of HFA (not shown in Figure 5.41). The crystal is further stabilised by a number of C-H···O bonds, including an intramolecular hydrogen bond between the amide oxygen atom and the hydrogen on C15 of NIC B, effecting the planarity of the NIC B molecule.

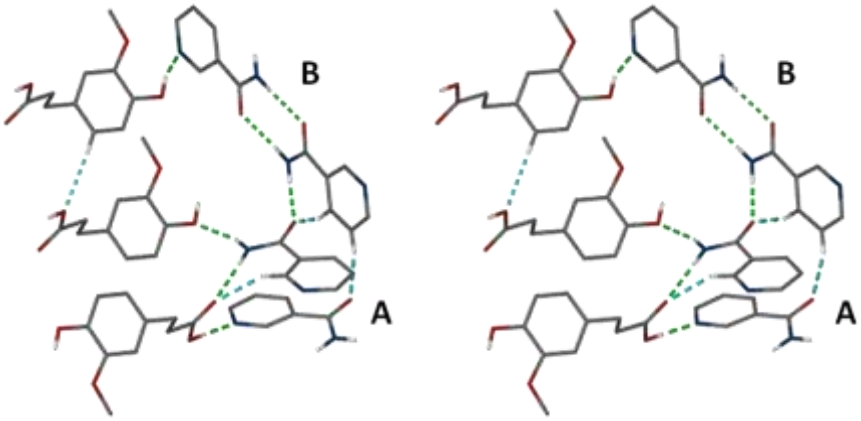

Figure 5.42: A stereodiagram of the hydrogen bonding interactions in HFA·NIC. C-H···O interactions are shown in cyan, while the classical hydrogen bonds are shown in green. Aliphatic/aromatic hydrogen atoms that are not involved in hydrogen bonding have been omitted for clarity.

The hydrogen bonding motifs generate a three-dimensional network within the crystal. Figure 5.43 shows a projection down the *c*-axis illustrating the intricate hydrogen bonding network. The intramolecular interactions are shown. No π-π stacking is evident. Table 5.19 lists the hydrogen bonding parameters.

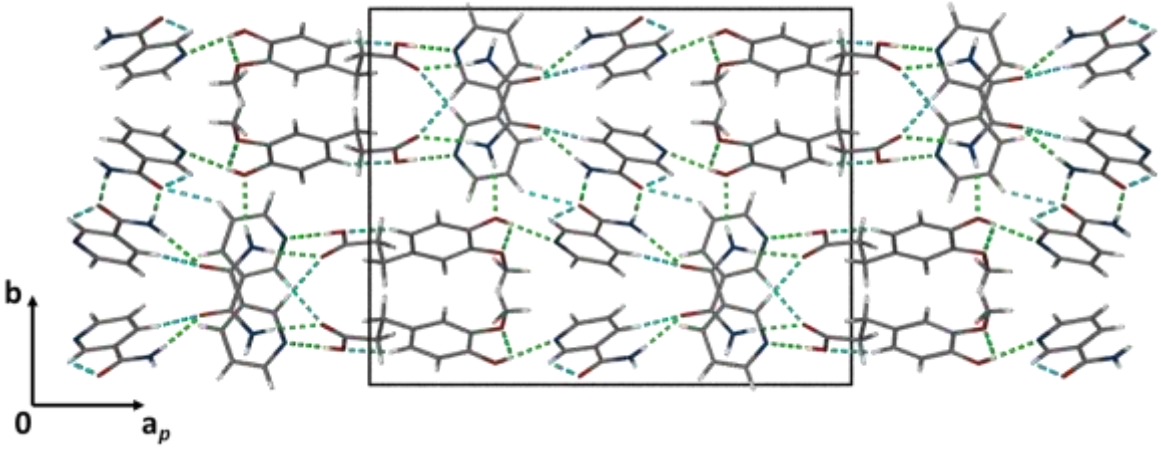

Figure 5.43: A projection down the *c*-axis showing the hydrogen bonding interactions in HFA·NIC.

Table 5.19: Hydrogen bonding parameters of HFA·NIC

D-H···A	D-H (Å)	H···A (Å)	D···A (Å)	D-H···A (°)	Symmetry Operation
O1-H1···O2	0.84	2.23	2.687(2)	114	-
O1-H1···N1B	0.84	2.00	2.687(2)	139	-
O4-H4···N1A*	0.84	1.81	2.646(2)	178	2-x,1/2+y,3/2-z
N2A-H2A1···O1	0.88	2.15	3.007(2)	164	-
N2A-H2A2···O3*	0.88	2.11	2.980(2)	170	2-x,1-y,1-z
N2B-H2B1···O5B*	0.88	2.01	2.880(2)	168	1-x,1-y,-1-z
N2B-H9B2···O5A*	0.88	2.04	2.891(2)	163	1-x,1-y,-z
C5-H5···O4*	0.95	2.56	3.456(2)	158	x,y,-1+z
C15A-H15A···O3*	0.95	2.31	3.140(2)	146	2-x,1-y,1-z
C12A-H12A···O5B*	0.95	2.51	3.289(2)	140	x,1/2-y,1/2+z
C14B-H14B···O5B	0.95	2.38	2.740(2)	102	-
C13B-H13B···O5A*	0.95	2.37	3.281(2)	161	1-x,1-y,-z

*The atom to which the symmetry operation applies.

Molecular geometry

The HFA aromatic ring and its substituents are coplanar, all torsion angles being between 2° and -2°. Atom numbering is shown in Figure 5.40. The acid tail of HFA is free to rotate leading to the torsion angles C3-C4-C7-C8 = 73.4(2)°, C4-C7-C8-C9 = 167.1(2)°, C7-C8-C9-O3 = -14.9(3)°. NIC A contains a planar aromatic ring while the amide substituent is twisted out of the plane (C15-C14-C16-N2 = 15.6(2)° and C13-C14-C16-O5 = 13.7(2)°). NIC B is planar, having all torsion angles < 1 °, aided by the intramolecular hydrogen bond C15-H15···O5.

Crystal packing

The HFA and NIC molecules pack in columns (Figure 5.44). The hydrogen bonding interactions between HFA and NIC A result in HFA-NIC columns which align antiparallel along the *b*-axis. The ends of these HFA-NIC columns interact with NIC B, forming columns of NIC B parallel to the *c*-axis. These columns are linked by the amide-amide homosynthon to form a wall of NIC B molecules in the *bc*-plane. The NIC A molecules stack in an antiparallel manner while the NIC B molecules and the HFA molecules each pack in a herringbone fashion, all parallel to the *c*-axis.

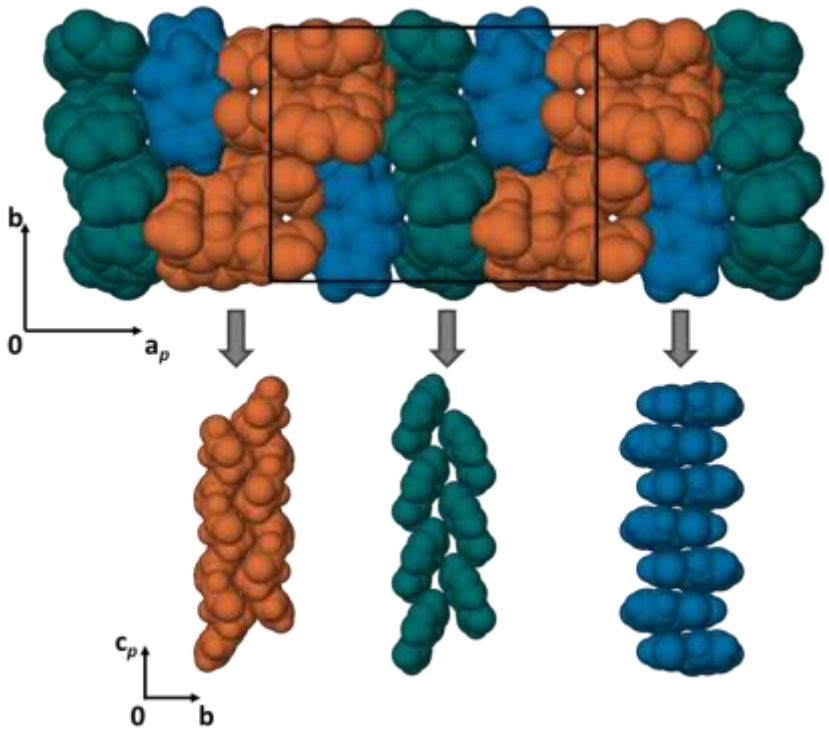

Figure 5.44: A projection of the packing of HFA·NIC down the *c*-axis (top). HFA is shown in orange, NIC A in blue and NIC B in teal. The isolated columns illustrate the packing patterns viewed down the *a*-axis (bottom).

Comparative PXRD

The calculated and experimental traces of HFA·NIC are compared in Figure 5.45. The peak positions match very well, although preferred orientation of the experimental sample leads to some differences in peak intensities. The match between the two traces indicates that the bulk material is homogeneous and is structurally identical to the crystal chosen for single crystal X-ray diffraction.

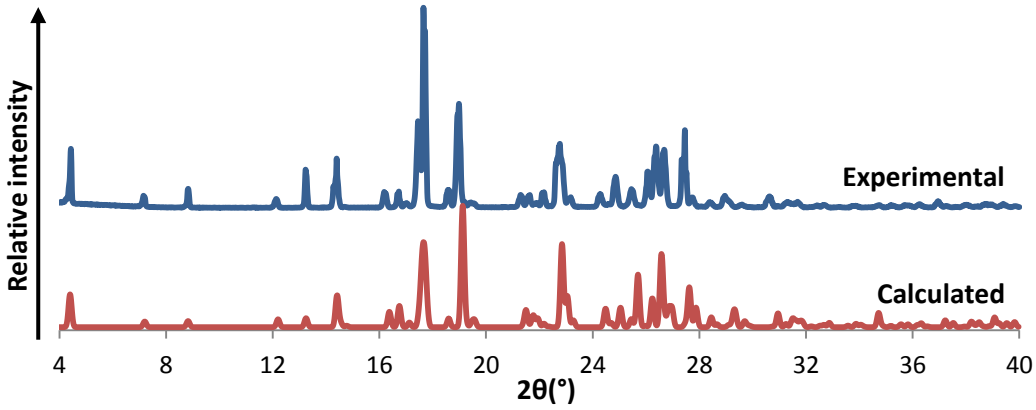

Figure 5.45: PXRD pattern of the cocrystal obtained by coprecipitation and the PXRD pattern calculated from the crystal structure.

***p*-COUMARIC ACID AND ISONICOTINAMIDE (PCA·ISO)**

Thermal analysis

HSM photographs of a single crystal of PCA·ISO show that the PCA·ISO crystal is stable up to 179 °C when it begins to melt (Figure 5.46). It is completely melted by 182 °C.

32 °C **179 °C** **180 °C** **182 °C**

Figure 5.46: Representative HSM photographs of PCA·ISO

The DSC analysis (Figure 5.47) shows a sharp endothermic event at 175 °C. This temperature differs from the melting points of the starting materials (PCA: 214 °C; ISO: 155-157 °C) confirming the formation of a new phase. Decomposition occurs after melting. TG analysis indicates a large mass loss at an onset temperature of 178 °C. No mass loss due to the loss of solvent or hydroxycinnamic acid molecules is evident prior to decomposition (Figure 5.47).

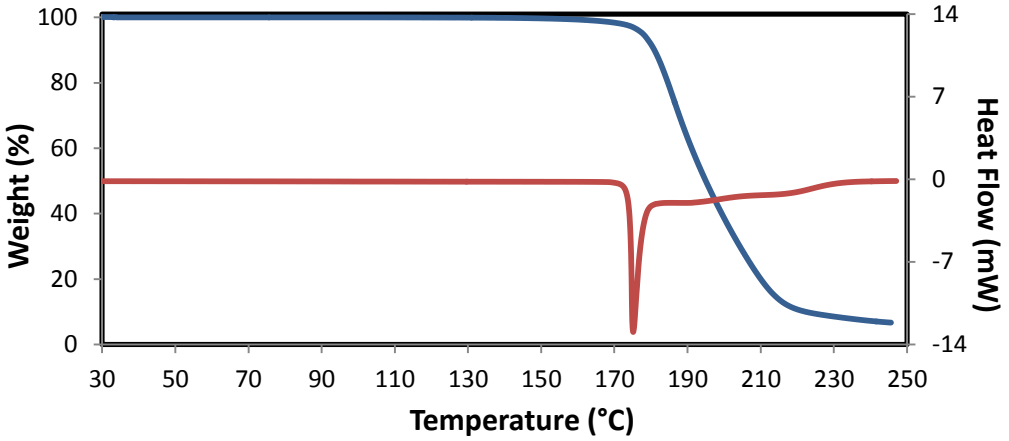

Figure 5.47: TGA (blue) and DSC (red) traces of PCA·ISO

^{1}H Nuclear Magnetic Resonance Spectroscopy

^{1}H NMR spectroscopy was used to determine the stoichiometry of the cocrystal obtained through integration of the proton signals of PCA and ISO for a sample of the cocrystal dissolved in DMSO-d_6 (Table 5.20). A stoichiometry of 1:1 was found for PCA·ISO (see Appendix B for full spectrum). The experimental/theoretical integration ratio of ISO indicates that it is in slight excess due to the paucity of the sample (reducing accuracy) and possible contamination from excess ISO.

Table 5.20: Integrals of the protons of PCA and ISO used to confirm the stoichiometry of PCA·ISO

Proton	δ (ppm)	Multiplicity	J (Hz)	Integration	Experimental/ Theoretical	
2 x C-$\underline{H}_a$ (ISO)	8.726	dd	^{3}J = 4.36 ^{5}J = 1.68	2.321	1.2	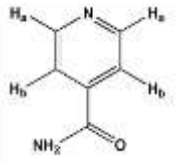
2 x C-$\underline{H}_b$ (ISO)	7.774	dd	^{3}J = 4.40 ^{5}J = 1.68	2.447	1.2	
C-$\underline{H}_A$ (PCA)	6.291	d	^{3}J = 15.93	1.000*	1	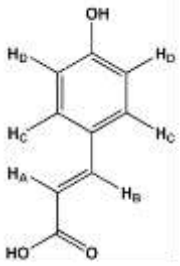
2 x C-$\underline{H}_D$ (PCA)	6.802	d	^{3}J = 8.64	2.000	1	

*Reference integral

Single crystal X-ray analysis

A single, colourless crystal was selected from the mother liquor, dried and placed under Paratone N oil.[13] X-ray intensity data were collected on the Bruker APEX DUO II diffractometer. The crystal system was determined to be triclinic (Laue symmetry $\bar{1}$). The experimental value of the mean $|E^2 - 1|$ was 1.039 (expected 0.968 for centrosymmetric and 0.736 for non-centrosymmetric) confirming the space group as $P\bar{1}$. The crystallographic data and refinement parameters for the structure are listed in Table 5.21.

Table 5.21: Data collection and refinement parameters for PCA·ISO

Chemical Formula	**$C_9H_8O_3 \bullet C_6H_6N_2O$**
Formula weight / g mol^{-1}	286.28
Crystal system	Triclinic
Space group	$P\bar{1}$ (No. 2)
a / Å	6.979(1)
b / Å	7.418(1)
c / Å	14.684(1)
α / °	79.954(1)
β / °	80.132(2)
γ / °	62.126(1)
Volume / $Å^3$	658.1(1)
Z	2
Calculated density / g cm^{-3}	1.445
μ (MoKα) / mm^{-1}	0.106
F (000)	300
Temperature of data collection / K	173(2)
Crystal size / mm^3	0.04 x 0.19 x 0.24
Theta range scanned / ˚	$1.4 \leq \theta \leq 28.5$
Index ranges	h: -9, 9; k: -9, 9; l: -19, 19
Total number of reflections	11510
No. of independent reflections	3297
No. of reflections with $I > 2\sigma(I)$	2785
No. of parameters	192
R_{int}	0.031
R_1 ($I > 2\sigma(I)$)	0.0402
wR_2 ($I > 2\sigma(I)$)	0.1155
S	1.041
Coefficients in weighting scheme	a = 0.0628, b = 0.1705
$(\Delta/\sigma)_{mean}$	< 0.001
Δρ excursions / e $Å^{-3}$	-0.27 and 0.30

Structure solution and refinement

SHELXS-97 was used to solve the structure of PCA·ISO.[16] The solution revealed the non-hydrogen atoms of the ASU (one PCA molecule and one ISO molecule) (Figure 5.48). All of the non-hydrogen atoms were assigned according to the difference Fourier map and refined isotropically on F^2 using SHELXH-97.[17] After subsequent refinements it was confirmed that the isotropic temperature factors of the non-hydrogen atoms were well-behaved and these atoms were allowed to refine anisotropically.

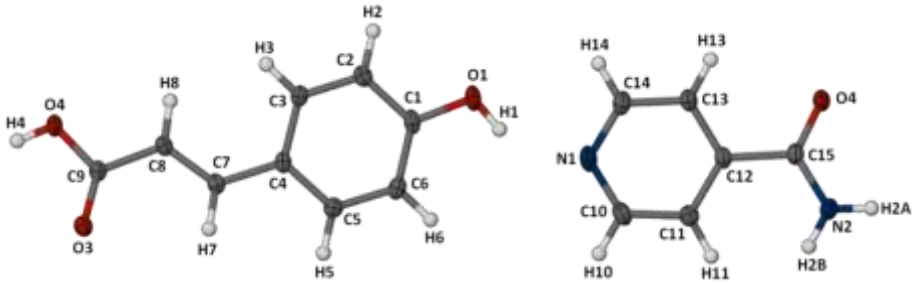

Figure 5.48: The asymmetric unit of PCA·ISO. Thermal ellipsoids are drawn at the 50% probability level, while the hydrogen atoms are shown as spheres of arbitrary radii.

All of the hydrogen atoms were successfully located from the difference electron density map in accordance with the known R-H bond lengths.[19] There was no evidence of proton transfer from the hydroxyl group of PCA to the pyridyl-N of ISO in the difference Fourier map. Based on the positions of the observed peaks, all of the aromatic hydrogen atoms were added in idealised positions in a riding model (AFIX 43). The hydroxyl hydrogen atoms were placed using the rotating group method (AFIX 147) and the instruction AFIX 93 was used to place the NH_2 hydrogen atoms on ISO. The temperature factors for the hydrogen atoms were 1.2 times those of their parent atoms.

Hydrogen bonding

A heteromeric hydrogen bonded ring is formed between the amide group of ISO and the acid group of PCA [$R_2^2(8)$]. The amide-acid units form a homosynthon with a centrosymmetrically related acid-amide unit, having graph set classification $R_4^2(8)$. Subsequent PCA-ISO units are linked by a hydrogen bonding interaction between the pyridyl-N of ISO with the *p*-hydroxyl group of PCA, resulting in the formation of molecular ribbons. Two π-π stacking interactions sustain the crystal: one within the ribbon (Cg2···Cg1' = 3.7554(8) Å; Cg1': -1+x, 1+y, z) and the other linking the ribbons (Cg1···Cg2 = 3.6862(8) Å) (Figure 5.49). Table 5.22 gives the hydrogen bonding parameters.

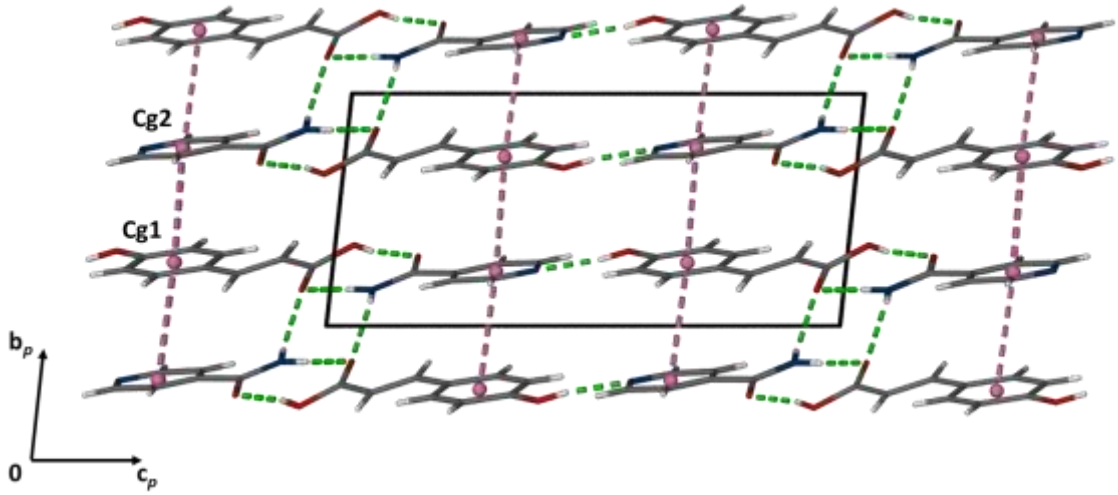

Figure 5.49: A projection down the *a*-axis of the hydrogen bonded columns formed (interactions shown in green) and the π-π stacking interactions (shown in pink) in PCA·ISO.

Table 5.22: Hydrogen bonding parameters of PCA·ISO

D-H···A	D-H (Å)	H···A (Å)	D···A (Å)	D-H···A (°)	Symmetry Operation
O1-H1···N1*	0.82	1.96	2.695(1)	149	-x,-y,1-z
O2-H2···O4*	0.82	1.78	2.586(2)	166	2-x,-y,-z
N2-H2A···O3*	0.86	2.21	3.041(2)	162	2-x,-y,-z
N2-H2B···O3*	0.86	2.23	2.988(2)	147	X, -1+y,z

*The atom to which the symmetry operation applies.

Molecular geometry

The torsion angle magnitudes of the aromatic ring of PCA are less than 1°. Some rotation in the acid tail of PCA leads to the torsion angles C3-C4-C7-C8 = -13.3(2)°, C4-C7-C8-C9 = 179.2(1)° and C7-C8-C9-O3 = -6.2(2)°. Figure 5.48 shows the atom labels used for PCA and ISO. The pyridyl ring of ISO is planar (|torsion angles| < 1.2°) while the amide substituent is twisted out of the plane, with C11-C12-C15-N2 = -13.5(2)° and C13-C12-C15-O4 = -12.4(2)°.

Crystal packing

The crystal structure is sustained by a number of hydrogen bonding interactions and two π-π stacking interactions. The hydrogen bonding interactions form columns of PCA-ISO units linked by the heterosynthon between the pyridyl-N of ISO with the *p*-hydroxyl group of PCA. Figure 4.50 shows the stacking of the molecules in PCA·ISO. The orange molecules form one ribbon of PCA·ISO molecules, blue molecules show an adjacent ribbon. The orange and blue ribbons are linked by π···π stacking interactions between PCA and ISO aromatic rings propagating parallel to the *b*-axis.

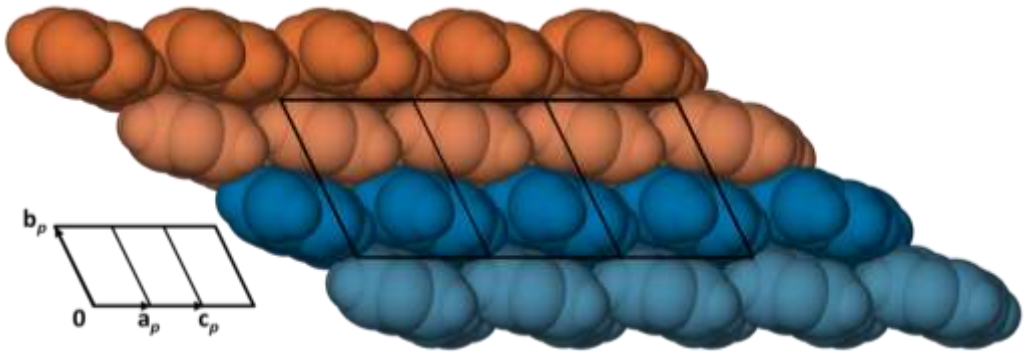

Figure 5.50: A projection of the packing of PCA·ISO. The columns are shown in orange and blue.

Comparative PXRD

To test the integrity of the material, the experimental PXRD pattern was compared with that calculated from the single crystal X-ray structure (Figure 5.51). A small shift in some peak positions of the experimental trace to lower 2θ values is due to the low temperature used in the data collection during single crystal X-ray diffraction (173 K). The two traces otherwise match very closely and the bulk material is homogeneous.

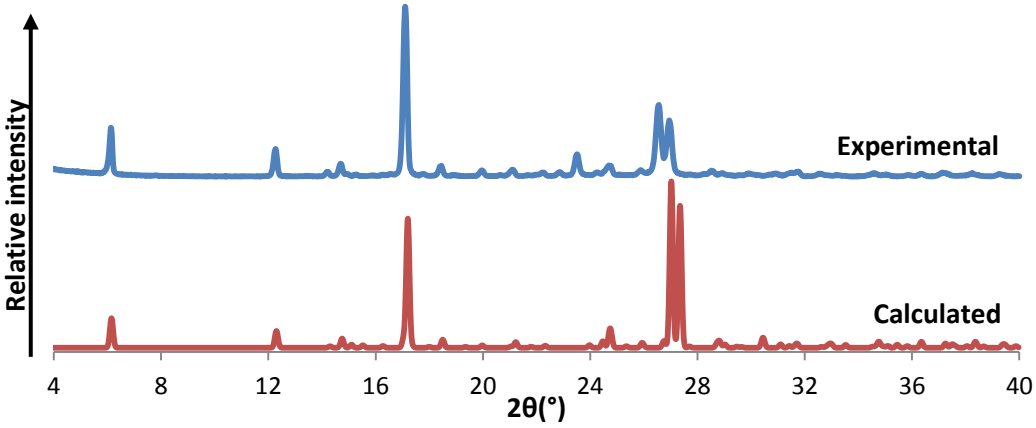

Figure 5.51: PXRD pattern of the cocrystal obtained by coprecipitation and the PXRD pattern calculated from the crystal structure.

p-COUMARIC ACID AND NICOTINAMIDE (PCA·NIC)

Thermal analysis

HSM photographs of a single crystal of PCA·NIC indicate that the crystal is clear at 30 °C and thermally stable until melting starts at 169 °C. While the crystal is melting, some bubbling occurs at 171 °C, interpreted as being due to the release of decomposition products (Figure 5.52).

30 °C **169 °C** **171 °C** **175 °C**

Figure 5.52: Representative HSM photographs of PCA·NIC

A sharp melt endotherm appears at 161 °C in the DSC curve (Figure 4.2.53). The melting point differs from those of the starting materials (PCA: 214 °C; NIC: 128-131 °C) confirming the formation of a new phase. The decomposition event, occurring at ~166 °C, directly follows melting. No solvent or hydroxycinnamic acid mass loss is evident prior to decomposition. The DSC results confirm the interpretation of the HSM observations.

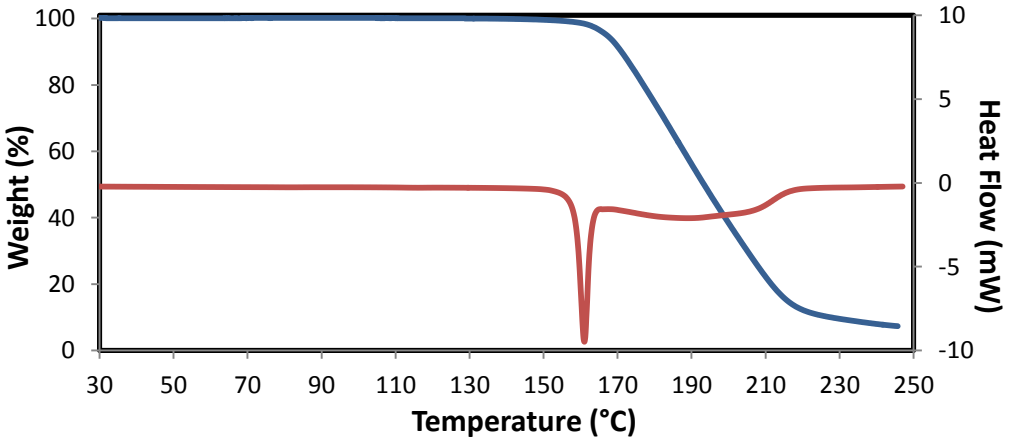

Figure 5.53: TGA (blue) and DSC (red) traces of PCA·NIC

^{1}H Nuclear Magnetic Resonance Spectroscopy

A small sample of the PCA·NIC cocrystal was dissolved in DMSO-d_6 and the ^{1}H NMR spectrum was recorded (data in Table 5.23). Through the integration of the signals of PCA and NIC it was found that the stoichiometry of the cocrystal was 1:1 (see Appendix B for full spectrum).

Table 5.23: Integrals of the protons of PCA and NIC used to confirm the stoichiometry of PCA·NIC

Proton	δ (ppm)	Multiplicity	J (Hz)	Integration	Experimental/ Theoretical	
C-$\underline{H}_a$ (NIC)	8.709	dd	^{3}J = 4.78 ^{4}J = 1.82	0.994	1	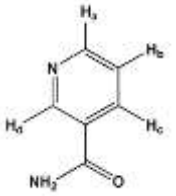
C-$\underline{H}_c$ (NIC)	8.214	dt	^{3}J = 7.88 ^{4}J = 2.40	1.104	1.1	
C-$\underline{H}_d$ (NIC)	9.039	dd	^{4}J = 2.20 ^{4}J = 0.92	1.000*	1	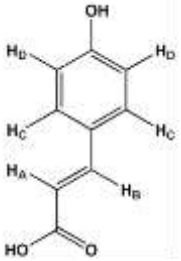
C-$\underline{H}_A$ (PCA)	6.291	d	^{3}J = 15.93	1.080	1.1	
2 x C-$\underline{H}_D$ (PCA)	6.802	d	^{3}J = 8.60	2.136	1.1	

*Reference integral

Single crystal X-ray analysis

Crystal data such as crystal system, space group and unit cell parameters were determined for the chosen crystal of PCA·NIC using X-ray intensity data collected on the Bruker APEX DUO II diffractometer. The single, colourless crystal used for analysis was selected from the mother liquor, dried on filter paper and mounted on a nylon loop using Paratone N oil.[13] The space group $P2_1/n$ (alternative setting of $P2_1/c$) was identified by the reflection conditions *hkl: none; h0l: h + l = 2n; 0k0: k = 2n* upon examining the digital precession photographs using the program LAYER.[14]

Structure solution and refinement

The non-hydrogen atoms were revealed after the structure was solved using direct methods with the program SHELXS-97.[16] The atoms were assigned accordingly and refined isotropically on F^2 using SHELXH-97.[17] The ASU was found to consist of three PCA molecules and three NIC molecules (Figure 5.54). The non-hydrogen atoms were allowed to refine anisotropically once it was established that the isotropic thermal parameters of the atoms were stable.

The crystallographic data and refinement parameters for the structure are listed in Table 5.24.

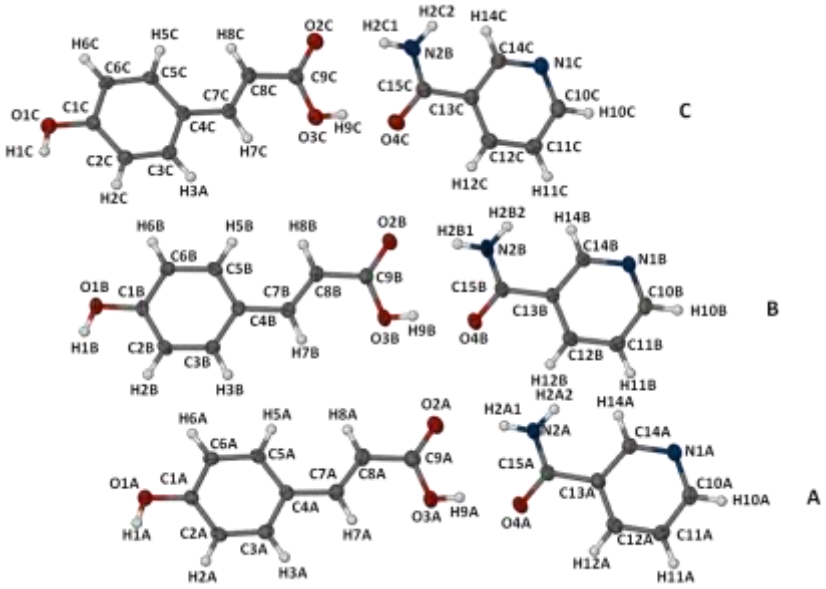

Figure 5.54: The asymmetric unit of PCA·NIC. Thermal ellipsoids are drawn at the 50% probability level, while the hydrogen atoms are shown as spheres of arbitrary radii.

Table 4.2.24: Data collection and refinement parameters for PCA·NIC complex formula

Chemical Formula	**$C_9H_8O_3 \bullet C_6H_6N_2O$**
Formula weight / g mol^{-1}	286.28
Crystal system	Monoclinic
Space group	$P2_1/n$ [alternative setting of $P2_1/c$ (No. 14)]
a / Å	17.009(1)
b / Å	7.251(1)
c / Å	34.291(2)
β / °	101.425(1)
Volume / $Å^3$	4145.5(4)
Z	12
Calculated density / g cm^{-3}	1.376
μ (MoKα) / mm^{-1}	0.101
F (000)	1800
Temperature of data collection / K	173(2)
Crystal size / mm^3	0.12 x 0.15 x 0.28
Theta range scanned / °	1.5 ≤ θ ≤ 28.3
Index ranges	h: -22, 22; k: -4, 9; l: -45, 43
Total number of reflections	22114
No. of independent reflections	10326
No. of reflections with I > 2σ(I)	6097
No. of parameters	568
R_{int}	0.041
R_1 (I > 2σ(I))	0.0511
wR_2 (I > 2σ(I))	0.1308
S	0.987
Coefficient in weighting scheme	a = 0.0573
$(Δ/σ)_{mean}$	< 0.001
Δρ excursions / e $Å^{-3}$	-0.24 and 0.28

All H atoms were located in difference Fourier maps and were included in the model in geometrically calculated positions. The aromatic hydrogen atoms were added using the AFIX 43 instruction (riding model) while the hydroxyl hydrogen atoms were placed using the AFIX 83 command, which places the hydrogen atom such that the best hydrogen bond is formed with the best acceptor to give a tetrahedral geometry. AFIX 93 was used to place the primary amide protons. The temperature factors for the hydrogen atoms were fixed at 1.2 times those of their parent atoms. There was no evidence of proton transfer between the *p*-hydroxyl hydrogen atom of PCA and the pyridyl-N of ISO in any of the three independent cocrystal units.

The ASU consists of three crystallographically unique PCA-NIC pairs. The phenolic rings of the three PCA molecules overlap when the crystal structure is viewed parallel to the *a*-axis. The PCA molecules extend in the *c*-direction and interact with the respective NIC molecules in three different orientations (Figure 5.55). The mean planes of A and B are inclined at 7.4(5)° to each other, the angle between the mean planes of B and C is 19.9(5)° and the interplanar angle between C and A is 26.2(5)°.

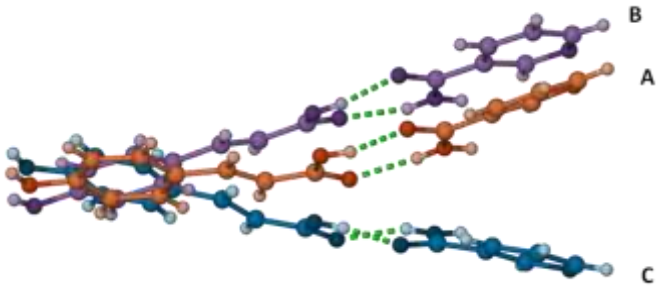

Figure 5.55: The orientations of the three crystallographically unique PCA-NIC pairs.

Hydrogen bonding

Each of the PCA and NIC molecules (A, B and C) form heteromeric rings [$R_2^2(8)$] through the hydrogen bonding interactions of the acid groups of PCA and the amide groups of NIC to form cocrystal units A, B and C. These units are linked by the hydrogen bonded heterosynthon formed between the *p*-hydroxyl group of PCA and the pyridyl N of NIC forming an undulating ribbon extending in the *c*-direction. The hydrogen bond between the *anti*-H of the amide of NIC and the carbonyl O of PCA [$R_4^2(8)$] results in the pairs A-A', B-C' and C-B' (Figure 5.56). Pair A-A' is formed through a centre of inversion while pairs B-C' and C-B' are related by a twofold screw axes parallel to *b*. The formation of these pairs link the ribbons ABC and A'C'B', which propagate in the *b*-direction, as shown in Figure 5.57. Table 5.25 gives the hydrogen bonding parameters.

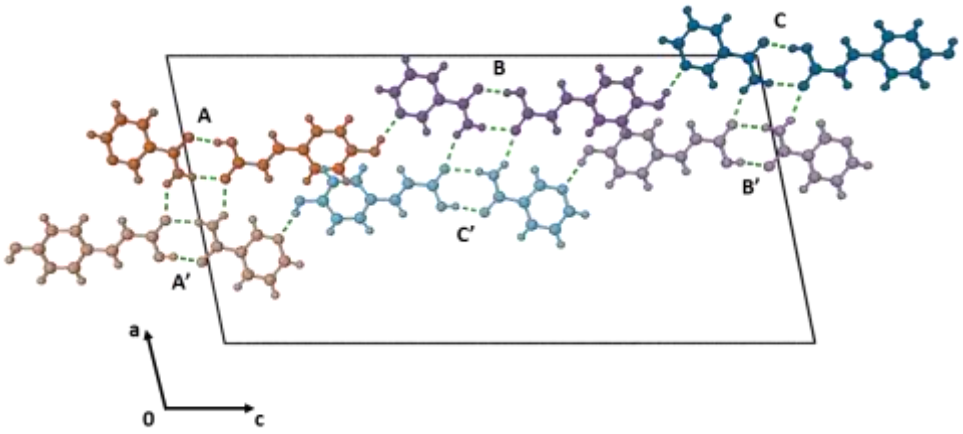

Figure 5.56: The hydrogen bonded ribbon formed in PCA·NIC. The PCA···NIC units are shown in different colours: A in orange, B in purple and C in blue.

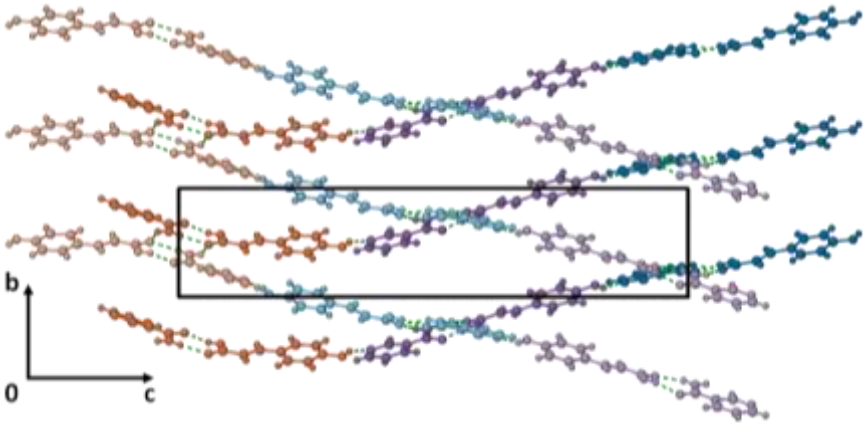

Figure 5.57: The hydrogen bonded ribbons formed in PCA·NIC. The PCA···NIC units are shown in different colours: A in orange, B in purple and C in blue.

Table 5.25: Hydrogen bonding parameters of PCA·NIC

D-H···A	D-H (Å)	H···A (Å)	D···A (Å)	D-H···A (°)	Symmetry code
O1A-H1A···N1B*	0.84	1.90	2.701(2)	158	1/2+x,3/2-y,1/2+z
O1B-H1B···N1C*	0.84	1.97	2.760(2)	157	1/2+x,1/2-y,1/2+z
O1C-H1C···N1A*	0.84	1.89	2.708(2)	162	-1/2+x,3/2-y,1/2+z
O2A-H9A···O4A	0.84	1.81	2.623(2)	164	-
O2B-H9B···O4B	0.84	1.86	2.690(2)	169	-
O2C-H9C···O4C	0.84	1.79	2.614(2)	167	-
N2A-H2A1···O3A	0.88	2.02	2.887(2)	170	-
N2A-H2A2···O3A*	0.88	2.22	2.899(2)	134	1-x,1-y,-z
N2B-H2B1···O3B	0.88	1.98	2.844(2)	167	-
N2B-H2B2···O3C*	0.88	2.13	2.943(2)	153	-x,1-y,-z
N2C-H2C1···O3C	0.88	2.03	2.870(2)	160	-
N2C-H2C2···O3B*	0.88	2.09	2.897(2)	153	-x,1-y,-z
C7A-H7A···O2A	0.95	2.40	2.765(2)	102	-
C7B-H7B···O2B	0.95	2.49	2.823(2)	100	-
C7C-H7C···O2C	0.95	2.42	2.775(2)	102	-
C10B-H10B···O1C*	0.95	2.51	3.120(2)	122	1/2+x,3/2-y,-1/2+z
C10C-H10C···O1A*	0.95	2.41	3.152(2)	135	-1/2+x,1/2-y,-1/2+z
C12A-H12A···O4C*	0.95	2.56	3.382(2)	144	1-x,1-y,-z

*The atom to which the symmetry operation applies.

Molecular geometry

Differences in the conformation of each of the PCA and NIC molecules result in the occurrence of three distinct PCA-NIC cocrystal units comprising the ASU. These differences occur around the rotatable bonds (involving the acid tail of PCA and the amide moiety of NIC). The aromatic moiety of each molecule is planar. Tables 5.26 and 5.27 list the torsion angles that define the conformation of each molecule.

Table 5.26: Torsion angles for the PCA molecules

Torsion angle (°)		PCA A	PCA B	PCA C	
C2-C3-C4-C7	τ_1	178.9(2)	177.2(2)	-176.1(2)	
C3-C4-C7-C8	τ_2	-175.0(2)	-166.9(2)	-176.3(2)	
C5-C4-C7-C8	τ_3	4.5(3)	12.0(3)	6.5(3)	
C7-C4-C5-C6	τ_4	-179.5(2)	-178.1(2)	174.8(2)	
C4-C7-C8-C9	τ_5	175.9(2)	-179.5(2)	179.0(2)	
C7-C8-C9-O2	τ_6	-173.7(2)	-177.3(2)	-169.2(2)	
C7-C8-C9-O3	τ_7	6.0(3)	3.2(3)	10.8(3)	

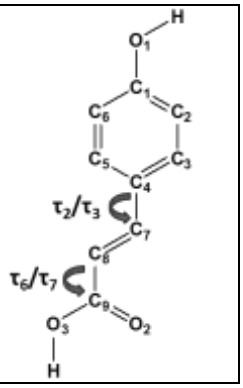

Table 5.27: Torsion angles for the NIC molecules

Torsion angle (°)		NIC A	NIC B	NIC C	
C12-C13-C15-N2	τ_8	-163.3(2)	-174.9(2)	161.5(2)	
C14-C13-C15-N2	τ_9	18.4(3)	5.0(3)	-19.2(3)	
C12-C13-C15-O4	τ_{10}	16.2(3)	4.2(3)	-17.5(3)	
C14-C13-C15-O4	τ_{11}	-162.1(2)	-175.8(2)	161.7(2)	

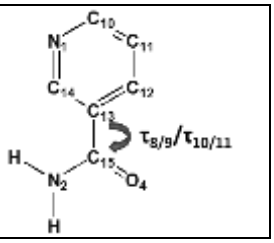

Crystal packing

Undulating ribbons are formed by the hydrogen bonding interactions between PCA-NIC units A, B and C. Figure 5.58 shows how these ribbons stack anti-parallel in columns. Successive C dimers (related by a crystallographic centre of inversion) stack parallel to the *b*-axis. The linked A and B dimers stack anti-parallel such that the aromatic rings of PCA A are stacked one on the other. The crystal propagates in the *a*-direction by the formation of tetramers A-A, B-C and C-B and adjacent columns are aligned in an offset manner.

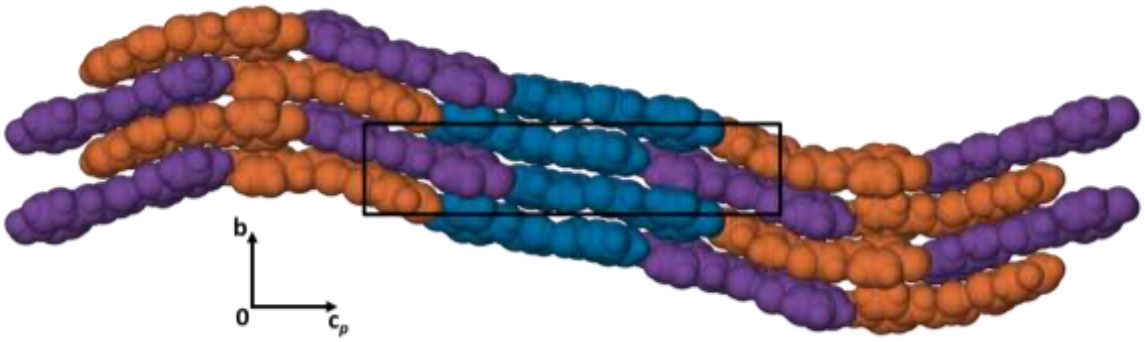

Figure 5.58: A space-filling diagram showing the packing in the crystal of PCA·NIC. The units are shown in different colours: A in orange, B in purple and C in blue.

Comparative PXRD

The calculated and experimental PXRD patterns of PCA·NIC are shown in Figure 5.59. The experimental pattern shows some shift of the peak positions to lower 2θ values. This may be due to some unit cell shrinkage as the calculated pattern is based on the structure of a crystal analysed at low temperature while the experimental PXRD is performed at room temperature. The two patterns are nonetheless in good agreement. The match between the experimental and calculated PXRD patterns indicates that the crystal chosen for analysis is representative of the bulk material. A match was found between the PXRD pattern of the 1:1 cocrystal obtained in this study and the PXRD pattern for the PCA·NIC cocrystal published by Bevill *et al*.[7]

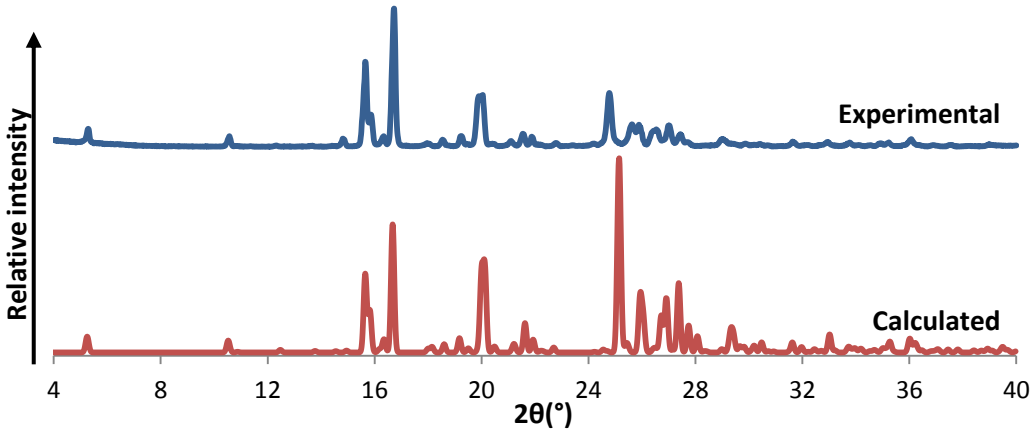

Figure 5.59: PXRD pattern of the PCA·NIC cocrystal obtained by coprecipitation and the PXRD pattern calculated from the crystal structure.

***p*-COUMARIC ACID AND NICOTINAMIDE [$(PCA)_2$·NIC]**

Thermal analysis

HSM analysis of $(PCA)_2$·NIC was carried out at 10 °C/min. Melting begins at 179 °C and some bubbling is apparent at 181 °C. This bubbling was interpreted as being due to the release of decomposition products (Figure 5.60).

30 °C **179 °C** **181 °C** **183 °C** **185 °C**

Figure 5.60: Representative HSM photographs of $(PCA)_2$·NIC.

The DSC analysis (Figure 5.61) shows a sharp endotherm at 174 °C indicating melting. The melting point is different from either of the melting points of the starting materials (PCA: 214 °C; NIC: 128-131 °C) confirming the formation of a new crystalline phase. Decomposition follows directly after cocrystal

fusion. TG analysis confirms that no solvent or hydroxycinnamic acid molecules are lost prior to decomposition, which begins at the onset temperature of 150 °C (Figure 5.61).

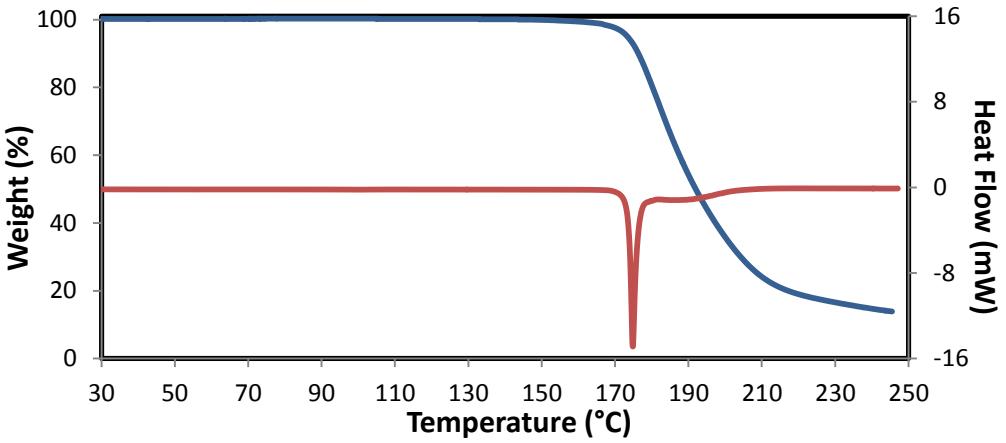

Figure 5.61: TGA (blue) and DSC (red) traces of $(PCA)_2$·NIC

^{1}H Nuclear Magnetic Resonance Spectroscopy

The ^{1}H NMR spectrum was obtained for a sample of the cocrystal $(PCA)_2$·NIC dissolved in DMSO-d_6 (data listed in Table 5.28). Integration of the peak signals of PCA and NIC, respectively, revealed a 2:1 stoichiometry (see Appendix B for full spectrum).

Table 5.28: Integrals of the protons of PCA and NIC used to confirm the stoichiometry of $(PCA)_2$·NIC

Proton	δ (ppm)	Multiplicity	J (Hz)	Integration	Experimental/ Theoretical	
C-$\underline{H}_a$ (NIC)	8.711	dd	^{3}J = 4.77 ^{4}J = 1.65	0.961	1	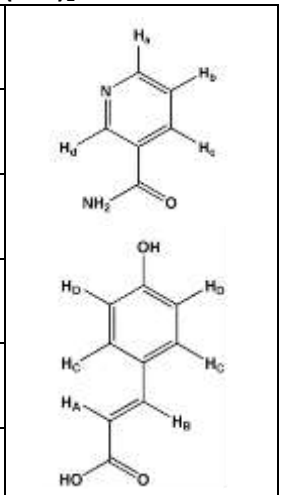
C-$\underline{H}_c$ (NIC)	8.214	dt	^{3}J = 7.89 ^{4}J = 2.02	1.090	1	
C-$\underline{H}_d$ (NIC)	9.040	d	^{4}J = 1.65	1.000*	1	
C-$\underline{H}_A$ (PCA)	6.291	d	^{3}J = 15.96	2.115	2.1	
2 x C-$\underline{H}_D$ (PCA)	6.802	d	^{3}J = 8.62	4.800	2.4	

*Reference integral

Single crystal X-ray analysis

After an appropriate single crystal was selected from the mother liquor and placed into Paratone N oil[13] X-ray intensity data were collected on the Bruker APEX DUO II diffractometer. Program LAYER[14] indicated that the Laue symmetry of the diffraction pattern was 2/*m* and hence the crystal system was indicated as being monoclinic. Conditions limiting possible reflections were as follows: *hkl*: none; *h0l*: *l* = 2*n*; *0k0*: *k* = 2*n*. These indicated the space group $P2_1/c$ unequivocally.[20]

The crystallographic data and refinement parameters for the structure are listed in Table 5.29.

Table 5.29: Data collection and refinement parameters for $(PCA)_2$·NIC

Chemical Formula	**$(C_9H_8O_3)_2 \bullet C_6H_6N_2O$**
Formula weight / g mol^{-1}	450.44
Crystal system	Monoclinic
Space group	$P2_1/c$ (No. 14)
a / Å	9.587(1)
b / Å	6.866(1)
c / Å	32.097(3)
β / °	91.009(2)
Volume / $Å^3$	2112.3(3)
Z	4
Calculated density / g cm^{-3}	1.416
μ (MoKα) / mm^{-1}	0.105
F (000)	944
Temperature of data collection / K	173(2)
Crystal size / mm^3	0.12 x 0.16 x 0.28
Theta range scanned / °	$2.1 \leq \theta \leq 28.4$
Index ranges	h: -12, 12; k: -9, 9; l: -41, 42
Total number of reflections	17428
No. of independent reflections	5268
No. of reflections with $I > 2\sigma(I)$	3758
No. of parameters	302
R_{int}	0.030
R_1 ($I > 2\sigma(I)$)	0.0439
wR_2 ($I > 2\sigma(I)$)	0.1165
S	1.022
Coefficients in the weighting scheme	a = 0.0526, b = 0.539
$(\Delta/\sigma)_{mean}$	< 0.001
Δρ excursions / e $Å^{-3}$	-0.23 and 0.25

Structure solution and refinement

SHELXS-97 was used to solve the structure by direct methods.[16] The resulting difference Fourier map revealed the non-hydrogen atoms which make up the ASU. The atoms were assigned accordingly and refined isotropically on F^2 using SHELXH-97.[17] The ASU was found to consist of two PCA molecules and one NIC molecule (Figure 5.62). The non-hydrogen atoms were later refined anisotropically as the refinement of the isotropic temperature factors was stable.

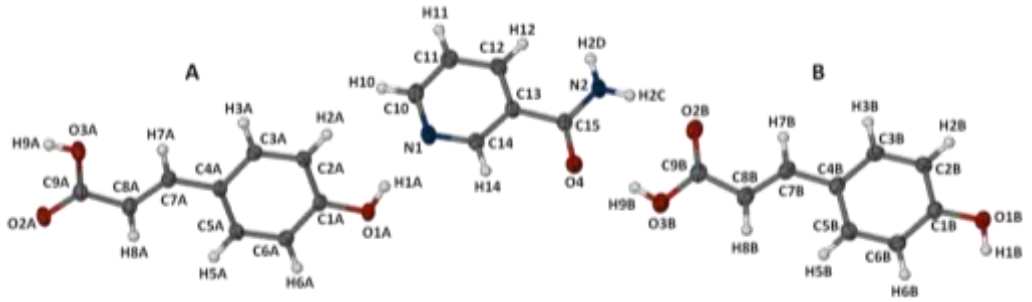

Figure 5.62: The asymmetric unit of $(PCA)_2$·NIC. Thermal ellipsoids are drawn at the 50% probability level, while the hydrogen atoms are shown as spheres of arbitrary radii.

Hydrogen atoms were identified in successive difference Fourier maps. A riding model (AFIX 43) was used to place the aromatic hydrogen atoms, based on the positions of the peaks found. The hydroxyl hydrogen atoms were placed using the rotating model (AFIX 147) and the AFIX 93 command was used to place the amide protons. The difference Fourier map did not indicate transfer of a hydrogen atom from the hydroxyl groups of PCA to the pyridyl-N or the amino group of NIC. The U_{iso} parameters for the hydrogen atoms were maintained at 1.2 times those of their parent atoms.

Hydrogen bonding

An acid-amide heterosynthon [$R_2^2(8)$] is formed between the carboxylic acid group of PCA molecule B and the amide group of NIC (Figure 5.62). The *anti*-H of the amide of NIC forms a hydrogen bond with the carbonyl O of the acid group of PCA molecule A. The interaction between the acidic groups of PCA molecule A and the centrosymmetrically related PCA molecule takes the form of a homosynthon [$R_2^2(8)$]. The formation of the homosynthon results in a distinct polymeric unit made up of two centrosymmetrically related $(PCA)_2$·NIC units which extend to form columns. Further stability is provided by a number of C-H···O hydrogen bonds. The units are linked by the hydrogen bonds formed between the pyridyl N of ISO, the p-hydroxyl group of PCA molecule A and the *p*-hydroxyl group of PCA molecule B (Figure 5.63). Table 5.30 contains the hydrogen bond parameters for $(PCA)_2$·NIC.

Table 5.30: Hydrogen bonding parameters of $(PCA)_2$·NIC

D-H···A	D-H (Å)	H···A (Å)	D···A (Å)	D-H···A (°)	Symmetry code
O1B-H1B···O1A*	0.84	1.89	2.713(2)	165	-x,-1/2+y,1/2-z
O1A-H1A···N1*	0.84	1.85	2.679(2)	168	-1+x,1/2-y,-1/2+z
O3B-H9B···O4	0.84	1.79	2.618(2)	170	-
O3A-H9A···O2A*	0.84	1.81	2.645(2)	170	1-x,1-y,1-z
N2-H2D···O2B	0.88	2.04	2.895(2)	165	-
N2-H2C···O2A*	0.88	2.23	3.091(2)	166	1+x,y,z
C7B-H7B···O2B	0.95	2.45	2.815(2)	103	-
C7A-H7A···O3A	0.95	2.32	2.718(2)	104	-
C12-H12···O2A*	0.95	2.50	3.368(2)	152	1+x,y,z
C10-H10···O1B*	0.95	2.59	3.413(2)	146	1+x,1/2-y,1/2+z
C14-H14···O4	0.95	2.43	2.764(2)	100	-

*The atom to which the symmetry operation applies.

The structure is further sustained by two weak π-π stacking interactions which link the polymeric units within a column (Cg1···Cg3^{b} = 4.179(1) Å and Cg2···Cg3 = 3.917(1) Å; symmetry operation *b*: 1-x, 1-y, 1-z) (Figure 5.64). The molecules that link the units in the (1 2 0) plane extend themselves in the (1 -2 0) plane, the angle between these planes being 39.4(5)° (Figure 5.65).

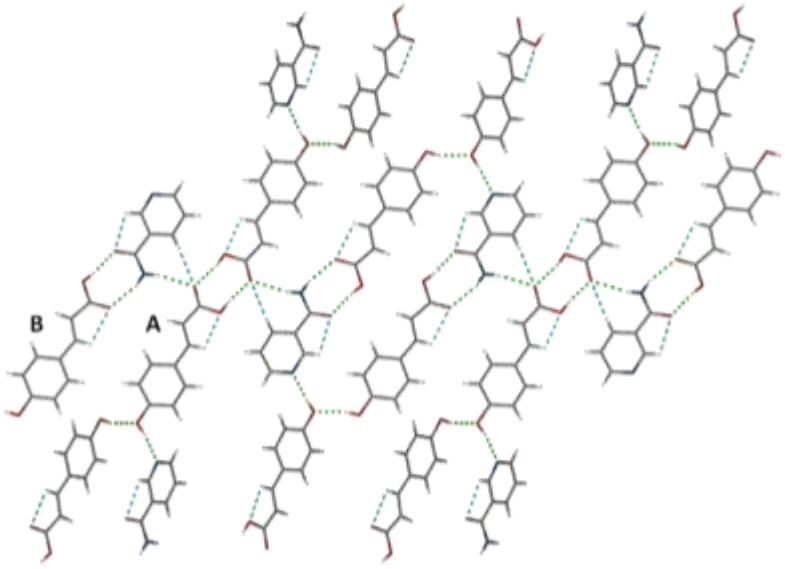

Figure 5.63: A projection onto the (1 2 0) plane showing the polymeric units formed in $(PCA)_2$·NIC. C-H···O interactions are shown in cyan.

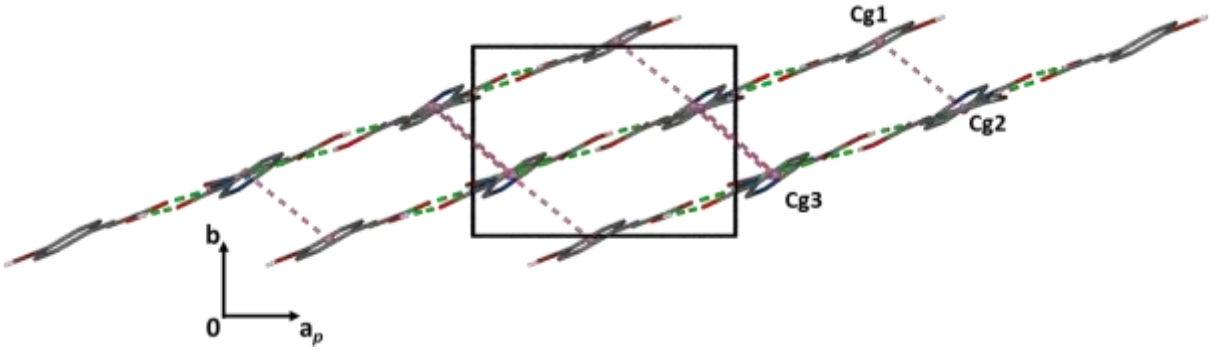

Figure 5.64: The view down the *c*-axis showing the π-π stacking interactions (pink) formed in $(PCA)_2$·NIC.

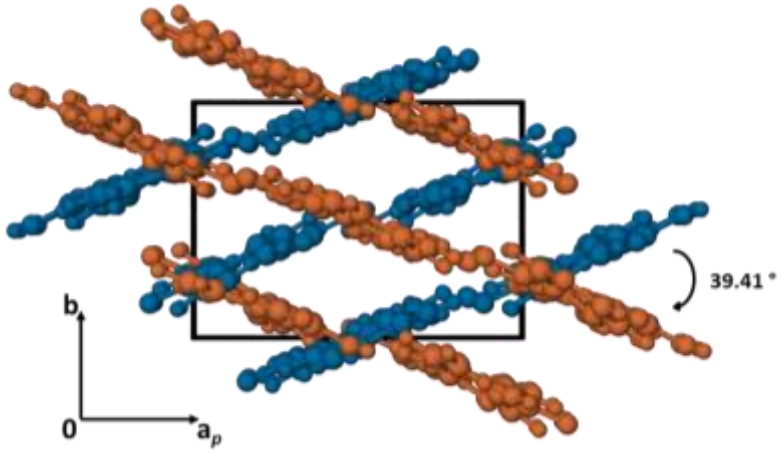

Figure 5.65: A packing diagram illustrating the orientation of two columns relative to each other viewed down the *c*-axis. The molecules parallel to the (1 2 0) plane are shown in orange while the molecules parallel to the (1 -2 0) plane are shown in blue.

Molecular geometry

The aromatic ring of PCA molecule A is planar, having torsion angle magnitudes smaller than 1.8°. The double bond is slightly twisted [C5A-C4A-C7A-C8A = 4.9(2)°] due to some rotation around the C4-C7 bond and the acid group is planar. Similarly, the torsion angle magnitudes for the aromatic ring of PCA molecule B are smaller than 1°, indicating planarity. The double bond is twisted around the C4-C7 bond to give a torsion angle of -7.2(2)° while the acid group is planar. There is some twisting of the amide moiety of NIC relative to the planar pyridyl ring such that C14-C13-C15-O4 = 11.0(2)° and C12-C13-C15-N2 = 11.0(2)°.

Crystal packing

Figure 5.66 illustrates the molecular sheets of PCA and NIC molecules formed by a number of hydrogen bonding interactions. The sheets stack by π-π interaction in an ABAB sequence.

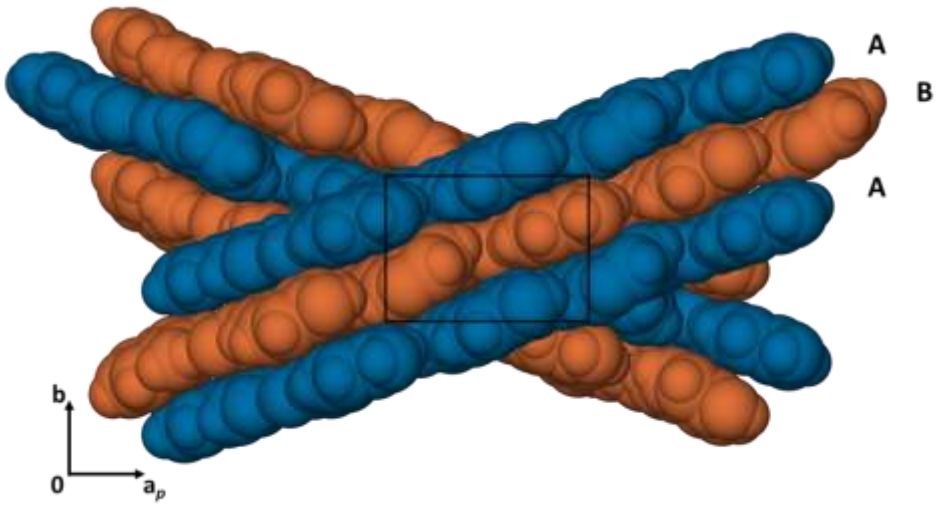

Figure 5.66: A space-filling packing diagram of $(PCA)_2$·NIC viewed down the *c*-axis.

Comparative PXRD

By comparing the calculated and experimental PXRD traces of $(PCA)_2$·NIC (Figure 5.67) it was determined that the bulk material is the same as the representative specimen chosen for single crystal X-ray diffraction. Peak shifts to slightly higher angular values in the calculated pattern are consistent with the expected unit cell shrinkage on cooling the single crystal from 294 K to 173 K. This product was not obtained from dry co-grinding. Both the experimental and calculated PXRD patterns match the PXRD pattern of the 2:1 *p*-coumaric acid-nicotinamide cocrystal investigated by Bevill *et al*.[7]

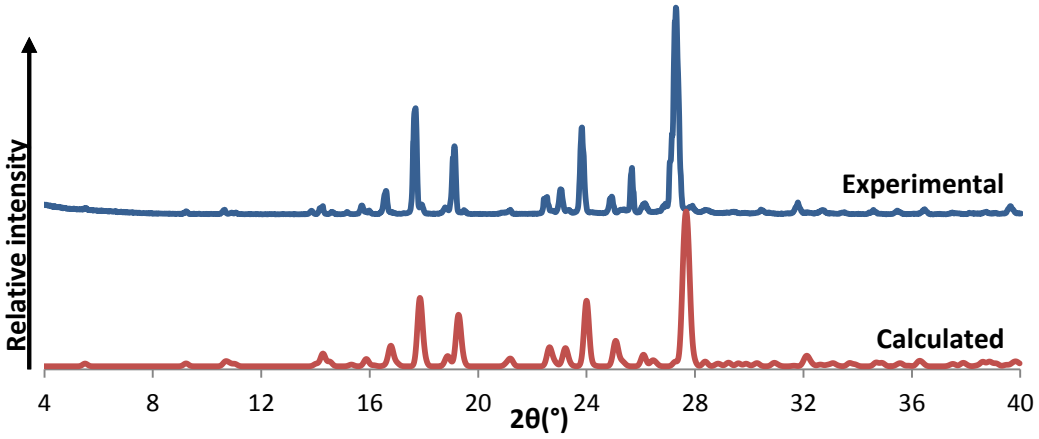

Figure 5.67: PXRD pattern of the cocrystal sample obtained by coprecipitation and the PXRD pattern calculated from the crystal structure.

SOLUBILITY STUDIES

The effect of cocrystallisation on the solubility of hydroxycinnamic acids was investigated using ^{1}H NMR spectroscopy, due to peak overlap of the components in UV-vis spectroscopy. DMSO was used as a known reference sample as its signal in ^{1}H NMR appears upfield in the spectrum and does not overlap with the hydroxycinnamic acid or coformer signals. The comparison of a DMSO signal of known concentration with the hydroxycinnamic acid and coformer signals enabled quantitative analysis of the cocrystals. Results were obtained for the cocrystals FA·NIC, PCA·NIC and $(PCA)_2$·NIC. The solubility measurements made are kinetic as only one measurement was recorded at one point in time.

An excess of the cocrystal was added to 1.5 mL of D_2O and allowed to stir for 24 hours at 25 °C. The cocrystal solution was filtered and 900 µL was transferred to an NMR tube. The DMSO was diluted in D_2O to a known concentration and 100 µL was added to the cocrystal solution. The sample was analysed and the hydroxycinnamic acid, coformer and DMSO signals were identified in the resultant ^{1}H NMR spectrum. The comparison of the hydroxycinnamic acid and coformer peak integrations with that of DMSO at 2.710 ppm enabled the concentration of each component to be determined.

Analysis of the ^{1}H NMR spectra revealed that FA·NIC (formed in a 1:1 ratio in the solid state) had a hydroxycinnamic acid to coformer ratio of 5:6 in solution and the concentration of each component was calculated to be 7.9 g/L for FA and 6.0 g/L for NIC. The aqueous solubility of FA has been reported to be 0.78 g/L,[21] therefore cocrystallisation affords a minimum solubility enhancement for FA of 10 times under the conditions studied. Similar results were obtained for PCA·NIC and $(PCA)_2$·NIC, as listed in Table 5.34.

Table 5.34: ^{1}H NMR results for the solubility determination of cocrystals FA·NIC, PCA·NIC and $(PCA)_2$·NIC at 25 °C.

Cocrystal	Ratio in solid	Ratio in solution	Hydroxycinnamic acid concentration g/L	Literature value g/L at 25 °C	Minimum solubility enhancement of hydroxycinnamic acid	Coformer concentration g/L
FA·NIC	1:1	5:6	7.9	0.78[21]	10 x	6
PCA·NIC	1:1	2:1	15.1	1.53*	10 x	5.2
$(PCA)_2$·NIC	2:1	5:6	3.1	1.53*	3 x	2.8

*S_0 value obtained from phase solubility experiments.

These results for the three samples studied clearly indicate that the solubility of the hydroxycinnamic acid component was enhanced by the formation of the cocrystal. The ratio of hydroxycinnamic acid to coformer was not maintained from solid to solution state for cocrystals FA·NIC and $(PCA)_2$·NIC, as predicted by Guzmán *et al.*[22] on the basis of the 'spring and parachute' effect. This effect describes the phenomenon of solubility enhancement of an insoluble compound due to the presence of a solubilizing agent (in this case the coformer in a cocrystal with hydroxycinnamic acid) – the 'spring' – followed by the 'parachute', where the insoluble compound precipitates out of the solution, leaving the more soluble component behind. This was, however, not the case for PCA·NIC where a higher proportion of hydroxycinnamic acid than coformer is observed. This is unusual and may be due to a change in the component interactions with the effect that NIC precipitates out of the solution.

CONCLUSION

The present chapter described cocrystals obtained with hydroxycinnamic acids and the coformers nicotinamide and isonicotinamide. Overall, the hydrogen bonds noted for the cocrystals or hydrates generated are dependent on the coformer. Coformers containing strong nitrogen acceptor and donor groups were found to interact preferentially with the oxygen functional groups of the hydroxycinnamic acids, supporting the argument that the N-H···O and O-H···N heterosynthons are favoured when these groups are present. The cocrystals formed between PCA and NIC reported here, namely PCA·NIC and the 2:1 form $(PCA)_2$·NIC, have been reported by Bevill *et al.*[7] In their account, published after the present study was underway, cocrystal identification was established using PXRD, DSC and ^{1}H NMR spectroscopic techniques; however, no X-ray structural data or solubility studies were previously reported for these phases.

Chapter 6 details the cyclodextrin inclusion complex formation of four hydroxymethoxyacetophenone isomers with both native and derivatised CDs, in solution and solid state.

REFERENCES

1. G. Springuel, B. Norberg, K. Robeyns, J. Wouters and T. Leyssens, *Cryst. Growth Des*., 2012, **12**, 475-484.
2. Cambridge Structural Database and Cambridge Structural Database System, Version 5.37, May 2016, Cambridge Crystallographic Data Centre, University Chemical Laboratory, 12 Union Road, Cambridge, England.
3. M. C. Etter, *Acc. Chem. Res.*, 1990, **23**, 120.
4. T. R. Shattock, K. K. Arora, P. Vishweshwar and M. J. Zaworotko, *Cryst. Growth Des*., 2008, **8**, 4533-4545.
5. (a) J. Bernstein, R. E. Davis, L. Shimoni and N.-L. Chang, *Angew. Chem. Int. Ed. Engl.*, 1995, **34**, 1555-1573, (b) M. C. Etter, J. C. MacDonald and J. Bernstein, *Acta Cryst*., 1990, **B46**, 256-262.
6. D. Braga, S. L. Giaffreda, K. Rubini, F. Grepioni, M. R. Chierotti and R. Gobetto, *Cryst. Eng. Comm.*, 2007, **9**, 39-45.
7. M. J. Bevill, P. I. Vlahova and J. P. Smit, *Cryst. Growth Des*., 2014, **14**, 1438-1448.
8. H. D. Clarke, K. K. Arora, H. Bass, P. Kavuru, T. T. Ong, T. Pujari, L. Wojtas and M. J. Zaworotko, *Cryst. Growth Des*., 2010, **10**, 2152-2167.
9. C. B. Aakeröy, A. M. Beatty, and B. A. Helfrich, *Angew. Chem. Int. Ed*., 2001, **40**, 3240-3242.
10. Z. Tan, E. Zhu, L. Luo, Z. Lin and R. Yan, *Acta Cryst. E*, 2011, **E67**, o424.
11. N. Schultheiss, M. Roe and S. X. M. Boerrigter, *Cryst. Eng. Comm.*, 2011, **13**, 611-619.
12. N. Ravikumar, G. Gaddamanugu, and K. Anand Solomon, *J. Mol. Struct.*, 2013, **1033**, 272-279.
13. Paratone N oil (Exxon Chemical Co., TX, USA).
14. L. J. Barbour, *J. Appl. Cryst.*, 1999, **32**, 351-352.
15. XPREP, *Data Preparation and Reciprocal Space Exploration*, Version 5.1, ©Bruker Analytical X-ray Systems, 1997.
16. Sheldrick, G. M., *SHELXS-97, Program for Crystal Structure Solution*, Institut für Anorganische Chemie der Universität, Tammanstrasse, D-3400 Göttingen, Germany, 1997.
17. G. M. Sheldrick, *Acta Cryst*., 2008, **A64**, 112-122.
18. J. A. Cowan, J. A. K. Howard, G. J. McIntyre, S. M.-F. Lo and I. D. Williams, *Acta Cryst.*, 2003, **B59**, 794-801.
19. F. H. Allen, O. Kennard, D. G. Watson, L. Brammer, A. Guy Orpen and R. Taylor, *J. Chem. Soc., Perkin Trans. 2*, 1987, S1-S19.
20. M. Kfoury, D. Landy, L. Auezova, H. Greige-Gerges and S. Fourmentin, *Beilstein J. Org. Chem*., 2014, **10**, 2322-2331.
21. F. L. Mota, A. J. Queimada, S. P. Pinho and E. A. Macedo, *Ind. Eng. Chem. Res.*, 2008, **47**, 5182-5189.
22. H. R. Guzmán, M. Tawa, Z. Zhang, P. Ratanabanangkoon, P. Shaw, C. R. Gardner, H. Chen, J. P. Moreau, O. Almarsson and J. F. Remenar, *J. Pharm. Sci.,* 2007, **96,** 2686-2702.

Chapter 6: A study of the complexation of a series of isomeric acetophenone derivatives by native and methylated cyclodextrins in the solid state and in aqueous solution

The inclusion complexes of a series of isomeric acetophenone isomers, namely 2-hydroxy-4-methoxy acetophenone (2H4M), 2-hydroxy-5-methoxy acetophenone (2H5M), 2-hydroxy-6-methoxy acetophenone (2H6M) and 4-hydroxy-3-methoxy acetophenone (4H3M) with the native cyclodextrins (CDs) β- and γ-CD are reported in this chapter. The chemical structures of the four guest compounds are shown in Chapter 1 (p. 7). To complement this study the interactions between each guest and each host were also studied in solution using proton nuclear magnetic resonance spectroscopy (^{1}H NMR). The inclusion complexes formed between the guests and derivatised CDs were also investigated using heptakis(2,3,6-tri-O-methyl)-β-CD (TRIMEB or TMB), hexakis(2,3,6-tri-O-methyl)-α-CD (TRIMEA or TMA) and heptakis(2,6-di-O-methyl)-β-CD (DIMEB or DMB). Crystalline products were obtained and analysed using single crystal X-ray diffraction, powder X-ray diffraction, thermal analysis and ^{1}H NMR spectroscopy.

INCLUSION COMPLEX FORMATION OF ISOMERIC ACETOPHENONE DERIVATIVES WITH NATIVE CDs

Preparation by means of kneading experiments

Equimolar amounts of host and guest were used to prepare inclusion complexes of each guest, 2H4M, 2H5M, 2H6M and 4H3M, and the native CDs γ- and β-CD, respectively. For kneading experiments 0.120 mmol was used. The experiments were carried out by transferring the host and guest into a mortar and kneading the two compounds together while adding water dropwise, such that a paste-like consistency was maintained, for a minimum of 10 minutes. The kneaded product was allowed to dry and analysed using PXRD.

The PXRD patterns of the kneaded products were compared to those of the known isostructural series.[1] Complexation was confirmed for all of the host-guest combinations except for 4H3M and β-CD.

Complex formation with γ-CD

Inclusion complexes formed between small molecules and γ-CD are well known to crystallize in the tetragonal space group $P42_12$, as discussed in Chapter 4. The unit cell dimensions are $a = b \approx 23.8$ Å and $c \approx 23.2$ Å.[2] These common crystallographic features of γ-CD complexes with different guests are reflected in the PXRD patterns, making confirmation of complex formation easy (Figure 6.1).

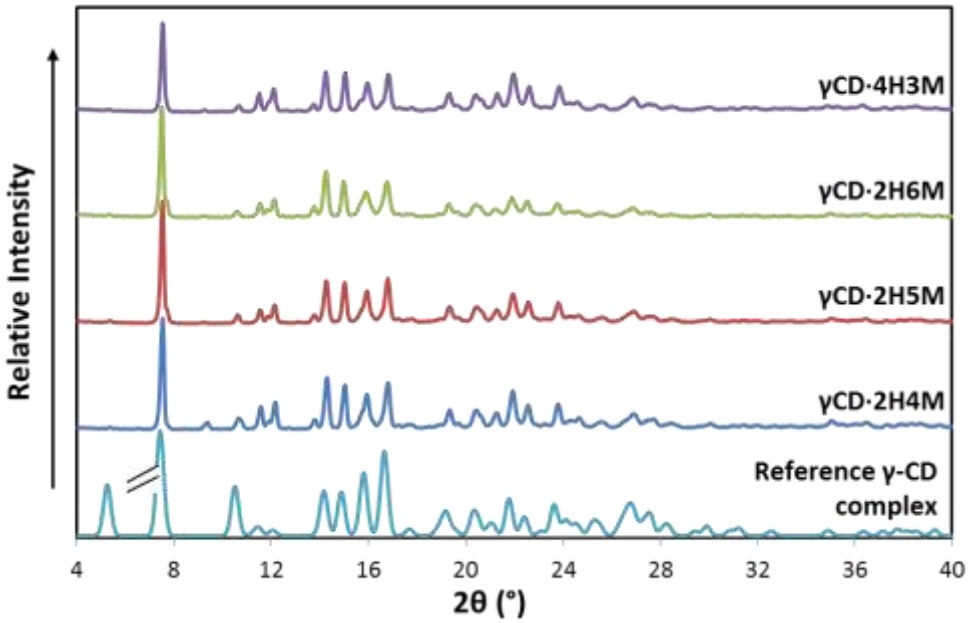

Figure 6.1: Experimental PXRD patterns of the kneaded product of each hydroxyacetophenone guest with γ-CD and reference PXRD pattern to determine complex formation.

Complex formation with β-CD

The PXRD patterns of βCD·2H4M, βCD·2H5M and βCD·2H6M appeared to match complexes found in the isostructural series. The reference traces for the P1 (triclinic) and C2 (monoclinic) channel type structures

are shown. These are, as discussed in Chapter 4, related by a metric transformation.[3] While discriminating between the two possible space groups is not possible from the traces below, they nevertheless confirm that inclusion complexes were formed. The trace for the product βCD·4H3M matched the pattern of hydrated β-CD. However, as shown below, this is a genuine inclusion complex. Figure 6.2 shows the experimental PXRD patterns and the matching isostructural series patterns.

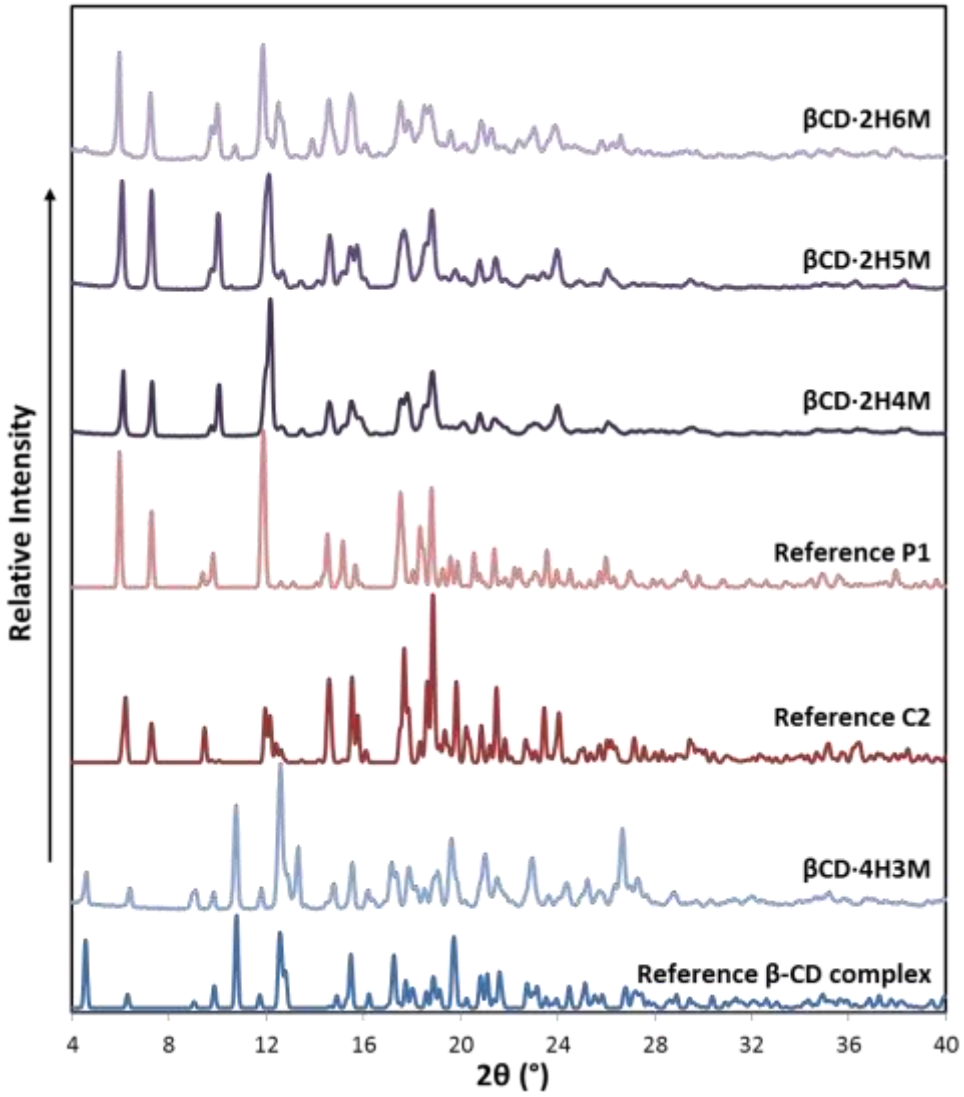

Figure 6.2: Experimental PXRD patterns of the kneaded product of each hydroxyacetophenone guest with β-CD and reference PXRD patterns to determine complex formation.

Preparation of γ-CD inclusion complex crystals

All co-precipitation experiments were performed using a 1:1 host to guest ratio (0.1204 mmol). The host was dissolved in distilled water (3-4 ml) at 60 °C. The guest was then added to the host solution and the solution was stirred until the solution cleared. The resulting solution was filtered and allowed to cool at room temperature. Crystals were obtained for the vials containing 4H3M and 2H4M and microcrystalline precipitates for the vials containing 2H5M and 2H6M, thus the method of slow cooling was used to obtain single crystals suitable for X-ray diffraction. After preparing the host-guest solutions as above, the

vials were sealed and placed in a Dewar flask of hot water, covered with cotton wool and tin foil and allowed to cool slowly over two days.

Single crystal X-ray diffraction and PXRD were used to confirm the complex formation of γCD·2H4M, γCD·2H5M, γCD·2H6M and γCD·4H3M by both preparative methods. All of the inclusion complexes formed were found to be isostructural with the $P42_12$ γ-CD inclusion complex series and were further analysed using thermal analysis and ^{1}H nuclear magnetic resonance spectroscopy.[2] The reproduction of some these inclusion complexes was challenging with the result that some analyses were not performed (HSM for γCD·2H6M and γCD·4H3M).

Thermal analysis and stoichiometry

The TGA traces (Appendix C) of the γ-CD inclusion complexes show an initial mass loss over the range 25 °C to 110 °C, except for the complex γCD·4H3M for which the mass loss continues to 150 °C. This mass loss corresponds to the loss of water from the complex crystals. A second mass loss step corresponding to the loss of the guest from the complex is evident over a wide range from the end of the first mass loss and leading into decomposition which begins at *ca* 275 °C. The DSC traces (Appendix C) are in accordance with the TGA findings and show a large, broad initial endotherm from 25 °C to 150 °C, coinciding with the water loss event. A very broad endotherm follows from 150 °C to 275 °C leading to decomposition. Table 6.1 lists the results of the thermal analysis as well as the results of ^{1}H NMR used to determine the stoichiometry of the γ-CD inclusion complexes. The ^{1}H NMR spectra can be found in Appendix B.

Table 6.1: Percentage mass losses and quantitative results of thermal analysis and ^{1}H NMR spectroscopy of the γ-CD inclusion complexes of the hydroxymethoxy acetophenone isomers

	γCD·2H4M	**γCD·2H5M**	**γCD·2H6M**	**γCD·4H3M**
No. of replicates	2	2	1	3
Water % mass loss	13.8 ± 1.8	13.1 ± 0.1	14.7	14.8 ± 0.4
No. of water molecules per CD	14.5 ± 2.2	13.0 ± 0.1	13.5	14.1 ± 0.5
Guest % mass loss	14.0 ± 0.1	15.2 ± 1.0	13.0	7.6 ± 0.5
No. of guest molecules per CD	1.52 ± 0.1	1.7 ± 0.1	1.6	0.8 ± 0.1
^{1}H NMR H:G	1:1.4	1:1.4	1:1.4	1:1.4
Proposed complex formulae	**$C_{48}H_{80}O_{40}$ $\cdot(C_9H_{10}O_3)_{1.4}$ $\cdot 14.5H_2O$**	**$C_{48}H_{80}O_{40}$ $\cdot(C_9H_{10}O_3)_{1.4}$ $\cdot 13.1H_2O$**	**$C_{48}H_{80}O_{40}$ $\cdot(C_9H_{10}O_3)_{1.4}$ $\cdot 14.7H_2O$**	**$C_{48}H_{80}O_{40}$ $\cdot(C_9H_{10}O_3)_{1.4}$ $\cdot 14.8H_2O$**

HSM was used to observe the physical changes in the crystals of γCD·2H4M and γCD·2H5M upon heating (Figures 6.3 and 6.4).

25 °C **130 °C** **270 °C** **293 °C** **317 °C**

Figure 6.3: HSM photographs of γCD·2H4M.

The crystal is colourless at 25 °C and after heating some fracturing was evident. Bubbling started at 130 °C as the water vaporises and escapes from the crystal. The crystal begins to discolour at 270 °C corresponding to the start of decomposition.

30 °C **100 °C** **286 °C**

Figure 6.4: HSM photographs of γCD·2H5M.

The crystal is clear at room temperature. The crystal fractures as it is heated, possibly due to water loss. At 280 °C the crystal begins to decompose indicated by the discolouration of the crystal and bubbling as the decomposition products escape.

Preparation of β-CD inclusion complex crystals

The host (0.1204 mmol) was added to 5 ml distilled deionised water and allowed to stir. The guest (20 mg) was then added and the solution was stirred with heating up to 60 °C. A small amount of EtOH was added to aid dissolution. The solution was then filtered, covered with parafilm and allowed to evaporate between 20 °C and 25 °C. Crystals were obtained for the solutions containing the guests 2H4M and 2H5M, while a microcrystalline powder resulted from the βCD·2H6M vial. The method of slow cooling was used to obtain large crystals, prepared as for the γ-CD experiments. Single crystals resulted from all host-guest solutions. Both co-precipitation and slow cooling experiments were performed using a 1:1 host to guest ratio. Confirmation of the complex formation of βCD·2H4M, βCD·2H5M, βCD·2H6M and βCD·4H3M was achieved using single crystal X-ray diffraction and PXRD. The complexes βCD·2H4M and βCD·2H5M were found to be isostructural, matching the isostructural series for the β-CD inclusion complexes that crystallize in the space group C2, and the complexes βCD·2H6M and βCD·4H3M were isostructural with the known reference isostructural series crystallizing in P1. Single crystal X-ray diffraction data were collected for the four complexes and they were further analysed using thermal analysis and ^{1}H NMR spectroscopy. The reproduction of some these inclusion complexes was challenging with the result that some analyses were not performed.

Thermal analysis and stoichiometry

TGA, DSC and HSM data were collected for the inclusion complexes βCD·2H4M, βCD·2H5M and βCD·2H6M. The TGA traces (Appendix C) indicate that water is lost over the range 25 °C to 110 °C, followed by a second mass loss step from 110 °C to 275 °C corresponding to the loss of the guest. Decomposition begins shortly after, at *ca* 285 °C. The DSC traces (Appendix C) show a large, multistep initial endotherm from 25 °C to 150 °C, coinciding with the water loss event observed in the TGA traces. For βCD·2H4M and βCD·2H5M a very broad endotherm follows from 150 °C to 275 °C leading to decomposition, while βCD·2H6M shows a small endotherm at 227 °C indicating a phase change. This phase change may be a result of the guest molecules leaving the crystal leading to a reorganisation of the CD molecules. Decomposition followed at 280 °C. ^{1}H NMR was performed on the crystals of βCD·2H4M for which the results confirmed a 1:1 host to guest ratio (Appendix B). Table 6.2 lists the results of the thermal analysis of the β-CD inclusion complexes as well as the proposed complex formulae for each complex, followed by the presentation and analysis of the HSM photographs.

Table 6.2: Percentage mass losses and quantitative results of thermal analysis of the β-CD inclusion complexes of the hydroxymethoxy acetophenone isomers

	βCD·2H4M	**βCD·2H5M**	**βCD·2H6M**
No. of replicates	3	3	3
Water % mass loss	10.9 ± 3.8	9.2 ± 0.4	17.2 ± 2.7
No. of water molecules	8.8 ± 3.6	8.2 ± 0.4	17.0 ± 3.2
Guest % mass loss	10.9 ± 0.5	12.0 ± 0.8	5.2 ± 0.4
No. of guest molecules	1.0 ± 0.1	1.1 ± 0.1	0.5 ± 0.1
Proposed complex formulae	**$C_{42}H_{70}O_{35}\cdot C_9H_{10}O_3 \cdot 8.8H_2O$**	**$C_{42}H_{70}O_{35}\cdot C_9H_{10}O_3 \cdot 8.2H_2O$**	**$C_{42}H_{70}O_{35}\cdot C_9H_{10}O_3 \cdot 17.0H_2O$**

30 °C **50 °C** **75 °C** **290 °C**

Figure 6.5: HSM photographs of βCD·2H4M.

30 °C **55 °C** **75 °C** **290 °C**

Figure 6.6: HSM photographs of βCD·2H5M.

The βCD·2H4M and βCD·2H5M crystals behave similarly when heated (Figures 6.5 and 6.6). The clear room-temperature crystals begin to fracture as they are heated and by 75 °C the crystals turn opaque indicating water loss. At 290 °C the crystals begin to darken indicating decomposition.

30 °C **110 °C** **125 °C** **240 °C** **310 °C**

Figure 6.7: HSM photographs of βCD·2H6M.

The crystal of βCD·2H6M is clear at room temperature and begins to fracture as the crystal is heated (Figure 6.7). Bubbles appear at 110 °C, indicating water loss. As the water escapes the crystal it turns opaque at *ca* 240 °C which corresponds to the phase transformation recorded in the DSC. At 300 °C the crystal begins to decompose indicated by the darkening of the microcrystalline material.

Data collection and space group determination

Single crystal X-ray diffraction intensity data were collected using a Bruker KAPPA APEX II DUO diffractometer. For each inclusion complex a chosen single crystal was surface-dried and coated in Paratone N oil.[4] Program LAYER was used to determine the crystal systems and space groups of the crystals.[5] The reflections of the complexes βCD·2H4M and βCD·2H5M were found to belong to Laue class 2/m indicating the monoclinic system, while those for βCD·2H6M and βCD·4H3M were found to belong to Laue class $\bar{1}$ indicating the triclinic system. Two space groups were indicated for the triclinic system and the P1 space group was chosen due to the chirality of the host. There were similarly two possible space groups for the monoclinic system (C2 and C2/m) based on the systematically absent reflections and the C2 space group was chosen as the host molecule is chiral.

Crystal structure solution and refinement

The data files were prepared using XPREP and isomorphic replacement was used to solve the structures.[6] The atom coordinates of the host backbone were used from the .RES file for ZUZXOH to solve the structures for βCD·2H4M and βCD·2H5M and atom coordinates from the .RES file for AGAZOX to solve the βCD·2H6M and βCD·4H3M structures.[7,8] The non-hydrogen atoms were refined isotropically and the glucopyranose units were labelled G1 to G7 for the C2 structures and A1-A7/B1-B7 for the P1 structures (Figure 6.8a).

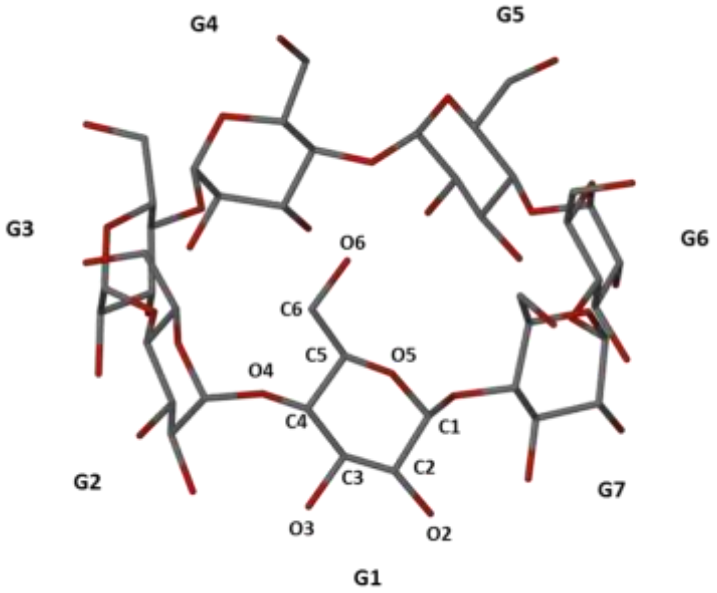

Figure 6.8a: Labelling of the host molecule in the C2 structure. The glucopyranose units are labelled A and B in the P1 structure.

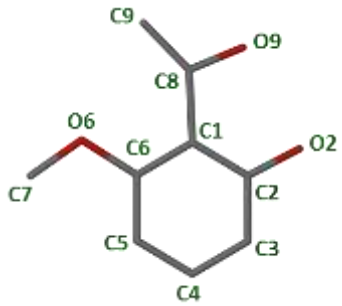

Figure 6.8b: Atom labels used for the guest molecule 2H6M.

SHELXH-97 was used to refine the structures.[9] The remaining host non-hydrogen atoms were assigned and any disordered atoms were assigned partial site occupancy factors (s.o.f.s) of x and 1-x, respectively. The ordered non-hydrogen atoms with satisfactory U_{iso} values were refined anisotropically. The host hydrogen atoms were placed in idealised positions using a riding model except for the hydroxyl hydrogen atoms which were placed using a hydrogen bond searching model (AFIX 83). All hydrogen atoms were refined isotropically with U_{iso} values 1.2 times that of the parent atoms. Table 6.3 lists the refinement parameters and crystal data for the four β-CD inclusion complexes.

Electron density peaks not related to either the host or guest were assigned as water molecules provided that the hydrogen bond criteria were satisfied. Some water O atoms were found to have partial occupancy, having neighbouring O atoms in close proximity and/or high U_{iso} values. In order to settle both the U_{iso} and s.o.f. values the U_{iso} was allowed to refine freely until it settled, after which it was set and the s.o.f. was allowed to refine freely. Hydrogen atoms of the water O atoms were not found.

Table 6.3: Refinement parameters, crystal data and proposed complex formulas for βCD·2H4M, βCD·2H5M, βCD·2H6M and βCD·4H3M.

Name	**βCD·2H4M**	**βCD·2H5M**	**βCD·2H6M**	**βCD·4H3M**
Complex Formula	**$C_{42}H_{70}O_{35}\cdot C_9H_{10}O_3 \cdot 7.9H_2O$**	**$C_{42}H_{70}O_{35}\cdot (C_9H_{10}O_3)_2 \cdot 8.9H_2O$**	**$C_{42}H_{70}O_{35}\cdot (C_9H_{10}O_3)_{0.5} \cdot 24.9H_2O$**	**$C_{42}H_{70}O_{35}\cdot (C_9H_{10}O_3)_{0.5} \cdot 24.6H_2O$**
Formula weight / g mol^{-1}	1444.02	1627.30	2884.82	2879.42
Crystal system	Monoclinic	Monoclinic	Triclinic	Triclinic
Space group	C2	C2	P1	P1
a / Å	19.245(3)	19.218(2)	17.930(2)	17.933(2)
b / Å	24.419(4)	24.510(2)	15.399(2)	15.468(2)
c / Å	15.757(3)	15.923(1)	15.321(2)	15.277(2)
α / °	90	90	102.843(2)	102.939(2)
β / °	109.522(3)	109.014(2)	113.450(2)	113.239(2)
γ / °	90	90	99.490(2)	99.612(2)
Volume / $Å^3$	6979(2)	7091(1)	3629(1)	3637(1)
Z	4	4	1	1
Calculated density / g cm^{-3}	1.374	1.524	1.320	1.314
μ (MoKα) / mm^{-1}	0.123	0.134	0.121	0.120
F (000)	2650	2692	1541	1401
Temperature / K	173(2)	173(2)	173(2)	173(2)
Crystal size / mm^3	0.21 x 0.18 x 0.11	0.17 x 0.12 x 0.09	0.24 x 0.23 x 0.10	0.18 x 0.15 x 0.11
Theta ranges scanned / °	1.7 ≤ θ ≤ 27.2	2.2 ≤ θ ≤ 27.5	2.1 ≤ θ ≤ 27.6	2.1 ≤ θ ≤ 27.1
Index ranges	h: -24, 23; k: -31, 31; l: -20, 20	h: -24, 20; k: -31, 31; l: -18, 20	h: -23, 23; k: -20, 20; l: -19, 19	h: -22, 22; k: -19, 19; l: -19, 19
Total number of reflections	28928	27503	69678	51815
No. of independent reflections	7912	8334	16721	15857
No. of reflections with I > 2σ(I)	6740	7308	15389	13636
No. of parameters	721	758	1531	1504
R_{int}	0.024	0.023	0.031	0.027
S	1.717	1.870	1.546	1.330
R_1 (I > 2σ(I))	0.1215	0.1354	0.1054	0.0964
wR_2	0.3704	0.3860	0.3079	0.2955
Weighting scheme	a = 0.2, b = 0.0	a = 0.2, b = 0.0	a = 0.2, b = 0.0	a = 0.2, b = 0.0
Δρ excursions / e $Å^{-3}$	-0.64 and 1.10	-0.83 and 1.89	-0.96 and 2.15	-0.58 and 2.00

The guest molecules were found to be highly disordered within the cavity of the cyclodextrin making elucidation impossible, except for βCD·2H6M where the guest was modelled. This resulted in incomplete crystal structures leading to the high values for the weighting scheme parameter as seen in Table 6.3. The absence of guest modelling in β-CD inclusion complexes with a channel-type packing arrangement of the host is not uncommon.[10] The electron densities do, however, give an indication of the location of the guest molecule. The guest in βCD·2H4M appears to exist within the CD cavity while in βCD·2H5M there are two areas of electron density clusters which indicate that one guest molecule penetrates at the primary rim and the other at the secondary rim. The electron density of the guest molecules in both βCD·2H6M and βCD·4H3M occur at the interface between the two CDs of a β-CD dimer. Due to the above limitations, only the structure of βCD·2H6M will be discussed in further detail.

β-CD INCLUSION COMPLEX WITH 2-HYDROXY-6-METHOXYACETOPHENONE (βCD·2H6M)

Modelling of the guest molecule

The electron density peaks within the host cavity were examined and the phenyl ring of the guest molecule was identified by its hexagonal shape. The atoms were assigned and the AFIX 66 command was applied to the ring to make it rigid. The methoxy and hydroxyl groups were then assigned followed by the assignment and refinement of the acetyl group. The guest molecule labels are shown in Figure 6.8b. Some distance constraints were applied to ensure reasonable geometry. The guest was refined isotropically as some atoms possessed large U_{iso} values due to further unresolved disorder of the guest. Hydrogen atoms were added in idealised positions using a riding model or hydrogen bond search model, with U_{iso} values 1.2 to 1.5 times that of the parent atoms.

Molecular structure

The asymmetric unit (ASU) consists of two β-CD molecules which form a head-to-head dimer, one 2H6M molecule and 24.9 water molecules (Figure 6.9a and b). The guest molecule is not included within the CD cavities but rather exists at the interface of the dimer.

(a) 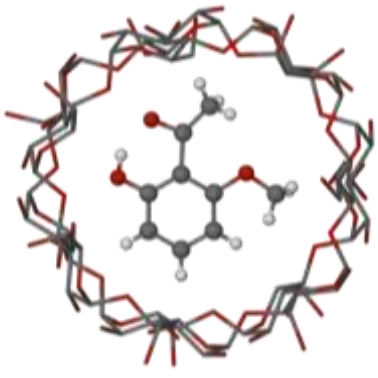 **(b)** 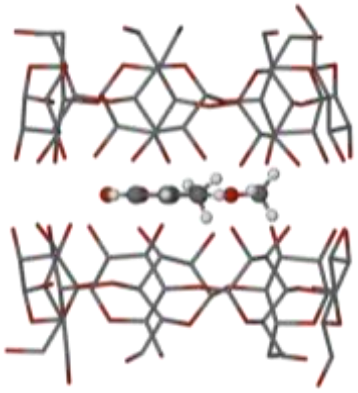

Figure 6.9: The ASU of βCD·2H6M viewed from (a) above and (b) side-on. Hydrogen atoms of the host are omitted for clarity.

Geometrical analysis

Host Geometry

The geometrical parameters that describe the conformation of the two independent host molecules are listed in Table 6.4. The O4 heptagon is generally described by certain geometric parameters namely the radii (*r*), the glycosidic O4(n)···O4(n+1) distance (*D*), the O4(n-1)···O4(n)···O4(n+1) angle (*α*), the O4(n-1)···O4(n)···O4(n+1)···O4(n+1) torsion angle (*d*), the deviation from atoms O4n from the least-squares O4 plane (*α*), the tilt angles (τ_1 and τ_2) and the intersaccharidic angles (*φ*). All of the glucopyranose units are in the $^4C_1$ chair conformation.

Table 6.4: O4-heptagon, *τ* and *φ* parameters of the βCD·2H6M structure

Residue	*r* (Å)	*D* (Å)	*α* (°)	*φ* (°)	*d* (°)	*α* (Å)*	τ_1 (°)	τ_2 (°)
A1	5.018	4.317	129.2	117.2(4)	0.81	0.005	11.4(1)	5.2(3)
A2	4.928	4.452	130.3	118.3(5)	-0.44	0.000	5.0(1)	3.0(2)
A3	5.055	4.330	128.9	117.5(5)	-0.01	0.008	3.8(1)	2.3(2)
A4	5.204	4.324	123.9	119.6(5)	1.36	-0.002	6.3(2)	3.0(3)
A5	4.875	4.499	133.1	116.6(4)	-2.83	-0.022	4.7(1)	2.0(3)
A6	5.009	4.262	128.5	117.3(4)	2.83	0.038	13.7(2)	7.9(1)
A7	5.158	4.412	126.1	118.4(4)	-1.82	-0.027	5.6(1)	1.4(2)
Mean	**5.04**	**4.37**	**128.6**	**117.8**	**1.44‡**	**0.020‡**	**7.2**	**3.5**
B1	5.129	4.251	125.4	118.7(5)	2.85	-0.011	7.5(2)	4.3(2)
B2	4.961	4.465	130.5	116.4(4)	-4.08	0.050	6.2(2)	1.9(2)
B3	4.968	4.276	129.2	117.5(4)	2.51	-0.047	13.4(2)	7.2(3)
B4	5.068	4.385	127.2	118.2(5)	-0.22	0.006	5.1(1)	1.8(2)
B5	5.016	4.297	129.2	117.2(4)	-0.53	0.020	13.3(2)	4.2(1)
B6	4.996	4.403	128.3	118.0(5)	0.06	-0.002	4.2(1)	2.2(2)
B7	4.970	4.393	130.2	117.3(5)	-0.71	-0.015	6.3(1)	4.0(3)
Mean	**5.02**	**4.35**	**128.6**	**117.6**	**1.57‡**	**0.028‡**	**8.0**	**3.7**

*Average e.s.d. = 0.003 Å, ‡Root mean square

The values for *r*, *D* and *α* fall within the expected ranges, indicating little distortion of the host, and compare favourably with the values obtained for other β-CD inclusion complexes.[3] The average intersaccharidic bond angles correspond well with the literature value for the β-CD structure of 117.7°.[11] The small deviation of the O4 atoms from the mean O4 plane (*α*) is small and thus there is no significant curvature of the host molecule. This is supported by the relatively small degree of deviation in the torsion angle (d) between successive O4 atoms. The two tilt angles (τ_1 and τ_2) describe the orientation of the glucopyranose residues. All of the tilt angles are positive, fairly small and cover a narrow range (3.75° to 13.73° for A and 4.20° to 13.44° for B when examining τ_1), with the result that the secondary rim is not considerably wider than the primary rim.

The torsion angle O5-C5-C6-O6 describes rotation around the C5-C6 bond and therefore the orientation of the C6-O6 bond. A positive torsion angle indicates that the C6-O6 bond is directed towards the CD cavity while a negative value indicates directionality away from the CD cavity. All of the C6-O6 bonds are (-)-*gauche* on both host A and host B with the exception of the bonds on glucopyranose units A1, A4 and B5 which are (+)-*gauche*.

Hydrogen bonding interactions

There are seven intramolecular hydrogen bonds in each of the β-CD molecules involving O3(n)···O2(n+1), often referred to as flip-flop hydrogen bonds, contributing to the rigidity and symmetry of the respective host molecules.[12] The dimer is held together by seven intermolecular hydrogen bonds of the type O3(A)···O3(B). A number of interdimer O6(A)···O6(B') interactions (some facilitated by water O atoms) give form to the greater crystal structure. These interactions are typical of dimeric β-CD complexes and fall within the expected ranges.[3] An extended hydrogen bonding network is formed involving water O···O close contacts and water-host interactions. There are no hydrogen bonding interactions between the guest and host molecules. The guest has an intramolecular O-H···O hydrogen bond which results in a ring with graph-set notation $S_1^1(6)$.[13] The O···H bond distance is 1.72 Å, the O···O bond distance is 2.47 Å and the bond angle is 147.0°.

Guest inclusion

As mentioned previously, the guest is included in the host molecules at the dimer interface (Figure 6.10). The formation of a dimer creates a large hydrophobic environment and any guest molecule would be expected to occupy more space within the cavity. However, the area between two β-CD molecules is likely to be the most hydrophobic region in the dimer.[3] In βCD·2H6M the primary driving force of inclusion is exclusively hydrophobic as evidenced by the lack of hydrogen bonding between the host and guest molecules. In this position the guest molecule remains planar. This type of inclusion was also found by Lien, *et al*. using the guest *N*-methylanthranilic acid, which is of similar size and polarity to 2H6M.[14]

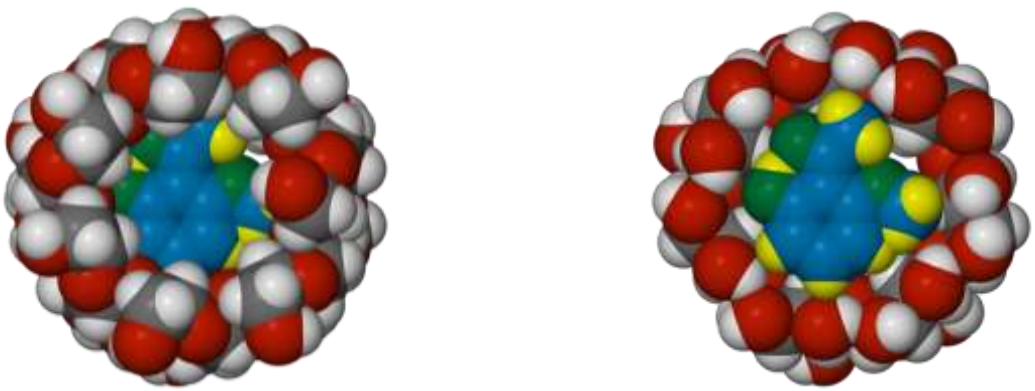

Figure 6.10: CPK diagrams of the βCD·2H6M complex dimer (left) and the complex dimer with the top host molecule removed (right).

Crystal packing

The β-CD dimers stack in a head-to-head fashion having an intermediate channel type packing arrangement.[3] The channels propagate infinitely in the *a*-direction. Layers of dimers are formed which lie parallel to the *b*-*c* plane (Figure 6.11). The layers and columns are held together by inter- and intra-layer hydrogen bonds, as well as by hydrogen bonds between the host molecules and the water molecules present in the interstitial spaces between columns.

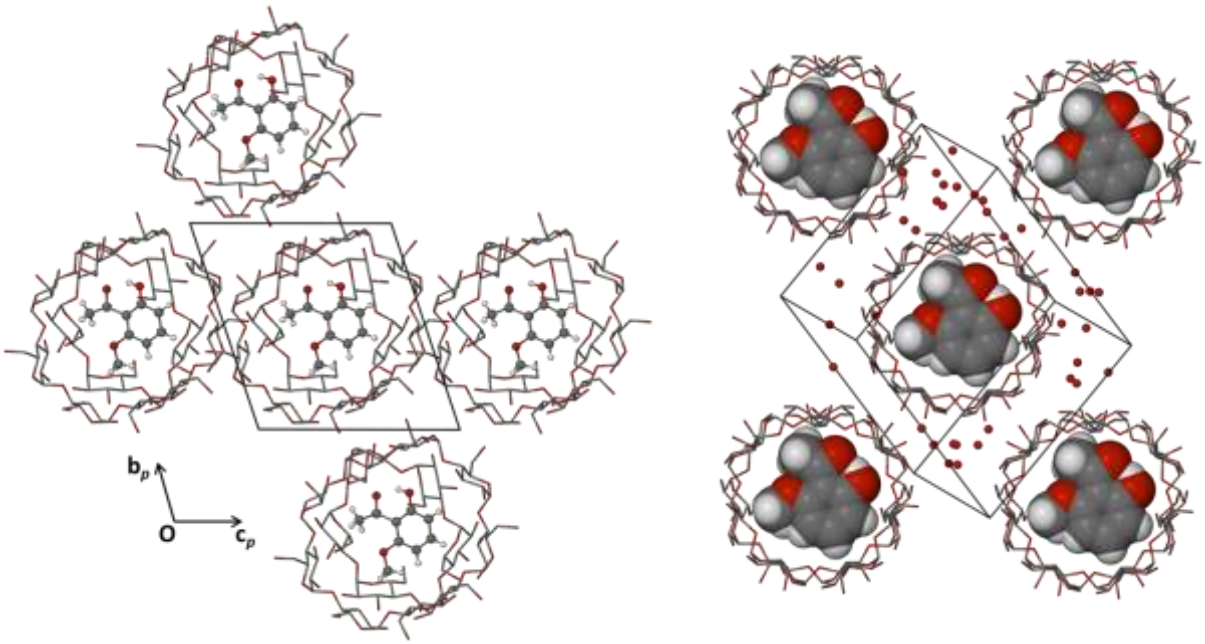

Figure 6.11: Packing diagrams of βCD·2H6M viewed down the *a*-axis (left) and down the dimer columns (right)

β-CD INCLUSION COMPLEXES WITH THE REMAINING GUESTS (βCD·2H4M, βCD·2H5M AND βCD·4H3M)

The structure of βCD·4H3M is isostructural with βCD·2H6M, with the host molecules forming a head-to-head dimer within similar unit cell parameters.

The structures of βCD·2H4M and βCD·2H5M also form head-to-head β-CD dimers in which the two CD molecules are related by a crystallographic two-fold axis. Intramolecular hydrogen bonds involving the distances O3(n)···O2(n+1) keep the host molecule symmetrical and inflexible. The dimer is held together by O3(A)···O3(A') intermolecular hydrogen bonds. Interdimer O6(A)···O6(B') interactions link adjacent dimers and contribute to the extended hydrogen bonding network of the water molecules, which exist in the interstitial space between complex units. The geometry of the β-CD molecule is typical of this type of complex.[3] The packing type in these crystals is channel-type such that the dimers are stacked parallel to the *c*-axis to form infinite channels, which are slightly shifted at the interdimeric interface.

SOLUTION-STATE STUDIES OF COMPLEXATION BETWEEN HYDROXYMETHOXYACETOPHENONE ISOMERS AND NATIVE CDs

Solution ^{1}H Nuclear Magnetic Resonance (NMR) spectroscopy

NMR spectroscopy is a very sensitive technique which can successfully be used to study CD inclusion phenomena in solution. The host-guest interaction can be clearly identified by the induced chemical shift of certain protons as a result of complexation and by changing various parameters of the NMR experiment. This chemically induced shift (CIS) is calculated by subtracting the chemical shift for a particular proton of the complexed molecule from that of the uncomplexed molecule ($\Delta\delta_{obs} = \delta_{free} - \delta_{obs}$).[15] Appendix D shows partial 500 MHz ^{1}H NMR spectra of the pure compounds and of the equilibrium mixtures for each guest with β- and γ-CD, respectively. Assignment of the CD protons was in accordance with a number of reliable sources.[16-18] The experiments were carried out in D_2O so as to avoid the exclusion of the guest from the CD cavity by larger deuterated solvent molecules. In some cases, a small amount of MeOD was added to aid dissolution. The numbering of the CD protons is shown in Figure 6.12. Figure 6.13 shows the structures of the guest molecules, using subscripts a, b and c to identify different chemical environments on the phenyl protons.

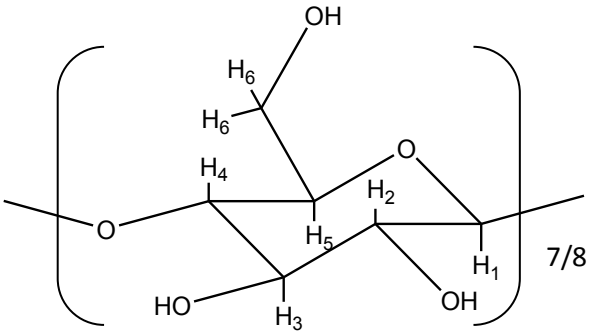

Figure 6.12: An α-glucopyranose unit including proton numbering

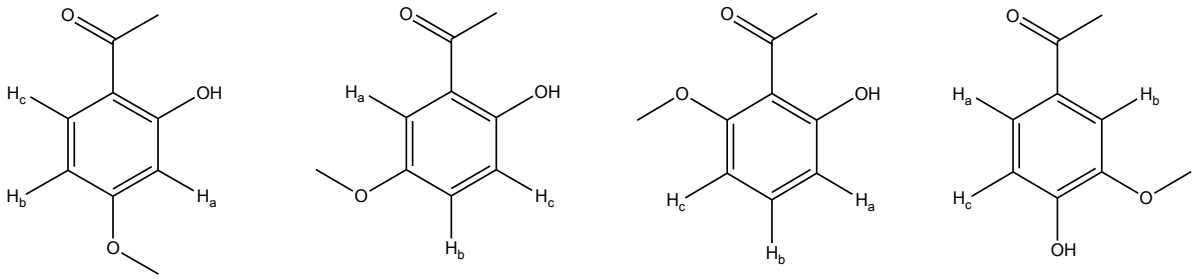

Figure 6.13: Chemical structures of the hydroxymethoxy acetophenone guest molecules.

The CD protons H_3 and H_5 are located inside the host cavity allowing interaction with the guest molecule. H_6 is located on the narrow (primary) rim of the CD and due to C_6 being relatively free to rotate around the C5-C6 bond, depending on the mode of complexation, the H_6 protons may or may not interact with the small guest molecules. H_1, H_2 and H_4 are situated on the exterior of the CD and therefore no significant interaction with an included guest molecule is generally observed. In the ^{1}H NMR spectra recorded, the only chemical shifts noted were for those of the affected protons and no distinct peaks were observed for the free molecules and the bound molecules (i.e. there was no change in multiplicity) indicating that the complexation process is dynamic. This requires that the guest experiences a fast exchange between its free and bound states (relative to the NMR time scale) and this exchange rate must exceed the reciprocal of the largest shift difference for any guest proton.[19] Figure 6.14 shows the partial ^{1}H NMR spectra of β-CD, as well as γ-CD, and the complexes formed with each guest at 1:1 [H]/[G] ratio illustrating the respective host proton shifts. Note the shift of protons H_3 and H_5 in each case. In general, guest protons that are located deep within the CD cavity will experience the largest CISs. The protons of the guest molecules outside the CD cavity will be less affected. A large peak at 4.7 ppm seen in the spectra is due to residual HDO molecules in the D_2O solvent. This peak was used as an internal standard in measuring the chemical shifts of the CD with or without the guest present. The CD hydroxyl protons may be exchanged with the D_2O and disappear from their normal spectral positions. The digital resolution is 0.00025 ppm/point. The β-CD complexes studied are designated β-CD·2H4M, β-CD·4H3M, β-CD·2H5M and β-CD·2H6M while the γ-CD complexes studied are designated γ-CD·2H4M, γ-CD·4H3M, γ-CD·2H5M and γ-CD·2H6M.

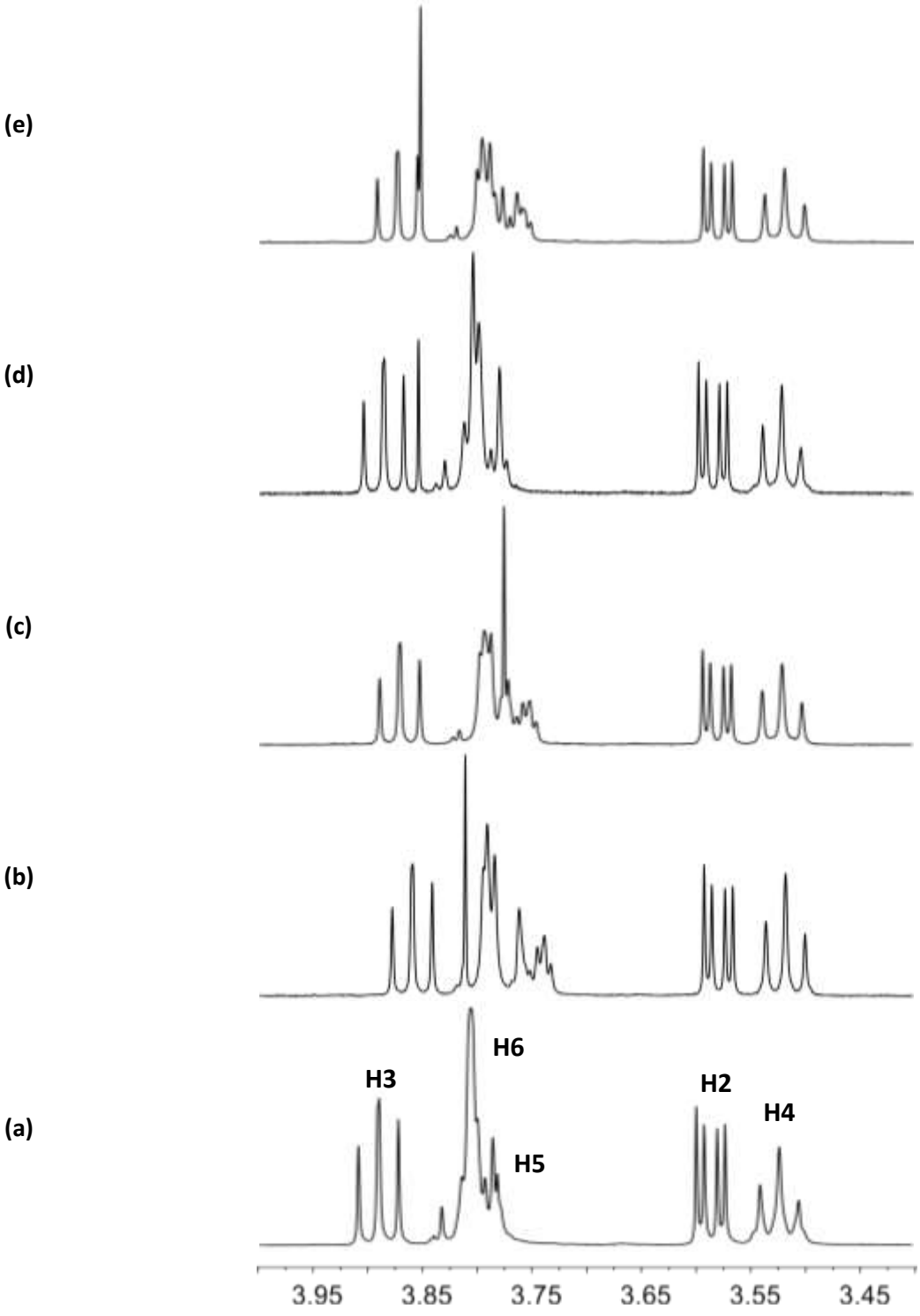

Figure 6.14a: Partial ^{1}H NMR spectra (500 MHz) of (a) pure β-CD, and of solutions of mixtures of β-CD and guests in 1:1 molar ratio, the respective guests being (b) 2H4M, (c) 2H5M, (d) 2H6M and (e) 4H3M at 298 K.

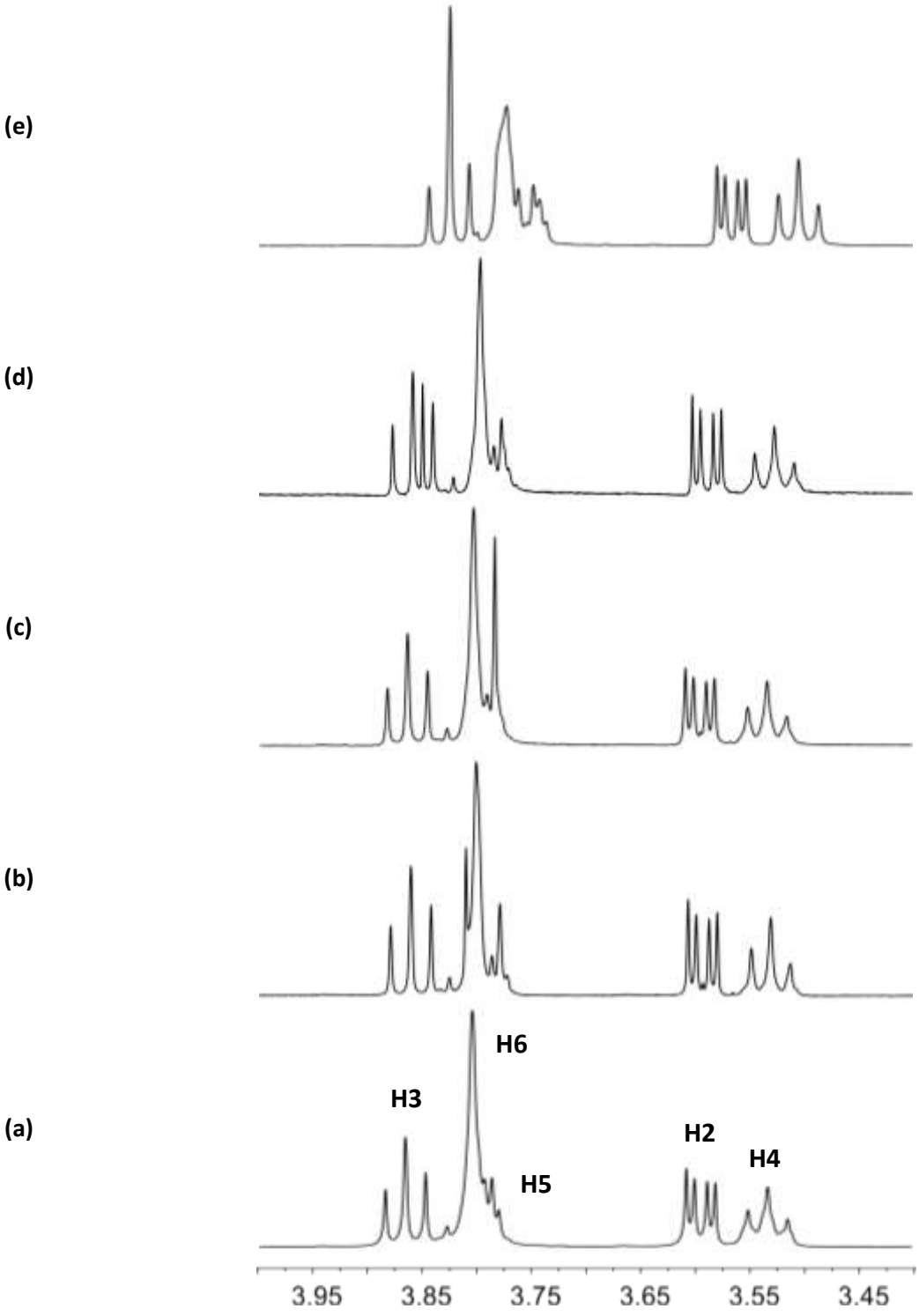

Figure 6.14b: Partial ^{1}H NMR spectra (500 MHz) of (a) pure γ-CD, and of solutions of mixtures of γ-CD and each guest in a 1:1 molar ratio, the respective guests being (b) 2H4M, (c) 2H5M, (d) 2H6M and (e) 4H3M at 298 K.

Stoichiometry (Continuous Variation Method)

The stoichiometries of the inclusion complexes were determined by the method of continuous variation, as explained in Chapter 2.[20] The stock solutions prepared for the β-CD experiments were made up to 3 mM for all host/guest solutions except the β-CD·2H6M solution, which was made to 2 mM due to the poor solubility of the guest in D_2O. Changes in the chemical shifts of the CD protons H_3 and H_5 were followed as these protons showed significant CIS values. As different molecules have different modes of inclusion, each guest proton has different CIS values and the protons with the largest CIS values were monitored in each case. Job plots for the host and guest for each complex are shown in the Figures 6.15 and 6.16 below. The Job plots for both β-CD and guest molecules are nearly symmetrical, with a maximum occurring at r = 0.5, where r is the ratio of either the host or the guest molar ratio and the total molar ratio such that r = a/(a+b). This indicates that only one type of complex was formed in each case and that the complexes have a 1:1 stoichiometry over the studied concentration range.

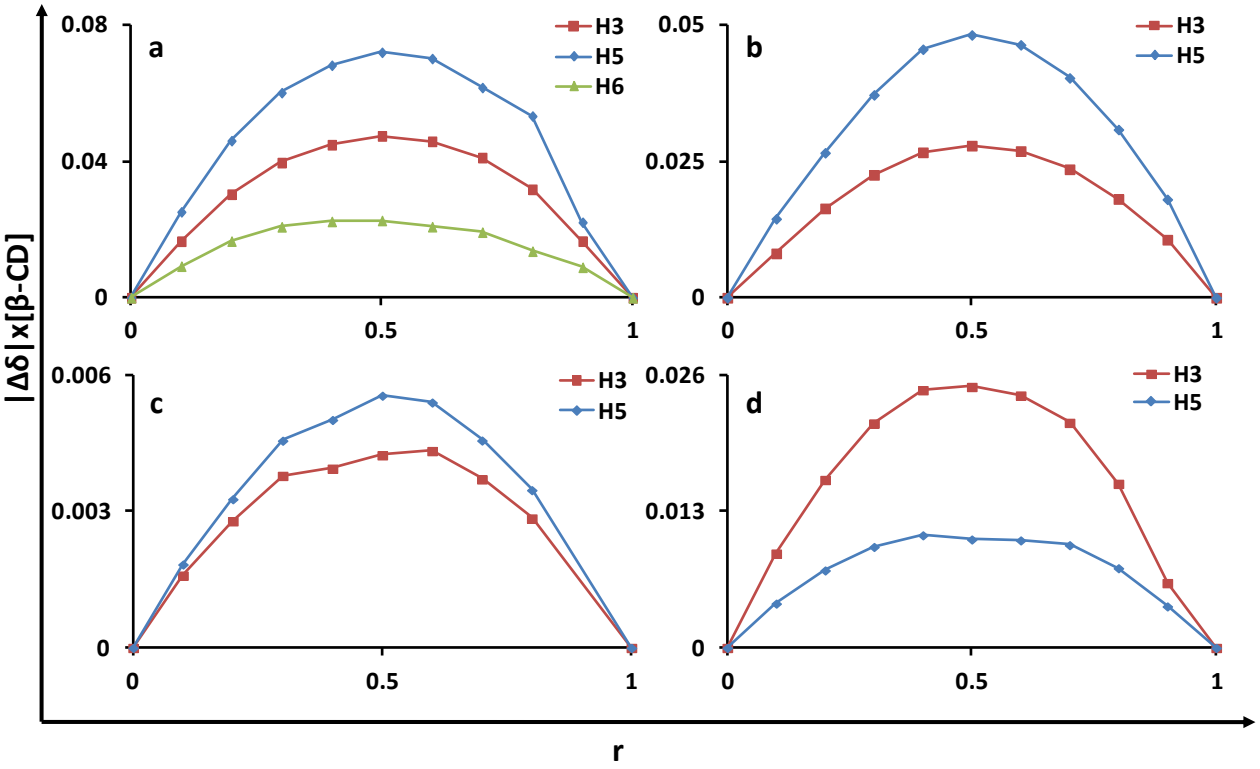

Figure 6.15: Job plots for protons of β-CD in the (a) β-CD·2H4M, (b) β-CD·2H5M, (c) β-CD·2H6M and (d) β-CD·4H3M complexes.

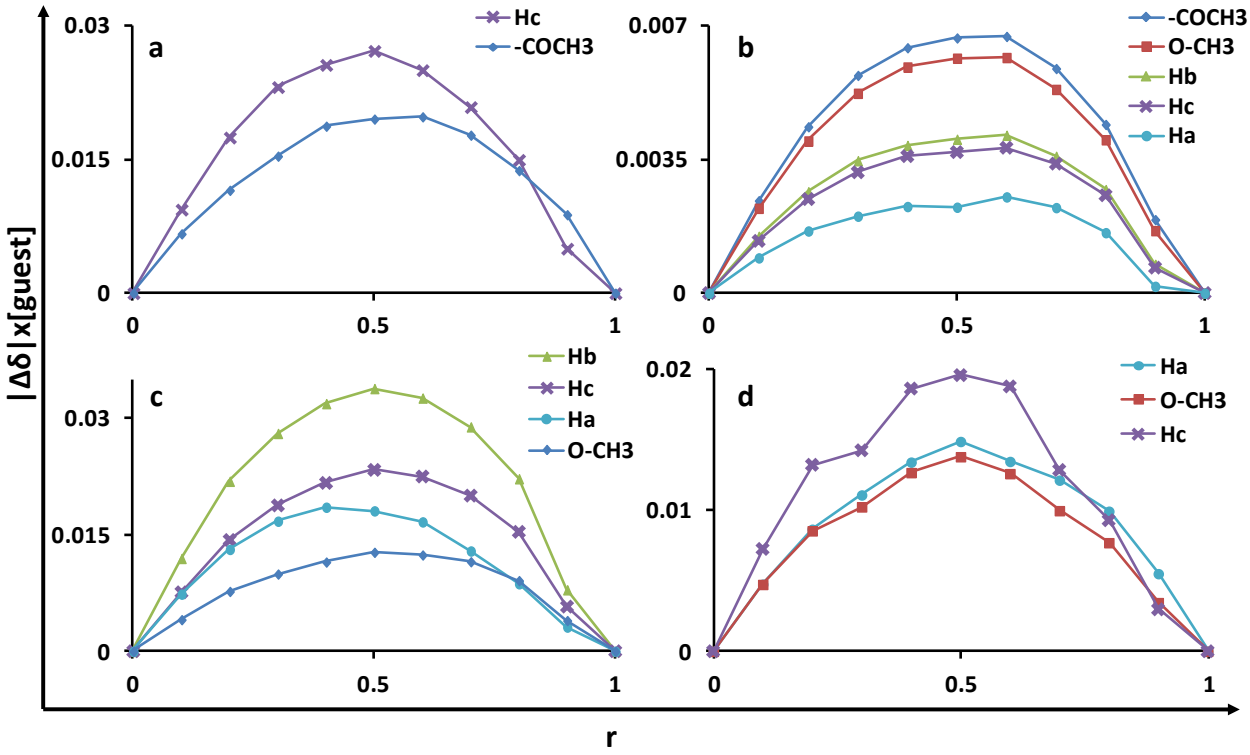

Figure 6.16: Job plots for protons of the respective guest molecules in the (a) β-CD·2H4M, (b) β-CD·2H5M, (c) β-CD·2H6M and (d) β-CD·4H3M complexes.

The stock solutions prepared for the γ-CD experiments were made up similarly to those for the experiments involving β-CD. The total concentration of the solutions γ-CD·2H4M, γ-CD·2H5M and γ-CD·2H6M were held constant at 2 mM. Where necessary a small amount of MeOD was added to aid dissolution. The total concentration of 4H3M and γ-CD was held at 5 mM. Significant shifts were observed for the host protons H_3 and H_5 for γ-CD·2H4M over the whole concentration range, indicating that inclusion does take place. However, the guest protons showed an upfield shift as the concentration of the guest increased to 1 mM but changed to a downfield shift from 1 mM to 2 mM. This suggests an interaction with the exterior of the CD cavity, supported by the CIS values recorded for host proton H_1 over the host concentration range 1 mM to 0.2 mM. While Job plot analysis was possible from the shifts of the host H_3 and H_5 protons, the varying shifts observed for the host protons H_1 as well as the guest protons indicate interaction between the guest and both the exterior and interior of the CD. For this reason association constant calculations were not pursued for γ-CD·2H4M. The results for γ-CD·2H5M showed very small changes in the chemical shifts of host and guest protons over the concentration range studied and Job plot analysis was not possible. The CIS values observed for the guest protons are similar to those observed for γ-CD·2H4M as well as for protons H_1 and H_4, and association constant calculations were consequently not performed. The CIS value of the host proton H_3 for γ-CD·2H6M showed significant shifts as did the guest protons O-CH_3 of 2H6M. These CIS values were used to construct the Job plot. The maximum chemical shift variations observed for the guest protons of γ-CD·4H3M were found to be smaller than the CIS values of the protons on the exterior of the CD molecule, indicating that the guest

molecules interact with both the interior and exterior of the CD molecule. The chemical shift of a guest proton represents a weighted average of both interactions and therefore only the host protons H_3 and H_5 were used to obtain the stoichiometry of each complex. Figure 6.17 shows that the Job plot of the complex γCD·4H3M is symmetrical with a maximum occurring at r = 0.5, indicating uniform complex formation with a 1:1 stoichiometric ratio of host to guest over the concentration range studied. The data points of the Job plots a and b appear to be more scattered; however, due to the very small CIS values recorded (of the order 10^{-3} ppm) it can be concluded that within experimental error only 1:1 stoichiometric ratios of host to guest are formed in solution.

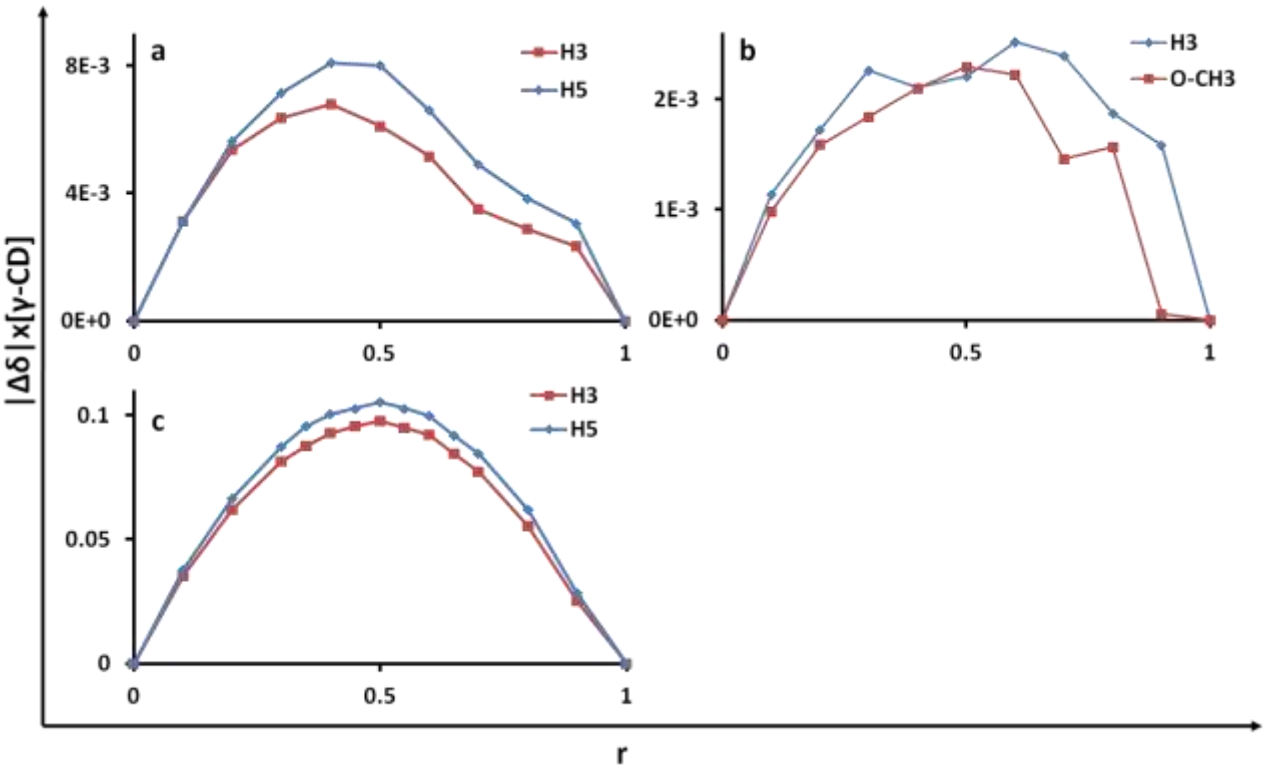

Figure 6.17: Job plots for protons of γ-CD in the (a) γ-CD·2H4M, (b) γ-CD·2H6M (H_3 of γ-CD and O-CH_3 of 2H6M) and (c) γ-CD·4H3M complexes

Asymmetric Job plot shapes may be due to the small concentrations used, as well as the very small CIS values recorded in all cases compared to the expected error in measurement. Where very small chemical shift variations were observed, subtraction of the internal standard peak (HDO) was used to improve the experimental data.

Comments on Modes of Inclusion

Interactions between host and guest molecules result in a change in the position of the complex proton shift relative to the free molecule proton shift, giving a CIS value. Structural information may be obtained from the CIS values observed. A negative CIS value is a downfield shift while a positive CIS value is an upfield shift. The upfield shifts are caused by the shielding of protons due to a change in local polarity within the β-CD cavity and indicate weak van der Waals interactions. Downfield shifts indicate that the

proton is interacting with a strongly electron withdrawing atom such as oxygen. The smaller CIS values for some protons indicate that these protons are not included in the CD cavity. The CD protons show only upfield shifts which are caused by the magnetic anisotropy effects due to the inclusion of molecules with electron-rich groups.[21] The largest contribution to this effect is the aromatic benzene ring of the guest molecule. The magnetic anisotropy is called the 'ring-current' effect and affects protons that are located above or below the electron cloud (H_3 and H_5).[22] In some cases the proton CIS could not be observed due to the proton peak being obscured by other proton peaks.

Table 6.5 shows the maximum observed CIS values of both host and guest protons for each complex formed with β-CD. The CIS values recorded for the β-CD protons with each guest molecule included are in the order $H_5 > H_3 > H_6$, suggesting that the guest molecule for each complex is located near the primary rim.[23] While the CIS values for the H_6 host protons are not large, the observed shifts indicate some interaction with guest protons. In all cases, the guest is located deep within the cavity (inserted either via the primary or secondary rim) and may protrude slightly from the primary end of the host to interact with H_6. An indication of the extent of insertion is given by the significant shifts that both H_3 and H_5 experience.[24] The guest protons experience both upfield and downfield shifts.

Table 6.5: Maximum observed CIS values (Δδ) for complexes formed with β-CD (in ppm)*

	H_1	**H_2**	**H_3**	**H_4**	**H_5**	**H_6**
β-CD·2H4M	0.0147	0.0113	0.0553	0.0097	0.0840	0.0309
β-CD·2H5M	0.0097	0.0081	0.0355	0.0030	0.0601	0.0217
β-CD·2H6M	0.0026	0.0021	0.0080	0.0020	0.0092	N/A
β-CD·4H3M	0.0078	0.0065	0.0300	0.0031	0.0423	0.0171
	H_a	**H_b**	**H_c**	**O-CH_3**	**-$COCH_3$**	
β-CD·2H4M	-0.0058	-0.0037	0.0313	-0.0058	-0.0222	
β-CD·2H5M	0.0246	-0.0399	-0.0253	N/A	-0.0136	
β-CD·2H6M	-0.0046	-0.0074	-0.0068	-0.0111	-0.0121	
β-CD·4H3M	-0.0159	-0.0242	-0.0029	-0.0158	3×10^{-5}	

*The entry N/A indicates that these signals could not be clearly resolved due to peak overlap

For the complex β-CD·2H4M it is clear from the observed CIS of the H_c proton and the acetyl protons of the guest molecule that these protons interact with the CD, indicating that the acetyl moiety of the molecule is included in the CD cavity. The CIS for H_c is a downfield shift, suggesting that it is in the vicinity of an oxygen atom, while the acetyl protons shift upfield and interact with the host by van der Waals forces.[21] Figure 6.18 illustrates the proposed mode of inclusion of 2H4M in β-CD.

The complex β-CD·2H5M has CIS values which indicate that almost all of the guest protons interact significantly with the protons found in the β-CD cavity (H_3 and H_5). Some interaction with H_6 is also evident. The greatest changes in chemical shift in the guest protons occur for protons H_b and H_c, while smaller changes can be seen for the proton H_a and the acetyl protons. All protons experience an upfield

shift and interact with the host by van der Waals forces.[21] Figure 6.19 illustrates the proposed mode of inclusion of 2H5M in β-CD.

The changes in chemical shift for the complex β-CD·2H6M are an order of magnitude smaller than those of the other complexes. This may indicate that the interactions between host and guest are very weak, although the guest is relatively deeply included within the CD cavity as the CIS values for H_3 and H_5 show some interaction with the guest. Also, all the guest protons experience a CIS, suggesting that the guest molecule does not have only one mode of inclusion but may enter and exit the CD in different orientations. It is however evident that the predominant interactions occur for the methoxy and acetyl protons. The upfield CIS values of the guest protons indicate that only van der Waals interactions occur between the host cavity and guest molecule.[21] Figure 6.20 illustrates the proposed mode of inclusion of 2H6M in β-CD.

The CIS values for the complex β-CD·4H3M suggest that a greater portion of the guest molecule is inserted in the CD cavity, as protons H_a and H_b as well as the methoxy protons show significant CIS changes. All affected guest protons experience an upfield shift indicating that weak van der Waals forces hold the guest in the cavity. Host protons H_3, H_5 and H_6 show significant shifts, indicating that the guest is deeply inserted in the CD cavity. Figure 6.21 illustrates the proposed mode of inclusion of 4H3M in β-CD.

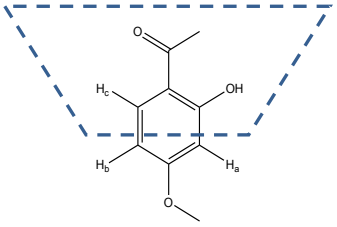

Figure 6.18: Proposed position of 2H4M in the β-CD cavity

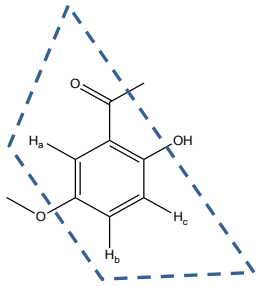

Figure 6.19: Proposed position of 2H5M in the β-CD cavity

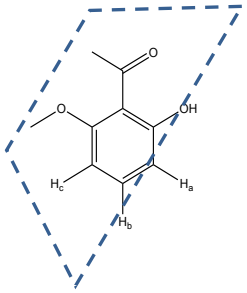

Figure 6.20: Proposed position of 2H6M in the β-CD cavity

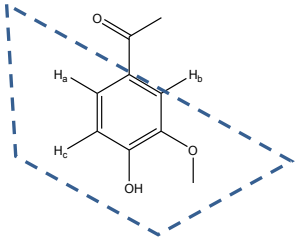

Figure 6.21: Proposed position of 4H3M in the β-CD cavity

Table 6.6 shows the maximum observed CIS values of both host and guest protons for each complex formed with γ-CD. The maximum CIS values for the guest protons are similar to those of the exterior CD protons, indicating that interactions occur between the guest molecule and both the exterior and the interior of the CD cavity. For this reason it is difficult to assign modes of inclusion with confidence. It can, however, be confirmed that inclusion does occur in each case as the CIS values of the host protons H_3 and H_5 are larger than those for the exterior protons.

Table 6.6: Maximum observed CIS values (Δδ) for complexes formed with γ-CD (in ppm)

	H_1	H_2	H_3	H_4	H_5	H_6
γ-CD·2H4M	0.0104	0.0067	0.0198	0.0090	N/A	N/A
γ-CD·2H5M	0.0033	0.0013	0.0086	0.0026	N/A	0.0050
γ-CD·2H6M	0.0046	0.0024	0.0098	0.0038	0.0119	0.0075
γ-CD·4H3M	0.0545	0.0483	0.0746	0.0481	0.0802	N/A
	H_a	H_b	H_c	$O\text{-}CH_3$	$\text{-}COCH_3$	
γ-CD·2H4M	-0.0123	-0.0073	-0.0068	N/A	-0.0012	
γ-CD·2H5M	0.0027	0.0041	0.0045	N/A	0.0051	
γ-CD·2H6M	0.0002	-0.0028	-0.0055	N/A	N/A	
γ-CD·4H3M	0.0345	0.0283	0.0218	N/A	0.0303	

*The entry N/A indicates that these signals could not be clearly resolved due to peak overlap

The complex γ-CD·2H6M shows very low CIS values and a ROESY experiment was performed to confirm the interaction between the host and guest molecules. Figure 6.22 shows that there is an interaction between H_a of the guest and H_3 of the host.

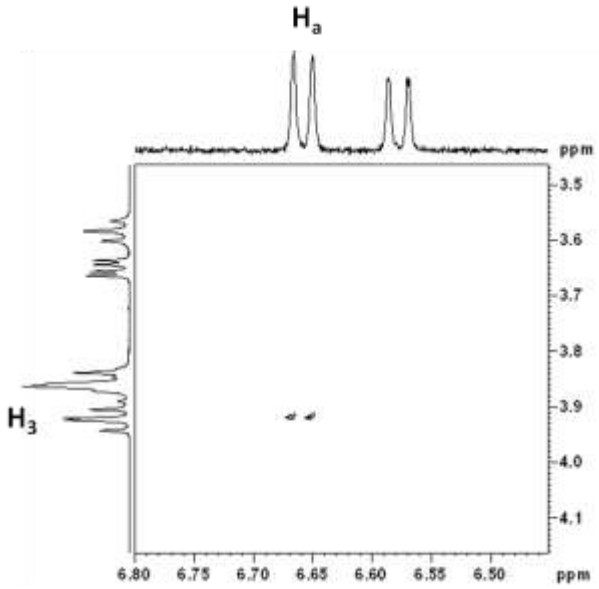

Figure 6.22: 2D-NMR (ROESY) spectrum of the inclusion complex γ-CD·2H6M ([γ-CD] = 1.5 mM, [2H6M] = 1.5 mM)

Association constant determination

Association constants were evaluated in order to determine the extent of the intermolecular host-guest interactions between each guest molecule and β-CD. These association constants, K, were found by using equation (10) in Chapter 2, where [X] is the concentration of the host or guest of a sample and $[M] = [G]_t + [H]_t$:

$$\Delta\delta_{obs}^{(X)} = \frac{\Delta\delta_c^{(X)}}{2[X]_t} \times \left\{ [M] + \frac{1}{K} \pm \left[\left([M] + \frac{1}{K} \right)^2 - 4[H]_t[G]_t \right]^{\frac{1}{2}} \right\} \quad (10)$$

The protons studied were those shown in the Job plot analyses, where changes in the chemical shifts were observed as a function of the parameter r. The association constant, K, was calculated for each complex using a non-linear least-squares analysis of the observed changes in chemical shift (Δδ) of each guest and β-CD NMR lines for the affected protons as a function of the concentration of β-CD. The program CONSTEQ was used successfully in this regard.[25] The protons studied and resulting K values are listed in Table 6.7, as are the correlation coefficients (R), the error loss function (E) and the calculated CIS (Δδ).

Table 6.7: The association constant results for each complex formed with β-CD

	β-CD·2H4M	**β-CD·2H5M**	**β-CD·2H6M**	**β-CD·4H3M**
Protons studied	H_3, H_5 H_c, O-CH_3	H_3, H_5 H_b, H_c	H_3, H_5 H_b, CH_3, -$COCH_3$	H_3 H_a, H_b, -$COCH_3$
Association constant, K	224 M^{-1}	154 M^{-1}	145 M^{-1}	336 M^{-1}
Correlation coefficient, R	0.9995	0.9993	0.9983	0.9996
Error loss function, E	2.54 X 10^{-5}	3.03 x 10^{-5}	5.716 X 10^{-6}	2.62 X 10^{-6}
$\Delta\delta_{H3}$ (ppm)	0.1515	0.1153	0.0387	0.0677
$\Delta\delta_{H5}$ (ppm)	0.2303	0.1973	0.0466	-
$\Delta\delta_{Ha}$ (ppm)	-	0.0814	-	-0.0319
$\Delta\delta_{Hb}$ (ppm)	-	- 0.1395	- 0.0363	-
$\Delta\delta_{Hc}$ (ppm)	0.0858	- 0.0922	-	- 0.0452
$\Delta\delta_{O\text{-}CH3}$ (ppm)	- 0.0607	- 0.0498	- 0.0547	-
$\Delta\delta$-$_{COCH3}$ (ppm)	-	-	- 0.0595	- 0.0348

The mode and extent of inclusion (as previously described) are factors which contribute to the strength of the host-guest association and therefore the value of the association constant. The stability ranking for the complexes (where stability refers to the degree of association between the host and guest molecules at equilibrium) based on the association constants is β-CD·4H3M > β-CD·2H4M > β-CD·2H5M > β-CD·2H6M.

Due to the low degree of association between the guests and γ-CD, the experimental method was modified to obtain more reliable association constant data. In the equation above, the maximum ratio of [H]/[G] is 9 and [H] + [G] = [M] = constant. However, the data obtained in these experiments referred to a ratio [H]/[G] >> 10 and the equation was modified accordingly. Where [M] was used previously, it is replaced explicitly with $[H]_t + [G]_t \neq$ constant. Only the guest proton CIS values were used. The program ConstEQV was used to evaluate the association constant and is a modified version of ConstEQ.[25] The

protons studied and resulting K values are listed in Table 6.8, together with the correlation coefficients (R), the error loss function (E) and the calculated CIS (Δδ).

Table 6.8: The association constant results for each complex formed with γ-CD

	γ-CD·2H6M	**γ-CD·4H3M**
Protons studied	H_a, H_c	H_a, H_b, H_c, O-CH_3
Association constant, K	65.6 M^{-1}	124.7 M^{-1}
Correlation coefficient, R	0.9989	0.9989
Error loss function, E	2.51 x 10^{-5}	3.31 X 10^{-4}
$\Delta\delta_{Ha}$ (ppm)	0.0523	0.1243
$\Delta\delta_{Hb}$ (ppm)	-	0.2268
$\Delta\delta_{Hc}$ (ppm)	-0.0448	0.0724
$\Delta\delta_{O\text{-}CH3}$ (ppm)	-	0.0643
$\Delta\delta$-$_{COCH3}$ (ppm)	-	-

The association constant values are generally very low, indicating a weak association between the host and each guest in solution. The stability ranking for the complexes based on the association constants is γ-CD·4H3M > γ-CD·2H6M.

Discussion

While it is possible for more than one mode of guest inclusion to exist in solution as well as for stoichiometric ratios to be greater than 1:1 simultaneously, the results clearly show a 1:1 host:guest ratio in solution for all inclusion complexes formed. These modes of inclusion may be directly or indirectly attributed to the hydrophobicity of the guest molecules as this is a primary driving force of CD inclusion.[26] In most cases it is clear that the guest is deeply included in the CD cavity as indicated by observed changes in chemical shift of the host H_3 and H_5 protons, while still only weakly interacting with this part of the CD as suggested by the very low CIS values (order of magnitude 10^{-2} - 10^{-3} ppm) and the low association constant values obtained.

A study was performed by Sun *et al*.[27] to determine the stoichiometry and association constants of the complexes formed in solution for each of the guests 2H4M, 2H5M and 4H3M interacting with β- and γ-CD, respectively. The method employed by Sun *et al*. was isothermal titration calorimetry (ITC). ITC measures the changes in enthalpy of a sample due to the non-covalent interaction occurring between two molecules in solution. The data obtained are used to determine stability constants, the enthalpy of the interaction, entropy and Gibbs free energy.[28] This method makes use of different approximations in the calculations compared to the method used in this project, which may lead to large differences in results. Sun *et al*. found that the β-CD·2H4M and β-CD·4H3M complexes had 1:1 stoichiometry in solution while 2H5M appeared to form two distinct complexes with β-CD in solution, namely a 1:1 host-guest complex as well as a 2:1 host-guest complex. From the data obtained in this project, only

complexes with 1:1 host-guest stoichiometry were detected. For complexes formed with γ-CD only 1:1 stoichiometries were observed in both studies.

Recently, a publication by Fielding *et al.*[29] described the NMR and ITC investigation of the interaction between a number of hydroxymethoxyacetophenone isomers and β-CD. By constructing a titration curve and fitting the data to a computer model (assuming 1:1 stoichiometry), association constants were obtained using ^{1}H NMR spectroscopy. ITC experiments were carried out to complement the study.

The association constants reported by Sun *et al*. and Fielding *et al*. for complexes formed with β-CD are listed in Table 6.9 below.

Table 6.9: Association constants for β-CD complexes formed in solution

Guest	Complex ratio (H:G)	K (M^{-1})	K (M^{-1})[a]	K (M^{-1})[b]	K (M^{-1})[c]
2H4M	1:1	224	3.33×10^{3}	310	230
2H5M	1:1	154	661.8	190	130
	2:1	-	4.06×10^{6}	-	-
2H6M	1:1	145	-	100	90
4H3M	1:1	336	937.7	110	120

[a]Sun *et al*. ITC results; [b]Fielding *et al*. NMR results; [c]Fielding *et al*. ITC results

In this study the stability ranking for the complexes based on the association constants is β-CD·4H3M > β-CD·2H4M > β-CD·2H5M > β-CD·2H6M while the stability ranking obtained by Sun *et al*. was β-CD·2H4M > β-CD·4H3M > β-CD·2H5M and by Fielding *et al*. was β-CD·2H4M > β-CD·2H5M > β-CD·4H3M > β-CD·2H6M. There are discrepancies between the studies regarding which complex is the most stable. These discrepancies may be due to the different techniques that were used (ITC and ^{1}H NMR spectroscopy). The ^{1}H NMR method used by Fielding *et al*. required a very low concentration of host while the guest concentration was allowed to vary from 0 to 7 mM. All of the studies indicate that the least stable complex in solution is β-CD·2H6M.

The association constants found by Sun *et al*. for complexes formed with γ-CD are listed in Table 6.10 below, along with the values obtained in the present study.

Table 6.10: Association constants for γ-CD complexes formed in solution

Guest	Complex ratio (H:G)	K (M^{-1})	K (M^{-1})[d]
2H4M	1:1	-	94.4
2H5M	1:1	-	73.4
2H6M	1:1	65.6	-
4H3M	1:1	124.7	1.6×10^{4}

[d]Sun *et al*. ITC results

Comparing the results obtained by Sun *et al*. and those obtained in this study, the complex γ-CD·4H3M consistently has the largest association constant.

The results obtained in the present study are a reflection of the interaction of the guest molecule with the host. The interactions are based on the energy contributions of the enthalpic release of water from the cavity of the CD and entropy from the hydrophobic interactions which occur between the host and guest. Due to the fact that there is no relief of conformational strain on the CD in solution as a result of inclusion, the results for both the β-CD and γ-CD experiments are similar.[30] The trends observed for the association constants obtained in this study, as well as research by other groups on this work, support the hypothesis that in the case of small aromatic guest molecules, hydrophobicity is not the only driving force for the inclusion (or lack of inclusion) but the geometry and size of the guest molecule also play a large role.[31]

Comparison between the solid state and aqueous solution inclusion complexes

There are no obvious similarities in the inclusion complex formation process between the native CD host molecules studied and the hydroxymethoxyacetophenones. The host to guest ratios in each state were different, being 1:1, 1:2 and 2:1 in the solid state when the host was β-CD and a 1:1 ratio in solution. The apparent modes of inclusion of the guest within the host cavity differed and it cannot be confirmed that similar host-guest interactions exist in either state. It appears that the dynamic inclusion of the guest is a common feature, leading to multiple interactions between the guest hydrogen atoms with H_3 and H_5 of the host in solution and significant disorder of the guest molecule within the host cavity in the solid state. There is evidence that hydrophobic interactions play a significant role in the inclusion process in both the solid state and in solution.

INCLUSION COMPLEX FORMATION BETWEEN HYDROXYMETHOXYACETOPHENONE ISOMERS AND DERIVATISED CDs

Preparation of single crystals

Inclusion complex crystals were obtained by dissolving the host (0.1203 mmol) in cold distilled de-ionised water (5 mL) at low temperature (*ca* 4°C). Once the solution cleared, an equimolar amount of the guest was added to the solution and it was allowed to stir vigorously at the same low temperature overnight. The solution was filtered, sealed in a vial and placed either in an oven at 60 °C or an oil bath at 70 °C to crystallise. Although solutions were prepared for all four of the hydroxyacetophenone guest molecules with TRIMEA, TRIMEB and DIMEB, crystals of only five inclusion complexes were obtained. Table 6.11 presents masses and temperature conditions used.

Table 6.11: Masses and temperature conditions used to obtain complex crystals.

Host	Guest	M_{host} (mg)	M_{guest} (mg)	Oven temperature (°C)
TMB	2H4M	84	20	60
TMB	2H5M	84	20	70
TMB	4H3M	84	20	70
DMB	4H3M	80	20	60
TMA	2H5M	74	20	70

TRIMEB INCLUSION COMPLEXES WITH 2-HYDROXY-4-METHOXY ACETOPHENONE, 2-HYDROXY-5-METHOXY ACETOPHENONE AND 4-HYDROXY-3-METHOXY ACETOPHENONE (TMB·2H4M, TMB·2H5M AND TMB·4H3M)

Thermal Analysis

The TGA and DSC traces for the three TMB inclusion complexes are shown in Figure 6.23 (a), (b) and (c). The TGA traces of the three TMB complexes show a small mass loss over the range of 30 °C to 100 °C corresponding to water loss, which is also observed as small endotherms in the same temperature range in the DSC results. The percentage mass losses are 1.0 ± 0.2 for TMB·2H4M, 2.5 ± 0.9 for TMB·2H5M and 2.8 ± 0.1 for TMB·4H3M. The recorded water loss yielded the number of water molecules per CD molecule as 0.9 ± 0.2 for TMB·2H4M, 2.3 ± 0.8 for TMB·2H5M and 2.6 ± 0.1 for TMB·4H3M, respectively, per complex unit (n = 2 for each inclusion complex). A mass loss corresponding to the loss of the respective guest molecules is observed over the temperature range 100 °C to 280 °C. The percentage mass losses are 11.4 ± 2.2 for TMB·2H4M, 10.3 ± 0.7 for TMB·2H5M and 10.4 ± 0.1 for TMB·4H3M. The loss was calculated to be 1.1 ± 0.3 guest molecules for TMB·2H4M, 1.0 ± 0.1 for TMB·2H5M and 1.0 ± 0.1 for TMB·4H3M, respectively, per complex unit (n = 2 for each inclusion complex). The mass loss was soon followed by decomposition at *ca*. 300 °C. DSC analysis showed a sharp endotherm at 141 ˚C for TMB·2H4M, 163 ˚C for TMB·2H5M and 148 ˚C for TMB·4H3M representing fusion of the complex. The melting endotherms of each complex occur at the temperature at which the guest molecules are

released. The decomposition of the remaining residues appears to begin at 280 ˚C, 200 °C and 250 °C for the complexes TMB·2H4M, TMB·2H5M and TMB·4H3M, respectively.

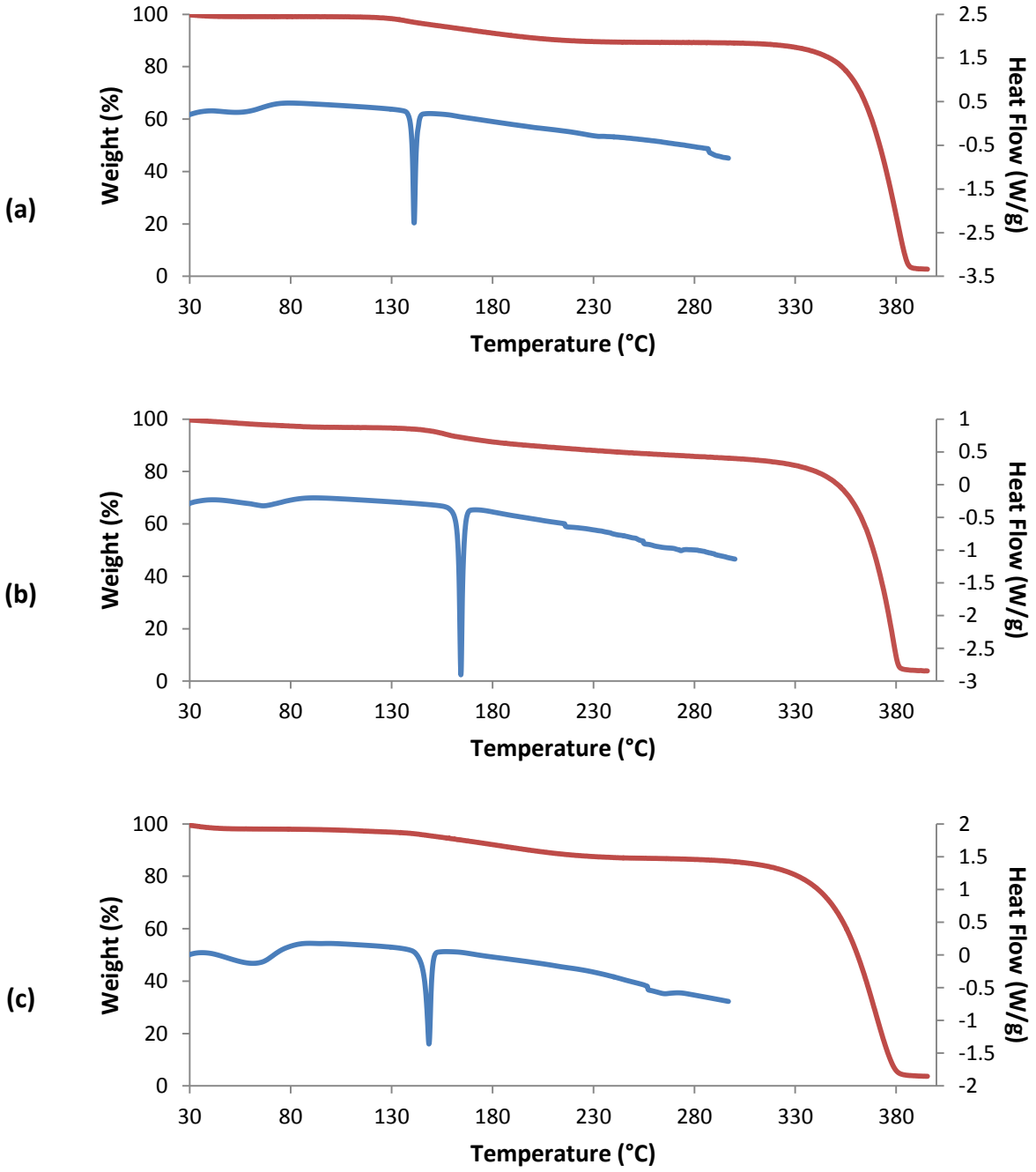

Figure 6.23: DSC (blue) and TGA (red) curves showing thermal events and decomposition of (a) TMB·2H4M, (b) TMB·2H5M and (c) TMB·4H3M

Photographs of the thermal behaviour of the crystals were taken using HSM. The HSM photographs are shown in Figure 6.24. TMB·2H4M began bubbling at 93 °C and started to melt at 137 °C. TMB·2H5M started bubbling at 78 °C and the crystal became opaque as it continued to release gas until melting occurred at 160 °C. The crystal of TMB·4H3M appeared to fracture as the heat increased although no bubbling occurred. The crystal began to melt at 153 °C.

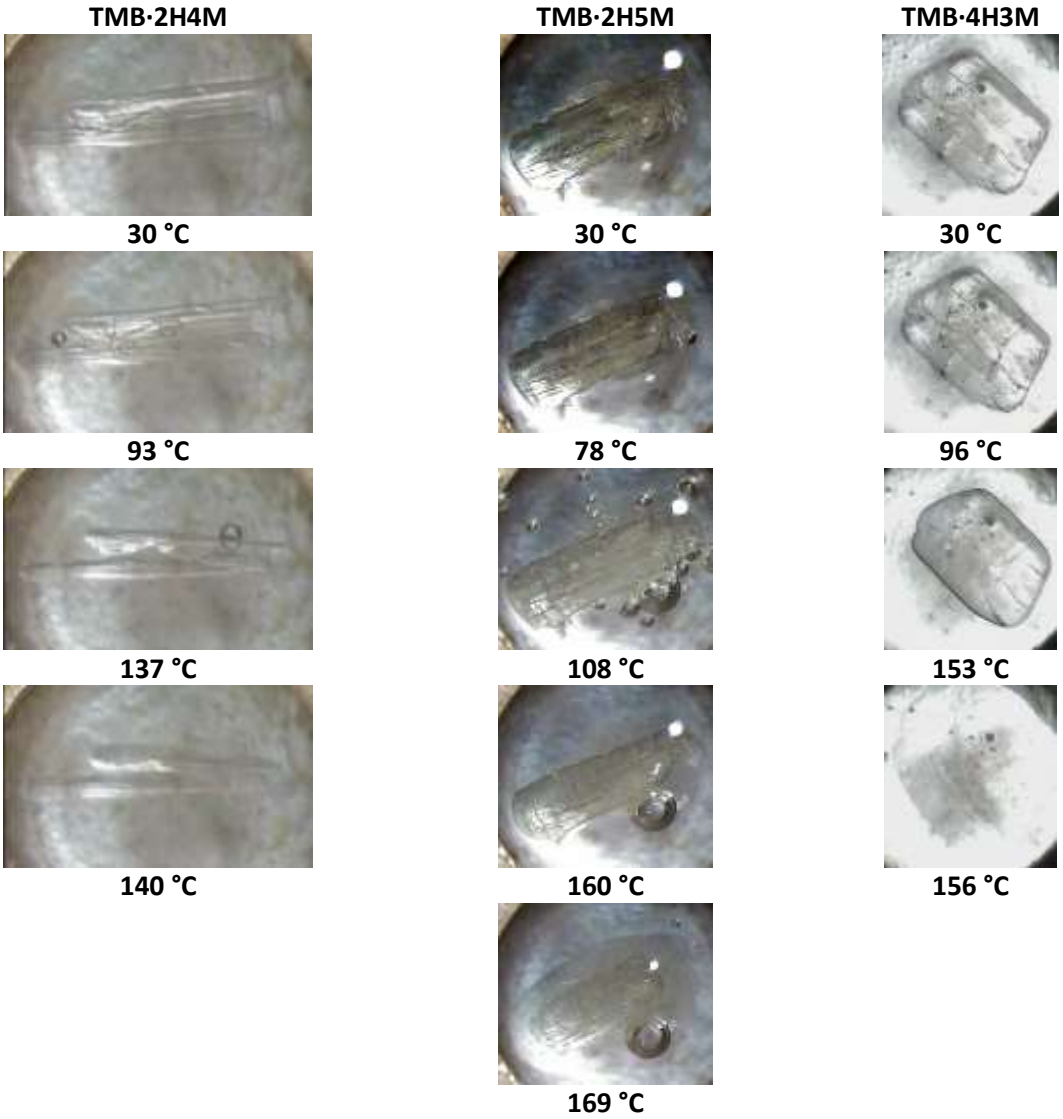

Figure 6.24: HSM photographs of the complexes TMB·2H4M, TMB·2H5M and TMB·4H3M

Single crystal X-ray analysis of the isostructural complexes TMB·2H4M and TMB·4H3M

Space group determination

The X-ray diffraction patterns from single crystals of both TMB·2H4M and TMB·4H3M were found to have Laue symmetry *mmm* by examining the intensity data as simulated precession photographs with the program LAYER[5], indicating an orthorhombic crystal system. Further inspection of the reciprocal lattices showed the reflection conditions for *hkl: none, h00: h = 2n, 0k0: k = 2n, 00l: l = 2n* indicating an $P2_12_12_1$ as the host molecules are chiral.

The crystallographic data and refinement parameters for each structure are listed in Table 6.12.

Table 6.12: Crystallographic data for the complexes TMB·2H4M and TMB·4H3M.

	TMB·2H4M	**TMB·4H3M**
Complex Formula	**$C_{63}H_{112}O_{35}·C_9H_{10}O_3·H_2O$**	**$C_{63}H_{112}O_{35}·C_9H_{10}O_3·2.6H_2O$**
Formula weight	1613.72	1642.53
Crystal system	Orthorhombic	Orthorhombic
Space group	$P2_12_12_1$ (No.19)	$P2_12_12_1$ (No.19)
a / Å	10.862(1)	10.869(2)
b / Å	25.610(3)	26.052(6)
c / Å	30.210(3)	29.526(6)
Volume / $Å^3$	8404(2)	8361(3)
Z	4	4
Calculated density / g cm^{-3}	1.275	1.302
μ (MoKα) / mm^{-1}	0.103	0.107
F (000)	3472	3521
Temperature / K	173(2)	173(2)
Crystal size / mm^3	0.32 x 0.16 x 0.02	0.42 x 0.40 x 0.18
Theta ranges scanned / °	$1.3 \leq \theta \leq 27.2$	$2.1 \leq \theta \leq 25.9$
Index ranges	h: -10, 13; k: -32, 32; l: -38, 30	h: -12, 13; k: -16, 31; l: -36, 33
Total number of reflections	47848	54628
No. of independent reflections	18653	16016
No. of reflections with $I > 2\sigma(I)$	14071	14774
No. of parameters	1040	1031
R_{int}	0.029	0.033
S	1.014	1.115
R_1	0.0462	0.0830
No. of reflections omitted	19	0
wR_2	0.1158	0.2478
Weighting scheme	a = 0.0538, b = 2.0979	a = 0.1078, b = 23.4255
Δρ excursions / e $Å^{-3}$	-0.41, 0.40	-0.47, 0.63

Structure determination and refinement

TMB·2H4M was found to be isostructural with the complex TRIMEB·psoralen·H_2O (CSD refcode BIFGIH).[32] The coordinates of the non-hydrogen atoms of the host molecule skeleton were used to solve the TMB·2H4M structure by isomorphous replacement. Atoms O2, O3, O6, C7, C8 and C9 were deleted, as well as the water molecule, and reassigned after refinement showed the electron density peaks reappearing. Full-matrix least-squares methods were used to refine the starting model using SHELXH-97.[9] Initially all atoms were refined isotropically. Two electron density peaks were identified as not being part of the host or guest molecules and were assigned as water molecules. The water molecules were found to possess high U_{iso} values and the s.o.f. values were fixed to 0.5 for both O1W and O2W. Three host

atoms were disordered over two positions and were refined with partial site occupancy factors (s.o.f.s) of x and 1 – x respectively. The initial value of x was set to 0.5 and allowed to refine freely. This value converged for all disordered atoms as shown in Table 6.13.

Table 6.13: Site occupancy factors for disordered host atoms in TMB·2H4M

Atom x	x	Atom 1-x	1-x
O321/C821	0.53(1)	O322/C822	0.47
O231/C731	0.52(1)	O232/C732	0.48

TMB·4H3M was found to be isostructural with TMB·2H4M. The atomic coordinates of the non-hydrogen atoms of the host molecule skeleton of TMB·2H4M were used to solve the TMB·4H3M structure by isomorphous replacement. Full-matrix least-squares methods were used to refine the starting model using SHELXH-97 and all atoms were initially refined isotropically.[9] Three electron density peaks were identified as not being part of the host or guest molecules and were assigned as water molecules. The atoms were assigned s.o.f. values proportional to the height of their density peaks such that the total number of water molecules matched that of the TGA results (0.97 for OW1, 0.92 for OW2 and 0.71 for OW3). Three host atoms (C631/O631/C931) were found to be disordered over two positions, the final s.o.f. value was 0.73(2).

All non-hydrogen atoms were allowed to refine anisotropically except for the disordered atoms and all water molecules which refined isotropically. Hydrogen atoms were placed on the host in fixed geometric positions using a riding model and were refined isotropically with temperature factors set to 1.2 times that of the parent atoms. Methyl hydrogen atoms were placed using the AFIX 137 command (rotating group refinement strategy) with isotropic temperature factors set to 1.5 times that of the parent atoms. Hydrogen atoms were placed on the disordered methyl groups in the same manner except that the s.o.f.s were set to be the same as for the disordered parent atoms.

The methylglucose residues were named G1 – G7. Each carbon atom was labelled with a number 1-9 and the corresponding oxygen atom was labelled accordingly as shown in Figure 6.25. The guest molecules were labelled as shown in Figure 6.25. Disordered atoms were named by the residue on which the atom exists, the atom number and the number 1 for the major position or 2 for the minor position.

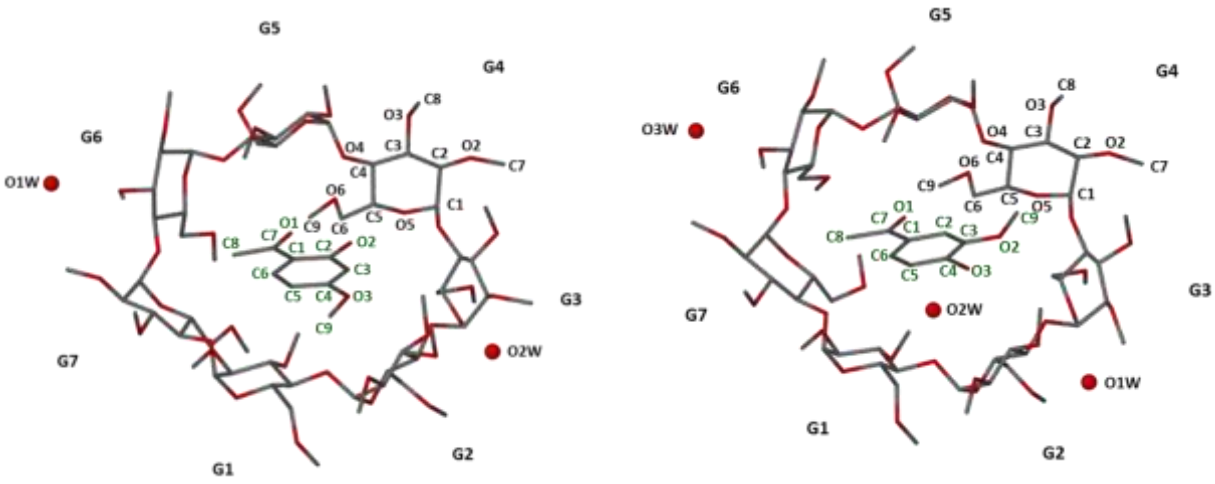

Figure 6.25: The TMB·2H4M (left) and TMB·4H3M (right) complexes viewed from the wider secondary face. The host numbering is shown in black and the guest numbering shown in green. Hydrogen atoms and disordered atoms are omitted for clarity.

The atoms of the guest molecules were assigned for each complex and no disorder was evident. The non-hydrogen guest atoms were refined anisotropically. Guest hydrogen atoms were placed using a riding model. The AFIX 137 command was used to assign methyl hydrogen atoms with isotropic temperature factors set to 1.5 times that of the parent atom. The phenyl hydrogen atoms were placed using the AFIX 43 commands with isotropic temperature factors set to 1.2 times that of the parent atom. The hydroxyl hydrogen atom was placed in an idealised hydrogen bond position using the AFIX 83 command.

The asymmetric unit of the TMB·2H4M complex consists of one TRIMEB molecule, one 2H4M molecule and one water molecules while the asymmetric unit of the TMB·4H3M complex consists of one TRIMEB molecule, one 4H3M molecule and 2.6 water molecules.

Geometrical Analysis

Host geometry

The geometrical parameters describing each macrocycle, which were discussed previously, are listed in Tables 6.14 and 6.15.

Table 6.14: Geometric parameters of the TRIMEB molecule in the complex TMB·2H4M.

Residue	*r* (Å)	*D* (Å)	*α* (°)	*φ* (°)	*d* (°)	D_3 (Å)	*α* (Å)	τ_1 (°)	τ_2 (°)
G1	4.677	4.472	132.7	116.6(2)	9.8	3.286	-0.425(2)	0.1(1)	6.0(1)
G2	5.353	4.209	122.4	117.5(3)	14.0	3.166	0.042(2)	10.3(1)	10.5(2)
G3	5.325	4.399	117.6	118.3(2)	-29.9	3.132	0.527(2)	25.2(1)	25.7(2)
G4	4.357	4.499	142.2	114.7(2)	4.9	3.560	-0.367(2)	40.2(1)	47.1(1)
G5	4.979	4.229	127.1	117.1(2)	21.6	3.782	-0.349(2)	13.8(1)	13.8(2)
G6	5.524	4.274	114.6	119.0(2)	-14.1	3.463	0.522(2)	25.6(1)	25.1(1)
G7	4.761	4.581	135.2	116.3(2)	-10.9	3.403	0.050(2)	35.0(1)	39.9(1)
Mean	**5.00**	**4.38**	**127.4**	**117.1**	**16.9**	**3.40**	**0.38**	**21.5**	**24.0**

Table 6.15: Geometric parameters of the TRIMEB molecule in the complex TMB·4H3M.

Residue	*r* (Å)	*D* (Å)	*α* (°)	*φ* (°)	*d* (°)	D_3 (Å)	*α* (Å)	τ_1 (°)	τ_2 (°)
G1	4.700	4.535	131.1	117.3(5)	10.5	3.271	-0.442(4)	0.6(2)	7.7(2)
G2	5.274	4.271	125.7	117.2(5)	14.1	3.224	0.004(4)	9.3(2)	10.5(4)
G3	5.471	4.385	112.8	117.5(5)	-30.5	3.357	0.535(4)	29.9(2)	29.4(4)
G4	4.302	4.547	144.8	114.3(5)	7.4	3.746	-0.355(4)	42.5(2)	50.8(2)
G5	4.949	4.134	127.6	117.1(5)	17.6	3.877	-0.339(4)	12.8(1)	13.3(3)
G6	5.526	4.325	115.1	118.7(5)	-6.7	3.283	0.439(4)	18.1(2)	18.8(2)
G7	4.773	4.502	135.3	116.6(5)	-16.8	3.586	0.158(4)	41.1(2)	44.1(2)
Mean	**5.00**	**4.39**	**127.5**	**117.0**	**16.6**	**3.48**	**0.37**	**22.0**	**24.9**

The macrocycle symmetry of the host TMB is described by *r*, *D* and *α*. The radii of TMB·2H4M and TMB·4H3M span similar ranges of 4.36 to 5.52 Å and 4.30 to 5.53 Å, respectively. The glycosidic distances are also very similar, ranging between 4.21 and 4.58 Å for TMB·2H4M and between 4.13 and 4.54 Å for TMB·4H3M. The glycosidic angles of TMB·2H4M and TMB·4H3M span larger ranges namely 114.6° to 142.2° and 112.8° to 144.8°. These values illustrate that the macrocycles are elliptical in shape.

The host O4-heptagon of both complexes has a saddle shape when viewed side-on as shown in Figure 6.26. The degree of the curvature is described by *d* and *α*. The torsion angles (*d*) for TMB·2H4M span the range -29.9° to 21.6° with a root mean square (rms) average of 16.9° while the TMB·4H3M torsion angles range from -30.5° to 17.6° with a rms of 16.6°.

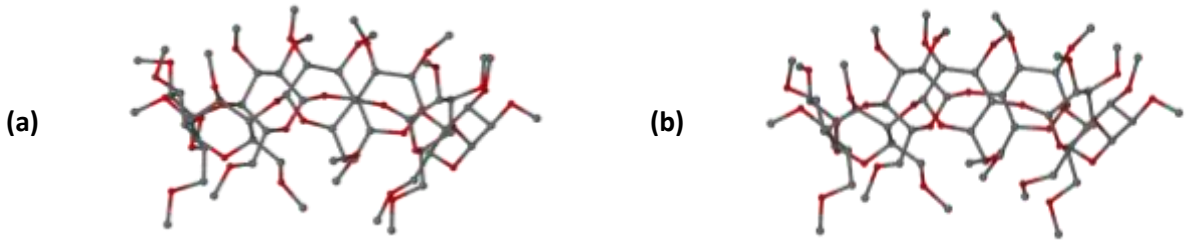

Figure 6.26: The TRIMEB molecule in (a) TMB·2H4M and (b) TMB·4H3M illustrating its saddle-like curvature. The minor components of the disordered atoms are not included in the figures. Hydrogen atoms and the minor components of disordered atoms were omitted for clarity.

The tilt angles (τ_1 and τ_2) are positive for each complex indicating that the methylglucose units are tilted towards the inside of the cavity such that the primary face is relatively "closed". The intersaccharidic

angles (φ) range between 114.7° and 119.0° for TMB·2H4M and between 114.3° and 118.7° for TMB·4H3M.

The torsion angles O5-C5-C6-O6 and C5-C6-O6-C9 describe the orientation of the C6-O6 and O6-C9 bonds which may be directed towards or away from the CD cavity. The complex TMB·2H4M has five bonds in the (-)-*gauche* orientation on residues G1, G2, G3, G4 and G5 and (+)-*gauche* on residues G6 and G7. All O6-C9 bonds are *trans* to the corresponding C5-C6 bonds, except in residue G5 where the bond lies *anticlinal*. The complex TMB·4H3M has four bonds in the (-)-*gauche* orientation on residues G1, G2, G4 and G5, (+)-*gauche* on residues G6 and G3 and (+)-*anticlinal* on residue G7. All O6-C9 bonds are *trans* to the corresponding C5-C6 bonds, except in residues G5 and G7 where the bonds lie *synclinal*.

Guest geometry

The guest geometry is best described by three torsion angles C2-C1-C7-O1, C6-C1-C7-C8 and C9-O3-C4-C5 in TMB·2H4M and C9-O2-C3-C2 in TMB·4H3M. These torsion angles are shown in Figure 6.27 for TMB·2H4M and in Figure 6.28 for TMB·4H3M. These torsion angles indicate that the guest molecules are nearly planar after inclusion into the CD cavity.

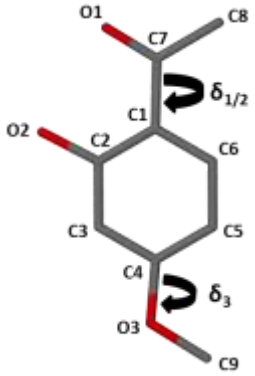

δ_1 C2-C1-C7-O1 = 5.0(6)°
δ_2 C6-C1-C7-C8 = 3.9(6)°
δ_3 C9-O3-C4-C5 = -7.4(6)°

Figure 6.27: Torsion angles δ_1, δ_2 and δ_3 of 2H4M

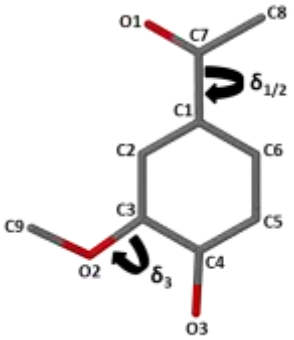

δ_1 C2-C1-C7-O1 = -1(1)°
δ_2 C6-C1-C7-C8 = -2(1)°
δ_3 C9-O2-C3-C2 = -12(1)°

Figure 6.28: Torsion angles δ_1, δ_2 and δ_3 of 4H3M

In the TMB·2H4M complex the guest molecule is embedded in the CD cavity with the O-methyl moiety pointing toward the primary rim and the acetyl and hydroxyl groups located close to the secondary rim of the CD. The angle between the plane through the phenyl ring and the mean O4 least-squares plane of the host molecule is 86.4(5)°. The guest molecule in the TMB·4H3M complex is positioned in the CD cavity such that the hydroxyl group is located close to the primary rim of the CD, with the acetyl moiety protruding from the secondary rim. The angle between the plane through the phenyl ring and the mean O4 least-squares plane is 78.7(5) °. Figures 6.29 to 6.32 show the CPK diagrams of the TMB·2H4M and TMB·4H3M complex structures illustrating the orientation of the guests within the host cavities and interactions between the host and guest molecules. The guest molecule is shown in different colours: carbon atoms are blue, oxygen atoms are green and hydrogen atoms are yellow.

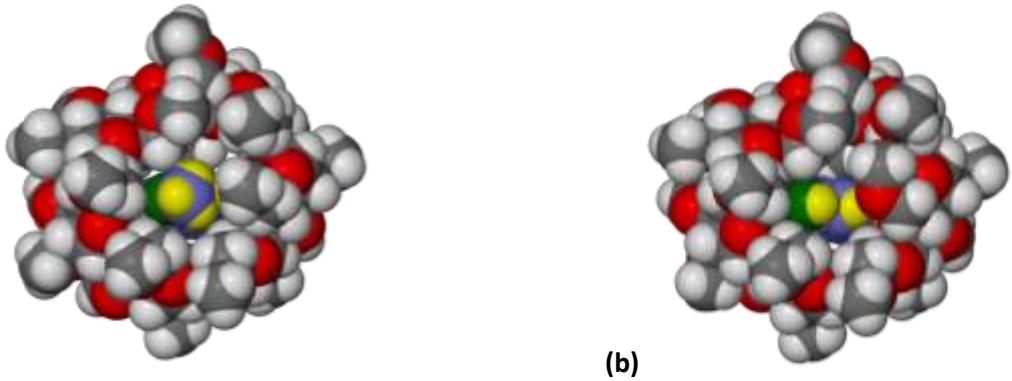

(a) (b)

Figure 6.29: Space-filling diagram of the TMB·2H4M (a) and TMB·4H3M (b) complex structures viewed from the primary rim

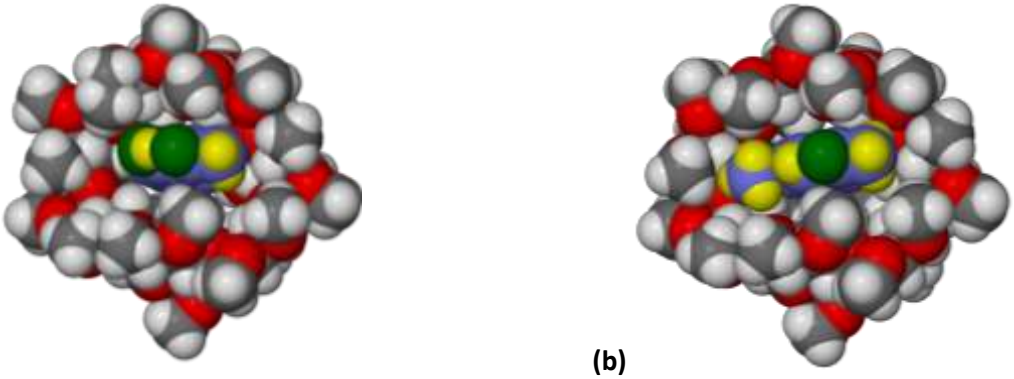

(a) (b)

Figure 6.30: Space-filling diagram of the TMB·2H4M (a) and TMB·4H3M (b) complex structures viewed from the secondary rim

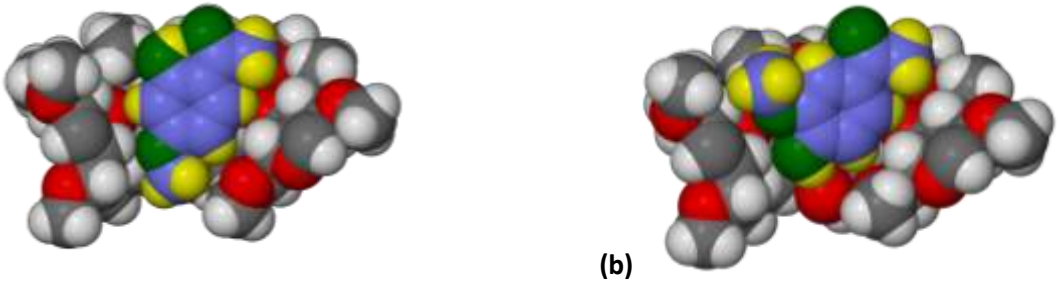

(a) (b)

Figure 6.31: Sectioned space-filling diagram of the TMB·2H4M (a) and TMB·4H3M (b) complex structures viewed from the side

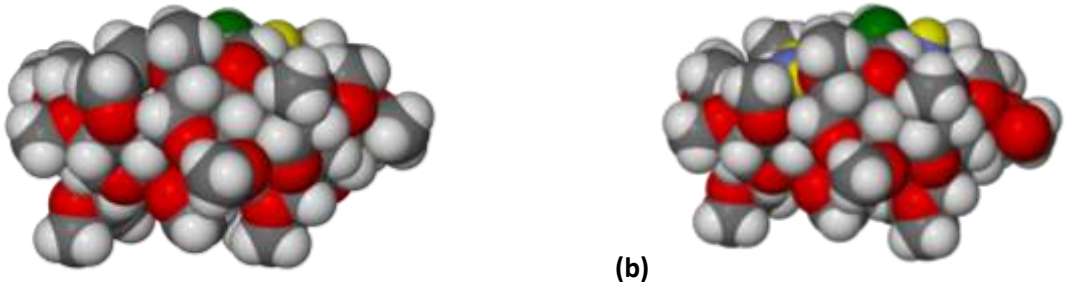

(a) (b)

Figure 6.32: Space-filling diagram of the TMB·2H4M (a) and TMB·4H3M (b) complex structures viewed from the side

Hydrogen bonding interactions

Host-guest intermolecular interactions and guest intramolecular interactions

The TMB·2H4M complex has only one host-guest hydrogen bond, namely C5G3-H5G3···O3, with a O···H distance of 2.60 Å, a C···O distance of 3.533(4) Å and a bond angle of 156°. This hydrogen bond weakly binds the guest molecule to the CD, in addition to other attractive forces such as van der Waals. One intramolecular guest hydrogen bond exists in TMB·2H4M**:** O2-H2···O1. The O···H bond distance is 1.85 Å, the O···O bond distance is 2.591(5) Å and the bond angle is 146°. The intramolecular hydrogen bond can be described by graph-set notation as $S_1^1(6)$[13] (Figure 6.33).

In the TMB·4H3M complex the guest molecule is bound to the CD by two C-H···O hydrogen bonds and one water mediated hydrogen bond (Table 6.16). The presence of water in the columns adds stronger O···O interactions, bridging the host and guest as well as two consecutive guest molecules. This is discussed further below. There are no guest intramolecular interactions (Figure 6.34).

Table 6.16: Intermolecular host-guest hydrogen bond distances and angles for TMB·4H3M.

D-H···A	D-H (Å)	H···A (Å)	D···A (Å)	D-H···A (°)
C5-H5···O4G7	0.95	2.58	3.510(10)	166
C6-H6···O6G7	0.95	2.58	3.311(8)	134
C5G4-H5G4···O2	1.00	2.52	3.502(10)	167

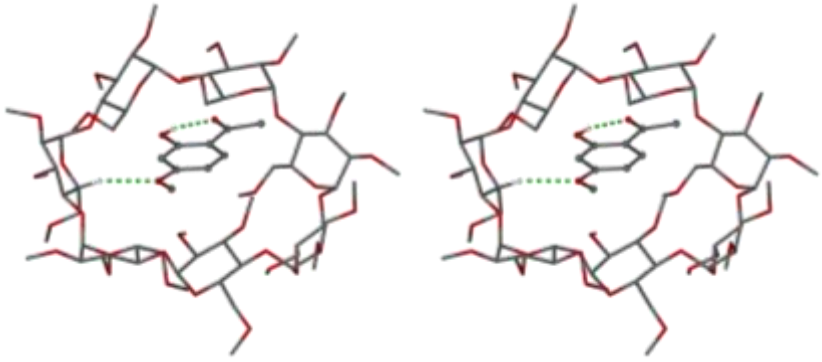

Figure 6.33: Stereoview of the intermolecular C-H··O bond between the host and guest, as well as the intramolecular hydrogen bond in the guest for the TMB·2H4M structure. Only hydrogen atoms involved in the hydrogen bonding are shown.

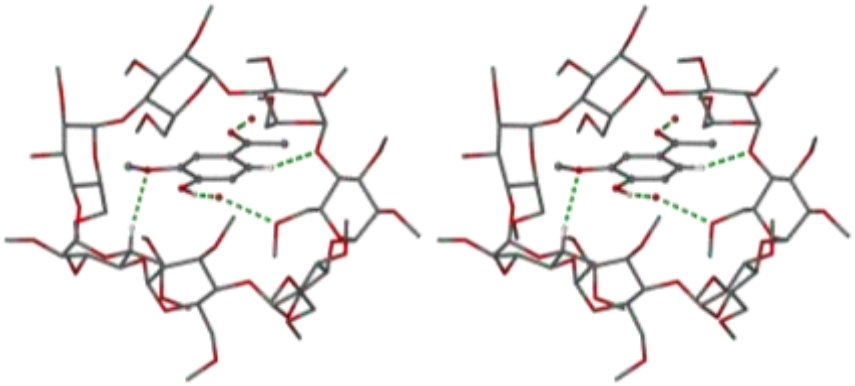

Figure 6.34: Stereoview of the intermolecular host-guest hydrogen bonds, as well as the water mediated host-guest interaction. Only hydrogen atoms involved in the hydrogen bonding are shown.

Host intermolecular interactions

The host intermolecular interactions in the structures of TMB·2H4M and TMB·4H3M are listed in Tables 6.17 and 6.18, respectively. They are relatively strong, occurring between host molecules making the crystal structure more rigid.

Table 6.17: Intermolecular host hydrogen bond distances and angles for TMB·2H4M

D-H···A	D-H (Å)	H···A (Å)	D···A (Å)	D-H···A (°)
C1G1-H1G1···O6G5[a]	1.00	2.54	3.446(4)	150
C2G1-H2G1···O5G6[a]	1.00	2.51	3.501(4)	170
C2G6-H2G6···O6G1[b]	1.00	2.44	3.340(4)	149
C7G6-H7GZ···O6G1[b]	0.98	2.58	3.357(4)	137

Symmetry operations: [a]1-x,-1/2+y,3/2-z; [b]1-x,1/2+y,3/2-z

Table 6.18: Intermolecular host hydrogen bond distances and angles for TMB·4H3M

D-H···A	D-H (Å)	H···A (Å)	D···A (Å)	D-H···A (°)
C2G6-H2G6···O6G1[c]	1.00	2.47	3.384(9)	151
C6G7-H6GB···O3G3[d]	0.99	2.50	3.400(10)	151
C1G1-H1G1···O6G5[e]	1.00	2.55	3.357(8)	137

Symmetry operations: [c]1-x,1/2+y,3/2-z; [d]1/2-x,1-y,1/2+z; [e]1-x,-1/2+y,3/2-z

Water-water, water-host and water-guest interactions

The hydrogen bonds involving water interactions in the TMB·2H4M structure are listed in Table 6.19. Three occur between host C-H donors and water O acceptors. The remaining four are considered to be close contacts as the hydrogen atoms of the water molecules could not be modelled and no specific hydrogen bonds could be identified. However, based on the distances between the water O atoms (as donors) and host or other water O atoms (as acceptors), potential intermolecular interactions can be identified.

Table 6.19: Various water intermolecular interactions in TMB·2H4M

D···A	H···A (Å)	D···A (Å)	D-H···A (°)
O1W-H1W2···O2W[f]	2.15	2.926(3)	153
O1W-H1W1···O6G2[f]	2.05	2.900(6)	171
O1W···O321	2.05	2.853(5)	157
O2W-H2W1···O3G6[g]	1.95	2.741(6)	145
C1G2-H1G2···O2W	2.40	3.131(7)	130
C822···O1W[f]	2.52	2.452(11)	119

Symmetry operations: [f]1/2+x,1/2-y,1-z; [g]1-x,-1/2+y,3/2-z

The hydrogen bonds involving water interactions in the 4H3M·TMB structure are listed in Table 6.20. Similarly to TMB·2H4M, close contacts can be identified between water O atoms and acceptor O atoms of nearby molecules.

Table 6.20: Various water intermolecular interactions in TMB·4H3M

D···A	H···A (Å)	D···A (Å)	D-H···A (°)
O1W···O3W[h]	-	2.897(5)	-
O2W···O1[i]	-	2.823(5)	-
O3-H3···O2W	1.84	2.655(8)	163
O1W···O3G6	-	2.874(8)	-
O3W-H19···O3G2	1.99	2.829(9)	177
O3W-H4···O6G2[j]	2.11	2.930(9)	165
O2W ···O6G7	-	2.798(9)	-
C1G2-H1G2···O1W	2.39	3.188(11)	136
C7G3-H7G8···O3W	2.59	3.219(11)	123

Symmetry operations: [h]1/2+x,1/2-y,1-z; [i]1-x,y,z; [j]3/2-x,1-y,-1/2+z

The water molecules have two different functions in the crystal structures. In TMB·2H4M the two water molecules exist in the interstitial spaces between the complex units and interact with each other as well as with oxygen atoms and carbon atoms on the surrounding host molecules (Figure 6.35).

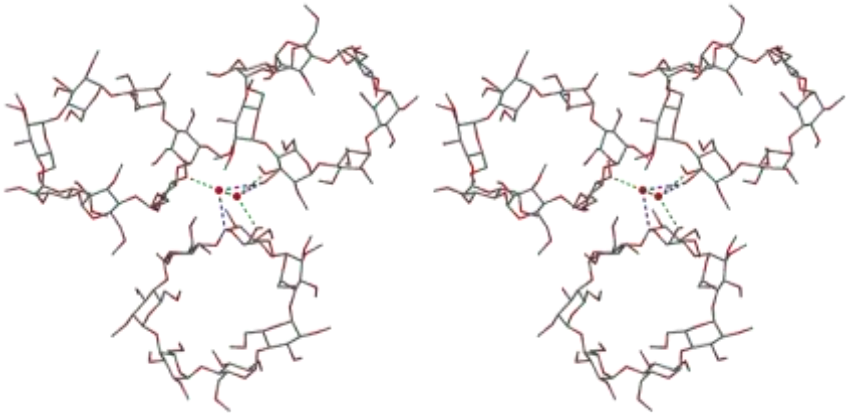

Figure 6.35: The intermolecular hydrogen bonds and close contacts which link the hosts and water molecules in TMB·2H4M. O···O close contacts are shown in green while the C-H···O hydrogen bonds are shown in cyan. Hydrogen atoms are omitted for clarity.

Two of the water molecules in TMB·4H3M serve the same purpose as those in TMB·2H4M (Figure 6.36a). However, TMB·4H3M has an additional disordered water molecule (O2W1/O2W2) situated at the primary end of the host molecule which stabilises the inclusion complex by forming a bridging hydrogen bond between O3-H3 of the guest molecule and O6G7 of the host. It also forms hydrogen bonds with two consecutive guest molecules, adding stability to the columns in the complex (Figure 6.36b). While the methoxyl group 'plugs' the primary end of the CD in TMB·2H4M**,** a water molecule fulfils this role in TMB·4H3M.

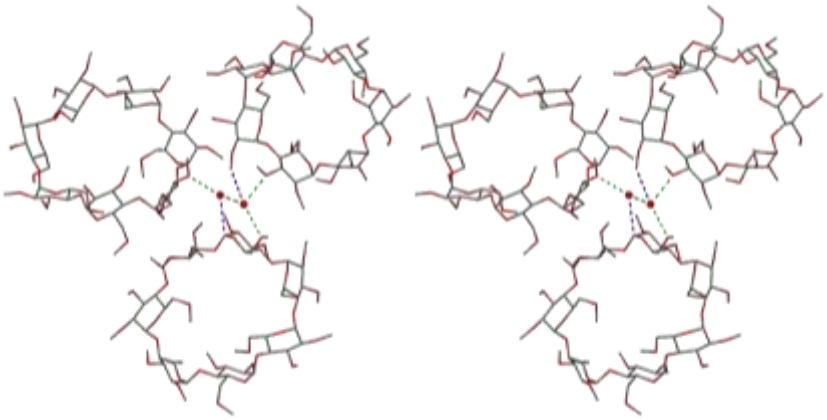

Figure 6.36a: The intermolecular hydrogen bonds and close contacts which link the hosts and water molecules in TMB·4H3M. O···O close contacts are shown in green while the C-H···O hydrogen bonds are shown in cyan. Hydrogen atoms are omitted for clarity.

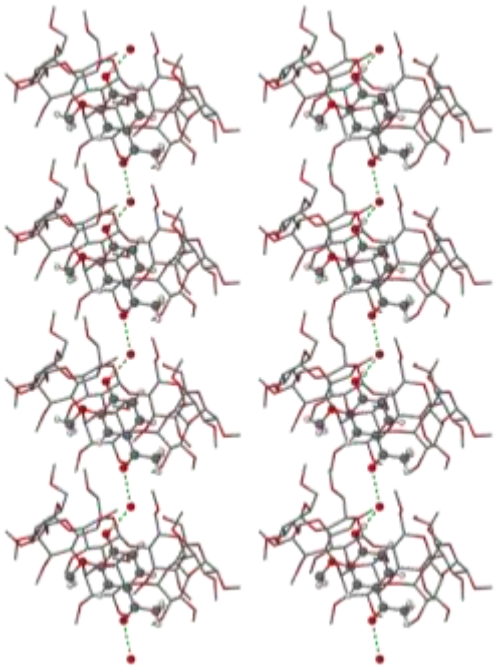

Figure 6.36b: The stereodiagram shows the O···O close contacts and O-H···O hydrogen bonds linking consecutive guest molecules in the CD columns along the *a*-axis. Only hydrogen atoms involved in hydrogen bonding are shown.

Weak host intramolecular close contacts

Both structures contain weak intramolecular close contacts of the form C-H···O, tabulated in Appendix E. These close contacts have reasonable hydrogen bond distances between donors and acceptors but typically less than ideal bond angles (100.0° ≤ D-H···A ≤ 120.0°). While these contacts may seem insignificant when considered individually, the cumulative effect of several such interactions does contribute to the shape of the macrocycle.[33]

Crystal packing

Both TMB·2H4M and TMB·4H3M complexes pack in infinite columns along the *a*-axis with the complex units stacked head-to-tail. Figures 6.37a and 6.38a for TMB·2H4M and TMB·4H3M, respectively, show the infinite columns viewed down the *a*-axis. Figures 6.37b and 6.38b show stereodiagrams illustrating how the columns form layers in the *a*-*c* plane. The columns of the CD molecules in TMB·2H4M form undulating channels while the CDs of TMB·4H3M pack in a cage-type packing arrangement.

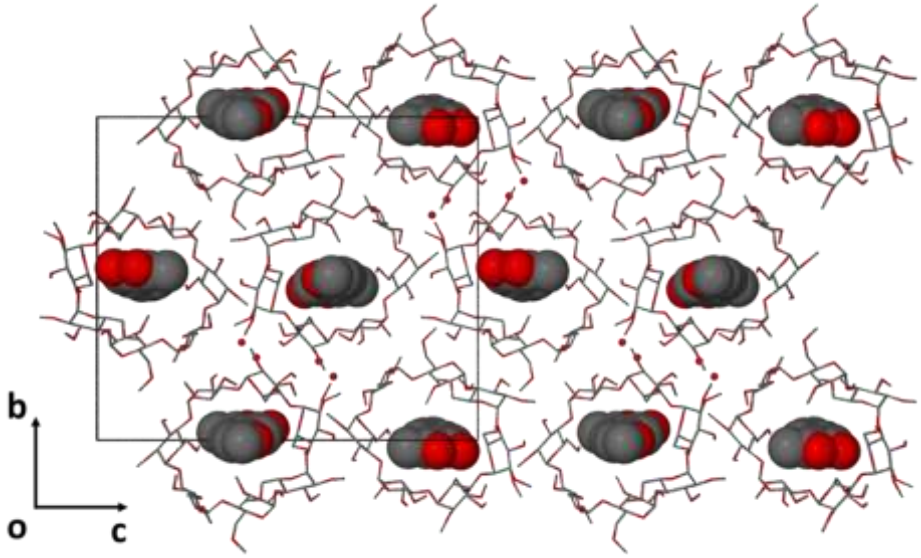

Figure 6.37a: Packing diagram of the TMB·2H4M structure projected down the *a*-axis. The guest molecule is shown in space-filling representation, water oxygen atoms are shown as dots and the host molecules as stick diagrams. Hydrogen atoms omitted for clarity.

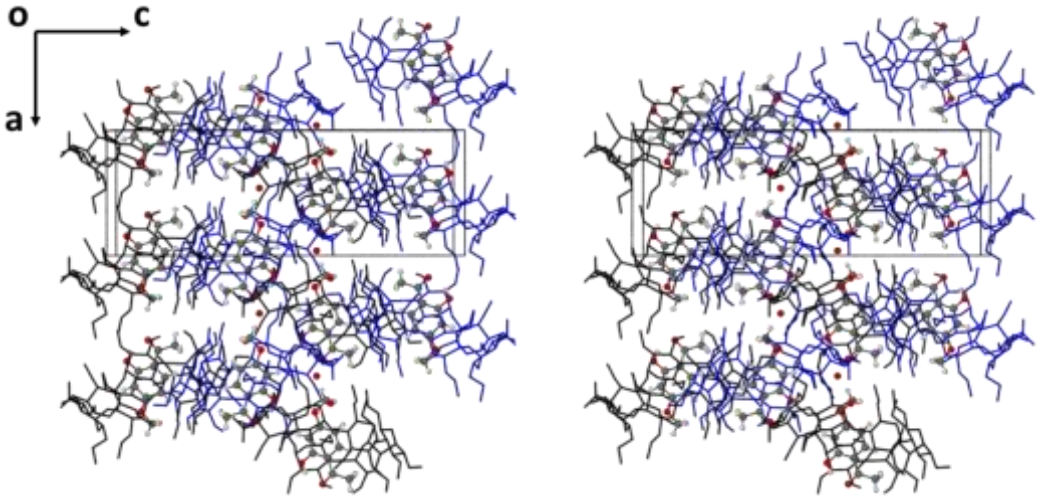

Figure 6.37b: A stereodiagram of the packing arrangement in TMB·2H4M viewed down the *b*-axis. The host molecules are shown as stick diagrams, with the layer in the foreground shown in blue and the layer in the background shown in black. The guest molecules and water oxygen atoms are depicted in a ball-and-stick fashion. Hydrogen atoms are omitted for clarity.

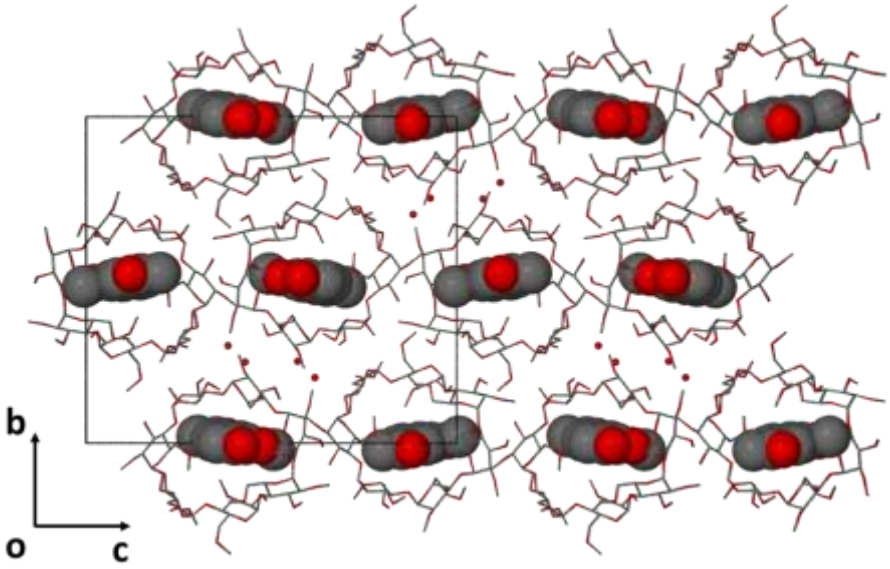

Figure 6.38a: Packing diagram of the TMB·4H3M structure projected down the *a*-axis. The guest molecule is shown in space-filling style, water oxygen atoms are shown as filled circles and the host molecules as stick diagrams. Hydrogen atoms are omitted for clarity.

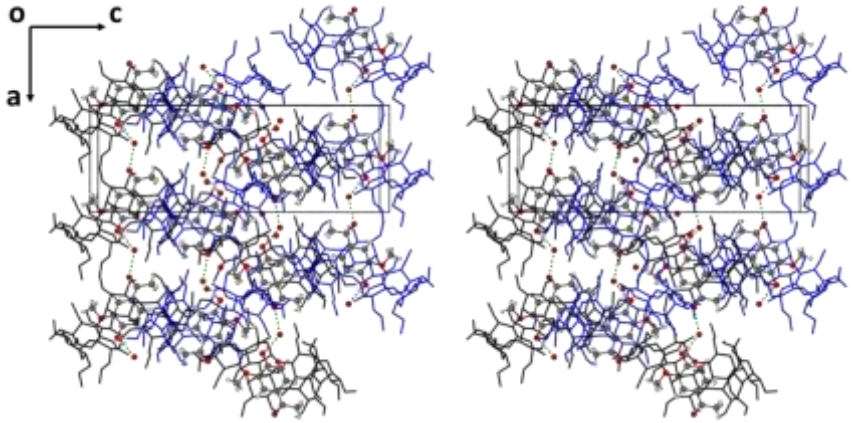

Figure 6.38b: A stereodiagram of the packing arrangement in TMB·4H3M viewed down the *b*-axis. The host molecules are shown as stick diagrams, with the layer in the foreground shown in blue and the layer in the background shown in black. The guest molecules and water oxygen atoms are depicted in a ball-and-stick fashion. Hydrogen atoms are omitted for clarity.

Comparative PXRD analysis

PXRD was used to determine the homogeneity of the crystalline products TMB·2H4M and TMB·4H3M. Figures 6.39 and 6.40 show the experimental PXRD patterns of the complexes as well as the patterns calculated from the crystal structure. In both cases the experimental patterns match the calculated patterns indicating that the sample used for single crystal X-ray diffraction is representative of the bulk material.

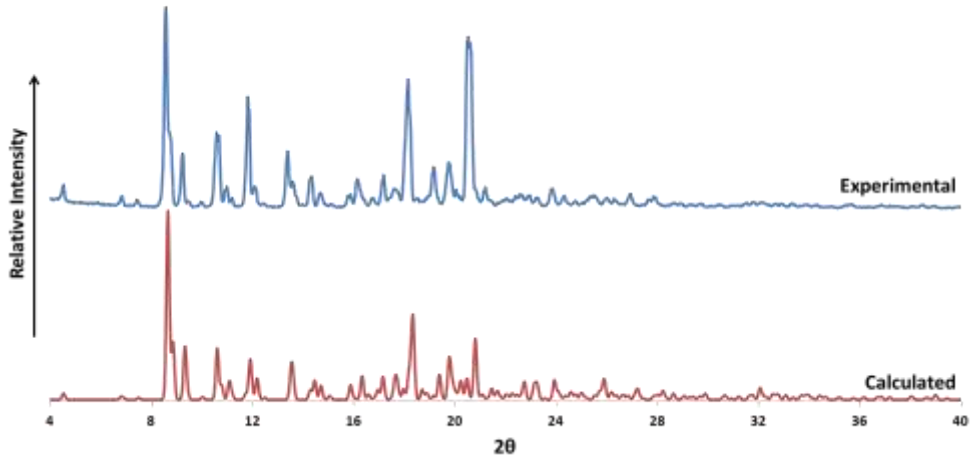

Figure 6.39: The PXRD trace of the experimental product and the pattern calculated from the single crystal X-ray structure of TMB·2H4M.

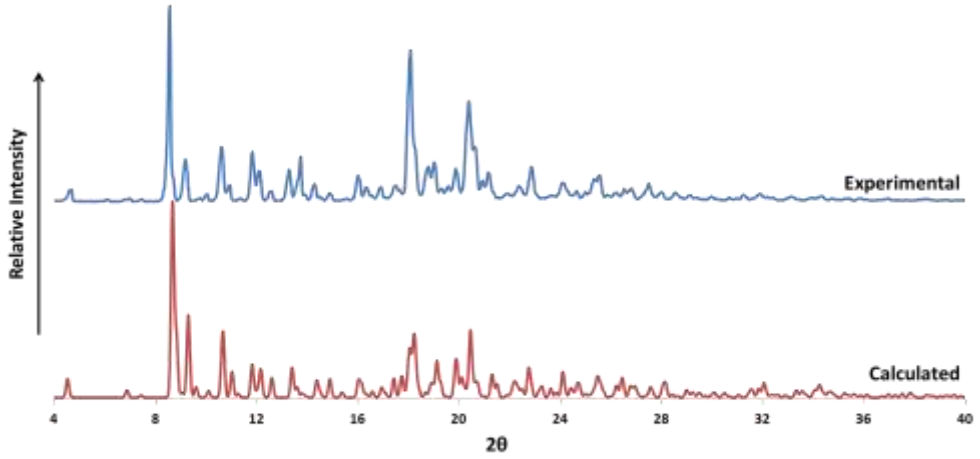

Figure 6.40: The PXRD trace of the experimental product and the pattern calculated from the single crystal X-ray structure of TMB·4H3M.

Single crystal X-ray analysis of the complex TMB·2H5M

Space group determination

The Laue symmetry of the diffraction pattern of TMB·2H5M was found to be $\bar{1}$ by examining the intensity data as simulated precession photographs with the program LAYER.[5] This indicated that the complex crystallizes in the triclinic system (space group possibilities P1 and P $\bar{1}$). Since the host molecule is chiral, the space group P1 was assigned and single crystal X-ray intensity data were collected accordingly. The crystallographic data and refinement parameters for the crystal are listed in Table 6.21.

Table 6.21: Crystallographic data for the complex TMB·2H5M.

Complex Formula	**$C_{63}H_{112}O_{35}\cdot C_9H_{10}O_3\cdot 2.05H_2O$**
Formula weight	1632.62
Crystal system	Triclinic
Space group	P1 (No.1)
a / Å	10.687(1)
b / Å	14.569(2)
c / Å	27.670(3)
α / °	89.980(2)
β / °	81.178(2)
γ / °	86.213(2)
Volume / $Å^3$	4248(1)
Z	2
Calculated density / g cm^{-3}	1.273
μ (MoKα) / mm^{-1}	0.104
F (000)	1749
Temperature / K	173(2)
Crystal size / mm^3	0.36 x 0.31 x 0.21
Theta ranges scanned / °	$2.0 \leq \theta \leq 26.5$
Index ranges	h: -13, 13; k: -18, 18; l: -34, 34
Total number of reflections	40891
No. of independent reflections	30765
No. of reflections with $I > 2\sigma(I)$	27201
No. of parameters	2066
R_{int}	0.033
S	1.044
R_1	0.0555
No. of reflections omitted	30
wR_2	0.1536
Weighting scheme	a = 0.0695, b = 2.9909
Δρ excursions / e $Å^{-3}$	-0.41, 0.76

Structure determination and refinement

TMB·2H5M was not found to be isostructural with any TRIMEB inclusion complex and the unit cell and space group data indicated the presence of two inclusion complex units in the asymmetric unit. Therefore the structure was solved using the program SHELXD, which uses Patterson and direct methods to orientate and position fragments of known geometry.[9] A final CC of 86.47 was obtained after a few minutes. The resulting solution revealed most of the non-hydrogen atoms of the host and guest molecules as well as atoms which were identified as water oxygen atoms, as they were not attached to

either the host or the guest molecule. The electron density peaks which appeared on the difference Fourier map after full-matrix least-squares refinement using SHELXH-97 were assigned such that the parameters describing the host and guest molecules converged within a few refinement cycles.[9] Three fully occupied water molecules were identified, one of which was later found to be disordered over two positions. Two further water oxygen atoms were identified but they were found to be unstable after refinement, having a high U_{iso} value when the s.o.f. was unity. It was therefore assigned a U_{iso} value equal to the average U_{iso} values of the other four water O atoms and the s.o.f. was allowed to refine freely. The s.o.f.s were 0.80 for O2W and 0.30 for O5W after numerous refinement cycles. Initially all atoms were refined isotropically.

A number of host atoms were found to be disordered over two positions and were refined with partial s.o.f.s of x and 1 – x respectively. The initial value of x was set to 0.5 and allowed to refine freely. This value converged for all disordered atoms as shown in Table 6.22.

Table 6.22: Site occupancy factors for disordered host atoms and water oxygen atoms for TMB·2H5M

Residue	Atom x	x	Atom 1-x	1-x
A	C671/O671/C971	0.82(1)	C672/O672/C972	0.18
A	O351/C851	0.64(2)	O352/C852	0.36
A	C751	0.63(2)	C752	0.37
B	C721	0.61(2)	C722	0.39

All non-hydrogen atoms were allowed to refine anisotropically except for the water molecules as well as disordered host atoms, which refined isotropically. Hydrogen atoms were placed on the host in fixed geometric positions using a riding model and were refined isotropically with temperature factors set to 1.2 times that of the parent atoms. Methyl hydrogen atoms were placed using the AFIX 137 command (rotating group refinement strategy) with isotropic temperature factors set to 1.5 times that of the parent atoms. Hydrogen atoms were placed on the disordered methyl groups in the same manner except that the s.o.f. s were set to be the same as for the disordered parent atoms.

The methylglucose residues were named A1 – A7 for one crystallographically independent host molecule and B1 - B7 for the other. Each host carbon atom was labelled with a number 1-9 and the corresponding oxygen atom was labelled accordingly, as shown in Figure 6.41 (a). The guest molecules were labelled as shown in Figure 6.41 (b), corresponding to its host molecule A or B. Disordered atoms were named by the residue on which the atom exists, the atom number and the number 1 for the major position or 2 for the minor position. Water molecules were labelled with a number and the letter “W”.

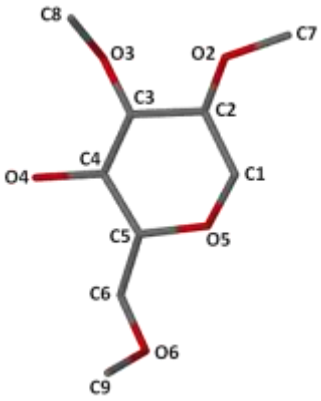

(a)

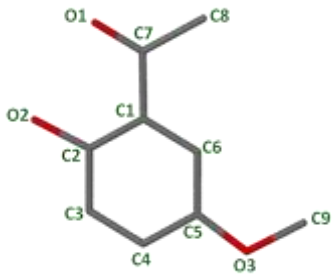

(b)

Figure 6.41: Labelling of residues on the host molecules (a) and a representative guest molecule showing the labelling (b). Hydrogen atoms and disordered atoms are omitted for clarity.

The atoms of the guest molecules were assigned for each complex and no disorder was observed. The non-hydrogen guest atoms were refined anisotropically. Guest hydrogen atoms were placed using a riding model. The AFIX 137 command was used to assign methyl hydrogen atoms with isotropic temperature factors set to 1.5 times that of the parent atom. The phenyl hydrogen atoms were placed using the AFIX 43 commands with isotropic temperature factors set to 1.2 times that of the parent atom. The hydroxyl hydrogen atoms were placed in an idealised hydrogen bond position using the AFIX 83 command.

The asymmetric unit of the TMB·2H5M complex consists of two TRIMEB molecules, two 2H5M molecules and 4.1 water molecules.

Geometrical Analysis

Host geometry

Table 6.23 (a and b) shows the values of the properties which describe the macrocycle symmetry: the radii (r), the glycosidic distance (*D*), the angle (*α*), the torsion angle (*d*), the O2(n)-O3(n-1) distances (D_3) and the root mean square of the deviation of the O4 atoms from the least-squares O4 plane (*α*), the tilt angle (*τ*) and the intersaccharidic angles (*φ*).

Table 6.23a: The geometric parameters describing the macrocycle A.

Residue	*r* (Å)	*D* (Å)	*α* (°)	*φ* (°)	*d* (°)	D_3 (Å)	*α* (Å)	τ_1 (°)	τ_2 (°)
A1	4.665	4.434	132.3	117.4(3)	16.30	3.383	-0.421(2)	7.0(1)	8.6(1)
A2	5.334	4.182	122.5	118.7(3)	5.30	3.144	0.244(2)	11.5(1)	12.0(2)
A3	5.311	4.388	117.7	118.2(3)	-31.41	3.048	0.395(2)	21.4(1)	23.1(2)
A4	4.299	4.507	143.0	113.6(3)	15.74	3.521	-0.484(3)	32.8(1)	39.3(2)
A5	5.029	4.236	125.3	117.8(3)	17.43	3.693	-0.175(2)	14.4(1)	17.6(2)
A6	5.489	4.228	115.3	117.9(3)	-19.58	3.783	0.558(2)	38.8(1)	37.7(1)
A7	4.719	4.584	135.5	115.1(4)	-6.10	3.403	-0.116(2)	30.2(1)	33.9(1)
Mean	**4.98**	**4.37**	**127.4**	**116.9**	**17.93**	**3.42**	**0.37**	**22.3**	**24.7**

Table 6.23b: The geometric parameters describing the macrocycle B

Residue	*r* (Å)	*D* (Å)	*α* (°)	*φ* (°)	*d* (°)	D_3 (Å)	*α* (Å)	τ_1 (°)	τ_2 (°)
B1	4.234	4.448	142.8	112.9(3)	20.70	3.435	0.615(2)	32.0(1)	41.5(2)
B2	5.128	4.251	121.4	118.4(3)	21.42	3.776	0.250(2)	15.4(1)	18.6(2)
B3	5.404	4.227	117.1	117.4(3)	-22.55	4.001	-0.694(2)	45.9(1)	44.6(1)
B4	4.697	4.580	134.7	116.2(3)	-10.18	3.371	0.079(2)	30.9(1)	37.4(1)
B5	4.673	4.494	131.8	117.1(3)	18.13	3.385	0.550(2)	6.8(1)	9.2(1)
B6	5.397	4.137	120.7	117.5(3)	10.63	3.290	-0.237(2)	13.4(1)	14.5(2)
B7	5.255	4.504	117.6	118.4(4)	-43.35	3.339	-0.562(2)	33.0(1)	33.2(2)
Mean	**4.97**	**4.38**	**126.6**	**116.7**	**23.32**	**3.52**	**0.48**	**25.3**	**28.4**

The macrocycles are elliptical in shape as the radii of A and B are in the ranges 4.30 - 5.49 Å and 4.23 - 5.40 Å, respectively. The glycosidic distances range between 4.18 and 4.58 Å for A and between 4.14 and 4.58 Å for B. The glycosidic angles of A and B span larger ranges, namely 115.3° - 143.0° and 117.1° – 142.8° respectively.

The saddle shapes of both O4-heptagons are illustrated in Figure 6.42. The degree of the curvature is described by the torsion angle (*d*) (-31.4° to 17.4° for A and -43.3° to 21.4° for B) and the deviation of the O4 atoms from the least-squares O4-plane (*α*). All of the O4 atoms of A deviate significantly from the least-squares O4 plane.

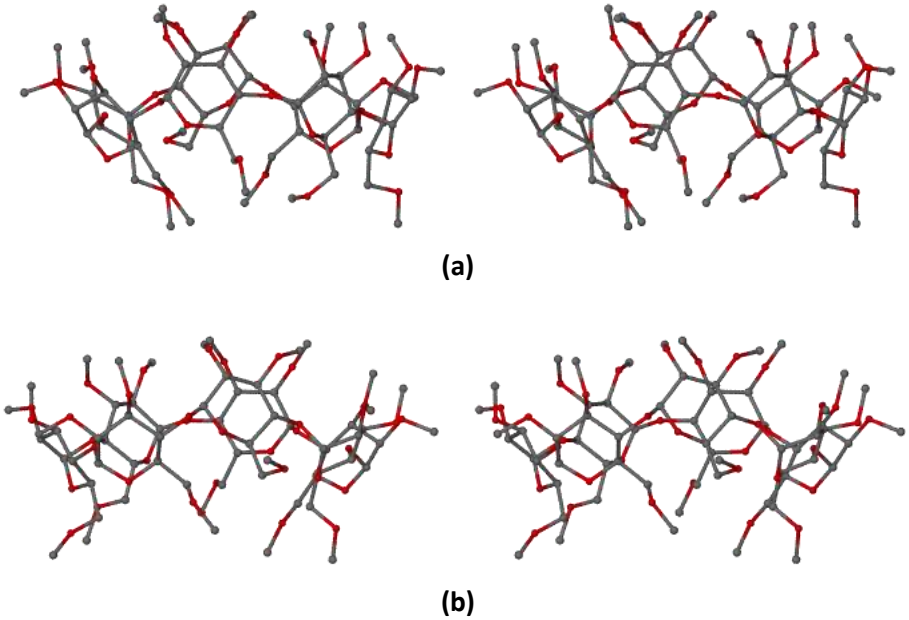

Figure 6.42: Stereoscopic view of the TRIMEB molecule A (a) and B (b) illustrating its saddle-like curvature. Hydrogen atoms and the minor components of disordered atoms are omitted for clarity.

The tilt angles (τ_1 and τ_2) are positive for each complex indicating that the methylglucose units are tilted towards the inside of the cavity such that the primary face is relatively "closed". The intersaccharidic angles (*φ*) range between 113.6° and 118.7° for A and between 112.9° and 118.4° for B.

Four of the torsion angles O5-C5-C6-O6 for the complex A possess the (-)-*gauche* orientation on residues A1, A3, A4 and A5 and these bonds are directed away from the CD cavity. The other three C6-O6 bonds are (+)-*gauche* on residues A2, A6 and A7 and are therefore directed towards the CD cavity. All O6-C9 bonds are *trans* to the corresponding C5-C6 bonds, except in residues A2 and A5 where the bonds lie (+)-*gauche*. The O6-methyl moiety on A2 is therefore orientated such that the methyl group partially "closes" the primary side of the CD, along with those on A6 and A7. The O6-methyl on residue A5 is directed severely away from the CD cavity due to steric hindrance. A1 and A3 are also directed away from the CD cavity. The complex B has six bonds in the (-)-*gauche* orientation on residues B1, B2, B3, B5, B6 and B7, but (+)-*gauche* on residue B4. All O6-C9 bonds are *trans* to the corresponding C5-C6 bonds, except in residues B2 on which the bond lies *synclinal* and B7 where the O6-C9 bond lies *anticlinal*. The O6-methyl moiety on residue B4 partially blocks the primary end of the CD while the O6-methyl moieties on B5 and B7 are directed acutely away from the CD cavity.

Guest geometry

The guest geometry is best described by three torsion angles C2-C1-C7-O1, C6-C1-C7-C8 and C9-O2-C5-C6. These torsion angles are shown in Figure 6.43. These torsion angles indicate that the guest molecules adopt planar conformations after inclusion into the CD cavity.

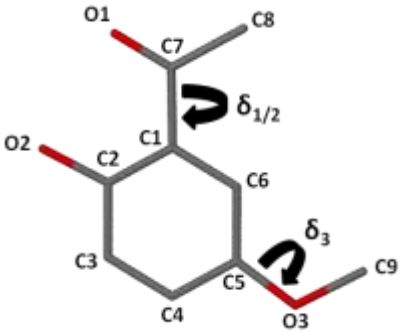

	A	B
δ_1	C2-C1-C7-O1 = 3(1)°	C2-C1-C7-O1 = 3(1)°
δ_2	C6-C1-C7-C8 = 7(1)°	C6-C1-C7-C8 = 2(1)°
δ_3	C9-O3-C5-C6 = 0(1)°	C9-O3-C5-C6 = -2(1)°

Figure 6.43: Torsion angles δ_1, δ_2 and δ_3 of 2H5M in complex unit A and B

The guest molecule in TMB·2H5M is embedded in the CD cavity with its methoxyl moiety pointing toward the primary rim and the acetyl group and the hydroxyl group located close to the secondary rim of the CD. The angle between the plane through the phenyl ring and the mean O4 least-squares plane is 86.2(5)° in complex A and 82.6(5)° in complex B. The angle between the mean O4 least-squares planes of the two complex units is 3.7(5) ° and the angle between the planes through the two guest phenyl rings is 42.9(5)°. To illustrate the position of the guest molecule within the host cavity CPK diagrams of the complex units A and B were generated (Figure 6.44 to 6.49).

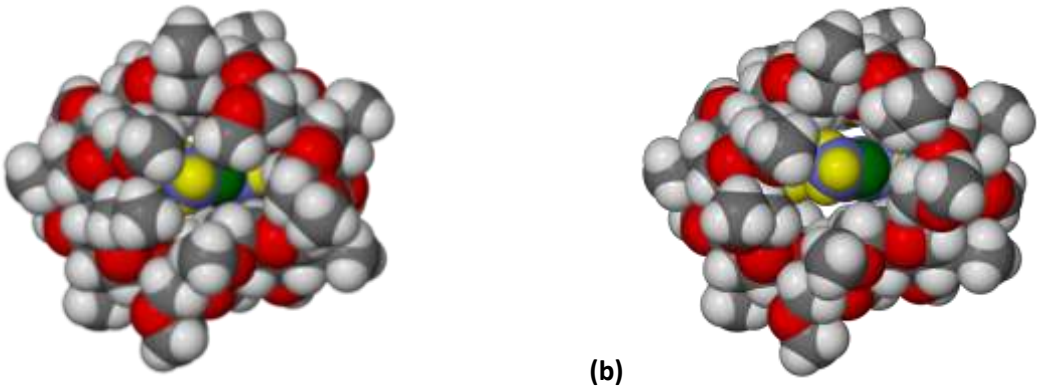

(a) (b)

Figure 6.44: Space-filling diagram of the A (a) and B (b) complex structures viewed from the primary rim

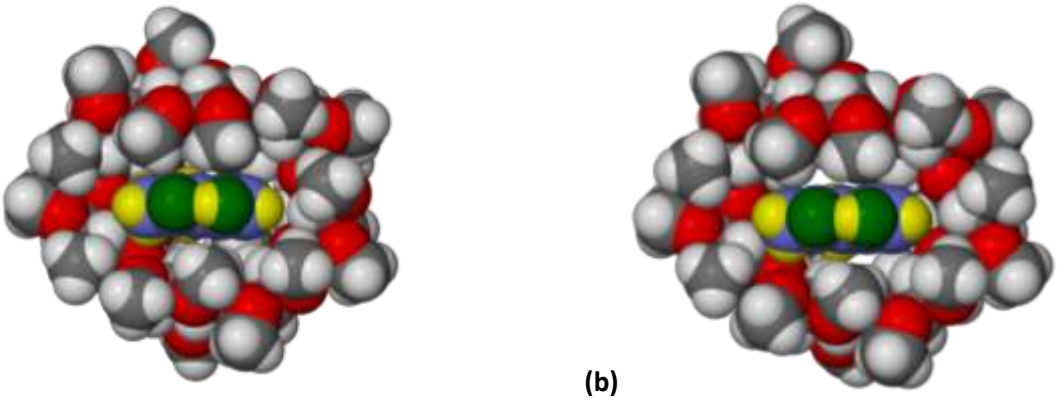

(a) (b)

Figure 6.45: Space-filling diagram of the A (a) and B (b) complex structures viewed from the secondary rim

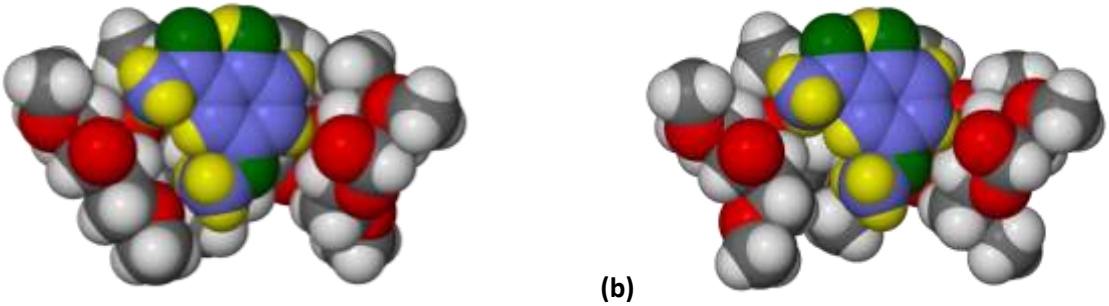

(a) (b)

Figure 6.46: Sectioned space-filling diagram of the A (a) and B (b) complex structures viewed from the side

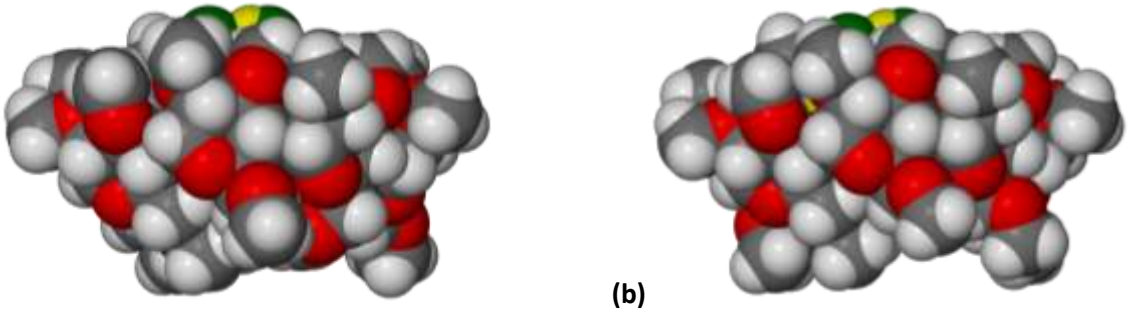

(a) (b)

Figure 6.47: Space-filling diagram of the A (a) and B (b) complex structures viewed from the side

Hydrogen bonding interactions

Guest intramolecular interactions

The guest molecules in both A and B contain one intramolecular hydrogen bond namely O1A-H1A···O3A and O1B-H1B···O3B, respectively (Figure 6.48). For both guest molecules the hydrogen bond can be described by graph set notation as $S_1^1(6)$.[13] Table 6.24 shows the geometric parameters of the hydrogen bonds.

Table 6.24: The geometric parameters of the intramolecular hydrogen bonds in the two guest molecules.

D-H···A	D-H (Å)	H···A (Å)	D···A (Å)	D-H···A (°)
O2A-H2A···O1A	0.84	1.83	2.563(8)	144
O2B-H2B···O1B	0.84	1.82	2.549(7)	145

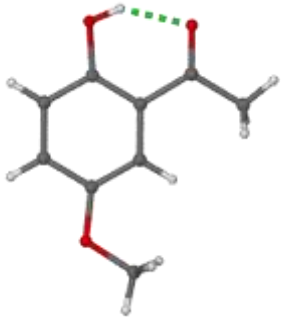

Figure 6.48: The intramolecular hydrogen bond in the guest in complex unit A. The hydrogen bond in the complex unit B occurs in the same manner.

Host intermolecular interactions

There are two C-H···O intermolecular hydrogen bonds between the two CD molecules A and B in the asymmetric unit. C2A7-H2A7···O6B3 has an O···H distance of 2.56 Å, a C···O distance of 3.489(6) Å and a bond angle of 154°. C4A6-H4A6···O6B2 has an O···H distance of 2.51 Å, a C···O distance of 3.490(6) Å and a bond angle of 167°. Seven additional intermolecular hydrogen bonds exist in the crystal by symmetry. These are listed in Table 6.25. These hydrogen bonds contribute to the overall structure of the crystal and keep the close-packed molecules in place.

Table 6.25: Various intermolecular C-H···O hydrogen bonds between host molecules.

D	A	D-H	H···A (Å)	D···A (Å)	D-H···A (°)
C2A4	O6A1[a]	1.00	2.47	3.444(5)	165
C6A2	O3B7[b]	0.99	2.55	3.450(7)	150
C9A3	O3B6[c]	0.98	2.58	3.528(8)	162
C9A5	O6B3[a]	0.98	2.46	3.411(6)	165
C1B4	O6A5[d]	1.00	2.40	3.381(5)	167
C2B1	O6B5[a]	1.00	2.39	3.392(7)	176
C9B4	O3B4[a]	0.98	2.51	3.131(8)	121

Symmetry operations: [a]x,1+y,z; [b]x,y,1+z; [c]x,1+y,1+z; [d]x,-1+y,z

Water-water and water-host interactions

The interactions listed in Table 6.26 are considered to be attractive close contacts, the water O atoms being donors, and host or other water O atoms being acceptors. There are no interactions between the water molecules and guest molecules. The water molecules fill the interstitial spaces between the complex units, adding to the structural integrity of the crystal.

Table 6.26: Various intermolecular interactions involving oxygen atoms of water in TMB·2H5M.

D	A	D···A (Å)
O1W	O2W	2.848(10)
O1W	O5A1	2.903(6)
O1W	O6A4[e]	2.903(8)
O2W	O3B3	2.955(9)
O3W	O3A6	2.998(9)
O3W	O4W	2.790(10)
O4W	O5W[f]	3.089(19)
O4W	O6B1	2.888(8)
O4W	O5B5[g]	3.005(7)
O5W	O5B1[h]	2.904(18)
O5W	O6B1[h]	2.948(18)
O5W	O2B2	2.987(17)

Symmetry operations: [e]x,y-1,z; [f]x-1,y,z; [g]x,y+1,z; [h]x+1,y,z

Weak attractive interactions involving host and guest atoms

Two weak C-H···O interaction exists between the guest and host, namely C9A2-H9A4···O3A (O···H = 2.61 Å, C···O = 3.507(10) Å and the bond angle = 153°) and C8B-H8B1···O4B4 (O···H = 2.57 Å, C···O = 3.469(9) Å and the bond angle = 155°). Various weak intramolecular hydrogen bonds and close contacts exist in the host molecules A and B, respectively. They are of the type C-H···O and contribute to the shape of the macrocycle. The geometric parameters of these interactions are tabulated in Appendix E. These close contacts have reasonable hydrogen bond distances between donors and acceptors but typically less than ideal bond angles (100° ≤ D-H···A ≤ 150°). Those that have more favourable bond angles are weakened by a longer than normal (but still acceptable) bond lengths.

Crystal packing

Both A and B pack in infinite columns along the *a*-axis with the complex units stacked head-to-tail. The columns lie anti-parallel to each other (Figure 6.49). The rows of A units and B units propagate in the *c* direction (Figure 6.50). The CDs of complex unit A form undulating channels while the CDs of complex unit B form cages.

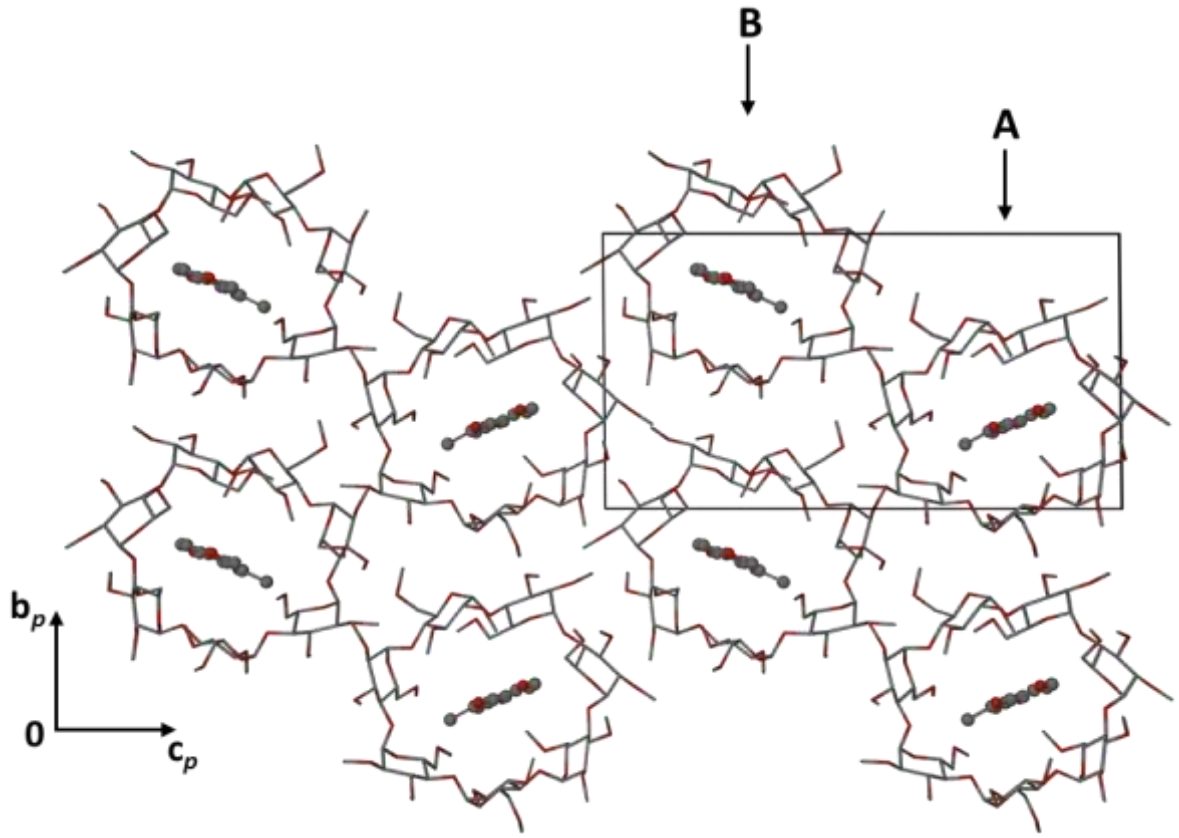

Figure 6.49: Packing diagram of the TMB·2H5M structure projected down the *a*-axis. The guest molecule is shown as ball-and-stick and the host molecules as stick diagrams. Hydrogen atoms are omitted for clarity.

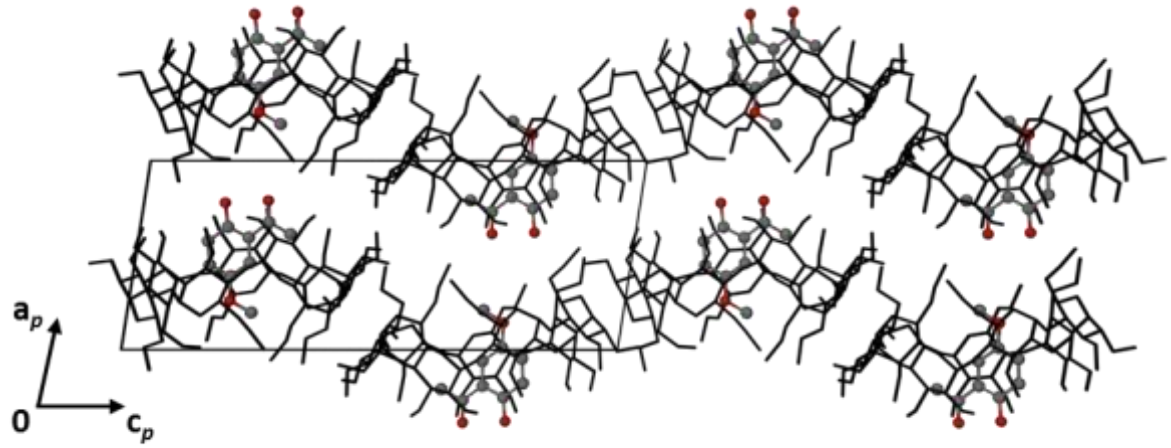

Figure 6.50: The packing arrangement in TMB·2H5M viewed down the *b*-axis. The host molecules are shown as stick diagrams in black. The guest molecules are depicted in a ball-and-stick fashion. Hydrogen atoms are omitted for clarity.

Comparative PXRD analysis

The calculated and experimental PXRD patterns of the TMB·2H5M complex were compared to determine whether the single crystal used for X-ray analysis is representative of the bulk material (Figure 6.51). Good agreement between the two indicates that the product is pure. Differences in the relative intensities between the two patterns are due to preferred orientation.

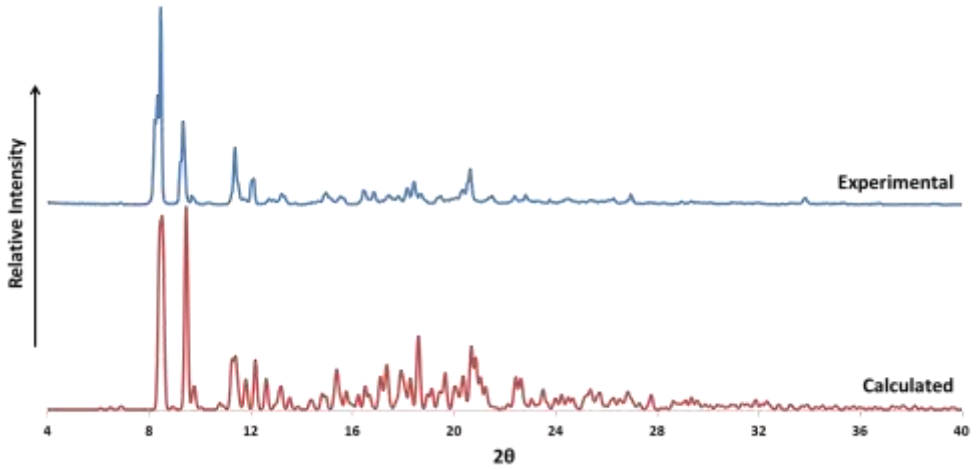

Figure 6.51: The PXRD trace of the experimental product and the pattern calculated from the single crystal X-ray structure of TMB·2H5M.

DIMEB INCLUSION COMPLEX WITH 4-HYDROXY-3-METHOXY ACETOPHENONE (DMB·4H3M)

Thermal analysis

TGA, DSC and HSM were used to determine the thermal behaviour of DMB·4H3M (see Figures 6.52 and 6.53). The TGA analysis of DMB·4H3M shows a mass loss of 11.1 % ± 0.1 % (n = 2) with an onset temperature of 180 °C. The mass loss equates to 1.0 ± 0.1 guest molecules per complex unit. The mass loss corresponds to the endotherm observed in the DSC curve over the range 170 °C - 210 °C. This endotherm appears sharper than is expected for a guest loss possibly due to the ordered nature of the crystalline material. A shoulder appearing on this endotherm is likely due to a phase transformation upon guest loss, which can be seen in the HSM photographs. No clear melting point was observed. Decomposition occurs after 330 °C.

25 °C 203 °C 220 °C 260 °C

Figure 6.52: HSM photographs of the complex DMB·4H3M.

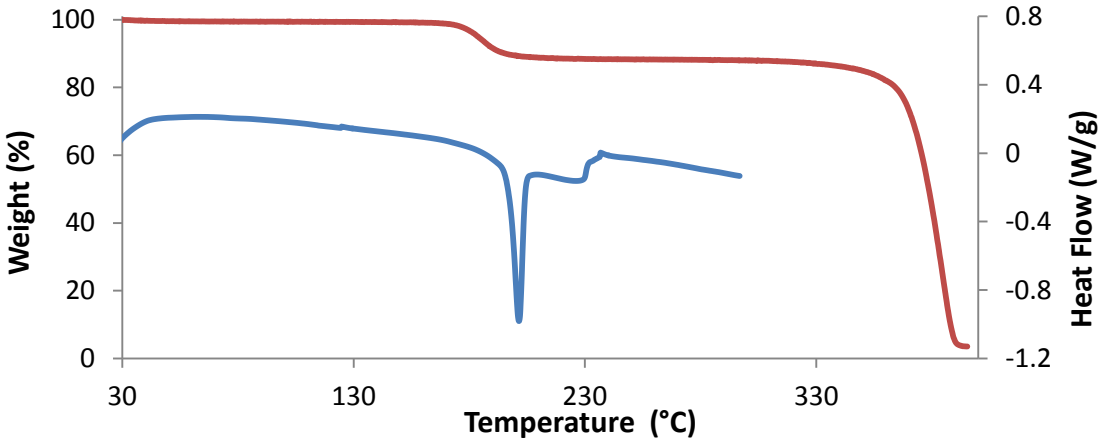

Figure 6.53: TGA (red) and DSC (blue) traces for the DMB·4H3M complex.

Single crystal X-ray analysis

Space group determination

Initial unit cell data suggested that an inclusion complex had been formed. The Laue group of the intensity-weighted reciprocal lattice was found to be *mmm* using the program LAYER,[5] revealing orthorhombic symmetry. Further inspection of the intensity data showed the reflection conditions to be *hkl: none, h00: h = 2n, 0k0: k = 2n, 00l: l = 2n*, indicating the space group $P2_12_12_1$. The data files were prepared for refinement using XPREP.[6] From density considerations it was determined that Z = 4. The crystallographic data and refinement parameters for the complex structure are listed in Table 6.27.

Structure determination and refinement

The crystal structure was solved by direct methods using the program SHELXD as no isostructural DIMEB complex (having similar unit cell dimensions) was found on the CSD.[9] A final CC of 87.69 was obtained and the solution revealed most of the non-hydrogen atoms of the host and guest molecules. Full-matrix least-squares methods were used to refine the starting model using SHELXH-97.[9] The difference electron density map resulting from the first refinement revealed most of the remaining host and guest atoms. To begin with, only host atoms were assigned in order to optimise the guest peak positions and the subsequent refinement cycles yielded difference Fourier maps which revealed all non-hydrogen atoms. Initially all atoms were refined isotropically.

Table 6.27: Crystallographic data for the complex DMB·4H3M.

Complex Formula	**$C_{56}H_{98}O_{35}\cdot C_9H_{10}O_3$**
Formula weight	1497.51
Crystal system	Orthorhombic
Space group	$P2_12_12_1$ (No.19)
a / Å	11.206(1)
b / Å	14.679(1)
c / Å	45.624(2)
Volume / $Å^3$	7505.1(6)
Z	4
Calculated density / g cm^{-3}	1.325
μ (MoKα) / mm^{-1}	0.109
F (000)	3208
Temperature of data collection / K	173(2)
Crystal size / mm^3	0.28 x 0.21 x 0.11
Theta ranges scanned / ˚	$1.9 \leq \theta \leq 26.6$
Index ranges	h: -14, 13; k: -17, 18; l: -56, 54
Total number of reflections	58957
No. of independent reflections	15535
No. of reflections with $I > 2\sigma(I)$	13394
No. of parameters	947
R_{int}	0.030
S	1.030
R_1	0.0485
No. of reflections omitted	11
wR_2	0.1275
Weighting scheme	a = 0.0643, b = 3.2436
Δρ excursions / e $Å^{-3}$	-0.38 and 0.61

After placing all host and guest atoms, further refinement revealed that ten host atoms were disordered over two positions. These atoms were refined with partial s.o.f.s of x and 1 – x respectively. The initial value of x was set to 0.5 and allowed to refine freely. This value converged for all disordered atoms as shown in Table 6.28. The O-methyl tail on C671-O671 was found to be further disordered at a third site, thus the s.o.f.s were set to 0.75 for the major component and 0.25 for the minor component.

Table 6.28: Site occupancy factors for disordered host atoms.

Atom x	**x**	**Atom x-1**	**1-x**
C831	0.63(1)	C832	0.37
C651/O651/C851	0.68(1)	C652/O652/C852	0.32
C671/O671	0.75	C672/O672	0.25
C871 + C872	0.50 + 0.25	C873	0.25

Atoms with stable isotropic thermal parameters were allowed to refine anisotropically, with the exception of atoms of the disordered atoms, which were refined isotropically. When it was noted that

that these atoms refined well with anisotropic temperature factors, hydrogen atoms were placed on the host in fixed geometric positions using a riding model and were refined isotropically with U_{iso} set to 1.2 times that of the parent atoms. Methyl hydrogen atoms were placed using the AFIX 137 command (rotating group refinement strategy) with isotropic temperature factors set to 1.5 times that of the parent atoms. Hydrogen atoms were placed on the disordered methyl groups in the same manner, except that the s.o.f.s were set equal to those of their disordered parent atoms. The host hydroxyl hydrogen atoms were placed based on their hydrogen bond potential using AFIX 83, where the placement of the hydrogen is determined by the angle and direction of potential hydrogen bond formers. The temperature factors of these hydrogen atoms were allowed to refine freely. Figure 6.54 shows the atoms labels used for the host and guest molecules. The disordered atoms were labelled by parts.

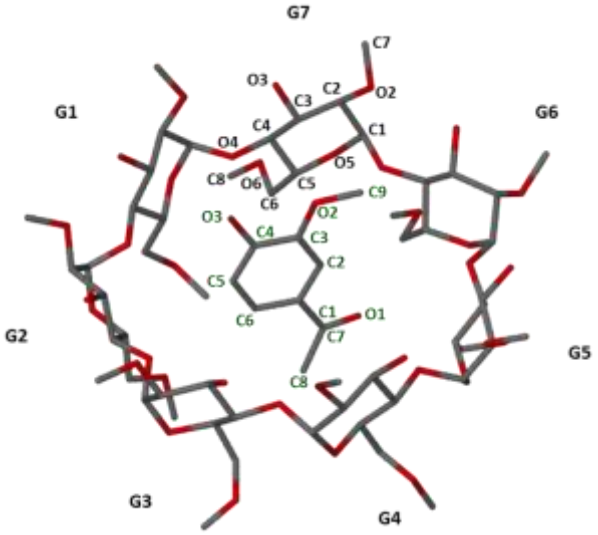

Figure 6.54: The DMB·4H3M complex viewed from the wider secondary face. The host numbering is shown in black and the guest numbering in green. Hydrogen atoms are omitted for clarity.

After assigning the host atoms, the highest peaks visible on the difference Fourier map were for those of the guest molecule and the atoms were assigned accordingly. No obvious disorder was seen. Once the guest non-hydrogen atoms were placed and refined satisfactorily an AFIX 66 command was applied to the six phenyl carbon atoms to keep them in an idealised geometry and to prevent atom shifting during refinements. The non-hydrogen guest atoms were refined anisotropically and were found to be stable as such. Guest hydrogen atoms were placed using a riding model. The aceto-methyl hydrogen atoms as well as the O-methyl hydrogen atoms were placed using the AFIX 137 command with isotropic temperature factors set to 1.5 times that of the parent atom. The phenyl hydrogen atoms were placed using the AFIX 43 (describing the aromatic C-H hydrogen atom) and AFIX 65 commands (describing the consequent non-hydrogen atoms of the rigid aromatic ring). The electron density map revealed a density attached to the hydroxyl oxygen and based on the bond length (c.a. 0.97 Å) it was determined to be a hydrogen atom.

The directionality of the bond was noted and the hydroxyl hydrogen atom was placed using the AFIX 83 command.

The asymmetric unit of the DMB·4H3M complex comprises one DIMEB molecule, one guest molecule included in the DIMEB cavity and no water molecules.

Geometrical analysis

Host geometry

Table 6.29 shows the geometric parameters associated with the O4-heptagon and gives information regarding the general shape of the DIMEB host molecule.

Table 6.29: The geometric parameters of the O4-heptagon of the host molecule

Residue	*r* (Å)	*D* (Å)	*a* (°)	*φ* (Å)	*d* (°)	D_3 (Å)	*α* (Å)*	τ_1 (°)	τ_2 (°)
G1	5.214	4.246	125.4	118.2(2)	-0.03	2.821(3)	0.164	11.0(1)	11.2(2)
G2	5.281	4.348	123.3	119.2(2)	-13.09	2.834(4)	0.123	17.3(1)	18.9(3)
G3	4.748	4.548	134.1	117.8(2)	12.02	2.889(3)	-0.260	6.8(1)	10.9(1)
G4	4.914	4.348	131.4	119.0(3)	1.41	2.846(4)	0.048	1.6(1)	3.9(1)
G5	5.424	4.216	119.6	119.9(3)	-5.62	2.809(4)	0.179	16.5(1)	17.7(1)
G6	4.970	4.570	131.6	117.8(2)	-3.35	2.965(4)	-0.081	17.8(1)	20.9(2)
G7	4.764	4.436	133.1	117.3(2)	9.45	2.885(4)	-0.173	6.8(1)	7.8(1)
Mean	**5.05**	**4.39**	**128.3**	**118.47**	**8.02**‡	**2.87**	**0.147**‡	**11.0**	**13.1**

*Average e.s.d. = 0.002 Å, ‡Root-mean-square deviation

The O4-heptagon of the DMB·4H3M complex deviates significantly from that of a regular heptagon. This deviation is determined by examining the *r*, *D*, and *a* parameters. The host molecule appears to be curved when viewed side-on in Figure 6.55, the degree of the curvature is measured by the torsion angle O4(n-1)···O4(n)···O4(n+1)···O4(n+1) (*d*) and the deviation of the O4 atoms from the least-squares O4 plane (*α*).

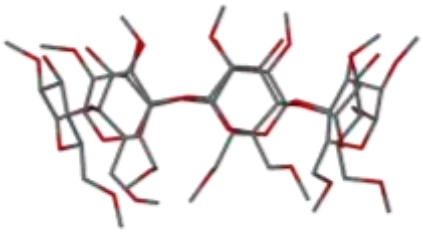

Figure 6.55: View from the side of the DIMEB molecule illustrating its curvature. Hydrogen atoms and the minor components of disordered atoms were omitted for clarity.

The O4 parameters are a result of the orientation of each individual methylglucose residue. These parameters are the tilt angle between the O4 plane and the mean plane through the atoms O4(n)···C4(n)···C1(n)···O4(n-1) (*τ*), the intersaccharidic bond angle C1(n-1)···O4(n)···C4(n) (*φ*) and the torsion angle O6(n)···C6(n)···C5(n)···O5(n) (*ω*) which describes the orientation of the C6-O6 bond with

respect to the cavity. The tilt angle τ_2 has an average of 13.1° with a range of 3.9 to 20.9°. All of the values are positive indicating that the methylglucose units are tilted towards the inside of the cavity on the primary face. The intersaccharidic bond angles have an average of 118.5° and are slightly larger than those observed for β-CD molecules. The smallest bond angles are seen for units G3, G6 and G7 which are found on the longitudinal ends of the macrocycle and indicate the degree of curvature of the elongated CD.

Three orientations are evident for the C6-O6 bonds, namely (-)-*gauche* for G3, G4, G5 (major position), G6 and G7 (minor position), (+)-*gauche* for G1, G5 (minor position) and G7 (major position) and (+)-*anticlinal* for G2. All O6-C8 bonds are *trans* to the corresponding C5-C6 bonds, except in residue G1 where the bond lies *gauche* and in residues G3 and G7 (major positions) where the bonds lie *anticlinal*.

Guest geometry

The guest planarity can be described by three torsion angles C6-C1-C7-O1, C2-C1-C7-C8 and C9-O2-C3-C4. These torsion angles are shown in Figure 6.56.

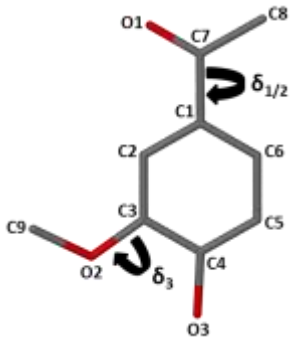

δ_1 C6-C1-C7-O1 = 167.8(5)°
δ_2 C2-C1-C7-C8 = 170.4(5)°
δ_3 C9-O2-C3-C4 = 178.6(4)°

Figure 6.56: Torsion angles δ_1, δ_2 and δ_3 of 4H3M

The guest molecule is completely embedded in the CD cavity with the acetyl moiety of the molecule located at the primary rim of the CD and the hydroxyl and O-methyl moieties are located at the secondary rim. The angle between the plane through the phenyl ring and the mean O4 least-squares plane is 71.4(5)°. CPK diagrams allow for examination of the special arrangement of the host and guest molecules (Figure 6.57 to 6.60).

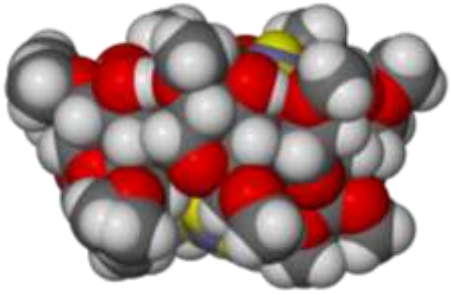

Figure 6.57: Space-filling diagram of the DMB·4H3M structure viewed from the side.

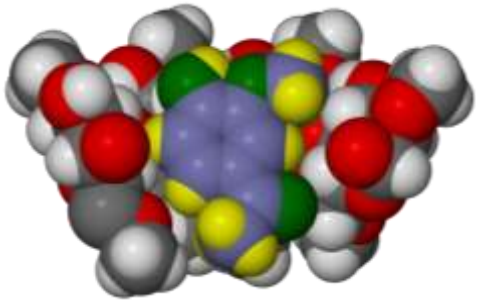

Figure 6.58: Sectioned space-filling diagram of the DMB·4H3M structure viewed from the side.

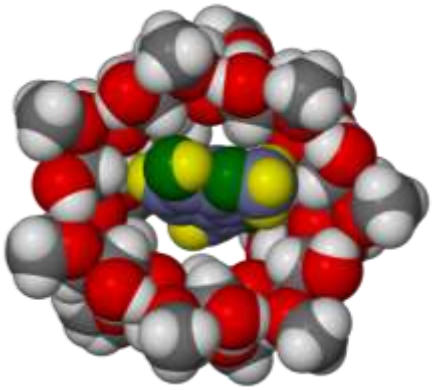

Figure 6.59: Space-filling diagram of the DMB·4H3M structure viewed from the secondary rim.

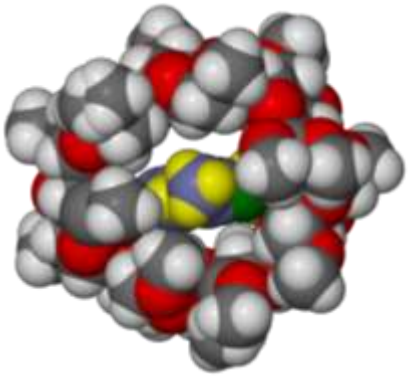

Figure 6.60: Space-filling diagram of the DMB·4H3M structure viewed from the primary rim.

Hydrogen bonding interactions

Two types of hydrogen bonds occur in the complex, namely intra- and intermolecular hydrogen bonds. The intramolecular hydrogen bonds contribute to the structural integrity of the individual molecules while the intermolecular hydrogen bonds contribute to the integrity of the crystal structure.

Strong intramolecular host hydrogen bonds

There are seven strong O2(n)-H···O3(n-1) intramolecular hydrogen bonds. Due to the *cis* orientation of the methylglucose units, the O2 and O3 atoms are on the same side of the CD. The O2 atoms are able to interact with the O3-H hydroxyl groups of the contiguous methyl-glucose unit, adding to the shape and rigidity of the CD.[34] The hydrogen bond lengths and angles are listed in Table 6.30. Figure 6.61 shows the hydrogen bond interactions.

Table 6.30: O2(n)···O3(n-1) hydrogen bond distances and angles

D-H···A	D-H (Å)	H···A (Å)	D···A (Å)	D-H···A (°)
O3G1-H31···O2G2	0.84	2.11	2.834(4)	145
O3G2-H32···O2G3	0.84	2.07	2.889(3)	164
O3G3-H33···O2G4	0.84	2.05	2.846(4)	158
O3G4-H34···O2G5	0.84	2.07	2.809(4)	147
O3G5-H35···O2G6	0.84	2.23	2.965(4)	146
O3G6-H36···O2G7	0.84	2.06	2.885(4)	166
O3G7-H37···O2G1	0.84	2.08	2.821(3)	146

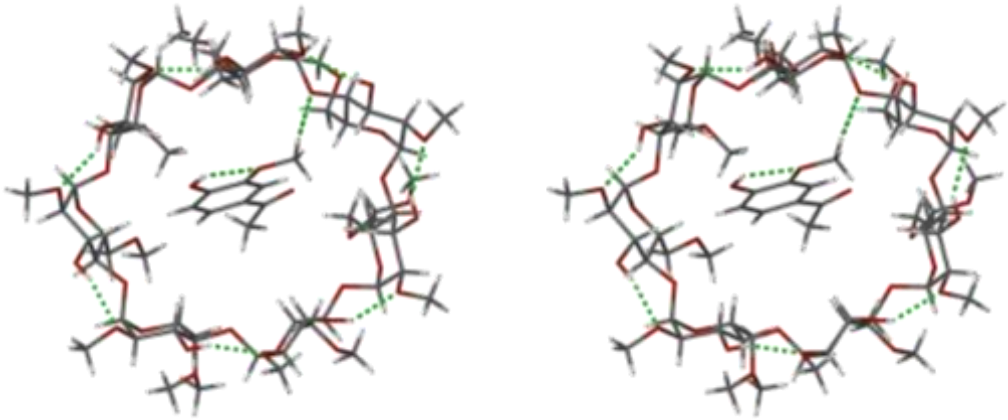

Figure 6.61: Stereodiagram illustrating the intramolecular host O2(n)-···O3(n-1) interactions, the host-guest interaction with symmetry x,y,z and the intramolecular guest interaction.

Weak intramolecular host hydrogen bonds

For some residues there are weak hydrogen bonds and close contacts which are either responsible for the structure of the host or a result of the crystal packing. The geometric parameters of these hydrogen bonds and close contacts are listed in the Appendix E.

For some residues (G3, G4, G5 and G6) the C6-O6 bond is held in the (-)-*gauche* orientation by a contact C4-H···O6 (refer to Figure 6.51 for methylglucose unit labels). However, these contacts are very weak due to poor geometry (*c.a.* 100°).[33] On residue G1 the C6-O6 bond is held in the (+)-*gauche* position by a weak hydrogen bond C8(G1)-H···O6(G2). On residues G1, G4, G5, G6 and G7 the O-methyl C7 forms a hydrogen bond with the corresponding O3 atom. Close contacts are formed on residues G2 and G6 such to form hydrogen bonds C5(n)-H···O4(n-1). Hydrogen bonding interactions are also formed of the type C6(n)-H···O5(n+1).

Intermolecular host hydrogen bonds

There are four intermolecular hydrogen bonds which contribute to the crystal packing, holding the host molecules in close proximity. These interactions are listed in Table 6.31. The hydrogen bond interactions occur between a donor carbon atom of one CD molecule and an acceptor oxygen atom on a symmetry generated CD molecule. These interactions are somewhat weak but nevertheless contribute cumulatively to the crystal structure.

Table 6.31: Hydrogen bond distances and angles in the DMB·4H3M structure

D-H···A	D-H (Å)	H···A (Å)	D···A (Å)	D-H···A (°)
C1G2-H1G2···O2G3 [a]	1.00	2.56	3.373(4)	138
C2G4-H2G4···O3G7 [b]	1.00	2.43	3.328(4)	150
C2G5-H2G5···O6G6 [c]	1.00	2.42	3.374(5)	158
C8G6-H8G8···O3G5 [d]	0.98	2.55	3.412(6)	146

Symmetry operations: [a] -½+x, ½-y, -z; [b] x, 1+y, z; [c] 1-x, ½+y, ½-z; [d] 1-x, -½+y, ½-z

Intermolecular host-guest and intramolecular guest hydrogen bonds

Three hydrogen bonds exist between the host and guest molecules. These interactions are listed in Table 6.32. One of the interactions occurs between the host and its included guest molecule while the other two interactions occur between a guest molecule of one complex unit and the host molecule of a symmetry-generated host molecule.

Table 6.32: Intermolecular host-guest hydrogen bond distances and angles

D-H···A	D-H (Å)	H···A (Å)	D···A (Å)	D-H···A (°)
C2G2-H2G2···O3 [e]	1.00	2.52	3.258(5)	130
C9-H9C···O4G6	0.98	2.47	3.442(5)	174
O3-H3···O3G2 [f]	0.84	2.11	2.651(4)	121

Symmetry operations: [e] -½+x, ½-y, -z; [f] ½+x, ½-y, -z

Only one intramolecular hydrogen bond exists in the guest molecule, namely that between the hydroxyl hydrogen atom and the oxygen atom of the methoxy group, O3-H3···O2, for which D-H = 0.84 Å, H···A = 2.18, D···A = 2.645(4) Å and D-H···A = 115°. Figure 6.62 shows the hydrogen bonds involving the guest molecule. The intramolecular hydrogen bond can be described by graph-set notation[13] as $S_1^1(5)$.

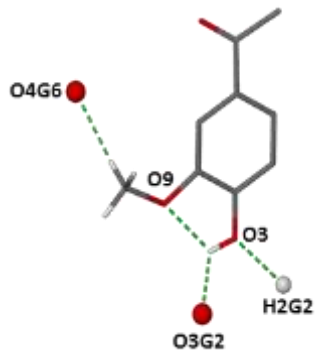

Figure 6.62: The inter- and intramolecular hydrogen bonds involving the guest molecule. Hydrogen bonds are shown in green and only hydrogen atoms involved in hydrogen bond interactions are shown.

Crystal packing

The packing arrangement in this complex is described as a being a modified herringbone type pattern.[34] Figure 6.63 shows that the complex units appear to form infinite columns when viewing the cell with a projection down the *a*-axis. Figure 6.64 shows the herringbone type packing motif when a projection down the *b*-axis is viewed, where the complex units form cages and stack in a head-to-tail fashion.

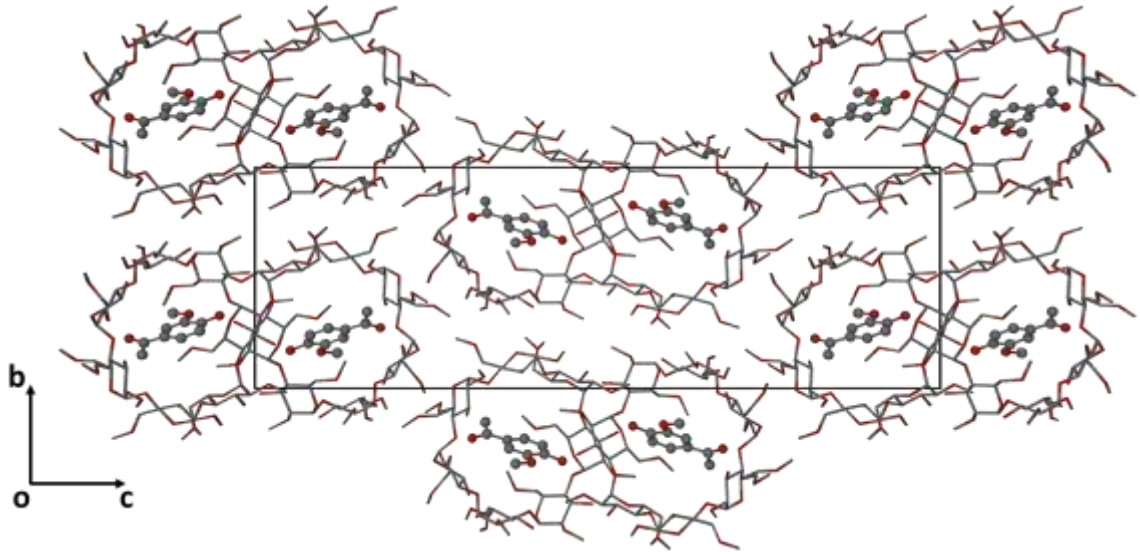

Figure 6.63: Stereo packing diagram of the DMB·4H3M structure projected down the *a*-axis. Hydrogen atoms omitted for clarity.

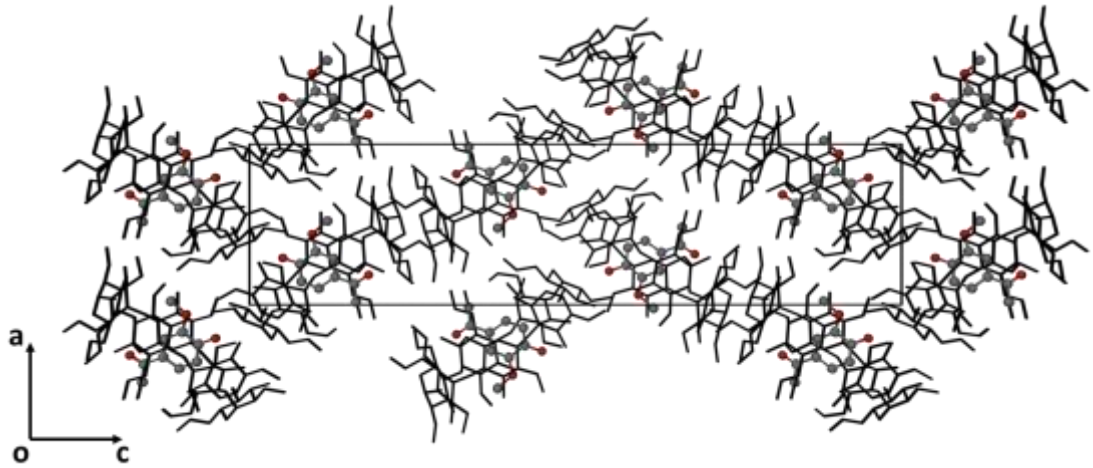

Figure 6.64: Stereo packing diagram of the DMB·4H3M structure projected down the *b*-axis. Hydrogen atoms omitted for clarity.

Comparative PXRD analysis

The experimental PXRD trace of the DMB·4H3M complex was compared to the trace calculated from the crystal structure. A good match indicates that the single crystal used for X-ray analysis is representative of the bulk material (Figure 6.65). The relative intensities between the two patterns may show differences due to preferred orientation.

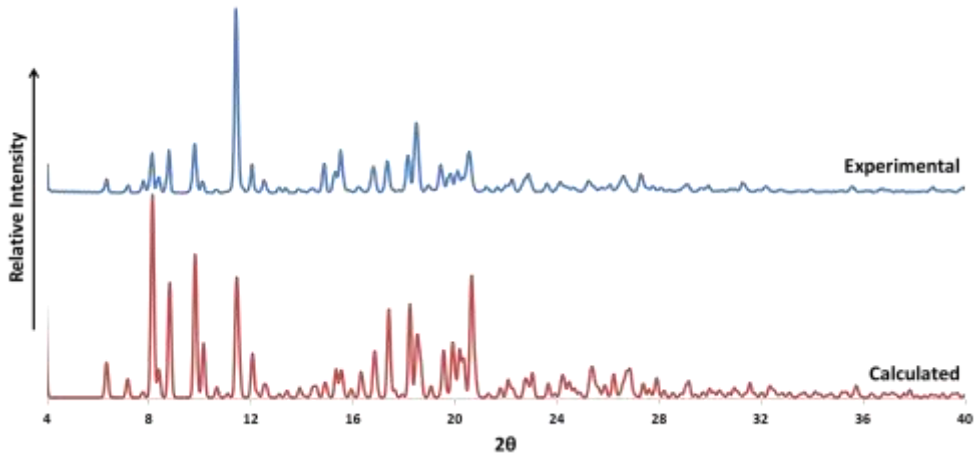

Figure 6.65: The PXRD trace of the experimental product and the pattern calculated from the single crystal X-ray structure of DMB·4H3M.

TRIMEA INCLUSION COMPLEX WITH 2-HYDROXY-5-METHOXY ACETOPHENONE (TMA·2H5M)

Thermal Analysis

The thermal behaviour of the complex TMA·2H5M was analysed using TGA, DSC and HSM. There is no indication of a mass loss in the TGA due to water loss (Figure 6.66). The mass loss recorded over the range 135 °C to 250 °C (11.9 ± 0.8 %, n = 4,) corresponds to a loss of 1.0 ± 0.1 guest molecules per complex unit. This mass loss is also indicated by the bubbling seen in the HSM photographs (Figure 6.67). A sharp endotherm in the DSC trace (Figure 6.66) at 172 °C may be due to a phase transformation as the host molecules rearrange after the loss of the guest. This phase transformation may be seen physically in the HSM photographs by the formation of a new crystalline material on the complex crystal. The DSC then appears to show erratic noise from 180 °C onwards, repeating this experiment three times revealed that this noise is not artificial and requires further investigation by modulated DSC and variable temperature PXRD. The sample decomposes at *ca.* 300 °C.

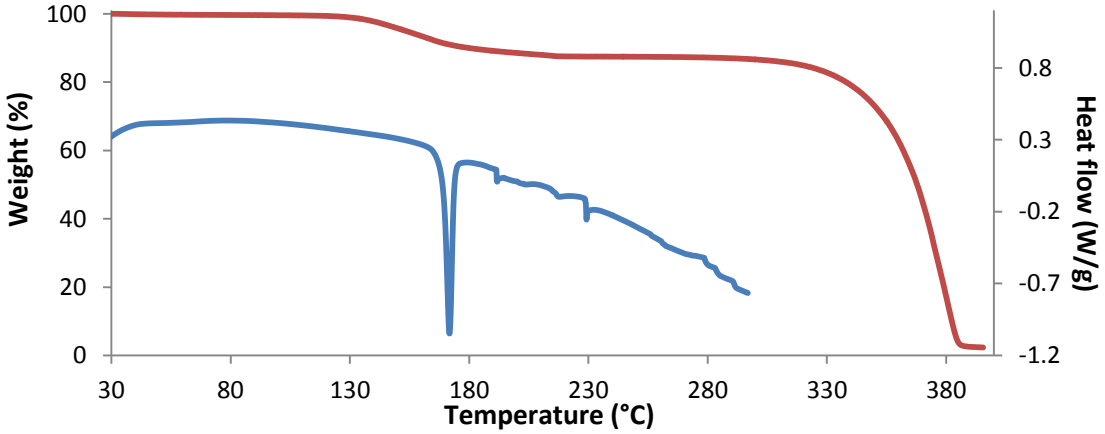

Figure 6.66: TGA (red) and DSC (blue) traces for the TMA·2H5M complex.

27 **167** **178** **194** **215** **237**

Figure 6.67: HSM photographs of the complex TMA·2H5M

Single crystal X-ray analysis

Space group getermination

The preliminary unit cell data suggested the formation of the inclusion complex TMA·2H5M. X-ray intensity data were collected for the crystal. Program LAYER[5] indicated the Laue symmetry *6/m*. Examination of the intensity data revealed the general reflection conditions *000l: l = 2n* indicating the hexagonal space group $P6_3$. From density considerations it was determined that Z = 6. Program XPREP[6] was used to prepare the data files for structure solution and refinement. The crystallographic data and refinement parameters for the structure are listed in Table 6.33.

Structure determination and refinement

An initial search of the CSD did not reveal any isostructural TRIMEA complexes and the structure of TMA·2H5M was solved using direct methods as implemented in the program SHELXD.[9] The final solution had a correlation coefficient of 85.29, showing most of the non-hydrogen host atoms and some guest non-hydrogen atoms. The full-matrix least-squares method was used in SHELXH-97 to refine the structure and the non-hydrogen host and guest atoms were assigned in successive difference Fourier maps.[9] Initially all atoms were refined isotropically and once they were found to have stable temperature factors they were refined anisotropically.

Table 6.33: The crystallographic and refinement parameters for the complex TMA·2H5M

Complex Formula	**$C_{54}H_{96}O_{30}•C_9H_{10}O_3•0.24H_2O$**
Formula weight	1395.07
Crystal system	Hexagonal
Space group	$P6_3$ (No. 173)
a / Å	24.228(3)
c / Å	22.070(5)
Volume / $Å^3$	11219(3)
Z	6
Calculated density / g cm^{-3}	1.239
μ (MoKα) / mm^{-1}	0.100
F (000)	4498
Temperature / K	173(2)
Crystal size / mm^3	0.27 x 0.14 x 0.06
Theta range scanned / ˚	1.9 ≤ θ ≤ 24.7
Index ranges	h: -28, 28; k: -28, 28; l: -25, 25
Total number of reflections	76558
No. of independent reflections	12751
No. of reflections with I > 2σ(I)	9206
No. of parameters	892
R_{int}	0.047
S	1.018
R_1	0.0469
No. of reflections omitted	30
wR_2	0.1336
Weighting scheme	a = 0.0693, b = 3.2932
Δρ excursions / e $Å^{-3}$	-0.28, 0.45

Six host atoms were found to be disordered over two positions. These atoms were refined with partial s.o.f.s of x and 1 – x respectively. The initial value of x was set to 0.5 and allowed to refine freely. These values settled as shown in Table 6.34. The disordered atoms were refined isotropically. Some of the bonds involving these disordered atoms were constrained to reasonable bond lengths.

Table 6.34: Site occupancy factors for disordered host atoms

Atom x	**x**	**Atom x-1**	**1-x**
C621/O621/C921	0.71(1)	C622/O622/C922	0.29
C911	0.69(1)	C912	0.31
C741	0.58(4)	C742	0.42
C931	0.59(5)	C932	0.41

Hydrogen atoms were placed on the primary and secondary host carbon atoms in fixed geometric positions using a riding model and were refined isotropically with temperature factors set to 1.2 times

that of the parent atoms. The AFIX 137 command was used to place the methyl hydrogen atoms with isotropic temperature factors set to 1.5 times that of the parent atoms. One electron density peak of height 0.7 eÅ^{-3} was identified as not being part of the host or guest molecules. It was found to adhere to hydrogen bonding parameters and was assigned as a water oxygen atom. The temperature factor of this atom was found to be very high and the s.o.f. adjusted such that a more reasonable temperature factor was obtained. The final s.o.f. was 0.20 for O1W and the U_{iso} settled at 0.113 Å^2. This was not evident in the TGA as the expected mass loss percentage would fall within experimental error. The hydrogen atoms of the partial water molecule were not located.

The phenyl ring of 2H5M was assigned and constrained to a rigid hexagon using the AFIX 66 command. The acetyl, methoxy and hydroxyl moieties were identified and assigned. A riding model was used to place guest hydrogen atoms. The methyl hydrogen atoms were placed using the AFIX 137 command with isotropic temperature factors set to 1.5 times that of the parent atom. The phenyl hydrogen atoms were placed using the AFIX 43 and the hydroxyl hydrogen atom was placed using the AFIX 147 command, both being refined with a U_{iso} value 1.2 times that of the parent atom.

The methylglucopyranose residues were named G1 - G6. Each carbon atom was labelled with a number 1 - 9 and the corresponding oxygen atom was labelled accordingly as shown in Figure 6.68a. The guest molecule was labelled as shown in Figure 6.68b.

The asymmetric unit of the TMA·2H5M complex contains one TRIMEA molecule, one guest molecule and 0.20 water molecules.

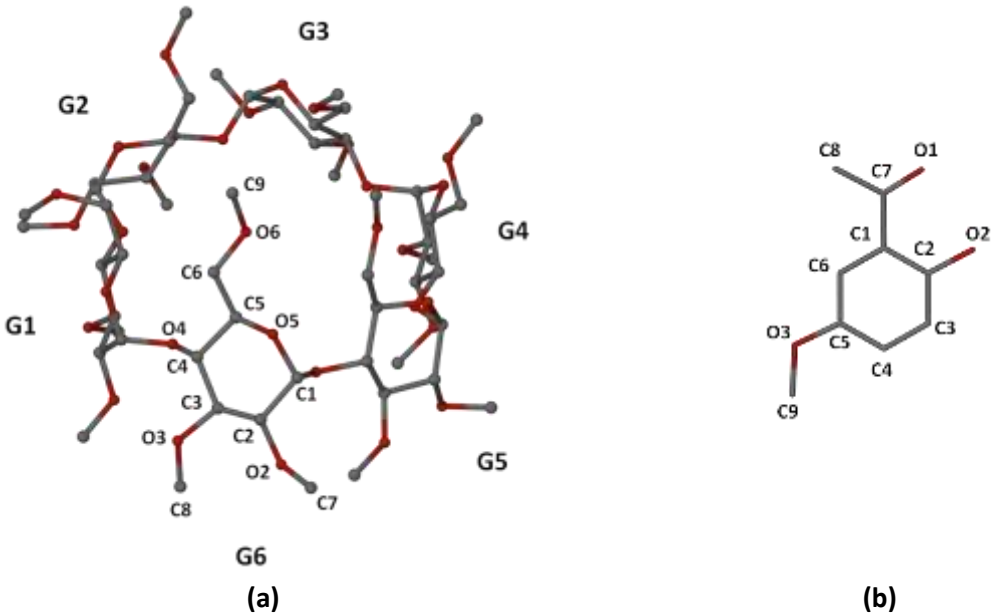

Figure 6.68: The labelling of residues on the host molecule (a) and the labelling of the guest molecule (b). Hydrogen atoms and disordered atoms are omitted for clarity.

Geometrical Analysis

Host geometry

Table 6.35 shows the geometric parameters associated with the O4 hexagon. These parameters are described in Chapter 1. Upon evaluating the *r*, *D*, *a* and *d* parameters the host molecule appears to have an overall round shape with a slight narrowing at the intersaccharide angle of G2 and G5. The deviations of the O4 atoms from the mean O4 plane give an indication of the curvature of the host molecule (Figure 6.69). The tilt angles (τ_1 and τ_2) are positive resulting in an inward tilt of the residues on the primary end.

Table 6.35: The geometric parameters of the host molecule O4 heptagon.

Residue	*r* (Å)	*D* (Å)	*a* (°)	*φ* (°)	*d* (°)	D_3 (Å)	*α* (Å)	τ_1 (°)	τ_2 (°)
G1	4.152	4.476	120.9	118.1(3)	20.98	3.313	-0.311(2)	2.0(1)	3.8(5)
G2	4.469	4.046	113.2	119.0(4)	-14.26	3.529	0.363(2)	25.8(1)	24.4(3)
G3	4.202	4.419	122.6	117.3(4)	-3.13	3.422	-0.094(2)	33.3(1)	35.9(2)
G4	4.125	4.289	122.3	118.0(4)	14.56	3.663	-0.240(2)	2.3(1)	2.6(6)
G5	4.449	4.144	114.1	119.2(4)	-7.55	3.350	0.290(2)	19.5(1)	19.8(3)
G6	4.193	4.311	122.9	117.6(3)	-10.30	3.401	-0.008(2)	30.0(1)	32.1(2)
Mean	**4.27**	**4.28**	**119.3**	**118.18**	**12.09**	**3.44**	**0.23**	**16.1**	**19.8**

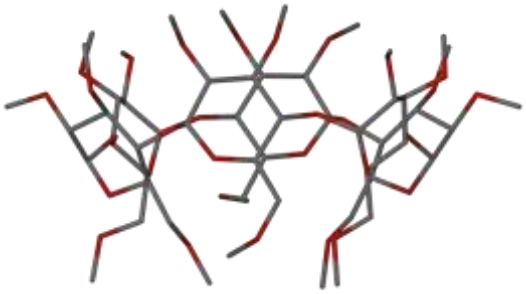

Figure 6.69: View from the side of the TRIMEA molecule illustrating its curvature. Hydrogen atoms and the minor components of disordered atoms are omitted for clarity.

Four of the O5-C5-C6-O6 torsion angles for the complex TMA·2H5M adopt the (+)-*gauche* orientation on residues G1, G2, G3 and G6 while the other two C6-O6 bonds are in a (-)-*gauche* orientation on residues G4 and G5. All O6-C9 bonds are *trans* to the corresponding C5-C6 bonds, except in residues G1 and G4 where the bonds lie (-)-*anticlinal* and (+)-*gauche,* respectively. The O6-methyl moieties on G2, G3 and G6 are directed such that the methyl group partially "closes" the primary side of the CD. The O6-methyl groups on residues G4 and G5 are directed away from the CD cavity due to steric hindrance.

Guest geometry

Examination of the torsion angles of the guest molecule shows that it is planar. Three torsion angles (C6-C1-C7-O1, C2-C1-C7-C8 and C9-O2-C3-C4) describe this planarity (Figure 6.70).

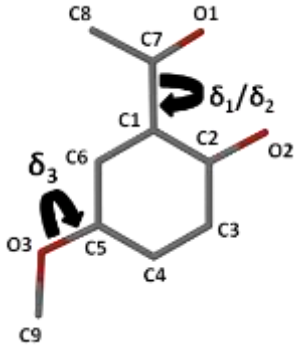

δ_1 C6-C1-C7-O1 = -174.6(7)°
δ_2 C2-C1-C7-C8 = -170.1(7)°
δ_3 C9-O3-C5-C6 = 173.8(6)°

Figure 6.70: Torsion angles δ_1, δ_2 and δ_3 of 2H5M

The methoxy group of 2H5M is included in the CD cavity while the acetyl and hydroxyl substituents protrude from the secondary rim. The angle between the mean O4 plane and the plane through the phenyl of the guest is 86.2(5)°. Figures 6.71 to 6.74 are space-filling diagrams illustrating the orientation of the guest within the host cavity and interactions between the host and guest molecules of the TMA·2H5M complex structure.

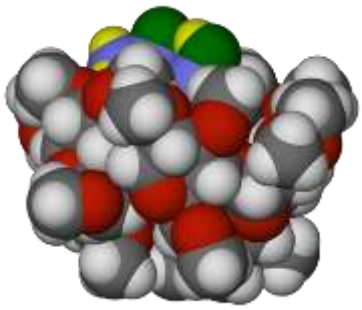

Figure 6.71: Space-filling diagram of the TMA·2H5M structure viewed from the side.

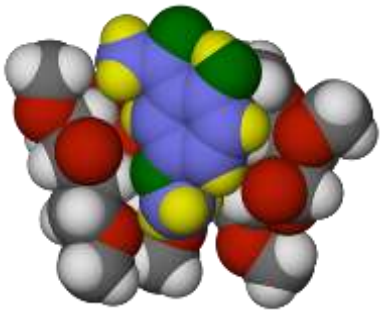

Figure 6.72: Sectioned space-filling diagram of the TMA·2H5M structure viewed from the side.

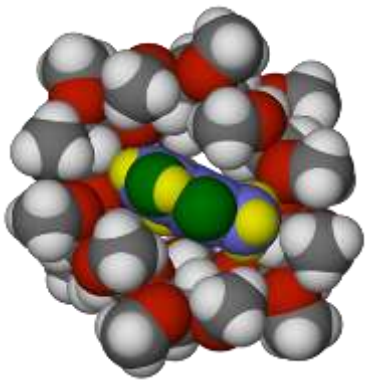

Figure 6.73: Space-filling diagram of the TMA·2H5M structure viewed from the secondary rim.

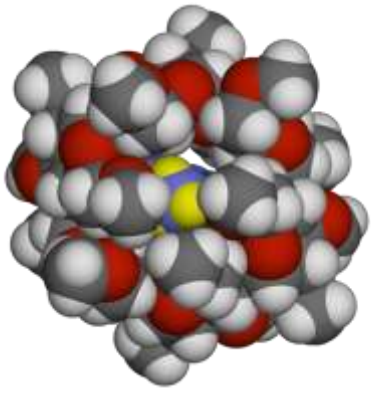

Figure 6.74: Space-filling diagram of the TMA·2H5M structure viewed from the primary rim.

Hydrogen bonding interactions

Guest intramolecular interactions

An intramolecular hydrogen bond, described by graph-set notation[13] as $S_1^1(6)$, exists in the guest molecule. This interaction is O2-H2···O1 (Figure 6.75) having an O···H distance of 1.88 Å, an O···O distance of 2.600(7) Å and a bond angle of 144°.

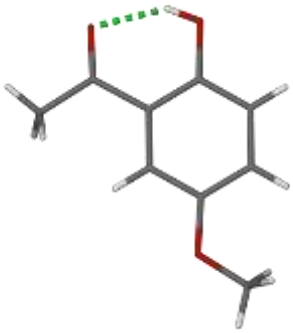

Figure 6.75: The intramolecular hydrogen bond in the guest for the complex TMA·2H5M.

Host intra- and intermolecular interactions

The intra- and intermolecular interactions in the complex TMA·2H5M are of the type C-H···O. Two host intermolecular hydrogen bonds exist, the parameters are listed in Table 6.36. A number of weak C-H···O intramolecular interactions contribute to the stability and shape of the macrocycle and are tabulated in Appendix E.

Table 6.36: The intermolecular interactions between host molecules

D-H···A	D-H	H···A (Å)	D···A (Å)	D-H···A (°)
C2G5-H2G5···O3G2[a]	1.00	2.60	3.559(7)	161
C7G6-H7GA···O5G2[a]	0.98	2.42	3.199(10)	136

Symmetry operator: [a]1+x-y,x,1/2+z

Host-guest intermolecular interactions

Two weak host-guest C-H···O interactions occur, namely C8B-H8B1···O2B4 (O···H = 2.53 Å, C···O = 3.490(10) Å, C-H···O = 168°) and C5G3-H5G3···O3 (corresponding data: 2.47 Å, 3.423(7) Å and 160°).

Water-water and water-host interactions

Three water oxygen atoms are related bya 3-fold rotation axis, forming an equilateral triangle with sides 2.11(5) Å. These water oxygen atoms exist in the interstitial space between complex units and form a hydrogen bond interaction with atom O3G4 of the host (O···O = 2.78(3) Å).

Crystal packing

The CD complex units pack around a 6-fold screw axis of the type 6_3. Three complex units (blue) are arranged in the same plane around a 3-fold rotation axis. Another three complex units (green) are arranged around a 3-fold rotation axis, lying staggered and half a unit cell above the blue units (Figure 6.76). The six complex units are arranged around the *c*-axis (Figure 6.77).

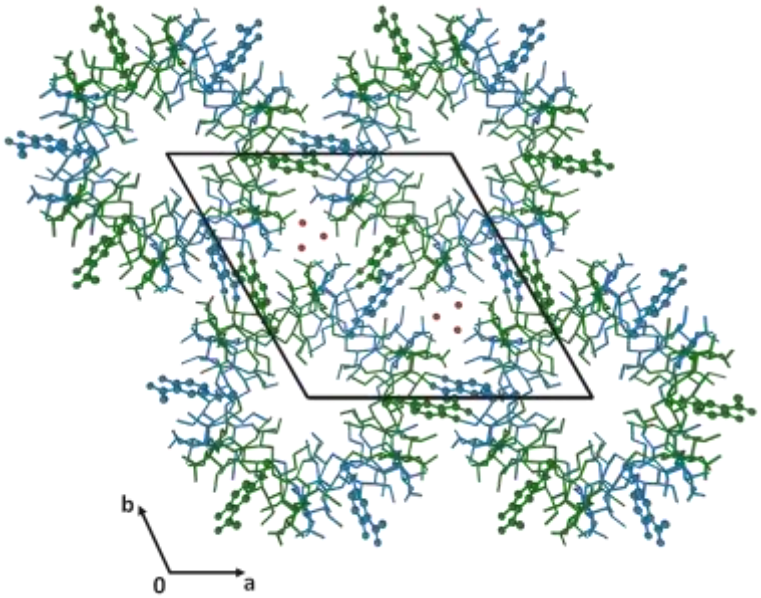

Figure 6.76: Packing diagram of the TMA·2H5M structure projected down the *c*-axis. The guest molecules and water oxygen atoms are represented as ball-and-stick and the host molecules as stick diagrams. Hydrogen atoms omitted for clarity.

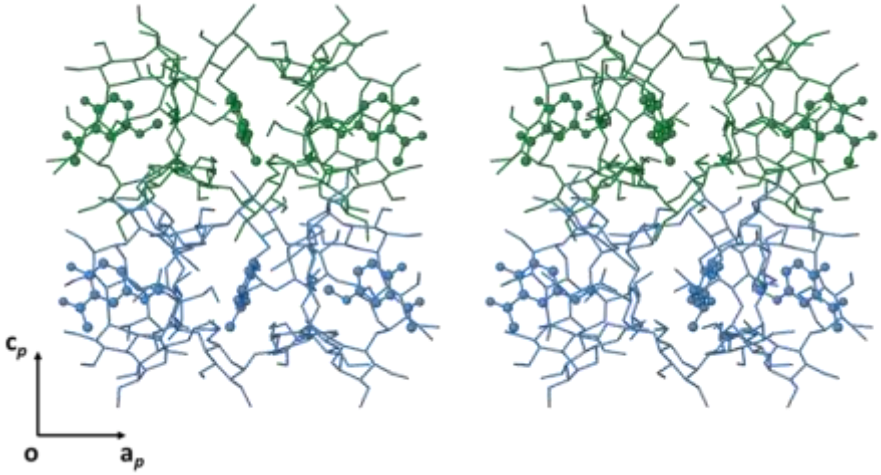

Figure 6.77: Stereodiagram of TMB·2H5M illustrating the layers of complex units arranged around the *c*-axis.

Comparative PXRD analysis

The calculated and experimental PXRD patterns shown in Figure 6.78 correlate well, indicating that the bulk material is the same as the single crystal used for X-ray analysis. The close match between the peak positions (2θ) is evidence of a pure product.

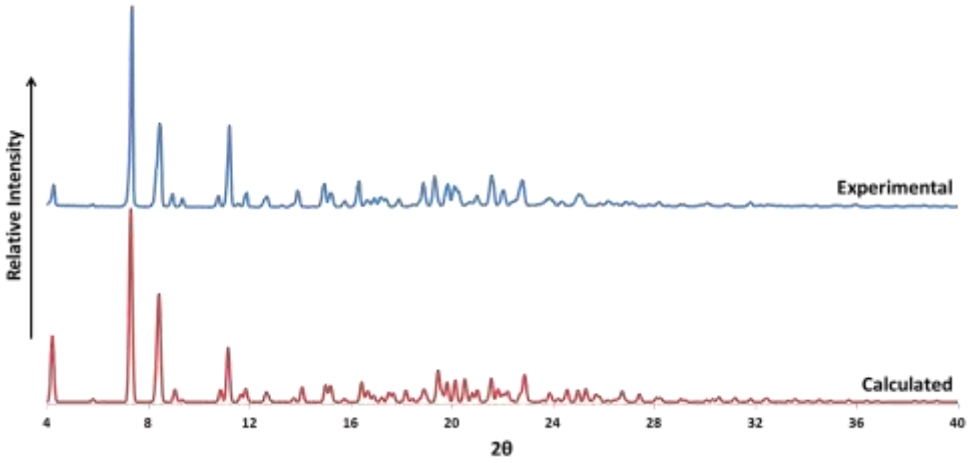

Figure 6.78: The PXRD trace of the experimental product and the pattern calculated from the single crystal X-ray structure of TMA·2H5M.

DISCUSSION

In this section complex formation was confirmed for each guest 2H4M, 2H5M, 2H6M and 4H3M with γ-CD both by the method of kneading and by coprecipitation/slow cooling. Complexes were also formed for each guest with β-CD by coprecipitation/slow cooling, however, kneading only yielded three out of the four guests forming complexes. These guests were also found to interact with γ- and β-CD in solution forming 1:1 host to guest complexes. Inclusion complexes were formed between the guests and a number of derivatised CDs, yielding five new inclusion complexes. Two of these complexes were found to be isostructural, namely TMB·2H4M and TMB·4H3M.

REFERENCES

1. M. R. Caira, *Rev. Roum. Chim*., 2001, **46**, 371-386.
2. T. Steiner and W. Saenger, *Acta Cryst.*, 1998, **B54**, 450-455.
3. D. Mentzafos, I. M. Mavridis, G. Le Bas and G. Tsoucaris, *Acta Cryst*., 1991, **B47**, 746-757.
4. Paratone N oil (Exxon Chemical Co., TX, USA).
5. L. J. Barbour, *J. Appl. Cryst*., 1999, **32**, 351-352.
6. XPREP, *Data Preparation and Reciprocal Space Exploration*, Version 5.1, ©Bruker Analytical X-ray Systems, 1997.
7. D. Mentzafos, I. M. Mavridis and M. B. Hursthouse, *Acta Cryst.*, 1996, **C52**, 1220-1223.
8. J. M. Alexander, J. L. Clark, T. J. Brett, and J. J. Stezowski, *Proc. Natl. Acad. Sci. U.S.A.*, 2002, **99**, 5115-5120.
9. G. M. Sheldrick, *Direct Methods for Solving Macromolecular Structures*, Kluwer Academic Publishers, Dordrecht, 1998.
10. Cambridge Structural Database and Cambridge Structural Database System, Version 5.36, May 2015, Cambridge Crystallographic Data Centre, University Chemical Laboratory, 12 Union Road, Cambridge, England
11. F. W. Lichtenthaler and S. Immel, *Liebigs Ann.*, 1996, 27-37.
12. W. Saenger and T. Steiner, *Acta Cryst.*, 1998, **A54**, 798-805.
13. M. C. Etter, J. C. MacDonald and J. Bernstein, *Acta Cryst*., 1990, **B46**, 256-262.
14. N. R. Lien and J. R. Telford, *Carbohydr. Chem.*, 2009, **344**, 2606-2608.
15. K. Hirose, *J. Inclusion Phenom. Macrocyclic Chem.*, 2001, **39**, 193-209.
16. H.-J. Schneider, F. Hacket, V. Rüdiger and H. Ikeda, *Chem. Rev.*, 1998, **98**, 1755-1785.
17. M. E. Amato, K. B. Lipkowitz, G. M. Lombardo and G. C. Pappalardo, *Magn. Reson. Chem.*, 1998, **36**, 693-705.
18. T. D. Thi, K. Nauwelaerts, M. Froeyen, L. Baudemprez, M. Van Speybroeck, P. Augustijns, P. Annaert, J. Martens, J. Van Humbeeck and G. Van Den Mooter, *J. Pharm. Sci.*, 2010, **99**, 3863-3873.
19. F. Djedaini, S. Lin, B. Perly and D. Wouessidjewe, *J. Pharm. Sci.*, 1990, **79**, 643-646.
20. P. Job, *Ann. Chim.*, 1928, **10**, 113-199.
21. F. J. B. Veiga, C. M. Fernandes, R. A. Carvalho and C. F. G. C. Gerlades, *Chem. Pharm. Bull.*, 2001, **49**, 1251-1256.
22. M. Otagiri, K. Uekama and K. Ikeda, *Chem. Pharm. Bull.*, 1975, **23**, 188-195.
23. H. M. Cabral Marques, J. Hadgraft, I. W. Kellaway and W. J. Pugh, *Int. J. Pharm.*, 1990, **63**, 267-274.
24. K. S. Cameron, D. Fletcher and L. Fielding, *Mag. Res. Chem.*, 2002, **40**, 251-260.

25. C. Floare, F. Balibanu and M. Bogdan, *Studia Universitatis Babes-Bolyai, Physica, Special Issue*, 2005, **L. 4a**, 451-454.
26. D. Bardelang, J.-L. Clement, J.-P. Finet, H. Karoui and P. Tordo, *J. Phys. Chem.* 2004, **108**, 8054-8061.
27. D.-Z. Sun, L. Li, X.-M. Qiu, M. Liu and B.-l. Yin, *J. Solution Chem.*, 2006, **35**, 1537-1549.
28. L. Wadsö, Y. Li, and X. Li, *J. Chem. Ed.*, 2011, **88**, 101-105.
29. L. Fielding, S. C. McKellar and A. J., Florence, *Magn. Reson. Chem.*, 2011, **49**, 405-415.
30. L. Liu and Q.-X. Guo, *J. Inclusion Phenom. Macrocyclic Chem.*, 2002, **42**, 1-14.
31. Y. Inoue and M. V. Rekharsky, *Chem. Rev.*, 1998, **98**, 1875-1917.
32. M. R. Caira, F. Giordano and S. L. Vilakazi, *Supramol. Chem.*, 2004, **16**, 389-393.
33. G. R. Desiraju, *Acc. Chem. Res.*, 1996, **29**, 441-449.
34. E. J. C. de Vries and M. R. Caira, *Carbohydr. Res.*, 2008, **343**, 2433-2438.

Chapter 7: Conclusion

SUMMARY

A number of nutraceuticals with antioxidant properties were modified using supramolecular chemistry methods. A brief summary of the results obtained is presented below:

- Three inclusion complexes were obtained with the guest molecule *trans*-resveratrol and the host molecules TRIMEB, TRIMEA and DIMEB, respectively, namely TMB·RES, TMA·RES and DMB·RES.
- Inclusion complexes were obtained by kneading and coprecipitation with hydroxycinnamic acids and β-CD (yielding β-CD·FA, β-CD·HFA, β-CD·HCA and β-CD·PCA) as well as γ-CD (yielding γ-CD·CAF, γ-CD·HCA, γ-CD·FA, γ-CD·HFA, and γ-CD·PCA). Sinapic acid did not from inclusion complexes with either β- or γ-CD; instead, the attempted preparations of new complexes of SA with the native CDs produced crystals of the guest alone. An investigation into inclusion complex formation of the hydroxycinnamic acid guests with three derivatised CDs resulted in the inclusion complexes TMB·HFA, TMB·PCA, TMA·FA and TMA·PCA. 'Exclusion' or 'partial inclusion' complexes were also produced, namely DMB·CAF, DMB·FA, DMB·HFA and DMB·PCA.
- Isothermal titration calorimetry (ITC) was used to investigate the thermodynamics of the interactions between each of the hydroxycinnamic acid guest molecules and the native CDs, β- and γ-CD, respectively, in aqueous solution.
- Cocrystallisation was attempted with the hydroxycinnamic acid guests and the coformers nicotinamide and isonicotinamide. Seven cocrystals and one cocrystal hydrate were obtained.
- Four isomeric acetophenone derivatives 2H4M, 2H5M, 2H6M and 4H3M formed inclusion complexes with both β- and γ-CD by coprecipitation/slow cooling. Kneading yielded β-CD inclusion complexes with three of the four guests, as well γ-CD complexes with all four guests. Five inclusion complexes were obtained with the derivatised CDs, namely TMB·2H4M, TMB·4H3M, TMB·2H5M, DMB·4H3M and TMA·2H5M.
- The interactions between each guest molecule 2H4M, 2H5M, 2H6M and 4H3M and the native CDs, β- and γ-CD, respectively, were studied in aqueous solution using ^{1}H NMR spectroscopy. The host-guest ratio was found to be 1:1 for all complexes and the association constants were evaluated.
- Crystalline products were characterised using single crystal X-ray diffraction, PXRD, TGA, DSC, HSM and ^{1}H NMR spectroscopy.
- Phase solubility experiments were performed to determine the solubility enhancement effected by CD inclusion. Semi-quantitative solubility experiments were carried out on three of the eight cocrystals produced.

A total of 40 X-ray crystal structures (nine γ-CD inclusion complexes, seven β-CD inclusion complexes, 16 inclusion complexes with derivatised CDs and eight cocrystals) were determined and described in this study.

CRYSTAL STRUCTURES

While the X-ray structures elucidated are novel, some of the inclusion complexes and cocrystals are not new, in the sense that they have been of interest in the area of nutraceuticals for some time and therefore have been previously studied to some extent. However, the earlier treatments focused on these compounds in powder form only, or exclusively in solution, while others were investigated by theoretical methods.[1-15] Therefore this thesis contribution is highly significant for the potential application of these compounds in solid form, providing details of explicit molecular structures and the intermolecular interactions present in these phases.

The CD inclusion complexes with *trans*-resveratrol (RES) revealed a very unusual supramolecular hydrogen bonding motif between the 1,3-benzenediol moiety of RES and the surrounding water molecules such that a "crown" of water molecules is formed on the 1,3-benzenediol ring. This unique feature is common to all three RES structures.

The phenomenon of "mutual induced fit" is illustrated by the conformations of the derivatised host molecules and each guest molecule, whereby the conformation of each component is dependent on the other.[16] This is a manifestation of the lock and key model introduced by Fischer in 1894, where an active site may be accessed by a substrate which fits the site.[17] Koshland expanded upon this model by determining that the conformation of active sites may change to allow a better fit of a substrate.[18]

The structures TMB·HFA and TMB·PCA are extraordinarily similar, from guest inclusion mode to crystal packing, and they may be considered 'nearly isostructural' as the *c*-axis of TMB·PCA is somewhat longer than that of TMB·HFA. Examination of the packing diagrams reveals that the cause of this elongation is the presence of six additional water molecules, disrupting the close packing of complex units (as seen in TMB·PCA). Similarly the structures of DMB·HFA and DMB·PCA are nearly isostructural, where the larger HFA molecule extends further from the CD cavity into the intermolecular space between complex units, causing the *c*-axis of DMB·HFA to be elongated when compared to that of DMB·PCA.

Another remarkable result was the discovery of the exclusion complexes DMB·CAF and DMB·FA, in which the guest molecules exist in the interstitial space between the CD molecules. A O6-methoxyl group on one DMB molecule is included within the cavity of a neighbouring DMB molecule and repetition of this motif leads to a column of DMB molecules. The guest molecules and most of the water molecules exist in

distinct pockets between the helical host columns. Each guest molecule engages in a hydrogen bond with an adjacent host molecule as well as with the water O atom, linking the host and guest molecules.

INVESTIGATIONS IN AQUEOUS SOLUTION

Phase solubility experiments were performed with RES and the native CDs β- and γ-CD, as well as the derivatised CDs TMB, DMB, HP-β-CD and RAMEB. Solubility enhancements were observed for all host-guest combinations, with β-CD effecting a 26-fold increase and RAMEB effecting a maximum solubility increase of 63 times that of free RES. The association constants were calculated and ranged from 410 M^{-1} for γ-CD to 11600 M^{-1} for DMB.

The ITC technique was used to determine the thermodynamic parameters and association constants for the complexation between hydroxycinnamic acids and both β- and γ-CD. The guest molecules were found to interact with β-CD in a 1:1 host-guest ratio, with association constants in the order of hundreds (246 - 774 M^{-1}). These results are comparable with those obtained from the phase solubility experiments performed with CAF and β-CD (K = 660 M^{-1}) and FA with β-CD (K = 500 M^{-1}). The complexation between the guest molecules and β-CD was found to be enthalpy-driven, except in the case of SA and β-CD, where complexation was entropy-driven. CAF interacts with γ-CD in a 1:1 host-guest ratio (K = 475 M^{-1}) while PCA, FA and SA interact with γ-CD in a 2:1 molar ratio. The association constants for complexation of the guests with γ-CD were in the order of hundreds (228-543 M^{-2}). The formation of 2:1 complexes in solution was found to be enthalpy-driven while formation of the 1:1 complex was entropy-driven.

The interactions between the acetophenone derivatives and the hosts β- and γ-CD in solution were studied using ^{1}H NMR spectroscopy. Job Plot analysis of each complex formed with β-CD revealed 1:1 stoichiometries. The association constants were calculated to be 224 M^{-1} for β-CD·2H4M, 154 M^{-1} for β-CD·2H5M, 145 M^{-1} for β-CD·2H6M and 336 M^{-1} for β-CD·4H3M. Similarly for γ-CD, interactions were confirmed to be 1:1 with 2H6M and 4H3M, respectively, with association constants being 67 M^{-1} for γ-CD·2H6M and 125 M^{-1} for γ-CD·4H3M. Due to the low concentrations of host and guest used no reliable results were obtained for γ-CD·2H4M and γ-CD·2H5M.

Semi-quantitative solubility studies were performed for the cocrystals FA·NIC, PCA·NIC and $(PCA)_2$·NIC. The results showed that the solubility of the antioxidant component was significantly enhanced by the formation of the cocrystal in each case.

FUTURE WORK

Towards the end of this project an inclusion complex of caffeic acid with TMA was obtained and analysed with single crystal X-ray diffraction. The structure was solved (space group $P2_12_12_1$, a = 15.6, b = 20.8,

c = 23.6 Å) but due to time constraints the inclusion complex was not further characterised. This study should be completed in order to publish the results.

After generating seven cocrystals and a hydrate with hydroxycinnamic acids (HCAs) and the coformers nicotinamide and isonicotinamide, an attempt was made to measure the resulting solubility enhancement of the acid component rendered by these products. A semi-quantitative method was employed and results were obtained for three of the eight samples, indicating a minimum but positive solubility enhancement. Due to time constraints ^{1}H NMR spectroscopy was used to analyse the samples as the experiments did not need optimisation using this method. In order to obtain more accurate results measurements should be taken over a period of time using a technique such as high performance liquid chromatography. Periodic measurements may also give insight into any changes in HCA:coformer ratios that may be inconsistent with the 'spring and parachute' effect.[19]

In cocrystal formation the use of different solvents or multi-solvent systems may result in more stable products or cocrystal polymorphs, a valuable result in the field of pharmaceuticals/nutraceuticals. Future studies exploring the use of different solvents may also facilitate the formation of supramolecular synthons between the hydroxycinnamic acids and other coformers.

Variable-temperature PXRD is a useful tool to distinguish the different polymorphic phases that result when a complex or cocrystal is heated. This aspect was not pursued in the present study, but for the instances in which thermal analysis did indicate a heat-induced phase transformation for several inclusion complexes and the cocrystal FA·NIC, this technique may in the future shed light on the products of phase transformation.

REFERENCES

73. C. Lucas-Abellán, M. T. Mercader-Ros, M. P. Zafrilla, J. A. Gabaldón and E. Núñez-Delicado, *Food Chem. Toxicol.*, 2011, **49**, 1255–1260.
74. C. Lucas-Abellán, M.I. Fortea, J.A. Gabaldón, E. Núñez-Delicado, *Food Chem.*, 2008, **111**, 262-267.
75. F. Kayaci and T. Uyar, *J. Agric. Food Chem*., 2011, **59**, 11772–11778.
76. S. Divakar, *J. Agric. Food Chem.,* 1990, **38**, 940-944.
77. J.- Y. Tsao, C.- P. Wu, H.- H. Tsai, K.- C. Peng, P.- Y. Lin, S.- Y. Su, L.- D. Chen, F.- J. Tsai and Y. Tsai, *J. Incl. Phenom. Macrocycl. Chem*., 2012, **72**, 405-411.
78. C. Chen, X. Xu, Y. Li and H. Ma, *Trop. J. Pharm. Res.,* 2015, **14**, 1565-1571.
79. Y. Tsai, H.- H. Tsai, C.- P. Wu and F.- J. Tsai, *Food Chem*., 2010, **120**, 837-841.
80. M.- E. Cuvelier, H. Richard and C. Berset, *Biosci. Biotech. Biochem.*, 1992, **56**, 324-325.
81. S. Divakar and M. M. Maheswaran, *J. Incl. Phenom. Mol. Recog. Chem.*, 1997, **27**, 113-126.
82. M. Zhang, J. Li, L. Zhang and J. Chao, *Spectrochim. Acta Mol. Biomol. Spectrosc.*, 2009, **71**, 1891-1895.
83. M. Strazisar, S. Andrensek and A. Smidovnik, *Food Chem*., 2008, **110**, 636-642.
84. J. Wang, Y. Cao, B. Sun and C. Wang, *Food Chem*., 2011, **124**, 1069-1075.
85. B. Liu, J. Zeng, C. Chen, Y. Liu, H. Ma, H. Mo and G. Liang, *Food Chem*., 2016, **194**, 1156-1163.
86. P. Górnaś, G. Neunert, K. Baczyński and K. Polewski, *Food Chem*., 2009, **114**, 190-196.
87. S. Haiahem, L. Nouar, I. Djilani, A. Bouhadiba, F. Madi and D. E. Khatmi, *C. R. Chimie*, 2013, **16**, 372-379.
88. A. Cooper, M. Nutley, E. J. MacLean, K. Cameron, L. Fielding, J. Mestres and R. Palin, *Org. Biomol. Chem.*, 2005, **3**, 1863-1871.
89. E. Fischer*, Berichte der Deutschen chemischen Gesellschaft zu Berlin*, 1894, **27**, 2985-2993.
90. D. E. Koshland. Jr., *Proc. Natl. Acad. Sci. USA,* 1958, **44**, 98.
91. H.R. Guzmán, M. Tawa, Z. Zhang, P. Ratanabanangkoon, P. Shaw, C. R. Gardner, H. Chen, J. Moreau, O. Almarsson and J. F. Remenar, *J. Pharm. Sci.,* 2007, **96,** 2686-2702.